The Role of Bone Morphogenetic Protein (BMP) Signalling in Lung Cancer and Lung Regeneration

By

Jennifer L Gilbert
B.A. (Mod)

A thesis submitted to
The National University of Ireland, Maynooth
for the degree of

Doctor of Philosophy

Department of Biology
National University of Ireland
Maynooth

NUI MAYNOOTH
Ollscoil na hÉireann Má Nuad

January 2009

Supervisor: Dr. Shirley O'Dea

Abbreviations

1-NN	1-nitronaphthalene
AAH	atypical adenomatous hyperplasia
AATD	alpha-1 antitrypsin deficiency
AAV	adeno-associated virus
ActR	activin receptor
Ad	adenovirus
ALK	activin like kinase
APS	ammonium persulphate
AQP5	aquaporin 5
ATCC	american type culture collection
BAC	bacterial artificial chromosome
BADJ	bronchoalveolar duct junction
BAMBI	BMP and activin membrane-bound inhibitor
BASC	bronchial alveolar stem cell
BEAS	bronchial epithelial airway cell
B-gal	beta galactosidase
BME	beta mercaptoethanol
BMP	bone morphogenic protein
BMPR	bone morphogenic protein receptor
BOOP	bronchiolitis obliterans organizing pneumonia
Bp	base pair
BrdU	5-bromo-2'-deoxyuridine
BSA	bovine serum albumin
caBMPR	constitutively active BMP receptor
CC10	Clara cell 10 (aka CCSP)
CCSP	clara cell specific protein
cDNA	complimentary DNA
COPD	chronic obstructive pulmonary disease
Crmp2	collapsing response mediator protein 2
CYP450	cytochrome 450 mono-oxygenase enzyme

DAPI	4’,6-diamidino-2-phenylindole
DEPC	diethylenepyrocarbonate
DMEM	dulbecco’s modified eagle’s media
DMEM:F12	dulbecco’s modified eagle’s media and hams F12
DMSO	dimethylsulphoxide triphosphate
DNA	deoxyribonucleic acid
dnBMPR	dominant negative BMP receptor
DNMT	DNA methyltransferase
DSFM	defined serum free media
DTT	dithiothreitol
E 9.5	embryonic day 9.5
EBAO	ethidium bromide/ acridine orange
ECL	enhanced chemiluminescence
ECM	extracellular matrix
EDTA	ethylenediaminetetraacetic acid
EGF	epithelial growth factor
EGFR	epithelial growth factor receptors
EMT	epithelial to mesenchymal transition
ER	endoplasmic reticulum
ERK	extracellular signal related kinase
EtOH	ethanol
FACS	fluorescent-activated cell sorting
FBS	fetal bovine serum
FGF	fibroblast growth factor
FPAH	familial pulmonary arterial hypertension
GAP	GTPase activating proteins
GAPDH	glyceraldehyde 3-phosphate dehydrogenase
GCV	ganciclovir
GDP	guanine diphosphate
GEF	guanine nucleotide exchange factor
GFP	green fluorescent protein

GGT	gamma-glutamyl transferase
GST	glutathione S transferase
GTP	guanine triphosphate
HC	hydrocortisone
HDAC	histone deacetylase
HGF/SF	hepatocyte growth factor/ scatter factor
HIV	human immunodeficiency virus
HLH	helix loop helix
HRP	horseradish peroxidise
Id	inhibitor of differentiation
IgE	immunoglobulin E
IκB	inhibitor of kappa B
IPAH	idiopathic pulmonary hypertension
IPF	idiopathic pulmonary fibrosis
I-Smad	inhibitory Smad
JNK	Jun N-terminal kinase
K5	cytokeratin 5
kb	kilobase
KDa	kilo dalton
LCM	laser capture microdissection
LDH	lactate dehydrogenase
LoxP	locus of cross-over P1
LSL	loxP-stop-loxP
MADH4	mad homology domain 4
MAECs	mouse airway epithelial cells
MAPK	mitogen activated protein kinase
MET	mesenchymal-epithelial transition
MeOH	methanol
$MgCl_2$	magnesium chloride
MH1	mad homology domain 1
μm	micrometer

MMP	matrix metalloprotease
MMR	mis-match repair
mRNA	messenger ribonucleic acid
MTS	3-(4,5-dimethylthiazol-2-yl)-5-(3-carboxymethoxyphenyl)-2-(4-sulfophenyl)-2H-tetrazolium)
Myc	myelocytomatosis viral oncogene
NaCl	sodium chloride
NSC	neural stem cells
NEB	neuroendocrine bodies
NFκB	nuclear factor kappa B
ng	nanogram
NSCLC	non-small cell lung cancer
O_3	ozone
OD	optical density
OP-1	osteogenic protein 1
Ova	ovalbumin
PAH	polycyclic aromatic hydrocarbon
PASMC	pulmonary arterial smooth muscle cells
PI3K	phosphoinositide 3-kinase
PBS	phosphate buffered saline
PCNA	proliferating cell nuclear antigen
PCR	polymerase chain reaction
PFA	paraformaldehyde
Pfu	plaque forming units
pg	picogram
PI	propidium iodide
P-smad	phospho-smad
Rb	retinoblastoma
RNA	ribonucleic acid
rpm	revolutions per minute
R-Smad	receptor smad

RTK	receptor thyrosine kinase
RT-PCR	reverse transcriptase polymerase chain reaction
SBE	smad binding element
SDS	sodium dodecyl sulphate
SCLC	small cell lung cancer
Smad	mothers against decapentaplegic homology
SP-A	surfactant protein A
SP-B	surfactant protein B
SP-C	surfactant protein C
SP-D	surfactant protein D
STAT	signal transducers and activators of transcription protein
SV40	simian virus 40
TBS	tris buffered saline
TGFβ	transforming growth factor β
TFGβR	transforming growth factor β receptor
TIC	tumour initiating cells
TKI	tyrosine kinase inhibitors
TSC	tumour stem cells
UV	ultraviolet
vCE	variant Clara cells
VSV-G	vesicular stomatitis virus glycoprotein
XIAP	X-linked inhibitor of apoptosis protein
YAC	yeast artificial chromosome
ZEB	zinc finger E-box binding homeobox protein

Publications

Gilbert, J.L., Purcell, J., Strappe, P., McCabe, M., O'Brien, T. and O'Dea, S. (2008) Comparative evaluation of viral, non-viral and physical methods of gene delivery to normal and transformed lung epithelial cells. Anti-Cancer Drugs. 19(8):783-788.

Jin N., Gilbert J.L., Broaddus R.R., DeMayo F.J., Jeong J.W. (2007)
Generation of a Mig-6 conditional null allele. Genesis. 45(11): 716-721

Summary

Bone morphogenetic proteins (BMPs) are members of the transforming growth factor beta (TGFβ) super-family of signalling molecules. BMPs play crucial roles in developing and adult tissues during processes including proliferation, differentiation, apoptosis and epithelial-mesenchymal transition (EMT). However, little is known regarding the role of BMPs in adult lungs during health and disease. In the present study, the role of BMP signalling in lung cancer and lung regeneration processes was examined.

Early lung cancer tumours were isolated by laser capture microdissection from K-ras^{G12D} mouse lungs and microarray analysis was carried out on RNA from the purified populations of cells. Microarray and qPCR analyses revealed differential BMP pathway expression during early tumour formation. BMPR expression was decreased compared to normal lung epithelial cells while BMP4, BMP5, Smad4 and Id-1 expression were increased.

We hypothesized BMPR-IB plays an anti-proliferative role during early tumour progression. To characterise the function of BMPR-IB in lung cells, the gene was cloned from mouse lung cDNA and an over-expression vector was generated. Viral and non-viral delivery methods were assessed for their ability to efficiently transfect normal and tumour-derived lung cells. Lipofectamine-2000 was the most efficient non-viral method of gene delivery. This mode of transfection was utilised to transfect BMPR-IB gene into the human BEAS-2B cell line, which is devoid of endogenous BMPR-IB expression. The effects of BMPR-IB expression on proliferation, BMP signalling, and differentiation were assessed. BMPR-IB expression caused a reduction in viable cell number, an increase in non-viable cell number and an increase in cell death by apoptosis. Given the loss of expression of BMPR-IB at the early stages of cancer, these data suggest that BMPR-IB may have anti-proliferative properties during this stage in cancer.

The role of BMP signalling in lung regeneration processes was also examined in the 1-NN acute lung damage. BMP signalling was up-regulated during the inflammatory stage of lung damage. These data suggest that the BMP pathway plays an integral role during regeneration and disease processes in the adult lung.

1. Introduction

1.1. The Lungs

The lungs are the primary organs responsible for gas exchange. Air is inhaled into the lungs via the nasal cavity or oral cavity and passes through the conducting airways to the alveolar region where gas exchange occurs. The conducting airways are composed of the trachea, bronchi, bronchioles and terminal bronchioles, and function in filtering and delivering air to the alveolar region (Figure 1.1 (Sun, S *et al.*, 2007)). The cells lining the conducting airways are heterogeneous and differ by location from proximal to distal regions. Through the process of inhalation the epithelial cells of the lung are constantly exposed to environmental toxins that can damage the epithelial barrier. Damage to the epithelial cells caused by toxins, infection or genetic mutations can lead to an array of lung diseases including cancer, asthma, fibrosis and cystic fibrosis.

The lungs develop as an outgrowth from the foregut endoderm and undergo branching morphogenesis through a number of stages: endoderm (3-7 weeks), pseudoglandular (5-17 weeks), canalicular (16-26 weeks), saccular (24-38 weeks), and alveolar (32- 18 months post natal). The proximal region gives rise to the larynx and trachea and the distal portion branches and gives rise to the right and left bronchi (Warburton, D *et al.*, 2006). Branching from the bronchi occurs in an organised pattern and continues up to 20 weeks in humans (Metzger, RJ *et al.*, 2008). Alveolarisation begins at 20 weeks gestation in humans and continues up to 7 years of age in the growing child. During development the cells of the conducting airways undergo differentiation to produce the numerous cells types of the airways. The factors that influence the differentiation of epithelial cells during development are many and include autocrine and paracrine signals from the epithelial cells themselves and from the cells within the underlying mesenchymal layer.

The adult lung has an alveolar surface of 70 m^2 and an alveolar thickness of 1 μm. The gas diffusion surface is juxtaposed to the capillary network. The oxygen from inhaled air diffuses into the capillaries and carbon dioxide diffuses out of the capillaries and is exhaled from the lungs. The proximal conducting airways are mainly composed of

ciliated cells, secretory cells (goblet cells, serous cells, Clara cells) and basal cells. Ciliated cells contain cilia on the apical surface of the cell membrane and are considered to be terminally differentiated cells. Ciliary action serves to remove pathogens and debris from inhaled air immobilised in the mucus layer. Goblet cells are responsible for secreting heavy mucus proteins, which in association with the cilia compose the mucocillary clearance for removing pathogens and debris from the lungs. These cells are in high abundance in the larger airways. Clara cells, which are more abundant in the lower airways, are identified as non-ciliated cells with abundant smooth endoplasmic reticulum. Clara cells have many important functions in the lung including roles in inflammation, detoxifying the lungs and lung regeneration. These cells will be discussed in more detail in section 1.3.

1.2. Lung Disease

Lung disease results in significant morbidity and mortality in the human population. Worldwide mortality from respiratory diseases is second only to cardiovascular disease. Respiratory diseases appear three times on the list of top ten causes of death in the Western world, according to the WHO (World Health Organisation), these include: lung cancer, lower respiratory infections and chronic obstructive pulmonary disease. The causes of lung disease are numerous and include inherited or acquired genetic defects, environmental toxins and pathogens.

Genetically inherited lung diseases can be sub-divided into simple diseases with one known defective gene, including cystic fibrosis and alpha-1-anti-trypsin; or complex genetic diseases with many defective genes including asthma. Cystic fibrosis (CF) is the most common lethality inherited disease among Caucasians (Griesenbach, U *et al.*, 2006). This disease affects all epithelial cells but the main disease pathology impacts on lung function. Mutations in the cystic fibrosis transmembrane receptor (CFTR) gene, a chloride ion channel, results in a disease pathology that includes increased mucus formation and a reduction in mucocilary clearance. These patients are prone to bacterial

colonisation, which results in chronic infection and inflammation, leading to irreversible alteration to lung architecture (Sibley, CD *et al.*, 2006). α1-antitrypsin deficiency manifests as liver cirrhosis and pulmonary emphysema. This disease is caused by a point mutation in the SERPINA1 gene, which truncates the anti-protease and renders it defective. Defective protein is sequestered in the liver; the lack of circulating α1-antitrypsin exposes the lungs to enzymatic damage by neutrophil elastase, which causes early onset of emphysema (Fregonese, L *et al.*, 2008). Asthma is a chronic inflammatory lung disease. The symptoms of the disease include airway obstruction, bronchial hyper-responsiveness and inflammation, which contribute to architectural changes (Warrier, MR and Hershey, GK, 2008). The disease pathology occurs when an allergen evokes a Th_2 response which, in turn, recruits eosinophils via IL-5 production, B cells via IL-4 and IL-13 production and mast cells via IL-9 production. This acute inflammatory response initiates a cascade of events that result in persistent inflammation and hyper-responsiveness. Repeat episodes of the acute inflammatory response result in progressive remodelling of the airway. Numerous genetic susceptibility markers have been associated with the onset of asthma, these include ADAM33, DPP10, PHF11, SETDB2, GPRA and SPINK5 (Blumenthal, MN, 2005).

Many lung diseases are attributed to environmental toxins from inhaled air. Tobacco smoke, containing more than 60 carcinogens (including polycyclic aromatic hydrocarbons and benzopyrimidine), is the main risk factor for chronic obstructive pulmonary disease (COPD). COPD is characterised by an obstruction in airflow due to chronic bronchitis, emphysema or chronic inflammation and is the fourth leading cause of adult deaths in the United States (Mannino, DM, 2002). It is a heterogeneous disorder that manifests with many symptoms, and disease pathology associated with irreversible remodelling of the airways (Mannino, DM, 2002). Lung cancer is the leading cause of cancer deaths in the western world; 90% of lung cancer cases are due to smoking, but because only 10% of smokers develop the disease there is thought to be genetic susceptibility element involved in this disease. This disease will be discussed in further detail in section 1.6. Other environmental toxins such as nitro-naphthalenes and ozone are found in high abundance in urban areas and can lead to airway damage. These chemicals

are by-products of diesel combustion. These chemicals cause lung damage that will be described further in section 1.5.

1.3. Clara cells

Clara cells are the most abundant cell type of the distal airways. These cells are identified as non-ciliated columnar cells with high abundance of smooth endoplasmic reticulum and under a light microscope appear to bleb at the apical region. This blebbing appearance is due to the high abundance of secretory granules that are important in lung homeostasis and during lung disease. Due to their cellular properties and secretory proteins, Clara cells have key functions in modulation of immune responses, regulation of lung regeneration and protection against environmental agents as discussed in section 1.3, 1.4, 1.5.

During homeostasis, Clara cells are responsible for the secretion of surfactant protein (SP-) A, B and D, but not SP-C which is specifically expressed by type II pneumocytes (Kalina, M *et al.*, 1992). Surfactant proteins are secreted by both Clara cells and alveolar epithelial cells; these proteins form a film on top of the epithelial lining and function in maintaining normal lung physiology and immune defence. SP-B is a phospholipid responsible for maintaining alveolar and airway surface tension. Mutations in this gene are associated with respiratory distress syndrome in new born babies (Beck, DC *et al.*, 2000). SP-A and SP-D surfactant proteins are involved in the innate immune response. Both proteins function in opsonisation of pathogens, by binding directly to microbes and causing their aggregation, and modulating the immune response (McCormack, FX and Whitsett, JA, 2002). SP-A and SP-D stimulate phagocytosis by alveolar macrophage and modulate the release of cytokines and reactive oxygen species from these cells. Administration of recombinant SP-D into an airway hyper-responsiveness (AHR) mouse model resulted in the reduction of the immune response. SP-D has been shown to cause an induction of anti-inflammatory cytokines (IL-10) and Th1 cytokines (IL-12 and IFNγ)

inhibition of histamine release from basophils, inhibition of T-cell proliferation, and reduction of eosinophils expression in the BALF of AHR (Takeda, K *et al.*, 2003). These immune modulatory properties of surfactant proteins have spurred the investigation of their use as therapeutics for chronic lung disease.

The most abundant secretory protein from Clara cells in the airways is the 16 kDa Clara cell specific protein (CCSP). Mouse models of CCSP ablation have alluded to the possible functions of the Clara cells during lung injury and chronic inflammation. CCSP has an important function in protection against intrapulmonary inflammation, both as a physical barrier and as an immunomodulator. CCSP ablation studies in mice resulted in ultra structural changes in the Clara cells and altered secreted proteins from these cells (Stripp, BR *et al.*, 2002). CCSP functions in protecting the lung from oxidant-induced damage (Plopper, CG *et al.*, 2006). Ozone challenge of CCSP knock-out mice result in increase susceptibility to damage. CCSP is also an important immunomodulator. Levels of CCSP expression are reduced in a number of acute and chronic lung infections. Acute lung inflammation caused by lipopolysaccharide resulted in a reduction in CCSP expression (Arsalane, K *et al.*, 2000). CCSP levels were also seen to be reduced in mice after *Pseudomonas aeruginosa* infection (Hayashida, S *et al.*, 2000). CCSP is an inhibitor of phospholipase A_2, in this way it acts as a negative regulator of inflammation (Facchiano, A *et al.*, 1991). Therefore during acute lung injury, when inflammatory response is stimulated, the level of CCSP is attenuated. In conclusion, low levels of CCSP expression are associated with chronic inflammation. Treatment of $CCSP^{-/-}$ mice with ovalbumin resulted in an increased inflammatory response compared to wild type mice (Wang, SZ *et al.*, 2001). Studies are required to examine the endogenous level of CCSP expression of asthmatics to establish if a deficiency in CCSP is contributing to the asthma phenotype. Examination of COPD patients revealed a decrease in CCSP expression in patients with severe COPD (Braido, F *et al.*, 2007). Healthy smokers have high levels of CCSP suggesting the protein has a protective effect against the development of COPD. Therefore low levels of CCSP can be used as a predictive or prognostic factor of COPD. A complex array of transcriptional regulators are responsible for the attenuation of CCSP after oxidant induced lung injury (Ramsay, PL *et al.*, 2003).

These regulators might be important targets for the amelioration of chronic lung diseases, such as COPD and asthma, which are deficient in CCSP expression.

Another characteristic of Clara cells is their high abundance of cytochrome P450 monooxygenase enzymes (CYP450). These enzymes confer onto Clara cells an important role in detoxifying environmental pollutants inhaled into the airways. The ability of Clara cells to metabolise pollutants expose them to harmful toxins. CYP450s metabolise an array of environmental toxins including polycyclic aromatic hydrocarbons (PAH). PAH are found in high abundance in cigarette smoke and can contribute to the development of lung cancer by producing DNA adducts that inactivate tumour suppressor genes or activate oncogenes. Lung cancer is described in more detail in section 1.6. Other environmental pollutants that are metabolised by Clara cells are the naphthalenes. Naphthalene and nitro-naphthalene are by-products of diesel combustion and therefore found in high abundant in urban areas. Acute lung injury animal studies have shown the ability of nitro-naphthalene to cause exfoliation of the Clara cells from the basement membrane. These studies will be discussed in more detail in section 1.5. The ability of naphthalene to ablate Clara cells has been utilised for the study of lung progenitor cell populations. Naphthalene ablation studies have revealed how indispensible Clara cells are for airway regeneration. These studies will be discussed in more detail in section 1.4.

1.4. Lung Regeneration

The epithelial lining of the conducting airways has a low mitotic rate in steady state. Nevertheless, epithelial cells have the ability to increase their proliferation rate and repair the epithelial lining following injury (Figure 1.2). The lung is composed of a heterogeneous population of cells, the composition of cells differ from proximal to distal regions. In line with the heterogeneity of cell populations, there are distinct stem cells that are responsible for regional differences in the repair process. A stem cell which, by definition, has low proliferation in steady state can proliferate and self-renew upon injury and can differentiate into other cell phenotypes. Differing from a stem cell, a transit-

amplifying (TA) or progenitor cells have a more limited ability to proliferate and differentiate compared to stem cells. Numerous injury models have been used to identify the tissue specific stem cells of the lung. One model used employs the conditional ablation of Clara cells by the administration of gancyclovir to CCSP-thymidine kinase expressing transgenic mice. Gancyclovir, an inert compound, is metabolised to a toxin by thymidine kinase and therefore ablates Clara cells by CCSP conditional expression. The second method utilised in many studies involves the acute administration of the toxin naphthalene to ablate CYP450 expressing Clara cells. Because Clara cells comprise the majority of cells populating the epithelial surface, ablation by either method causes major damage in the airways of the lungs.

The tracheobronchial epithelium is lined predominantly with ciliated and nonciliated secretory cells (Clara, basal and goblet cells). There have been numerous suggestions as to the cells responsible for regeneration of the bronchial epithelium; these included either secretory or ciliated cells (Evans, MJ *et al.*, 1986; Liu, JY *et al.*, 1994). A convincing report by Hong *et al* showed the importance of basal cells for the regeneration of the bronchial epithelium (Hong, KU *et al.*, 2004). Ablation of Clara cells by gancyclovir administration to CCSP-thymidine kinase expressing mice and acute naphthalene administration caused an increase in BrdU (proliferation marker) and GSI-B4 lectin (basal cell marker) double labelled cells. Therefore basal cells hyperproliferated in response to Clara cells damage. Examination of time points after Clara cells depletion resulted in the identification of a small number of CCSP (Clara cell marker) and K14 (basal cell marker) double positive cells, showing the ability of basal cells to differentiate into Clara cells. Transgenic mice expressing the LacZ reporter gene under the control of K14 promoter and regulated in a temporal manner by administration of Tamoxifen, were generated. Treatment of this mouse with naphthalene and Tamoxifen resulted in β-galactosidase expression in basal cells in conjunction with Clara cell depletion. Examination of late recovery time points (days 12 and 20) allowed characterisation of cells expressing β-galactosidase that originated as K14 expressing basal cells. This experiment resulted in the identification of β-galactosidase stained cells no longer expressing K14 or basal cell morphology, and that were cuboidal or ciliated in

morphology. A small population of cells expressing β-galactosidase also expressed CCSP. Basal cell proliferation in the trachea and primary bronchi in response to Clara cells damage was also observed by Rawlins *et al* (Rawlins, EL *et al.*, 2007). Therefore basal cells of the bronchial airway can proliferate and differentiate into ciliated cells and Clara cells, and are important for the repair of the bronchial epithelium.

The bronchiolar airways are mainly composed of cuboidal non-ciliated secretory cells (Clara cells), with fewer ciliated cells and a sparse population of neuroendocrine cells localised to clusters (Jeffery, PK and Reid, L, 1975). Both the naphthalene damage model (mentioned above and described in detail in section 1.5) and the gancyclovir CCSP-thymidine kinase model ablating Clara cells in the lungs of mice have resulted in an increase in pulmonary neuroendocrine cells (PNEC) within the neuroendocrine bodies (NEB) (Peake, JL *et al.*, 2000; Reynolds, SD *et al.*, 2000a). Cells in this region become hyperproliferative after Clara cell damage and have the capacity to self renew. Longevity studies in these models show PNECs do not have the ability to regenerate damaged airways (Hong, KU *et al.*, 2001; Reynolds, SD *et al.*, 2000b). Therefore PNEC are progenitor cells with the ability to proliferate in response to damage but do not have the ability to differentiate and repopulate the airways.

Ciliated cells are terminally differentiated cells that do not proliferate in response to epithelial damage. Recent studies show conflicting data as to the ability of ciliated cells to act as progenitor cells in the lung. Park *et al* suggest ciliated cells are progenitor cells in the lung with the ability to proliferate in response to a pneumonectomy and re-differentiate into Clara cells in response to naphthalene injury (Park, KS *et al.*, 2006). Transgenic mouse model studies in which mice express LacZ reporter gene in a FoxJ1-Cre specific conditional manner have shown ciliated cells cannot proliferate and do not trans-differentiate into other cell phenotypes (Rawlins, EL *et al.*, 2007).

Clara cells are the main transit amplifying cell of the bronchiolar airways (Evans, MJ *et al.*, 1978; Evans, MJ *et al.*, 1986). Identification of the progenitor cell of the distal airway has come from Clara cell ablation studies. Elimination of susceptible Clara cells by acute

naphthalene exposure results in the proliferation of naphthalene resistant Clara cells which reside in the neuroendocrine body (NEB). These variant Clara cells are morphologically distinct from other Clara cells in that they do not express the CYP450 enzyme, CYP2F2, and are therefore resistant to the toxic effects of naphthalene. Naphthalene treatment of mice result in proliferation and differentiation of variant Clara cells to allow repopulation of the conducting airways (Hong, KU *et al.*, 2001). Complete ablation of CCSP expressing cells including variant Clara cells, by administration of gancyclovir to CCSP-thymidine kinase expressing mice, demonstrates the requirement of variant Clara cells for the regeneration of the airway epithelium. Administration of naphthalene to these transgenic mice result in the proliferation of PNEC cells, but repopulation of the airways is not possible because of the deficiency of variant Clara cells (Hong, KU *et al.*, 2001).

Another population of naphthalene resistant Clara cells have been found in the most distal regions of the conducting airways, at the bronchiolar alveolar duct junction (BADJ). Again Clara cell ablation studies have identified a naphthalene resistant population of Clara cells that proliferated in response to injury. The naphthalene resistant population of Clara cells at the BADJ are also known as bronchioalveolar stem cells (BASC). BASCs are not associated with calcitonin gene-related peptide (CGRP) expressing pulmonary neuroendocrine cells (PNEC), nor are they localised to NEB (Giangreco, A *et al.*, 2002). BASCs co-express CCSP, Clara cell marker, and SP-C, Type II pneumocyte marker. The increased incidence of BASC in response to both naphthalene (targets Clara cell ablation) and bleomycin (targets Type II cell ablation) injury suggests its involvement in regeneration of terminal bronchioles and alveolar regions (Kim, CF *et al.*, 2005). These cells were isolated by fluorescent activated cell sorting (FACS) and *in vitro* analysis was carried out. Single BASCs have the ability to undergo many rounds of proliferation to form colonies and have the ability to differentiate into cells expressing CCSP (Clara cells), surfactant protein C (SP-C) (Type II pneumocytes) and aquaporin 5 (AQ5) (Type I pneumocytes). Therefore BASCs have the ability to proliferate in response to injury and differentiate into many cell lineages, suggesting they are the stem cell of the distal lung.

In the alveolar regions Type II pneumocytes have long been regarded as the progenitor cells. Bleomcyin (induces lung fibrosis) studies have shown Type II pneumocytes have the ability to proliferate and differentiate into Type I pneumocytes. Furthermore, intratracheal administration of Type II pneumocytes can reverse bleomycin induced fibrosis (Serrano-Mollar, A *et al.*, 2007).

The mechanisms that allow cellular repair after injury lead to dysregulation of steady state growth and differentiation processes. Changes in cellular signalling during the repair process involve hyperproliferation. Constant exposure to damaging agents such as pollutants that promote dysregulation of proliferation or differentiation of epithelial cells increase the risk of developing diseases such as cancer.

1.5. 1-Nitronaphthlene Lung Injury Model

Polycyclic aromatic hydrocarbons (PAH) are environmental pollutants that constitute a high percentage of airbourne particles in urban areas of the United States, Europe and Central America (Calderon-Segura, ME *et al.*, 2004). In certain cell types, PAH are metabolised by enzymes to toxins that bind DNA and proteins, altering their function. Naphthalenes are the most abundant PAH in the atmosphere. These pollutants are products of diesel combustion and are also found in cigarette smoke. 1-Nitronaphthalene (1-NN) is a PAH that forms following the nitration of naphthalene by nitric oxide, or directly from diesel combustion. Studies have shown 1-NN to be a lung toxin causing respiratory distress in rats and mice.

1-NN is an inert compound that is metabolised by CYP450 enzymes to electrophilic metabolites that are toxic to the cell. The non-ciliated cells of the lung have the highest levels of cytochrome 450 mono-oxygenase (CYP450) in the body and are therefore the primary target of 1-NN toxicity. Studies were carried out showing that pre-treatment of animals with CYP450 inhibitors, prior to 1-NN administration, caused a reduction in 1-

NN induced cellular damage. Inhibition of CYP2B (CYP450 isozyme 2B) by chemical inhibitors such as *p*-xylene and *O, O,* S-trimethylphosphorodithioate [OOS-MeP(S)] resulted in protection from 1-NN lung damage (Verschoyle, RD *et al.*, 1993). Foy and Schatz showed that inhalation of *m*-xylene caused a dose related reduction of CYP2B1, CYP4B1 and CYP2E1 enzymes which was sustained for 2 days (Foy, JW and Schatz, RA, 2004). Simultaneous exposure of rats to *m*-xylene and 1-NN prevented the increase of LDH (lactate dehydrogenase) and GGT (gamma-glutamyl transferase) in bronchoalveolar lavage fluid and prevented epithelial denuding caused by 1-NN.

Long-term exposure to naphthalene has caused adenoma formation in mice but not rats and acute exposure to naphthalene caused epithelial cell damage in mice but not rats (Frank, DB *et al.*, 2005). Naphthalene shows species selective toxicity, due to the levels and isoforms of CYP450 in Clara cells. Baldwin *et al* conducted experiments to determine the specific CYP450 required to metabolise both naphthalene and 1-NN (Frank, DB *et al.*, 2005). They found the rate of epithelial damage correlates with the rate of metabolism of the toxicant. Naphthalene was readily broken down to its toxic components by the high levels of CYP2F4 active in Clara cells. 1-NN however, is metabolised by a different isoform, CYP2B1 (Verschoyle, RD *et al.*, 1993). CYP2F2 was shown to be capable of metabolizing both napththalene and 1-NN (Shultz, MA *et al.*, 1999). Therefore, naphthalene toxicity in mice compared to rats is due to higher levels of CYP2F4. The level of 1-NN toxicity is also species specific. The airways of rats and mice undergo similar pathology after 1-NN treatment; however, rats are more sensitive to lower doses of 1-NN compared to mice. Also 1-NN treatment of neonates and adults reveal a higher susceptibility of neonates of both mice and rats compared to adults (Fanucchi, MV *et al.*, 2004).

Terminal bronchioles of mice contain 75 % non-ciliated cells and terminal bronchioles of rats contain 63 % Clara cells (Fanucchi, MV *et al.*, 2004). It is this high predominance of CYP450 containing cells that causes the conducting airways to be the main target of 1-NN toxicity. Toxicity occurs as early as 1 hour post 1-NN treatment. Electron microscopy investigation showed smooth endoplasmic reticulum and mitochondrion

distortion in non-ciliated cells 1 hour after administration (Sauer, JM *et al.*, 1997). 6 hrs after administration the pathology worsens with severe mitochondrial distortion, vacuolisation of the cytoplasm, and loss of non-ciliated cells from more distal bronchioles. At this stage ciliated cells appeared to be vacuolated and with distended mitochondria. There was also severe edema and pneumonitis in these airways with inflammatory infiltration and necrosis and denuding of the epithelial membrane. At 24 hrs the distal conducting airways were almost exfoliated of epithelial cells (Sauer, JM *et al.*, 1997). To date no study has been carried out examining the damage/ repair process past the 48 hr time point.

Ozone (O_3) is an environmental pollutant that has been well characterised as contributing to acute and chronic respiratory damage. Ozone exposure has been shown to cause airway inflammation, acute lung injury and lung function impairment among others (Mudway, IS and Kelly, FJ, 2000). O_3 is generated by a photochemical reaction between O_2 and sunlight, generating O_3, and its production is enhanced by PAH. Although O_3 exposure protects the lungs against further O_3 insult, the toxic effects caused by 1-NN are enhanced by ozone, both of which commonly co-exist in urban areas. It is therefore important to understand the effect of the exposure of both these pollutants on the lungs. Studies have been carried out examining the lungs of 1-NN animals pre-exposed to ozone. Ozone causes an increase in CYP450 2B activity and consequently 1-NN metabolism in Clara cells of the conducting airways (Paige, RC *et al.*, 2000a). Pre-treatment of animals with ozone caused an increase in ciliated cell toxicity with 1-NN (Paige, RC *et al.*, 2000b). A comprehensive study was carried out to identify the proteins adducted by 1-NN metabolites after ozone pre-exposure. Calreticulin, which functions in the regulation of immune responses, cell migration and adhesion, was adducted in ozone pre-exposed animals and not in the controls. This was the only differential protein adduct between animals pre-treated with ozone or filtered air and subsequently treated with 1-NN, and therefore is responsible for the sensitivity seen in ozone pre-exposed animals (Wheelock, AM *et al.*, 2005).

Schmelzer *et al* have analysed the immune cell infiltration and cytokine secretion after 1-NN administration to animals that were pre-exposed to filtered air or ozone (Schmelzer, KR *et al.*, 2006). Rats exposed to both ozone and 1-NN demonstrated an immune response equivalent to an allergic response, which are high levels of GM-CSF and IL-1β 2 hrs after 1-NN administration. Rats exposed to 1-NN alone produced an immune response indicative of an acute inflammatory response, with high levels of IFN-γ and IL-10 at early time points. The damaging effects of 1-NN have been well characterised for early time points after administration. However, little is known about the molecular mechanisms that occur during the damage and repair process in this lung damage model.

1.6. Lung Cancer

Lung cancer is the leading cause of cancer deaths in the Western world. Approximately 85 % of lung cancer cases arise in smokers or former smokers (Meuwissen, R and Berns, A, 2005). However, only 10 % of heavy smokers will develop lung cancer, suggesting there are genetic factors contributing to the development of the disease. The mortality rate is very high with 85 % of patients dying within 5 years of diagnosis. The reason for this poor prognosis is the lack of early detection methods. Most lung cancers are identified at an advanced stage, which is not acquiescent to standard surgical therapies or radiotherapies. There is a great need for early detection methods to identify the disease at a curative stage, and also a need for more effective drugs for treating the disease.

Environmental factors are the main contributors to lung cancer; these include exposure to radon, asbestos, other air pollutants and most significantly cigarette smoke. The latter is the main risk factor leading to the onset of lung cancer. Cigarette smoke contains over 60 carcinogens, 20 of which are associated with lung cancer development. The most prominent carcinogens are the polycyclic aromatic hydrocarbons (PAH). These carcinogens, as described earlier (section 1.5) are metabolised by CYP450 in the Clara cells of the lung to toxic metabolites that bind DNA and form DNA adducts. DNA adducts can generally be repaired, but chronic exposure to these carcinogens increases

the likelihood of generating mutations in critical genes. Critical mutations resulting from DNA adducts include the constitutive activation of oncogenes, as in the case of K-ras^{G12D} mutations, or rendering tumour suppressor genes inactive, as it the case for p53. Genetic susceptibility has a role in lung cancer development in smokers, inherited mutations in genes responsible for the metabolism of tobacco carcinogens or DNA repair may affect smokers' susceptibility to lung cancer. Predisposing mutations in glutathione S transferase (GST) genes which are responsible for metabolizing tobacco carcinogens have been associated with lung cancer susceptibility (Lee, KM *et al.*, 2008). Mutations in DNA methyltransferase genes (DNMT1 and DNMT3B), which have a role in DNA repair, have also been associated with PAH mutation susceptibility (Leng, S *et al.*, 2008).

15 % of lung cancer patients cannot attribute the disease onset to smoking. A genetic linkage analysis associated the risk of developing lung cancer with mutations in the 6q 23-25 locus (Bailey-Wilson, JE *et al.*, 2004). Further analysis must be carried out on this locus association, but if mutations in this region have a high association with predisposition to lung cancer, it can be used as a potential screening mechanism. A recent study associated α-1 antitrypsin deficiency carriers (AATD) as being 70 % -100 % more likely to develop lung cancer (Yang, P *et al.*, 2008). Microarray studies comparing genetic mutations in adenocarcinomas of smokers versus non-smokers show a difference in gene clustering, suggesting that different signalling pathways are effected (Powell, CA *et al.*, 2003).

1.6.1. Lung Cancer Histology

Lung cancer can be divided into two main classes, small cell lung cancer (SCLC) and non-small cell lung cancer (NSCLC). SCLC, which accounts for 20 % of lung cancer cases, occurs in the neuroendocrine cells of the lung. These tumours metastasise early, resulting in poor prognosis for this disease (Meuwissen, R *et al.*, 2003). This form of lung cancer is strongly associated with smoking. NSCLC is the most common type of lung cancer encountered, accounting for 80 % of cases. This class of cancer is sub-divided into

squamous cell carcinoma, adenocarcinoma and large cell carcinoma. Adenocarcinoma is the most common form of lung cancer found in never smokers. SCLC and NSCLC differ in histology and in molecular mutations. SCLC mutations occur most frequently in 4p, 4q, 5q12, 10q and 13q14 loci. The areas that are most frequently effected in NSCLC include 9p12 and 8p21. A study carried out by Wistuba *et al* found that of 22 mutational hotspots in lung cancer patients, only 2 were common to both SCLC and NSCLC (Wistuba, II *et al.*, 2002).

Lung cancer progression is well studied in squamous cell carcinoma (SCC). SCC accounts for 35 % of all lung cancer cases. The early form of the disease initiates as hyperplasia, progressing to metaplasia and dysplasia and then development into a well differentiated carcinoma (Figure 1.3). The hyperplasia (a proliferation of cells) can occur in basal and goblet cells. This disease can be diagnosed by keratinisation in the tumour. Adenocarcinoma accounts for 35 % of lung cancers; these frequently metastasise and are fast growing. The precursor cell for adenocarcinoma is less well characterised. It is believed the atypical adenomatous hyperplasia foci are the precursor for adenocarcinoma (Pankiewicz, W *et al.*, 2007). The precursor feature of this disease is atypical adenomous hyperplasia (AAH) and bronchoalveolar carcinomas then progressing into a tumour (Figure 1.3). This tumour is identified by large mucin production. The large cell carcinomas only account for 10% of lung cancers. These tumours are identified by elimination of the features of other lung cancers. They do not show any keratinisation or neuroendocrine feature, nor do they stain for mucin.

1.6.2. Molecular Pathways Involved in Lung Cancer

1.6.2.1. Cell Cycle Regulators

The retinoblastoma (Rb) protein is responsible for the regulation of cell cycle progression from G1 to S phase. In its hypo-phosphorylated active form, Rb can bind to and inhibit E2F transcription factors from progressing into the DNA synthesis phase of the cell cycle (S phase). Phosphorylation of Rb by Cyclin D or Cyclin E inhibits its regulation of the E2F transcription factors and cell cycle progression occurs. Therefore the Cyclin- cyclin

dependent kinase (CDK) activation complex are tightly regulated by cyclin dependent kinase inhibitors (CDKI). Included in the class of CDKI is p16 (also known as $p16^{INK4a}$, p14, CDKN2A), which binds to and inhibits CDK4, which in turn is the cognate kinase of Cyclin D. In this way p16 indirectly maintains Rb in a hypo-phosphorylated state. Expression of the tumour suppressor gene Rb is lost in 90 % of SCLC and 15-30 % in NSCLC (Reissmann, PT *et al.*, 1993; Shimizu, E *et al.*, 1994). p16 expression is lost approximately 50 % of NSCLC and almost never lost in SCLC (Brambilla, E *et al.*, 1999; Wistuba, II *et al.*, 2001). Loss of p16 expression can be caused by promoter methylation, mis-sense mutation or homozygous deletion. Therefore a molecular difference between lung cancer classes is that loss of retinoblastoma is prominent in SCLC while loss of p16 expression is prominent in NSCLC (Sekido, Y *et al.*, 2003).

Cyclin D is over expressed in ~45 % of NSCLC (Brambilla, E *et al.*, 1999). Increase in Cyclin D expression is highly associated with atypical adenomas hyperplasia. The pattern of Cyclin D expression changes throughout the disease progression, with increased expression found in AAH, decrease expression found in early stages of adenocarcinoma and increased expression in later stages of adenocarcinoma (Pankiewicz, W *et al.*, 2007). These changes in expression through the development of adenocarcinoma highlight the complexity of the disease.

1.6.2.2. p53 Mutations in Lung Cancer

The tumour suppressor gene p53 is the most frequently mutated gene in human cancers. It is a transcription factor involved in a labyrinth of cellular pathways associated with DNA damage and repair. p53 is activated in response to stress stimuli or DNA damage. It activates down stream targets, the outcome of which includes the transient halt in cell cycle at either G1 or G2 and the activation of DNA damage molecules, and the induction of senescence or apoptosis. The loss of p53 regulation leads to the inappropriate progression of cell cycle with damaged DNA. p53 mutations have been found in approximately 50 % of NSCLC and 90 % SCLC (Tammemagi, MC *et al.*, 1999).

Upstream regulators of p53 include p14 and HDM (Sekido, Y *et al.*, 2003). p14 is a splice variant gene product of the p16 gene. Like p16 it is a tumour suppressor and can enhance the stability of p53 by binding to HDM, the p53 inhibitor.

Mutations arising in the p53 gene are linked to DNA adducts formed from the metabolism of carcinogens from cigarettes. There are numerous mutational hotspots in the p53 gene, generally G-T transversions at DNA adducts. Two polymorphisms have been found in codon 72 of the p53 gene that is thought to increase the incidence of certain lung cancers. A proline substitution of codon 72 has been associated with an increased risk of developing adenocarcinoma and an arginine substitution has been linked with increased risk of developing squamous cell carcinoma due to tobacco toxins (Robles, AI *et al.*, 2002). Other mis-sense mutational hotspots occur in the p53 gene at the DNA binding domain; these include codon 273, 248, 249, 245 and 158 (Jackson, JG and Pereira-Smith, OM, 2006). DNA adducts on the hotspots more frequently occur in smokers (33 %) compared to non-smokers (15 %).

1.6.2.3. EGFR and Therapeutics

In recent years many epidermal growth factor receptors (EGFR) targeted therapies have shown great potential for treatment of NSCLC. EGFR, a member of the receptor tyrosine kinase family, is activated by ligand binding and in turn activates a broad range of signalling pathways including PI3K (phosphoinositol 3 kinase), MAPK (mitogen activated protein kinase) and STAT (Signal transducers and activators of transcription protein), which regulate proliferation, survival, metastasis and differentiation of epithelial cells. EGFR (also known as Herceptin 1) expression is up-regulated in 30 % of NSCLC. Clinical trials for NSCLC are currently ongoing to test tyrosine kinase inhibitors (TKI) which can bind to and inhibit tyrosine kinase receptor activity.

EGFR mutations occur most frequently in lung cancer patients who were never smokers, female, Asian and that have an adenocarcinoma phenotype (Zhang, X and Chang, A, 2008). Clinical trials using TKI, namely gefinitib and erlotinib, have shown increased

survival in 10 % of the total patient population. However, there is a sub-class of individuals that benefit greatly from TKI treatment. Screening is ongoing to characterise these patients. Patients that have highest survival with TKI have an in-frame mutation in codon 19, a lysine to arginine point mutation at position 858, or an increase in EGFR copy number (Lynch, TJ *et al.*, 2004; Zhang, X and Chang, A, 2008). Mutations in K-ras correlate with lack of sensitivity for TKI treatment due to constitutively active K-ras being downstream of EGFR.

A case study of a lung cancer patient carried out by Kobayashi et al found a deletion in the 747-752 nucleotide regions of EGFR. This patient was responsive to gefinitib, but relapse occurred 24 months after remission (Kobayashi, S *et al.*, 2005). Analysis of the EGFR found that the same deletion was preserved in the lung cells but there was an additional nucleotide change which corresponded to a threonine to methionine transition. The methionine residues is bulkier then the threonine and sterically inhibited the drug from binding to its activating pocket. This new mutation rendered the gefinitib inactive and the patient unresponsive, hence the relapse. The molecular data explains why gefinitib appears to work in a small population of patients. In this way the gefinitib is a mutation specific medicine and screening of the mutations will aid diagnosis.

1.6.2.4. K-ras Mutations in Lung Cancer

The Ras family of GTPase proteins includes H, N- and K-ras all of which share a strong protein homology. Mutations in *ras* genes are implicated in approximately 30 % of all human cancers (Schubbert, S *et al.*, 2007). The Ras proteins share 100 % homology in their amino terminal domains, with less than 15 % homology in their carboxy domains. This protein family is highly conserved from yeast to mammals, which highlight their essential role in eukaryotic cellular function. The molecular make up of these *ras* genes, including omission of a TATA motif in their promoter domain, is characteristic of house keeping genes. Murine knock-out models revealed N- and H- ras are not essential for embryo development, while K-ras is essential for mouse embryo development (Koera, K *et al.*, 1997).

Ras proteins reside in the inner surface of the plasma membrane and function as a guanine diphosphate (GDP)/ guanine triphosphate (GTP) switch. Inactive forms of Ras have a conformation such that they can bind GDP. The switch to the active form, which binds GTP, is facilitated by guanine nucleotide exchange factor (GEF). Activated Ras is returned to an inactive form by the actions of GTPase activating proteins (GAP); proteins which facilitate the intrinsic Ras GTPase activity. Common mutations in Ras, namely at codon 12, 13 or 61, effect the GTPase activity of the proteins and in turn render the protein in a constitutively active form (Malumbres, M and Pellicer, A, 1998).

K-ras mutations are more common in smokers than non-smokers, and are found in 30-50 % of adenocarcinoma lung cancer histologies. The most common mutation is the glycine to aspartic acid transversion at codon 12 which renders the protein constitutively active. EGFR and K-ras mutations are mutually exclusive, that is patients rarely have both mutations. K-ras signalling is down-stream of EGFR signalling, therefore K-ras mutations render patients insensitive to tyrosine kinase inhibitor treatments (Figure 1.4) (Zhang, X and Chang, A, 2008).

1.6.3. Mouse Models for Lung Cancer

1.6.3.1. Mouse Models

Transgenic animal models have transformed the ability to study gene function *in vivo.* Mouse models can be generated to over express or delete a gene in a spatial and temporal manner. The ability to spatially regulate the expression of a transgene is important in an organ such as the lung, due to the heterogeneity of the cells. Two promoters have been extensively utilised in lung gene targeted expression: surfactant protein C (SP-C) and Clara cell specific promoter (CCSP) (Kwak, I *et al.*, 2004). The SP-C promoter is specifically expressed in type II pneumocytes in the alveolar region of the lung, while CCSP is expressed in the Clara cells of the conducting airways. Transgene expression under the control of these promoters allows cell specific expression of the transgene. One limitation of promoter controlled gene expression is the lack of control over the timing of

transgene expression, which is dependent on the expression pattern of the endogenous promoter. Both SP-C and CCSP (expressed from day 14 of gestation) are expressed during lung development and in the adult lung; therefore, these promoters constitutively express the transgene.

Several ligand inducible systems are currently utilised in gene expression experiments, these include the lac operator-repressor system (Cronin, CA *et al.*, 2001), the ecdysone-regulated gene switch (Saez, E *et al.*, 2000) and the progesterone GAL4/ UAS inducible system (Wang, XJ *et al.*, 1999). The most commonly used ligand inducible transgenic system for the generation of temporally expressed transgenic mice is the tetracycline inducible system. There are two varieties of the tetracycline regulated system; pTet-Off whereby addition of the tetracycline antibiotic (namely doxycycline) inhibits the expression of the transgene, and the pTet-On system where administration of the antibiotic induces expression of the transgene (Figure 1.5). The pTet-On system differs from the pTet-Off system by four amino acid substitutions in the reverse tetracycline-controlled transcriptional activator (rtTA) gene. Doxycycline binds to rtTA and causes a conformational change which allows binding to the tet operator (also known as tetracycline response element- TRE). Thus, the pTet-On system allows rapid induction of transgene expression in the presence of the inducible antibiotic, doxycycline. Although the tetracycline inducible system was first used *in vitro,* there are many tetracycline inducible transgenic mouse models. The advantage of temporal expression with this system is that it can overcome the problems associated with, for example, a strong mitogenic signal during lung development (Roelen, BA *et al.*, 2003). Tissue specific induction can be coupled with the tetracycline inducible system to generate temporal and spatial regulation of transgene expression (Floyd, HS *et al.*, 2005; Floyd, HS *et al.*, 2006).

Another level of control of transgene expression has been afforded with the development of the Cre-LoxP system. Cre (causes recombination) protein targets recombination between LoxP (locus of crossover P1) DNA sites to remove the DNA sequence within the LoxP sites. In this way an endogenous gene can be flanked with LoxP sites and

removed in a Cre specific manner. Another application for this system is to insert a stop cassette, flanked by LoxP sites, upstream of a transgene allowing removal of the stop cassette and expression of the transgene in a Cre specific manner. A combination of the promoter specific expression and the Cre-LoxP system presents an increased level of controlled transgene expression.

Recombineering or recombinogenic engineering is a form of chromosome engineering which involves recombination into plasmids, BACs (bacterial artificial chromosome) or YACs (yeast artificial chromosome). This method is more efficient for the generation of transgenic animals compared to conventional sub-cloning methods due to the minimal restriction digests and ligation required. Recombineering is carried out in bacteria. The ability to homologously recombine a linear fragment in bacteria is due to the presence of the *Red* genes encoded on a pro-phage. The *Red* genes include *exo, bet* and *gam.* The *exo* gene encodes a protein with 5'-3' exonuclease activity for single stranded DNA (ssDNA). The *bet* gene encodes a protein responsible for promoting annealing of the ssDNA to its homologous region. The prophage also encodes a *gam* gene which inhibits the activity of the RecBCD exonuclease complex endogenous to the bacteria. RecBCD encodes an ATP dependent exonuclease activity which acts on linear double stranded DNA. Homologous recombination activity is not constitutive in the bacteria; it is regulated by a temperature sensitive repressor gene. The *Red* genes responsible for the recombination are expressed by a strong phage promoter $P_{L.}$ This promoter however, is regulated by *cI857* repressor. The repressor activity is eliminated by heat shock, to allow expression of the *Red* genes and therefore homologous recombination (Copeland, NG *et al.*, 2001; Warming, S *et al.*, 2005; Yu, D *et al.*, 2000).

1.6.3.2. K-ras Mouse Models for Lung Cancer

The generation of animal models to study lung cancer has had 3 benefits: firstly, the contribution to understanding of the molecular biology of lung cancer; secondly, the development of early cancer diagnostic methods; thirdly, their use for development and validation of lung cancer therapeutics for pre-clinical trials. Numerous lung cancer mouse

models have been generated to mimic human lung cancer. These models include spontaneous generation of lung cancer in susceptible strains, carcinogen induced lung cancer and the generation of transgenic mice for the development of lung cancer.

The susceptibility of strains of mice to develop spontaneous tumours is highly correlated with their susceptibility to carcinogens. Mouse strains such as A/J and SWR are highly susceptible, while Balb/c is mildly susceptible and C57BL/6 is resistant to spontaneous development of lung cancer (Malkinson, AM, 2001). The carcinogens commonly used to induce lung cancer include polycyclic aromatic hydrocarbons (PAH) and urethane that are found in tobacco smoke. Animals exposed to carcinogens develop mutations in oncogenes such as K-ras and tumour suppressor genes such as p53 (Li, EE *et al.*, 1994; Malkinson, AM, 2001). However, the use of carcinogens does not restrict tumour development to the lungs and causes a variety of mutations within targeted cells. To overcome this uncontrolled environment, transgenic mouse models have been developed to express an oncogene or ablate a tumour suppressor gene (Meuwissen, R and Berns, A, 2005).

One well characterised transgenic model of lung cancer involves the expression of K-ras oncogene in the epithelial cells of the lung. K-ras^{G12D} mouse model was first generated by a hit-and-run technique whereby a transgenic mouse could undergo spontaneous recombination to replace the wild-type K-ras with K-ras^{G12D} oncogene. The K-ras mutation resulted in reduced survival and various tumour types developing especially in the lungs where 100 % of mice developed early onset lung tumours (Johnson, L *et al.*, 2001). However, the lack of reproducibility of tumours in this model lead to the development of the LSL-K-ras model.

LoxP-Stop-LoxP (LSL) - K-ras transgenic mouse model contains the K-ras oncogene downstream of a floxed stop cassette, such that in the absence of Cre recombinase the oncogene is not expressed (Figure 1.6). Intranasal administration of adenoviral-Cre (Ad-Cre) vector lead to the development of hyperplasia and adenoma lesions in the lungs of these transgenic mice 6 weeks post Ad-Cre administration (Johnson, L *et al.*, 2001).

Varying amounts of Ad-Cre were administered and a proportional increase in tumour burden was seen with increasing viral load. Similarly, the sporadic expression of LSL-K-ras^{G12V} using intranasal administration Ad-Cre also resulted in a similar development of tumour lesion in the epithelial cells of the lung 6 weeks post Ad-Cre administration. The development of hyperplasia and adenomas that developed in both studies mimics the early stages of human lung cancer development (Johnson, L *et al.*, 2001; Meuwissen, R *et al.*, 2001).

A transgenic mouse was developed to control the spatial expression of the K-ras oncogene. CCSP allows expression of the Cre recombinase specifically in the Clara cells of the lung. The LSL transcriptional repression site upstream of the constitutively active K-ras^{G12D} is removed in the presence of Cre recombinase, by recombination of the LoxP sites. In this way, the constitutive K-ras mutant gene is expressed in the Clara cells of the lungs of these mice. Characterisation of LSL-K-ras^{G12D} mice noted the development of cancer at 3 months of age with hyperplasia lesions begining to form in the airways and alveolar regions (Ji, H *et al.*, 2006). These lesions become more prominent as the disease progresses and adenomas begin to form in the alveolar regions. These adenomas can be classified as papillary, solid or mixed adenomas.

The two systems described above each have their own advantages. Intra-tracheal infection of Ad-Cre allows sporadic activation of the mutant gene in the epithelial cells of the lung. This is reflective of human cancers where tumours develop in foci and progress over time into adenocarcinoma. The CCSP-Cre model causes expression of the mutant gene in every Clara cell of the lung. In this way there are numerous lesions obliterating the architecture of the lung. These mice tend to die from suffocation before the adenocarcinoma develops. However, this model is advantageous for experimental examination since the disease burden is consistent in every animal.

1.6.4. Mig-6 Tumour Suppressor Gene

Mitogen-inducible gene 6, *Mig-6,* (also known as, ERBB receptor feedback inhibitor 1(*Errfi1*), receptor-associated late transducer (RALT), and gene 33) is an immediate early response gene to stress stimuli, cytokines and growth factors (Makkinje *et al.*, 2000, Zhang et al 2007). *Mig-6* contains many protein-protein interaction sites including cdc42/Rac interacting and binding domain (CRIB), src homology 3 domain (SH3), 14-3-3 protein binding motif, proline rich domain and epidermal growth factor (EGF) interacting domain. Interaction with proteins via these specific interaction domains results in the regulation of a plethora of biological processes which includes cell cycle regulation, apoptosis, cytoskeleton remodelling, and stress responses, revealing the complexity of *Mig*-6 signalling. *Mig-6* can interact with members of the ErbB family and has been shown to negatively regulate the ErbB signalling pathway (Anastasi, S *et al.*, 2005; Fiorini, M *et al.*, 2002; Xu, D *et al.*, 2005).

Mig-6 is expressed in many tissues including the uterus, liver, lung, kidney, heart, brain and skeletal tissue (Saarikoski, ST *et al.*, 2002; van Laar, T *et al.*, 2001). This gene encodes a 50 kDa protein and is located on human chromosome 1p36, a locus associated with frequent genetic alterations in human cancer. Ablation of *Mig-6* in mice lead to many phenotypes including the development of joint abnormalities especially in the knees, ankles and temporal-mandibular joint (Zhang, YW *et al.*, 2005), and abnormalities in the skin especially on the footpads and at the ear tag where there is evidence of tumourigenesis. The loss of *Mig-6* leads to over expression of EGFR signalling, resulting in hyperplasia phenotype in many organs including the skin, uterus and the lung. Epithelial hyperplasia, adenoma, and adenocarcinoma in organs such as the lung, gallbladder, and bile duct have also been shown to occur in *Mig-6* null mice (Zhang *et al.*, 2007). This tumour suppressor gene function in mice (Ferby *et al.*, 2006; Tseng *et al.*, 2005) is also observed in humans (Fujii *et al.*, 2002; Girard *et al.*, 2000; Nomoto *et al.*, 1998). Loss of *Mig-6* expression has been correlated with poor prognosis in breast cancer patients (Anastasi, S *et al.*, 2005), and loss of expression has been shown in NSCLC cell lines and primary tumours (Zhang, YW *et al.*, 2007).

1.6.5. Adherence Junctions

Adhesion molecules are involved in many processes including embryogenesis, epithelial integrity, inflammation and carcinogenesis. Adhesion molecules are aberrantly expressed in many stages of malignancy and contribute to defective proliferation, disorganisation of cell morphology and tumour migration and invasion (Charalabopoulos, K *et al.*, 2004). Adhesion molecules belong to a number of different super-families namely cadherins, integrins and immunoglobulins. The cadherin family is the most influential adherence super-family on biological processes. Classical cadherins are single-span calcium dependent transmembrane proteins. Epithelial (E)-cadherin is specifically expressed in the epithelial cells. The cytoplasmic domain interacts with catenin molecules (α-, β-, and γ- catenin and p120). The most accepted adherence complex is composed of β-catenin binding E-cadherin, recruiting α-catenin which in turn binds actin filaments (Figure 1.7). Recruitment of the actin network to E-cadherin results in epithelial cell integrity and polarity. Recently Myosin VI, an actin-based motor, has been found recruited to the E-cadherin complex when the cell-cell contacts of the epithelial monolayer has matured (Maddugoda, MP *et al.*, 2007). It is likely that the complex of proteins associated with the E-cadherin complex will depend on cellular context and will influence cell signalling.

E-cadherin is an accepted tumour suppressor gene. Loss of function of this adhesion molecule has been noted in many solid tumours and is a poor prognostic factor (Beavon, IR, 2000). *In vitro* studies have shown the importance of E-cadherin in sequestering β-catenin at the membrane thereby preventing its involvement in the Wnt signalling (Gottardi, CJ *et al.*, 2001). Aberrant β-catenin expression has been implicated in many epithelial cancers including NSCLC, colorectal cancer, prostate cancer and breast cancer (Junior, JP *et al.*, 2008; Zhang, H and Xue, Y, 2008). Loss of the tumour suppressor gene APC, which inhibits Wnt signalling, pre-disposes patients to the hereditary familial adenomatous polyopsis cancer. E-cadherin and its interacting catenin molecules are important for inhibition of proliferation by β-catenin/ Wnt signalling. Adherent cells in culture halt in G1 cell cycle when they reach confluency. Loss of E-cadherin or any of the catenin components can overcome this contact inhibition. In an *in vivo* setting, loss of any of the cell-cell adhesion molecules promotes cancer invasion and metastasis. During

injury, cells on the epithelial membrane proliferate to re-populate the denuded membrane. The rate of proliferation during injury is strictly regulated and contact inhibition by adhesion molecules is thought to control this process. E-cadherin has been implicated in the induction of p27 which halts the cell cycle at G1 (Motti, ML *et al.*, 2005). In this way E-cadherin acts as an important regulator molecule which can tip the balance between normal proliferation and abnormal proliferation.

β-catenin is part of the E-cadherin complex that is involved in cell-cell adhesion and cell polarity. This protein is expressed in the developing embryo, and the homozygous null mouse model is embryonic lethal. β-catenin has a critical role in establishing cell fate in the proximal and distal regions of the epithelial lining and conditional deletion of β-catenin in epithelial cells of the lung impedes lung branching morphogenesis and alveolar airway differentiation (Mucenski, ML *et al.*, 2003). β-catenin has diverse roles; as well as its role in cell adhesion, it also acts as a transcriptional activator in the Wnt signalling pathway. Aberrant expression of β-catenin has been correlated with oncogenesis and poor prognosis in numerous cancers (Junior, JP *et al.*, 2008; Zhang, H and Xue, Y, 2008). Over expression of β-catenin caused hyperproliferation and atypical differentiation of lung epithelial cells (Mucenski, ML *et al.*, 2003).

1.6.6. PCNA

Proliferating cell nuclear antigen (PCNA) is essential for cell proliferation, with a specific role during DNA replication and DNA mismatch repair. PCNA belongs to the well conserved family of DNA β-sliding clamps. A homotrimer of PCNA forms a ring like structure that encircles DNA. PCNA functions as a cofactor to secure polymerase to DNA in order to allow DNA synthesis. The presence of this protein has been shown to increase progression of DNA polymerase protein, thereby enhancing proliferation (Moldovan, GL *et al.*, 2007).

Due to the constant exposure to environmental carcinogens, DNA in the epithelial cells of the lung has the potential to accumulate mutations over time, increasing susceptibility to

many lung diseases. Mismatch repair plays an essential role in DNA damage response preventing replication of mutated DNA. PCNA has been shown to interact with proteins involved in mismatch repair process (MMR), increasing their specific binding to mismatch DNA. The PCNA clamp is also important for the DNA processing in the MMR process (Marti, TM *et al.*, 2002). PCNAs role in DNA repair and processing can be inhibited by p21, a key regulator of growth arrest, and induced by p53, the tumour suppressor gene. p21 can act as a negative regulator of DNA replication by competitively binding PCNA and preventing DNA replication and mismatch repair, but not nucleotide excision repair process. Examination of PCNA in breast cancer patients has correlated PCNA over expression with reduced overall survival and reduced disease free survival (Stuart-Harris, R *et al.*, 2008). The p21-PCNA interaction domain has been determined and can be a potential target for small molecule therapy for cancer (Zheleva, DI *et al.*, 2000). Activation of p21 following DNA damage may inhibit DNA replication through inhibition of PCNA. In turn, defective p21 can not inhibit PCNA DNA replication.

1.7. BMP Pathway

Bone morphogenetic proteins are a group of conserved signalling molecules that belong to the TGFβ signalling super-family. The components of the BMP pathway were first identified by their ability to induce ectopic bone formation (Wozney, JM *et al.*, 1988). This family of signalling molecules is involved in events including neurogenesis, hematopoiesis, bone formation, limb development and lung formation in the developing embryo. The BMP pathway regulates cellular events such as proliferation, differentiation and angiogenesis. To date there have been 20 BMP related proteins identified. BMP 2-7 are ligands that bind to a type I and type II serine threonine kinase heterodimer receptor complexes to initiate the intracellular response (Figure 1.8). BMP have pleitrophic effects during development and maintenance of tissues.

BMP ligands are produced as immature precursor proteins composed of a pro-domain and a mature protein. The pro-peptide which renders the protein in its inactive form is

detached by proteolytic cleavage during secretion, resulting in the mature carboxy protein (Chang, H *et al.*, 2002). There are 3 main subgroups of BMP ligands based on sequence homology: growth differentiation factor 5 group (includes GDF5, GDF6, and GDF7), osteogenic protein 1 group (includes OP1, BMP5, BMP6, BMP7, BMP8) and BMP2/4 group (includes BMP2, BMP4) (Wu, X *et al.*, 2007). BMP ligands have distinct biological activities, diverse expression patterns and differential affinities for BMP receptors. BMP2 and BMP4 ligands are the most extensively studied in relation to their function during embryogenesis and lung disease, these ligand share 90 % amino acid homology. BMP4 is widely expressed during embryogenesis, with high levels being detected as early as E3.5 during mouse development. Homozygous null mutants of BMP4 die between E6.5 and E9.5 due to lack of mesodermal differentiation (Winnier, G *et al.*, 1995). BMP2 ablation causes embryonic lethality at E7.5 to E10.5, resulting in cardiac developmental defects (Zhang, H and Bradley, A, 1996).

BMP ligands bind with varying affinities to heterodimer complexes of serine threonine kinase receptors, composed of type I and type II receptors. There are 3 type I receptors capable of BMP signalling: activin like kinase 2 (ALK2), BMPR-IA (also known as ALK3), BMPR-IB (also known as ALK6). Three BMP type II receptors have been described to date: BMPR-II (BMP receptor type II), ActRIIA (activin receptor type II A), and ActRIIB (activin receptor type II B). BMPR-IA, BMPR-IB and BMPR-II are exclusive to BMP signalling, while ALK2, ActRIIA and ActRIIB are capable of BMP and activin signalling. BMP2 and BMP4 ligands preferentially signal through receptor complexes composed of BMPR-II and either BMPR-IA or BMPR-IB. Members of OP-1 sub-family of ligands preferentially signal through ALK2 and BMPR-IB, and members of the GDF5 family signal through BMPR-IB (Miyazono, K *et al.*, 2005). BMPs have different affinities for the type I receptors, thereby increasing the complexity of BMP signalling.

Of the three type II receptors, BMPR-II is specific for BMP2/ 4 signalling. There are two forms of BMPR-II, short form (Liu, F *et al.*, 1995) and a long form (Rosenzweig, BL *et al.*, 1995). The long form contains a long C-terminal tail that is not present in the short

form. The 1038 amino acid long form is composed of an extracellular domain, a transmembrane domain, an intracellular domain comprised of the kinase domain and the C-terminal domain rich in serine and threonine residues (Rosenzweig, BL *et al.*, 1995). Type II receptors (70-80 kDa) are much larger than type I receptors (50-55 kDa) and lack the glycine serine rich domains that are found in type I receptors. The ability of BMP receptors to bind Smad proteins is well characterised. There has been recent evidence to show the C-terminal domain of BMPR-II can interact with other families of proteins initiating a number of Smad independent pathways. BMPR-II has been shown to interact with a high number of signalling proteins including those involved in transcription regulation (LIMK, p50 (NFkB pathway)), cytoskeleton regulation (SemF) and MAP kinase signalling pathway (Hassel, S *et al.*, 2004).

BMPR heterodimers which are localised to the cell surface as pre-formed complexes induce Smad dependent signal transduction (Nohe, A *et al.*, 2002). BMPR can also localise to the membrane as homodimers and upon ligand binding, heteromeric complexes form, signalling via a Smad independent pathway (Nohe, A *et al.*, 2002). BMP ligands have a high affinity for type I receptors, and downstream signalling is specific to the ligand receptor combination complex. Formation of the ligand receptor complex results in the constitutively active type II receptor phosphorylating the glycine-serine (GS) rich domain of a type I receptor, which in turn activates the intracellular signalling molecules. BMPR-IA is ubiquitously expressed during embryo development and transgenic knock out mice are embryonic lethal due to lack of mesodermal formation (Mishina, Y *et al.*, 1995). Also, BMPR-II homozygous null mice are embryonic lethal, indicating the importance of these receptors and BMP signalling in embryonic development. BMPR-IB null phenotype results in viable animals with skeletal defects (Yi, SE *et al.*, 2000).

On receptor activation, the canonical signalling pathway disseminates through the cytoplasm to the nucleus via the Smad proteins. There are three functional classes of Smad proteins: receptor Smads (Smad 1, 5, 8); co-operating/ common Smad (Smad 4); inhibitory Smads (Smad 6 & 7). Smad proteins are composed of highly conserved regions

namely an amino terminal MH1 (MAD homologous region 1) domain and an MH2 domain at the C-terminus, which flank a highly variable linker region. The SSXS motif in the MH2 domain of the receptor Smads is phosphorylated by activated type I receptor, Smad 4 does not contain this domain and is, therefore, not a target of receptor activation.

Activated type I receptor phosphorylates a receptor Smad (R-Smad) which in turn form a complex with the common Smad (co-Smad). This R-Smad/ co-Smad hetero-oligomeric complex can translocate to the nucleus where it regulates transcription of target genes by binding to a Smad binding element (SBE) in promoters of target genes. Smad proteins are coupled to different receptors; Smad 1, 5, 8 are specific for the BMP pathway while receptor Smad 2 and 3 are common to the TGF-β and activin signalling pathway. Smad 4 is common to both the BMP and TGF- β signalling pathway.

The importance of BMP signalling during embryonic development is evident from the embryonic lethality, due to homozygous null mutants of many components of the BMP pathway. Smad 4 homozygous null mice are embryonic lethal between day 6.5 and day 8.5, due to defects in epiblast proliferation and mesoderm formation (Yang, X *et al.*, 1998). Smad 1 mice show defects at day 7 post coitus which lead to embryonic lethality by day 10 due to the lack of placental development (Tremblay, KD *et al.*, 2001). Smad 5 null mice are embryonic lethal between day 9.5 and 11.5, due to defects in left-right asymmetry (Chang, H *et al.*, 2000).

Several levels of regulation are in place to control the potent pleiotrophic effects of BMP signalling. Regulation of BMP signalling include: inhibition of BMP-ligand interaction; presence of non-signalling receptors which compete for ligand binding; degradation of signalling molecules; and inhibition of Smad signalling. BMP ligands can be impeded from binding their cognate receptor by antagonistic proteins in the extracellular region. These antagonists include chordin, noggin, and gremlin, among others which have a high affinity for BMP ligands. BMP signalling can be inhibited by non-signalling pseudo-receptors which compete with signalling receptor for ligand binding. Pseudo receptors such as BAMBI (BMP and activin membrane-bound inhibitor) are composed of an extra

cellular domain capable of ligand binding, but lack the intracellular kinase domain required for signalling (Gazzerro, E and Canalis, E, 2006). To add yet another level of complexity to the regulation of BMP signalling, co-receptors can enhance BMP signalling. BMP co-receptors, RGMa and DRAGON, have recently been identified. These molecules can bind directly to BMP2 and BMP4, associated with type I and type II receptors and enhance BMP signalling. These co-receptors are members of the glycosylphosphatidylinositol-anchored repulsive guidance family of molecules (Samad, TA *et al.*, 2005). RGMa co-receptor has been shown to enhance BMP signalling via ActRII in BMPR-II deficient pulmonary arterial smooth muscle cells (PASMC) (Xia, Y *et al.*, 2007). Another mode of potential regulation at a receptor level is the ubiquitin mediated proteosomal degradation of BMP receptors. The process of ubiquitination requires three proteins: ubiquitin-activating enzymes (E1), ubiquitin conjugating enzymes (E2), and ubiquitin ligase (E3). E3 ubiquitin ligases are responsible for defining substrate specificity and subsequent degradation. Dullard targets BMPR-II for ubiquitination and proteosomal degradation and it also acts as a phosphatase acting on BMPRI, thereby inhibiting BMP signal transduction (Satow, R *et al.*, 2006). Smad ubiquitin regulatory factor 1 (Smurf 1) is an E3 ubiquitin ligase that can interact with R-Smad proteins and mediate their degradation. The inhibitory Smads also negatively regulate BMP signalling. Smad 6 is a specific inhibitor of BMP signalling, while Smad 7 acts as an inhibitory protein for TGF-β/ activin and BMP signalling. Inhibitory Smads physically impede the signal transduction by either binding to type I activated receptor, thereby competing with receptor Smads; or by binding to activated receptor Smads and inhibiting the formation of the hetero-oligomeric complex with Smad 4 (Hanyu, A *et al.*, 2001; Hata, A *et al.*, 1998). In the nucleus, activation of BMP target genes is regulated by a number of transcriptional activators (CBP, p300) and repressors (Ski, Sno, Myc). Other modes of BMP signalling regulation include cross-talk with other signalling pathways such as MAPK and Wnt; this is described further in section 1.7.2.

1.7.1. BMP Pathway in Lung Disease

Significant progress has been made understanding the involvement of BMP signalling pathway in embryonic development. Embryonic lethality of many homozygous null pathway components highlights the importance of this pathway. However, there are many unanswered questions as to the involvement of this pathway in adult diseases. An emerging body of evidence has suggested dysregulation of BMP signalling in many human diseases including carcinogenesis, inflammatory diseases, such as asthma, and idiopathic pulmonary arterial hypertension (IPAH). BMP proteins cross talk with many other signalling pathways; it is this complexity that has hindered the understanding of its involvement in human disease.

1.7.1.1. Cancer

Mutations in BMP receptors have been implicated in the development of colorectal cancer, gliomas, pancreatic and prostate cancers, among others. Genetic linkage studies have been carried out on cancer patients to try identifying genes responsible for the development of the cancer. A genetic analysis of juvenile polyopsis patients revealed Smad 4 and BMPR-IA germ-line mutations in approximately 20 % of patients (Howe, JR *et al.*, 2004). Juvenile polyopsis is an autosomal dominant syndrome which predisposes patients to gastrointestinal and colorectal cancers. Loss of BMP signalling correlates with progression of colorectal cancer. Early stage adenoma samples expressed normal BMPR-IA, BMPR-IB, BMPR-II, and Smad4, and showed phosphorylated Smad in the nuclei of the cells. Examination of a more advanced stage of carcinoma in situ found a loss of BMPR-II and Smad 4 expression and a loss of phosphorylated Smad (Kodach, LL *et al.*, 2008a). A comprehensive study by Lee *et al* found glioblastoma tumour initiating cells (TIC) to have similar characteristics to early embryonic neural stem cells (NSC) (Lee, J *et al.*, 2008). Neither cells differentiated in the presence of BMP2 ligand, both proliferated in the presence of BMP2 ligand, and neither expressed BMPR-IB. These characteristics differed from later embryonic NSC and adult NSC, which undergo differentiation and inhibition of growth in the presence of BMP2 ligand, and express BMPR-IB. Early embryonic NSCs express BMPR-IB at later embryonic stages. TICs did

not express BMPR-IB due to aberrant genomic methylation and therefore remained in a perpetual state similar to early embryonic NSC. Hypermethylation of BMPR-IB in glioblastoma tumour initiating cells maintained the tumour cells in a pro-proliferative, dedifferentiated state. Expression of BMPR-IB transgene in the TICs restored their differentiation capabilities.

Both up- and down- regulation of BMP ligands have been associated with human cancers. A comprehensive analysis of BMP ligand expression in normal prostate tissue and prostate cancer tissue revealed variable BMP expression in all samples, but BMP2 and BMP4 were predominantly expressed in prostate carcinoma tissues (Bobinac, D *et al.*, 2005). Expression levels of BMP2 but not BMP4 were shown to be highly over expressed in non-small cell lung cancer samples (Langenfeld, EM *et al.*, 2003). Increased expression of BMP4 ligand was demonstrated in colonic carcinomas compared to normal tissue and early stage adenomas; while BMP receptor expression remained unchanged (Deng, H *et al.*, 2007).

BMP signalling has also been implicated with angiogenesis, a stage associated with tumour progression. Smad 1 or Smad 5 homozygous knock out mouse models are embryonic lethal due to defects in angiogenesis. The angiogenic function of BMP signalling is recapitulated in adult disease. BMP2 ligand stimulated blood vessel formation in A549 tumours in a nude mouse model. Also anti-sense targeted deletion of BMP2 expression resulted in a reduction in blood vessel formation in an *in vitro* assay (Langenfeld, EM and Langenfeld, J, 2004). These studies show the involvement of BMP signalling in all stages of cancer progression.

1.7.1.2. EMT

Epithelial to mesenchymal transition is a normal developmental process during embryogenesis. However, aberrant expression of this process has been associated with metastatic phenotypes in human cancers. Cancers of epithelial origin account for approximately 90 % of human malignancies (Kiemer, AK *et al.*, 2001). Therefore it is of

upmost importance that we understand the progression of epithelial cell to a metastatic carcinoma. Epithelial cells undergo a multi-step process to become a carcinoma. The first step involves indefinite proliferation in order to form a well differentiated tumour mass, termed benign. These cells may loose their epithelial phenotype and acquire a mesenchymal phenotype through a process known as epithelial to mesenchymal transition (EMT). A major event in EMT is the loss of tight cell-cell adhesion that is characteristic of epithelial cells (Burdsal, CA *et al.*, 1991). This loss of adhesion molecule is lead by the down regulation of E-cadherin, and its associated molecule β-catenin. Expression of E-cadherin is regulated by hypermethylation of the promoter and at a transcriptional level by binding of co-repressors such as snai1, snai2, zeb1, zeb2, δEF1 and twist to the E-box in the promoter region (Peinado, H *et al.*, 2007). Epithelial cells loose their structure and apical/ basal polarity due to a loss of cytokeratins, and gain an elongated front-back polarity of mesenchymal cells (Hay, ED, 1995). Loss of epithelial markers is in conjunction with a gain of mesenchymal markers such as desmin and N-cadherin adhesion molecules and α-smooth muscle actin, fibronectin, collagen. This mesenchymal phenotype confers increased mobility potential to the cells. Matrix metalloproteins such as MMP1, 2, 3, 7 and 14 are frequently up-regulated during EMT. These proteins allow epithelial cells to detach from one another and to invade the basement membrane, to metastasise and invade other organs. BMP signalling is involved in the EMT process. Expression of BMP6 ligand in breast cancer cell lines increases E-cadherin expression attenuating the metastatic phenotype. Expression of E-cadherin and BMP6 are inversely correlated to δEF1 a transcriptional repressor of E-cadherin, that promotes a metastatic phenotype (Yang, S *et al.*, 2007).

1.7.1.3. Fibrosis

Idiopathic pulmonary fibrosis (IPF) is a progressive fatal disease that is characterised by an increase in fibroblast, accumulation of extracellular matrix and lung remodelling (Katzenstein, AL *et al.*, 2008). IPF is thought to be caused by epithelial injury after which the lung architecture is not properly restored (Geiser, T, 2003). Examination of human specimens from both lung and kidney fibrotic disease patients have found an associated

with increased Gremlin, a BMP ligand antagonist (Myllarniemi, M *et al.*, 2008). TGFβ-1 and Gremlin expression are positively correlated in human fibrotic diseases. Treatment of human A549 cells with TGFβ-1 caused an induction of Gremlin (Koli, K *et al.*, 2006). Gremlin has been shown to be up-regulated in human IPF and also in the asbestos induce mouse model. This correlated with down regulation of BMP signalling, as observed by reduced P-Smad 1/5/8; and increased TGFβ signalling, as observed by increased p-Smad 2 activation (Myllarniemi, M *et al.*, 2008). BMP7 has the ability to inhibit renal fibrosis progression. A mouse model has shown the ability of BMP7 to halt the progression of the disease, and slightly increase the glomerular filtration rate of the kidney (Morrissey, J *et al.*, 2002). TGFβ induces Gremlin which, in turn, inhibits the fibrotic inhibitory effect of BMP7 thereby allowing a positive feedback loop for fibrosis.

1.7.1.4. Pulmonary Arterial Hypertension

Pulmonary arterial hypertension (PAH) is a potentially fatal disease that causes elevation of pulmonary arterial pressure which may result in hypertrophy and right heart failure. PAH is histologically characterised by proliferation of pulmonary-artery smooth muscle and endothelial cells (Rubin, LJ, 1997). This is a rare disease affecting females preferentially over males, with a mean age of onset at 36 years (Ghamra, ZW and Dweik, RA, 2003). Onset of PAH may be sporadic, idiopathic PAH (IPAH), or inherited, familial PAH (FPAH). Inheritance of FPAH is autosomal dominant and account for 6% of diagnosed PAH cases (Aldred, MA *et al.*, 2006). 50% of patients with familial cases and 10-40% of sporadic cases have mutations in the BMPR-II gene (Aldred, MA *et al.*, 2006). Numerous BMPR-II mutations have been observed; these include partial gene deletions, mis-sense, splice-site, nonsense and frame-shift mutations (Machado, RD *et al.*, 2001; Thomson, JR *et al.*, 2000). Mis-sense mutations have been shown to occur in conserved regions inhibiting ligand binding, or disrupting kinase activity of the receptor. Other mutations cause truncation in the transcript resulting in nonsense mediated decay. As proof of the ability of dysfunctional BMPR-II to cause PAH, a transgenic mouse model expressing dominant negative BMPR-II in smooth muscle cells resulted in increased arterial pressure in the animals (West, J *et al.*, 2004). Ablation of BMPR-II

expression in pulmonary smooth muscle cells does not inhibit BMP signalling, rather signalling occurs through ActRII receptor which preferentially binds BMP6 and BMP7 (Yu, PB *et al.*, 2005). Re-introduction of wild-type BMPR-II into pulmonary arterial smooth muscle cells deficient in BMPR-II, restored their ability to inhibit proliferation and induce differentiation in a ligand dependent manner (Yu, PB *et al.*, 2005). Microarray analysis carried out on cells isolated from transgenic mice expressing an inducible dominant negative form of BMPR-II revealed attenuation of smooth muscle differentiation, a decrease in angiogenesis related genes, and changes in matrix, motility and cell cycle genes that concur with the disease pathology. There was an increase in cytokine genes in female mice, due to other unknown factors. Increased inflammation exacerbates the disease pathology and might explain the increase incidence of PAH in females (Tada, Y *et al.*, 2007).

1.7.2. BMP Non-Canonical MAPK Signalling Pathway

BMP signalling via the ligand induced receptor complex has been shown to initiate the non-canonical BMP signalling through the mitogen-activated protein kinase (MAPK) signalling pathway. The MAPK signalling pathway is a highly conserved family of kinases that transduce signals from the membrane to the nucleus. The MAPK signalling pathway is controlled by phosphorylation of a cascade of proteins; MAPK kinase kinase, MAPK kinase, MAPK. MAPK are controlled by a diverse array of biological processes including proliferation, differentiation, migration and apoptosis, and are activated by phosphorylation on threonine and tyrosine residues in their conserved T-X-Y motif (Wada, T and Penninger, JM, 2004).

There are three sub-groups within the MAPK family of proteins: c-Jun NH2-terminal kinase (JNK); p38-MAPK; extracellular signal-regulated kinase (ERK). JNK and p38-MAPK family of proteins respond to external stimuli including DNA damage, heat shock, UV damage, and other forms of stress, while the ERK family of proteins responds mainly to growth stimuli. The function of these proteins is diverse and contradicting

outcomes have been noted for each. The JNK and p38-MAPK proteins have been associated with enhancing cell survival, growth and differentiation, but also promoting cell death (Wada, T and Penninger, JM, 2004). Although JNK and p38-MAPK have pro-apoptotic roles, their oncogenic function has been found over expressed in a number of cancers. Up-regulation of the ERK pathway has been noted in many types of cancer and has been associated with tumour proliferation and survival.

The MAPK pathway is downstream of EGFR signalling and ras GTPase activity. These components are frequently mutated in lung cancers and lead to the uncontrolled induction of MAPK signalling. Due to the prevalence of their defective signalling in human cancers intense research has been carried out to identify pharmaceutical interventions to attenuate the pro-survival signalling.

Non-canonical BMP pathway signals through the MAPK intracellular signalling cascade. MAPK is activated by BMP ligand binding to a ligand induced heteromeric receptor complex, rather that a pre-formed receptor complex which signals through the canonical pathway (Nohe, A *et al.*, 2002). The exact dynamics of how BMP-MAPK pathways interact is unknown. Studies on the role of MAPK signalling report conflicting results. A study conducted by Gaella *et al* demonstrated that BMP2 ligand activates both p38 and ERK signalling cascades. They illustrated that MAPK is necessary for and positively regulates BMP2 induced osteoblast differentiation in C2C12 cells (Gallea, S *et al.*, 2001). In contrast Vinals *et al* report that BMP2 activates p38 MAPK cascade but not ERK cascade and that p38 negatively regulates BMP2 induced osteoblast differentiation in C2C12 cells (Vinals, F *et al.*, 2002). MAPK signalling has been shown to negatively regulate BMP signalling by phosphorylating Smad1 protein in the linker domain, thereby targeting it for ubiquitination (Sater, AK *et al.*, 2003). On the contrary BMP ligands can inhibit p38 signalling depending on the concentration of ligand. Low doses of BMP7 stimulated p38 signalling in a renal medullary cell line, while high doses inhibited p38 signalling (Hu, MC *et al.*, 2004). These conflicting results reveal the requirement for further understanding of how the BMP signalling pathway and MAPK pathway interact.

1.8. Gene Therapy for the Lung

Gene therapy is defined as the delivery of a nucleic acid to correct a defective gene. During the past decade many clinical trials have been carried out assessing the efficacy and safety of gene delivery vectors. These vectors can be broken into two main categories; viral and non-viral. The main viral vector repertoire for gene delivery to the airway epithelium includes adenovirus, adeno-associated virus, retrovirus and sendai virus. The range of non-viral vectors in lung delivery trials comprise mainly of liposomes, polypsomes and nano-particles.

The lack of efficiency of *in vivo* trials has highlighted the difficulties associated with gene delivery to the lungs. The lungs have evolved to inhibit pathogen entry; therefore there are numerous barriers to intratracheal gene delivery (Figure 1.9). A successful gene delivery vector must overcome the thick mucus layer, the mucocillary clearance and the hindering glycocalyx layer before reaching the apical membrane of the epithelial cell (Montier, T *et al.*, 2004). *In vivo* cationic non-viral vector are often eliminated by opsonisation in negatively charged particles in the mucocillary layer. Viral vectors may be eliminated from the airways by immune cells that recognise them as foreign. The apical membrane of lung epithelial cells has very few receptors on their surface to allow entry of viral vectors. Viruses modified with capsid proteins that can bind apical receptors have a high tropism to those epithelial cells. Once inside the cell, a successful vector must escape the endosomal compartment and move through the cytoplasm to the nucleus. Some viral vectors have the capacity to transduce non-dividing cells; other viral vectors and non-viral vectors can only transduce dividing cells because they require nuclear break-down for entry into the nucleus. To achieve long-term transgene expression an ideal vector would integrate into the host cell genome. Many viral and non-viral vector methods are being improved to achieve success in human trials.

1.8.1. Adeno-Associated Virus

Recombinant AAV (rAAV) vectors have become a popular choice for gene therapy due to the number of advantageous properties they possess. The wild type vector is not associated with any human disease and therefore has no risk of adverse effects. Recombinant vectors do not contain any viral gene therefore do not evoke an inflammatory response. AAV vectors have the potential to confer long-term gene expression; this can overcome the need for repeat administration, which may be hampered by neutralising antibodies. A limitation of the vector is its size, rAAV vectors can contain DNA up to 4.5 kb. For cancer gene therapy this is not an issue since there are numerous targets of suitable size.

Wild type AAV is a 4.6 kb, non-enveloped, single stranded DNA dependo-parvovirus that can potentially integrate into a genome allowing long-term expression (Owens, RA, 2002). Since the discovery of AAV as a contaminant of adenovirus stocks, numerous serotypes (AAV1-9) have been isolated from humans and other primates (Gao, G *et al.*, 2005; Gao, GP *et al.*, 2002). rAAV vectors only contain *cis* elements and inverted terminal repeats, flanking a gene of interest. All *trans* acting proteins required for replication, which are the *rep* and *cap* genes, are provided by the packaging cell lines, which are used to generate the rAAV vectors. The AAV capsid equips the vector with a cell tropism. The rAAV vector can be pseudotyped with a capsid protein that has a higher tropism for a cell type of interest. For example, the AAV2 vector has been pseudotyped with the capsid protein from AAV5 and AAV6 both of which have a higher tropism for the cells of the lung compared to AAV2 capsid (De, B *et al.*, 2004; Halbert, CL *et al.*, 2001; Seiler, MP *et al.*, 2006). Unlike the wild type AAV the recombinant vector does not have the ability to integrate into the host genome, due to the removal of the *rep* gene from the recombinant vector. However, the rAAV vector can form concatamers in the nucleus conferring long-term expression (Yang, J *et al.*, 1999).

The numerous AAV serotypes which have been cloned show distinctly different cell tropisms. Cell tropism is conferred by receptors on the cell surface membrane which

AAV binds to allowing entry into the cell. The receptor by which AAV2 enters the cell is the heperan sulphate proteoglycan (HSP), this is expressed on the basolateral surface of the epithelial cell (Duan, D *et al.*, 1998) and is therefore not easily accessible from the luminal region of the lung. The abundance of its co-receptors $\alpha_v\beta_5$ also influences the tropism for specific cells. AAV5 has been found to have higher tropism for the lungs compared to AAV2, due to the expression of its 2,3-*N*-linked sialic acid receptor on the apical surface of airway epithelial cells (Walters, RW *et al.*, 2001; Zabner, J *et al.*, 2000). *In vivo* studies have shown the increased efficiency of up to 50 fold for AAV5 delivery to the lungs compared to AAV2 due to the apical expression of AAV5 receptor (Sumner-Jones, SG *et al.*, 2006; Zabner, J *et al.*, 2000). The exact mechanism by which AAV6 enters epithelial cells is unknown. AAV6 has been shown to bind, but its entry is not dependent on, heperan (Halbert, CL *et al.*, 2001) and it has been shown to enter into cells by a sialic acid dependent and independent pathway (Seiler, MP *et al.*, 2006). The efficiency by which AAV6 can transduce both human and mouse airway cells is far greater than AAV2 (Halbert, CL *et al.*, 2001). AAV6 and AAV5 have been shown to transfect human airway cells with equal efficiency but AAV6 had a higher transfection rate in mouse airway cells compared to AAV5 (Seiler, MP *et al.*, 2006).

Phase I and II clinical trials have been carried out to test the safety of AAV recombinant vectors. Delivery of AAV2 vector to cystic fibrosis (CF) patients has reported the safety of this gene therapy vector. Anti-AAV-neutralising antibodies were reported in patients that received high doses which may interfere with repeat administration (Flotte, TR *et al.*, 2003). Moss *et al* reported the safe re-administration of AAV-CFTR to patients, anti-AAV-antibodies did not have a deleterious effect (Moss, RB *et al.*, 2004). Cystic fibrosis disease pathology had improved after the first administration, as seen by the reduction of IL8 in the sputum and improved lung function, this beneficial effect was not seen after the second or third administration. Early stage clinical trials with AAV2 vectors have shown the vectors to be well tolerated but not efficient at transfecting the cells and diminishing disease symptoms. Promising results from animal studies using AAV5 and AAV6 mean clinical trials with these serotypes are imminent.

1.8.2. Lentivirus

Lentivirus belongs to the retrovirus family of RNA viruses that reverse transcribe their genome into DNA to allow stable integration into the genome of the host. The retroviruses family can be sub-divided into the simple (e.g. murine leukemia virus-MLV) and a complex form (e.g. human immunodeficiency virus-HIV). The genome of both sub-groups contains gag, pol and env genes; the complex retroviruses, contain additional genes. In order to ensure recombinant vectors are safe, some viral genes were removed from the recombinant vector. The *psi* gene which is responsible for packaging is not present in the gene therapy vector to ensure the vector cannot replicate in host cells (Dalba, C *et al.*, 2005).

MLV was the first retrovirus developed for gene therapy. This virus can integrate into the genome of the host to confer long-term transgene expression, but it can only transduce diving cells. This selective ability to transduce dividing cells makes it an ideal candidate for cancer gene therapy. First generation MLV vectors were replication incompetent, *in vivo* animal trials were not very successful due to the inefficiency of transfection by this vector. More recently replication competent retroviral (RCR) vector have been generated and studies have shown their ability to transfect tumour cells *in vitro* and *in vivo* (Solly, SK *et al.*, 2003; Wang, WJ *et al.*, 2003). However, the unrestricted replication of these RCR vectors has the potential to augment disease pathology.

Clinical trials for X-linked SCID (adenosine deaminase severe combined immunodeficiency) utilised *ex vivo* delivery of MLV-interleukin-γ-chain gene transfer into autologous $CD34^+$ bone marrow derived cells to alleviate the disease pathology (Hacein-Bey-Abina, S *et al.*, 2003). However, due to the ability of the vector to randomly integrate some patients developed leukaemia. The lack of success from these trials has tarnished the image of retroviral use for gene therapy.

HIV, human immunodeficiency virus, was the first well characterised lentivirus. The wild type HIV virus is associated with human disease and for this reason was overlooked as a potential gene therapy vector. The recombinant HIV is an ideal candidate for gene

delivery because of its ability to integrate into the genome and permit long-term transgene expression. While lentivirus does not have a natural tropism for the lung, high transduction efficiencies have been achieved *in vitro* by pseudotyping with the vesicular stomatitis virus G glycoprotein (VSV-G) capsid protein (Copreni, E *et al.*, 2004). VSV-G induces clathrin dependent endocytosis into the cell (Lichty, BD *et al.*, 2004). The pseudotyped capsid protein enables viruses to transduce a wide range of cell types, including lung epithelial cells.

Relatively few studies have examined lentiviral transduction of lung cells. HIV-VSV-G is significantly more efficient at transducing mouse alveolar cells than rat airway cells *in vitro* (Borok, Z *et al.*, 2001). HIV and FIV (feline immunodeficiency virus) pseudotyped with envelope proteins of Ebola virus can transduce human and mouse lung cells *in vitro* and *in vivo* with high efficiency (Kobinger, GP *et al.*, 2001; Medina, MF *et al.*, 2003; Sinn, PL *et al.*, 2005; Sinn, PL *et al.*, 2003). But again safety issues concerning a gene therapy vector containing components of two human pathogens have prevented extensive studies. No clinical trials have been carried out using a HIV based gene therapy vector. Due to the adverse effects of previous trials based on MLV vector there are concerns about the biosafety of these vectors. A study conducted to address this problem showed replication competent MLV inserted into 481 immune deficient mice showed no adverse effects, also no adverse effects were seen after lentiviral administration into 149 mice (Bauer, G *et al.*, 2008).

1.8.3. Non-Viral Vectors

The methods of non-viral based gene delivery that have been developed include physical and chemical approaches. The physical gene therapy methods developed include electroporation, injection, magnetism, ultrasound and gene gun bombardment (Gazdhar, A *et al.*, 2006; Wolff, JA *et al.*, 1990; Xenariou, S *et al.*, 2006; Xenariou, S *et al.*, 2007; Yang, NS *et al.*, 1990). Chemical approaches for gene delivery utilise synthetic or naturally occurring materials that carry genetic material. The main chemical components for gene delivery are liposomes and polysomes. Liposomes are mainly composed of

cationic lipids, which have the ability to condense DNA, and neutrally charged lipids, which are considered helper lipids for the formation of liposomes. Polysomes are composed of positively charged polymers that can be linear or branched configuration. Polymers that have been utilised for gene delivery to date include polyethylenimine (PEI) cationic proteins (polylysine, protaine, histones) and polypropylamine dendrimers; among others (Mennesson, E *et al.*, 2005; Schatzlein, AG *et al.*, 2005). Non-viral vectors are generally considered to be less efficient at transfecting cells compared to viral methods of gene delivery. However, non-viral vectors have benefits over viral vectors in that they are less immunogenic and can deliver large size genes compared to viral vectors.

DNA delivery of cationic liposomes enters the cell by fusion with lipids in the cellular membrane. The net positive charge on cationic lipids, facilitated by the neutral charge of the helper lipid, allows release from the endosomal compartment within the cell (Farhood, H *et al.*, 1995; Xu, Y and Szoka, FC, Jr., 1996). The proton sponge hypothesis has been used to describe the method by which polymers escape the endosomal compartment. Ions enter the endosome to protonate the polymer and cause swelling and eventual rupture of the organelle (Sonawane, ND *et al.*, 2003). The inefficient gene delivery associated with non-viral vector transfer has spurred the development of improved vectors. Cationic liposomes and polysomes have a positive net charge and are readily opsonised by negatively charged particles *in vivo,* reducing their efficiency as gene delivery vectors. To overcome this lack of stability *in vivo*, liposomes and polysomes are regularly complexed to PEG (polyethylene glycol) or negatively charged molecules, to yield a more efficient transfection rate (Walsh, M *et al.*, 2006). Another mode of improvement to non-viral gene transfer is the development of antibody targeted vectors. Immunoliposomes can be engineered to contain monoclonal antibodies conjugated to liposomes. Targeted vectors have two added advantageous, that is they can target specific cells and their interaction with the specific cell is increased improving the potential for internalisation (Torchilin, V, 2008).

In vivo trials have been carried out testing the efficacy of some lipid and polymer based therapies. Human clinical trials with GL67 lipid based gene delivery resulted in an immune response as seen by "flu" like symptoms in 4 of 8 patients tested (Ruiz, FE *et al.*, 2001). This study identified that liposome based gene delivery results in a mild immunological response in human patients. *In vitro* and *in vivo* trials have shown cationic polymers to cause some cytotoxicity (Gebhart, CL and Kabanov, AV, 2001; Lee, CC *et al.*, 2008). Cationic polymers have been associated with anti-tumour effects. Although the mechanism is not fully understood, cationic polymers have been shown to cause anti-tumour effect by stimulating the immune system, by enhancing apoptosis and by inhibiting multi-drug resistance (reviewed in (Akhtar, S, 2006)). Non-viral vectors are currently being developed and improved to enhance their efficacy for gene therapy.

1.9. Experimental Aims

Given the importance of BMP signalling during lung development and given its aberrant expression in human diseases we hypothesised that BMP signalling is important during damage and repair processes in the adult lung. Therefore, several experimental questions were posed in this study.

Firstly, little is known about BMP signalling during lung cancer progression. Given the role of BMP signalling in many other types of epithelial cancers, we hypothesised components of the BMP pathway were aberrantly expressed during lung cancer progression. The K-ras^{G12D} lung cancer model was utilised to characterise BMP signalling during the early stages of lung cancer.

Secondly, BMPR-IB expression was found down-regulated in lung cancer and many other cancer types. We hypothesised that BMPR-IB has an anti-proliferative function during the early stages of lung cancer. To investigate this hypothesis the BMPR-IB gene was cloned from mouse lung cDNA and an over expression vector was generated. *In*

vitro analysis of the effects of BMPR-IB expression on cell proliferation and differentiation will be assessed by transient transfection into lung epithelial cell lines.

Thirdly, in the event of the above studies identifying a therapeutic target, we wished to establish an efficient gene delivery method to target lung epithelial cells. Many studies have compared the efficiency of either non-viral vectors or viral vectors at transfecting epithelial cells, but no study has simultaneously compared a range of non-viral and viral vectors for their efficiency at transfecting lung epithelial cells. To this end we compared a range of non-viral and viral vectors to establish an efficient method of gene delivery to lung epithelial cells.

Fourthly, BMP signalling is important for regulation of proliferation and differentiation during lung development. We hypothesised that these BMP signals are recapitulated in the adult lung during the repair process. In order to investigate this, the rat nitronaphthalene model of epithelial injury was utilised. BMP signalling was characterised during the injury and repair stages in this model.

2. Materials and Methods

2.1. Materials

2.1.1. Reagents

Product	Cat no.	Company	Address
1kb ladder	15615-016	Invitrogen	Paisley, UK
100bp ladder	G210A	Promega	Madison, WI, USA
2-Methylbutane	32, 040-4	Aldrich	Dublin, Ireland
Acetone	A3396	Sigma	Dublin, Ireland
Agarose	A9439	Sigma	Dublin, Ireland
Alkaline phosphatase, calf intestinal	M02905	NEB	Hertfordshire, UK
Ammonium persulfate	A3678	Sigma	Dublin, Ireland
Antigen unmasking solution	H-3300	Vector Labs	Dublin, Ireland
B-mercaptoethanol	M-3148	Sigma	Dublin, Ireland
Bio-Rad Bradford protein assay	30098	Bio-rad	Herts, UK
Bis-Acrylamide	161-0158	Bio-Rad	Herts, UK
Blocking serum (Goat)	G9026	Dako	Dublin, Ireland
Blocking serum (Rabbit)	R 9133	Sigma	Dublin, Ireland
Bovine Serum Albumin	10270-106	Sigma	Dublin, Ireland
BMP4 recombinant protein	314-BP	R&D Systems	Oxford, UK
Cell Titer -Cell Proliferation Assay	G3580	Promega	Madison, WI, USA
Chloroform	C2432	Sigma	Dublin, Ireland
Complete mini protease Inhibitor Cocktail	12371600	Roche Diagnostics	Dublin, Ireland
Crystal violet stain	61123	Fluka	Dublin, Ireland
DAPI	D9542	Sigma	Dublin, Ireland
DEPC water tablets	D5758	Sigma	Dublin, Ireland
Developer	P7042-5GA	Sigma	Dublin, Ireland
DMSO	154938	Sigma	Dublin, Ireland
DMEM:F12	31330	Gibco	Paisley, UK
DNase (for RT-PCR)	18068-015	Invitrogen	Paisley, UK
DNase (for MAEC prep)	13738000	Sigma	Dublin, Ireland
dNTP (set of dATP, dCTP, dGTP, dTTP)	10297-117	Invitrogen	Paisley, UK
Doxycycline	631311	Clontech	Dublin, Ireland
ECL reagent	RPN2209	Amersham	Buckinghamshire, UK
Effectene	301425	Qiagen	West Sussex, UK
Ethanol molecular grade	E7148-1GA	Sigma	Dublin, Ireland
Ethidium bromide	E-2515	Sigma	Dublin, Ireland
Ethylene diamine tetra acetic acid (EDTA)	100935V	Sigma	Dublin, Ireland

Farramount Aqueous Mounting Media	S3025	DAKO	Galway, Ireland
Fetal bovine serum	B2019	Sigma	Dublin, Ireland
Fibronectin	F4759	Sigma	Dublin, Ireland
Fixer	P7167-5GA	Kodak	Dublin, Ireland
Fluoroscein FDG	F-1930	Molecular probes	Paisley, UK
Formaldehyde 37% v/v	F8775	Sigma	Dublin, Ireland
G418	G1264	Sigma	Dublin, Ireland
Gene Juice	70967-5	Novagen	Dublin, Ireland
Glass cloning cylinder	C1059-1EA	Sigma	Dublin, Ireland
Glycerol	G-6279	Sigma	Dublin, Ireland
HAMS:F12	31765	Gibco	Paisley, UK
HEPES	H4034	Sigma	Dublin, Ireland
Hyperfilm ECL	RPN3114K	Amersham	Buckinghamshire, UK
Insulin-Transferrin-Selenium	51500-056	Gibco	Paisley, UK
Isopropanol	I-9516	Sigma	Dublin, Ireland
L-Glutamine	25030-024	Gibco	Paisley, UK
Liopfectamine 2000	11668027	Invitrogen	Paisley, UK
Luciferase assay system	E1500	Promega	Madison, WI, USA
M199 basal media	41150	Gibco	Paisley, UK
Marvel			Maynooth, Ireland
MagiMark XP	LC5602	Molecular probes	Dublin, Ireland
Methanol	34885	Sigma	Dublin, Ireland
M-MLV Reverse Transcriptase	28025-013	Invitrogen	Paisley, Ireland
Nitrocellulose Membrane	RPN68D	Amersham	Buckinghamshire, UK
OCT	4583	Tissue Tek	Surrey, UK
Oligo (12-18) dT primers	18418-012	Invitrogen	Paisley, UK
OptiMEM	11058-021	Gibco	Paisley, UK
Orthoboric Acid	274094Q	BDH	Dublin, Ireland
Paraffin wax	26154	VWR	Dublin, Ireland
Paraformaldehyde	P6148	Sigma	Dublin, Ireland
Penicillin/Streptomycin	15070-063	Gibco	Paisley, UK
Phosphate Buffered Saline	P-4417	Sigma	Dublin, Ireland
Phusion High Fidelity Taq	F-530S	NEB	Hertfordshire, UK
Picopure RNA isolation kit	KIT0204	Arcturus	California, USA
Poly-Acryl Carrier	PC152	MRC	Cincinnati, OH, USA
Potassium acetate	P1190-100G	Sigma	Dublin, Ireland
Potassium chloride	P4504-500G	Sigma	Dublin, Ireland
Propidium iodide	81845	Sigma	Dublin, Ireland
Qiagen maxi prep kit	12163	Qiagen	West Sussex, UK
Qiagen mini prep kit	27106	Qiagen	West Sussex, UK
Qiashredder	79656	Qiagen	West Sussex, UK
RIPA buffer	R0278	Sigma	Dublin, Ireland
RNase OUT	10777-019	Invitrogen	Paisley, UK
SeeBlue Protein Ladder	LC5625	Invitrogen	Paisley, UK
Sodium Acetate	S3272	Sigma	Dublin, Ireland

Sodium Chloride	S7653	BDH	Lennox, Dublin
Sodium Dodecyl Sulphate	L6026	Sigma	Dublin, Ireland
Sucrose	84097	Fluka	Dublin, Ireland
Superfect	301305	Qiagen	West Sussex, UK
Sybr Green PCR kit	204143	Qiagen	West Sussex, UK
Taq Polymerase	M1861	Invitrogen	Paisley, UK
TEMED	T9281	Sigma	Dublin, Ireland
TGS loading buffer (2X)	LC2676	Invitrogen	Paisley, UK
TGS running buffer (10X)	161-0772	Bio-Rad	Herts, UK
Transblot filter paper	1703968	Bio-Rad	Herts, UK
Tris	271195Y	BDH	Lennox, Dublin
Trizol	15596-018	Invitrogen	Paisley, UK
Trypsin-EDTA	15400-054	Gibco	Paisley, UK
Trypsin type I	T8003	Sigma	Dublin, Ireland
Tween-20	27,434-8	Aldrich	Dublin, Ireland
Xylene	102936H	BDH	Dublin, Ireland

2.1.2. Instrumentation

ABI 7700 qPCR thermo cycler	Applied Biosystems	California, USA
Bioanalyser	Agilent Technologies	California, USA
Densitometer	Bio-Rad	Herts, UK
Digital Camera (Olympus C-310)	Olympus	Ennis, Ireland
FACS Calibur (Becton Dickinson)	BD Biosciences	California, USA
Fluorescent Microscope (Olympus)	Mason Technology	Dublin, Ireland
NanoDrop 1000 Spectrophotometer	Thermo Scientific	Surrey, UK
Spectrophotometer-Biometra Gene Ray	Mason Technology	Dublin, Ireland
Tecan Plate Reader	Unitech	Dublin, Ireland
Trans-Blot SD Semi Dry Transfer Cell	Bio-Rad	Herts, UK
UV Microscope	Nikon	Surrey, UK
Western Blotting Electrophoresis Rig	Bio-Rad	Herts, UK

2.1.3. Primers

Gene	Species	Sequence	Product (bp)	Anneal Temp (°C)
BMPR-IA	Hu/Mse	F: 5'- ATGACCAGGGAGAAACCACA -3' R: 5'- ATTCTATTGTCCGGCGTAGC -3'	105	55
BMPR-IB- 1	Hu/Mse	F: 5'- ACTCAAGGCAAACCAGCAAT -3' R: 5'- TCTGTTCAAGCTCTCGTCCA -3'	204	58
BMPR-IB- 2	Hu/Mse	F: 5'- AAATGTGGGCACCAAGAAAG- 3' R: 5'- ACAGGCAACCCAGAGTCATC- 3'	171	58
BMPR-II	Hu/Mse	F: 5'- GCCCGCTTTATAGTTGGAGA -3' R: 5'- AGCAAGACGGCAAGCGATTA -3'	144	55 & 58
Smad7	Hu/Mse	F: 5'- TCCAGATACCCGATGGATTT -3' R: 5'- GGGCCAGATAATTCGTTCC -3'	94	55
Id-1	Hu/Mse	F: 5'- GCAAAGTGAGCAAGGTGGAG -3' R: 5'- ATCGTCGGCTGGAACACAT -3'	191	55 & 58
Snail2	Hu/Mse	F: 5'- CCTGGTCAAGAAGCATTTCA -3' R: 5'- CCTTGGAGGAGGTGTCAGAT -3'	278	55 & 58
GAPDH	Hu/Mse	F: 5'- CTGCACCACCAACTGCTTAG -3' R: 5'- CCAGGAAATGAGCTTGACAAA -3'	487	55 & 58
E-cadherin	Hu/Mse	F: 5'- GGCTGGACCGAGAGAGTT -3' R: 5'- CTGCTTGGCCTCAAAATCC -3'	350	58
Crmp2	Hu	F: 5'-CTCGTTTCCAGATGCCTGAT- 3' R: 5'- TTATGCCACTCGCTGATGTC- 3'	207	55
rtTA		F: 5'-GCTGTGGGGCATTTTACTTTAG- 3' R:5'-CGATGGTAGACCCGTAATTGTT- 3'	262	58

Key: Mse: Mouse

Hu: Human

Cloning Primers

Primer	Sequence	Anneal Temp(ºC)
BMPRII-F	*5'- CGGATCC*CTCTGCAGCTAGGTCCTCTCAT	60
BMPRII-R	*5'- AGCGGCCGC*GCTGACAGGAGGATAAAGCAGT	60
BMPR-II-F-*EcoR I*	5'- *GGAATTCGAA*ATGACTTCCTCGCTGCAG	60
BMPR-II-R-*Xho I*	5'- *CCTCGAG*TCCCAGACAGTTCATTCC	60
BMPR-IB-F-*BamH I*	5'- *CGGATCC*GAAATGCTCTTACGAAGCTCT	60
BMPR-IB-R-*EcoR I*	5'- *GAATTC*TCCGAGTTTAATGTCCTGGGAC	60
Mig6-F-*Sac II*	5'- *GAACCGCGG*GGGCACAATGTCAACAGCAGGAGT	60
Mig-6-R-*BamH I*	5'- *GCAGGATCC*TTGCCACTTGACATTGTTCTACGA	60

(Italic indicate restriction site nucleotides**)**

2.1.4. Antibodies

Antibody/Clone	**Raised in**	**IF conc.**	**WB conc.**	**Company**
E-cadherin/36	Mouse	1/200	1/2000	BDB
α-catenin/5	Mouse	1/50	1/250	BDB
β-catenin/14	Mouse	1/200	1/500	BDB
γ-catenin/15	Mouse	1/200	1/1000	BDB
BMPR-IA/H-60	Rabbit	1/20	1/200	SC
BMPR-IB	Goat	1/20	1/250	R&D
BMPR-II	Goat	1/20	1/100	R&D

p-Smad1/5/8	Rabbit	1/50	1/1000	CST
Smad4/B-8	Mouse	1/100	1/100	SC
Myc tag	Mouse	1/1000	1/1000	CST
P-ERK1/2	Rabbit	1/1000	1/1000	CST
T-ERK1/2	Rabbit	1/1000	1/1000	CST
Mig-6	Mouse	1/50	1/200	Sigma
PCNA	Mouse	1/3000	1/3000	Sigma

Key:

BDB: BD Biosciences

SC: Santa Cruz

CST: Cell Signalling Technology

R & D: R & D Systems

2.2. Methods

2.2.1. Cell Culture

2.2.1.1. Culture Media

A549, BEAS-2B and MLE-12 cell lines were cultured in serum containing media composed of 1:1 Hams F12: M199, 5 % FBS, 2 mM L-glutamine. Defined serum free media contained 1:1 Hams F12 and M199 basal medium, 100 ng/µl hydrocortisone, 10 ng/µl EGF, 1 % L-glutamine, 1 % penicillin/streptomycin, 1 % Insulin-Transferrin-Selenium.

2.2.1.2. Primary Cell Isolation

Primary mouse airway epithelial cells (MAECs) were extracted from the lungs of 5-6 week old C3H mice. Lungs were perfused with saline via the heart to remove excess blood cells. Pre-warmed trypsin was instilled into the lungs through the trachea and incubated for 15 minutes at 37 ºC. Lungs were macerated to release the epithelial cells that had been digested from the airway membrane. These cells were treated with DNase. The cells were plated on a non-tissue culture 10 cm^2 Petri dish in defined serum free media (section 2.2.1.1). This step allowed differential attachment of blood cells and fibroblasts, while the airway epithelial cells remained in suspension. The MAECs were harvested from the suspension. MAECs were isolated in clumps; therefore cell counts were not feasible. In order to ensure equal seeding densities, an aliquot of cells were taken prior to seeding and using the Cell Titer 96® AQ_{ueous} One Solution Cell Proliferation Assay (section 2.2.1.7), an absorbance value was obtained. Cells were seeded in culture medium (1:1 Hams F12: M199, 5 % FBS, 2 mM L-glutamine, 100 U/ml penicillin and 100 µg/ml streptomycin). Cells were seeded either onto fibronectin-coated 24-well tissue culture inserts or 8 well chamber slides.

2.2.1.3. Cell Lines

The SV-40 transformed human lung epithelial cell line, BEAS-2B (ATCC) was cultured in tissue culture flasks in 1:1 ratio of Dulbecco's modified Eagle's media and Hams F12 (DMEM: F12) supplemented with 5 % fetal bovine serum (FBS) and 1 % L-glutamine. The human lung adenocarcinoma cell line A549 (ATCC) was cultured in DMEM: F12 containing 5 % FBS and 1 % L-glutamine. The mouse MLE-12 (ATCC) cell line was derived from an adenoma tumour of an SP-C SV40 transgenic mouse, these cells were maintained in DMEM: F12 containing 5 % FBS and 1 % L-glutamine. All cells were incubated at 37 °C with 5 % CO_2 and 95 % air.

2.2.1.4. Freezing Cells for Liquid Nitrogen Stock

Cells in the logarithmic phase of growth (70-90 % confluency) were removed from tissue culture flasks by the cleaving action of the enzyme trypsin-EDTA. The cells were centrifuged into a pellet and resuspended in 500 µl of FBS. 500 µl of a 1: 9 solution of DMSO: FBS was added to the cells in serum. The final concentration of cells was approximately 5 x 10^6 cells/ml. The cells were stored in a cryovial at -80 ºC for 2 weeks then transferred to the liquid nitrogen where they were stored long-term.

2.2.1.5. Thawing Cells from Liquid Nitrogen Stock

Cells were taken from the liquid nitrogen and thawed for 1 minute in a 37 ºC water bath. The cell suspension was added to pre-warmed media containing 5 % FBS and centrifuged at 1200 rpm for 5 minutes to pellet the cells. The supernatant containing the DMSO was removed and the cell pellet was resuspended in pre-warmed media containing 5 % FBS and seeded into a 75cm^2 tissue culture flask.

2.2.1.6. Cell Viability Assay

For assessment of cell viability, counts were carried out using ethidium bromide/ acridine orange (EBAO) staining. Cell counts were carried out using a haemocytometer under the UV microscope; live cells appeared green and dead cells appeared orange.

2.2.1.7. MTS Assay

The CellTiter 96® AQ_{ueous} Assay was used to identify the number of live cells from a Clara preparation. In this assay the tetrazolium compound, MTS (3-(4, 5-dimethylthiazol-2-yl)-5-(3-carboxymethoxyphenyl)-2-(4-sulfophenyl)-2H-tetrazolium)) was reduced to soluble formazan product by dehydrogenase enzyme from metabolically active cells. The product formed resulted in a colour change which was measured at OD_{450}. The OD_{450} value was directly proportional to the number of live cells in the sample. Media only was used to set the background level. Cells were seeded at a constant OD for repeatable results.

2.2.1.8. Cell Migration Assay

Cells were seeded at approximately 90,000 cells/ well in a 24 well tissue culture plate, on Day -1. Cells were untransfected (no-vector), transfected with pcDNA4 (empty-vector) or BMPR-IB-pcDNA4 on Day 0. The cell monolayer was wounded with a sterile 200 µl pipette tip to generate a cell-free area of approximately 500 µm in width. Cell debris was removed by rinsing with PBS. Defined serum free medium was added to the cells with or without BMP4 ligand (100 ng/ml). After 24 hrs in culture, cells were fixed with ice cold methanol for 5 min, air dried and stained with crystal violet solution. Phase-contrast photomicrographs of five fields of view per scrape were acquired using an inverted microscope equipped with a digital camera (Olympus C-310). Cells in each field of view were counted and the average number of cells that had migrated into the wounded area was determined.

2.2.1.9. Cell Cycle Analysis

Cells were rinsed in PBS, fixed in 70 % ethanol and stored at -20 ºC. Prior to analysis, cells were rinsed in PBS containing 1 % FBS and re-suspended in propidium iodide staining solution containing 40 µg/ml propidium iodide, 100 µg/ml RNase solution in PBS. Cells were

incubated for 30 minutes at 37 ºC and analysed using a FACScan Flow Cytometer using Cell Quest software.

2.2.1.10. Antibiotic Concentrations

An antibiotic kill curve was carried out on BEAS-2B cells to identify the concentration at which doxycycline (Dox) was toxic to the cells. Cells were seeded at a density of 5 x 10^4 cells/ well in a 24 well plate. Media containing 1 µg/ml, 5 µg/ml, 10 µg/ml, 20 µg/ml and 40 µg/ml were each added to the cells. The media was changed every 2 days. Cell counts were carried out on day 0, 4, 8 and 12 to determine the level of toxicity caused by the different concentrations of the antibiotic.

An antibiotic kill curve was carried out on BEAS-2B cells to identify the concentration at which hygromycin B caused cell death. Cells were seeded at a density of 5 x 10^4 cells/well in a 24 well plate. Media containing 25 µg/ml, 50 µg/ml, 100 µg/ml, 150 µg/ml and 200 µg/ml were each added to the cells. The media was changed every 2 days. Cell counts were carried out on day 0, 4, 8 and 12 to determine the level of toxicity caused by the different concentrations of the antibiotic.

An antibiotic kill curve was carried out on BEAS-2B cells to identify the toxic concentration of G418 antibiotic. This concentration was then used to generate stable cell clones which contained the transfected plasmid. 5 x 10^4 cells/well were seeded into a 24 well plate and treated with 0, 125, 250, 500, 750 and 1000 µg/ml of G418. Cell counts were carried out on day 0, 4, 8 and 12.

2.2.2. Flow Cytometry

2.2.2.1. CMV-GFP Transfection Flow Cytometry Analysis

GFP expressing plasmids and viruses were transfected into cells, in order to measure the efficiency of transfection GFP expression was measured using a flow cytometer. Cells

were removed from the cell culture vessel using trypsin, and suspended in PBS containing 1 % paraformaldehyde. Cells were stored on ice until analysed by flow cytometry. Endogenous levels of GFP were measured on FL-1 setting of Cell Quest software which measures fluorescence in the 450-500 nm. The background level of autofluorescence was set with untreated cells. The transfection efficiencies were then measured for each experiment by determining the percentage of the population that expressed GFP higher than the negative control.

2.2.2.2. CCSP-GFP Flow Cytometry Analysis

$CCSP^{Cre}$ mice were crossed with $Rosa^{GFP}$ to generate mice that expressed GFP specifically in the Clara cells of the lung. MAECs were isolated (section 2.2.1.2) and examined by flow cytometry to establish if GFP expressing cells could be isolated by FACS sorting. MAECs from $CCSP^{Cre}$ control mice, which do not express GFP, were used as a negative control. The percentage of cells expressing GFP higher than the negative control was quantified.

2.2.2.3. CCSP-LacZ Flow Cytometry Analysis

Unlike GFP, expression of β-galactosidase (β-gal) required a substrate for visualisation on a flow cytometer. The fluorescent substrate utilised in these experiments was the FDG (fluoroscein di-β -D-galactopyranoside) substrate. The β-galactosidase protein hydrolysed the FDG substrate to an FMD (fluorescein monogalactoside) and then to a strongly fluorescing fluoroscein, which emits at 514 nm.

Cells were isolated and pooled from 3-5 $CCSP^{Cre}$ $Rosa^{LacZ}$ animals (section 2.2.1.2). 1 x 10^6 cells per 100 µl were stored on ice. 100 µl of a 2mM FDG substrate was incubated for 10 minutes in a 37 ºC water bath. This pre-warmed substrate was added to the cells and incubated for 1 minute in a 37 ºC water bath. The cells were put back on ice and 1.8 ml of propidium iodide (1:100 dilution made in staining solution (PBS, 4% FBS, 10mM HEPES)) was added to the tube as a counter stain. Cells were kept on ice before and during the FACS analysis. Cells from $CCSP^{Cre}$ mice, which did not express LacZ,

underwent the same staining process and were used as a negative control to set the fluorescent background on the flow cytometer.

2.2.3. Immunofluorescence

2.2.3.1. Preparation and Fixation of Cells

Immunofluorescence was carried out to investigate the localisation of protein expression in cells. Cells were grown for immunofluorescence on either tissue culture inserts in 24 well tissue culture plates or in 8 well chamber slides. Cells taken for immunofluorescence were fixed in ice-cold 100 % methanol for 5 minutes at -20 ºC. The fixed cells were air-dried and stored at -20 ºC until immunofluorescence was carried out.

2.2.3.2. Preparation of PFPE Tissue for Immunofluorescence

Immunofluorescence was carried out on tissue sections to identify the localisation of protein expression in paraformaldehyde fixed paraffin embedded (PFPE) 3µm tissue sections. The tissue slices were de-waxed by 5-10 minute incubation in xylene. The tissue slices were re-hydrated for 2 minutes in 90 % EtOH, 2 minute incubation in 75 % EtOH and 2 minute incubation in 75 % EtOH. The antigen retrieval process was carried out by boiling the slides three times for 5 minutes in antigen unmasking solution.

2.2.3.3. Immunofluorescence Procedure

The tissue or cells were incubated with appropriate animal serum (20 %) for 20 minutes at room temperature to block the IgG receptors. Serum was replaced by appropriate primary antibody diluted in TBS (see section 2.1.4 for dilutions) and incubated at 4 ºC overnight. Unbound primary antibody was washed off in TBS/ 0.1 % Tween-20 before the addition of the secondary antibody. Secondary antibody was diluted in 20 % animal serum (see section 2.1.4 for dilutions) and incubated at room temperature for 30 minutes. Unbound secondary antibody was washed off in TBS/ 0.1 % Tween-20 for 10 minutes.

Cells/ tissue were counter stained with 1/200 DAPI diluted in TBS, incubated for 10 minutes at room temperature. DAPI was removed by washing briefly in dH_2O before mounting in Faramount aqueous mounting medium. Immunofluorescence staining was viewed under a fluorescence microscope. As a negative control cells and tissue were treated with secondary antibody only, to ensure there was no non-specific staining by the secondary antibody (Figure 2.1).

2.2.4. Western Blot Analysis

2.2.4.1. Cell Lysis and Protein Quantification

Cells were removed from tissue culture plates by scraping into sterile, ice cold PBS and centrifuged at 1500 rpm for 5 minutes. Total protein was extracted by lysing the cell pellet in ice cold RIPA buffer (150 mM NaCl, 1% Igepal CA-630, 0.5 % sodium deoxycholate, 0.1 % v/v SDS, 50 mM Tris pH 8.0) which contained a 1X protease inhibitor cocktail. Protein was stored at -80 ºC.

2.2.4.2. Protein Assay

Protein quantification was carried out using the Bio-rad Bradford protein assay, according to manufacturer's guidelines. Briefly, BSA was diluted in sterile dH_2O to generate standards which ranged from 0 to 1.4 µg/ml. Standards and samples were mixed with Bio-rad reagent in a 96 well plate, incubated at room temperature for 5 minutes, and measured at 620 nm. The standards were used to generate a standard curve from which protein quantification was determined.

2.2.4.3. SDS- PAGE Electrophoresis

Sodium dodecyl sulphate polyacrylamide gel electrophoresis (SDS-PAGE) was run according to Mini-PROTEAN 3 Cell protocol (Bio-rad). Resolving and stacking gels were made according to section 2.2.4.6. The gels were polymerised by the addition of

Figure 2.1 secondary control

TEMED and ammonium persulphate (APS). An equal volume of loading buffer (25 µl BME in 500 µl 2X loading buffer) was added to 20 µg of protein. The samples were boiled for 5 minutes and loaded on the SDS-PAGE gel along with a molecular weight protein ladder (MagiMark XP and/or See Blue Protein Ladder). Electrophoresis was carried out using the Laemmli buffer system. The gels were run in 1X TGS running buffer (section 2.2.4.6.1) at a constant 130 volts until the highest molecular weight protein entered the gel.

2.2.4.4. Semi-Dry Electro Blotting

Proteins were transferred from an SDS-PAGE gel onto a nitrocellulose membrane using a Bio-Rad Transblot SD Semi Dry Transfer Cell. Extra thick blot paper and nitrocellulose membrane were equilibrated in transfer buffer. The gel was assembled between the blot paper and membrane on the Semi Dry Transfer Cell as follows: blot paper, nitrocellulose paper, SDS-PAGE gel, blot paper. Proteins were transferred to the nitrocellulose membrane for 45 minutes at a constant 25 volts.

2.2.4.5. Immunoblotting

The nitrocellulose membrane blots were incubated in a blocking buffer which was made of either 5 % milk powder or 5 % bovine serum albumin (BSA), to block non-specific binding. [Blots used to detect phosphorylated proteins were blocked in 5 % BSA-TBS; all other blots were blocked in 5 % Marvel-TBS.] The blocking buffer was replaced by the primary antibody and incubated at 4 ºC overnight. Unbound antibodies were removed by washing in TBS/ 0.1 % Tween-20. Blots were then incubated in horseradish peroxidase (HRP) conjugated secondary antibody for 1 hour at room temperature. Unbound secondary antibody was removed by washing in TBS/ 0.1 % Tween-20 buffer prior to the addition of ECL (enhanced chemiluminescence) Western blot detection reagent. The protein was visualised by exposing the blot to a chemiluminescence film (Hyperfilm ECL) in an x-ray film cassette. The chemiluminescence film was developed and fixed in Kodak developer and fixer reagents. The protein signal on the film was visualised and analysed.

2.2.4.6. Western Blot Reagents

SDS-PAGE Gels:	**Resolving gel**		**Stacking gel**
	10 %	**12 %**	**4 %**
dH_2O	4.1 ml	3.4 ml	3.05 ml
30 % Bis/acrylaminde	3.3 ml	4.0 ml	650 µl
1.5 M Tris-HCl, pH 8.8	2.5 ml	2.5 ml	
0.5 M Tris HCl, pH 6.8			1.25 ml
10 % SDS	100 µl	100 µl	50 µl
10 % ammonium persulphate	50 µl	50 µl	25 µl
TEMED	5 µl	5 µl	5 µl

2.2.4.6.1. Running Buffer (1X TGS buffer)

Dilute 10X TGS (Tris, Glycine, SDS) buffer with dH_2O to a 1X working concentration.

2.2.4.6.2. Transfer Buffer (Towbin buffer)

Tris-HCl	1.515 g
Glycine	7.2 g
MeOH	100 ml

2.2.5. Animals and Tissue Collection

2.2.5.1. Animals

Transgenic mice were maintained at Baylor College of Medicine, Texas, in the designated animal care facility in accordance with the institutional guidelines for care and use of laboratory animals. C3H mice were maintained at National University of Ireland, Maynooth in the designated animal care facility in accordance with the institutional

guidelines. Ethical approval was gained from local authorities for use of animals in these studies. Mice were sacrificed by interperitonelial injection of pentabarbitone.

2.2.5.2. Tissue Collection

2.2.5.2.1. Paraformaldehyde Fixed Paraffin Embedded Tissue

Perfused lungs were instilled with either 4 % or 1 % paraformaldehyde, and incubated overnight at 4 ºC. The lungs were then moved to 70 % EtOH for an overnight incubation at 4 ºC. The lungs were dehydrated in 70 % EtOH (30 min), 80 % EtOH (30 min), 95 % EtOH (30 min), 100 % EtOH (45 min) three times, xylene (1 hour) three times and incubated in paraffin (1 hour at 60 ºC) three times. The lobes were then embedded in paraffin wax. This paraformaldehyde fixed paraffin embedded tissue was sliced to 3 µm on a microtome.

2.2.5.2.2. Cryopreserved Tissue

Lungs were perfused with PBS via the heart to removed blood from the blood vessels. A 1:1 ratio of OCT: 10 % sucrose solution was instilled down the trachea into the lungs to preserve the architecture during freezing. The lobes of the lung were separated and each lobe was placed in OCT embedding medium in a cryomould, the lobe was kept flat against the bottom to maximise the area of lung to be cut. The lobe was frozen in liquid nitrogen cooled 2-methylbutane for approximately 10 seconds and stored at -80 ºC until required.

2.2.5.2.3. Cryosectioning for Laser Capture Microdissection

Frozen lobes were maintained at -20 ºC and sectioned at 7 µm on a cryotome. Sections adhered to room temperature, sterile, uncoated and uncharged microscope slides.

Sections were immediately fixed in 70 % EtOH for 30 seconds, followed by washing in DEPC water. The sections were fixed by dehydrating in 80 % EtOH, 90 % EtOH (3 washes, 2 minutes each), 100 % EtOH (3 washes, 2 minutes each), and xylene (3 washes, 2 minutes each). Sections were stored in xylene until used in laser capture microdissection (2 hrs max). All reagents used were from newly opened vials and all water used was RNase free to prevent RNase contamination of the tissue slices. The first one of six serial sections was stained with hematoxylin and eosin for histological reference.

2.2.6. Laser Capture Microdissection

The Arcturus PixCell II Microdissection system (www.arcturus.com) was used to isolate purified populations of normal lung airway cells from non-cancerous mice ($CCSP^{Cre}$) and cancer pathologies from the lungs of lung cancer mice ($CCSP^{Cre}$ LSL-K-ras^{G12D}). The microscope and all utensils used were decontaminated with RNase Away. The purified population of cells were isolated under the supervision of a pathologist. This microdissection system works as follows: the laser beams through the cap and distorts the thin ethylene vinyl acetate plastic filament at the bottom of the cap such that the cells of interest are picked up from the tissue on the microscope slide onto the cap (Figure 2.2). The following parameters were used for the isolation of these cells: laser spot size 7.5 µm, pulse power 50 mW, pulse width 0.75 ms and a threshold voltage of 205 mV.

2.2.7. RNA Isolation

2.2.7.1. Arcutrus PicoPure RNA Isolation

Cells captured by LCM were extracted from the Arcturus macro-cap by incubation in 50 µl of extraction buffer at 42 ºC for 30 minutes. The cells were stored at -80 ºC until RNA was to be isolated. RNA isolation was carried out according to the Arcturus PicoPure RNA isolation protocol. Briefly, RNA was bound to a pre-conditioned purification

Figure 2.2

column by centrifugation. The RNA was washed in 70 % EtOH and wash buffer 1. The RNA was treated with DNase, for 15 minutes at room temperature, to remove any genomic contamination. The column was washed in wash buffer 2 and dried by centrifugation before elution in 13 µl of elution buffer. The RNA was aliquoted, to prevent any degradation due to freeze thawing, and stored immediately at -80 ºC.

2.2.7.2. Trizol RNA Isolation

Cells were removed from culture in 1 ml of Trizol with 5 µl of polyacryl carrier. RNA was extracted according to the Invitrogen Trizol protocol. Briefly, 200 µl chloroform was added to 1ml of Trizol, shaken vigorously for 15 seconds and allowed to stand for 2 minutes prior to centrifugation at 12,000 g for 15 minutes at 4 ºC. The aqueous phase (containing RNA) was carefully removed to an eppendorf and 500 µl isopropanol was added, inverted to mix and incubated for 15 minutes at room temperature prior to centrifugation at 12,000 g for 10 minutes at 4 ºC. The supernatent was removed and the visible pellet was rinsed with 70 % EtOH. The pellet was resuspended in 17µl DEPC water. RNA was stored in aliquots at -80 ºC.

2.2.8. RNA Analysis

2.2.8.1. Bioanalyser

Quality assurance of LCM isolated RNA was carried out by the RNA core at Baylor College of Medicine so the RNA was of high standard for microarray analysis. The quantity of RNA was determined with a nanodrop which has a sensitivity of 2-3700 ng/ µl. The purity and integrity of the RNA was assessed on an Agilent 2100 Bioanalyser, using Bioanalyser RNA 6000 Pico Assay (Agilent, CA).

RNA samples selected for microarray analysis contained no alveolar contamination, contained more than 100 pg/µl of RNA, showed clear 18S and 18S peaks with minimum

noise between the peaks suggesting no contamination. These samples were independently confirmed by Dr Linda White at the RNA core at Baylor College of Medicine.

2.2.8.2. UV spectrophotometer

RNA samples were diluted 1/ 50 in DEPC water and read at 260 nm for quantification. A 260 nm absorbance value of 1 unit equates to 40 µg/ml of RNA concentration. Therefore the following calculation was used to quantify RNA:

$$\text{Concentration RNA } (\mu g/\mu l) = \text{Abs}_{260} \times 40 \times \text{dilution factor (50)}$$

2.2.9. Microarray

Cells extracted by laser capture microdissection yielded picogram (pg) and nanogram (Roberts, AB *et al.*) quantities of RNA. These samples required amplification to achieve the minimum starting material for microarray analysis. The NuGen Pico Amplification System (NuGen, California, US) was used to amplify the RNA isolated from laser capture microdissected samples. This Ribo-SPIA based system results in a double stranded DNA product which was more stable for microarray analysis than cDNA. However, this amplification method was unsuccessful due to incompatibility issues between the RNA isolation method C(Arcturus PicoPure Isolation) and the NuGen Pico amplification kit. To overcome this incompatibility issue, the Arcturus RiboAmp HS amplification kit (Arcturus, California, US) was used to amplify the RNA. Arcturus RiboAmp HS allows amplification of 100-500pg of total RNA (Figure in 2.2). This two round amplification method was successful. The amplified cDNA was labelled with biotin and hybridised to Affymetrix Mouse Genome 430 2.0 GeneChip arrays (Affymetrix, CA, USA). High through-put gene array analysis was performed on an Affymetrix platform using a Mouse 2.0 430 CHIP- analyses expression of 39,000 transcripts expressed by the mouse. The RNA quality analysis, amplification and microarray were carried out at Baylor College of Medicine, Houston, Texas, USA. Microarray analysis was carried out by Dr. Chad Creighton at Baylor College of Medicine. The following criteria for genes listed had to pass three filters: lower bound of

90 % confidence interval, fold-change greater than 1.2, and an absolute value of difference between groups means greater than 80.

2.2.10. PCR

2.2.10.1. Primers

Primers were designed using the Primer 3 programme (http://biotools.umassmed.edu/bioapps/primer3_www.cgi). When restriction enzyme sites were added to primers the Tm and % GC were calculated using DANA oligo calculator (http://mbcf.dfci.harvard.edu/docs/oligocalc.html). Forward and reverse primers were designed to have similar melting temperatures and similar GC content.

2.2.10.2. Primer Design for Cloning

2.2.10.2.1. Human BMPR-II Cloning Primer Design

Human primers were designed against the BMPR2 cDNA sequence NM_001204. Primers, BMPR-II- F1 and BMPR-II- R1, were designed within the 5' and 3' untranslated region, respectively. The forward primer was designed to include a *BamH* I restriction enzyme site and the reverse primer included a *Not* I restriction site, to allow sub-cloning into the pTRE plasmid.

2.2.10.2.2. Mouse BMPR-IB Cloning Primer Design

Primer BMPR-IB-F was designed to include the start codon of sequence NM_007560, with a Kozak sequence and *BamH* I restriction site upstream. Primer BMPR-IB-R was designed to include a point mutation to change the termination codon to a glycine residue and contained an *EcoR* I restriction site for sub-cloning.

2.2.10.3. Typical PCR

Conditions for standard PCR were as follows:

		(Final Conc.)
5 X Go Taq Flexi PCR Buffer	10 µl	1X
50 mM $MgCl_2$	3-5 µl	3 mM – 5 mM
10 mM dNTP mix	1 µl	200 µM each dNTP
Forward Primer (10µM)	1 µl	200 nM
Reverse Primer (10µM)	1 µl	200 nM
Go Taq Flexi Polymerase (5U/ µl)	0.25 µl	1.25 units
cDNA	0.5 µl	
DEPC-treated water	to 50 µl	

2.2.10.4. Cloning PCR

Cloning PCRs were carried out using Phusion high fidelity polymerase to ensure minimal errors during gene amplification. The PCR reaction was carried out as recommended in the protocol. A 50 µl total reaction volume contained 1X HF buffer, 1 mM $MgCl_2$, 200 µM of each dNTP, 500 nM of each primer, 1 % DMSO, 1 unit of DNA polymerase, and approximately 500 ng of template DNA. The PCR cycle was carried out as follows: 98 ºC for 90 seconds, (98 ºC for 30 seconds, 60 ºC for 30 seconds, 72 ºC for 2.5 minutes) 35 cycles, 72 ºC for 10 minutes.

2.2.10.5. Bacterial PCR

Diagnostic PCR was carried out directly on bacterial colonies. The PCR reaction contained 1X buffer, 1 mM $MgCl_2$, 200 µM each dNTP, 500 nM each primer, 1 unit taq polymerase (Invitrogen), swab of bacterial culture and 0.08 % Tween-20 detergent. The PCR cycle was carried out as follows: (95 ºC for 1 minute, 50 ºC for 2 minutes, 72 ºC for 2 minutes), (95 ºC for 1 minute, 56 ºC for 1 minutes, 72 ºC for 1 minute) for 30 cycles, 72 ºC for 5 minutes.

2.2.10.6. Quantitative PCR

The qPCR machine ABI 7700 (Applied Biosystems, CA, USA), was used to validate microarray results. Real time PCR was carried out on RNA samples captured by LCM, using TaqMan RNA to C_t 1 step kit (Invitrogen). 500 pg of RNA was analysed in a one step real time PCR using DNA probes against 18S as a standard, *Mig-6*, Id-1, Smad4, BMP4, BMP5, BMPR-IA, BMPR-IB and BMPR-II. Probes were purchased from Applied Biosystems.

2.2.10.7. RT-PCR

RNA was isolated as per section 2.2.7.2. RNA (500 ng) was treated with DNase to remove genomic contamination. RNA was incubated with 0.5 - 1 unit of DNase I, 1X DNase buffer in a 10 µl total volume. The DNase treatment was incubated for 20 minutes at room temperature. The enzyme reaction was inactivated by the addition of 1 µl of 25 mM EDTA and subsequent incubation at 65 ºC for 10 minutes. Genomic controls were set up to ensure the DNase treatment was successful and there was no genomic carry over. These controls were DNase treated but not synthesised to cDNA. GAPDH PCR ensured the samples were free from genomic contamination.

To each DNase treated RNA sample, 1 µl of 50 µM oligo dT and 1 µl of 10 mM dNTPs was added, incubated at 65 ºC for 5 minutes and subsequently cooled on ice. 10X reaction buffer, 25 mM $MgCl_2$, 0.1 M DTT, RNase OUT, and Superscript III reverse transcriptase were added to the samples to synthesis the RNA into cDNA. The mixture was incubated for 50 minutes at 50 ºC and the reaction was inactivated at 85 ºC for 5 minutes.

2.2.10.8. Agarose Gel Electrophoresis of PCR Products

0.8 - 2 % (w/v) agarose gels were made by dissolving 0.8 - 2 g agarose in 100 ml TAE buffer (40 mM Tris, 0.35 % v/v Acetic Acid, 0.5 mM EDTA). 3 µl of ethidium bromide [10 mg/ ml] was added per 100 ml of agarose to visualise the DNA. The gel was cast and set at room temperature. DNA was electrophoresed such that sufficient separation

occurred. A DNA ladder was run adjacent to the samples to allow determination of the product size. Gels were visualised under UV light.

2.2.11. Plasmids

2.2.11.1. Tetracycline Inducible Plasmids

pTet-On plasmid expresses the reverse tetracycline regulator under the control of a CMV promoter (Figure 9.1). The pTRE-Luciferase plasmid expresses the Luciferase reporter gene under the control of the tetracycline response element and a minimal CMV promoter (Figure 9.2). The pTRE2hyg plasmid contains the tetracycline response element and minimal CMV promoter upstream of a multiple cloning site to allow insertion of a gene of interest (Figure 9.3). These plasmids were purchased from Clontech.

2.2.11.2. TOPO Cloning Plasmids

PCR amplified products, with a thymidine 5' overhang nucleotide, are ligated to pCR2.1-TOPO cloning vector (Figure 9.4). Blunt ended PCR amplified DNA fragments were ligated into the pCR-Blunt II-TOPO cloning vector (Figure 9.5). TOPO cloning was carried out according to manufacturer's guidelines (Invitrogen).

2.2.11.3. pCMV-Script

PCR amplified DNA fragments were ligated into the pCMV-Script cloning vector (Figure 9.6). pCMV-Script cloning was carried out according to manufacturer's guidelines (Stratagene).

2.2.11.4. pcDNA4

PCR amplified DNA fragments were ligated into pcDNA4 cloning vector (Invitrogen) into the multiple cloning site (Figure 9.7).

2.2.11.5. p1647 Rosa-PolyA-FRT-Neo

This plasmid was constructed in a pBluescript backbone (Figure 9.8). This plasmid contained a multiple cloning site for the insertion of a gene of interest. The FRT-neomycin- FRT region allowed antibiotic selection, and removal of the antibiotic resistance gene. The gene of interest region and FRT-neo region were flanked by 5' and 3' DNA regions that were homologous to sequences in the Rosa Luciferase backbone. These regions were required for the homologous recombination of the gene of interest into the Rosa Luciferase backbone.

2.2.11.6. Rosa Luciferase Backbone

This plasmid was composed of a strong CAGGS promoter which allowed expression of a puromycin selection cassette; this was known as the stop cassette (Figure 9.9). The stop cassette was flanked by LoxP regions on either side. The LoxP-Stop cassette was located 5' of the luciferase gene. The DNA sequences flanking the luciferase reporter gene were homologous to the 5' and 3' DNA sequences in the p1647 Rosa-PolyA-FRT-Neo plasmid. Homologous recombination at these regions replaced the luciferase gene with the gene of interest. The Rosa Luciferase backbone plasmid contained large regions of DNA which were homologous to the Rosa26 locus. This region allowed homologous recombination of linearised plasmid into the Rosa locus in the mouse genome.

2.2.11.7. pCyclinD$_1$-GFP

pCyclin D_1-GFP vector was generated previously in the lab by sub-cloning the Cyclin D_1 promoter upstream of *Aeuqorea Victoria* enhanced GFP gene, in the pEGFP-1 promoterless vector (Figure 9.10). Therefore GFP expression was driven by the Cyclin D_1 promoter, an early cell cycle gene. The GFP has a long half life and its expression persisted for over 24 hrs.

2.2.11.8. pMGFP

pMGFP plasmid, purchased from Promega, contained a GFP gene from *Montastrea cavernosa* (known as MGFP). The MGFP is under the constitutive control of the CMV promoter, which had been modified for eukaryotic cell expression (Figure 9.11).

2.2.12. Plasmid Preparation

2.2.12.1. Mini/ Maxi Preparation of Plasmid from E. coli

Small scale preparations (mini-prep) of plasmid were carried out using either Machery-Nagel kit or the Qiagen mini prep kit. Large scale preparations (maxi prep) of plasmid were carried out using the Qiagen maxi prep kit. Procedures were carried out according to manufacturers' protocols.

2.2.12.2. DNA Purification

Purification of DNA from a PCR reaction and purification of a DNA band from an agarose gel was carried out using the Machery Nagel DNA purification kit, according to the manufacturer's protocol.

2.2.12.3. Generation of Plasmid Stocks

E.coli transformed with plasmid was grown over night at 37 ºC and 200 rpm, in LB media containing antibiotic selection. 500 µl of bacteria was diluted in an equal volume of 30 % glycerol solution and stored at -80 ºC.

2.2.12.4. Antibiotic Selection

Ampicillin was used at a concentration of 25 µg/ml. Kanamycin was used at a concentration of 30 µg/ml. Tetracycline was used at a concentration of 12.5 µg/ml.

2.2.13. DNA: Sub-Cloning

2.2.13.1. Restriction Site Design

When inserting restriction sites on primers for sub-cloning purposes the following requirements were followed: the restriction sites were chosen such that they do not have a recognition sequence in the gene of interest, they can cut the gene of interest from the donor plasmid and they can cut the recipient plasmid. Where possible, restriction sites were chosen such that they were compatible for double digestion.

2.2.13.2. Restriction Digest

Diagnostic digests typically contained 0.5 - 5 µg of DNA in a total volume of 20 µl. Restriction digests were carried out on 10-50 µg of DNA in a total volume of 100 µl when the DNA was required for sub-cloning. Restriction enzymes, buffers and BSA were used according to manufacturers' guidelines.

2.2.13.3. Alkaline Phosphatase Treatment

Plasmid backbones were treated with calf intestinal alkaline phosphatase (CIP) in order to remove 5' phosphate groups so as to prevent self ligation. Dephosphorylation was carried out according to NEB guidelines. Briefly, DNA was incubated with Buffer 3, CIP in a total volume of 20 µl. The reaction took place at 37 ºC for 1 hour. In order to remove the CIP enzyme, which can not be heat inactivated, the DNA was purified using a Machery-Nagel DNA purification column.

2.2.13.4. T4 DNA Polymerase

T4 DNA polymerase treatment produced blunt ended products from DNA with 5' or 3' overhangs. T4 DNA polymerase had 5' to 3' DNA polymerase activity whereby it filled in an overhang in the presence of dNTP. T4 DNA polymerase treatment was carried out on DNA in the presence of 1X T4 polymerase buffer, 0.1 mM dNTP, T4 DNA polymerase, DNA (10-20 µg), T4 DNA polymerase (1 unit/µg), in a total volume of 100

µl. The treatment was carried out at 11 ºC for 15 minutes and the enzyme was heat inactivated at 75 ºC for 20 minutes.

2.2.13.5. T4 Polynucleotide Kinase Treatment

T4 polynucleotide kinase (PNK) treatment was carried out on the hBMPR2-F1R1 blunt ended PCR product in order to add a phosphate group to the 5' end of the DNA strands. The gel purified PCR product was incubated with PNK and T4 DNA ligase buffer, which contained ATP required for the reaction, for 30-60 minutes at 37 ºC.

2.2.13.6. Ligation

Ligations were carried out at 1:1, 1:2, 1:3 and/or 1:4 ratios in a total volume of 10 µl with a vector DNA concentration of 50 ng. Ligations were either carried out at room temperature for 2-4 hrs or overnight at 4 ºC using T4 DNA ligase (NEB).

2.2.13.7. pCMV-Script Cloning

Gel purified blunt ended BMPR2 PCR product was ligated into pCMV-Script cloning vector according to manufacturer's protocol. Briefly, pCMV-Script plasmid was digested with *Srf* I restriction enzyme. Blunt ended PCR product was ligated to the blunt ended pCMV-Script plasmid. The ligation product was transformed into competent bacteria and colonies are selected for on antibiotic containing LB agar plates.

2.2.13.8. TOPO Cloning

5 µl gel purified blunt ended PCR product was ligated into 1 µl of Blunt II- TOPO cloning vector in the presence of 1 µl of salt solution for 5 minutes at room temperature. 5 µl of PCR product containing an A overhang nucleotide was ligated to pCR2.1 TOPO cloning vector in the presence of 1 µl salt solution, and incubated for 5 minutes at room temperature. 2 µl of the ligation product was transformed into TOP 10 chemically

competent *E.coli*. Clones were selected by overnight incubation on antibiotic containing LB agar plates.

2.2.13.9. DNA Extraction from Agarose Gels

DNA required for sub-cloning was isolated from 0.8 % low melting point TAE agarose gels, after electrophoresis. DNA purification was carried out using a Qiaquick gel extraction kit (Qiagen) or the Machery-Nagel Gel Extract II purification kit; both protocols were utilised according to manufacturer's protocol.

2.2.13.10. Purification of DNA

DNA purification of PCR products was carried out according to the Qiaquick PCR purification kit (Qiagen) or Machery-Nagel PCR clean-up kits (Machery-Nagel); procedures were carried out as per manufacturer's instructions.

2.2.13.11. Seuqnecing Analysis

Sequencing analysis was carried out externally by the sequencing core at Baylor College of Medicine, Houston, Texas and by Co-Genics, UK.

2.2.14. Recombineering

2.2.14.1. Growth and Maintenance of Bacteria

E.coli was grown on LB agar culture plates at 37 ºC with appropriate antibiotic selection for the plasmid. Liquid cultures were grown in LB broth, in an orbital shaker at 200 rpm overnight. For long-term storage, 30 % (v/v) glycerol was added to fresh liquid cultures and stored at -70 ºC. DY380 bacteria used for bacterial recombineering were grown at 30ºC on LB plates or in LB broth. All other bacteria were grown at 37 ºC on LB plates or in LB broth.

2.2.14.2. Bacterial Recombineering

Competent DY380 bacteria were prepared by culturing 5 ml of cells in LB media to an OD_{600} of 0.4-0.6. Bacteria were then incubated in a 42 ºC shaking water bath for 15 minutes followed by 10 minute incubation in an ice bath. Cells were pelleted by centrifugation at 8,800 rpm for 8 minutes at 4 ºC. Cells were washed twice in 1 ml ice cold 10 % glycerol. The final cell pellet was re-suspended in 50 µl of ice cold 10 % glycerol.

50 µl of heat shocked cells were added to an ice-cold electroporation cuvette. Approximately 1 µg of DNA was added to the cells and electroporated for 3 seconds using the bacterial setting on a BioRad electroporator. 800 µl of SOC media was added and the cells are incubated for 1.5 hrs at 30 ºC for DY380 bacterial cells, after which time the cells were plated on antibiotic selection plates as appropriate.

2.2.14.3. Transformation of Chemically Competent Bacteria

Chemically competent bacteria, XL-1 Blue (Strategene) and TOP10 (Invitrogen), were purchased as ultra-competent bacterial cells. These cells were transfected with plasmid DNA according to manufacturer's guidelines. Briefly, cells were thawed on ice, and after the addition of β-mercaptoethanol cells were incubated on ice for 10 minutes. DNA was then added to the bacteria and subsequently incubated for 30 minutes on ice. The cells underwent heat shock at 42 ºC for 30 seconds before the addition of pre-heated SOC media. Cells were incubated for 1 hrs at 37 ºC and 300 rpm before being plated on antibiotic selection plates.

2.2.14.4. Electroporation

50 µl of ice cold competent cells and approximately 1 µg of DNA were added to an ice cold electroporation cuvette (BioRad). The DNA was electroporated into the cells using a 3 second pulse. 800 µl of SOC media was added to the cuvette to retrieve the cells. The cells were incubated for 1.5 hrs at 30 ºC for DY380 bacteria or 1.5 hrs at 37 ºC for 294-FLP bacteria. Post incubation, bacteria were plated on antibiotic selection plates.

2.2.15. Transfections

2.2.15.1. $CaPO_4$ Transfection

Cells were seeded in a 10 cm^2 tissue culture grade Petri dish. 7 µg plasmid DNA was incubated in 500 µl DEPC water at 37 ºC for 1 hour. 60 µl 2 M $CaCl_2$ was added dropwise to the DNA and mixed by vortexing. The $CaCl_2$-DNA solution was added dropwise to 2X HBS solution and mixed by vortexing. This solution was incubated at room temperature for 30 minutes. Cells were rinsed in PBS and the DNA complex was added to the cells and incubated at 37 ºC for 4 hrs. After the incubation the media was removed from the cells and 5 ml of 10 % sterile glycerol solution (in 1X HBS) was added to the cells for 3 minutes. The glycerol was removed, the cells were rinsed twice and 5 % serum containing medium was added. Cells were incubated for 2 days before the addition of the antibiotic selection media.

2.2.15.2. Lipid Transfections

Non-viral vectors were tested for their ability and efficiency to transfect airway epithelial cells. Conditions were optimised for epithelial cell delivery of commercially available vectors namely Lipofectamine 2000 (Invitrogen), Superfect (Qiagen) and Effectene (Qiagen). Optimum conditions were determined by varying the concentration and ratios of each vectors delivered to airway epithelial cells. The efficiency of transient transfection was compared for each vector.

Briefly, cells were seeded at 9 x 10^4 cells/well, in a 24 well tissue culture plate, and transfected 48 hrs later. DNA and vector were complexed together at room temperature and incubated with cells. After 6 hrs incubation, 200 µl of 5 % FBS containing media was added on top of the lipoplex mixture and further incubated over night. The cells were harvested after 24 and 48 hrs to carry out cell counts to determine levels of toxicity and to carry out flow cytometry analysis to determine the efficiency of transgene expression.

2.2.15.3. Viral Transfections

2.2.15.3.1. AAV Transfections

AAV vector production was carried out as previously described (McMahon, JM *et al.*, 2006). For AAV transfection cells were plated at a concentration of 3.5 x 10^5 cell/well in 24-well tissue culture plates. Following 48 hr attachment, supernatants were removed and cells were rinsed once in OptiMEM. 400 µl OptiMEM containing 5 x 10^7, 5 x 10^8 or 5 x 10^9 plaque forming units (pfu) of AAV2-GFP, AAV5-GFP or AAV6-GFP were added and cells were incubated for 5 hr at 37°C, 5% CO_2 and 95% air. Supernatants were removed and culture medium was added. Cells were harvested at 24 and 48 hrs and analysed for GFP expression and cell viability.

2.2.15.3.2. Lentiviral Transfections

Third generation recombinant HIV-1 based lentivirus pseudotyped with VSV-G envelope and expressing GFP under the control of PGK promoter was prepared as described previously (McMahon, JM *et al.*, 2006). Cells were plated at a concentration of 3.5 x 10^3 cells/well in a 24-well plate and transduced 48 hrs later. Cells were transduced with 7.5 x 10^4, 1.5 x 10^5 or 2.25 x 10^5 pfu in 400 µl OptiMEM. GFP analysis and cell viability was performed as for AAV transfections.

2.2.15.4. BMPR-IB Over Expression Experimental Set Up

9 x 10^4 BEAS-2B cells were seeded in duplicate wells of a 24 well plates per treatment for RNA isolation. 1 x10^5 MLE-12 cells were seeded in duplicate wells of a 24 well plate per treatment for RNA isolation.

4 x 10^5 BEAS-2B cells were seeded in one well of a 6 well plate per treatment for protein isolation. 4.3 x 10^5 MLE-12 cells were seeded in one well of a 6 well plate per treatment, for protein isolation.

3.15×10^4 BEAS-2B cells were seeded in a well of an 8 well chamber slide per treatment for immunofluorescence analysis. 3×10^4 MLE-12 cells were seeded per well of an 8 well chamber slide, per treatment for immunofluorescence analysis.

The treatments included: cell only untransfected control, cell only untransfected control treated with BMP4 ligand, empty vector (pcDNA4 mock transfected) control, empty vector (mock transfected) control treated with BMP4 ligand, BMPR-IB-pcDNA4 transfected cells, BMPR-IB-pcDNA4 transfected cells treated with BMP4 ligand.

2.2.16. Statistical Analysis

Results were expressed as the mean ± the standard error of the mean (SEM). Where two treatments were compared, the Student's T-test for unpaired data was carried out to determine statistical significance. Results were considered statistically significant when the p-value was less than 0.05.

3. BMP Signalling in the K-ras^{G12D} Lung Cancer Mouse Model

3.1. Introduction

The $CCSP^{Cre}$ LSL-K-ras^{G12D} mouse model of lung cancer was utilised to assess the differential expression of BMP signalling in early stages of lung cancer. Aberrant gene expression of BMP pathway components has been shown in numerous cancers including breast, prostate, colorectal and pancreatic cancers (described in detail in section 1.7.1). Few reports characterise the differential expression of BMP pathway in lung cancers and there are no reports of BMP signalling in the $CCSP^{Cre}$ LSL-K-ras^{G12D} mouse model of lung cancer.

As described in section 1.6.3 the K-ras^{G12D} mouse model was generated in the Rosa26 mice (Soriano, P, 1999), briefly Cre recombinase was expressed by the CCSP promoter. The Cre enzyme binds to LoxP sites upstream of the gene of interest and removes the transcription inhibition sequence (Stop) allowing expression of the gene of interest, which in these studies included K-ras^{G12D} and/or, GFP or LacZ. CCSP was specifically expressed in the Clara cells of the conducting airways (Figure 3.1A). $CCSP^{Cre}$ LSL-K-ras^{G12D} mice express a constitutively active form of K-ras mutant gene. These mice develop lung tumours originating from the Clara cells (Figure 3.1B).

The $CCSP^{Cre}$ LSL-K-ras^{G12D} expressing mice form bronchiolar and alveolar hyperplasia at 3 months of age, the number and severity of lesions increased with age in these mice, with adenomas forming at later stages (Figure 3.2). In order to understand the molecular mechanisms occurring at the early stages of cancer, we isolated and analysed purified populations of proliferating cells from mouse lungs. Firstly, flow cytometry was utilised to identify Clara cells expressing a reporter transgene, with the view to isolating cells by flow cytometry cell sorting (FACS). These mice, $CCSP^{Cre}$ $Rosa^{GFP}$ and $CCSP^{Cre}$ $Rosa^{LacZ}$, co-expressed the reporter genes GFP and LacZ respectively. Isolation of these cells by FACS would allow analysis of gene expression of the early stages of hyperplasia and metaplasia in these animals. Secondly, laser capture microdissection, a method of isolating a purified population of cells, was employed to isolate hyperplasia and adenoma cells from the lungs of the $CCSP^{Cre}$ LSL-K-ras^{G12D} mice.

One major reason, leading to the poor prognosis for lung cancer patients, is the lack of early detections methods. Numerous studies are being carried out to identify biomarkers with which to identify early stages of lung cancer. In order to identify biomarkers, we must gain further understanding of the signalling pathways affected in lung cancer. Global gene expression profiling was carried out on hyperplasia and adenoma samples from the $CCSP^{Cre}$ LSL-K-ras^{G12D} mouse model to identify novel gene targets. Due to the lack of information about BMP signalling during lung cancer, the K-ras mouse model was utilised to characterise BMP signalling during early lung cancer progression.

3.2. Results

3.2.1. Reporter Gene Identification in MAECs

In the $CCSP^{Cre}$ LSL-K-ras^{G12D} mouse model of lung cancer, Clara cells become hyperproliferative and develop into early cancer lesions. In order to identify early markers of lung cancer prior to tumour development, mice can be generated to co-express K-ras^{G12D} and a reporter gene, namely GFP or LacZ under the control of the Clara cell specific promoter (CCSP). In this experiment the ability to isolate Clara cells based on GFP and LacZ expression was tested.

Cells were isolated from $CCSP^{Cre}$ and $CCSP^{Cre}$ $Rosa^{GFP}$ mice using the standard primary cell isolation protocol. These cells were analysed by flow cytometry to identify GFP expression. Cells isolated from $CCSP^{Cre}$ mice were used as a negative control because they did not express the GFP reporter gene. GFP expression was not detected from either control ($CCSP^{Cre}$) or potential GFP expressing mice ($CCSP^{Cre}$ $Rosa^{GFP}$) (Figure 3.3 A & B). As detection of the GFP reporter gene from CCSP ^{Cre} Rosa ^{GFP} cells proved difficult, an alternative method of identification was tested.

Cells were isolated from CCSP^{Cre} Rosa^{LacZ} mice using the standard primary cell isolation protocol. Indirect flow cytometry was carried out using a fluorescent FDG (fluoroscein di-β -D-galactopyranoside) substrate to identify β-galactosidase expression. Cells isolated from CCSP^{Cre} mice which did not express β-galactosidase were used as a negative control (Figure 3.3C). Flow cytometry identified 17% of CCSP^{Cre} Rosa^{LacZ} cells expressing the transgene (Figure 3.3D).

These experiments demonstrated that LacZ was a more readily detectable marker in lung epithelial cells compared to GFP. Expression of the reporter gene can be used for future cell sorting experiments to isolate cells co-expressing a transgene and the reporter gene.

3.2.2. Laser Capture Microdissected Cells

At 3 months of age the Clara cells of the CCSP^{Cre} LSL-K-ras^{G12D} mouse lungs become hyper proliferative and form heterogenous hyperplasia lesions in the bronchioles and in the alveolar regions. The types of lesions that have been found in these lungs include atypical adenomatous hyperplasia (AAH), bronchiolar hyperplasia, and solid, papillary or mixed adenomas. In order to understand the differential gene expression pattern between these early cancer lesions, laser capture microdissection was used to isolate a purified population of cells from each of the pathologies and normal airway controls.

Lungs were harvested from control (CCSP^{Cre}) and K-ras ^{G12D} (CCSP^{Cre} LSL-K-ras^{G12D}) expressing mice and laser capture microdissection was carried out to isolate cells from normal airways and cancer pathologies (Figure 3.4). Normal airways were isolated from CCSP^{Cre} control mice. Hyperplasia, AAH, papillary adenoma and mixed adenomas were isolated from CCSP^{Cre} LSL-K-ras^{G12D} mice under the supervision of a pathologist (Figure 3.4). Ninety laser captured samples were taken from 22 mice. These mice consisted of 10 control mice (CCSP^{Cre}) and 12 K-ras^{G12D} mice (CCSP ^{Cre} LSL-K-ras^{G12D}) (Figure 3.5).

3.5

RNA was isolated from 80 laser captured samples. The amount of RNA in each sample was quantified on a NanoDrop^{TM} (Thermo Sceintific, CA, USA) and the quality of the samples were analysed on an Agilent 2000 Bioanalyser (Agilent, CA, USA) (Figure 3.6 A). Many of the samples did not pass the quality control due to low mRNA concentration or low mRNA quality, that is poor 260/280 ratio or poor 260/230 ratio. Only high quality samples were sent for microarray analysis (Figure 3.6 B). Three RNA samples of normal airway isolated from control mice (CCSP^{Cre} LSL-K-ras^{G12D}); 3 RNA samples of hyperplasia, 2 RNA samples of AAH, 3 RNA samples of papillary adenoma and 1 RNA sample of solid adenoma isolated from K-ras^{G12D} expressing mice (CCSP^{Cre} LSL-K-ras^{G12D}) were sent for microarray analysis carried out at the RNA core facility at Baylor College of Medicine.

Difficulties arising during the laser capture procedure included contamination of non-specific cells on the cap. These non-specific regions were mainly alveolar regions that bound non-specifically (not captured by the laser) to the cap due to the delicate architecture of the region (Figure 3.7). Samples that were chosen for microarray analysis did not contain alveolar contamination.

Another difficulty of LCM was the degradation of the RNA during the fixing and capturing process. A positive tissue control was analysed to establish if degradation was occurring during the laser capturing process. This “scrape” control tissue was prepared for LCM along with the sample tissue. The entire cryosectioned tissue slice was scraped into a tube for RNA isolation, and did not undergo LCM. The scrape control samples were of high quantity (Figure 3.8). The lack of consistent quality in LCM RNA samples indicated that the processing and capturing procedure had a deleterious effect on the RNA quality. The tissue slices were maintained in xylene prior to laser capture; a de-humidifier was used to reduce the levels of humidity in the room. This reduced water contamination on the samples and activation of RNases in the cells of the tissue.

3.2.3. Microarray Analysis

Analyses were carried out on results from the Affymetrix microarray. Supervised clustering was carried out normalising the normal airway samples to a value of 1, and expressing differential RNA levels from hyperplasia and adenoma samples to the normal airways. A heat map was generated showing genes that formed similar differential pattern in hyperplasia and adenoma samples (analysis carried out by Dr Craig Creighton, Baylor College of Medicine). The heat map demonstrated 8 different gene expression patterns (Figure 3.9). In these expression patterns normal airways were at a value of 1, and hyperplasia and adenoma patterns are as follows: A) up-regulated in hyperplasia and unchanged in adenoma; B) down-regulated in hyperplasia and unchanged in adenoma; C) unchanged in hyperplasia and up-regulated in adenoma; D) unchanged in hyperplasia and down-regulated in adenoma; E) up-regulated in both hyperplasia and adenoma; F) down-regulated in both hyperplasia and adenoma; G) up-regulated in hyperplasia but down-regulated in adenoma; H) down-regulated in hyperplasia and up-regulated in adenoma.

In order to establish if functional pathways were differentially affected between hyperplasia and adenoma, the gene list was analysed using Babelomics bioinformatics programme (Al-Shahrour, F *et al.*, 2005). The FatiGO+ tool within this programme allowed analysis of functional enrichment comparing two different groups of genes (Al-Shahrour, F *et al.*, 2007). FatiGO+ uses gene ontology (GO) annotations to allocate a function to each gene. Using FatiGO+ programme, differential gene expression between hyperplasia and adenoma was compared, to seek enrichment for biological differences between the two pathologies. Three separate gene onotology lists were retrieved from this programme: cellular components, biological processes and molecular functions. The subgroups within the main three functional groups become more complex with increasing levels of description. Due to the functional diversity of genes, many genes appear within more than one functional group.

Genes up-regulated in hyperplasia were compared to genes up-regulated in adenoma.

There were a significant number of genes responsible for cell communication up-regulated in adenoma samples compared to hyperplasia ($p = 0.03$). There was an increase in genes responsible for cell activation in adenoma but not hyperplasia samples ($p = 0.058$). There was little difference between other functional groups within the biological process gene ontology group (Figure 3.10). Many genes up-regulated in both hyperplasia and adenoma samples compared to normal airway belonged to metabolic process: that is primary metabolic processes, macromolecule processes, and cellular metabolic processes. Within the cellular component functional annotation group there was significant increase in membrane bound organelle genes in hyperplasia compared to adenoma ($p = 0.02$). There is no other significant functional difference between genes up-regulated in hyperplasia and adenoma. There was a similarly large increase in genes responsible for producing cell components in both hyperplasia and adenoma compared to normal control (Figure 3.11). This concurs with the hyper proliferative stage these cells were in. There was no significant difference between genes activated in hyperplasia and adenoma within the molecular function gene ontology annotation (data not shown).

A comparison was carried out for genes down-regulated in hyperplasia and genes down-regulated in adenoma. Within the biological process gene annotation, there was a significant increase in macromolecular process in the hyperplasia samples compared to the adenoma samples ($p = 0.036$) (Figure 3.12). There was no significant differential gene expression between hyperplasia and adenoma samples with the biological process or cellular component gene ontologys (Figure 3.13).

3.2.4. Characterisation of Pre-Cancer Lesions

In order to validate the tumour status of the hyperplasia and adenoma samples, analysis was carried out to characterise known tumour associated proteins. Examination of PCNA (proliferative cell nuclear antigen), a cell cycle protein, E-cadherin an adhesion protein and *Mig-6* a tumour suppressor protein was carried out on K-ras ^{G12D} and normal samples.

The Clara cells of the CCSP^{Cre} LSL K-ras^{G12D} mice undergo uncontrolled cell cycle due to the K-ras^{G12D} mutant gene. PCNA is active during cell cycle. Immunofluorescence was carried out in normal and K-ras^{G12D} tissue sections to visualise the levels and localisation of PCNA in the airways and cancer pathologies. As expected there was little PCNA activity in normal airway epithelium, indicative of the low steady state division that occurs in normal lungs. There was increased PCNA expression in hyperplasia and adenoma samples indicative of the increased proliferation occurring in those pathologies (Figure 3.14). PCNA expression was localised to the nuclei of the cells.

Loss of tumour suppressor gene, *Mig-6*, leads to the development of cancers including lung cancer (Zhang, YW *et al.*, 2007). Real time PCR analysis for *Mig-6* expression was carried out on RNA samples isolated by laser captured microdissection. *Mig-6* expression was normalised to 18S in each sample. *Mig-6* mRNA expression was found to be decreased in both hyperplasia ($p < 0.05$) and adenoma samples ($p < 0.01$) compared to normal airways (Figure 3.15). Immunofluorescence was carried out to verify the protein level of *Mig-6*. A reduction of *Mig-6* fluorescence in hyperplasia regions and a further reduction in adenoma regions was evident (Figure 3.16). From these analyses it can be deduced that the *Mig-6* protein expression is attenuated at the early stages of lung cancer.

E-cadherin is expressed in epithelial cells; it functions as a cell-cell adhesion molecule and is down-regulated in cancer cells to allow migration and metastasis. Expression of E-cadherin was examined in the K-ras^{G12D} lung cancer tissue and control tissue. E-cadherin protein was localised to the cell adherence junction membranes, as expected. The level of

fluorescence intensity of E-cadherin appears higher in normal airway epithelial cells and was reduced in hyperplasia and reduced further in adenoma (Figure 3.17).

β-catenin, a component of the E-cadherin adherence complex and Wnt signalling pathway, was examined by immunofluoresence. β-catenin protein was localised to the cell adhesion junction membrane. The intensity of protein expression appears to be higher in the cells of the normal airways with decreasing fluorescent intensity in hyperplasia and adenoma cells (Figure 3.18).

3.2.5. Involvement of the BMP Pathway in Early Lung Cancer

The BMP pathway has been implicated in numerous cancers. Microarray analysis revealed 1.5 fold increase in BMPR-IB expression in hyperplasia and 0.7 fold reduction in adenoma samples (Figure 9.18). This prompted further investigation of BMP signalling in the K-ras lung cancer model.

Validation of microarray results were carried out on independent laser captured samples. Real time PCR validation of independent samples verified a significant loss of BMPR-IB in hyperplasia ($p < 0.05$) and adenoma ($p < 0.05$) (Figure 3.19). Immunofluorescence analysis of control and K-ras^{G12D} lung tissue for BMPR-IB expression was carried out. BMPR-IB protein expression was localised to the cytoplasmic region of epithelial cells of normal airways, but was not detected in cells of hyperplasia or adenoma pathologies (Figure 3.20).

Human lung adenocarcinoma tissues slices were received as a kind gift from Dr. Ken O' Byrne from St. James Hospital. Lung adenocarcinoma tissues from lung cancer patients undergoing surgical resection were paraformaldehyde fixed, paraffin embedded and sectioned into 3μm tissue slices at St. James Hospital. Serial sections were cut and H & E staining was carried out on the first of 5 sections, and the cancer pathologies were identified by a pathologist. BMPR-IB immunofluorescence staining was carried out on

tissue from 3 different patients. Photomicrographs were taken of BMPR-IB staining in the adenocarcinoma regions. BMPR-IB staining was predominantly localised to the nucleus of the adenocarcinoma cells (Figure 3.21). Unfortunately we did not have earlier tumour pathologies or normal airways to compare the level of BMPR-IB expression. However, compared to the mouse adenoma tissue samples, there was BMPR-IB expression in the human adenocarcinoma cells.

Further analyses into the involvement of BMP signalling was carried out on the K-ras ^{G12D} tissue samples. Real time PCR analysis was carried out to observe the expression of BMPR-IA and BMPR-II in normal, hyperplasia and adenoma. There was no reduction in BMPR-IA expression in hyperplasia samples; however, a decrease in BMPR-IA expression in adenoma samples was evident but this reduction was not statistically significant (Figure 3.22). There was a significant loss of BMPR-II expression in hyperplasia ($p < 0.05$) and adenoma ($p < 0.01$) samples (Figure 3.22).

Mouse K-ras^{G12D} RNA was analysed for other components of the BMP pathway. BMP2, a ligand of the pathway, has been found dysregulated in human lung cancers (Langenfeld, EM *et al.*, 2003). Real time PCR analysis of the BMP4 ligand revealed an increase in expression of this ligand in early cancer lesions. BMP4 mRNA expression was increased in hyperplasia ($p < 0.05$) and adenoma ($p < 0.05$) samples (Figure 3.23). Expression of BMP5 ligand which has been implicated in bone metastasis was analysed in lung cancer and normal samples. Real time PCR analysis resulted in a significant increase in BMP5 mRNA expression in hyperplasia ($p < 0.05$) and in adenoma samples ($p < 0.01$) (Figure 3.23). Analysis of the co-Smad (Smad 4) which is involved in BMP and TGF-β signalling, was an increased in hyperplasia ($p < 0.05$) and adenoma (not statistically significant) (Figure 3.24). Expression of the transcription factor Id-1, an immediate early gene target of the BMP pathway, was examined. There was increased expression of Id-1 in hyperplasia ($p < 0.05$) and adenoma, although not statistically significant (Figure 3.24).

One method of detecting activated canonical BMP signalling is to identify phosphorylated receptor smad protein that is p-Smad 1, 5, 8. Immunofluorescence for p-Smad was carried out on K-ras^{G12D} and control tissue sections. Low level expression of p-Smad was detected in normal airway epithelium (Figure 3.25). By overlaying DAPI nuclear counter-stain and p-Smad stained images, increased p-Smad was observed in the nuclei and cytoplasm in hyperplasia samples (Figure 3.26 B) compared to normal airway control (Figure 3.26 A). A further increased of nuclear p-Smad was observed in adenoma pathologies, indicating increased BMP pathway activation in this early lung cancer lesion (3.26 C).

Analysis of BMP signalling in K-ras^{G12D} tumour samples revealed a decrease in receptor expression, but an increase in BMP ligand production, an increase in Id-1 (a BMP target gene), and an increase in p-Smad, indicating activated BMP signalling in these early tumour pathologies. These results are summarised in figure 3.27.

3.3. Discussion

The primary reason for poor prognosis in lung cancer patients is the lack of early detection methods. While early screening methods have increased the survival rate for breast cancers (Cox, B, 2008), little progress has been made to increase the survival rate for lung cancer patients. The five year survival rates for breast, colon and prostate cancers are 4-6 times greater than lung cancer due to screening methods and therefore patients benefit from early treatment (Belinsky, SA, 2004). Currently there is no definitive screening method for identifying lung cancer at the early stages of the disease. Current screening methods require the tumours to be in an advanced stage, large enough for visualisation on a CT or PET scan or central in the lung for facilitating a biopsy (Guessous, I *et al.*, 2007). There have been recent developments in increasing the sensitivity of CT scanning, but this procedure is very costly. An ideal low cost, non-invasive screening method for lung cancer would involve the identification of biomarkers in sputum, blood or cells (Chorostowska-Wynimko, J and Szpechcinski, A, 2007). In order to identify novel early lung cancer biomarkers the molecular signals that change at the early stages of lung cancer progression must first be identified. In this chapter, the K-ras^{G12D} lung cancer mouse model is used to identify early lung cancer biomarkers and to characterise the expression of the BMP signalling in early lung cancer.

The lungs are composed of a heterogenous population of cells. In order to understand the molecular mechanisms occurring during cancer progression, it is necessary to analyse a purified population of cells. Transgenic mice expressing a reporter gene under the control of the CCSP promoter were utilised to assess the validity of using flow cytometry to isolate a purified population of cells. Using the flow cytometry technique, Clara cells could potentially be isolated based on their reporter gene expression prior to tumour formation. Flow cytometry was not successful at detecting GFP expression from transgenic mice, that is, cells from CCSP^{Cre} Rosa^{GFP} mice did not express GFP compared to control CCSP^{Cre} mice. The utility of cell isolation based on GFP transgene expression has been demonstrated by numerous groups. Basal cells have been successfully isolated from transgenic mice expressing GFP under the control of the K5 keratin promoter

(Schoch, KG *et al.*, 2004). Type II pneumocytes have been successfully isolated from the lung based on a GFP reporter gene expression. Transgenic mice expressing GFP under the control of SP-C promoter result in GFP expressing alveolar epithelial cells (Kotton, DN *et al.*, 2005).

The ability to isolate cells based on β-galactosidase reporter gene expression was also examined. LacZ reporter gene expression is widely used to identify cells in whole mount lungs by colorimetric identification (Li, H *et al.*, 2008). However, a fluorescent substrate for the β-galactosidase protein allows identification of the reporter protein by flow cytometry (Fiering, SN *et al.*, 1991). Clara cells from $CCSP^{Cre}$ $Rosa^{LacZ}$ mice were visualised by flow cytometry. 17% of $CCSP^{Cre}$ $Rosa^{LacZ}$ Clara cells expressed β-galactosidase. The LacZ expression from Clara cells was lower than expected; the MAEC preparation used was comprised of approximately 80% Clara cells (McBride, S *et al.*, 2000). One reason for the low detection may be due to the substrate used. The FDG substrate was optimised on prokaryotic cultures. Future experiments would benefit from the use of C_{12}-FDG substrate, which is more sensitive for β-galactosidase in mammalian cells (Plovins, A *et al.*, 1994).

The use of the recently developed codon optimised Cre recombinase in mouse models should improve the efficiency with which reporter or transgenes are expressed. The Cre recombinase used to generate reporter mouse models in these experiments was derived from the bacteriophage P1 system. This Cre has not been codon optimised for mammalian systems and represents another mode for improvement for cell isolation based on reporter gene expression (Gu, H *et al.*, 1993; Shimshek, DR *et al.*, 2002).

The ability to isolate cells based on reporter gene expression would increase the need for mouse models expressing both transgene and reporter gene. In the case of the $K\text{-}ras^{G12D}$ lung cancer mouse model, expression of $K\text{-}ras^{G12D}$ could coincide with the expression of a reporter gene. The Clara cells could then be isolated before the cells hyperproliferate, and analysed for RNA and protein expression patterns.

Due to the heterogeneity of cells in the lung and during carcinoma, LCM has become a popular technique for isolating tumour cells. In our study LCM was carried out to isolate a purified population of cells from early cancer pathologies including normal airway, hyperplasia and adenoma pathologies. Miura *et al* utilised LCM to isolate adenocarcinoma tissue from both smokers and non-smokers. Microarray analysis was carried out on the tissues and 45 genes were found to delineate smokers from non-smokers. Also 27 genes were differentially expressed between non-survivors and survivors 5 years post surgery (Miura, K *et al.*, 2002).

Recent advances in genomics, especially the sequencing of the human and other organisms' genomes, have proved revolutionary for the characterisation of diseases at a molecular level. DNA microarrays exploits this sequencing data allowing large scale analysis of genes altered during disease. DNA microarrays contain oligonucleotide probes at predefined locations on a chip, upon hybridisation the nucleotides bind to their single stranded complimentary DNA. In this way, genome wide screening studies can be carried out looking at genes up or down-regulated during disease state. In our study of the 12 samples used for microarray analysis, 7 samples produced interpretable results from the microarray procedure. The ability to successfully carry out microarray analysis on small numbers of LCM mouse airway cells has also been shown by Betsuyaku *et al* (Betsuyaku, T and Senior, RM, 2004). In our study gene expression profiles were examined for normal airway, hyperplasia and adenoma samples. The generated heat map allowed clustering of expression patterns of DNA. Gene function analysis was carried out on the microarray gene list in order to assign enriched gene function to genes differentially expression between hyperplasia and adenoma samples. Gene function was assigned a gene ontology category (GO). Gene Ontology categories were developed to standardise gene description based on biological processes, molecular function and cellular localisation. From our studies, genes altered in adenoma samples were enriched with genes involved in cell communication, cell activation, membrane bound organelles, macromolecular metabolic processes and establishment of localisation. These functions are indicative of a well differentiation and high proliferative cell population.

Mig-6 is located at human chromosome 1p36, this locus is thought to contain putative tumour suppressor genes and is frequently altered in many types of cancers (Hunt, JL, 2008; Nomoto, S *et al.*, 2000; Thiagalingam, S *et al.*, 2002). Loss of locus 1p36 has been found in human lung cancer cell lines including both NSCLC and SCLC, and in 50% of primary human lung cancers (Nomoto, S *et al.*, 2000). Loss of *Mig-6* expression in mice result in development of multi tissue carcinogenesis (Jin, N *et al.*, 2007; Zhang, YW *et al.*, 2007). In our study loss of *Mig*-6 expression was found in hyperplasia and adenoma samples at an RNA and protein level. *Mig-6* is a negative regulator of EGFR signalling, it binds to an inhibits the kinase domain of EGFR and ERBB2 (Zhang, X *et al.*, 2007b). EGF family of protein receptors are key targets for lung cancer therapy. Tyrosine kinase inhibitors (gefinitib and erlonitib) have been developed to inhibit phosphorylation of the receptors. However, response to these drugs has been variable. Studies have been ongoing to identify factors that allow sensitivity to these drugs. To date an in-frame mutation (exon 19 746-753) and substitution (L858R) correlate with EGFR-TKI sensitivity (Zhang, X and Chang, A, 2008). Screening methods are being developed to identify patients that will respond to TKI treatments, for the remaining lung cancer patients other methods of therapy will need to be developed. *Mig-6* EGF inhibitor is an excellent potential candidate for cancer gene therapy for NSCLC. Expression of this tumour suppressor extends to other organs including the skin, uterus, gall baldder, bile duct (Jin, N *et al.*, 2007; Zhang, YW *et al.*, 2007), increasing its potential utility as a therapeutic. However, a study has shown that exogenous expression of *Mig-6* in MCF7 breast cancer cell line resulted in the inhibition of apoptosis (Xu, J *et al.*, 2005).

The K-ras mouse model expresses a mutant gene (K-ras^{G12D}) and therefore renders the Clara cells in a constant state of proliferation. The intensity of PCNA staining was increased in hyperplasia and adenoma samples. This indicated the increased level of proliferation compared to the steady state lung. The development and progression of epithelial cancers are a result of alterations in signals promoting cellular proliferation and cellular death. Cell cycle regulators such as PCNA have the potential to be utilised as tumour dependent or tumour independent biomarkers. Within the early stages of biomarker detection PCNA was identified as a potential biomarker for lung cancer

progression. A positive correlation was made between increased PCNA intensity and increased lung cancer stage, suggesting PCNA could be used as a biomarker in small biopsy samples (Lee, JS *et al.*, 1992) Our data corroborates this finding that PCNA expression is correlated with increased tumour progression and has the potential to act as a biomarker for the identification of early lung cancer lesions. PCNA has been implicated as a biomarker for many types of cancers including eosophagal, testicular and breast cancer (D'Andrea, MR *et al.*, 2008; Kimos, MC *et al.*, 2004; Malkas, LH *et al.*, 2006). Because PCNA is a marker of proliferation, it is an indicator of cancer progression for all tumour types, expression of PCNA and a tissue specific marker confers tissue specific tumour progression identification. For example loss of esophagin expression and gain of PCNA expression in the eosophagal epithelium is an indicator of eosphoageal cancer progression (Kimos, MC *et al.*, 2004). Correlation studies have also been carried out to identify the use of PCNA as an indicator of prognosis. Increased PCNA was associated with shorter survival in breast cancer patients (Stuart-Harris, R *et al.*, 2008). Co-expression and correlation studies of PCNA expression with lung cancer specific markers may be used as potential biomarkers and prognostic factors of lung cancer progression.

3.3.1. Cellular Adhesion

Cell adhesion is essential for the establishment and maintenance of an epithelial phenotype. There are numerous studies describing the loss of cell adhesion molecules in human carcinomas, these include prostate (Umbas, R *et al.*, 1992), colon (Dorudi, S *et al.*, 1993), breast (Oka, H *et al.*, 1993), pancreatic (Winter, JM *et al.*, 2008) and lung cancer (Charalabopoulos, K *et al.*, 2004; Kato, Y *et al.*, 2005). The epithelial adhesion molecule, E-cadherin, is necessary for tight cell-cell adhesion which is a characteristic of epithelial cells. In the present study a decrease in E-cadherin protein was found in advancing tumour pathologies of K-ras^{G12D} lung tissue. E-cadherin has been found to be down-regulated in many carcinomas; here we show attenuated E-cadherin expression at pre-carcinoma stages of tumour progression. Recently the molecular mechanism for loss of E-cadherin expression in cells expressing oncogenic K-ras was deciphered (Wang, XQ *et al.*, 2008). *In vitro* analysis of K-ras^{G12V} expression caused downstream activation of

ERK. ERK signalling was responsible for the induction of MMP9, which is responsible for cleaving E-cadherin protein (Symowicz, J *et al.*, 2007). Although differential expression of MMP proteins was not detected in our microarray analysis, independent investigation may identify an increase in their gene expression.

The microarray analysis revealed Myosin VI, an actin-based motor, to be down-regulated in hyperplasia and adenoma samples. This molecule is recruited to the E-cadherin adhesion complex when the cell-cell contacts of epithelial monolayers mature (Maddugoda, MP *et al.*, 2007). Therefore loss of E-cadherin expression and some associated complex proteins verifies the loss of cell-cell adhesion at the proliferative stages of cancer formation. E-cadherin expression is regulated at a number of different levels. Transcriptional regulation of the gene is achieved in 3 ways: transcriptional repression, mutation (Chun, YS *et al.*, 2001), or hypermethylation of the promoter (Toyooka, S *et al.*, 2001). Transcriptional repressors such as Twist, Snail and ZEB bind to the E-cadherin promoter and inhibit the transcriptional activation of the gene. These transcription factors are up-regulated in many cancers therefore have an inhibitory effect on E-cadherin expression (Blanco, MJ *et al.*, 2002; Terauchi, M *et al.*, 2007). E-cadherin is also regulated at the protein level. Matrix metalloproteinase (MMP) proteins that are up-regulated during cancer cleave the E-cadherin protein. MMP are responsible for the degradation of the extracellular matrix, they function in attenuating E-cadherin expression contributing to their potent role in tumour invasion and cancer progression.

Loss of E-cadherin expression may be utilised as a biomarker of cancer progression. Nawrocki-Raby *et al* reported that E-cadherin fragments were shed from epithelial cells into serum of lung cancer patients. This shedding is due to the cleavage of the E-cadherin protein by proteases. This soluble E-cadherin has been shown to up-regulate matrix metalloproteinases thereby promoting tumour invasion (Nawrocki-Raby, B *et al.*, 2003). The soluble E-cadherin could act as a potential marker of tumour identification and progression (De Wever, O *et al.*, 2007). Other components of the E-cadherin adhesion complex include α- , β- , γ-, p120 catenins. Expression of these catenin proteins has been shown to be down-regulated in cancers including NSCLC (Kato, Y *et al.*, 2005; Liu, Y *et*

al., 2007). Our examination suggests β-catenin is down-regulated at the early stages of lung cancer progression. Analysis of the lesions in the K-ras lung cancer mouse model suggests a down regulation of E-cadherin expression at the early hyperproliferative stages of cancer. It is interesting to see a down regulation of this adhesion molecule at such an early stage and may act as a potential prognostic marker of lung carcinomas. Future studies would be of benefit to establish if soluble E-cadherin exists in this mouse model, to be used as a biomarker.

Microarray analysis also revealed a loss of expression of a number of protocadherins: Pcdha4, Pcdha6, Pcdha7, Pcdha5 and Pcdha11. Protocadherins are a sub-cadherin family of proteins that to date are found to be predominantly expressed in the central nervous system. Like all members of the cadherin superfamily they function in cell-cell adhesion. Loss of expression of some protocadherins have been implicated in a number of cancers and are considered to be candidate tumour suppressor genes (Imoto, I *et al.*, 2006). Loss of protocadherin 20 (PCDH20) expression by hyerpmethylation was found in NSCLC cell lines and was associated with shorter survival rates. Re-introduction of the gene into NSCLC cell lines resulted in a reduction of colony formation, validating its importance in tumour progression (Imoto, I *et al.*, 2006). Inactivation of protocadherin 8 (PCDH8) by epigenetic silencing or mutations have been found in breast cancers (Yu, JS *et al.*, 2008). On the contrary other protocadherins have been shown to promote cancer progression. Protocadherin-PC is up-regulated in some prostate cancer cell lines. *In vitro* expression of this genes results in the induction of Wnt signalling, which is associated with proliferation and cell survival, and the promotion of malignant phenotype of a prostate cancer cell line (Terry, S *et al.*, 2006; Vacherot, F *et al.*, 2005).

Overall, loss of cell-cell adhesion molecules appears to promote oncogenesis in epithelial cancers by disrupting cell-cell adhesion required for tissue organisation, conferring motility to the cancer cells.

3.3.2. BMP Signalling

The BMP pathway has been implicated in a number of cancers including prostate, pancreatic, glioblastoma, breast and colon cancer. The BMP signalling pathway and the TGF-β super-family have known growth suppressive activity *in vitro* and *in vivo* (Grady, WM *et al.*, 1998; Huang, SC *et al.*, 2000; Markowitz, SD and Roberts, AB, 1996). Few studies have been carried out on the involvement of the BMP signalling in lung cancer (Langenfeld, EM *et al.*, 2005; Langenfeld, EM *et al.*, 2003; Langenfeld, EM and Langenfeld, J, 2004). This study characterised the expression of BMP pathway components in early lung cancer tumours. A loss of BMP receptor expression but increased pathway activity has been found in the K-ras^{G12D} lung cancer tumours.

Independent validation studies showed no differential BMPR-IA expression in the hyperplasia samples; however, a decrease in BMPR-IA was shown in the adenoma samples. Previous studies have shown a decrease in functional BMPR-IA expression in juvenile polyopsis, where loss of BMPR-IA expression is due to mutations in the gene which predispose patients to colorectal cancer (Howe, JR *et al.*, 2008; Howe, JR *et al.*, 2004). Transgenic mouse model studies have verified that loss of BMPR-IA resulted in the expansion of progenitor cells and eventual formation of polyopsis in the intestine of conditional BMPR-IA$^{-/-}$ mice (He, XC *et al.*, 2004). The increase in proliferation in the intestinal region was due to the lack of inhibition on the Wnt signalling. Conditional loss of BMPR-IA expression in the intestine of mice is associated with an increase in phospho-PTEN expression, an increase in phospho-Akt expression and an increase in nuclear β-catenin. Therefore, BMP signalling was shown to be necessary for negatively regulating the proliferative Wnt signalling, via PTEN regulation, to maintain normal homeostasis in the intestines. These studies suggest BMPR-IA is a growth inhibitory factor and attenuation of its expression contributes to proliferation of cancer cells.

BMPR-IB expression was down-regulated in hyperplasia and adenoma samples in K-ras^{G12D} expressing lungs. The loss of BMPR-IB expression is consistent with previously described studies on glioblastoma (Lee, J *et al.*, 2008; Norton, JD, 2000). BMPR-IB expression was found to be epigenetically silenced in glioblastoma tumour initiating

cells. Hypermethylation of BMPR-IB rendered the cancer cells in a constant state similar to early embryonic neural stem cells, incapable of differentiation. Re-expression of BMPR-IB in the glioblastoma cell line restored their differentiation ability and reduced their tumourigenicity. Therefore, in human glioblastoma cells, loss of BMPR-IB contributed to their tumourigenicity. It has been shown in our investigations and investigations by others that BMPR-IB is endogenously expressed in airway epithelial cells. However, BMPR-IB expression was down-regulated during tumour progression. The role by which BMPR-IB expression was attenuated in the K-ras model is unknown but perhaps the mechanism is similar to the epigenetic silencing described by Lee *et al.* On the contrary to studies which identified down regulation of BMPR-IB in cancer cells, an increase of BMPR-IB has been found in poorly differentiated breast cancers (Helms, MW *et al.*, 2005). Expression of BMPR-IB in the breast cancer tumours was associated with proliferation, poor tumour differentiation and cancer progression.

Loss of BMPR-IB protein has been correlated with an increase in tumour grade in prostate cancer (Kim, IY *et al.*, 2000). Well-differentiated cancers were positive for BMPR-IB, BMPR-IA and BMPR-II expression but there was a significant loss of BMPR expression in poorly differentiated prostate cancers. In the present mouse lung tumour study, BMPR-IB expression was attenuated at the early hyperplasia and adenoma stages of tumourigenicity. However, BMPR-IB was expressed in human lung adenocarcinoma cells, and its expression was localised to the nuclei of the cells. Although nuclear localisation of membrane receptor is not a novel occurrence, BMPR have not been identified in the nucleus. Several transmembrane receptors have been reported in the nucleus, these include EGFR (epidermal growth factor receptor), FGFR (fibroblast growth factor receptor) and NGFR (nerve growth factor receptor), among others (Clevenger, CV, 2003). However, the exact mechanism of how membrane receptors migrate to and enter the nucleus has not been elucidated. In the nucleus, the receptors appear to function as co-regulators of target genes (Lin, SY *et al.*, 2001). Although BMPR have not been identified in the nucleus, BMPR-IA has been associated with SF 3b4, a protein involved in the spliceosome in the nucleus (Nishanian, TG and Waldman, T, 2004; Watanabe, H *et al.*, 2007). The potential role of nuclear BMP receptor function

will be discussed further in section 6.3. Without normal human tissue samples, it is impossible to establish whether BMPR-IB expression is altered compared to normal human airway cells. Future studies into the characterisation of BMPR-IB differential expression during lung tumour progression will contribute to the understanding of this disease.

BMPR-II was found to be down-regulated in hyperplasia and adenoma lesions in the present K-ras^{G12D} lung cancer study. This down regulation was shown by real time PCR, though not at a protein level due to the lack of sensitive antibodies to mouse BMPR-II. Loss of BMPR-II has been associated with increased progression of prostate cancers. Well differentiated prostate cancers expressed the BMPR-II while poorly differentiated prostate cancers showed loss of BMPR-II expression (Kim, IY *et al.*, 2000; Kim, IY *et al.*, 2004). BMPR-II expression is also lost in colorectal cancer due to microsatellite instability (Kodach, LL *et al.*, 2008b). The loss of BMPR-II in colorectal cancer correlates with progression of adenomas to carcinomas and occurs at the early stage of cancer progression, supporting our findings (Kodach, LL *et al.*, 2008b). *In vivo* mouse models of conditional BMPR-II ablation, verified that loss of BMPR-II expression results in hyperproliferation of epithelial cells in the colon (Beppu, H *et al.*, 2008).

The present study has shown, for the first time, the loss of BMP receptor expression in lung cancer. These results concur with numerous other reports of BMPR loss in various types of human cancers. The loss of BMPR expression appears to be correlated with tumour progression in other cancer types and if that is the case with lung cancer, loss of BMPR maybe a potential biomarker for identifying lung cancer at the early stages of progression.

In contrast to the loss of BMP receptor expression there appears to be an increase in expression of other components of the BMP pathway including BMP4 and BMP5 ligand, Smad4 co-operating Smad and Id-1, a gene target of the BMP pathway. Over expression of the BMP4 ligand has been observed in breast cancer tissue (Alarmo, EL *et al.*, 2007), eosophageal squamous cell carcinoma (van Baal, JW *et al.*, 2008), prostate cancer (Li,

ZL *et al.*, 2006) and colorectal cancer (Madoz-Gurpide, J *et al.*, 2006). Numerous *in vitro* studies have described how cell lines undergo a metastatic phenotype in the presence of exogenous BMP4 ligand (Molloy, EL *et al.*, 2008; Montesano, R, 2007; Theriault, BL *et al.*, 2007). Therefore over expression of the BMP ligand appears to cause differentiation into a metastatic phenotype. One study has examined the expression of the BMP ligands in NSCLC and has found only BMP2 to be over expressed (Langenfeld, EM *et al.*, 2005). We have reported an increase in BMP4 expression in the hyperplasia and adenoma cells. It would be interesting to assess the level of BMP4 expression in the bronchoalveolar lavage (BALF) of these mice, as it may be used as a prognostic biomarker for early lung cancer.

Smad4, which has been described as a tumour suppressor, is found on the chromosome region 18q21, which is frequently deleted in cancers including lung cancers (Xu, X *et al.*, 2000). Loss of Smad4 expression has been identified in colon cancer (Beck, SE *et al.*, 2007; Kodach, LL *et al.*, 2007; Xu, WQ *et al.*, 2007), pancreatic cancer (Algul, H and Schmid, RM, 2008) and lung cancer (Nagatake, M *et al.*, 1996). Xu *et al* suggest that a reduction in Smad4 expression is a sign of malignancy and progression in colorectal cancer (Xu, WQ *et al.*, 2007). However, over expression of Smad4 has been found in intestinal metaplasia, the precursor to gastric cancer (Barros, R *et al.*, 2008), prostate cancer (Sheehan, GM *et al.*, 2005), and hepatocellular carcinoma (Torbenson, M *et al.*, 2002). We have shown over expression of Smad4 in hyperplasia and adenoma samples. Perhaps Smad4 was over expressed in our model because the cells were well differentiated and are not yet at a carcinoma or metastatic stage.

BMP activation was seen to occur in the K-ras^{G12D} lung cancer tissue, as indicated by increased localisation of nuclear p-Smad in hyperplasia and adenoma cells. Minimal p-Smad staining in the cytoplasmic region of some normal epithelial cells was observed and indicates low level pathway activation during homeostasis. Increased p-Smad staining was evident in cells of the hyperplasia and adenoma lesions with staining in the nucleus of hyperplasia cells, and increased nuclear staining in the adenoma cells. This indicates an increase in BMP pathway activation in early cancer lesions. The increase in

p-Smad activation in conjunction with the decrease in receptor expression seems to be paradoxical. However, studies have shown that loss of BMPR-II expression in pulmonary smooth muscle cells, by conditional ablation, results in an augmentation of BMP signalling after BMP6 and BMP7 stimulation. This result was due to redundancy in BMPR type II signalling. BMP ligands preferentially signalled via BMPR-II in wild type cells, but signalled via ActRII (Activin receptor type II) in BMPR-II deficient cells (Yu, PB *et al.*, 2005). In our study, we have shown a significant reduction in BMPR-II and BMPR-IB receptors. BMPR-IA expression was reduced but not to the extent of BMPR-II and BMPR-IB; therefore, BMPR-IA could potentially activate the BMP signalling pathway in conjunction with Activin type II receptors.

The transcription factor Id-1, a target of BMP signalling, was up-regulated in hyperplasia and adenoma K-ras^{G12D} samples. Id-1 is known to be an activator of proliferation, by preventing p21 inhibition of CyclinD. CyclinD is subsequently liberated to hyperphosphorylate retinoblastoma allowing progression into the S phase of cell cycle (Norton, JD, 2000). Augmentation of Id-1 expression has been identified in many cancer types including squamous cell carcinoma, melanoma, colorectal adenocarcinoma, pancreatic cancer, neuroblastoma and prostate cancer, among others (Fong, S *et al.*, 2004). Id-1 expression in carcinomas correlate with increased tumour grade and poor clinical outcome in many cancer types (Fong, S *et al.*, 2004). Expression of Id-1 has also been associated with anti-cancer drug resistance. Expression of Id-1 conferred anti-apoptotic resistance to cancer cells in the presence of several anti-cancer drugs. The anti-cancer drugs inactivate cells via several different pathways, suggesting Id-1 expression is common to many signalling pathways during cancer progression. *In vitro* studies have shown Id-1 to be a potential target to overcome anti-cancer drug resistance in many cancer cell types (Zhang, X *et al.*, 2007a). The identification of Id-1 at the early stages of lung cancer progression in the K-ras^{G12D} tumour samples indicates the early expression of this cancer prognosis factor. Therefore Id-1 could be used as a potential biomarker for lung cancer patients.

The exact molecular mechanism of lung carcinogenesis is incompletely understood. Never-the-less, the development and progression of lung cancer likely involves multiple steps and factors. In this regard the results of the present study suggest that loss of BMPRs play an important role during lung carcinogenesis. This study has also identified aberrant expression of other BMP signalling components at the early proliferative stages of lung cancer. This is the first study that implicates BMP signalling as a potential biomarker for lung cancer.

4. Generation of Expression Plasmids

4.1. Introduction

Aberrant BMP receptor expression has been characterised in a number of human diseases, including diseases of the lungs. The exact molecular mechanisms of aberrant BMPR expression remain unknown. Tetracycline inducible BEAS-2B cell line was established to generate cells that could be used to temporally induce a transgene. In this chapter BMPR-II and BMPR-IB expression vectors were generated to study the effect of over expressing these receptors in lung epithelial cells. Also a *Mig-6* expression vector was constructed for the generation of a *Mig-6* expressing transgenic mouse.

The BEAS-2B cell line was utilised for the establishment of the tetracycline inducible system. These cells were originally generated from normal bronchial epithelial cells which were transformed with an adenovirus-12 SV40 hybrid virus, rendering them immortal (Reddel, RR *et al.*, 1988). BEAS-2B cells retained characteristics of well differentiated epithelial cells but were non-tumourgenic when injected subcutaneously into mice. The tetracycline inducible system has not been previously generated in the BEAS-2B normal transformed cell line.

Mutations in the BMPR-II gene have been identified in idiopathic and familial pulmonary hypertension cases (Humbert, M, 2008). Trangenic mouse models expressing a dominant negative form of BMPR-II have verified that loss of BMPR-II expression causes the pulmonary hypertension disease phenotype (Ramos, MF *et al.*, 2008). However, the molecular mechanism of how BMPR-II mutations contribute to the development of the disease is not yet elucidated. Loss of BMPR-II has also been shown to occur in human cancers, with loss of receptor expression correlating with disease progression (Kim, IY *et al.*, 2000). Also unpublished studies by our lab have identified augmentation of BMPR-II expression in human chronic inflammatory lung diseases including chronic obstructive pulmonary disease (COPD), bronchiolitis olibterans organizing pneumonia (BOOP) and sarcoidosis. Therefore BMPR-II aberrant expression has been identified in a number of human diseases. In this chapter BMPR-II cDNA was cloned from human lung epithelial cells and inserted under the control of the strong constitutive CMV promoter to generate

a BMPR-II over expression vector. The over expression vector has the potential to elucidate the function of BMPR-II in disease models.

Numerous studies have identified a loss of BMP receptor expression in many human cancers, suggesting an anti-tumourigenic role for these receptors (Kim, IY *et al.*, 2000; Lee, J *et al.*, 2008). The study on the K-ras^{G12D} lung cancer model corroborated loss of BMPR-IB expression in early tumour progression. BMPR-IB gene and protein expression was attenuated in hyperplasia and adenoma stages of early lung cancer progression. In order to establish if BMPR-IB expression has potential anti-tumourigenic function, a BMPR-IB expression vector was generated. BMPR-IB was cloned from primary mouse lung epithelial cells and expressed under the control of the CMV promoter.

Loss of *Mig-6* expression was found in hyperplasia and adenoma tissue in the K-ras^{G12D} model of lung cancer. In this chapter a *Mig-6* over expression vector was constructed for the generation of a *Mig-6* over expressing transgenic mouse. As described in section 1.6.4 transgenic mouse models with *Mig-6* ablation develop tumours in numerous organs, indicating that *Mig-6* functions as a tumour suppressor. In order to establish if *Mig-6* has the potential to inhibit or delay the onset of tumour development in cancer models, an over expression vector was generated. The *Mig-6* cDNA was cloned from mouse uterine cells. *Mig-6* was sub-cloned into the Rosa-luciferase vector which contains homologous regions and allows homologous recombination into the Rosa βgeo 26 locus. The Rosa26 locus is a region in the mouse genome which was first identified by gene trapping, homozygous mutations in this gene result in viable normal mice. This locus has become extensively utilised for the generation of transgenic mouse models. Rosa βgeo 26 mice contain β-galactosidase gene and neomycin gene chimera under the control of the endogenous constitutive Rosa promoter (Soriano, P, 1999). The Rosa-luciferase vector allows easy insertion of genes of interest into the Rosa βgeo 26 locus for the generation of transgenic mice.

This chapter describes the molecular cloning of a number of expression vectors. Research using these vectors has the potential to elucidate mechanisms of human disease pathologies.

4.2. Strategies

4.2.1. Strategy for the Generation of a Tetracycline Inducible System

Firstly, antibiotic kill curves for G418 (antibiotic selection for pTet-On), hygromycin B (antibiotic selection for pTRE-2hyg) and doxycycline (inducible antibiotic) were set up to establish the toxic concentrations. BEAS-2B cells were transfected with pTet-On and selected for stable integration of the plasmid. The functionality of the rtTA transactivator expression from the pTet-On plasmid was assessed by co-transfection with the luciferase reporter plasmid, pTRE-luciferase. Selection of a pTet-On cell line was based on its ability to express high levels of luciferase in the presence of doxycycline with little background luciferase expression in the absence of doxycycline.

4.2.2. Generation of pTet-On Clones

Two methods of transfection were utilised for the generation of pTet-On stable clones. The transfection techniques used were $CaPO_4$ and Lipofectamine 2000. The $CaPO_4$ chemical transfection method (section 2.2.15.1) was utilised prior to the establishment of the more efficient less toxic Lipofectamine 2000 method of transfection (section 2.2.15.2).

Trial #1: The calcium phosphate transfection procedure was used to transfect the pTet-On plasmid into the BEAS-2B cell line. Transfected cells were grown in media containing G418 to select for cells transfected with the pTet-On plasmid. Selection was complete after 2 weeks with complete cell death except for colonies that contained stable

integration of pTet-On. Serial dilutions were used to isolate individual clones which were resistant to G418 and therefore contained the integrated pTet-On plasmid.

Trial #2: pTet-On plasmid was transfected into the human BEAS-2B cell lines using Lipofectamine 2000 transfection method. Stable clones were selected in G418 media for 2 weeks. During the selection period substantial cell death occurred by day 9 and stably transfected cells began to grow in colonies. Individual colonies were isolated using cloning cylinders.

Each clone was transferred from either 96 well plates (Trial #1) or 10cm^2 petri dishes (Trial #2) into 6 well culture dishes. Clones from confluent 6 wells were relocated into 75cm^2 tissue culture flasks; frozen stocks of each clone were generated from confluent 75cm^2 flasks. Cells were thawed for functional analysis of their stably integrated pTet-On plasmid by transfection with pTRE-luciferase in the presence and absence of doxycycline.

4.2.3. Cloning Strategy for the Generation of pCMV-BMPR-II

Human BMPR-II was cloned from BEAS-2B cDNA and inserted into pCMV-Script vector. The resulting pCMV-BMPR-II vector was validated by sequence analysis and functional assays including RT-PCR, immunofluorescence and Western blot analysis to ensure the plasmid expressed the BMPR-II cDNA.

4.2.4. Cloning Strategy for the Generation of pBMPR-IB-pcDNA4

Mouse BMPR-IB was cloned from mouse airway epithelial cell cDNA and inserted into the TOPO-Blunt II cloning vector (Figure 10.5), for ease of sequencing and sub-cloning. BMPR-IB was sub-cloned from the TOPO vector into the pcDNA4 vector (Figure 10.7). pcDNA4 vector expressed BMPR-IB under the control of a CMV promoter and provided a myc epitope at the 3' terminal of the gene. The myc epitope provided a method of easy identification of the expression vector, using an anti-myc antibody. The myc epitope also

allows purification of the gene and its interacting proteins using immunoprecipitation assays. BMPR-IB-pcDNA4 vector was validated by sequence analysis and functional assays including RT-PCR, immunofluorescence and Western blot analysis to ensure BMPR-IB expression.

4.2.5. Cloning Strategy for Mig-6 Expression Vector

Mig-6 was cloned from cDNA isolated from a mouse uterus and inserted in pCR2.1 TOPO cloning vector. *Mig-6* was excised from the TOPO vector and inserted into the multiple cloning site of the Rosa cassette down-stream of an SV40 promoter (Figure 4.14). The *Mig-6* Rosa cassette plasmid was verified by restriction digest and sequencing analysis. The *Mig-6* Rosa cassette plasmid contains 450 bp regions flanking the *Mig-6* gene which are homologous to regions in the Rosa-luciferase vector flanking the luciferase gene (Figure 4.14). These homologous regions allow recombination of the *Mig-6* gene, from the *Mig-6* Rosa cassette, into the location of the luciferase gene of the Rosa-luciferase vector (Figure 4.21). Verification of insertion of the *Mig-6* gene into the Rosa vector was carried out using restriction digest analysis and sequencing analysis. The recombineered Rosa *Mig-6* vector (RRM) was microinjected into mouse embryonic stem cells for the generation of a transgenic animal. The Rosa vector contains a LoxP-Stop-LoxP region upstream of the *Mig-6* gene. This vector contains homologous regions to the Rosa βgeo 26 gene that has been described in Soriano 1999 (Soriano, P, 1999). The Rosa vector is used to insert a transgene into the Rosa βgeo 26 locus in mouse embryonic stem cells for the generation of transgenic mice (Figure 4.22).

4.3. Results

4.3.1. Characterisation of pTet-On System

4.3.1.1. Antibiotic selection

An antibiotic kill curve was generated to establish the optimal concentration for plasmid selection in the BEAS-2B cell line. Optimal conditions were established such that cell death would begin to occur within 4 days, with complete cell death after approximately 2 weeks (Figure 4.1). A concentration of 500 µg/ml of G418 was chosen for initial pTet-On plasmid selection and the 250 µg/ml concentration was chosen for continual plasmid

selection (Figure 4.1A). 25 µg/ml concentration of hygromycin B was chosen to select for pTRE-2hyg plasmid (Figure 4.1B). A dose response was set up testing concentrations of doxycycline. It was found that 5 µg/ml doxycycline was quite toxic to the cells (Figure 4.1C). Therefore a dose response range of 1-3 µg/ml would be tested to induce the tetracycline inducible system.

4.3.1.2. Validation of pTet-On Inducible System

To initially validate the pTet-On system in BEAS-2B cells, the pTet-On plasmid and pTRE-luciferase reporter plasmid were transiently co-transfected. BEAS-2B cells were transfected with pTet-On, pTRE-luciferase, and pTet-On plus pTRE-Luciferase in the absence of doxycycline to ensure there was no background luciferase expression generated by the plasmids alone. The co-transfection experiment was activated with 1 µg, 2 µg, 3 µg and 5 µg doxycycline to find the optimal concentration of doxycycline for activation of the luciferase reporter. From the antibiotic kill curve experiment (Figure 4.1C) 5 µg of doxycycline was toxic to the cells, > 80 % cell death after 8 days. As expected, this concentration resulted in less luciferase expression compared to the lower concentrations of the antibiotic. There was little difference in luciferase expression with 1 µg (5.6×10^5 ($\pm$ 9.3×10^4)), 2 µg (5.8×10^5 ($\pm$ 1×10^5)) or 3 µg (6.5×10^5 ($\pm$ 1.6×10^5)) of doxycycline (Figure 4.2). Therefore, the lowest concentration (1 µg) was chosen for

activation of pTRE-luciferase in the pTet-On stable cell lines. There was low level luciferase expression from the pTRE-luciferase sample alone (3.7×10^4 ($\pm$ 2.3×10^4)) and from the pTet-On plus pTRE-luciferase co-transfection (3.7×10^4 ($\pm$ 1.1×10^4)) in the absence of doxycycline; indicating the background level or "leakiness" of the system (Figure 4.2).

4.3.1.3. Characterising pTet-On Clones

The pTet-On BEAS-2B clones described in section 4.2.2 were grown in G418-containing media and were therefore presumed to contain a stably integrated pTet-On plasmid. However, depending on the random site of integration the reverse tetracycline transactivator (rtTA) protein maybe expressed at different levels. In order to test the level of rtTA expression, clones were transiently transfected with the reporter plasmid pTRE-luciferase. This plasmid contained the luciferase reporter gene under the control of the tetracycline response element (TRE) and minimal CMV promoter. An induced clone (+ doxycycline) was expected to express luciferase approximately 20 fold higher (recommended in the manufacturers manual) than the non-induced (- doxycycline) control.

BEAS-2B pTet-On clones were transfected with pTRE-luciferase in duplicate. Each control received no doxycycline (- Dox) and 1 μg doxycycline (+ Dox) was added to the treated samples. Luciferase expression was then measured in the control and doxycycline treated wells. Of the 24 (trial#1) (Figure 4.3) and 16 (trial#2) (Figure 4.4) BEAS-2B pTet-On clones tested, none expressed over 2 fold induction of the luciferase reporter in the presence of doxycycline.

In order to ensure these clones contained and expressed the pTet-On plasmid, 6 BEAS-pTet-On clones were chosen for RT-PCR analysis to establish whether the rtTA mRNA was being expressed. Three BEAS-2B pTet-On clones (B14, B15, and B19) resulted in an rtTA gene product (Figure 4.5). However, these clones did not functionally express the

rtTA protein required for the activation of the luciferase reporter in the presence of doxycycline.

4.3.2. Generation of BMPR-II Over Expression Vector

4.3.2.1. Generation of pCMV-BMPR-II

BMPR-II was cloned from BEAS-2B cDNA using the BMPR-II-F-*EcoR* I and BMPR-II-R-*Xho* I primers (section 2.1.3) (Figure 4.6 A). The blunt ended BMPR-II PCR product was inserted into the blunt ended *Srf* I site of the pCMV-Script cloning vector. Confirmation that the gene product had been sub-cloned into the vector in the correct direction was tested by amplifying the gene using the T3 forward and BMPR-II-R-*EcoR* I primers in a PCR reaction. A PCR product resulted when the BMPR-II gene had inserted in the correct direction. Of the 10 colonies tested 1 contained the BMPR-II gene in the correct orientation (Figure 4.6 B). This pCMV-BMPR-II vector was further tested by restriction digest with *Pvu* II (Figures 4.6 C). The correct plasmid resulted in three bands at 4719 bp, 2373 bp and 608 bp (Figure 4.6 D). The plasmid was sequenced to ensure it was in fact the BMPR-II gene.

4.3.2.2. Validation of pCMV-BMPR-II

In order to prove the functionality of the pCMV-BMPR-II over-expression vector, the plasmid was transiently transfected into the BEAS-2B cell line. Empty vector (pCMV-Script) was transiently transfected as a mock transfection control. The over expression of BMPR-II was analysed at the mRNA level by RT-PCR and at the protein level by immunofluorescence and Western blot analysis.

The level of BMPR-II mRNA expression was normalised to the level of GAPDH in each sample. RT-PCR expression was examined at day 1, 2 and 3 to establish if BMPR-II expression increased over time. The pCMV-BMPR-II expression vector caused

approximately 1.3 fold increase in BMPR-II expression compared to the pCMV-Script empty vector control (Figure 4.7).

Immunofluoresence, using an anti-BMPR-II antibody, was carried out to verify BMPR-II protein expression. Levels of protein expression were visualised in pCMV-BMPR-II transfected cells and were compared to pCMV-Script (empty-vector control) transfected cells. BMPR-II expression appeared higher in pCMV-BMPR-II transfected cells compared to the empty vector control (Figure 4.8).

Western blot analysis was carried out to quantify the level of BMPR-II protein expression from pCMV-BMPR-II plasmid. Densitometry was carried out on Western blots and the results showed no significant increase in the levels of BMPR-II expression in the pCMV-BMPR-II transfected cells compared to pCMV-Script transfected cells (Figure 4.9).

Transient expression of a CMV promoter driven expression vector would be expected to result in a large increase in gene and protein expression. From this RT-PCR, immunofluorescence and Western blot analysis it was clear that BMPR-II over expression was not occurring at a sufficiently high rate. After re-assessing the cloning strategy it was noticed that because the forward cloning primer was designed in the 5' region, there was a 200 bp sequence upstream of the start site. It was believed this 200 bp redundant sequence resulted in inefficient expression of the BMPR-II cDNA.

4.3.3. Generation of BMPR-IB-pcDNA4 Expression Vector

4.3.3.1. Cloning BMPR-IB from Lung Epithelial Cell cDNA

The forward cloning primer (BMPR-IB-F-*BamH I*) was designed against mouse BMPR-IB. This primer encoded the first 18 nucleotides of the coding sequence, and had an engineered *BamH I* restriction site (section 2.1.3). The reverse primer (BMPR-IB-R-*EcoR I*) was designed such that it introduced a point mutation into the stop codon (TGA to GGA). This point mutation changed the stop codon to a glycine amino acid. This

mutation was to permit transcription through the stop codon and into the myc epitope in the final pcDNA4 plasmid. The reverse primer also included an *EcoR I* restriction site for sub-cloning into the pcDNA4 vector. The BMPR-IB sequence was examined to ensure the engineered restriction sites were unique to the BMPR-IB cDNA; neither *BamH I* nor *EcoR I* restriction sites were found in the BMPR-IB coding sequence. The mouse BMPR-IB was cloned from normal mouse airway epithelial cell cDNA (Figure 4.10A).

4.3.3.2. Generation of BMPR-IB-TOPO Vector

BMPR-IB PCR product was inserted into the TOPO Blunt II shuttling vector for ease of sequencing and sub-cloning (Figure 4.10B). The BMPR-IB-TOPO Blunt II ligation product was transformed into XL1 blue competent bacteria. Resulting colonies were screened for correctly ligated BMPR-IB-TOPO vectors. Plasmids were isolated from the colonies and digested with the *EcoR* I restriction enzyme. Positive clones resulted in two DNA products: 3.5 kb TOPO Blunt II vector and 1.5 kb BMPR-IB gene (Figure 4.11 A). Positive BMPR-IB-TOPO clones were analysed by *Hind* III restriction digest to ensure the BMPR-IB gene had inserted in the correct orientation (Figure 4.11 B). Correctly orientated clones resulted in two bands: 3566 bp and 1462 bp. Incorrectly orientated clones resulted in two bands: 4861 bp and 167 bp. BMPR-IB clone T6 contained BMPR-IB in the correct orientation.

4.3.3.3. Generation of BMPR-IB-pcDNA4 Vector

The BMPR-IB gene was excised from the BMPR-IB clone T6 (contained in pCR BluntII TOPO vector) with *EcoR* I and *BamH* I restriction enzymes, and inserted into an *EcoR* I and *BamH* I digested pcDNA4 vector. The ligated vector was transformed into XL1 Blue competent *E .coli* and colonies were screened for a correctly ligated product. *EcoR* V diagnostic digest was carried out; correctly ligated plasmids contained two bands: 5900 bp and 700 bp (Figure 4.12). A positive clone (BMPR-IB-pcDNA4) was sent for sequence analysis (OriGene, Kent, UK). The sequencing results showed two point mutations in the cDNA sequence of the BMPR-IB (Figure 4.13). These point mutations

occurred in the third nucleotide of the codon and did not change the encoded amino acid. Therefore, the point mutations were synonomous and coded for the correct protein. The sequencing results also verified that the stop codon had been mutated to glycine in the gene as intended.

4.3.4. Generation of Mig-6 Over Expression Plasmid

4.3.4.1. Generation of Mig-6 TOPO Vector

Mig-6 was cloned from mouse uterus cDNA using primers *Mig-6*-F-*Sac* II and *Mig-6*-R-*Bam*H I (section 2.1.3) (Figure 4.14 A), and inserted into pCR2.1-TOPO cloning vector (4.14 B). Resulting colonies were screened for the insertion of the 1.5 kb *Mig-6* cDNA into the 3.9 kb pCR2.1-TOPO vector. All of the 6 pCR2.1-TOPO *Mig-6* colonies screened contained the insert and resulted in a 5.4 kb linearised DNA product (Figure 4.14 C).

4.3.4.2. Generation of Rosa Mig-6 Cassette Plasmid

Mig-6 was digested from the pCR2.1-TOPO vector using *Sac* II and *Bam*H I restriction enzymes (Figure 4.15 A). *Mig-6* was inserted between the *Sac* II and *Bam*H I restriction sites of the Rosa cassette (Figure 4.15 B) to generate the Rosa *Mig-6* cassette. The Rosa *Mig-6* cassette contained 5' and 3' regions homologous to the Rosa-luciferase vector which allowed homologous recombination between the homologous regions. The *Mig-6* gene preceded a polyA (polyadenylation) sequence and a FRT-neo-FRT sequence. The FRT-neo-FRT sequence conferred kanamycin resistance to prokaryote cells and neomycin resistance to eukaryotes cells, this gene could be easily removed in the presence of the FRT recombinase.

A correct Rosa *Mig-6* cassette plasmid was determined by *BamH* I restriction digest analysis. *BamH* I linearised the plasmid and two clones resulted in a correct sized DNA

band of 7.5 kb (Figure 4.15 C). Positive Rosa *Mig-6* cassette clones: RM3 and RM5 were digested with *Hind* III to ensure the *Mig-6* insert was in the correct orientation. *Hind* III digest of a correctly orientated product resulted in a 3715bp, 3433 bp and 330 bp band (Figure 4.16 A). Clone RM5 resulted in the correct restriction digest map (Figure 4.16 B).

4.3.4.3. Generation of Recombineered Rosa Mig-6 Vector

The Rosa *Mig-6* cassette fragment was excised from the vector backbone with *Sac* I and *Kpn* I from the positive Rosa *Mig-6* cassette plasmid (Figure 4.17 A). The Rosa *Mig-6* cassette was electroporated into DY380 bacteria containing the Rosa luciferase plasmid. Homologous recombination occurred between the linear Rosa *Mig-6* cassette and the luciferase region of the Rosa luciferase plasmid, such that the luciferase gene was replaced with the *Mig-6* cassette (Figure 4.20). Electroporated bacteria were selected for their ability to grow on tetracycline (encoded on the Rosa luciferase plasmid) and kanamycin (encoded on the Rosa *Mig-6* cassette) containing LB agar plates. These positive colonies underwent homologous recombination between the Rosa luciferase plasmid and the Rosa-*Mig-6* cassette in order to grow on selective media (Figure 4.17 B). Resulting colonies were initially screened by PCR for the presence of the *Mig-6* cDNA. All colonies screened contained *Mig-6* cDNA (Figure 4.18 A). Clones were linearised with *Pac* I and vectors resulting in a single DNA product of > 12kb were analysed further (Figure 4.18 B). Diagnostic digest was carried out on clones. Correctly inserted *Mig*-6 cassettes resulted in 9883bp, 4593bp, 3558bp, 3433bp, 327bp digest products (Figure 4.19 A). One clone RRM34 (Recombineered Rosa *Mig-6* clone 34) resulted in the correct banding pattern. Clone RRM34 was digested with *BamH* I restriction digest enzyme, using RM (Rosa *Mig-6* cassette plasmid) as a positive control and Rosa-Luciferase as a negative control for the presence of the *Mig-6* gene at 1.5kb (Figure 4.19 B).

Sequencing analysis across the entire gene revealed that the plasmid was completely correct (data not shown). This plasmid was then used for the generation of a *Mig-6* over expression mouse model. RRM34 vector was linearised with *Pac* I and microinjected into mouse embryonic stem (ES) cells for the generation of a transgenic mouse. The ES cells

originated from Rosa βgeo 26 mice (Soriano, P, 1999). The RRM34 plasmid contains regions homologous to the Rosa βgeo 26 locus to allow homologous recombination. In this way the LoxP-Stop-LoxP-*Mig-6* vector was inserted into the mouse chromosome in a specific region (Figure 4.21).

4.4. Discussion

The advancement of genomics over the past decade, especially the sequencing of the human and mouse genomes have advanced the identification of genes involved in development and disease. However, the mechanism by which these genes cause disease is not fully elucidated. Studies into the K-ras^{G12D} mouse model revealed the aberrant expression of BMPR-II, BMPR-IB and *Mig*-6 (Chapter 3). As described previously these genes are implicated in a number of human disease processes (section 1.6.4 and 1.7.1). This chapter describes the generation of cloning vectors for over expressing BMPR-II, BMPR-IB and *Mig-6* genes in order to utilise these vectors in understanding their involvement in lung disease.

The tetracycline inducible system is widely used to differentially express genes in a temporally controlled manner. This system has been used for gene ablation and over expression in mice to study lung disease (Cheng, DS *et al.*, 2007; Sisson, TH *et al.*, 2006; Sisson, TH *et al.*, 2002). For the most part *in vitro* tetracycline inducible system has been carried out in HeLa and HEK 293 cell lines. Currently, there is no known BEAS-2B tetracycline inducible cell line. In this chapter the pTet-On system (Clontech) was used to establish tetracycline inducible BEAS-2B cell lines. None of the 40 pTet-On clones tested induced luciferase reporter protein in the presence of doxycycline. This lack of luciferase induction indicates the poor expression of rtTA from all of these clones. This system required random integration of the pTet-On plasmid. All expanded clones sustained growth in G418 containing media, and therefore contained the plasmid. Three of six clones that were selected expressed rtTA mRNA. However, expression of the transactivator gene was dependent on the random integration of the plasmid. An ideal

pTet-On clone should have expressed low levels of luciferase reporter protein in the absence of doxycycline and approximately 20 fold induction of luciferase reporter expression in the presence of the doxycycline. In this study, 10 of 40 clones expressed background levels of luciferase higher than 10,000 RLU. This high background of luciferase expression demonstrates the leakiness of the pTet-On system. This tetracycline inducible system was inefficient in the BEAS-2B cell line. More clones would have had to be isolated and characterised in order to identify a positive pTet-On clone. This system may benefit from the use of the pTRE-Tight vector which provides tight control of the gene of interest's expression.

An inducible system has added advantages of temporal control of transgene expression. However, due to the inefficiency of the tetracycline inducible system BMPR-II and BMPR-IB over expression vectors were generated to study their effects in airway epithelial cells.

BMPR-II was sub-cloned into pCMV-Script cloning vector. This vector was verified by restriction analysis and sequence analysis demonstrating the correct gene was cloned. Functional analysis of this plasmid revealed the lack of over expression of BMPR-II when transiently transfected into BEAS-2B cells. This lack of over expression may have been due to the 200bp sequence at the 5' end of the start site. This 200bp region was included in the 5' UTR (untranslated region) when the forward cloning primer was designed. Another possibility for the lack of over expression may be due to the large size of the cDNA; the BMPR-II cDNA is 3.3kb in size.

BMPR-II expression vector was generated in order to use the vector as a tool for characterising the effect of BMPR-II over expression in lung cells. To date a number of groups have generated a dominant negative BMPR-II (dnBMPR-II) plasmid which lacks the intracellular signalling domain of the receptor (Hagen, M *et al.*, 2007; Pouliot, F *et al.*, 2003; Tada, Y *et al.*, 2007; West, J *et al.*, 2004). The dnBMPR-II vector revealed loss of BMPR-II signalling in smooth muscle cells produced a pulmonary hypertension phenotype in transgenic mice (West, J *et al.*, 2004). Expression of dnBMPR-II in breast

cancer cells caused resistance to BMP2 induced proliferation. This suggested BMPR-II expression in breast cancer cells contributes to BMP2 induced proliferation and cell survival (Pouliot, F *et al.*, 2003). To date no group has published the use of BMPR-II full length cDNA for use in *in vitro* assays. Atypical BMPR-II expression has been seen in inflammatory diseases such as COPD (chronic obstructive pulmonary disease), sarcoidosis, BOOP (bronchiolitis obliterans organizing pneumonia), ARDS (acute respiratory distress syndrome) (O'Dea, unpublished data) and asthma (Kariyawasam, HH *et al.*, 2008). The BMPR-II plasmid was generated to establish if BMPR-II over expression contributed to inflammation. These studies would elucidate the role of BMPR-II over expression seen in human chronic inflammatory diseases. BMPR-II expression is lost in many types of cancer, including lung cancer (Chapter 3), prostate cancer (Kim, IY *et al.*, 2000), and colorectal cancer (Kodach, LL *et al.*, 2008b). BMPR-II expressing plasmid would be utilised to re-express BMPR-II in lung cancer cells devoid of its expression, to establish if signalling via this receptor could inhibit or delay cancer progression.

The BMPR-IB-pcDNA4 plasmid was verified using restriction digest and sequence analysis. Functionality of this expression plasmid was validated by RT-PCR, immunofluorescence and Western blot analysis (section 0). Similar to BMPR-II, BMPR-IB expression is attenuated in numerous types of cancers including glioblastoma (Lee, J *et al.*, 2008), prostate cancer (Kim, IY *et al.*, 2000), and lung cancer (Chapter 3). This over expression plasmid was used to characterise the function of BMPR-IB over expression in the lung airway cell line devoid of endogenous BMPR-IB expression (Chapter 6). If loss of BMPR-IB expression correlated with increased tumour grade, then perhaps re-expression of BMPR-IB would inhibit or delay tumour progression.

Mitogen-inducible gene 6, *Mig-6,* can interact with members of the ErbB family and has been shown to negatively regulate the ErbB signalling pathway (Fiorentino et al., 2000; Anastasi et al., 2003; Xu et al., 2005). Ablation of *Mig-6* in mice leads to the development of animals with epithelial hyperplasia, adenoma, and adenocarcinoma in organs like the lung, gallbladder, and bile duct (Zhang *et al.*, 2007(Jin, N *et al.*, 2007).

Also *Mig-6* expression is lost in a number of cancer types. In this chapter a *Mig-6* expression plasmid was constructed in order to generate transgenic animals expressing the *Mig-6* gene under the control of the constitutive CAGGS (β-actin) promoter. Future work includes the generation of transgenic mice expressing both K-ras^{G12D} and *Mig-6* to establish the tumour suppressor effect of *Mig-6*. It is believed that *Mig-6* expression would delay the onset of tumour formation due to its tumour suppressive function. These studies are ongoing. The outcome of these studies will indicate if *Mig-6* expression can be utilised as a therapeutic target for treating lung cancer.

5. Comparative Gene Delivery to Lung Epithelial Cells

5.1. Introduction

Cancer gene therapies have been developed to intercept cell division. These include the introduction of anti-sense oligonucleotide or dominant negative plasmids of oncogenes; re-introduction of wild type tumour suppressor genes; or suicide gene therapy to selectively kill cancer cells. Therefore potential molecular targets for cancer gene therapy are plentiful. It is the need for efficient and safe methods of gene delivery that causes a bottleneck in clinical gene therapy success. Previous gene therapy trials have compared the efficiency of either liposomes or viral vectors for the delivery of genes to lung epithelial cells. To date there has been no study comparing a range of non-viral to viral vector delivery to lung cells. This study compares the efficiency of delivery to normal murine lung cells (MAECs), adenocarcinoma derived mouse lung cell line (MLE-12) and adenocarcinoma derived human lung cell line (A549).

Comparative studies were conducted measuring the transfection efficiencies and toxicities of a range of the most commonly used viral vectors (AAV2, AAV5, AAV6 and HIV-VSV-G), commercial non-viral vectors (Effectene (Qiagen), SuperFect (Qiagen) and Lipofectamine 2000 (Invitrogen)) using a green fluorescent protein (GFP) reporter transgene. Initial studies were carried out to optimise read-out parameters, that is, the choice of transgene and the choice of cell fixative. Preliminary experiments were carried out using wide ranges of concentrations of each non-viral and viral vector to determine narrower ranges of optimal transfection efficiencies. Optimum transfection rates were then compared across the range of transfection vectors. Transfection efficiency comparisons were made between primary mouse airway epithelial cells (MAECs), a mouse adenocarcinoma derived cell line (MLE-12) and a human adenocarcinoma derived cell line (A549).

5.2. Results

5.2.1. Validation of Flow Cytometry

Positive cell lines expressing pCyclinD$_1$-GFP were generated by a previous member of the lab. These clones were tested for positive GFP expression to optimise the flow cytometry procedure for endogenous GFP expression. Ten A549-pCyclinD$_1$GFP clones were expanded and analysed for GFP expression in a flow cytometer. A549 cells alone were used as a negative control to set background fluorescence level of these cells. The pCyclinD$_1$-GFP clone 1A was the only clone that expressed the GFP transgene at a level higher than the negative control (Figure 5.1).

5.2.2. GFP Plasmid Comparison

The CyclinD$_1$-GFP plasmid allowed conditional expression of the *Aeuqorea victoria* GFP gene under the transcriptional control of the CyclinD$_1$ promoter, which is expressed early during cell cycle progression. pMGFP permits expression of the *Montastrea cavernosa* GFP gene under the transcriptional control of the constitutively active CMV promoter. Comparative analysis of transient transfection expression from pCyclinD1-GFP and pMGFP was carried out. pMGFP resulted in a higher transfection efficiency and a higher fluorescent intensity compared to the pCyclinD$_1$-GFP plasmid (Figure 5.2). From these results pMGFP plasmid was chosen for subsequent transfection studies.

5.2.3. Optimisation of Non-Viral Vector Delivery

To optimise Lipofectamine 2000, A549 cells were treated with a range of lipid concentrations. The concentration ranged from 0.4 µg to 5 µg, untreated cells served as a negative control. Cell counts were carried out on these cells and it was found that high concentrations of Lipofectamine 2000 caused cell death. 0.4 µg of Lipofectamine 2000 caused little to no cell death compared to the higher concentrations (Figure 5.3 A). This quantity of lipid was then complexed to 500 ng, 750 ng or 1000 ng of pMGFP plasmid to establish the optimum concentration of lipid: DNA complex required to achieve high

transfection efficiency. 750 ng of pMGFP complexed with 0.4µg of Lipofectamine 2000 resulted in high transfection efficiency; this concentration was used in transfection comparison studies.

In order to establish the optimum concentration of Superfect, various amounts of pMGFP plasmid and Superfect were complexed together. Of the conditions tested, 12 µg Superfect complexed to 0.58 µg plasmid resulted in the highest efficiency of GFP expression (8.2 (± 11.8) %). There was little to no expression from other quantities of Superfect (Figure 5.4).

A variety of plasmid and Effectene concentrations were complexed together to find the most efficient quantity of Effectene for transfecting A549 cells. The conditions that resulted in the highest expression, 47.2 (± 16.1) %, was composed of 0.66 µg pMGFP plasmid complexed to 1.28 µg enhancer and 1.6 µg Effectene (Figure 5.5).

5.2.4. Optimisation of Viral Gene Delivery

Varying concentrations of AAV2 plaque forming units (pfu) were used to identify the range at which A549 cells were transfected. Cells were seeded such that they were 90 % confluent (as for the lipid transfections). A range of viral titre concentrations ($5x10^6$ pfu, $5x10^7$ pfu, $5x10^8$ pfu, and $1x10^9$ pfu) were used to establish the most efficient concentration (Figure 5.6 A). Modest GFP expression resulted from these concentrations.

To improve the *in vitro* culture system the cell density was decreased to allow exposure of viral integrins on the basolateral membrane, that is the cells were seeded sub-confluent. The transfection rate for the low density cells improved the rate of transgene expression (Figure 5.6 B). The low cell density conditions were chosen for subsequent viral transfections. The three concentrations of AAV2 ($5x10^7$, $5x10^8$, $5x10^9$ pfu) were

used in further comparative studies. The cell density and AAV concentration established from these optimisation experiments were used to also compare AAV5 and AAV6 transfection efficiencies.

A range of HIV-VSV-G pfu concentrations were transfected into sub-confluent A549 cells. The range included: $7.5x10^4$, $1.5x10^5$, $2.25x10^5$, $3x10^5$, $4.5x10^5$, and 6.75 x 105 pfu. Three concentrations $7.5x10^4$, $1.5x10^5$, $2.25x10^5$ were chosen for comparative studies (Figure 5.7).

5.2.5. Transfection at 24 hr

The optimal conditions that were established for each transfection method were used to transfect primary mouse airway epithelial cells, MAECs, the mouse adenocarcinoma derived cell line, MLE-12, and the human adenocarcinoma derived cell line, A549 (Figure 5.8).

AAV6 was the most efficient vector at transfecting MAECs 23.7 (± 7.3) %. HIV-VSV-G was the second most efficient vector at transfecting MAEC 10.8 (± 1.6) %. Effectene was the third most efficient vector at transfecting MAECs, it was also the most efficient non-viral vector resulting in 7.0 (± 1.9) % transgene expression 24 hrs after transfection.

The vector that resulted in the highest transgene expression in MLE-12 cell line was AAV6, 68.2 (± 3.2) %. The second best transfection method to these cells was Lipofectamine 2000 which resulted in 55.9 (± 4.1) % transgene expression. HIV-VSV-G was the third most efficient transfection method for these cells 38.0 (± 3.3) %.

HIV-VSV-G resulted in the highest level of transgene expression for A549 cells 68.9 (± 3.4) %. Lipofectamine 2000 was the second most efficient method of transfection for this cell line with 65.1 (± 7.8) % transgene expression. The third most effective transfection vector was Effectene 32.9 (± 9.1) %.

Cell viability counts were carried out for each transfection method. Of the most efficient vectors tested, that is: AAV6, HIV-VSV-G, Lipofectamine 200 and Effectene, none caused a significant loss in cell number. Therefore the most efficient transfection vectors were not toxic to the cells (Figure 5.9).

5.2.6. Transfection at 48 hr

Transfection efficiencies were measured at 48 hrs to examine if transgene expression from certain vectors required time to be expressed and to see if the level of expression from vectors was maintained over a short period of 24 hrs (Figure 5.10).

At 48 hrs after transfection the rate of transgene expression in AAV6 transfected MAECs was reduced to 14.4 (± 10.9) %. Transgene expression from HIV-VSV-G transfection has increased to 26.0 (± 3.6) %, making it the most efficient vector at transfecting primary mouse cells. Effectene remained the most efficient non-viral vector with an increase in transgene expression to 9.4 (± 2.7) % at 48 hrs.

In MLE-12 cells, the level of AAV6-GFP expression had decreased to 56.0 (± 4.4) % at 48 hrs, but still remained the most efficient transfection vector. An increase in GFP expression with Lipofectamine 2000 transfection was observed in MLE-12 cells with a transfection efficiency of 61.5 (± 5.1) %. HIV-VSV-G remained the third most efficient vector with unchanged expression of 35.7 (± 5.7) %.

HIV-VSV-G transgene expression levels had increased to 81.3 (± 1.0) %, this was the highest transfection rate seen in any cell type with any vector. Lipofectamine 2000 expression level was sustained at 48 hrs with 64.9 (± 9.3) % GFP expression. Effectene remained the third most efficient method of transfection with a slight increase in expression to 37.6 (± 15.2) %.

As with 24 hrs the level of toxicity caused by the most efficient vector was not statistically significant (Figure 5.11).

5.3. Discussion

To date therapies used to treat lung cancer include surgical resection, chemotherapy and radiation. More recently monoclonal immunotherapies are used to treat non-small cell lung cancer patients. However, only a small percentage of patients respond to these therapies. Responsiveness to these therapies is dependent of the molecular profile of the mutations in the cancer (Zhang, X and Chang, A, 2008). Monoclonal therapies remain inefficient until comprehensive screening methods or sensitive biomarker identification assays are developed, to thoroughly identify patients that will benefit from monoclonal therapies. Another promising method of therapy to treat lung cancer patients is the area of cancer gene therapy. To date most lung gene therapy trials have been designed to re-introduction the cystic fibrosis transmembrane receptor genes (CFTR) mutated in cystic fibrosis (CF) patients (Griesenbach, U *et al.*, 2006). However, gene therapy has great potential for the treatment of lung cancer due to the numerous potential targets and the high rate of division of cancer cells (Choi, SH *et al.*, 2008; Gleave, ME and Monia, BP, 2005).

The constitutive growth of tumour cells is dependent on aberrant regulation of cell division and apoptotic pathways. Numerous therapies have been developed to intercept cell division in cancer cells, these include the introduction of anti-sense oligonucleotide or dominant negative oncogenes; re-introduction of wild type tumour suppressor genes; or suicide gene therapy to selectively kill cancer cells. In this study we have compared a range of viral and non-viral vectors for their efficiency at transfecting normal mouse airway epithelial cells (MAEC), mouse adenocarcinoma derived airway cell line (MLE-12), and human adenocarcinoma derived airway cell line (A549). As expected due to their high mitotic rates the cancer cell lines were transfected more efficiently than the normal airway cells. The enhanced ability for cancer cells to be transfected is advantageous for cancer gene therapy. In this study we also assessed if there were species differences in the efficiency of transfection to adenocarcinoma derived mouse MLE-12 cell line and the adenocarcinoma derived human A549 cell line.

Being the first serotype discovered, AAV2 has been extensively studied for gene delivery to the lungs. However, AAV5 and AAV6 have been shown to have higher tropism for the lung compared to AAV2 (Halbert, CL *et al.*, 2001; Seiler, MP *et al.*, 2006). Concurring with these reports AAV6 transfection resulted in the highest transgene expression of the serotypes tested.

A species difference for gene delivery vectors has been previously noted. Seiler *et al* reported AAV5 and AAV6 can transfect human primary airway epithelial cells with equal efficiency. However, AAV6 was capable of a 6 fold increase in transfection rates in mouse airway cells compared to AAV5 (Seiler, MP *et al.*, 2006). This Gilbert *et al* study shows AAV6 is more efficient at transfecting all cell types compared to AAV5. AAV5 entry into cells is dependent on the expression of sialic acid. The low rate of AAV5 transfection suggests this receptor is not expressed at high rates in the cells tested. AAV6 is more efficient at transfecting mouse cells compared to human cells. The receptor necessary for AAV6 binding and entry is not fully known, however, AAV6 entry into cells has been shown to be sialic acid dependent and independent (Seiler, MP *et al.*, 2006). The high transfection efficiency for mouse and not human cells suggested there is higher expression of AAV6 receptor on the mouse primary cells and mouse cell line compared to the human cell line.

HIV-VSV-G conferred the highest rate of transgene expression in the human cancer cell line and mouse primary cells. Although not the highest rate of transgene expression, HIV-VSV-G resulted in reasonable transgene expression in the mouse cell line. This gene therapy vector has the advantage to confer long-term gene expression because of its ability to integrate into the genome. The ability to randomly integrate into the genome however, has had deleterious effects. Clinical trials in which a retroviral gene therapy vector was delivered to ADA SCID (adenosine deaminase severe combined immunodeficiency) patients resulted in the development of leukaemia in 2 of these patients due to the random integration of the viral vector (Hacein-Bey-Abina, S *et al.*, 2003). This safety issue of random integration has hindered the progress of retroviral gene therapy trials.

Non-viral vectors, particularly Lipofectamine 2000, achieved high gene transfer efficiencies in the cell lines but not in primary cells. The low rate of transfection into primary cells is likely due to the low rate of cell cycle, as cell division within the primary cell cultures is slower than that of the cell lines. Lipid and polymer based vectors require the nuclear membrane to be degraded to allow entry of the plasmid into the nucleus, this characteristic is advantageous for cancer gene therapy. *In vivo* cancer xenograft mouse models have shown the ability of non-viral vectors to target tumour cells for elimination. Wild type p53 complexed to polymers such as cationic polymers or PEI have been successful at attenuating tumour cell growth and increasing animal survival in these models (Choi, SH *et al.*, 2008; Moffatt, S *et al.*, 2006; Zou, Y *et al.*, 2007).

High toxicity can counteract high transfection efficiencies for some vectors. In this study the best performing vectors did not result in significant reduction in cell viability. Moreover, AAV2 had a growth promoting effect on the human and mouse adenocarcinoma derived cell lines. This growth promoting effect of AAV2 would be a disadvantage for the use in cancer therapies.

Introduction of anti-sense or dominant negative plasmids have been developed to negate the effects of oncogene expression. This type of therapy has had success *in vitro* and in animal models. Expression of dominant negative growth factor receptors reduce proliferation rates induced by growth factor ligands. The dominant negative genes have the ability to compete with endogenous molecules to bind growth factors but they not initiate the intercellular signalling. Generation of adenoviral vector expressing IGF-IR dominant negative mutant reduces tumour growth in a cancer xenograft mouse model (Lee, CT *et al.*, 2003; Lee, CT *et al.*, 1996). Anti-sense therapy towards survival signals that confer chemo-resistance to tumours have progressed to clinical trials. These therapies although tolerated only result in modest effects. To advance the effectiveness of the anti-sense oligonucleotides, they are being tried in combination with other therapies (Gleave, ME and Monia, BP, 2005; Ramanarayanan, J *et al.*, 2004).

Loss of wild type expression of the tumour suppressor gene p53 has been implicated in over 50% of human cancers. Loss of this gene renders cells incapable of apoptosis in response to DNA damage. Re-introduction of p53 as a potential cancer gene therapy has been tested. Intra-tumoural injection of adenoviral vector expressing wild type p53 has been shown to be safe and effective in clinical trials (Schuler, M *et al.*, 1998).

Suicide gene therapy is based on the introduction the herpes simplex virus thymidine kinase (HSV-TK) gene which is capable of metabolising an inactive prodrug, gancyclovir, to a toxic product. Therefore transfected cells will be selectively killed by the toxic product. Studies have successfully administered AAV vectors expressing HSV-TK to oral squamous cell carcinomas, subsequent treatment with gancyclovir resulted in efficient tumour cell killing (Fukui, T *et al.*, 2001; Yamamoto, N *et al.*, 2005). NSCLC cell lines were subcutaneously injected into mice and tumours formed. Adenoviral delivery of HSV-TK-GFP was found to successfully transfect adenocarcinoma and large cell carcinoma lung cancer cell lines. Therefore adenoviral based HSV-TK therapy has the potential to treat NSCLC (Maatta, AM *et al.*, 2004).

Due to the heterogeneity and complexity of cancer there are a number of potential gene therapeutic approaches that can be taken. One limiting factor for successful gene therapy is the lack of efficacious vectors for gene delivery. In this study we have shown that HIV-VSV-G and Lipofectamine 2000 are efficient for *in vitro* gene delivery to human cancer cells. We have shown that AAV6, HIV-VSV-G and Lipofectamine 2000 are the most efficient vectors for gene delivery to mouse cancer cells. While AAV6, HIV-VSV-G and Effectene are most efficient vector for transfecting primary mouse airway cells.

6. Investigation of BMPR-IB Expression in Lung Epithelial cells

6.1. Introduction

The BMP pathway plays an important role in many biological processes including cellular proliferation, differentiation and cell death. Dysregulation of components of this pathway have been implicated in a number of human diseases, including cancer. BMPR-IB mRNA and protein expression were down-regulated during early lung cancer progression as demonstrated in the K-ras^{G12D} lung cancer mouse model (Chapter 3, section 3.2.5). In addition, BMPR-IB expression was observed in the nuclei of human lung adenocarcinoma cells (Chapter 3 section 3.2.5) suggesting BMPR-IB has an important function throughout cancer progression. Due to the loss of BMPR-IB at the early proliferative stages of cancer, we hypothesised that BMPR-IB has an anti-proliferative function therefore having potential tumour suppressor like properties at the early stages of cancer progression.

In order to test this hypothesis a BMPR-IB expression vector was generated, as described in Chapter 4 section 4.3.3. The mouse and human BMPR-IB sequence have 89% nucleotide homology and 98% amino acid homology. The mouse BMPR-IB was cloned with a view to generating a transgenic animal. Validation and characterisation of BMPR-IB expression was carried out in the human BEAS-2B cell line. The BEAS-2B cell line was originally generated from normal bronchial epithelial cells which were transformed with an adenovirus-12 SV40 hybrid virus, rendering them immortal (Reddel, RR *et al.*, 1988). These cells retain characteristics of well differentiated epithelial cells but are non tumourigenic when injected subcutaneously into mice. These cells were utilised in our study as they were hyperproliferative and did not express BMPR-IB. Previous studies were carried out on this cell line, characterising an epithelial-to-mesenchymal-like transition in the presence of BMP4 ligand (Molloy, EL *et al.*, 2008). Here, this model was utilised to characterise the effect of BMPR-IB expression during EMT. We hypothesised that BMPR-IB expression may alter proliferation in BEAS-2B cells and may alter BMP4 induced EMT

For the present study, BEAS-2B cells were transiently transfected with BMPR-IB-pcDNA4 vector (BMPR-IB vector); untransfected cells (no-vector) and pcDNA4 transfected cells (empty-vector) were used as controls in these experiments. Cells were cultured in the presence or absence of 100 ng/ml BMP4 ligand 24 hrs after transient transfection. RNA and protein were harvested on day 2 and day 4 after transfection. BMP pathway activation was characterised in response to BMPR-IB expression in the presence or absence of BMP4 ligand. The effects of BMPR-IB expression on proliferation, EMT like transitions and cell death were investigated.

The BMPR-IB plasmid was generated from mouse cDNA. In order to ensure effects caused in the BEAS-2B human cell line were not due to species differences, BMPR-IB was also transfected into the mouse MLE-12 cell line. The MLE-12 cell line was originally cloned from an adenocarcinoma derived from a SP-C $^{SV40/+}$ transgenic mouse model for lung cancer. MLE-12 cells were briefly assessed to establish if BMPR-IB expression could activate BMP signalling in these cells in the presence or absence of BMP4 ligand.

6.2. Results

6.2.1. Endogenous BMPR-IB Expression

From the literature it is evident that the BMPR-IB receptor is not as widely expressed as the BMPR-IA receptor. RT-PCR analysis was carried out to test the endogenous level of BMPR-IB expression in BEAS-2B and A549 cell lines. Two primers sets were designed against the coding sequence of the gene. BMPR-IB mRNA was detected in A549 cells but not in BEAS-2B cells, using both primer sets (Figure 6.1).

In order to analyse the endogenous protein expression of BMPR-IB in the cell lines and mouse lung samples available in the lab, anti- human/ mouse BMPR-IB antibody (R&D Systems) was used to detect protein expression by Western blot analysis. BMPR-IB

protein was detected in protein extracted from whole mouse lungs (Figure 6.2). Detectable levels of BMPR-IB protein was not observed in A549 or BEAS-2B human cell lines, or in MLE-12 or LA-4 mouse cell lines. BMPR-IB was detected in whole mouse lung positive control

6.2.2. Validation of BMPR-IB over Expression Plasmid

BEAS-2B cells did not express endogenous BMPR-IB mRNA or protein (section 6.2.1). This cell line was therefore used for transient transfection experiments to examine the effects of expressing BMPR-IB cDNA in proliferating lung epithelial cells.

The BMPR-IB-pcDNA4 expression plasmid was generated as described in Chapter 4 section 4.3.3. Functional analysis of the BMPR-IB-pcDNA4 expression vector was carried out by transient transfection into BEAS-2B cells using Lipofectamine 2000. No-vector control (cells only), empty-vector control (pcDNA4), and BMPR-IB vector (BMPR-IB-pcDNA4) were harvested for mRNA and protein to observe the level of BMPR-IB expression.

RT-PCR analysis revealed a high level of BMPR-IB expression generated by the BMPR-IB-pcDNA4 vector, while BMPR-IB was not expressed by the no-vector control or empty-vector control cells (Figure 6.3 A). Immunofluorescence, using anti-myc antibody, validated expression of BMPR-IB vector in BMPR-IB transfected cells and not in the control cells (Figure 6.3 B). Western blot analysis of BMPR-IB protein expression, using the anti-myc antibody, revealed a high level of expression of BMPR-IB vector (Figure 6.3 C). These results indicated the BMPR-IB-pcDNA4 expression vector could positively express the BMPR-IB receptor at an mRNA and protein level.

6.2.3. Localisation of BMPR-IB in BEAS-2B Cells

Confocal microscopy was carried out on BMPR-IB-pcDNA4 transfected cells to observe the localisation of BMPR-IB expression. BMPR-IB vector expression was detected by an anti-myc antibody and DAPI was utilised as a nuclear counter stain.

Confocal microscopy identified high levels of BMPR-IB protein expression in the perinuclear region of the cell, possibly the endoplasmic reticulum (Figure 6.4). Low levels of BMPR-IB expression were localised to areas in the cell membrane.

BMPR-IB expressing cells were treated with BMP4 to establish if the presence of ligand could trigger an increased BMPR-IB localisation to the cell membrane (Figure 6.5). BMP4 treatment of BMPR-IB transfected cells resulted in high levels of BMPR-IB expression adjacent to the nucleus, possibly the endoplasmic reticulum, with lower BMPR-IB expression in areas of the cell membrane and foci localised to the filipodia of cells. There were also levels of BMPR-IB expression in the nucleus the cells (Figure 6.5). Therefore BMPR-IB expression is not exclusive to the cell membrane, and treatment with BMP4, compared to the control, results in nuclear localisation of the receptor.

6.2.4. Duration of Transient Transfection

In order to establish the duration of the BMPR-IB vector expression after transient transfection a time course analysis was established.

Chapter 5 demonstrated that Lipofectamine 2000 was the most efficient non-viral commercially available method of transfection. The transfection ability of BEAS-2B was tested using conditions established for A549 cell line. The pMGFP reporter plasmid was transiently transfected into BEAS-2B and GFP expression was quantified by flow cytometry as an indication of transfection efficiency into this normal transformed human cell line. GFP was expressed in 74.2 (± 10.7) % of BEAS-2B cells (data not shown). This indicates a high transfection efficiency of Lipofectamine 2000 into the BEAS-2B cell line.

Untransfected (no-vector), mock transfected (empty-vector) and BMPR-IB-pcDNA4 (BMPR-IB vector) transfected cells were analysed on day 2, 4 and 7, post transfection for BMPR-IB mRNA expression (Figure 6.6). Day 2 no-vector control cells were normalised to a value of 1 and empty-vector and BMPR-IB vector transfected cells were expressed relative to the untreated control. Densitometry analysis carried out on day 2 RT-PCR demonstrated

no BMPR-IB expression from empty-vector transfected cells (1.9 (± 0.2)) and a significant increase in BMPR-IB transfected cells (152.2 (± 4.8)). On day 4 empty-vector control cells did not express BMPR-IB (1 (± 0.2)) compared to BMPR-IB expressing cells (89.6 (± 1.4)). By day 7 the expression of the BMPR-IB vector had decreased to 57.6 (± 2.7) but was still significantly higher than the empty-vector control. In summary there was a significant increase in BMPR-IB mRNA which was maintained at day 2, 4 and 7, post transfection.

Western blot analysis was utilised to validate the duration of protein expression after BMPR-IB vector transient transfection. Anti-myc antibody detected BMPR-IB-pcDNA4 the expression at day 2 and day 4, post transfection but the level of protein expression was no longer detectable on day 7 (Figure 6.7). Compared to empty-vector control (3.1 (± 1.5)) there was a significant increase in BMPR-IB-pcDNA4 protein expression (52.9 (± 18.1)) on day 2. Day 4 BMPR-IB vector (5.6 (± 1.3)) levels were reduced but remained significantly higher than the empty-vector (1.2 (± 0.4)). By day 7 vector expression was no longer detectable. Therefore functional analysis of transient transfection will only be carried out up to day 4 post transfection.

6.2.5. Activation of BMP Pathway

Transfected cells were cultured in defined serum free media to ensure a controlled culturing condition. Western blot analysis and RT-PCR were carried out to analyse expression of pathway activation in cells expressing BMPR-IB compared to empty-vector control.

p-Smad activation was quantified by Western blot analysis to investigate BMP pathway activation in the presence of BMPR-IB over expression. There was an increase in p-Smad activation 2 days after BMPR-IB expression; despite consistently higher p-Smad protein levels in cells over expressing BMPR-IB, the difference was not statistically significant (Figure 6.8). The expression level of p-Smad decreased consistently on day 4 post transfection compared to empty-vector control, but did not reach significance.

Id-1, an immediate early gene target of BMP signalling, was examined by RT-PCR to quantify pathway activation in the presence of BMPR-IB expression. BMPR-IB expression did not induce Id-1 expression compared to empty-vector control (Figure 6.9).
Smad7, an inhibitory Smad responsible for negative regulation of the BMP pathway, was quantified by RT-PCR. There was no change in Smad7 mRNA expression levels in the presence of BMPR-IB, compared to empty-vector control (Figure 6.10).

In summary BMP pathway appears to be activated, as indicated by increased p-Smad expression. However, neither Id-1 nor Smad7 gene targets were activated by autocrine signalling via BMPR-IB.

6.2.6. Effects on BMP Receptors

Canonical BMP signalling is dependent on BMP pathway activation through pre-formed complexes. Activation of the non-canonical pathway results when ligands induce receptor dimerisation. BEAS-2B cells do not express BMPR-IB endogenously therefore introducing BMPR-IB may change the dynamics of BMP receptor expression. Expression levels of BMPR-IA and BMPR-II in the presence of BMPR-IB expression vector were therefore observed.

BMPR-IA and BMPR-II mRNA expression did not change in the presence of BMPR-IB vector (Figure 6.11 & 6.12).

6.2.7. Effects of BMPR-IB on Proliferation and Cell Cycle

EBAO cell counts were conducted to assess the effects of BMPR-IB over expression on cell proliferation rates. Propidium iodide staining was carried out to establish the effects of BMPR-IB expression on cell cycle.

BMPR-IB expression vector caused a consistent reduction in viable cell number over three experimental repeats; however, the change did not reach statistical significance

(Figure 6.13 A). Day 2 BMPR-IB expression vector resulted in 7.3 x 10^4 (± 1.2 x10^4) viable cells, compared to empty-vector control which had 11 x 10^4 (± 1.2 x 10^4) viable cells. Therefore BMPR-IB expression caused a 0.5 fold reduction in viable cells compared to the empty-vector control. Day 4 post transfection BMPR-IB transfection resulted in 20 x 10^4 (± 6 x 10^4) viable cells compared to the empty-vector control which had 25 x 10^4 (± 7.2 x 10^4) viable cells. Therefore BMPR-IB expression resulted in 0.25 fold decrease in viable cells compared to the empty vector control.

In parallel with the consistent decrease in viable cells, there was an increase in non-viable cells in the presence of BMPR-IB expression (Figure 6.13 B). BMPR-IB expression resulted in 1.5 x 10^4 (± 0.6 x 10^4) non-viable cells, whereas the empty-vector control resulted in 1.1 x 10^4 (± 0.4 x 10^4) non-viable cells. Therefore BMPR-IB expression caused a 0.3 fold increase in non-viable cells 2 days after transfection. However, by day 4 there was a significant increase ($p < 0.05$) in non-viable cells due to BMPR-IB expression (4.6 x 10^4 (± 1.0 x 10^4)) compared to empty-vector control (1.6 x 10^4 (± 0.2 x 10^4)). This increase equates to a 1.8 fold increase of non-viable cells in BMPR-IB transfected cells compared to empty vector control.

To assess if the loss of viable cell number was caused by a halt in cell cycle, propidium iodide staining was carried out on cells transfected with empty-vector and BMPR-IB expressing vector. Cell cycle analysis of day 2 cells revealed no difference between cells that were dead, in G1/G0, in S-phase or in G2/M phase of the cell cycle (Figure 6.14 A). Day 4 analysis revealed no difference in cell cycle phase G0/G1, S-phase or G2/M (Figure 6.14 B). However, there was an increase in cell death in BMPR-IB transfected cells on day 4. This increase in cell death on day 4 concurs with the increase in non-viable cells observed from the EBAO cell counts.

Immunofluorescent pictures of DAPI stained nuclei were taken for empty-vector control and BMPR-IB vector expression. Apoptotic nuclei were apparent from their increased fluorescent intensity and morphology change that is a fragmentation of the DNA creating a vacuolar nucleus. Apoptotic cells were counted and the number was quantified as a

percentage of the entire population in 3 fields of view for 3 experiments. There was a significant increase ($p<0.05$) in apoptotic cells due to BMPR-IB expression (Figure 6.15).

6.2.8. The Effect of BMPR-IB Expression on Motility

Previous studies have observed BMPR-IB localised to filipodia of migrating endothelial cells (Pi, X *et al.*, 2007). A migration assay was carried out to establish if BMPR-IB was involved in cell migration. Cells were transfected with empty-vector control or BMPR-IB vector and a wound was established 24 hrs after transfection. Cells were fixed 24 hrs after the wound was established and stained with crystal violet stain. Cells counts were carried out on cells that had migrated into the denuded area in the well 24 hrs after the wound was established. There was a significant increased ($p < 0.01$) in the number of cells which migrated into the denuded area in BMPR-IB expressing cells compared to the empty-vector control (Figure 6.16).

6.2.9. BMP4 Effects on BMPR-IB Over Expressing BEAS-2B Cells

It has previously been shown that BMP4 treatment of BEAS-2B cells induces an epithelial to mesenchymal (EMT) like transition (Molloy, EL *et al.*, 2008). The EMT process is an important stage in late tumour progression. We have hypothesised that loss of BMPR-IB expression during early tumour development contributes to tumour progression. Therefore, we examined if re-expression of BMPR-IB using over expression vector in BEAS-2B could prevent the EMT like process from occurring in BMP4 treated BEAS-2B cells.

BMP4 ligand has been shown to induce a fibroblast like cell morphology in BEAS-2B cells after 6 days in culture (Molloy, EL *et al.*, 2008). Whereas the Molloy *et al* study utilised cells seeded at low density, BEAS-2B cells in the present culture system were 90 % confluent before the addition of BMP4. On day 2, BMP4 treatment of empty-vector control and BMPR-IB expressing cells appeared to induce a morphology change, with cells becoming more spindle like rather than cobblestoned as is the norm for epithelial

cells (Figure 6.17 A). By day 4, in the presence of BMP4, empty-vector control and BMPR-IB expressing cells had undergone a morphology change to a fibroblast like appearance (Figure 6.17 B). Therefore expression of BMPR-IB did not inhibit the BMP4 induced morphology change in BEAS-2B cells.

BMP4 caused a reduction in proliferation in BEAS-2B cells (Molloy, EL *et al.*, 2008). This reduction in proliferation was also evident in the current experimental system as BMP4 treatment caused a 1 fold reduction in viable cells in the presence of BMP4 ligand (Figure 6.18). However, BMP4 treatment of BMPR-IB expressing cells did not result in a reduction in cell number. In fact there was a 0.5 fold increase in cell number in the presence of BMP4 ligand. By day 4 in the empty-vector control, the reduction of viable cell number due to the presence of BMP4 ligand was no longer evident. The increase in cell number in BMPR-IB expressing cells in the presence of BMP4 ligand remained apparent at day 4. There was no difference in non-viable cell number due to the presence of BMP4 ligand on day 2. On day 4, in both empty-vector control and BMPR-IB expressing cells there was an increase in non-viable cells due to BMP4 treatment. However, the increase in non-viable cells was not statistically significant.

The levels of p-Smad activation increased after the addition of BMP4 ligand to no-vector control, empty-vector control and BMPR-IB vector expression (Figure 6.19). BMP4 ligand sustained p-Smad activation on day 4 in control and BMPR-IB expressing cells.

Immunofluorescence was carried out to observe the localisation of p-Smad in the cells. In empty-vector control cells in the absence of BMP4 ligand p-Smad was dispersed throughout the cell (Figure 6.20 A). In the presence of BMP4 ligand, p-Smad translocated to the nucleus of the empty-vector control cells, as expected (Figure 6.20 B). In contrast, in BMPR-IB expressing cells, p-Smad activation was evident in the absence of BMP4, due to the nuclear localisation of the protein (Figure 6.20 E). Nuclear p-Smad was also observed in BMPR-IB expressing cells treated with BMP4 ligand (Figure 6.20 F). Nuclear localisation of p-Smad is indicative of BMP canonical pathway activation.

Immunofluorescence was carried out to observe if BMPR-IB expression or BMP4 treatment caused abnormal localisation of BMPR-II and BMPR-IA endogenous receptor expression. BMPR-II protein was dispersed throughout the cells in empty-vector control with staining observed in the cytoplasm and nucleus of many cells (Figure 6.21 A). BMP4 treatment of empty-vector transfected cells resulted in the exclusion of BMPR-II from the nucleus (Figure 6.21 B). Cells expressing BMPR-IB both in the absence or presence of BMP4 resulted in cytoplasmic BMPR-II staining. That is BMPR-II staining in BMPR-IB minus BMP4 cells was similar to BMPR-IB plus BMP4 and empty-vector plus BMP4 cells (Figure 6.21 E & F). This suggests BMPR-IB expression causes BMPR-II expression similar to cells treated with BMP4.

Immunofluorescence analysis identified BMPR-IA expression dispersed throughout the cell with intense perinuclear staining in empty-vector control cells in the absence or presence of BMP4 (Figure 6.22 A & B). BMPR-IB transfected cells express endogenous BMPR-IA throughout the cells, with an increase in nuclear concentration compared to control cells (Figure 6.22 E). BMPR-IB expressing cells treated with BMP4 ligand increased the nuclear localisation of BMPR-IA, with some cells expressing BMPR-IA exclusively in the nucleus (Figure 6.22 F). This data suggests BMPR-IB expression causes nuclear localisation of BMPR-IA, and this localisation is enhanced in the presence of BMP4 ligand.

RT-PCR analysis of Id-1 was assessed as a measure of pathway activation (Figure 6.23) BMP4 ligand caused an increase of Id-1 in no-vector control, empty-vector control and BMPR-IB expressing cells. By day 4 the level of Id-1 expression remained higher in BMP4 treated cells compared to BMP4 untreated cells.

mRNA expression analysis of Smad7, an inhibitory Smad which is induced by BMP ligands to negatively regulate the pathway, was conducted as a measure of BMP pathway activation (Figure 6.24). BMP4 ligand caused an induction of Smad7 expression in no-

vector control, empty-vector control and BMPR-IB expressing cells on day 2. Smad7 induction by BMP4 ligand was sustained on day 4.

Another characteristic of BMP4 treatment of BEAS-2B cells is the reduction of E-cadherin expression. RT-PCR analysis was carried out comparing E-cadherin expression in empty-vector control and BMPR-IB expressing cells cultured in the absence or presence of BMP4 ligand (Figure 6.25). As expected BMP4 treatment caused a reduction in E-cadherin mRNA expression in no-vector and empty-vector control. E-cadherin expression was also reduced by 50 %, by BMP4 ligand in BMPR-IB expressing cells. Interestingly BMPR-IB alone, in the absence of BMP4 ligand caused a significant reduction of E-cadherin expression compared to empty-vector control, on day 2. The BMP4 induced reduction in E-cadherin expression remained evident on day 4. However, the reduction of E-cadherin expression caused by BMPR-IB expression alone was not sustained at day 4. On day 2 and day 4, E-cadherin protein expression was reduced by BMP4 ligand (Figure 6.26). The reduction in E-cadherin expression in BMPR-IB expressing cells that was seen at an mRNA level was not evident at the protein level. In fact on day 2 there was a 1.4 fold increase in E-cadherin protein in BMPR-IB expressing cells compared to empty-vector control in the absence of BMP4 ligand, this difference was not maintained at day 4. The down regulation of E-cadherin protein by BMP4 ligand was sustained at day 4 in no-vector control, empty-vector control and BMPR-IB expressing cells.

Immunofluorescence analysis of E-cadherin expression revealed nuclear staining of this protein in BEAS-2B cells. Neither BMPR-IB expression nor treatment with BMP4 ligand affected the localisation of the protein (Figure 6.27).

E-cadherin is regulated at many levels including at the transcriptional level and at the protein level. The decrease in E-cadherin mRNA in BMPR-IB expressing cells on day 2, lead to the investigation of E-cadherin transcriptional regulators. Examination was carried out on the expression of Snail2, a known transcriptional repressor of E-cadherin (Figure 6.28). Investigation of Snail2 mRNA in BMPR-IB expressing cells in the absence

of BMP4 resulted in 17% increase in expression compared to empty-vector control cells, on day 2. In the presence of BMP4, Snail2 mRNA expression was increased in no-vector control, empty-vector control and BMPR-IB expressing cells on day 2 (Figure 6.28). On day 4 the increase in Snail2 expression was sustained in the presence of BMP4. The day 2 pattern of Snail2 was the inverse of the pattern for E-cadherin mRNA expression suggesting Snail2 is responsible for E-cadherin regulation in BEAS-2B cells in the presence of BMPR-IB and BMP4 ligand.

A decrease in the E-cadherin cell-cell adhesion molecule is often associated with increase in motility. BMP4 has previously been shown to increase the motility of BEAS-2B cells (Molloy, EL *et al.*, 2008). Figure 6.16 revealed an increase in motility due to BMPR-IB alone. RT-PCR analysis was carried out to observe the mRNA expression of Crmp2, a gene involved in motility, in BMPR-IB expressing cells in the presence or absence of BMP4 ligand. Crmp2 is a protein involved in neuronal migration that has been found through proteomic studies to be regulated by BMP4 ligand (Moore, JB *et al,* unpublished). RT-PCR analysis revealed expression of BMPR-IB in the absence of exogenous BMP4 ligand resulted in an increase in Crmp2 expression on day 4 (Figure 6.29). On day 2, BMPR-IB expression resulted in a 0.4 fold increase in Crmp2 expression while on day 4, BMPR-IB expression resulted in 1 fold increase in Crmp2 expression, compared to empty vector control. An increase in Crmp2 expression was evident in the presence of BMP4 in no-vector control, empty-vector control and BMPR-IB expressing cells. This data suggests Crmp2 might be involved in the migration of BMPR-IB expressing cells.

6.2.10. Expression of BMPR-IB in MLE-12 Cells

BMPR-IB was transiently expressed in the human BEAS-2B cell line because these cells were a normal transformed cell line and because extensive studies had been carried out in the lab to characterise the effect of BMP4 signalling on these cells. However, BMPR-IB plasmid was generated from mouse cDNA. In order to establish if BMPR-IB had a similar effect in a mouse cell line, BMPR-IB-pcDNA plasmid was transfected into the

MLE-12 cell line. Western blot analysis identified no endogenous BMPR-IB expression in the MLE-12 cell line, therefore we analysed the effect of introducing this plasmid into the cells (Figure 6.2).

Firstly, to validate BMPR-IB mRNA and protein expression in the mouse MLE-12 cell line real time PCR, immunofluorescence and Western blotting were carried out on BMPR-IB transfected cells, using empty-vector transfected cells as a negative control. Real time PCR analysis revealed high levels of BMPR-IB expression in transfected cells (Figure 6.30 A). High levels of BMPR-IB protein expression were evident from immunofluorescence and Western blot analysis on day 2, using anti-myc antibody (Figure 6.30 B & C). The level of BMPR-IB protein expression was not detected by Western blot analysis on day 4, therefore downstream analyses were only carried out for day 2.

6.2.10.1. Localisation of BMPR-IB in MLE-12

Confocal microscopy illustrated high levels of BMPR-IB protein expression found adjacent to the nucleus (possibly the endoplasmic reticulum) and in the nucleus of MLE-12 cells in the absence of BMP4 ligand (Figure 6.31). The pattern of BMPR-IB expression was similar in the presence of BMP4 ligand; that is expression in the nucleus, perinuclear region and dispersed throughout the cytoplasm (Figure 6.32). There were low levels of BMPR-IB expression at the membrane of the cells.

6.2.10.2. Effects of BMPR-IB on Proliferation of MLE-12 Cells

To establish the effects of BMPR-IB expression on MLE-12 an MTS assay was carried out on no-vector control, empty-vector control and BMPR-IB-pcDNA4 transfected MLE-12 cells. An MTS assay was carried out on transfected cells to measure the metabolic activity as a measure of the quantity of active cells in the well, which is an indirect measure of proliferation. The lack of difference in MTS reading between treatments suggests that neither BMPR-IB expression nor BMP4 treatment negatively regulated proliferation in MLE-12 cells (Figure 6.33).

6.2.10.3. Effects of BMPR-IB on BMP Signalling in MLE-12 cells

Western blot analysis was carried out to investigate if BMPR-IB expression in the absence and presence of BMP4 could activate the BMP pathway in MLE-12 cells. BMPR-IB in the absence of BMP4 resulted in an increase in p-Smad, suggesting pathway activation without induction by exogenous ligand (Figure 6.34). Levels of phosphorylated Smad increased in the presence of BMP4 in no-vector control and empty-vector control. p-Smad immunofluorescence staining was high in BMPR-IB expressing cells both in the absence or presence of BMP4. This suggests autocrine activation of p-Smad in the absence of endogenous ligand in BMPR-IB expressing cells (Figure 6.35).

Real time PCR analysis was used to quantify Id-1 expression in BMPR-IB expressing cells cultured in the absence or presence of BMP4 ligand (Figure 6.36). BMPR-IB alone did not increase the expression of the BMP target gene. Administration of BMP4 resulted in Id-1 induction in both empty-vector control and BMPR-IB expressing cells. However, the level of Id-1 induction in BMPR-IB expressing cells in the presence of BMP4 was 0.4 fold greater than empty-vector control treated with BMP4.

Treatment of BMPR-IB expressing BEAS-2B cells with BMP4 ligand resulted in a nuclear localisation of BMPR-IA. Immunofluorescence was carried out to establish if BMPR-IA localised to the nucleus in BMPR-IB expressing MLE-12 cells. BMPR-IA expression in empty-vector control cells was localised to the cytoplasmic membrane, in cells cultured in the absence or presence of BMP4 (Figure 6.37 A & B). Expression of BMPR-IB both in the absence or presence of BMP4 caused an increase in BMPR-IA nuclear localisation (Figure 6.37 E & F).

6.2.10.4. E-cadherin Expression in BMPR-IB Expressing MLE-12 Cells

Real time PCR analysis was carried out on RNA isolated from empty-vector and BMPR-IB expressing cells cultured in the absence or presence of BMP4 ligand (Figure 6.38 A). E-cadherin mRNA levels increased 3.5 fold in BMPR-IB expressing cells compared to

empty-vector control in the absence of BMP4 ligand. Treatment of empty-vector control cells with BMP4 ligand resulted in an increase in E-cadherin mRNA. The level of E-cadherin mRNA expression in BMPR-IB expressing cells in the absence of BMP4 was similar to the BMPR-IB expressing in the presence of BMP4 ligand.

E-cadherin protein expression was quantified by Western blot analysis (Figure 6.38 B & C). BMPR-IB expression in the absence of ligand resulted in an augmentation of E-cadherin protein expression compared to empty-vector control, in the absence of BMP4 ligand. This pattern of expression paralleled that seen for mRNA expression. An increase in E-cadherin protein levels was evident in empty-vector control cells in the presence of BMP4 ligand compared to in the absence of BMP4 ligand. There was no additional increase in E-cadherin expression in BMPR-IB expressing cells with the addition of BMP4 ligand; however, the level of E-cadherin was comparable to the empty-vector control in the presence of BMP4.

Immunofluorescence was carried out to establish the localisation of E-cadherin (Figure 6.39). BEAS-2B unusually had nuclear E-cadherin staining. However, E-cadherin was localised to the cell membrane in the MLE-12 cell line. Expression of neither BMPR-IB nor treatment with BMP4 altered the localisation of the E-cadherin protein in these cells.

Figure 6.40 represents a summary of effects occurring in the presence of BMPR-IB expression and in the absence or presence of BMP4 ligand.

6.3. Discussion

Numerous studies have been conducted to understand the roles of BMPR-IB *in vitro* and *in vivo*. Several lines of evidence have implicated aberrant BMPR-IB expression in human disease. In Chapter 3 it was shown that loss of BMPR-II and BMPR-IB expression occurred at the early stages of tumour progression in the lungs of K-ras^{G12D} expressing mice. We hypothesised that BMPR-IB receptor possesses anti-proliferative properties, whereby loss of its expression at the early stages of cancer progression contributes to proliferation and tumour formation. To investigate this hypothesis BMPR-IB expression vector was generated, as described in Chapter 4. BMPR-IB vector was transiently transfected into BEAS-2B cells which are devoid of BMPR-IB endogenous expression, to investigate its tumour suppressor effect.

BMP receptors are widely expressed in mammalian cells. BMPR-IA and BMPR-IB are more closely related than other type I receptors. Although BMPR-IB is less widely distributed and is expressed at a later embryonic stage than BMPR-IA, these two receptors are co-expressed in many tissues in the developing embryo and in adult tissue (Dewulf, N *et al.*, 1995). BMPR-IB receptor expression has been noted in cells of the heart (Inai, K *et al.*, 2008), retina (Hocking, JC and McFarlane, S, 2007), colon (Kodach, LL *et al.*, 2007), neurons (Lee, J *et al.*, 2008) and the lung (Rosendahl, A *et al.*, 2002), among others. BMPR-IB is less widely expressed compared to BMPR-IA; BMPR-IB expression has not been detected in human thyroid (Suzuki, J *et al.*, 2005), BMRIA is expressed at higher levels in 2T3 osteoblast cell line (Chen, D *et al.*, 1998) and lung (Rosendahl, A *et al.*, 2002). Altered BMPR-IB expression has been discovered in disease phenotypes including rheumatoid arthritis (Marinova-Mutafchieva, L *et al.*, 2000), tracheoesophageal fistula (Crowley, AR *et al.*, 2006), and asthma (Rosendahl, A *et al.*, 2002). In this study BMPR-IB was found to be expressed in mouse lung. However, BMPR-IB protein expression was not detected in the lung epithelial cell lines A549, BEAS-2B and MLE-12. These cell lines are either derived from adenocarcinoma (A549 and MLE-12) or immortalised with SV40 T-antigen (BEAS-2B), resulting in perpetual

proliferation. Lack of BMPR-IB protein expression in these immortalised cells corresponds with BMPR-IBs potential function in negatively regulating proliferation.

In control BEAS-2B cells in the absence of exogenous BMP ligand stimulation, there is a baseline level of phosphorylated receptor mediated Smad 1, 5, 8 (p-Smad), indicative of pathway activation. BEAS-2B cell line can endogenously express both BMP2 and BMP4 ligand; these cells, therefore, have the potential to activate their own BMP signalling pathway in an autocrine manner. Immunofluorescence data revealed the disperse localisation of p-Smad throughout the empty-vector control cells. BMPR-IB expression resulted in an increase in receptor mediated Smad phosphorylation and induced a nuclear translocation of the protein, indicative of active signal transduction. In the presence of exogenous BMP4 ligand, there was a two fold increase in p-Smad activation in empty-vector control cells. BMP4 stimulation of BMPR-IB expressing cells resulted in an increase of p-Smad activation comparable to, but not exceeding, the BMP4 treated control. BMPR-IB expression did not contribute to an increase in p-Smad activation in the presence of BMP4 ligand compared to the control suggesting maximum Smad phosphorylation is achieved in control cells in the presence of BMP4 ligand. Baseline p-Smad expression, in MLE-12 empty-vector control cells, was localised to the nucleus. BMPR-IB expression resulted in an increase in receptor mediated Smad phosphorylation and nuclear localisation of the protein.

The data indicated an increase in the intensity of p-Smad expression in cells which occurred more frequently in BMPR-IB expressing cells and BMP4 treated cells, in both BEAS-2B and MLE-12 cell line. Examination of the DAPI stained nuclei identified the intensely stained cells as undergoing cell division or apoptosis. It appears that p-Smad is either expelled from the nucleus or prevented from entering the nucleus during these processes. Smad proteins reside in the cytoplasm and are phosphorylated by an activated type I BMP receptor. In the presence of the co-operating smad, Smad 4, the phosphorylated R-Smad is shuttled into the nucleus and activates a number of target genes. There are a number of regulatory mechanisms that restrict the p-Smad protein to the cytoplasm preventing their entry into the nucleus and subsequent gene regulation.

This suggests activated p-Smad may be sequestered in the cytoplasm and prevented from entering the nucleus and activating its target genes. One mode of possible p-Smad inhibition is caused by MAPK and GSK2 phosphorylation on the linker region of the R-smad, which targets the protein for ubiquitination by Smurf1 E3 ligase (Verheyen, EM, 2007).

p-Smad activation, induced by BMP4 ligand, caused the activation of BMP gene targets such as Id-1 and Smad7. p-Smad increase in BMPR-IB expressing cells, in the absence of BMP4 ligand, did not result in Id-1 or Smad7 activation. The inconsistency between p-Smad activation and BMP target activation may be due to the quantity of BMP4 ligand present. It has been previously shown that there is a threshold of BMP activation required to activate Smad canonical BMP signalling pathway. In the absence of sufficient BMP ligand, BMP signalling is activated through the non-canonical MAPK pathway. Low levels of BMP7 (0.25nM) increase p38-MAPK signalling, whereas high doses of BMP7 (10nM) cause an inhibition of MAPK and an activation of Smad1 dependent signalling (Hu, MC *et al.*, 2004). In the present study exogenous expression of BMP4 is sufficient to activate BMP signalling through Smad proteins thereby activating BMP target genes, however, autocrine levels of BMP ligand is not sufficient to activate BMP target genes in the presence of BMPR-IB over expression. Another possible reason for the lack of Id-1 and Smad7 activation may be due to alternative target gene activation. There are many other BMP pathway targets; examination of these other target genes was beyond the scope of this study.

BEAS-2B cells were transformed with the SV40 large T-antigen to generate an immortalised cell line. *In vitro* analysis of BMPR-IB expression in BEAS-2B cells resulted in a decrease in viable cell numbers and an increase in non-viable cell numbers. Propidium iodide analysis of BMPR-IB expressing BEAS-2B showed the loss of viable cell numbers was not due to a halt in cell cycle. The increase in non-viable cells, as determined by EBAO cell counts; the increase in apoptotic cell population, as determined by propidium iodide flow cytometry analysis; and the increase in apoptotic bodies in the BMPR-IB expressing cells as determined by DAPI microscopy indicate the involvement

of BMPR-IB in negatively regulating proliferation. We proposed BMPR-IB possess anti-proliferative properties, and the involvement of BMPR-IB in regulating apoptosis contributes to this hypothesis. Early studies characterising BMPR-IB expression in the developing embryo revealed its role in promoting apoptosis. In the developing limb constitutively active BMPR-IB (caBMPR-IB) expression causes an increase in cell death as seen by an increase in cartilage condensation. Whereas inhibition of signalling via BMPR-IB, achieved by expressing a dominant negative BMPR-IB (dnBMPR-IB), results in a reduction of apoptosis as visualised by an increase in webbing in the developing limb bud. These findings verify the involvement of BMPR-IB in apoptosis in the developing limb (Zou, H *et al.*, 1997). Expression of caBMPR-IB in the neural tube of the developing embryo resulted in an increase in apoptosis, indicated by an increase in caspase3 expression, and a halt in neural tube closure (Panchision, DM *et al.*, 2001). Expression of caBMPR-IA and dnBMPR-IA did not regulate apoptosis confirming that apoptosis is a specific function of BMPR-IB in the developing embryo. The role of BMPR-IB may also be linked to apoptosis as many reports show the loss of BMPR-IB during cancer progression, for example a decrease in BMPR-IB expression correlates with increased tumour grade in prostate cancer (Kim, IY *et al.*, 2000). Loss of BMPR-IB in tumour initiating cells renders the cells in a proliferative dedifferentiated state (Lee, J *et al.*, 2008). It has been suggested that BMPR-IB's negative effect on proliferation is restricted to stem and progenitor cells (Lee, J *et al.*, 2008). We have shown that BMPR-IB expression has the potential to negatively regulating proliferation by inducing apoptosis in a well differentiation immortalised cell line. The loss of BMPR-IB during the early proliferative stages of lung tumourigenesis implicates the potential of BMPR-IB re-expression in inducing apoptosis and negatively regulating proliferation in the early stages of lung cancer.

It has been shown in these and previous studies that BMPR-IB negatively regulates proliferation; it is also true that BMPR-IB positively regulates differentiation. The involvement of BMPR-IB in the differentiation process has been shown in early functional studies. Constitutively active BMPR-IB is responsible for the differentiation of progenitor cells into chondrocytes and osteoblast (Chen, D *et al.*, 1998; Gilboa, L *et al.*,

2000). Expression of dnBMPR-IB in 2T3 cells inhibit BMP2 induction of bone matrix formation while expression of dnBMPR-IA did not have this inhibitory effect on differentiation, suggesting BMPR-IB is involved in osteoblast differentiation whereas BMPR-IA is not. BMPR-IB is expressed downstream of BMPR-IA in neural progenitor cells, BMPR-IB expression is concurrent with the switch from proliferation to differentiation of neural progenitor cells (Panchision, DM *et al.*, 2001). Re-expression of BMPR-IB into poorly differentiated glioblastoma cells resulted in an increase in differentiation of these cells. These studies show the ability of BMPR-IB to induce differentiation of tumour initiating cells (Lee, J *et al.*, 2008). In the present study the BEAS-2B lung epithelial cells are terminally differentiation and therefore it was not possible to establish the involvement of BMPR-IB in lung epithelial differentiation. However, administration of BMP4 ligand to control and BMPR-IB expressing cells was used to investigate the role of BMPR-IB in differentiation. BMP4 has been shown to cause a trans-differentiation from epithelial to mesenchymal phenotype (EMT) in BEAS-2B cells (Molloy, EL *et al.*, 2008). We hypothesised that expressing BMPR-IB would prevent the EMT process in BEAS-2B cells. In the presence of the BMP4 ligand, BEAS-2B cells undergo a loss of E-cadherin expression and an increase in E-cadherin transcriptional repressors such as snail and twist, which are hallmarks of EMT during development and carcinogenesis (Molloy, EL *et al.*, 2008). Also BEAS-2B cells became more motile and cell morphology changed to be more mesenchymal, in the presence of BMP4. We hypothesised that if BMPR-IB acts as a positive regulator of differentiation then it would be able to prevent these EMT like changes from occurring in the BEAS-2B cell line.

The most evident effect of BMP4 ligand on BEAS-2B cells is the change in cell morphology from a cuboidal shape to a thin fibroblast like cell phenotype. In the presence of BMP4 ligand, on day 2 there appeared to be a less mesenchymal like morphology in BMPR-IB expressing cells compared to empty-vector control. However, by day 4 the mesenchymal like phenotype adopted by the BEAS-2B cells was exacerbated by BMPR-IB expression compared to the empty-vector control. The EMT transition occurring in BMPR-IB expressing cells may be due to BMP4 signalling via the

BMPR-IA receptor which remained endogenously expressed in the cells. This EMT effect via BMPR-IA may be too potent to be inhibited by BMPR-IB. In fact activation of the EMT like process via BMPR-IA may utilise BMPR-IB migratory function and pro-differentiation function to drive the mesenchymal phenotype at an accelerated rate. That is, once the EMT effect is initiated via BMPR-IA, BMPR-IB may contribute to the trans-differentiation.

BMP4 treatment of BEAS-2B cells causes a 15 fold reduction in E-cadherin expression (Molloy, EL *et al.*, 2008). The E-cadherin cell-cell adhesion molecule is down-regulated in many cancers and correlates with poor prognosis (Beavon, IR, 2000). BMPR-IB expressing BEAS-2B cells result in a down regulation of E-cadherin expression. Loss of E-cadherin expression is consistent with increased tumour grade and therefore conflicts with BMPR-IB function as a potential tumour suppressor. However, immunofluorescence data shows E-cadherin is localised to the nuclei of BEAS-2B cells. Although a function for nuclear E-cadherin is unknown, its nuclear localisation has previously been reported in cancer. Aberrant nuclear E-cadherin staining has been reported in Merkel cell carcinoma, epithelioid sarcoma, breast cancer carcinoma and Wilms disease of the kidney (Alami, J *et al.*, 2003; Han, AC *et al.*, 2000; Saito, T *et al.*, 2001; Sauer, T *et al.*, 2001). The loss of E-cadherin expression from the cell membrane is consistent with increased tumour grade; however, the existence of nuclear E-cadherin has only been noted during tumour progression. Therefore nuclear E-cadherin may have an oncogenic function. A reduction of E-cadherin mRNA expression in BMPR-IB expressing cells is in fact a down regulation of nuclear E-cadherin. This attenuation of oncogenic nuclear E-cadherin may support a potential tumour suppressor role for BMPR-IB. To add to the complexity of the role of E-cadherin in BEAS-2 B cells; BMP4 treatment causes a reduction in E-cadherin expression in no-vector control, empty-vector control and BMPR-IB vector treated cells. BMP4 treatment causes an increase an EMT like phenotype, which is dependent on epithelial cells loosing their cell-cell adhesion junctions thereby increasing their motility. However, attenuation of E-cadherin by BMP4 cannot be attributed to a loss in cell-cell adhesion and an increase in motility due to its nuclear localisation in these cells. E-cadherin is localised to the cell membrane in MLE-12 cells. Expression of

BMPR-IB resulted in an increase in E-cadherin mRNA and protein. The increase of E-cadherin by BMPR-IB supports the potential tumour suppressor role for BMPR-IB.

E-cadherin expression is tightly regulated at a transcriptional and post-translational level (described in section 1.6.5). The significant decrease in E-cadherin mRNA expression caused by BMP4 ligand correlates with an increase in Snail2 expression. Therefore the loss of E-cadherin expression in the presence of the BMP4 ligand is regulated by transcriptional repressors. The significant level of E-cadherin attenuation in BMPR-IB expressing cells does not correlate with a significant increase in Snail2 mRNA expression. Snail 2 is one of many transcriptional regulator of E-cadherin expression, and further investigation may reveal a number of transcriptional repressors contributing to the reduction in E-cadherin expression.

The loss of BMPR-IB expression at the early stages of tumour progression suggests BMPR-IB might have tumour suppressor properties. However, BMPR-IB expression has been shown in human lung adenocarcinoma tissue (Figure 3.21). This suggests BMPR-IB might have a positive effect on tumour progression at the later stages of cancer. Strong BMPR-IB expression has previously been shown to correlate with poor prognosis in breast cancer patients (Helms, MW *et al.*, 2005), verifying a potential tumour promoting function for BMPR-IB. These opposing roles for BMPR-IB can be explained by the stage of tumour progression. Lung tumours analysed from the K-ras^{G12D} mouse in chapter 3 were composed of well differentiated, proliferating cells. When lung cancer develops into a carcinoma the cells are less well differentiated and have the potential to metastasise to other areas of the body. The metastatic phenotype of a cancer is characterised by its ability to migrate, a process which BMPR-IB is involved in. The function of BMPR-IB in epithelial cells has not been elucidated; however, BMPR-IB has been shown to be necessary for endothelial cell migration and for angiogenesis. Treatment with BMP2 or expression of caBMPR-IB can result in the migration of mesenchymal cells. Conversely treatment with Noggin or expression of dnBMPR-IB inhibited migration of these mesenchymal cells (Inai, K *et al.*, 2008). Treatment of mouse embryonic endothelial cells with BMP6, which has a higher affinity for BMPR-IB, compared to BMPR-IA

(Brederlau, A *et al.*, 2004), caused an increase in myosin-X expression, a protein involved in filipodia formation. An increase in myosin-X expression in endothelial cells, induced by BMP6 ligand, correlates with an increase in filipodia formation and increased migration (Pi, X *et al.*, 2007). Stimulation of endothelial cells with BMP6 caused BMPR-IB to localise with myosin in the filipodia's formed by the cells. From this data BMPR-IB appears to be necessary for the induction of migration via BMP6 stimulation but also translocates to the migrating filipodia. In our study confocal microscopy revealed BMPR-IB protein localised to the filipodia of BEAS-2B cells treated with BMP4. The cell migration assay confirmed the increase in migration of BMPR-IB expressing cells compared to the empty-vector control. RT-PCR analysis revealed an increase in Crmp2 protein in BMPR-IB expressing BEAS-2B cells. Crmp2 (collapsing response mediator protein) is a transducer molecule for the semaphorin signalling pathway. This molecule plays a critical role in migration of cells, namely neurons and T lymphocytes (Charrier, E *et al.*, 2003; Vincent, P *et al.*, 2005). Crmp2 has been associated with a range of biological functions similar to BMPR-IB including proliferation, differentiation, apoptosis and migration (Charrier, E *et al.*, 2003). Therefore we hypothesis that re-expression of BMPR-IB in lung adenocarcinoma can increase the rate of cancer progression by contributing to the motility of cancer cells. Elucidation of the exact signals and mechanisms that control this migratory process will lead to a better understanding of BMPR-IB's potential role in migration and metastasis.

Confocal microscopy was carried out to establish the localisation of the BMPR-IB receptor in BEAS-2B cells. BMPR-IB staining was localised to pockets within the plasma membrane of BEAS-2B cells cultured in the absence of BMP4. The majority of BMPR-IB expression was localised to an area adjacent to the nucleus, which may possibly be the endoplasmic reticulum, an area where newly produced protein is post translationally modified before being transported to the area where they function. In MLE-12 cells BMPR-IB appeared dispersed throughout the cytoplasm. Activated BMP receptors undergo rapid internalisation, to negatively regulate the signal cascade. Receptors which are internalised either undergo recycling to the membrane or are transported to lysosomes for degradation (Katzmann, DJ *et al.*, 2001). A study conducted

by Hartung *et al* showed HA-BMPR-IB (BMPR-IB tagged at the amino terminal domain) undergoes constitutive endocytosis via clathrin coated pits, and has a half life of 14 minutes (Hartung, A *et al.*, 2006). Investigations into Smad dependent and independent signalling revealed receptors localised to different areas of the plasma membrane resulted in alternate downstream signalling. Pre-formed complexes of type I and type II receptor resided in non-raft regions of the plasma membrane, phosphorylated receptor mediated Smad proteins at the membrane, and undergo clathrin coated endocytosis for downstream signalling and target gene activation. Signalling through BMP induced signalling complexes require receptors to associate with rafts and caveolae at the membrane. The rapid rate of receptor endocytosis may explain the low levels of BMPR-IB observed at the membrane of our cells.

Immunofluorescence analysis of BMPR-IA and BMPR-II proteins in BEAS-2B cells revealed low membrane localisation of the proteins. As mentioned above receptors are rapidly internalised via clathrin coated pits. Internalisation of receptors functions to negatively regulate BMP pathway signalling. The main localisation of BMPR-IA and BMPR-II staining in BEAS-2B cells is cytoplasmic and perinuclear suggesting the receptors remain in the endoplasmic reticulum awaiting transport out to the membrane or have been endocytosed and reside in lysosomes awaiting degradation. However, BMPR-IA is localised to the plasma membrane of MLE-12 cell line. Previous reports have identified BMPR-IA localised to the cytoplasm and perinuclear areas of NTERA2 cells (derived from human testicular carcinoma) (Nishanian, TG and Waldman, T, 2004). Therefore the lack of plasma membrane staining seen in BEAS-2B may be due to the specific cell type. Interestingly BMPR-IB expressing BEAS-2B cells in the presence of BMP4 ligand had nuclear localised BMPR-IA. Also MLE-12 cells expressing BMPR-IB in the absence and presence of BMP4 ligand possessed nuclear localised BMPR-IA. Confocal analysis of BMPR-IB showed nuclear localisation of the receptor in BEAS-2B cells stimulated with BMP4 and in MLE-12 cells cultured in the presence or absence of the BMP4 ligand. Although the function of nuclear BMPR is unknown their nuclear localisation suggests they may act as transcriptional regulators. BMPR-IA has been shown to associate with SF 3b4, a protein involved in the spliceosome in the nucleus

(Nishanian, TG and Waldman, T, 2004; Watanabe, H *et al.*, 2007). BMPR-IA has been shown to function upstream of BMPR-IB, perhaps nuclear BMPR-IA is a component of the regulatory complex for BMPR-IB expression. This would explain the nuclear localisation of BMPR-IA in BMPR-IB expressing MLE-12 cells.

Lipofectamine 2000 transfection of pMGFP into BEAS-2B cells resulted in 70% transfection efficiency. This efficiency was assumed for BMPR-IB-pcDNA4. Even though the transfection efficiency was high, a dilution effect, from 30% of the cells which do not express the plasmid, was still occurring. Another technical difficulty with transient transfection is the heterogeneous expression of the plasmid. Transfected cells expressed different copy numbers of the BMPR-IB gene; this is evident in the fluorescent pattern in the anti-myc immunofluorescence. To overcome these technical difficulties, ideally stable cell lines would be established. Establishment of stable clones would ensure 100% of the population expresses the same copy number of the gene. Also different lines of stable transfectants can be established to express increasing copy number of the transgene. Future experiments would benefit from the generation of BMPR-IB expressing cell lines for further characterisation of the processes affected by this type I signalling receptor.

In our experimental system the BMP4 ligand was chosen to activate the BMP pathway because of its ability to stimulate an EMT-like effect in BEAS-2B cells, a process that occurs during tumour development. BMP ligands, however, have different binding affinities to BMP type I receptors as described in section 1.7. Of the three sub-groups of BMP ligands BMP2 and BMP4 ligands preferentially bind BMPR-IA and BMPR-IB (Chen, D *et al.*, 2004). Yet, BMP2 has been shown to preferentially bind BMPR-IA over BMPR-IB (Brederlau, A *et al.*, 2004). Ligands from the OP1 and GDF5 groups have also been found to bind with high affinity to BMPR-IB. Therefore the use of BMP4 ligand in these experiments may have a higher affinity for endogenous BMPR-IA receptor and not signal through the BMPR-IB over expressing receptor (Chen, HL and Panchision, DM, 2007; Panchision, DM *et al.*, 2001). That is, a BMPR-IB specific signalling effect may not be fully achieved due to the specificity of the ligand. To overcome this potential

difficulty of assessing the function of BMPR-IB expressing in lung epithelial cells, future experiments would benefit from the addition of ligands with a higher affinity for BMPR-IB compared to BMPR-IA. For example BMP6 or BMP7 have been shown to have a higher affinity for BMPR-IB compared to BMPR-IA (Brederlau, A *et al.*, 2004; Chen, D *et al.*, 2004). Also BMPR type I receptors have been reported to have different binding affinities to BMPR-II, in the presence of BMP-2, -4 and -7 (Rosenzweig 1995, Liu 1995, Nohno 1995). Therefore another method that would ensure signalling through BMPR-IB would be to knock down BMPR-IA. Attenuation of BMPR-IA by siRNA or use of a BMPR-IA$^{-/-}$ cell line would ensure BMP signalling occurs through BMPR-IB, and specific signalling outcomes could be determined.

BMPR-IB has been implicated in many biological processes. In this chapter we have shown BMPR-IB contributes to negative regulation of proliferation, positive regulation of apoptosis, positive regulation of differentiation and positive regulation of migration. We had hypothesised that BMPR-IB acts as a potential tumour suppressor like molecule, but the picture is a lot more complicated than this. Our results suggest that BMPR-IB may contribute to different functions depending on the tumour stage. The BMP pathway interacts with many other signal pathways and this cross-talk and interaction will influence the function of BMPR-IB expression and downstream targets. While our original hypothesis of BMPR-IB acting as a potential tumour suppressor in the early proliferative stages of lung cancer is consistent with some of our results, it has not been proven here. However, this remains a very interesting platform from which future studies can be conducted to address the specific function of BMPR-IB during each tumour stage.

7. Rat Nitronaphthalene Lung Damage Model

7.1. Introduction

Mechanisms of cellular damage caused by 1-NN in the lungs have been well characterised but little is known about the molecular mechanisms that drive the subsequent repair process in the airways. We hypothesised that the BMP signalling pathway that is expressed during lung development may also be important during the lung repair process after chemical damage in the adult lung. The rat 1-NN model of lung damage was used to assess this hypothesis.

Many cell proliferation studies have been carried out to study the effects of naphthalene damage on mouse lungs (reviewed in section 1.4). In this study 1-NN was used to induce Clara cell damage in rats. 1-NN is the most highly abundant nitro polycyclic aromatic hydrocarbon in the atmosphere. As described in section 1.5 it is a by-product of diesel combustion and is therefore found in high quantities in urban areas. Naphthalene which is also a by-product of diesel combustion becomes nitrosylated in the atmosphere to form nitronaphthalene (1-NN). Therefore 1-NN is a more physiologically relevant toxin in animal studies compared to the parent chemical compound naphthalene. Previous studies have shown the toxic effect of 1-NN on the lungs of rodents, causing epithelial damage (section 1.5). No study to date has observed the signalling pathway expression during the damage and repair process in the lungs. This study examines the effects of 1-NN on the lungs of rats; these model animals provide a large protein yield for examination.

Two animal groups were used in our model; 4 Sprague-Dawley rats per group were administered 50 mg/kg 1-NN in oleic oil vehicle or vehicle only and the lungs of the animals were harvested at 6, 24, 48 and 96 hrs post treatment. One animal per treatment/ time course was harvested for lung tissue and 3 animals were harvested by lysis lavage for protein. To validate the 1-NN injury model, lung tissue was stained with hematoxylin and eosin to observe the epithelial damage. Lysis lavage protein was examined for a marker of proliferation (PCNA) and differentiation (E-cadherin), to validate the time points at which lung damage and repair occur. Cell adhesion complex proteins were

examined for their involvement during epithelial repair. Expression of components of the BMP pathway, namely p-Smad, Smad4 and BMPR-IA, were characterised in this model.

7.2. Results

Injection of rats with 1-NN was carried out by our collaborators Dr. Alan Buckpitt (University California, Davis, California, USA). Protein, cells and tissue were harvested by Dr. Joanne Masterson (from Dr. Shirley O'Dea lab at the National University of Ireland, Maynooth) while carrying out a placement in Dr. Buckpitt's lab.

The lysis lavage procedure, carried out by Dr. Joanne Masterson, has previously been described in detail (Wheelock, AM *et al.*, 2004). This procedure allows high yield purified Clara cells from the epithelial airways with minimum contamination of other cell types compared to previous epithelial cell isolation methods.

7.2.1. 1-NN Induced Epithelial Cell Damage in Rat Airways

In order to validate the 1-NN model, rat lung tissue sections were stained with hematoxylin and eosin (H & E) to determine epithelial damage caused by 1-NN administration. Untreated control tissue sections were considered undamaged lung tissue (Figure 7.1 a & 7.1 b). No cellular damage was evident at 6 hrs in either vehicle control (Figure 7.1 c) or 1-NN treated (Figure 7.1 d) lungs. At 24 hrs the epithelial cells were as expected of healthy lungs, cuboidal and tightly packed in the vehicle control lung (Figure 7.1 e). In contrast 1-NN treatment caused exfoliation of the epithelial lining at the 24 hr time point (Figure 7.1 f). Thin flattened squamous cells were apparent at the basement membrane, in the location of lost columnar epithelial cells. At 48 and 96 hrs epithelial cells were present in the conducting airways (Figure 7.1 g & 7.1 i). However, in comparison to the vehicle control tissues; 1-NN treated epithelial cells were more flattened with less cytoplasmic columnar regions (Figure 7.1 h & 7.1 j).

7.2.2. 1-NN Induced Infiltration of Immune Cells

Bronchiolar alveolar lavage fluid (BALF) was recovered during the lysis lavage procedure. Cell counts were carried out to determine the number of inflammatory cells that had migrated to the lung after the 1-NN treatment at each time point. The untreated rat resulted in 1 x 10^4 cells/ml in BALF; this number of immune cells represented the untreated baseline. There was a significant increase in inflammatory cells at 6 hrs after 1-NN treatment compared to vehicle control (Figure 7.2). The number of inflammatory cells caused by 1-NN treatment reduced after this time point. Compared to the one untreated control animal, the oleic oil vehicle caused an increase in inflammatory cells at all time points. This indicated the vehicle was not without effect in these animals. However, the significant increase in BALF cells after 1-NN treatment compared to the vehicle control at the 6 hr time point signified the 1-NN treatment caused an enhanced inflammatory response compared to the oleic oil vehicle.

7.2.3. Cell Proliferation in Response to 1-NN

Proliferating cell nuclear antigen (PCNA) is involved in the S phase of the cell cycle. In normal healthy lungs epithelial cells have a low mitotic rate and this rate of division increases after epithelial damage in order to repair the epithelial membrane. In this rat lung repair model, the distal airways were denuded of their epithelial cells 24 hrs after 1-NN administration. PCNA was used to establish the time point at which cellular repair began after 1-NN induced epithelial damage.

Immunofluorescence was carried out on vehicle control and 1-NN treated rat lung tissue at the 6, 24, 48 and 96 hour time points in order to visualise the localisation of PCNA expression in the airways (Figure 7.3). PCNA expression was localised to the nuclei of epithelial cells. Although this procedure is not quantitative increased levels of PCNA expression were evident in 48 hr and 96 hr 1-NN treated airways. The airways of the untreated control rat resulted in a low level of PCNA expression that is representative of steady state lung mitosis (Figure 7.3 a). The airways of the 6 hr vehicle control animal (Figure 7.3 b) and the 6 hr 1-NN treated animal (Figure 7.3 c) had similarly low levels of

PCNA expression compared to the untreated control. Low levels of PCNA were apparent in the lungs of the 24 hr vehicle control (Figure 7.3 d) and 24 hr 1-NN treated (Figure 7.3 e) animals. Increased nuclear PCNA staining was apparent in the epithelial cells in the airways of 1-NN treated rats at 48 hr (Figure 7.3 g) compared to the 48 hr vehicle control (Figure 7.3 f). High levels of PCNA were also apparent in the 96 hr 1-NN treated lung (Figure 7.3 i) compared to the 96 hr vehicle control lung (Figure 7.3 h).

Western blot analysis was carried out on lysis lavage protein to quantify PCNA in vehicle control and 1-NN treated animals at 6, 24, 48 and 96 hour time points (Figure 7.4 A & B). The relative expression of PCNA for control and 1-NN treatment at each time point was graphed in Figure 7.4 C. The level of PCNA expression for untreated control was normalised to a value of 1 and the vehicle control and 1-NN treated values at each of the time points were expressed relevant to the untreated control (Figure 7.4 C). At the 6 hr time point PCNA expression did not differ between vehicle control (1.3 (± 0.3)) and 1-NN treatment (1.3 (± 0.2)). At 24 hrs there was a slight decrease in PCNA expression in 1-NN treated animals (1.3 (± 0.3)) compared to the vehicle control (1.7 (± 0.02)). At 48 hrs 1-NN caused an increased in PCNA expression (1.0 (± 0.6)) while vehicle control PCNA levels were 0.6 (± 0.1). The greatest PCNA increase occurred at 96 hrs after 1-NN treatment (2.2 (± 0.6)), compared to the vehicle control (1.0 (± 0.2)). Compared to the untreated control animal the levels of PCNA expression fluctuated; 6 hr and 24 hr protein had higher levels of PCNA compared to 48 hr and 96 hrs vehicle control animals. This increase in cell proliferation may be due to the oleic oil vehicle.

7.2.4. E-cadherin Expression was Affected by 1-NN Treatment

The cell-cell adhesion molecule, E-cadherin, is expressed in well differentiated epithelial cells. The level of E-cadherin expression in lung epithelial cells was quantified in 1-NN treated animals. Immunofluorescence analysis of E-cadherin expression revealed membranous staining in the epithelial cells of the airway in vehicle control and 1-NN treated animals (Figure 7.5). Western blot analysis was carried out on lysis lavage protein from the rats to quantify the amount of E-cadherin in the lungs during the time course.

Western blot analysis of E-cadherin resulted in a double band (Figure 7.6). E-cadherin is 120 kDa and is represented by the lower band. The upper band may be the E-cadherin precursor, a post translationally modified form of the protein or possibly even N-cadherin (Brady-Kalnay, SM *et al.*, 1998). Quantification of E-cadherin was carried out by analysing the densitometry values for the E-cadherin bands and normalising each to their respective actin value, average values were graphed for each time point and treatment (Figure 7.6 C). At 6 hrs there was a slight decrease in E-cadherin expression in 1-NN treated lungs (0.11 (± 0.04)) compared to vehicle control lungs (0.17 (± 0.06)) and at 24 hrs there was an increase in E-cadherin expression after 1-NN treatment (0.23 (± 0.01)) compared to the vehicle control (0.14 (± 0.04)), although these differences did not reach statistical significance. No difference was observed at the 48 hr time point between vehicle control (0.20 (± 0.06)) and 1-NN treated (0.22 (± 0.04)) lungs. At 96 hrs E-cadherin expression was significantly reduced ($p < 0.01$) in 1-NN treated lungs (0.06 (± 0.02)) compared to vehicle control (0.16 (± 0.01)). The reduction in E-cadherin at 96 hrs suggested the epithelial cells were not fully differentiated at this time point. The reduction in E-cadherin at 96 hrs concurred with the increase in PCNA at this time point, as a decrease in E-cadherin is necessary for epithelial cell division. E-cadherin values for vehicle controls at each time point did not differ suggesting the oleic oil vehicle did not have an effect on the expression of the cell-cell adhesion molecule.

7.2.5. Adhesion Complex Proteins are Differentially Expressed following 1-NN Treatment

The catenin proteins are required for the E-cadherin adherence junction complex. Western blot analysis was carried out to quantify α-, β-, and γ- catenin proteins from rat lysis lavage protein treated with vehicle control or 1-NN. There was a significant loss ($p < 0.05$) of α-catenin at 24 hrs post 1-NN treatment (0.3 (± 0.1)) compared to vehicle control (1.3 (± 0.5)) (Figure 7.7). There was a slight increase at 6 hrs and 96 hrs and a slight decrease at 48 hrs after 1-NN treatment compared to vehicle control. However, these differences were not statistically significant.

A significant increase ($p < 0.05$) of β-catenin was seen at 6 hrs after 1-NN administration (1.2 (± 0.2)) compared to vehicle control (0.3 (± 0.1)) (Figure 7.8). At 24 hrs there was a slight decrease in β-catenin expression due to 1-NN treatment; however, this was not statistically significant. A statistically significant decrease ($p < 0.01$) of β-catenin was seen 48 hrs after 1-NN administration (0.6 (± 0.1)) compared to vehicle control (1.5 (± 0.1)) at this time point. There was a slight increase of β-catenin at 96 hrs but this value was not statistically significant. The levels of β-catenin expression in the vehicle control animals differed throughout the time course, compared to the no-vehicle control baseline expression.

The expression of γ-catenin was examined for vehicle control and 1-NN treated animals. There was no significant differential expression of γ-catenin due to 1-NN administration, when compared to the vehicle control (Figure 7.9). Differential expressed γ-catenin was observed throughout the time course for vehicle control animals, compared to the no-vehicle control baseline expression.

7.2.6. BMP Signalling in 1-NN Treated Lungs

It has been established from observation of H & E stained tissue sections that maximum epithelial damage occurred 24 hrs after 1-NN treatment. Examination of PCNA levels during the time course indicated the highest level of cell proliferation occurred at 96 hrs post treatment. In order to establish if the BMP pathway is involved in the injury and repair process, protein expression was examined by immunofluorescence in rat tissue and by Western blot analysis in rat lysis lavage protein. Due to limited cross reactivity with our antibodies to rat protein, only BMPR-IA, Smad4 and p-Smad levels were examined.

Immunofluorescence analysis of mouse lung tissue show BMPR-IB protein expression localised to the apical membrane of the epithelial cells in the airways (Figure 7.10). Analysis of BMPR-IA expression revealed a significant increase ($p < 0.05$) in receptor protein expression at 6 hrs in 1-NN treated rats (0.56 (± 0.03) compared to vehicle control rats (0.22 (± 0.07)) (Figure 7.11). This time point was the point at which high levels of immune cells infiltrated the lungs (Figure 7.2). There was no significant difference in BMPR-IA expression when 1-NN rats were compared to vehicle control rats at 24, 48 or 96 hour time points.

Protein analysis for Smad 4 was carried out on the lung lysis lavage protein from vehicle control and 1-NN treated time course (Figure 7.12). There was no significant difference in Smad4 expression after 1-NN treatment compared to the vehicle control, at any time point. There was a low level of Smad4 expression at 6 hrs after vehicle control treatment, with increasing levels over 24, 48 and 96 hr time points. This pattern of increasing Smad4 expression corresponds with in the increase in inflammatory cells in the BALF, in vehicle control animals (Figure 7.2).

Immunofluorescence analysis of untreated control, vehicle control lung tissue or 1-NN treated lung tissues were examined for p-Smad localisation (Figure 7.13). p-Smad was localised to the apical region of the cytoplasm in the epithelial cells of the airways. Western blot analysis was carried out on lung lysis lavage protein to quantify activated p-

Smad 1/5/8 protein expression. Compared to the 1 untreated control animal both vehicle control and 1-NN treatments resulted in a decrease in p-Smad expression at 6 hrs. At 6 hrs post 1-NN treatment there was a significant increase of p-Smad (0.8 (± 0.05)) compared to vehicle control (0.5 (± 0.1)). 1-NN did not cause significant differential p-Smad activity at 24, 48 or 96 hrs compared to the vehicle controls at each of these time points. p-Smad densitometry values for vehicle control at all times points were normalised to a value of 1 and the 1-NN value at each time point was compared to the control (Figure 7.14). Compared to the vehicle control p-Smad activity was increased at 6 hrs with no differential expression at any other time point compared to their vehicle controls. The treatment alone appeared to cause a reduction in p-Smad expression after 6 hrs.

7.2.7. MAPK Signalling in 1-NN Treated Lungs

The MAPK pathway is involved in numerous biological processes, including cell proliferation, differentiation and apoptosis. Moreover, non-canonical BMP signalling, signals via the MAPK pathway. Rat lysis lavage protein was analysed for the activation of ERK, a member of the MAPK pathway. Total ERK was quantified via Western blot analysis and densitometry. Total ERK (T-ERK) antibody was used to identify T-ERK1 and T-ERK2 (Figure 7.15 A & B). Analysis of T-ERK1 revealed no significant difference in 1-NN treated rats compared to vehicle control at any time point (Figure 7.16 A). There was a statistically significant increase in total ERK2 at 48 hrs after 1-NN treatment (0.5 (± 0.04)) compared to vehicle control (0.2 (± 0.03)) (Figure 7.16 B). No difference in the expression levels of ERK2 was observed in 1-NN treated lungs and vehicle control lungs at 6, 24 or 96 hrs. Comparison of vehicle control and untreated control showed a decrease in T-ERK1 and T-ERK2 expression at 48 and 96 hrs due to vehicle administration.

The activated form of ERK, phospho-ERK (P-ERK), was quantified by Western blot analysis (Figure 7.17). There was a large increase in P-ERK1 (0.1 (± 0.026) compared to the vehicle control (0.02 (± 0.001)) 6 hrs after 1-NN administration (Figure 7.18 A). However, due to animal variation this increase was not statistically significant. P-ERK2 had also increased after 1-NN treatment (0.2 (± 0.07)) compared to vehicle control (0.011 (± 0.004)) (Figure 7.18 B). There is a slight decrease in P-ERK expression at 24 and 96 hrs and a slight increase at 48 hrs after 1-NN administration; however, these differences were not statistically significant. There is little variation in P-ERK expression due to vehicle control, as compared to untreated baseline levels

The differential expression of ERK signalling, as indicated in the results above, suggest this pathway is involved in the damage and repair process caused by 1-NN treatment.

The molecular effects of 1-NN treatment on lung epithelial injury and repair are summarised in Figure 7.19.

7.3. Discussion

Environmental pollutants which are in high abundance in urban areas are generally co-localised with many other airborne toxins. These pollutants pose a significant risk to respiratory health. Pollutants effect pulmonary function, induce airway inflammation, and cause airway hyper responsiveness contributing to pathogenesis or exacerbation of lung disease. Due to the increasing air pollutants in developed and developing countries it is necessary to understand the processes through which these toxins affect cells in the lungs. The environmental pollutant 1-NN, a by-product of diesel combustion which has been reported to be present in high concentration in urban areas of USA, Europe and South America, was used in this study to induce injury in the lungs of rats (Dihl, RR *et al.*, 2008). 1-NN like many airborne pollutants targets destruction of Clara cells by virtue of their high cytochrome 450 activity which metabolise inert chemical compounds to toxic metabolites. This study was conducted to characterise molecular processes occurring during the stages of injury and repair in the lungs of rats, and to identify if the BMP signalling pathway was involved in the repair process.

1-NN induces damage of epithelial cells in both the lung and liver; however, the lung is the primary target organ. The development of 1-NN lung toxicity can be sub-divided into two phases. Within the initial phase Clara cells undergo ultra structural changes due to high expression of CYP450 enzymes. The changes within the Clara occur as early as 1 hour after 1-NN administration, this detail was not detectable by our light microscope. The second phase of toxicity occurs 6 hrs after 1-NN administration and is characterised by increase immune cells and progressive damage to the Clara cells, which includes chromatin clumping, osmophilic granules, mitochondrial distension and severe cytoplasmic vacuolisation (Sauer, JM *et al.*, 1997). Analysis of BALF revealed a statistically significant increase of inflammatory cells at 6 hrs in 1-NN treated animals compared to vehicle control animals. Onset of respiratory distress has been noted at this time point in the 1-NN treated animals (Sauer, JM *et al.*, 1997). Although other compounds similar to 1-NN, for example naphthalene and 2-NN, cause Clara cell toxicity they do not induce respiratory distress. In our study hematoxylin and eosin stained lung

tissue sections illustrated epithelial cell toxicity, as noted by epithelial cell shedding from the basement membrane at the 24 hr time point (Figure 7.1f). A decrease in both non-ciliated cells and ciliated cells and an increase in vacuolated cells and squamous cells in response to 1-NN at 24 hrs post administration was noted in adult rats (Fanucchi, MV *et al.*, 2004). Non-ciliated Clara cells were directly targeted by their high CYP450 activity; ciliated cells were targeted either because of low level CYP450 expression or their close proximity to the necrotic Clara cells. The level of cellular toxicity is dependent on numerous factors including 1-NN dose, animal species and age of the animal. Fanucchi *et al* reported an increase in non-ciliated (Clara) cell toxicity with increasing 1-NN dose (12.5, 35, 50, 100 mg/kg). They also reported adult rats to be more susceptible to 1-NN treatment compared to adult mice. This difference in toxicity is due to species differences in CYP450 enzymes. Neonates of both rats and mice were shown to be more susceptible to 1-NN compared to adult animals (Fanucchi, MV *et al.*, 2004). The loss of tall cuboidal epithelial cells and a replacement of thin squamous cells were noted in our study at the 48 hr and 96 hr time points during the injury and repair process. Therefore our model concurs with those previously reported that surmountable epithelial damage occurs at 24 hrs post 1-NN administration, while the epithelial membrane appears to be intact although not fully repaired by 48 hrs, suggesting an active repair process occurring during this time scale.

Observation of PCNA expression levels during the time course identified the 48 hr time point as the initiation of cell proliferation and 96 hr time point as the peak of cell proliferation. Compared to other organs such as the intestines, the lungs have a very low mitotic rate during steady-state. However, progenitor cells in the lung have the ability to rapidly self renewal upon injury. In our lung injury model, damage to the epithelial cells of the conducting airways occur 24 hrs after 1-NN administration; this is noted by epithelial shedding from the basement membrane. The presence of thin epithelial cells 48 hrs and 96 hrs after 1-NN treatment illustrates the rapid response of airway cells to restore the epithelial lining. The epithelial barrier in the lungs protects the internal environment from pathogens and toxins in inhaled air. The high levels of PCNA expression at 48 hrs and 96 hrs, compared to vehicle control animals, indicate the

occurrence of epithelial repair. Interestingly, high PCNA expression occurs in clustered regions in the conducting airway after damage.

The clustering of proliferating cells in this damage model is consistent with previous studies that have been carried out to identify the local stem cells responsible for regenerating a denuded epithelial membrane. Cells lining the airways differ in composition between the trachea and the terminal bronchioles. This heterogeneity is necessary for homeostasis and results in different stem cells responsible for regenerating different areas of the airways. As reviewed in section 1.4 there are numerous cells responsible for regenerating the epithelial membrane in the airways. Within the conducting airways the basal cells have the capacity to self renewal in the absence of Clara cells (Hong, KU *et al.*, 2004). PNEC (pulmonary neuroendocrine cells) also have the capacity to self renew in the absence of Clara cells (Hong, KU *et al.*, 2001). However, the ability of the basal cells and PNEC to self renew is not consistent with regeneration of the airways due to the lack of differentiation of these cells. Therefore the regenerative capability of these cells is limited. Variant Clara cells which possess a low mitotic rate and a relatively undifferentiated state are located within the NEB (neuroendocrine bodies) and are responsible for proliferation and regeneration of the conducting airways. The cells responsible for regeneration at the terminal bronchiole junction are the pollutant resistant Clara cells which are not associated with the NEB and express SP-C and CC10 markers. In our study damage caused by 1-NN targets pollutant susceptible Clara cells, that is Clara cells expressing high levels of CYP450. Based on the previous studies it may be deduced that cells expressing PCNA at 48 hrs and 96 hrs after 1-NN administration are the progenitor cells that have been resistant to 1-NN toxic effects.

Differentiated, polarised epithelial cells express E-cadherin at their basolateral membrane, and for this reason E-cadherin was used as a marker of differentiation in these studies. Immunofluorescence analysis of vehicle control and 1-NN treatment validated the expression of E-cadherin at the epithelial membranes. Quantification of the protein expression resulted in decreased E-cadherin expression after 1-NN treatment at the 96 hr time point. The low level E-cadherin protein suggests that the epithelial cells are not fully

differentiated at this time point. The time point at which E-cadherin expression is attenuated coincides with high PCNA expression, to allow cell proliferation and regeneration. It is necessary for E-cadherin protein to be down-regulated to permit proliferation of epithelial cells

As described in section 1.6.5 the adherence junction complex is composed of cadherin and catenin proteins. Loss of catenin protein expression or E-cadherin expression has been associated with cancer progression, allowing cells to metastasise. Loss of the adherence junction protein expression results in a loss of cell to cell contact and therefore an enhancement in cell mobility. The adherence complex is directly linked to the actin cytoskeleton. Therefore loss of adherence junction complex proteins enhances cytoskeleton movement. In this lung repair model collectively α-catenin, β-catenin and E-cadherin expression is down-regulated by 1-NN treatment at 24, 48 or 96 hour time points, respectively. This down regulation in cell-cell adhesion complex may be to allow surviving cells to migrate to the denuded basement membrane during the repair process.

β-catenin, which binds to the cytoplasmic domain of the E-cadherin protein, was found to be significantly up-regulated at the 6 hr time point. This protein has been implicated in a number of biological was processes including cell adhesion, proliferation, and differentiation. Numerous studies have been carried out to inhibit β-catenin or its upstream regulators in wound healing assays, showing the necessity of β-catenin in this process (Cheon, SS *et al.*, 2006; Zhu, M *et al.*, 2007). The significant augmentation of β-catenin seen 6 hrs after 1-NN administration is consistent with these studies. At 6 hrs the 1-NN becomes toxic to the CYP2F2 expressing Clara cells. The up-regulation at the early time point suggests β-catenin is rapidly expressed under stress conditions. β-catenin can then function in epithelial squamation and migration of the 1-NN resistant cells along the denuded areas of membrane.

During embryogenesis β-catenin has been implicated in lung proliferation and differentiation processes. Expression of constitutively active β-catenin-Lef1 construct under the control of the lung specific SP-C promoter resulted in highly proliferative cells

which lack fully differentiated phenotypes (Okubo, T and Hogan, BL, 2004). A recent study of the naphthalene induced lung injury of dominant stabilised β-catenin transgenic mice ($Catnb^{\Delta(ex3)}$) reports that β-catenin expression in lung epithelial cells increase the population of progenitor stem cells and inhibit differentiation (Reynolds, SD *et al.*, 2008). In the developing embryo attenuation of β-catenin expression was correlated to the emergence of cellular differentiation. In adult transgenic mice, there was an increase in Clara cells with progenitor phenotype, that is, no secretory granules or smooth endoplasmic reticulum. This study showed the inability of transgenic epithelial cells to differentiate into Clara cells or ciliated cells after naphthalene injury. In our study β-catenin expression was significantly reduced at the 48 hour time point in 1-NN treated animals. In accordance with the above study β-catenin attenuation was necessary for the differentiation of the newly proliferating cells.

BMP signalling is emerging as an essential process contributing to numerous human diseases. Previous studies have reported the BMP activation, namely the presence of BMP2 and BMP4 ligands, in the airways of OVA murine models of asthma (Rosendahl, A *et al.*, 2002). BMP receptor basal activity is down-regulated in asthmatic patients compared to healthy individuals, however, allergen challenge resulted in a sustained up regulation of BMP pathway activation (Kariyawasam, HH *et al.*, 2008). Our lab has reported the activation of BMP pathway in allergic rhinitis patients (Molloy *et al,* unpublished data), supporting a role for BMP signalling during the inflammatory process of asthma. In this study BMP signalling was observed during lung injury. That is p-Smad expression was augmented and BMPR-IA was significantly up-regulated 6 hrs after 1-NN administration. The up-regulation of BMPR-IA concurs with previous studies showing augmentation of BMP receptor expression during inflammation (Kariyawasam, HH *et al.*, 2008; Rosendahl, A *et al.*, 2002). The increase of BMP signalling during inflammatory processes implicates this pathway in the pathogenesis of lung diseases such as acute lung injury and chronic lung injury. However, the role of BMP signalling in inflammation and repair is not yet known.

Some understanding of the role of the TGF-β super-family in tissue repair and inflammation comes from studies on skin wound healing. TGF-β is important for the stimulation of fibroblasts and for extracellular matrix production which can prevent invasion of pathogens after epithelial damage (Cutroneo, KR, 2007). The inflammatory process has been studied in detail and it has been found through genetic ablation studies that inflammatory cells of the immune system can be contribute to and negate wound repair processes (reviewed in (Martin, P and Leibovich, SJ, 2005). Ablation of macrophage, neutrophils and mast cells resulted in faster skin repair with reduced scaring compared to control animals (Martin, P *et al.*, 2003). Smad3 null mice, which do not propagate in TGF-β downstream signalling, resulted in speedier repair and reduced scarring (Ashcroft, GS *et al.*, 1999). These studies suggest TGF-β among other factors negatively contribute to tissue repair and must therefore be down-regulated in order to restore tissue homeostasis. Our results in combination with other studies suggest attenuation of BMP signalling after the 6 hr time point is important for the repair process. Future studies are required to investigate in detail the exact role of BMP signalling during inflammation.

MAPK pathway is involved in cell survival, proliferation and differentiation and inflammation among others. Augmentation of MAPK pathway activation has been reported in asthma patients, with the levels of pathway activation correlating with disease severity. Patients with severe asthma demonstrate strongly activated ERK1/2 and p38 signalling. *In vitro* inhibition of MAPK signalling in primary airway epithelial cells result in a reduction of chemokines, suggesting MAPK may be a therapeutic target for asthma patients (Liu, W *et al.*, 2008). It has been shown that inhibiting the MAPK pathway can lead to amelioration of the asthmatic pathology (Chialda, L *et al.*, 2005; Duan, W *et al.*, 2005). In our study P-ERK2 was significantly up-regulated 6 hrs after 1-NN administration, this time point correlates with the presence of inflammatory cells. These results implicate the involvement of ERK in the inflammation prior to epithelial repair. Due to the role of MAPK signalling in recruiting inflammatory cells it cannot be inferred whether MAPK activation is a down stream effect of the inflammation or an early

process activated for the repair of the epithelium lining, further studies would be required to validate this.

Throughout the time course experiment there appears to be differential expression of proteins in the vehicle control lysis lavage protein. It is difficult to say whether these disparities are due to normal pathway fluctuations during homeostasis or due to adverse effects of the oleic oil vehicle. To address this question an animal group of untreated control at each of the time points would be required. This control group was not provided and therefore the question as to whether the oleic oil vehicle causes damage in these animals could not be addressed. However, because the 1-NN is delivered in oleic oil, the vehicle control acts as an appropriate control to observe effects due to the 1-NN damage alone.

We hypothesised that the BMP signalling pathway is important during the lung repair process. This study identified an increase in BMP signalling during the inflammatory process prior to epithelial repair. From these and other studies we suggest that BMP signalling is important modulator of inflammation but must be down-regulated to allow epithelial repair and restore homeostasis. This study has also shown the importance of adherence junction proteins, which may contribute to migration during epithelial repair. A mass spectrometry global approach would identify more pathways differentially expressed during lung epithelial damage and repair. Studies into the differential expression of signalling pathways in this lung damage model may help identify drug targets for lung disease.

8. Conclusion

BMPs play important roles in biological processes such as proliferation, differentiation, apoptosis and epithelial to mesenchymal transition. All these biological process are important during development and during disease and cellular repair in adult lungs. Studies were conducted to characterise the role of BMP signalling during the disease process of cancer and during acute lung injury and repair.

Lung cancer is the leading cause of cancer deaths in the world. Despite advances in cancer survival for breast and prostate cancer, little advances have been made for lung cancer patients. The reason for the poor prognosis in lung cancer patients is the lack of early detection methods. Microarray analysis was carried out on pre-cancerous tumours to identify targets which may be potential biomarkers, and also to understand the development of lung cancer progression. Examination of known tumour suppressors revealed an increase in PCNA and a down regulation of *Mig-6* and E-cadherin expression at the early stages of lung cancer. This is the first report to show aberrant expression of these markers at such early stages of tumour development. These proteins have the potential to be used as biomarkers to identify lung cancer at the early stages.

Mig-6 has only recently been identified as having tumour suppressor properties. To further investigate this function a *Mig-6* expression vector was constructed for the generation of a transgenic mouse over expressing *Mig-6*. This mouse has recently been generated and verified by the DeMayo group at Baylor College of Medicine. Future work will include the generation of mice expressing oncogenic K-ras and over expressing *Mig-6* to investigate the ability of *Mig-6* to delay tumour progression. These studies will identify the potential of *Mig-6* as a therapeutic for the treatment of cancer.

The BMP signalling pathway is aberrantly expressed in a number of epithelial cancers. However, there is little known about the expression of BMP pathway in lung cancer. Our studies identified the differential expression of the BMP signalling pathway in murine lung cancer. BMPR-IB and BMPR-II expression was decreased compared to normal lung epithelial cells, while BMP4, BMP5, Smad4 and Id-1 expression were increased. The increase in BMP signalling was also evident by the increase in phosphorylated Smad

1/5/8 protein in hyperplasia and adenoma samples. The loss of receptor expression has been shown in other studies to correlate with increased tumour grade and poor prognosis. Given the loss of BMPR-IB in many epithelial cancers, we hypothesized that BMPR-IB has potential anti-proliferative function.

To investigate this hypothesis, BMPR-IB was cloned from mouse lung cDNA and an expression vector was generated. BMPR-IB was transiently transfected into the BEAS-2B transformed human cell line that were devoid of endogenous BMPR-IB expression. BMPR-IB expression resulted in a decrease in cell proliferation and an increase in cell death by apoptosis, suggesting it has anti-proliferative properties. However, given the expression of BMPR-IB in human adenocarcinoma tissue the role of BMPR-IB during cancer is complex. We hypothesize BMPR-IB re-expression during the late stages of cancer progression contributes to metastasis by influencing differentiation and migration. Future experiments will be conducted to investigate this role for BMPR-IB.

We hypothesized that BMP signalling has a role during lung repair. To investigate this, the 1-NN rat model of acute lung injury was investigated. The effects of 1-NN on lung epithelial cells have been investigated extensively, however, no study has been conducted to investigate signalling pathways that are differentially expressed during the damage and repair stages. We first identified the stages of proliferation and differentiation in the model. PCNA expression was up-regulated at 48 and 96 hrs after 1-NN administration suggesting high levels of cell proliferation occurring at this stage. The E-cadherin marker of epithelial differentiation was down-regulated at 96 hrs suggesting the epithelial monolayer was not fully differentiated at this stage. Extensive investigation into the involvement of the BMP pathway was not possible due to the lack of sensitive antibodies to rat BMP pathway components. However, there was an up regulation of BMPR-IA and p-Smad at 6 hrs after 1-NN administration which correlated with high inflammation in the lung at this time point. These results suggest BMP signalling is implicated in the inflammatory response after damage but may not be directly involved in epithelial cell repair.

Over all we have provided significant insights into the importance of BMP signalling during lung disease (Figure 8.1). Future aims would be to characterise BMP signalling in human lung cancer at different stages of progression, and to establish if BMP expression correlates with detection, prognosis or survival. Other important future aims would be to continue the investigation into the role of BMPR-IB as tumour suppressor by generating a transgenic mouse over expressing this gene to see if it can delay or prevent the onset of lung cancer progression.

9. Appendix

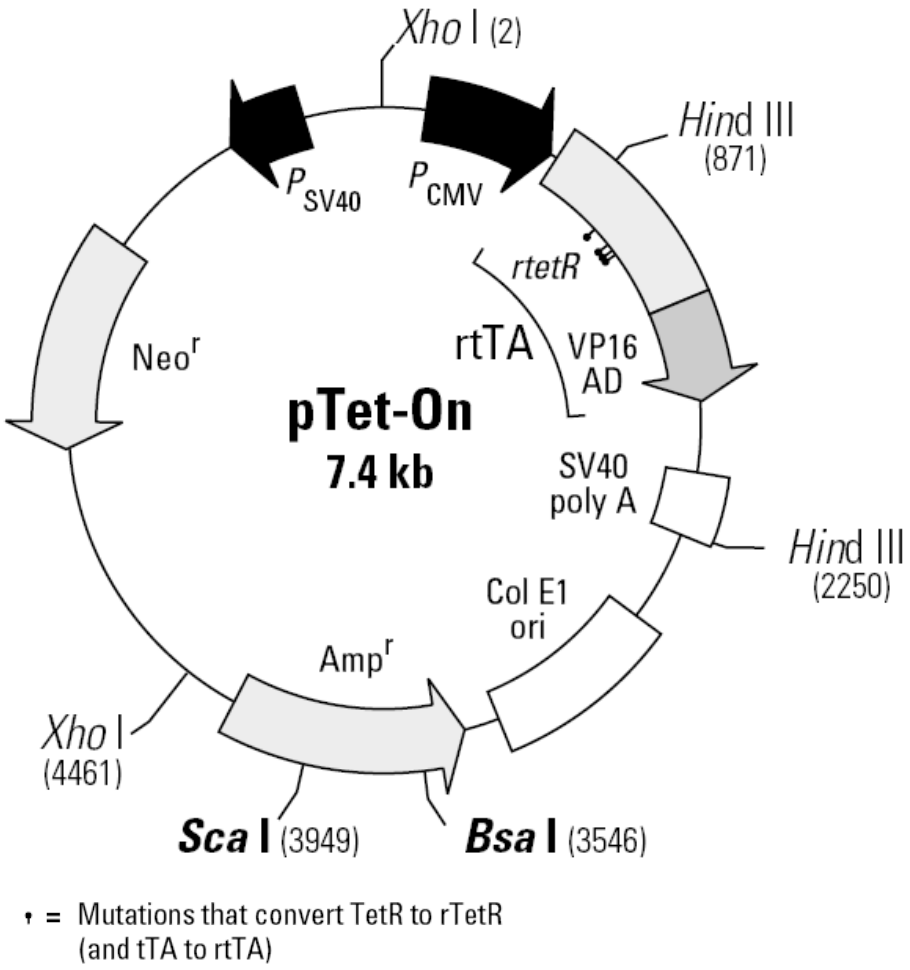

Figure 9.1: pTet-On plasmid map (Clontech)

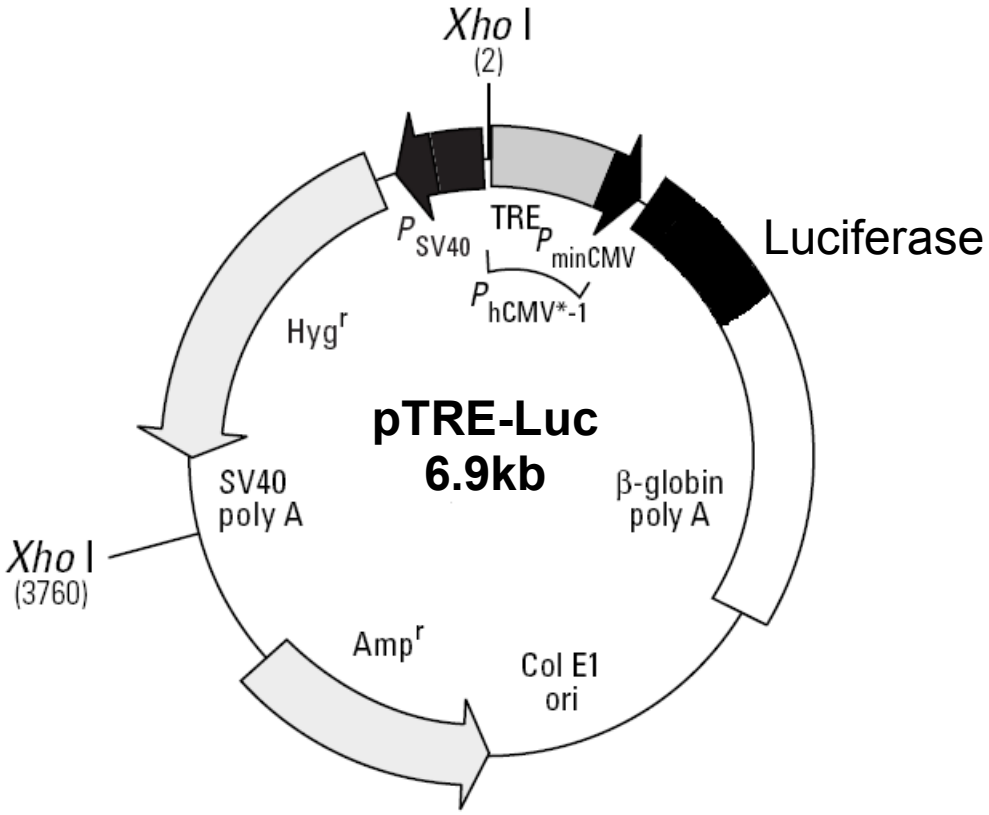

Figure 9.2: pTRE-Luciferase plasmid map (Clontech)

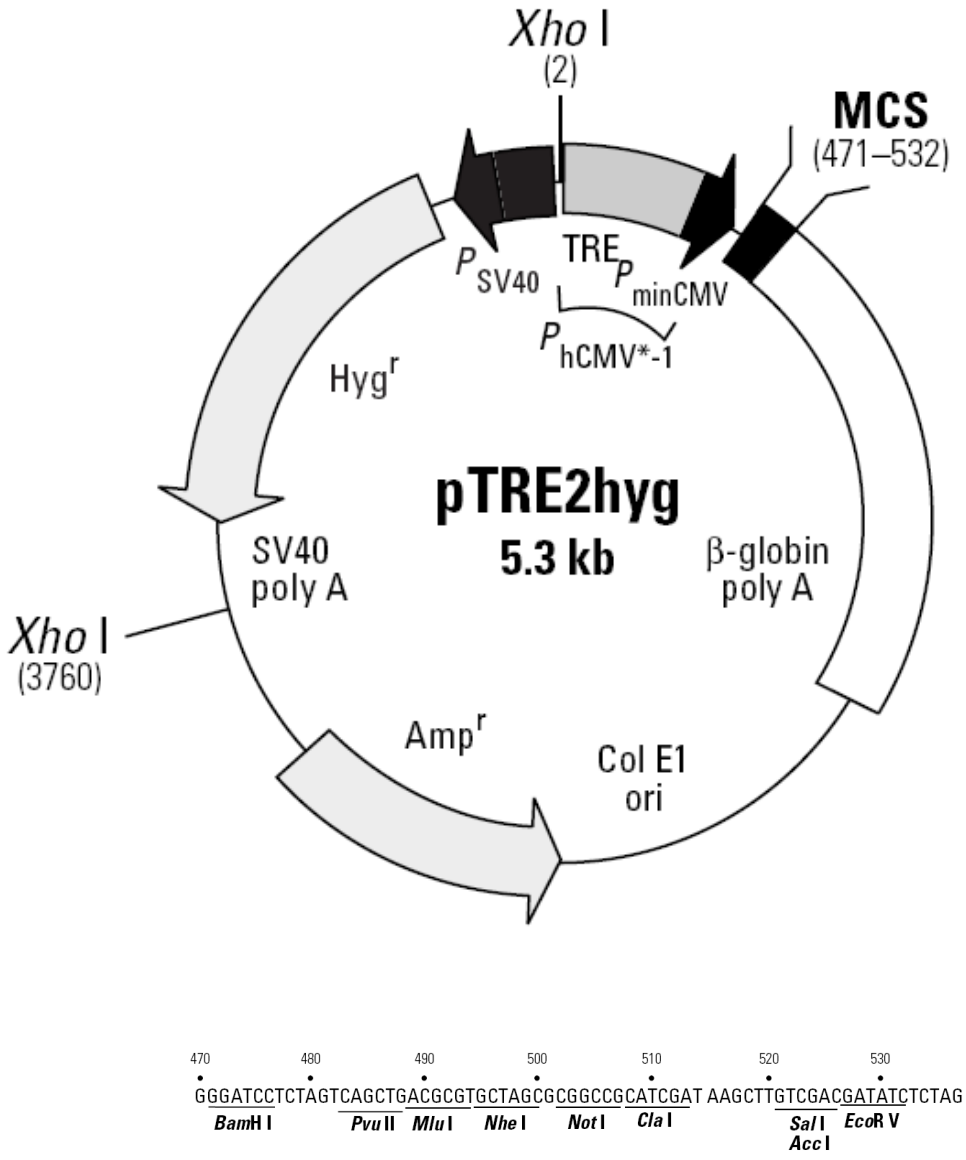

Figure 9.3: pTRE2hyg plasmid map (Clontech)

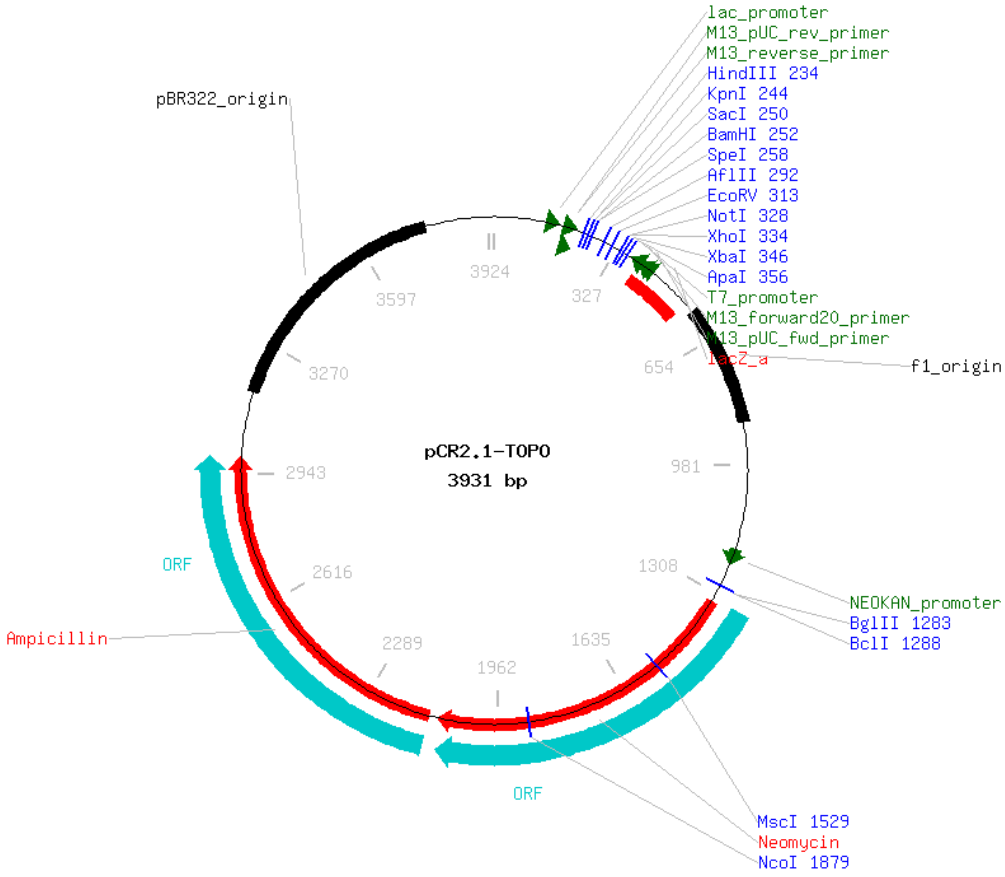

Figure 9.4: pCR2.1 TOPO cloning vector plasmid map (Invitrogen)

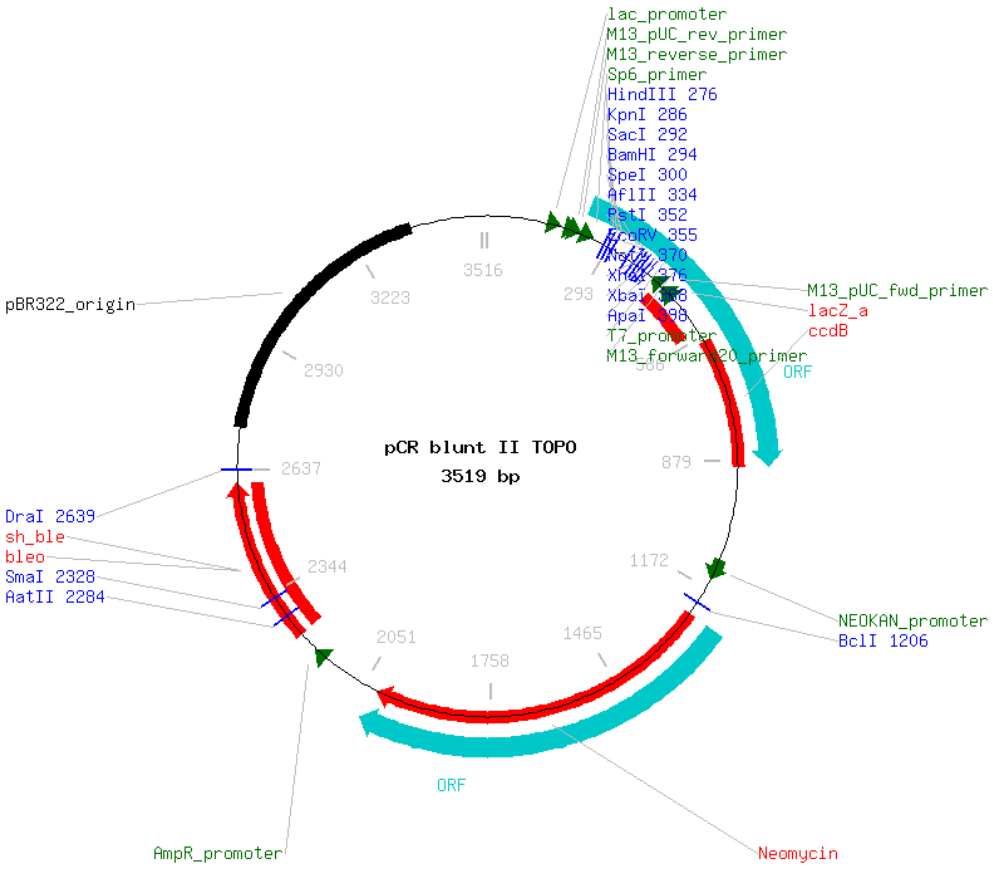

Figure 9.5: pCR BluntII TOPO cloning vector plasmid map (Invitrogen)

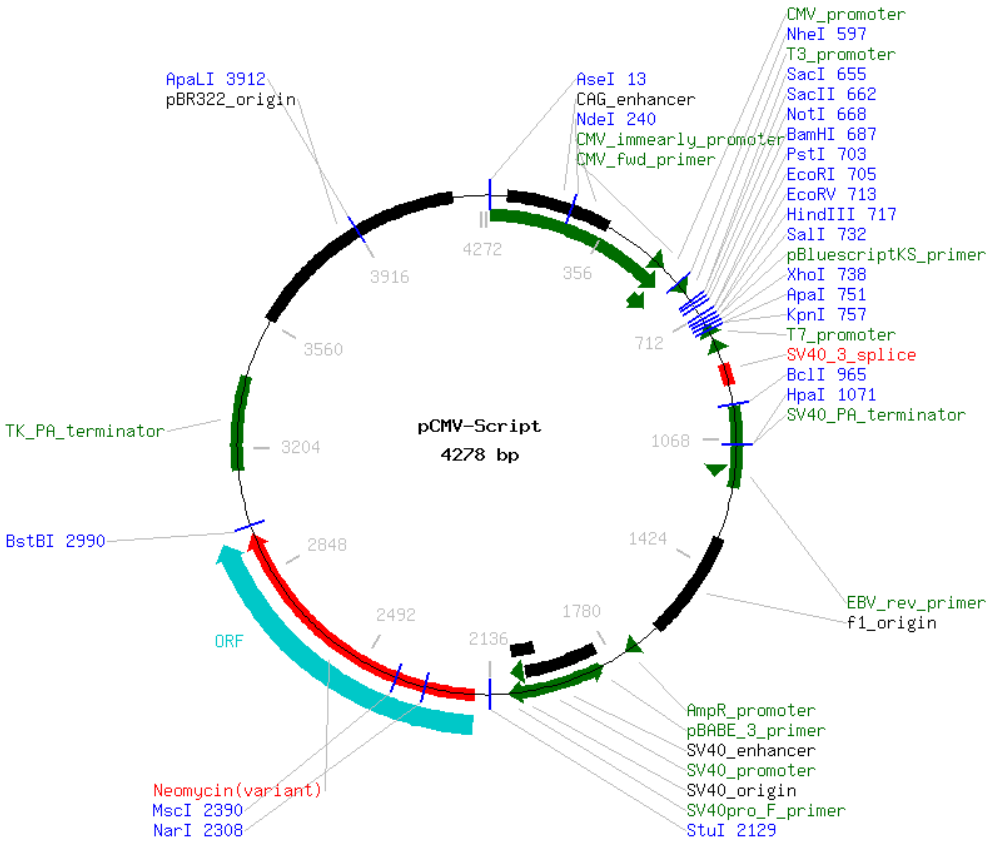

Figure 9.6: pCMV-Script cloning vector plasmid map (Stratagene)

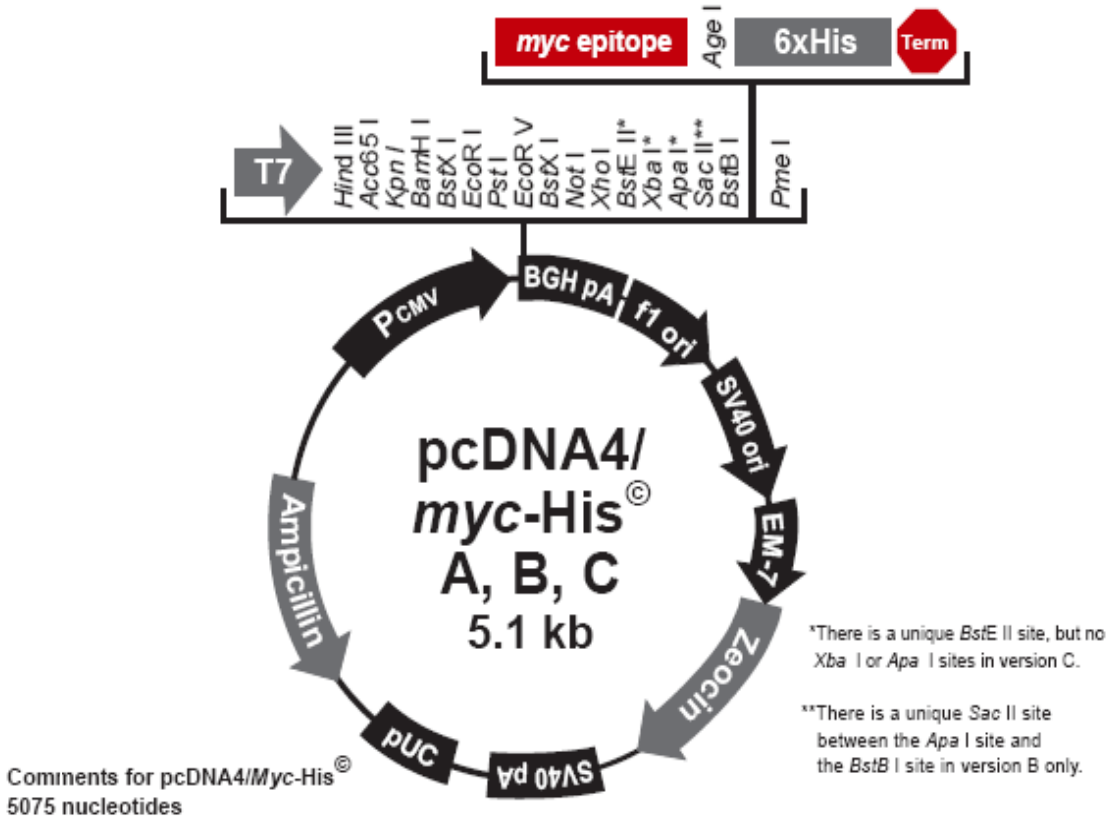

Figure 9.7: pcDNA4 plasmid map (Invitrogen)

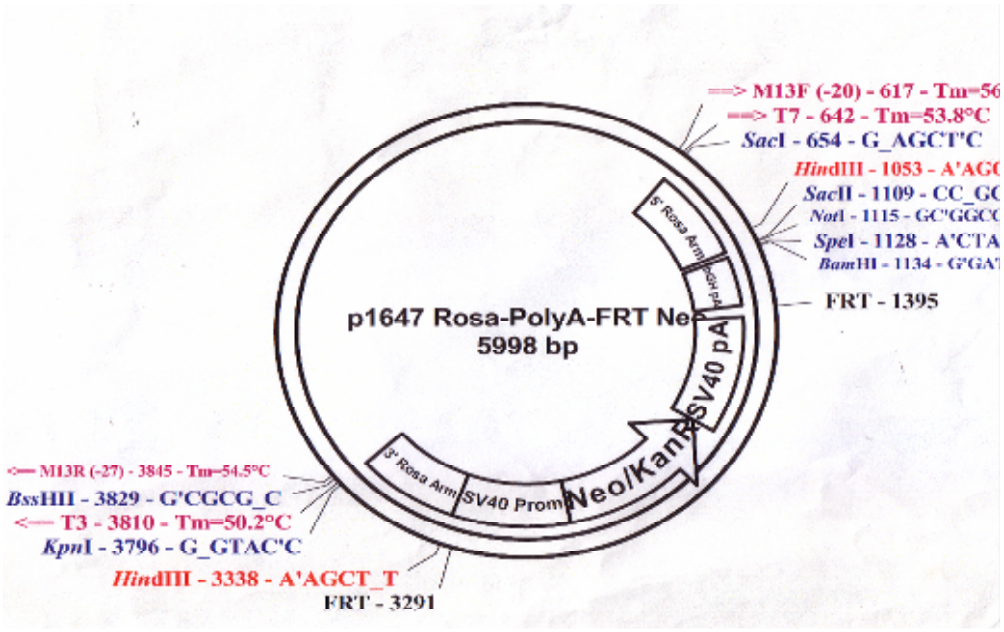

Figure 9.8: p1647 Rosa-PolyA-FRT-Neo plasmid map

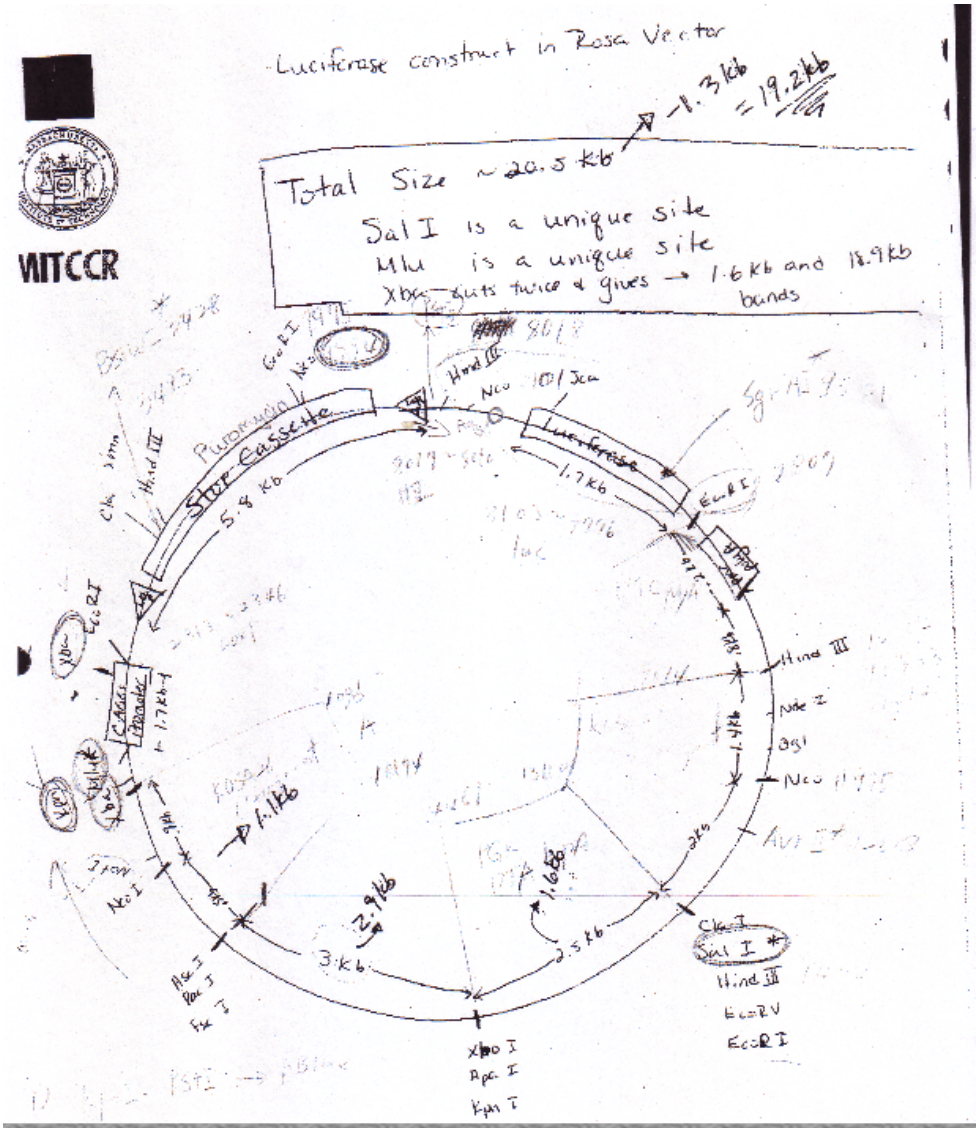

Figure 9.9: pRosa-luciferase

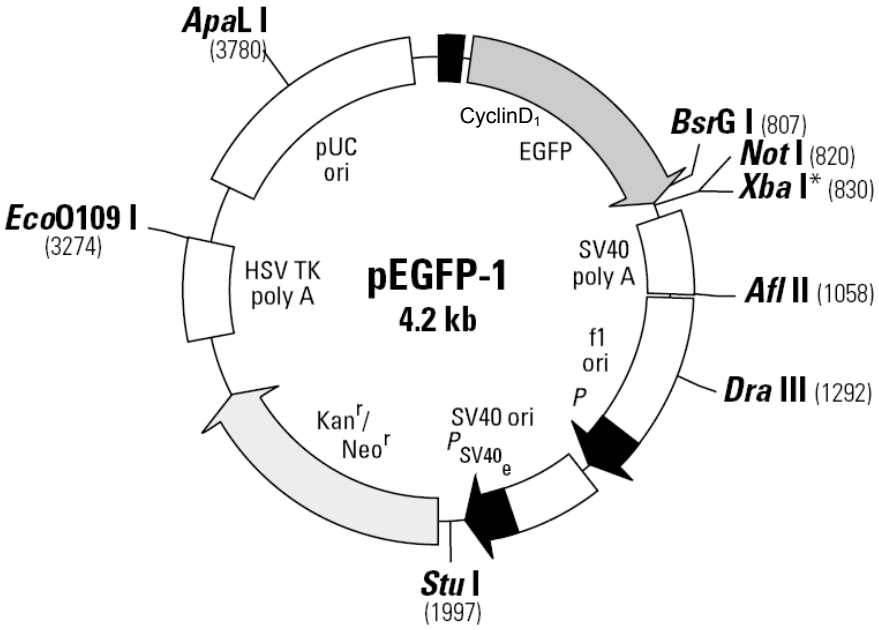

Figure 9.10: pCyclin-D$_1$-GFP plasmid map

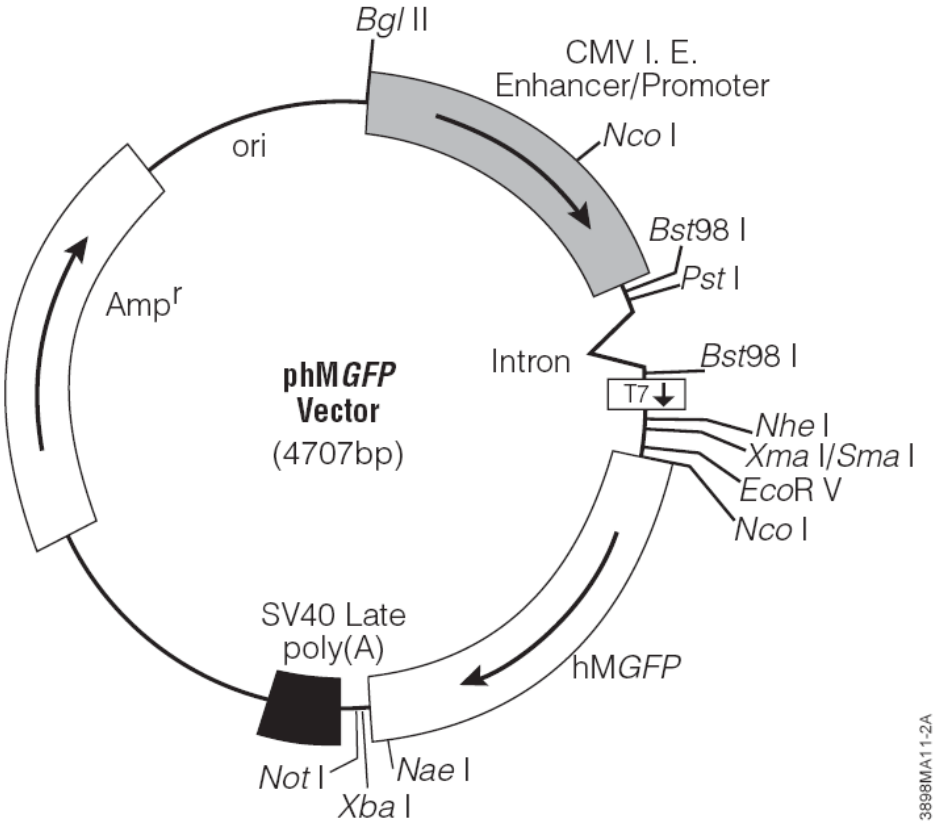

Figure 9.11: pMGFP plasmid map (Promega)

Pattern A

Gene Symbol	Gene Title	Fold Change hyper	aden
Ctsb	Cathepsin B	2.13	1.16
Dbi	diazepam binding inhibitor	2.15	1.24
Gaa	glucosidase, alpha, acid	1.81	1.10
Inhbb	inhibin beta-B	3.33	1.41
Npdc1	neural proliferation, differentiation and control gene 1	2.02	1.39
St6gal1	beta galactoside alpha 2,6 sialyltransferase 1	2.52	1.41
Cops7a	COP9 (constitutive photomorphogenic) homolog, subunit 7a (A. thaliana)	1.99	0.86
Atp11a	ATPase, class VI, type 11A	3.44	1.34
Hes6	hairy and enhancer of split 6 (Drosophila)	3.54	1.77
Apba3	amyloid beta (A4) precursor protein-binding, family A, member 3	1.51	0.92
Tmed3	Transmembrane emp24 domain containing 3	3.29	1.56
Zdhhc3	zinc finger, DHHC domain containing 3	14.53	4.10
Gtf3c2	general transcription factor IIIC, polypeptide 2, beta	3.38	1.27
Gusb	glucuronidase, beta	4.27	1.66
Pawr	PRKC, apoptosis, WT1, regulator	2.70	1.01
Aamp	angio-associated migratory protein	2.99	0.94
Bcl2	B-cell leukemia/lymphoma 2	14.03	1.18
Col1a1	procollagen, type I, alpha 1	4.56	2.08
Lmna	lamin A	2.01	1.22
Tmed1	transmembrane emp24 domain containing 1	1.72	0.87
Nfia	nuclear factor I/A	2.80	0.98
Zfp106	zinc finger protein 106	1.84	0.94
AA536749	Expressed sequence AA536749	2.20	0.83
Map1lc3a	microtubule-associated protein 1 light chain 3 alpha	1.90	0.88
Abp1	amiloride binding protein 1 (amine oxidase, copper-containing)	4.20	0.66
Afm	afamin	3.59	1.72
Rab22a	RAB22A, member RAS oncogene family	1.99	0.82
Slamf6	SLAM family member 6	1.40	1.18
Paf1	Paf1, RNA polymerase II associated factor, homolog (S. cerevisiae)	3.19	1.28
Chst12	carbohydrate sulfotransferase 12	3.19	1.15
Kcng4	potassium voltage-gated channel, subfamily G, member 4	2.26	1.05
Arl13b	ADP-ribosylation factor-like 13B	1.90	1.07
Hemk1	HemK methyltransferase family member 1	3.04	1.18
Cpn2	carboxypeptidase N, polypeptide 2	6.08	0.69
Klhl5	kelch-like 5 (Drosophila)	10.87	1.12
Sh2d4a	SH2 domain containing 4A	2.55	1.48
Yipf6	Yip1 domain family, member 6	2.70	1.20
Rsnl2	restin-like 2	8.79	1.23
Pag1	Phosphoprotein associated with glycosphingolipid microdomains 1	2.70	0.98
C77815	expressed sequence C77815	6.61	1.37
Klk9	kallikrein related-peptidase 9	3.35	0.90
Tmem16a	transmembrane protein 16A	3.24	1.74
Cnot6	CCR4-NOT transcription complex, subunit 6	4.47	1.34
AA536717	expressed sequence AA536717	1.84	1.19
Tmem153	transmembrane protein 153	2.38	0.85

AW049604	expressed sequence AW049604	1.92	1.03
Ankrd12	ankyrin repeat domain 12	2.73	1.16
Pcdh9	Protocadherin 9	3.72	0.84
Slc36a1	solute carrier family 36 (proton/amino acid symporter), member 1	7.47	2.28
Atp13a3	ATPase type 13A3	2.41	1.06
Pggt1b	protein geranylgeranyltransferase type I, beta subunit	4.30	1.53
Tpcn2	two pore segment channel 2	4.05	1.30
Tpte	transmembrane phosphatase with tensin homology	1.79	1.35
Zfp71-rs1	zinc finger protein 71, related sequence 1	2.04	0.85
Sulf1	sulfatase 1	4.06	0.81
Ppp1r3b	protein phosphatase 1, regulatory (inhibitor) subunit 3B	15.99	1.52
Ankrd37	ankyrin repeat domain 37	3.10	1.44
Cyb561	cytochrome b-561	1.80	0.87
Zrsr2	zinc finger (CCCH type), RNA binding motif and serine/arginine rich 2	5.32	1.23
Mif4gd	MIF4G domain containing	2.48	1.12
Tysnd1	trypsin domain containing 1	1.60	1.25
Poldip3	polymerase (DNA-directed), delta interacting protein 3	2.37	1.13
Zkscan1	zinc finger with KRAB and SCAN domains 1	3.57	1.00
Rbm9	RNA binding motif protein 9	1.83	0.94
Slc6a1	solute carrier family 6 (neurotransmitter transporter, GABA), member 1	1.76	1.06
Grb2	growth factor receptor bound protein 2	6.49	1.57
Kcna1	potassium voltage-gated channel, shaker-related subfamily, member 1	12.88	3.80
Pax9	paired box gene 9	1.68	0.86
Pcsk1	proprotein convertase subtilisin/kexin type 1	1.53	0.96
Supt6h	suppressor of Ty 6 homolog (S. cerevisiae)	1.97	1.08
Mapkbp1	mitogen activated protein kinase binding protein 1	3.57	1.59
Lrrfip2	leucine rich repeat (in FLII) interacting protein 2	3.09	1.74
Ptdsr	phosphatidylserine receptor	2.41	1.42
Lama5 /// LOC671909	laminin, alpha 5 /// similar to Laminin alpha-5 chain precursor	2.29	1.49
Tagln2 /// LOC672466	transgelin 2 /// similar to transgelin 2	4.60	1.57

Figure 10.12: Pattern A of the microarray heat map
RNA expression in normal airway control was normalised to a value of 1. The list indicates the gene symbol, the gene title and the fold change by which genes were up regulated in hyperplasia (hyper) cells but unchanged in adenoma (aden) cells.

Pattern B:

Gene Symbol	Gene Title	Fold Change hyper	aden
Cask	Calcium/calmodulin-dependent serine protein kinase (MAGUK family)	0.37	0.92
Nfkb2	nuclear factor of kappa light polypeptide gene enhancer in B-cells 2, p49/p100	0.28	0.81
Rpl30	ribosomal protein L30	0.26	0.99
Fibp	Fibroblast growth factor (acidic) intracellular binding protein	0.45	1.18
Mms19l	MMS19 (MET18 S. cerevisiae)-like	0.51	1.06
Csn1s1	casein alpha s1	0.68	0.93
Fkbp7	FK506 binding protein 7	0.13	0.96
Gnat1	guanine nucleotide binding protein, alpha transducing 1	0.45	0.91
Pfkfb1	6-phosphofructo-2-kinase/fructose-2,6-biphosphatase 1	0.63	1.06
Tgfbr3	Transforming growth factor, beta receptor III	0.49	0.80
Cntnap1	contactin associated protein-like 1	0.60	1.04
Peli1	Pellino 1	0.23	0.61
Cts8	cathepsin 8	0.40	0.75
Tubd1	tubulin, delta 1	0.33	0.97
Ndst4	N-deacetylase/N-sulfotransferase (heparin glucosaminyl) 4	0.51	0.78
Eid3	EP300 interacting inhibitor of differentiation 3	0.31	1.26
Kirrel3	kin of IRRE like 3 (Drosophila)	0.19	1.57
Cml2	camello-like 2	0.46	1.06
C77626	expressed sequence C77626	0.42	0.79
Mbnl2	Muscleblind-like 2	0.57	1.22
Igf2bp3	insulin-like growth factor 2 mRNA binding protein 3	0.20	0.59
Dock4	dedicator of cytokinesis 4	0.58	0.76
Auts2	autism susceptibility candidate 2	0.11	0.38
Lrrc24	leucine rich repeat containing 24	0.18	0.54
Ubqln1	ubiquilin 1	0.29	0.56
Phxr2	per-hexamer repeat gene 2	0.49	1.04
Prss7	protease, serine, 7 (enterokinase)	0.61	1.10
Rfxank	regulatory factor X-associated ankyrin-containing protein	0.61	0.91
Srpk3	serine/arginine-rich protein specific kinase 3	0.33	0.84

Figure 10.13: Pattern B of the microarray heat map
RNA expression in normal airway control was normalised to a value of 1. The list indicates the gene symbol, the gene title and the fold change by which genes were down regulated in hyperplasia (hyper) cells but unchanged in adenoma (aden) cells.

Pattern C

Gene Symbol	Gene Title	Fold Change hyper	aden
Entpd1	ectonucleoside triphosphate diphosphohydrolase 1	1.44	3.00
Dazl	deleted in azoospermia-like	1.01	2.26
Kng1	kininogen 1	4.40	31.12
Men1	multiple endocrine neoplasia 1	0.99	2.18
Pld1	phospholipase D1	2.70	9.54
Serpinb5	serine (or cysteine) peptidase inhibitor, clade B, member 5	1.40	6.28
Rgs19	regulator of G-protein signaling 19	1.67	4.69
Tspan31	tetraspanin 31	1.63	2.79
Txndc4	Thioredoxin domain containing 4 (endoplasmic reticulum)	0.93	1.72
B3galnt2	UDP-GalNAc:betaGlcNAc beta 1,3-galactosaminyltransferase, polypeptide 2	2.35	17.44
Utrn	utrophin	1.75	3.74
Olfr49	olfactory receptor 49	1.57	4.88
Sap30l	SAP30-like	1.30	1.95
Tmem141	transmembrane protein 141	1.55	2.63
Rassf7	Ras association (RalGDS/AF-6) domain family 7	1.11	1.92
Lass4	longevity assurance homolog 4 (S. cerevisiae)	1.24	1.85
Tmem86b	transmembrane protein 86B	1.24	2.37
Trpm4	transient receptor potential cation channel, subfamily M, member 4	1.27	2.21
Gucy2g	guanylate cyclase 2g	1.04	2.39
Osbp2	oxysterol binding protein 2	2.18	5.40
Tusc3	Tumor suppressor candidate 3	2.30	10.72
Msr2	macrophage scavenger receptor 2	1.11	1.89
Mrpl1	mitochondrial ribosomal protein L1	1.16	1.87
AA407782	expressed sequence AA407782	1.21	1.56
Tmc2	transmembrane channel-like gene family 2	1.08	1.89
Rfxdc2	regulatory factor X domain containing 2 homolog (human)	1.02	1.64
Atp10b	ATPase, Class V, type 10B	0.90	5.87
LOC675709	similar to Beta-1,4-galactosyltransferase 6 (Beta-1,4-GalTase 6) (Beta4Gal-T6) (b4Gal-T6) (UDP-galactose:beta-N-acetylglucosamine beta-1,4-galactosyltransferase 6) (UDP-Gal:beta-GlcNAc beta-1,4-galactosyltransferase 6)	1.00	3.01
Blr1	Burkitt lymphoma receptor 1	1.05	2.90
Crct1	cysteine-rich C-terminal 1	1.41	120.40
Acy1	aminoacylase 1	0.89	2.20
Scn9a /// LOC671835	sodium channel, voltage-gated, type IX, alpha /// similar to sodium channel 25	1.40	9.15

Figure 10.14: Pattern C of the microarray heat map
RNA expression in normal airway control was normalised to a value of 1. The list indicates the gene symbol, the gene title and the fold change by which genes were unchanged in hyperplasia (hyper) cells but up regulated in adenoma (aden) cells.

.

Pattern D

Gene Symbol	Gene Title	Fold Change hyper	aden
Myc	myelocytomatosis oncogene	1.13	0.13
Tmem168	transmembrane protein 168	0.82	0.57
AI324046	expressed sequence AI324046	0.85	0.22
Prdx6	peroxiredoxin 6	0.57	0.26
Cd55	CD55 antigen	0.49	0.12
Gnrhr	gonadotropin releasing hormone receptor	0.51	0.22
Mlf1	myeloid leukemia factor 1	0.85	0.28
Six4	sine oculis-related homeobox 4 homolog (Drosophila)	0.43	0.15
Cenpo	centromere protein O	0.79	0.27
Cacnb4	calcium channel, voltage-dependent, beta 4 subunit	0.60	0.33
D2Ertd750e	DNA segment, Chr 2, ERATO Doi 750, expressed	0.58	0.27
Heyl	hairy/enhancer-of-split related with YRPW motif-like	1.09	0.20
Slc35b4	solute carrier family 35, member B4	1.13	0.44
Ap3m2	adaptor-related protein complex 3, mu 2 subunit	0.83	0.53
Alg14	asparagine-linked glycosylation 14 homolog (yeast)	0.94	0.50
Tmem19	transmembrane protein 19	0.58	0.26
Loh12cr1	loss of heterozygosity, 12, chromosomal region 1 homolog (human)	0.79	0.12
Pdzd2	PDZ domain containing 2	1.13	0.62
2810404F17Rik	D-aspartate oxidase	0.68	0.10
Pgm2l1	phosphoglucomutase 2-like 1	0.61	0.32
Cage1	cancer antigen 1	0.40	0.12
Dnajc6	DnaJ (Hsp40) homolog, subfamily C, member 6	0.72	0.08
Eaf1	ELL associated factor 1	0.91	0.60
Mdh1b	malate dehydrogenase 1B, NAD (soluble)	0.75	0.18
Kremen1	kringle containing transmembrane protein 1	0.95	0.38
Arid4b	AT rich interactive domain 4B (Rbp1 like)	1.62	0.23
Prickle1	Prickle like 1 (Drosophila)	0.79	0.39
Dnahc7c	dynein, axonemal, heavy chain 7c	0.70	0.32
Stard6	StAR-related lipid transfer (START) domain containing 6	0.82	0.60
Plekhk1	pleckstrin homology domain containing, family K member 1	0.89	0.22
Clic6	chloride intracellular channel 6	0.76	0.28
Zfyve1	zinc finger, FYVE domain containing 1	1.08	0.18
AU021034	expressed sequence AU021034	0.31	0.08
Muc20	mucin 20	0.60	0.13
Dlgap1	discs, large (Drosophila) homolog-associated protein 1	0.85	0.48
Trpm3	transient receptor potential cation channel, subfamily M, member 3	1.35	0.44
Cdc42bpa	Cdc42 binding protein kinase alpha	1.02	0.72
Agps	Alkylglycerone phosphate synthase	1.43	0.23
Cdc14a	CDC14 cell division cycle 14 homolog A (S. cerevisiae)	0.37	0.03
Hs3st6	heparan sulfate (glucosamine) 3-O-sulfotransferase 6	0.81	0.03
Tmcc1	transmembrane and coiled coil domains 1	1.09	0.42
Gm1574	gene model 1574, (NCBI)	0.55	0.16
EG434128	predicted gene, EG434128	0.95	0.33
Atp8a1	ATPase, aminophospholipid transporter (APLT), class I, type 8A, member 1	0.99	0.37
Rab33a	RAB33A, member of RAS oncogene family	1.19	0.51

Zrsr2	zinc finger (CCCH type), RNA binding motif and serine/arginine rich 2	0.98	0.21
Dnttip2	deoxynucleotidyltransferase, terminal, interacting protein 2	0.66	0.43
Anxa8	annexin A8	1.15	0.32
Asgr1	asialoglycoprotein receptor 1	0.59	0.15
Fabp3	fatty acid binding protein 3, muscle and heart	0.77	0.31
Gli2	GLI-Kruppel family member GLI2	0.94	0.17
Hmgcs2	3-hydroxy-3-methylglutaryl-Coenzyme A synthase 2	0.36	0.13
Lhx3	LIM homeobox protein 3	1.25	0.47
Slc11a2	solute carrier family 11 (proton-coupled divalent metal ion transporters), member 2	0.84	0.50
Pou3f1	POU domain, class 3, transcription factor 1	1.06	0.24
Klrg1	killer cell lectin-like receptor subfamily G, member 1	0.87	0.55
Actr1a	ARP1 actin-related protein 1 homolog A (yeast)	1.09	0.33
Pcdha 4/6/7/5/11/	Protocadherin alpha 4, 6, 7, 5, 11,	0.71	0.39

Figure 10.15: Pattern D of the microarray heat map
RNA expression in normal airway control was normalised to a value of 1. The list indicates the gene symbol, the gene title and the fold change by which genes were unchanged in hyperplasia (hyper) cells but down regulated in adenoma (aden) cells.

Pattern E

Gene Symbol	Gene Title	Fold Change hyper	aden
Acox1	acyl-Coenzyme A oxidase 1, palmitoyl	2.35	1.77
Areg	amphiregulin	31.09	7.69
Arg2	arginase type II	4.66	10.16
Arpc1b	actin related protein 2/3 complex, subunit 1B	2.72	2.15
Phb2	prohibitin 2	2.62	3.57
Bmp1	bone morphogenetic protein 1	1.99	3.21
Tspo	translocator protein	2.85	2.60
Cebpa	CCAAT/enhancer binding protein (C/EBP), alpha	2.64	3.59
Celsr1	Cadherin EGF LAG seven-pass G-type receptor 1	3.14	2.89
Socs3	suppressor of cytokine signaling 3	10.43	7.12
Clu	clusterin	16.22	14.09
Clu	clusterin	5.69	4.99
Clu	clusterin	4.96	4.59
Clu	clusterin	5.34	4.39
Ctsh	cathepsin H	5.85	9.88
Fasn	fatty acid synthase	61.02	48.12
Lrp2	low density lipoprotein receptor-related protein 2	43.01	11.39
Cd74	CD74 antigen (invariant polypeptide of major histocompatibility complex, class II antigen-associated)	4.36	3.89
Il18rap	interleukin 18 receptor accessory protein	3.07	4.41
Itga7	integrin alpha 7	5.02	5.18
Itgb1bp1	integrin beta 1 binding protein 1	2.09	2.88
Napsa	napsin A aspartic peptidase	9.76	15.55
Kras	v-Ki-ras2 Kirsten rat sarcoma viral oncogene homolog	3.55	5.45
Lamb3	laminin, beta 3	2.21	2.69
Lcn2	lipocalin 2	24.35	35.70
Mal	myelin and lymphocyte protein, T-cell differentiation protein	8.67	10.90
Gtl2	GTL2, imprinted maternally expressed untranslated mRNA	38.16	138.84
Myh9	myosin, heavy polypeptide 9, non-muscle	2.53	2.87
Pcsk7	proprotein convertase subtilisin/kexin type 7	7.23	7.87
Ptprf	protein tyrosine phosphatase, receptor type, F	3.82	3.15
Ptprf	protein tyrosine phosphatase, receptor type, F	5.97	5.22
Scd1	stearoyl-Coenzyme A desaturase 1	5.82	2.79
Sftpc	surfactant associated protein C	1.88	2.68
Sftpc	Surfactant associated protein C	3.02	7.48
Slpi	secretory leukocyte peptidase inhibitor	7.14	11.76
Soat1	sterol O-acyltransferase 1	6.45	6.27
Soat1	sterol O-acyltransferase 1	28.68	15.26
Tnfaip1	tumor necrosis factor, alpha-induced protein 1 (endothelial)	2.22	2.11
Yipf3	Yip1 domain family, member 3	2.11	2.80
Nucb2	nucleobindin 2	2.53	5.65
Hip2	huntingtin interacting protein 2	4.09	2.77
Elovl1	elongation of very long chain fatty acids (FEN1/Elo2, SUR4/Elo3, yeast)-like 1	4.92	10.44
Elovl1	elongation of very long chain fatty acids (FEN1/Elo2, SUR4/Elo3, yeast)-like 1	2.84	3.93

Elovl1	elongation of very long chain fatty acids (FEN1/Elo2, SUR4/Elo3, yeast)-like 1	2.89	3.98
Phc2	polyhomeotic-like 2 (Drosophila)	3.16	3.62
Stard10	START domain containing 10	2.12	3.78
Rab9	RAB9, member RAS oncogene family	2.97	1.88
B4galt3	UDP-Gal:betaGlcNAc beta 1,4-galactosyltransferase, polypeptide 3	2.80	2.71
Slc22a17	solute carrier family 22 (organic cation transporter), member 17	1.59	2.33
Pno1	partner of NOB1 homolog (S. cerevisiae)	1.56	1.60
Atp6v1g1	ATPase, H+ transporting, lysosomal V1 subunit G1	2.50	2.84
Mrps15	mitochondrial ribosomal protein S15	1.74	2.19
Ubap1	ubiquitin-associated protein 1	2.28	1.91
Ergic1	endoplasmic reticulum-golgi intermediate compartment (ERGIC) 1	2.92	3.36
Tceb2	transcription elongation factor B (SIII), polypeptide 2	1.82	1.94
Zdhhc3	zinc finger, DHHC domain containing 3	11.55	15.57
Basp1	brain abundant, membrane attached signal protein 1	7.99	7.52
Lman1	lectin, mannose-binding, 1	2.11	1.83
Fuca1	fucosidase, alpha-L- 1, tissue	2.69	2.63
Phpt1	phosphohistidine phosphatase 1	4.25	5.21
Tmem56	transmembrane protein 56	2.82	1.90
Ptpn23	protein tyrosine phosphatase, non-receptor type 23	2.84	2.67
Otub1	OTU domain, ubiquitin aldehyde binding 1	5.46	3.69
Napa	N-ethylmaleimide sensitive fusion protein attachment protein alpha	2.13	3.48
Hdlbp	high density lipoprotein (HDL) binding protein	3.08	4.12
Aytl2	acyltransferase like 2	9.79	8.05
Aytl2	acyltransferase like 2	5.45	4.69
Tspan8	Tetraspanin 8	6.45	17.72
Aco1	aconitase 1	3.36	3.37
Aco1	aconitase 1	3.93	3.74
E2f5	E2F transcription factor 5	2.64	2.94
Fkbp10	FK506 binding protein 10	1.72	2.10
Fosb	FBJ osteosarcoma oncogene B	6.65	5.88
Hspa4	heat shock protein 4	2.19	2.00
Kpna3	karyopherin (importin) alpha 3	1.49	1.76
Lmna	lamin A	2.76	2.50
Marcks	Myristoylated alanine rich protein kinase C substrate	11.34	3.80
Pbx3	Pre B-cell leukemia transcription factor 3	17.34	6.92
pPtp4a3	protein tyrosine phosphatase 4a3	2.80	2.28
Scrg1	scrapie responsive gene 1	1.39	1.24
Sh3bp1	SH3-domain binding protein 1	3.93	3.29
Baz1b	bromodomain adjacent to zinc finger domain, 1B	4.06	2.13
Odz3	Odd Oz/ten-m homolog 3 (Drosophila)	3.43	2.26
D3Ertd300e	DNA segment, Chr 3, ERATO Doi 300, expressed	15.10	6.80
Ptges	prostaglandin E synthase	14.44	35.79
Wdr48	WD repeat domain 48	5.03	2.59
Acot7	acyl-CoA thioesterase 7	4.91	3.06
Ube2j2	ubiquitin-conjugating enzyme E2, J2 homolog (yeast)	1.72	2.13
D10Bwg1364e	DNA segment, Chr 10, Brigham & Women's Genetics 1364 expressed	2.07	2.79
Clcn5	chloride channel 5	1.38	1.72
Glp1r	glucagon-like peptide 1 receptor	1.82	2.59
Ipw	imprinted gene in the Prader-Willi syndrome region	2.53	2.58

Nedd10	neural precursor cell expressed, developmentally down-regulated gene 10	13.65	18.59
Cxcl15	chemokine (C-X-C motif) ligand 15	2.06	2.43
Cxcl15	chemokine (C-X-C motif) ligand 15	2.46	3.05
Ighmbp2	Immunoglobulin mu binding protein 2	3.40	2.70
Sort1	sortilin 1	6.42	4.18
Trf	transferrin	14.43	17.46
Abca7	ATP-binding cassette, sub-family A (ABC1), member 7	2.68	2.89
Ppap2c	phosphatidic acid phosphatase type 2c	2.98	5.61
Solh	Small optic lobes homolog (Drosophila)	4.40	3.86
Echdc2	enoyl Coenzyme A hydratase domain containing 2	2.42	2.45
Ppp2r2d	protein phosphatase 2, regulatory subunit B, delta isoform	1.81	1.80
Egfl6	EGF-like-domain, multiple 6	8.44	6.23
Retnla	resistin like alpha	3.33	1.87
Fads3	fatty acid desaturase 3	3.51	2.87
Fads3	fatty acid desaturase 3	3.14	3.16
Impg1	interphotoreceptor matrix proteoglycan 1	8.53	5.91
Pigy	phosphatidylinositol glycan anchor biosynthesis, class Y	1.60	2.15
Tmem35	transmembrane protein 35	5.25	8.57
Iah1	isoamyl acetate-hydrolyzing esterase 1 homolog (S. cerevisiae)	2.69	2.08
Ilf2	interleukin enhancer binding factor 2	1.95	3.39
Rab32	RAB32, member RAS oncogene family	3.92	5.88
Scgb3a1	secretoglobin, family 3A, member 1	7.23	6.52
Vars2l	valyl-tRNA synthetase 2-like	2.03	1.83
Noxo1	NADPH oxidase organizer 1	13.39	32.15
Jam4	junction adhesion molecule 4	3.39	3.95
Usp13	ubiquitin specific peptidase 13 (isopeptidase T-3)	1.89	2.24
Ibrdc3	IBR domain containing 3	14.16	8.93
Zdhhc20	zinc finger, DHHC domain containing 20	2.72	4.34
Slc38a3	solute carrier family 38, member 3	7.86	10.05
Abhd14b	abhydrolase domain containing 14b	1.84	1.86
Tanc2	Tetratricopeptide repeat, ankyrin repeat and coiled-coil containing 2	5.20	3.70
Arfgef2 /// LOC670796	ADP-ribosylation factor guanine nucleotide-exchange factor 2 (brefeldin A-inhibited) /// similar to ADP-ribosylation factor guanine nucleotide-exchange factor 2 (brefeldin A-inhibited)	3.89	3.97
Syt13	synaptotagmin XIII	2.05	2.31
Sorcs2	sortilin-related VPS10 domain containing receptor 2	2.90	2.99
Klb	klotho beta	3.09	1.99
AU018740	expressed sequence AU018740	3.93	3.74
Rabif	RAB interacting factor	1.78	2.50
Abtb2	ankyrin repeat and BTB (POZ) domain containing 2	3.65	3.55
Magi3	membrane associated guanylate kinase, WW and PDZ domain containing 3	5.32	4.37
AU015263	expressed sequence AU015263	6.97	10.22
Cog4	component of oligomeric golgi complex 4	2.17	2.71
Mapkapk3	mitogen-activated protein kinase-activated protein kinase 3	2.96	2.99
Gmpr2	guanosine monophosphate reductase 2	1.53	2.20
Kctd1	potassium channel tetramerisation domain containing 1	2.63	2.10
Coro2a	Coronin, actin binding protein 2A	1.74	2.06
Brunol4	bruno-like 4, RNA binding protein (Drosophila)	6.09	6.45
Epsti1	epithelial stromal interaction 1 (breast)	2.20	2.11

Mta3	Metastasis associated 3	2.06	1.49
Pqlc2	PQ loop repeat containing 2	5.82	7.59
D10Bwg1379e	DNA segment, Chr 10, Brigham & Women's Genetics 1379 expressed	1.77	1.45
Cd300a	CD300A antigen	4.45	3.69
Naprt1	nicotinate phosphoribosyltransferase domain containing 1	8.22	10.11
Mcat	malonyl CoA:ACP acyltransferase (mitochondrial)	1.80	1.66
Atp13a4	ATPase type 13A4	7.72	21.59
Lrfn4	leucine rich repeat and fibronectin type III domain containing 4	2.61	3.08
Smc5	structural maintenance of chromosomes 5	7.48	3.51
Fer1l3	fer-1-like 3, myoferlin (C. elegans)	3.04	2.89
B3gnt7	UDP-GlcNAc:betaGal beta-1,3-N-acetylglucosaminyltransferase 7	5.46	3.73
BC059842	cDNA sequence BC059842	3.43	6.58
BC059842	cDNA sequence BC059842	5.01	11.60
Zmpste24	zinc metallopeptidase, STE24 homolog (S. cerevisiae)	2.61	2.98
Fbxo44	F-box protein 44	1.86	2.53
Bud31	BUD31 homolog (yeast)	1.68	2.66
Fuk	fucokinase	2.05	2.40
Ttc13	tetratricopeptide repeat domain 13	2.56	3.80
Ttc13	tetratricopeptide repeat domain 13	3.07	4.22
St8sia6	ST8 alpha-N-acetyl-neuraminide alpha-2,8-sialyltransferase 6	15.01	34.02
Slc26a11	Solute carrier family 26, member 11	3.61	2.77
Pask	PAS domain containing serine/threonine kinase	1.63	1.43
Ppp2r2c	Protein phosphatase 2 (formerly 2A), regulatory subunit B (PR 52), gamma isoform	4.30	7.62
Klhdc1	kelch domain containing 1	3.25	2.43
Ctdspl2	CTD (carboxy-terminal domain, RNA polymerase II, polypeptide A) small phosphatase like 2	2.57	3.25
Cyp3a44	cytochrome P450, family 3, subfamily a, polypeptide 44	1.99	1.89
Tbc1d2	TBC1 domain family, member 2	5.85	8.30
LOC433351	hypothetical gene supported by AK081809	4.04	2.38
LOC637870	similar to Nedd4 WW binding protein 4	3.89	2.75
Adra2c	adrenergic receptor, alpha 2c	2.37	2.93
Akp5	alkaline phosphatase 5	6.56	8.12
Bcl3	B-cell leukemia/lymphoma 3	7.67	4.78
S100g	S100 calcium binding protein G	4.40	3.40
Cnn2	calponin 2	2.61	3.84
Dab1	disabled homolog 1 (Drosophila)	4.22	3.73
F13b	coagulation factor XIII, beta subunit	4.34	2.40
Il2rb	interleukin 2 receptor, beta chain	1.99	2.25
Lyzs	lysozyme	2.86	3.14
Naga	N-acetyl galactosaminidase, alpha	3.08	2.70
Lypla1	lysophospholipase 1	1.57	1.52
Prep	prolyl endopeptidase	1.84	1.87
Rgs16	regulator of G-protein signaling 16	15.21	8.66
Ring1	ring finger protein 1	2.21	1.90
Exoc4	exocyst complex component 4	2.56	3.37
Thbs2	thrombospondin 2	2.30	4.43
Rnf11	Ring finger protein 11	7.33	6.75
Txnl2	thioredoxin-like 2	1.70	1.75
Stx5a	syntaxin 5A	1.80	2.71

	39331	Septin 6	6.30	4.61
Mrpl24		mitochondrial ribosomal protein L24	1.96	1.69
Ptms		parathymosin	2.45	2.56
Ptms		parathymosin	3.01	3.24
Kcmf1		potassium channel modulatory factor 1	3.15	3.49
Ndfip2		Nedd4 family interacting protein 2	2.51	2.43
Kdelr3		KDEL (Lys-Asp-Glu-Leu) endoplasmic reticulum protein retention receptor 3	2.13	2.84
Serpina10		serine (or cysteine) peptidase inhibitor, clade A (alpha-1 antiproteinase, antitrypsin), member 10	4.63	2.75
Gtf3c1		general transcription factor III C 1	2.76	2.49
Capzb		capping protein (actin filament) muscle Z-line, beta	1.61	1.55
Clgn		calmegin	2.46	1.73
Egf		epidermal growth factor	2.24	2.28
Kcnq1		Potassium voltage-gated channel, subfamily Q, member 1	2.79	2.41
Ltbp2		latent transforming growth factor beta binding protein 2	5.62	8.53
Pbx2		pre B-cell leukemia transcription factor 2	3.32	5.05
Prkca		protein kinase C, alpha	3.26	4.54
Txnrd2		thioredoxin reductase 2	2.30	1.83
Chmp2b		chromatin modifying protein 2B	2.58	1.91
Ccdc101		coiled-coil domain containing 101	2.15	1.69
Nans		N-acetylneuraminic acid synthase (sialic acid synthase)	4.50	6.69
Cog8		component of oligomeric golgi complex 8	1.78	2.48
Adrbk1		adrenergic receptor kinase, beta 1	3.75	2.54

Figure 10.16: Pattern E of the microarray heat map
RNA expression in normal airway control was normalised to a value of 1. The list indicates the gene symbol, the gene title and the fold change by which genes were up regulated in both hyperplasia (hyper) cells and in adenoma (aden) cells.
.

Pattern F

Gene Symbol	Gene Title	Fold Change hyper	aden
Kcnd3	potassium voltage-gated channel, Shal-related family, member 3	0.13	0.23
Amy1	amylase 1, salivary	0.15	0.11
Cacnb2	calcium channel, voltage-dependent, beta 2 subunit	0.36	0.42
Runx1t1	runt-related transcription factor 1; translocated to, 1 (cyclin D-related)	0.22	0.11
Mb	myoglobin	0.09	0.06
Mpdz	Multiple PDZ domain protein	0.56	0.52
Myh6	myosin, heavy polypeptide 6, cardiac muscle, alpha	0.04	0.02
Myom2	myomesin 2	0.07	0.06
Ncam1	Neural cell adhesion molecule 1	0.31	0.18
Plcb1	phospholipase C, beta 1	0.39	0.59
Omd	osteomodulin	0.15	0.29
Nell2	NEL-like 2 (chicken)	0.27	0.13
Hspb8	heat shock protein 8	0.71	0.54
Ces3	carboxylesterase 3	0.31	0.21
Ces3	carboxylesterase 3	0.29	0.19
Defcr-rs12	defensin related cryptdin, related sequence 12	0.39	0.39
Slc26a3	solute carrier family 26, member 3	0.58	0.43
Myoz2	myozenin 2	0.08	0.04
C85319	expressed sequence C85319	0.56	0.60
Synpo2	synaptopodin 2	0.07	0.24
Stac2	SH3 and cysteine rich domain 2	0.71	0.65
Dpp10	dipeptidylpeptidase 10	0.10	0.08
A730046J16	hypothetical protein A730046J16	0.19	0.14
C630010N09	hypothetical protein C630010N09	0.71	0.63
Ogt	O-linked N-acetylglucosamine (GlcNAc) transferase (UDP-N-acetylglucosamine:polypeptide-N-acetylglucosaminyl transferase)	0.20	0.36
Cyp2a4 /// Cyp2a5	cytochrome P450, family 2, subfamily a, polypeptide 4 /// cytochrome P450, family 2, subfamily a, polypeptide 5	0.18	0.05
Dynll1 /// EG627788 /// LOC637840 /// LOC672375	dynein light chain LC8-type 1 /// predicted gene, EG627788 /// similar to dynein, cytoplasmic, light peptide /// similar to dynein, cytoplasmic, light peptide	0.75	0.64
Eml1 /// LOC634102	echinoderm microtubule associated protein like 1 /// similar to echinoderm microtubule associated protein like 1	0.61	0.75

Figure 10.17: Pattern F of the microarray heat map
RNA expression in normal airway control was normalised to a value of 1. The list indicates the gene symbol, the gene title and the fold change by which genes were down regulated in both hyperplasia (hyper) and adenoma (aden) cells.

Pattern G

Gene Symbol	Gene Title	Fold Change hyper	aden
Cd82	CD82 antigen	1.37	0.44
Fmr1	fragile X mental retardation syndrome 1 homolog	3.12	0.66
Gaa	glucosidase, alpha, acid	1.60	0.66
Gyk	glycerol kinase	1.31	0.83
Ptn	pleiotrophin	2.03	0.33
Punc	Putative neuronal cell adhesion molecule	1.73	0.73
Cp	ceruloplasmin	2.22	0.49
Cp	ceruloplasmin	2.43	0.51
Epha4	Eph receptor A4	2.09	0.44
Fgfr4	fibroblast growth factor receptor 4	1.54	0.72
Fzd3	frizzled homolog 3 (Drosophila)	1.24	0.58
Lnx1	ligand of numb-protein X 1	1.79	0.47
Myo1b	myosin IB	5.20	0.28
Ryr2	Ryanodine receptor 2, cardiac	1.52	0.70
Siah1a	seven in absentia 1A	1.53	0.48
Tuba-rs1	tubulin alpha, related sequence 1	1.28	0.69
Syt6	synaptotagmin VI	1.99	0.68
Sltm	SAFB-like, transcription modulator	2.02	0.61
Cnn3	calponin 3, acidic	1.55	0.73
Cnn3	calponin 3, acidic	1.60	0.68
Aldh7a1	aldehyde dehydrogenase family 7, member A1	1.67	0.56
Srfbp1	serum response factor binding protein 1	3.77	0.47
Stk35	serine/threonine kinase 35	1.24	0.68
Chd8	Chromodomain helicase DNA binding protein 8	1.83	0.33
Pot1b	protection of telomeres 1B	2.93	0.60
Wdr35	WD repeat domain 35	1.55	0.76
Glt8d2	glycosyltransferase 8 domain containing 2	1.40	0.73
Ccdc46	coiled-coil domain containing 46	2.00	0.61
Glis2	GLIS family zinc finger 2	1.32	0.86
Hmgn3	high mobility group nucleosomal binding domain 3	2.00	0.45
AA673488	expressed sequence AA673488	1.49	0.38
Tbcd	tubulin-specific chaperone d	1.74	0.57
AB056442	cDNA sequence AB056442	1.49	0.81
Gabrp	gamma-aminobutyric acid (GABA-A) receptor, pi	1.62	0.74
Fnip1	folliculin interacting protein 1	2.79	0.20
BC022687	cDNA sequence BC022687	1.65	0.60
Ccdc106	coiled-coil domain containing 106	1.99	0.60
Sytl1	synaptotagmin-like 1	1.46	0.72
BC038156	cDNA sequence BC038156	2.25	0.61
Prr11	proline rich 11	1.41	0.55
Mcc	mutated in colorectal cancers	1.86	0.24
Slc9a9	solute carrier family 9 (sodium/hydrogen exchanger), isoform 9	1.93	0.38
Apoa1	apolipoprotein A-I	2.57	0.41
Gria4	glutamate receptor, ionotropic, AMPA4 (alpha 4)	1.39	0.53
Kcnd2	Potassium voltage-gated channel, Shal-related family, member 2	2.19	0.72
Vav2	Vav2 oncogene	1.59	0.68

Abcd2	ATP-binding cassette, sub-family D (ALD), member 2	5.07	0.56
Mtmr7	myotubularin related protein 7	1.81	0.60
P140	P140 gene	3.33	0.44
Abcb9	ATP-binding cassette, sub-family B (MDR/TAP), member 9	1.21	0.72
Sdhc	succinate dehydrogenase complex, subunit C, integral membrane protein	1.46	0.65
Cab39l	Calcium binding protein 39-like	4.08	0.54
Brd1	bromodomain containing 1	1.42	0.77
Aars	alanyl-tRNA synthetase	1.92	0.63
Bmpr1b	bone morphogenetic protein receptor, type 1B	1.59	0.72
Ercc3	excision repair cross-complementing rodent repair deficiency, complementation group 3	2.49	0.66
Zfp207	zinc finger protein 207	1.30	0.56
Psmb3	proteasome (prosome, macropain) subunit, beta type 3	1.33	0.82
Cmtm3	CKLF-like MARVEL transmembrane domain containing 3	1.47	0.44
Tiparp	TCDD-inducible poly(ADP-ribose) polymerase	1.63	0.59

Figure 10.18: Pattern G of the microarray heat map
RNA expression in normal airway control was normalised to a value of 1. The list indicates the gene symbol, the gene title and the fold change by which genes were up regulated in hyperplasia (hyper) cells but down regulated in adenoma (aden) cells.

Pattern H

Gene Symbol	Gene Title	Fold Change hyper	aden
Ppil2	peptidylprolyl isomerase (cyclophilin)-like 2	0.72	1.21
Slain1	SLAIN motif family, member 1	0.68	1.59
Gprk5	G protein-coupled receptor kinase 5	0.74	1.78
Synj2	synaptojanin 2	0.81	1.67
Ube2s	ubiquitin-conjugating enzyme E2S	0.52	1.28
Oog1	oogenesin 1	0.57	1.59
Defcr3	defensin related cryptdin 3	0.79	1.31
Tmem54	transmembrane protein 54	0.61	1.60
Lrp2bp	Lrp2 binding protein	0.46	2.97
Rnf122	ring finger protein 122	0.36	1.58
Cep164	centrosomal protein 164	0.81	1.22
Slc35f1	solute carrier family 35, member F1	0.34	2.88
Gmds	GDP-mannose 4, 6-dehydratase	0.84	1.36
Klrb1f	killer cell lectin-like receptor subfamily B member 1F	0.63	1.75
Tmem161a	transmembrane protein 161A	0.44	2.15
Lman1l	lectin, mannose-binding 1 like	0.47	1.66
BC012278	cDNA sequence BC012278	0.82	1.54
Glra2	glycine receptor, alpha 2 subunit	0.37	1.52
C920021A13	hypothetical protein C920021A13	0.82	1.22
A4gnt	Alpha-1,4-N-acetylglucosaminyltransferase	0.85	1.45
Serpina11	serine (or cysteine) peptidase inhibitor, clade A (alpha-1 antiproteinase, antitrypsin), member 11	0.53	1.47
Vps4b	Vacuolar protein sorting 4b (yeast)	0.87	1.27
Tuba1 /// LOC544863	tubulin, alpha 1 /// similar to tubulin, alpha 1	0.76	1.28
Anks1b /// LOC544718	ankyrin repeat and sterile alpha motif domain containing 1B /// similar to AIDA-1b	0.85	1.52

Figure 10.19: Pattern H of the microarray heat map
RNA expression in normal airway control was normalised to a value of 1. The list indicates the gene symbol, the gene title and the fold change by which genes were down regulated in hyperplasia (hyper) cells but up regulated in adenoma (aden) cells.

```
bmpr2           ------------------------------------------------------------
primer1         ATTGTGATACGGGCAGGATCAGTCCACGGGAGAGAAGACGAGCCTCCCGGCTGTTTCTCC 60


bmpr2           ------------------------------------------------------------AT 2
primer1         GCCGGTCTACTTCCCATATTTCTTTTCTTTGCCCTCCTGATTCTTGGCTGGCCCAGGGAT 120
                                                                          **

bmpr2           GACTTCCTCGCTGCAGCGGCCCTGGCGGGTGCCCTGGCTACCATGGACCATCCTGCTGGT 62
primer1         GACTTCCTCGCTGCAGCGGCCCTGGCGGGTGCCCTGGCTACCATGGACCATCCTGCTGGT 180
                ************************************************************

bmpr2           CAGCACTGCGGCTGCTTCGCAGAATCAAGAACGGCTATGTGCGTTTAAAGATCCGTATCA 122
primer1         CAGCACTGCGGCTGCTTCGCAGAATCAAGAACGGCTATGTGCGTTTAAAGATCCGTATCA 240
                ************************************************************

bmpr2           GCAAGACCTTGGGATAGGTGAGAGTAGAATCTCTCATGAAAATGGGACAATATTATGCTC 182
primer1         GCAAGACCTTGGGATAGGTGAGAGTAGAATCTCTCATGAAAATGGGACAATATTATGCTC 300
                ************************************************************

bmpr2           GAAAGGTAGCACCTGCTATGGCCTTTGGGAGAAATCAAAAGGGGACATAAATCTTGTAAA 242
primer1         GAAAGGTAGCACCTGCTATGGCCTTTGGGAGAAATCAAAAGGGGACATAAATCTTGTAAA 360
                ************************************************************

bmpr2           ACAAGGATGTTGGTCTCACATTGGAGATCCCCAAGAGTGTCACTATGAAGAATGTGTAGT 302
primer1         ACAAGGATGTTGGTCTCACATTGGAGATCCCCAAGAGTGTCCCTATGAAGAATGAGTAG- 419
                ****************************************** ************ ****

bmpr2           AACTACCACTCCTCCCTCAATTCAGAATGGAACATACCGTTTCTGCTGTTGTAGCACAGA 362
primer1         ------------------------------------------------------------


bmpr2           TTTATGTAATGTCAACTTTACTGAGAATTTTCCACCTCCTGACACAACACCACTCAGTCC 422
primer1         ------------------------------------------------------------
bmpr2           CCACCTCATTCATTTAACCGAGATGAGACAATAATCATTGCTTTGGCATCAGTCTCTGTA 480
primer2         ------------------------------------------------------------


bmpr2           TTAGCTGTTTTGATAGTTGCCTTATGCTTTGGATACAGAATGTTGACAGGAGACCGTAAA 540
primer2         ------------------------------------------------------------


bmpr2           CAAGGTCTTCACAGTATGAACATGATGGAGGCAGCAGCATCCGAACCCTCTCTTGATCTA 600
primer2         ------------------------------------------------------------


bmpr2           GATAATCTGAAACTGTTGGAGCTGATTGGCCGAGGTCGATATGGAGCAGTATATAAAGGC 660
primer2         ------------------------------------------------------------


bmpr2           TCCTTGGATGAGCGTCCAGTTGCTGTAAAAGTGTTTTCCTTTGCAAACCGTCAGAATTTT 720
primer2         ---------------CAGCTTGCTGTAAAAGTGTTTTCCTTTGCAAACCGTCAGAATTTT 45
                             *   ****************************************

bmpr2           ATCAACGAAAAGAACATTTACAGAGTGCCTTTGATGGAACATGACAACATTGCCCGCTTT 780
primer2         ATCAACGAAAAGAACATTTACAGAGTGCCTTTGATGGAACATGACAACATTGCCCGCTTT 105
                ************************************************************

bmpr2           ATAGTTGGAGATGAGAGAGTCACTGCAGATGGACGCATGGAATATTTGCTTGTGATGGAG 840
primer2         ATAGTTGGAGATGAGAGAGTCACTGCAGATGGACGCATGGAATATTTGCTTGTGATGGAG 165
                ************************************************************

bmpr2           TACTATCCCAATGGATCTTTATGCAAGTATTTAAGTCTCCACACAAGTGACTGGGTAAGC 900
primer2         TACTATCCCAATGGATCTTTATGCAAGTATTTAAGTCTCCACACAAGTGACTGGGTAAGC 225
                ************************************************************

bmpr2           TCTTGCCGTCTTGCTCATTCTGTTACTAGAGGACTGGCTTATCTTCACACAGAATTACCA 960
primer2         TCTTGCCGTCTTGCTCATTCTGTTACTAGAGGACTGGCTTATCTTCACACAGAATTACCA 285
                ************************************************************
```

```
bmpr2           CGAGGAGATCATTATAAACCTGCAATTTCCCATCGAGATTTAAACAGCAGAAATGTCCTA 1020
primer2         CGAGGAGATCATTATAAACCTGCAATTTCCCATCGAGATTTAAACAGCAGAAATGTCCTA 345
                ************************************************************

bmpr2           GTGAAAAATGATGGAACCTGTGTTATTAGTGACTTTGGACTGTCCATGAGGCTGACTGGA 1080
primer2         GTGAAAAATGATGGAACCTGTGTTATTAGTGACTTTGGACTGTCCATGACGCTGACTG-- 403
                ********************************************** ********

bmpr2           AATAGACTGGTGCGCCCAGGGGAGGAAGATAATGCAGCCATAAGCGAGGTTGGCACTATC 1140
primer2         ------------------------------------------------------------

bmpr2           AGATATATGGCACCAGAAGTGCTAGAAGGAGCTGTGAACTTGAGGGACTGTGAATCAGCT 1200
primer2         ------------------------------------------------------------

bmpr2           TTGAAACAAGTAGACATGTATGCTCTTGGACTAATCTATTGGGAGATATTTATGAGATGT 1260
primer2         ------------------------------------------------------------

bmpr2           ACAGACCTCTTCCCAGGGGAATCCGTACCAGAGTACCAGATGGCTTTTCAGACAGAGGTT 1320
primer2         ------------------------------------------------------------

bmpr2           GGAAACCATCCCACTTTTGAGGATATGCAGGTTCTCGTGTCTAGGGAAAAACAGAGACCC 1380
primer3         ------------------------------------------------------------

bmpr2           AAGTTCCCAGAAGCCTGGAAAGAAAATAGCCTGGCAGTGAGGTCACTCAAGGAGACAATC 1440
primer3         ------------------------------------------------------------

bmpr2           GAAGACTGTTGGGACCAGGATGCAGAGGCTCGGCTTACTGCACAGTGTGCTGAGGAAAGG 1500
primer3         -----------GGGACAGGATGCAGAGGCTCGGCTTACTGCACAGTGTGCTGAGGAAAGG 49
                           **  ******************************************

bmpr2           ATGGCTGAACTTATGATGATTTGGGAAAGAAACAAATCTGTGAGCCCAACAGTCAATCCA 1560
primer3         ATGGCTGAACTTATGATGATTTGGGAAAGAAACAAATCTGTGAGCCCAACAGTCAATCCA 109
                ************************************************************

bmpr2           ATGTCTACTGCTATGCAGAATGAACGCAACCTGTCACATAATAGGCGTGTGCCAAAAATT 1620
primer3         ATGTCTACTGCTATGCAGAATGAACGCAACCTGTCACATAATAGGCGTGTGCCAAAAATT 169
                ************************************************************

bmpr2           GGTCCTTATCCAGATTATTCTTCCTCCTCATACATTGAAGACTCTATCCATCATACTGAC 1680
primer3         GGTCCTTATCCAGATTATTCTTCCTCCTCATACATTGAAGACTCTATCCATCATACTGAC 229
                ************************************************************

bmpr2           AGCATCGTGAAGAATATTTCCTCTGAGCATTCTATGTCCAGCACACCTTTGACTATAGGG 1740
primer3         AGCATCGTGAAGAATATTTCCTCTGAGCATTCTATGTCCAGCACACCTTTGACTATAGGG 289
                ************************************************************

bmpr2           GAAAAAAACCGAAATTCAATTAACTATGAACGACAGCAAGCACAAGCTCGAATCCCCAGC 1800
primer3         GAAAAAAACCGAAATTCAATTAACTATGAACGACAGCAAGCACAAGCTCGAATCCCCAGC 349
                ************************************************************

bmpr2           CCTGAAACAAGTGTCACCAGCCTCTCCACCAACACAACAACCACAAACACCACAGGACTC 1860
primer3         CCTGAAACAAGTGTC---------------------------------------------- 364
                ***************

bmpr2           ACGCCAAGTACTGGCATGACTACTATATCTGAGATGCCATACCCAGATGAAACAAATCTG 1920
primer3         ------------------------------------------------------------

bmpr2           CATACCACAAATGTTGCACAGTCAATTGGGCCAACCCCTGTCTGCTTACAGCTGACAGAA 1980
primer3         ------------------------------------------------------------

bmpr2           GAAGACTTGGAAACCAACAAGCTAGACCCAAAAGAAGTTGATAAGAACCTCAAGGAAAGC 2040
primer3         ------------------------------------------------------------
```

```
bmpr2           TCTGATGAGAATCTCATGGAGCACTCTCTTAAACAGTTCAGTGGCCCAGACCCACTGAGC 2100
primer3         ------------------------------------------------------------


bmpr2           AGTACTAGTTCTAGCTTGCTTTACCCACTCATAAAACTTGCAGTAGAAGCAACTGGACAG 2160
primer3         ------------------------------------------------------------

bmpr2           CAGGACTTCACACAGACTGCAAATGGCCAAGCATGTTTGATTCCTGATGTTCTGCCTACT 2220
primer4         ------------------------------------------------------------


bmpr2           CAGATCTATCCTCTCCCCAAGCAGCAGAACCTTCCCAAGAGACCTACTAGTTTGCCTTTG 2280
primer4         ------------------------------------------------------------


bmpr2           AACACCAAAAATTCAACAAAAGAGCCCCGGCTAAAATTTGGCAGCAAGCACAAATCAAAC 2340
primer4         -AC-CCAAAAATTCAACAAAAGAGCCCCGGCTAAAATTTGGCAGCAAGCACAAATCAAAC 58
                 ** ************************************************************


bmpr2           TTGAAACAAGTCGAAACTGGAGTTGCCAAGATGAATACAATCAATGCAGCAGAACCTCAT 2400
primer4         TTGAAACAAGTCGAAACTGGAGTTGCCAAGATGAATACAATCAATGCAGCAGAACCTCAT 118
                ************************************************************


bmpr2           GTGGTGACAGTCACCATGAATGGTGTGGCAGGTAGAAACCACAGTGTTAACTCCCATGCT 2460
primer4         GTGGTGACAGTCACCATGAATGGTGTGGCAGGTAGAAACCACAGTGTTAACTCCCATGCT 178
                ************************************************************


bmpr2           GCCACAACCCAATATGCCAATGGGACAGTACTATCTGGCCAAACAACCAACATAGTGACA 2520
primer4         GCCACAACCCAATATGCCAATGGGACAGTACTATCTGGCCAAACAACCAACATAGTGACA 238
                ************************************************************


bmpr2           CATAGGGCCCAAGAAATGTTGCAGAATCAGTTTATTGGTGAGGACACCCGGCTGAATATT 2580
primer4         CATAGGGCCCAAGAAATGTTGCAGAATCAGTTTATTGGTGAGGACACCCGGCTGAATATT 298
                ************************************************************


bmpr2           AATTCCAGTCCTGATGAGCATGAGCCTTTACTGAGACGAGAGCAACAAGCTGGCCATGAT 2640
primer4         AATTCCCGTCCTGACGAGCATGAGCCTTTACTGAGACCAGAGCA---------------- 342
                ****** ******* ********************** ******


bmpr2           GAAGGTGTTCTGGATCGTCTTGTGGACAGGAGGGAACGGCCACTAGAAGGTGGCCGAACT 2700
primer4         ------------------------------------------------------------


bmpr2           AATTCCAATAACAACAACAGCAATCCATGTTCAGAACAAGATGTTCTTGCACAGGGTGTT 2760
primer4         ------------------------------------------------------------


bmpr2           CCAAGCACAGCAGCAGATCCTGGGCCATCAAAGCCCAGAAGAGCACAGAGGCCTAATTCT 2820
primer4         ------------------------------------------------------------


bmpr2           CTGGATCTTTCAGCCACAAATGTCCTGGATGGCAGCAGTATACAGATAGGTGAGTCAACA 2880
primer4         ------------------------------------------------------------


bmpr2           CAAGATGGCAAATCAGGATCAGGTGAAAAGATCAAGAAACGTGTGAAAACTCCCTATTCT 2940
primer4         ------------------------------------------------------------


bmpr2           CTTAAGCGGTGGCGCCCCTCCACCTGGGTCATCTCCACTGAATCGCTGGACTGTGAAGTC 3000
primer4         ------------------------------------------------------------


bmpr2           AACAATAATGGCAGTAACAGGGCAGTTCATTCCAAATCCAGCACTGCTGTTTACCTTGCA 3060
primer4         ------------------------------------------------------------


bmpr2           GAAGGAGGCACTGCTACAACCATGGTGTCTAAAGATATAGGAATGAACTGTCTGTGA 3117
primer4         ------------------------------------------------------------
```

Figure 10.20 pCMV-BMPRII sequencing results
Sequencing results from pCMV-BMPRII plasmid were aligned to BMPRII cDNA sequence NM_ using the ClustalW programme. (BMPR2=BMPRII)

10. Bibliography

Akhtar, S. (2006) Non-viral cancer gene therapy: beyond delivery. Gene Ther, 13, 739-740.

Al-Shahrour, F., Minguez, P., Tarraga, J., Medina, I., Alloza, E., Montaner, D. and Dopazo, J. (2007) FatiGO +: a functional profiling tool for genomic data. Integration of functional annotation, regulatory motifs and interaction data with microarray experiments. Nucleic acids research, 35, W91-96.

Al-Shahrour, F., Minguez, P., Vaquerizas, J. M., Conde, L. and Dopazo, J. (2005) BABELOMICS: a suite of web tools for functional annotation and analysis of groups of genes in high-throughput experiments. Nucleic acids research, 33, W460-464.

Alami, J., Williams, B. R. and Yeger, H. (2003) Differential expression of E-cadherin and beta catenin in primary and metastatic Wilms's tumours. Mol Pathol, 56, 218-225.

Alarmo, E. L., Kuukasjarvi, T., Karhu, R. and Kallioniemi, A. (2007) A comprehensive expression survey of bone morphogenetic proteins in breast cancer highlights the importance of BMP4 and BMP7. Breast cancer research and treatment, 103, 239-246.

Aldred, M. A., Vijayakrishnan, J., James, V., Soubrier, F., Gomez-Sanchez, M. A., Martensson, G., Galie, N., Manes, A., Corris, P., Simonneau, G., Humbert, M., Morrell, N. W. and Trembath, R. C. (2006) BMPR2 gene rearrangements account for a significant proportion of mutations in familial and idiopathic pulmonary arterial hypertension. Human mutation, 27, 212-213.

Algul, H. and Schmid, R. M. (2008) Pancreatic cancer: a plea for good and comprehensive morphological studies. European journal of gastroenterology & hepatology, 20, 713-715.

Anastasi, S., Sala, G., Huiping, C., Caprini, E., Russo, G., Iacovelli, S., Lucini, F., Ingvarsson, S. and Segatto, O. (2005) Loss of RALT/MIG-6 expression in ERBB2-amplified breast carcinomas enhances ErbB-2 oncogenic potency and favors resistance to Herceptin. Oncogene, 24, 4540-4548.

Arsalane, K., Broeckaert, F., Knoops, B., Wiedig, M., Toubeau, G. and Bernard, A. (2000) Clara cell specific protein (CC16) expression after acute lung inflammation induced by intratracheal lipopolysaccharide administration. American journal of respiratory and critical care medicine, 161, 1624-1630.

Ashcroft, G. S., Yang, X., Glick, A. B., Weinstein, M., Letterio, J. L., Mizel, D. E., Anzano, M., Greenwell-Wild, T., Wahl, S. M., Deng, C. and Roberts, A. B. (1999) Mice lacking Smad3 show accelerated wound healing and an impaired local inflammatory response. Nature cell biology, 1, 260-266.

Bailey-Wilson, J. E., Amos, C. I., Pinney, S. M., Petersen, G. M., de Andrade, M., Wiest, J. S., Fain, P., Schwartz, A. G., You, M., Franklin, W., Klein, C., Gazdar, A., Rothschild, H., Mandal, D., Coons, T., Slusser, J., Lee, J., Gaba, C., Kupert, E., Perez, A., Zhou, X., Zeng, D., Liu, Q., Zhang, Q., Seminara, D., Minna, J. and Anderson, M. W. (2004) A major lung cancer susceptibility locus maps to chromosome 6q23-25. American journal of human genetics, 75, 460-474.

Barros, R., Pereira, B., Duluc, I., Azevedo, M., Mendes, N., Camilo, V., Jacobs, R., Paulo, P., Santos-Silva, F., van Seuningen, I., van den Brink, G., David, L., Freund, J. N. and Almeida, R. (2008) Key elements of the BMP/SMAD pathway

co-localize with CDX2 in intestinal metaplasia and regulate CDX2 expression in human gastric cell lines. The Journal of pathology.

Bauer, G., Dao, M. A., Case, S. S., Meyerrose, T., Wirthlin, L., Zhou, P., Wang, X., Herrbrich, P., Arevalo, J., Csik, S., Skelton, D. C., Walker, J., Pepper, K., Kohn, D. B. and Nolta, J. A. (2008) In vivo biosafety model to assess the risk of adverse events from retroviral and lentiviral vectors. Mol Ther, 16, 1308-1315.

Beavon, I. R. (2000) The E-cadherin-catenin complex in tumour metastasis: structure, function and regulation. Eur J Cancer, 36, 1607-1620.

Beck, D. C., Ikegami, M., Na, C. L., Zaltash, S., Johansson, J., Whitsett, J. A. and Weaver, T. E. (2000) The role of homodimers in surfactant protein B function in vivo. The Journal of biological chemistry, 275, 3365-3370.

Beck, S. E., Jung, B. H., Del Rosario, E., Gomez, J. and Carethers, J. M. (2007) BMP-induced growth suppression in colon cancer cells is mediated by p21WAF1 stabilization and modulated by RAS/ERK. Cellular signalling, 19, 1465-1472.

Belinsky, S. A. (2004) Gene-promoter hypermethylation as a biomarker in lung cancer. Nature reviews, 4, 707-717.

Beppu, H., Mwizerwa, O. N., Beppu, Y., Dattwyler, M. P., Lauwers, G. Y., Bloch, K. D. and Goldstein, A. M. (2008) Stromal inactivation of BMPRII leads to colorectal epithelial overgrowth and polyp formation. Oncogene, 27, 1063-1070.

Betsuyaku, T. and Senior, R. M. (2004) Laser capture microdissection and mRNA characterization of mouse airway epithelium: methodological considerations. Micron, 35, 229-234.

Blanco, M. J., Moreno-Bueno, G., Sarrio, D., Locascio, A., Cano, A., Palacios, J. and Nieto, M. A. (2002) Correlation of Snail expression with histological grade and lymph node status in breast carcinomas. Oncogene, 21, 3241-3246.

Blumenthal, M. N. (2005) The role of genetics in the development of asthma and atopy. Current opinion in allergy and clinical immunology, 5, 141-145.

Bobinac, D., Maric, I., Zoricic, S., Spanjol, J., Dordevic, G., Mustac, E. and Fuckar, Z. (2005) Expression of bone morphogenetic proteins in human metastatic prostate and breast cancer. Croatian medical journal, 46, 389-396.

Borok, Z., Harboe-Schmidt, J. E., Brody, S. L., You, Y., Zhou, B., Li, X., Cannon, P. M., Kim, K. J., Crandall, E. D. and Kasahara, N. (2001) Vesicular stomatitis virus G-pseudotyped lentivirus vectors mediate efficient apical transduction of polarized quiescent primary alveolar epithelial cells. J Virol, 75, 11747-11754.

Brady-Kalnay, S. M., Mourton, T., Nixon, J. P., Pietz, G. E., Kinch, M., Chen, H., Brackenbury, R., Rimm, D. L., Del Vecchio, R. L. and Tonks, N. K. (1998) Dynamic interaction of PTPmu with multiple cadherins in vivo. The Journal of cell biology, 141, 287-296.

Braido, F., Riccio, A. M., Guerra, L., Gamalero, C., Zolezzi, A., Tarantini, F., De Giovanni, B., Folli, C., Descalzi, D. and Canonica, G. W. (2007) Clara cell 16 protein in COPD sputum: a marker of small airways damage? Respiratory medicine, 101, 2119-2124.

Brambilla, E., Moro, D., Gazzeri, S. and Brambilla, C. (1999) Alterations of expression of Rb, p16(INK4A) and cyclin D1 in non-small cell lung carcinoma and their clinical significance. The Journal of pathology, 188, 351-360.

Brederlau, A., Faigle, R., Elmi, M., Zarebski, A., Sjoberg, S., Fujii, M., Miyazono, K. and Funa, K. (2004) The bone morphogenetic protein type Ib receptor is a major mediator of glial differentiation and cell survival in adult hippocampal progenitor cell culture. Molecular biology of the cell, 15, 3863-3875.

Burdsal, C. A., Alliegro, M. C. and McClay, D. R. (1991) Tissue-specific, temporal changes in cell adhesion to echinonectin in the sea urchin embryo. Developmental biology, 144, 327-334.

Calderon-Segura, M. E., Gomez-Arroyo, S., Villalobos-Pietrini, R., Butterworth, F. M. and Amador-Munoz, O. (2004) The effects of seasonal weather on the genotoxicity, cytokinetic properties, cytotoxicity and organochemical content of extracts of airborne particulates in Mexico City. Mutation research, 558, 7-17.

Chang, H., Brown, C. W. and Matzuk, M. M. (2002) Genetic analysis of the mammalian transforming growth factor-beta superfamily. Endocrine reviews, 23, 787-823.

Chang, H., Zwijsen, A., Vogel, H., Huylebroeck, D. and Matzuk, M. M. (2000) Smad5 is essential for left-right asymmetry in mice. Developmental biology, 219, 71-78.

Charalabopoulos, K., Gogali, A., Kostoula, O. K. and Constantopoulos, S. H. (2004) Cadherin superfamily of adhesion molecules in primary lung cancer. Experimental oncology, 26, 256-260.

Charrier, E., Reibel, S., Rogemond, V., Aguera, M., Thomasset, N. and Honnorat, J. (2003) Collapsin response mediator proteins (CRMPs): involvement in nervous system development and adult neurodegenerative disorders. Molecular neurobiology, 28, 51-64.

Chen, D., Ji, X., Harris, M. A., Feng, J. Q., Karsenty, G., Celeste, A. J., Rosen, V., Mundy, G. R. and Harris, S. E. (1998) Differential roles for bone morphogenetic protein (BMP) receptor type IB and IA in differentiation and specification of mesenchymal precursor cells to osteoblast and adipocyte lineages. The Journal of cell biology, 142, 295-305.

Chen, D., Zhao, M. and Mundy, G. R. (2004) Bone morphogenetic proteins. Growth factors (Chur, Switzerland), 22, 233-241.

Chen, H. L. and Panchision, D. M. (2007) Concise review: bone morphogenetic protein pleiotropism in neural stem cells and their derivatives--alternative pathways, convergent signals. Stem cells (Dayton, Ohio), 25, 63-68.

Cheng, D. S., Han, W., Chen, S. M., Sherrill, T. P., Chont, M., Park, G. Y., Sheller, J. R., Polosukhin, V. V., Christman, J. W., Yull, F. E. and Blackwell, T. S. (2007) Airway epithelium controls lung inflammation and injury through the NF-kappa B pathway. J Immunol, 178, 6504-6513.

Cheon, S. S., Wei, Q., Gurung, A., Youn, A., Bright, T., Poon, R., Whetstone, H., Guha, A. and Alman, B. A. (2006) Beta-catenin regulates wound size and mediates the effect of TGF-beta in cutaneous healing. Faseb J, 20, 692-701.

Chialda, L., Zhang, M., Brune, K. and Pahl, A. (2005) Inhibitors of mitogen-activated protein kinases differentially regulate costimulated T cell cytokine production and mouse airway eosinophilia. Respiratory research, 6, 36.

Choi, S. H., Jin, S. E., Lee, M. K., Lim, S. J., Park, J. S., Kim, B. G., Ahn, W. S. and Kim, C. K. (2008) Novel cationic solid lipid nanoparticles enhanced p53 gene transfer to lung cancer cells. Eur J Pharm Biopharm, 68, 545-554.

Chorostowska-Wynimko, J. and Szpechcinski, A. (2007) The impact of genetic markers on the diagnosis of lung cancer: a current perspective. J Thorac Oncol, 2, 1044-1051.

Chun, Y. S., Lindor, N. M., Smyrk, T. C., Petersen, B. T., Burgart, L. J., Guilford, P. J. and Donohue, J. H. (2001) Germline E-cadherin gene mutations: is prophylactic total gastrectomy indicated? Cancer, 92, 181-187.

Clevenger, C. V. (2003) Nuclear localization and function of polypeptide ligands and their receptors: a new paradigm for hormone specificity within the mammary gland? Breast Cancer Res, 5, 181-187.

Copeland, N. G., Jenkins, N. A. and Court, D. L. (2001) Recombineering: a powerful new tool for mouse functional genomics. Nature reviews, 2, 769-779.

Copreni, E., Penzo, M., Carrabino, S. and Conese, M. (2004) Lentivirus-mediated gene transfer to the respiratory epithelium: a promising approach to gene therapy of cystic fibrosis. Gene Ther, 11 Suppl 1, S67-75.

Cox, B. (2008) The effect of service screening on breast cancer mortality rates. Eur J Cancer Prev, 17, 306-311.

Cronin, C. A., Gluba, W. and Scrable, H. (2001) The lac operator-repressor system is functional in the mouse. Genes & development, 15, 1506-1517.

Crowley, A. R., Mehta, S. S., Hembree, M. J., Preuett, B. L., Prasadan, K. L., Sharp, S. W., Yew, H., McFall, C. R., Benjes, C. L., Tulachan, S. S., Gittes, G. K. and Snyder, C. L. (2006) Bone morphogenetic protein expression patterns in human esophageal atresia with tracheoesophageal fistula. Pediatric surgery international, 22, 154-157.

Cutroneo, K. R. (2007) TGF-beta-induced fibrosis and SMAD signaling: oligo decoys as natural therapeutics for inhibition of tissue fibrosis and scarring. Wound Repair Regen, 15 Suppl 1, S54-60.

D'Andrea, M. R., Lawrence, D., Nagele, R. G., Wang, C. Y. and Damiano, B. P. (2008) PCNA indexing as a preclinical immunohistochemical biomarker for testicular toxicity. Biotech Histochem, 83, 211-220.

Dalba, C., Klatzmann, D., Logg, C. R. and Kasahara, N. (2005) Beyond oncolytic virotherapy: replication-competent retrovirus vectors for selective and stable transduction of tumors. Current gene therapy, 5, 655-667.

De, B., Heguy, A., Leopold, P. L., Wasif, N., Korst, R. J., Hackett, N. R. and Crystal, R. G. (2004) Intrapleural administration of a serotype 5 adeno-associated virus coding for alpha1-antitrypsin mediates persistent, high lung and serum levels of alpha1-antitrypsin. Mol Ther, 10, 1003-1010.

De Wever, O., Derycke, L., Hendrix, A., De Meerleer, G., Godeau, F., Depypere, H. and Bracke, M. (2007) Soluble cadherins as cancer biomarkers. Clinical & experimental metastasis, 24, 685-697.

Deng, H., Makizumi, R., Ravikumar, T. S., Dong, H., Yang, W. and Yang, W. L. (2007) Bone morphogenetic protein-4 is overexpressed in colonic adenocarcinomas and promotes migration and invasion of HCT116 cells. Experimental cell research, 313, 1033-1044.

Dewulf, N., Verschueren, K., Lonnoy, O., Moren, A., Grimsby, S., Vande Spiegle, K., Miyazono, K., Huylebroeck, D. and Ten Dijke, P. (1995) Distinct spatial and

temporal expression patterns of two type I receptors for bone morphogenetic proteins during mouse embryogenesis. Endocrinology, 136, 2652-2663.
Dihl, R. R., Bereta, M. S., do Amaral, V. S., Lehmann, M., Reguly, M. L. and de Andrade, H. H. (2008) Nitropolycyclic aromatic hydrocarbons are inducers of mitotic homologous recombination in the wing-spot test of Drosophila melanogaster. Food Chem Toxicol, 46, 2344-2348.
Dorudi, S., Sheffield, J. P., Poulsom, R., Northover, J. M. and Hart, I. R. (1993) E-cadherin expression in colorectal cancer. An immunocytochemical and in situ hybridization study. The American journal of pathology, 142, 981-986.
Duan, D., Yue, Y., Yan, Z., McCray, P. B., Jr. and Engelhardt, J. F. (1998) Polarity influences the efficiency of recombinant adenoassociated virus infection in differentiated airway epithelia. Hum Gene Ther, 9, 2761-2776.
Duan, W., Chan, J. H., McKay, K., Crosby, J. R., Choo, H. H., Leung, B. P., Karras, J. G. and Wong, W. S. (2005) Inhaled p38alpha mitogen-activated protein kinase antisense oligonucleotide attenuates asthma in mice. American journal of respiratory and critical care medicine, 171, 571-578.
Evans, M. J., Cabral-Anderson, L. J. and Freeman, G. (1978) Role of the Clara cell in renewal of the bronchiolar epithelium. Laboratory investigation; a journal of technical methods and pathology, 38, 648-653.
Evans, M. J., Shami, S. G., Cabral-Anderson, L. J. and Dekker, N. P. (1986) Role of nonciliated cells in renewal of the bronchial epithelium of rats exposed to NO2. The American journal of pathology, 123, 126-133.
Facchiano, A., Cordella-Miele, E., Miele, L. and Mukherjee, A. B. (1991) Inhibition of pancreatic phospholipase A2 activity by uteroglobin and antiflammin peptides: possible mechanism of action. Life sciences, 48, 453-464.
Fanucchi, M. V., Day, K. C., Clay, C. C. and Plopper, C. G. (2004) Increased vulnerability of neonatal rats and mice to 1-nitronaphthalene-induced pulmonary injury. Toxicology and applied pharmacology, 201, 53-65.
Farhood, H., Serbina, N. and Huang, L. (1995) The role of dioleoyl phosphatidylethanolamine in cationic liposome mediated gene transfer. Biochimica et biophysica acta, 1235, 289-295.
Fiering, S. N., Roederer, M., Nolan, G. P., Micklem, D. R., Parks, D. R. and Herzenberg, L. A. (1991) Improved FACS-Gal: flow cytometric analysis and sorting of viable eukaryotic cells expressing reporter gene constructs. Cytometry, 12, 291-301.
Fiorini, M., Ballaro, C., Sala, G., Falcone, G., Alema, S. and Segatto, O. (2002) Expression of RALT, a feedback inhibitor of ErbB receptors, is subjected to an integrated transcriptional and post-translational control. Oncogene, 21, 6530-6539.
Flotte, T. R., Zeitlin, P. L., Reynolds, T. C., Heald, A. E., Pedersen, P., Beck, S., Conrad, C. K., Brass-Ernst, L., Humphries, M., Sullivan, K., Wetzel, R., Taylor, G., Carter, B. J. and Guggino, W. B. (2003) Phase I trial of intranasal and endobronchial administration of a recombinant adeno-associated virus serotype 2 (rAAV2)-CFTR vector in adult cystic fibrosis patients: a two-part clinical study. Hum Gene Ther, 14, 1079-1088.
Floyd, H. S., Farnsworth, C. L., Kock, N. D., Mizesko, M. C., Little, J. L., Dance, S. T., Everitt, J., Tichelaar, J., Whitsett, J. A. and Miller, M. S. (2005) Conditional

expression of the mutant Ki-rasG12C allele results in formation of benign lung adenomas: development of a novel mouse lung tumor model. Carcinogenesis, 26, 2196-2206.

Floyd, H. S., Jennings-Gee, J. E., Kock, N. D. and Miller, M. S. (2006) Genetic and epigenetic alterations in lung tumors from bitransgenic Ki-rasG12C expressing mice. Molecular carcinogenesis, 45, 506-517.

Fong, S., Debs, R. J. and Desprez, P. Y. (2004) Id genes and proteins as promising targets in cancer therapy. Trends in molecular medicine, 10, 387-392.

Foy, J. W. and Schatz, R. A. (2004) Inhibition of rat respiratory-tract cytochrome P-450 activity after acute low-level m-xylene inhalation: role in 1-nitronaphthalene toxicity. Inhalation toxicology, 16, 125-132.

Frank, D. B., Abtahi, A., Yamaguchi, D. J., Manning, S., Shyr, Y., Pozzi, A., Baldwin, H. S., Johnson, J. E. and de Caestecker, M. P. (2005) Bone morphogenetic protein 4 promotes pulmonary vascular remodeling in hypoxic pulmonary hypertension. Circulation research, 97, 496-504.

Fregonese, L., Stolk, J., Frants, R. R. and Veldhuisen, B. (2008) Alpha-1 antitrypsin Null mutations and severity of emphysema. Respiratory medicine, 102, 876-884.

Fukui, T., Hayashi, Y., Kagami, H., Yamamoto, N., Fukuhara, H., Tohnai, I., Ueda, M., Mizuno, M. and Yoshida, J. (2001) Suicide gene therapy for human oral squamous cell carcinoma cell lines with adeno-associated virus vector. Oral oncology, 37, 211-215.

Gallea, S., Lallemand, F., Atfi, A., Rawadi, G., Ramez, V., Spinella-Jaegle, S., Kawai, S., Faucheu, C., Huet, L., Baron, R. and Roman-Roman, S. (2001) Activation of mitogen-activated protein kinase cascades is involved in regulation of bone morphogenetic protein-2-induced osteoblast differentiation in pluripotent C2C12 cells. Bone, 28, 491-498.

Gao, G., Vandenberghe, L. H. and Wilson, J. M. (2005) New recombinant serotypes of AAV vectors. Current gene therapy, 5, 285-297.

Gao, G. P., Alvira, M. R., Wang, L., Calcedo, R., Johnston, J. and Wilson, J. M. (2002) Novel adeno-associated viruses from rhesus monkeys as vectors for human gene therapy. Proceedings of the National Academy of Sciences of the United States of America, 99, 11854-11859.

Gazdhar, A., Bilici, M., Pierog, J., Ayuni, E. L., Gugger, M., Wetterwald, A., Cecchini, M. and Schmid, R. A. (2006) In vivo electroporation and ubiquitin promoter--a protocol for sustained gene expression in the lung. J Gene Med, 8, 910-918.

Gazzerro, E. and Canalis, E. (2006) Bone morphogenetic proteins and their antagonists. Reviews in endocrine & metabolic disorders, 7, 51-65.

Gebhart, C. L. and Kabanov, A. V. (2001) Evaluation of polyplexes as gene transfer agents. J Control Release, 73, 401-416.

Geiser, T. (2003) Idiopathic pulmonary fibrosis--a disorder of alveolar wound repair? Swiss Med Wkly, 133, 405-411.

Ghamra, Z. W. and Dweik, R. A. (2003) Primary pulmonary hypertension: an overview of epidemiology and pathogenesis. Cleveland Clinic journal of medicine, 70 Suppl 1, S2-8.

Giangreco, A., Reynolds, S. D. and Stripp, B. R. (2002) Terminal bronchioles harbor a unique airway stem cell population that localizes to the bronchoalveolar duct junction. The American journal of pathology, 161, 173-182.

Gilboa, L., Nohe, A., Geissendorfer, T., Sebald, W., Henis, Y. I. and Knaus, P. (2000) Bone morphogenetic protein receptor complexes on the surface of live cells: a new oligomerization mode for serine/threonine kinase receptors. Molecular biology of the cell, 11, 1023-1035.

Gleave, M. E. and Monia, B. P. (2005) Antisense therapy for cancer. Nat Rev Cancer, 5, 468-479.

Gottardi, C. J., Wong, E. and Gumbiner, B. M. (2001) E-cadherin suppresses cellular transformation by inhibiting beta-catenin signaling in an adhesion-independent manner. The Journal of cell biology, 153, 1049-1060.

Grady, W. M., Rajput, A., Myeroff, L., Liu, D. F., Kwon, K., Willis, J. and Markowitz, S. (1998) Mutation of the type II transforming growth factor-beta receptor is coincident with the transformation of human colon adenomas to malignant carcinomas. Cancer research, 58, 3101-3104.

Griesenbach, U., Geddes, D. M. and Alton, E. W. (2006) Gene therapy progress and prospects: cystic fibrosis. Gene Ther, 13, 1061-1067.

Gu, H., Zou, Y. R. and Rajewsky, K. (1993) Independent control of immunoglobulin switch recombination at individual switch regions evidenced through Cre-loxP-mediated gene targeting. Cell, 73, 1155-1164.

Guessous, I., Cornuz, J. and Paccaud, F. (2007) Lung cancer screening: current situation and perspective. Swiss Med Wkly, 137, 304-311.

Hacein-Bey-Abina, S., Von Kalle, C., Schmidt, M., McCormack, M. P., Wulffraat, N., Leboulch, P., Lim, A., Osborne, C. S., Pawliuk, R., Morillon, E., Sorensen, R., Forster, A., Fraser, P., Cohen, J. I., de Saint Basile, G., Alexander, I., Wintergerst, U., Frebourg, T., Aurias, A., Stoppa-Lyonnet, D., Romana, S., Radford-Weiss, I., Gross, F., Valensi, F., Delabesse, E., Macintyre, E., Sigaux, F., Soulier, J., Leiva, L. E., Wissler, M., Prinz, C., Rabbitts, T. H., Le Deist, F., Fischer, A. and Cavazzana-Calvo, M. (2003) LMO2-associated clonal T cell proliferation in two patients after gene therapy for SCID-X1. Science, 302, 415-419.

Hagen, M., Fagan, K., Steudel, W., Carr, M., Lane, K., Rodman, D. M. and West, J. (2007) Interaction of interleukin-6 and the BMP pathway in pulmonary smooth muscle. American journal of physiology, 292, L1473-1479.

Halbert, C. L., Allen, J. M. and Miller, A. D. (2001) Adeno-associated virus type 6 (AAV6) vectors mediate efficient transduction of airway epithelial cells in mouse lungs compared to that of AAV2 vectors. J Virol, 75, 6615-6624.

Han, A. C., Soler, A. P., Tang, C. K., Knudsen, K. A. and Salazar, H. (2000) Nuclear localization of E-cadherin expression in Merkel cell carcinoma. Archives of pathology & laboratory medicine, 124, 1147-1151.

Hanyu, A., Ishidou, Y., Ebisawa, T., Shimanuki, T., Imamura, T. and Miyazono, K. (2001) The N domain of Smad7 is essential for specific inhibition of transforming growth factor-beta signaling. The Journal of cell biology, 155, 1017-1027.

Hartung, A., Bitton-Worms, K., Rechtman, M. M., Wenzel, V., Boergermann, J. H., Hassel, S., Henis, Y. I. and Knaus, P. (2006) Different routes of bone

morphogenic protein (BMP) receptor endocytosis influence BMP signaling. Molecular and cellular biology, 26, 7791-7805.
Hassel, S., Eichner, A., Yakymovych, M., Hellman, U., Knaus, P. and Souchelnytskyi, S. (2004) Proteins associated with type II bone morphogenetic protein receptor (BMPR-II) and identified by two-dimensional gel electrophoresis and mass spectrometry. Proteomics, 4, 1346-1358.
Hata, A., Lagna, G., Massague, J. and Hemmati-Brivanlou, A. (1998) Smad6 inhibits BMP/Smad1 signaling by specifically competing with the Smad4 tumor suppressor. Genes & development, 12, 186-197.
Hay, E. D. (1995) An overview of epithelio-mesenchymal transformation. Acta anatomica, 154, 8-20.
Hayashida, S., Harrod, K. S. and Whitsett, J. A. (2000) Regulation and function of CCSP during pulmonary Pseudomonas aeruginosa infection in vivo. American journal of physiology, 279, L452-459.
He, X. C., Zhang, J., Tong, W. G., Tawfik, O., Ross, J., Scoville, D. H., Tian, Q., Zeng, X., He, X., Wiedemann, L. M., Mishina, Y. and Li, L. (2004) BMP signaling inhibits intestinal stem cell self-renewal through suppression of Wnt-beta-catenin signaling. Nature genetics, 36, 1117-1121.
Helms, M. W., Packeisen, J., August, C., Schittek, B., Boecker, W., Brandt, B. H. and Buerger, H. (2005) First evidence supporting a potential role for the BMP/SMAD pathway in the progression of oestrogen receptor-positive breast cancer. The Journal of pathology, 206, 366-376.
Hocking, J. C. and McFarlane, S. (2007) Expression of Bmp ligands and receptors in the developing Xenopus retina. The International journal of developmental biology, 51, 161-165.
Hong, K. U., Reynolds, S. D., Giangreco, A., Hurley, C. M. and Stripp, B. R. (2001) Clara cell secretory protein-expressing cells of the airway neuroepithelial body microenvironment include a label-retaining subset and are critical for epithelial renewal after progenitor cell depletion. American journal of respiratory cell and molecular biology, 24, 671-681.
Hong, K. U., Reynolds, S. D., Watkins, S., Fuchs, E. and Stripp, B. R. (2004) Basal cells are a multipotent progenitor capable of renewing the bronchial epithelium. The American journal of pathology, 164, 577-588.
Howe, J. R., Chinnathambi, S., Calva, D., Bair, J., Pechman, B., Salamon, A., Tam, B. and Simon, L. (2008) A family with two consecutive nonsense mutations in BMPR1A causing juvenile polyposis. Cancer genetics and cytogenetics, 181, 52-54.
Howe, J. R., Sayed, M. G., Ahmed, A. F., Ringold, J., Larsen-Haidle, J., Merg, A., Mitros, F. A., Vaccaro, C. A., Petersen, G. M., Giardiello, F. M., Tinley, S. T., Aaltonen, L. A. and Lynch, H. T. (2004) The prevalence of MADH4 and BMPR1A mutations in juvenile polyposis and absence of BMPR2, BMPR1B, and ACVR1 mutations. Journal of medical genetics, 41, 484-491.
Hu, M. C., Wasserman, D., Hartwig, S. and Rosenblum, N. D. (2004) p38MAPK acts in the BMP7-dependent stimulatory pathway during epithelial cell morphogenesis and is regulated by Smad1. The Journal of biological chemistry, 279, 12051-12059.

Huang, S. C., Chen, C. R., Lavine, J. E., Taylor, S. F., Newbury, R. O., Pham, T. T., Ricciardiello, L. and Carethers, J. M. (2000) Genetic heterogeneity in familial juvenile polyposis. Cancer research, 60, 6882-6885.

Humbert, M. (2008) Update in pulmonary arterial hypertension 2007. American journal of respiratory and critical care medicine, 177, 574-579.

Hunt, J. L. (2008) Molecular testing in solid tumors: an overview. Archives of pathology & laboratory medicine, 132, 164-167.

Imoto, I., Izumi, H., Yokoi, S., Hosoda, H., Shibata, T., Hosoda, F., Ohki, M., Hirohashi, S. and Inazawa, J. (2006) Frequent silencing of the candidate tumor suppressor PCDH20 by epigenetic mechanism in non-small-cell lung cancers. Cancer research, 66, 4617-4626.

Inai, K., Norris, R. A., Hoffman, S., Markwald, R. R. and Sugi, Y. (2008) BMP-2 induces cell migration and periostin expression during atrioventricular valvulogenesis. Developmental biology, 315, 383-396.

Jackson, J. G. and Pereira-Smith, O. M. (2006) p53 Is Preferentially Recruited to the Promoters of Growth Arrest Genes p21 and GADD45 during Replicative Senescence of Normal Human Fibroblasts. Cancer research, 66, 8356-8360.

Jeffery, P. K. and Reid, L. (1975) New observations of rat airway epithelium: a quantitative and electron microscopic study. Journal of anatomy, 120, 295-320.

Ji, H., Houghton, A. M., Mariani, T. J., Perera, S., Kim, C. B., Padera, R., Tonon, G., McNamara, K., Marconcini, L. A., Hezel, A., El-Bardeesy, N., Bronson, R. T., Sugarbaker, D., Maser, R. S., Shapiro, S. D. and Wong, K. K. (2006) K-ras activation generates an inflammatory response in lung tumors. Oncogene, 25, 2105-2112.

Jin, N., Gilbert, J. L., Broaddus, R. R., Demayo, F. J. and Jeong, J. W. (2007) Generation of a Mig-6 conditional null allele. Genesis, 45, 716-721.

Johnson, L., Mercer, K., Greenbaum, D., Bronson, R. T., Crowley, D., Tuveson, D. A. and Jacks, T. (2001) Somatic activation of the K-ras oncogene causes early onset lung cancer in mice. Nature, 410, 1111-1116.

Junior, J. P., Srougi, M., Borra, P. M., Dall' Oglio, M. F., Ribeiro-Filho, L. A. and Leite, K. R. (2008) E-cadherin and beta-catenin Loss of Expression Related to Bone Metastasis in Prostate Cancer. Appl Immunohistochem Mol Morphol.

Kalina, M., Mason, R. J. and Shannon, J. M. (1992) Surfactant protein C is expressed in alveolar type II cells but not in Clara cells of rat lung. American journal of respiratory cell and molecular biology, 6, 594-600.

Kariyawasam, H. H., Xanthou, G., Barkans, J., Aizen, M., Kay, A. B. and Robinson, D. S. (2008) Basal expression of bone morphogenetic protein receptor is reduced in mild asthma. American journal of respiratory and critical care medicine, 177, 1074-1081.

Kato, Y., Hirano, T., Yoshida, K., Yashima, K., Akimoto, S., Tsuji, K., Ohira, T., Tsuboi, M., Ikeda, N., Ebihara, Y. and Kato, H. (2005) Frequent loss of E-cadherin and/or catenins in intrabronchial lesions during carcinogenesis of the bronchial epithelium. Lung cancer (Amsterdam, Netherlands), 48, 323-330.

Katzenstein, A. L., Mukhopadhyay, S. and Myers, J. L. (2008) Diagnosis of usual interstitial pneumonia and distinction from other fibrosing interstitial lung diseases. Human pathology, 39, 1275-1294.

Katzmann, D. J., Babst, M. and Emr, S. D. (2001) Ubiquitin-dependent sorting into the multivesicular body pathway requires the function of a conserved endosomal protein sorting complex, ESCRT-I. Cell, 106, 145-155.

Kiemer, A. K., Takeuchi, K. and Quinlan, M. P. (2001) Identification of genes involved in epithelial-mesenchymal transition and tumor progression. Oncogene, 20, 6679-6688.

Kim, C. F., Jackson, E. L., Woolfenden, A. E., Lawrence, S., Babar, I., Vogel, S., Crowley, D., Bronson, R. T. and Jacks, T. (2005) Identification of bronchioalveolar stem cells in normal lung and lung cancer. Cell, 121, 823-835.

Kim, I. Y., Lee, D. H., Ahn, H. J., Tokunaga, H., Song, W., Devereaux, L. M., Jin, D., Sampath, T. K. and Morton, R. A. (2000) Expression of bone morphogenetic protein receptors type-IA, -IB and -II correlates with tumor grade in human prostate cancer tissues. Cancer research, 60, 2840-2844.

Kim, I. Y., Lee, D. H., Lee, D. K., Kim, W. J., Kim, M. M., Morton, R. A., Lerner, S. P. and Kim, S. J. (2004) Restoration of bone morphogenetic protein receptor type II expression leads to a decreased rate of tumor growth in bladder transitional cell carcinoma cell line TSU-Pr1. Cancer research, 64, 7355-7360.

Kimos, M. C., Wang, S., Borkowski, A., Yang, G. Y., Yang, C. S., Perry, K., Olaru, A., Deacu, E., Sterian, A., Cottrell, J., Papadimitriou, J., Sisodia, L., Selaru, F. M., Mori, Y., Xu, Y., Yin, J., Abraham, J. M. and Meltzer, S. J. (2004) Esophagin and proliferating cell nuclear antigen (PCNA) are biomarkers of human esophageal neoplastic progression. International journal of cancer, 111, 415-417.

Kobayashi, S., Boggon, T. J., Dayaram, T., Janne, P. A., Kocher, O., Meyerson, M., Johnson, B. E., Eck, M. J., Tenen, D. G. and Halmos, B. (2005) EGFR mutation and resistance of non-small-cell lung cancer to gefitinib. The New England journal of medicine, 352, 786-792.

Kobinger, G. P., Weiner, D. J., Yu, Q. C. and Wilson, J. M. (2001) Filovirus-pseudotyped lentiviral vector can efficiently and stably transduce airway epithelia in vivo. Nat Biotechnol, 19, 225-230.

Kodach, L. L., Bleuming, S. A., Musler, A. R., Peppelenbosch, M. P., Hommes, D. W., van den Brink, G. R., van Noesel, C. J., Offerhaus, G. J. and Hardwick, J. C. (2008a) The bone morphogenetic protein pathway is active in human colon adenomas and inactivated in colorectal cancer. Cancer, 112, 300-306.

Kodach, L. L., Bleuming, S. A., Peppelenbosch, M. P., Hommes, D. W., van den Brink, G. R. and Hardwick, J. C. (2007) The effect of statins in colorectal cancer is mediated through the bone morphogenetic protein pathway. Gastroenterology, 133, 1272-1281.

Kodach, L. L., Wiercinska, E., de Miranda, N. F., Bleuming, S. A., Musler, A. R., Peppelenbosch, M. P., Dekker, E., van den Brink, G. R., van Noesel, C. J., Morreau, H., Hommes, D. W., Ten Dijke, P., Offerhaus, G. J. and Hardwick, J. C. (2008b) The bone morphogenetic protein pathway is inactivated in the majority of sporadic colorectal cancers. Gastroenterology, 134, 1332-1341.

Koera, K., Nakamura, K., Nakao, K., Miyoshi, J., Toyoshima, K., Hatta, T., Otani, H., Aiba, A. and Katsuki, M. (1997) K-ras is essential for the development of the mouse embryo. Oncogene, 15, 1151-1159.

Koli, K., Myllarniemi, M., Vuorinen, K., Salmenkivi, K., Ryynanen, M. J., Kinnula, V. L. and Keski-Oja, J. (2006) Bone morphogenetic protein-4 inhibitor gremlin is overexpressed in idiopathic pulmonary fibrosis. The American journal of pathology, 169, 61-71.

Kotton, D. N., Fabian, A. J. and Mulligan, R. C. (2005) Failure of bone marrow to reconstitute lung epithelium. American journal of respiratory cell and molecular biology, 33, 328-334.

Kwak, I., Tsai, S. Y. and DeMayo, F. J. (2004) Genetically engineered mouse models for lung cancer. Annual review of physiology, 66, 647-663.

Langenfeld, E. M., Bojnowski, J., Perone, J. and Langenfeld, J. (2005) Expression of bone morphogenetic proteins in human lung carcinomas. The Annals of thoracic surgery, 80, 1028-1032.

Langenfeld, E. M., Calvano, S. E., Abou-Nukta, F., Lowry, S. F., Amenta, P. and Langenfeld, J. (2003) The mature bone morphogenetic protein-2 is aberrantly expressed in non-small cell lung carcinomas and stimulates tumor growth of A549 cells. Carcinogenesis, 24, 1445-1454.

Langenfeld, E. M. and Langenfeld, J. (2004) Bone morphogenetic protein-2 stimulates angiogenesis in developing tumors. Mol Cancer Res, 2, 141-149.

Lee, C. C., Liu, Y. and Reineke, T. M. (2008) General structure-activity relationship for poly(glycoamidoamine)s: the effect of amine density on cytotoxicity and DNA delivery efficiency. Bioconjugate chemistry, 19, 428-440.

Lee, C. T., Park, K. H., Adachi, Y., Seol, J. Y., Yoo, C. G., Kim, Y. W., Han, S. K., Shim, Y. S., Coffee, K., Dikov, M. M. and Carbone, D. P. (2003) Recombinant adenoviruses expressing dominant negative insulin-like growth factor-I receptor demonstrate antitumor effects on lung cancer. Cancer Gene Ther, 10, 57-63.

Lee, C. T., Wu, S., Gabrilovich, D., Chen, H., Nadaf-Rahrov, S., Ciernik, I. F. and Carbone, D. P. (1996) Antitumor effects of an adenovirus expressing antisense insulin-like growth factor I receptor on human lung cancer cell lines. Cancer Res, 56, 3038-3041.

Lee, J., Son, M. J., Woolard, K., Donin, N. M., Li, A., Cheng, C. H., Kotliarova, S., Kotliarov, Y., Walling, J., Ahn, S., Kim, M., Totonchy, M., Cusack, T., Ene, C., Ma, H., Su, Q., Zenklusen, J. C., Zhang, W., Maric, D. and Fine, H. A. (2008) Epigenetic-mediated dysfunction of the bone morphogenetic protein pathway inhibits differentiation of glioblastoma-initiating cells. Cancer cell, 13, 69-80.

Lee, J. S., Lippman, S. M., Hong, W. K., Ro, J. Y., Kim, S. Y., Lotan, R. and Hittelman, W. N. (1992) Determination of biomarkers for intermediate end points in chemoprevention trials. Cancer research, 52, 2707s-2710s.

Lee, K. M., Kang, D., Clapper, M. L., Ingelman-Sundberg, M., Ono-Kihara, M., Kiyohara, C., Min, S., Lan, Q., Le Marchand, L., Lin, P., Lung, M. L., Pinarbasi, H., Pisani, P., Srivatanakul, P., Seow, A., Sugimura, H., Tokudome, S., Yokota, J. and Taioli, E. (2008) CYP1A1, GSTM1, and GSTT1 polymorphisms, smoking, and lung cancer risk in a pooled analysis among Asian populations. Cancer Epidemiol Biomarkers Prev, 17, 1120-1126.

Leng, S., Stidley, C. A., Bernauer, A., Picchi, M. A., Sheng, X., Frasco, M. A., Van Den Berg, D., Gilliland, F. D., Crowell, R. E. and Belinsky, S. A. (2008) Haplotypes

of DNMT1 and DNMT3B are associated with mutagen sensitivity induced by benzo[a]pyrene diol epoxide among smokers. Carcinogenesis.

Li, E. E., Heflich, R. H., Bucci, T. J., Manjanatha, M. G., Blaydes, B. S. and Delclos, K. B. (1994) Relationships of DNA adduct formation, K-ras activating mutations and tumorigenic activities of 6-nitrochrysene and its metabolites in the lungs of CD-1 mice. Carcinogenesis, 15, 1377-1385.

Li, H., Cho, S. N., Evans, C. M., Dickey, B. F., Jeong, J. W. and DeMayo, F. J. (2008) Cre-mediated recombination in mouse Clara cells. Genesis, 46, 300-307.

Li, Z. L., Liu, R. H. and Kong, C. Z. (2006) [Significance of expressions of bone morphogenetic protein 2 and 4 in prostatic carcinoma]. Zhonghua nan ke xue = National journal of andrology, 12, 126-128, 132.

Lichty, B. D., Power, A. T., Stojdl, D. F. and Bell, J. C. (2004) Vesicular stomatitis virus: re-inventing the bullet. Trends in molecular medicine, 10, 210-216.

Lin, S. Y., Makino, K., Xia, W., Matin, A., Wen, Y., Kwong, K. Y., Bourguignon, L. and Hung, M. C. (2001) Nuclear localization of EGF receptor and its potential new role as a transcription factor. Nature cell biology, 3, 802-808.

Liu, F., Ventura, F., Doody, J. and Massague, J. (1995) Human type II receptor for bone morphogenic proteins (BMPs): extension of the two-kinase receptor model to the BMPs. Molecular and cellular biology, 15, 3479-3486.

Liu, J. Y., Nettesheim, P. and Randell, S. H. (1994) Growth and differentiation of tracheal epithelial progenitor cells. The American journal of physiology, 266, L296-307.

Liu, W., Liang, Q., Balzar, S., Wenzel, S., Gorska, M. and Alam, R. (2008) Cell-specific activation profile of extracellular signal-regulated kinase 1/2, Jun N-terminal kinase, and p38 mitogen-activated protein kinases in asthmatic airways. The Journal of allergy and clinical immunology, 121, 893-902 e892.

Liu, Y., Xu, H. T., Dai, S. D., Wei, Q., Yuan, X. M. and Wang, E. H. (2007) Reduction of p120(ctn) isoforms 1 and 3 is significantly associated with metastatic progression of human lung cancer. Apmis, 115, 848-856.

Lynch, T. J., Bell, D. W., Sordella, R., Gurubhagavatula, S., Okimoto, R. A., Brannigan, B. W., Harris, P. L., Haserlat, S. M., Supko, J. G., Haluska, F. G., Louis, D. N., Christiani, D. C., Settleman, J. and Haber, D. A. (2004) Activating mutations in the epidermal growth factor receptor underlying responsiveness of non-small-cell lung cancer to gefitinib. The New England journal of medicine, 350, 2129-2139.

Maatta, A. M., Tenhunen, A., Pasanen, T., Merilainen, O., Pellinen, R., Makinen, K., Alhava, E. and Wahlfors, J. (2004) Non-small cell lung cancer as a target disease for herpes simplex type 1 thymidine kinase-ganciclovir gene therapy. International journal of oncology, 24, 943-949.

Machado, R. D., Pauciulo, M. W., Thomson, J. R., Lane, K. B., Morgan, N. V., Wheeler, L., Phillips, J. A., 3rd, Newman, J., Williams, D., Galie, N., Manes, A., McNeil, K., Yacoub, M., Mikhail, G., Rogers, P., Corris, P., Humbert, M., Donnai, D., Martensson, G., Tranebjaerg, L., Loyd, J. E., Trembath, R. C. and Nichols, W. C. (2001) BMPR2 haploinsufficiency as the inherited molecular mechanism for primary pulmonary hypertension. American journal of human genetics, 68, 92-102.

Maddugoda, M. P., Crampton, M. S., Shewan, A. M. and Yap, A. S. (2007) Myosin VI and vinculin cooperate during the morphogenesis of cadherin cell cell contacts in mammalian epithelial cells. The Journal of cell biology, 178, 529-540.

Madoz-Gurpide, J., Lopez-Serra, P., Martinez-Torrecuadrada, J. L., Sanchez, L., Lombardia, L. and Casal, J. I. (2006) Proteomics-based validation of genomic data: applications in colorectal cancer diagnosis. Mol Cell Proteomics, 5, 1471-1483.

Malkas, L. H., Herbert, B. S., Abdel-Aziz, W., Dobrolecki, L. E., Liu, Y., Agarwal, B., Hoelz, D., Badve, S., Schnaper, L., Arnold, R. J., Mechref, Y., Novotny, M. V., Loehrer, P., Goulet, R. J. and Hickey, R. J. (2006) A cancer-associated PCNA expressed in breast cancer has implications as a potential biomarker. Proceedings of the National Academy of Sciences of the United States of America, 103, 19472-19477.

Malkinson, A. M. (2001) Primary lung tumors in mice as an aid for understanding, preventing, and treating human adenocarcinoma of the lung. Lung cancer (Amsterdam, Netherlands), 32, 265-279.

Malumbres, M. and Pellicer, A. (1998) RAS pathways to cell cycle control and cell transformation. Front Biosci, 3, d887-912.

Mannino, D. M. (2002) COPD: epidemiology, prevalence, morbidity and mortality, and disease heterogeneity. Chest, 121, 121S-126S.

Marinova-Mutafchieva, L., Taylor, P., Funa, K., Maini, R. N. and Zvaifler, N. J. (2000) Mesenchymal cells expressing bone morphogenetic protein receptors are present in the rheumatoid arthritis joint. Arthritis and rheumatism, 43, 2046-2055.

Markowitz, S. D. and Roberts, A. B. (1996) Tumor suppressor activity of the TGF-beta pathway in human cancers. Cytokine & growth factor reviews, 7, 93-102.

Marti, T. M., Kunz, C. and Fleck, O. (2002) DNA mismatch repair and mutation avoidance pathways. Journal of cellular physiology, 191, 28-41.

Martin, P., D'Souza, D., Martin, J., Grose, R., Cooper, L., Maki, R. and McKercher, S. R. (2003) Wound healing in the PU.1 null mouse--tissue repair is not dependent on inflammatory cells. Curr Biol, 13, 1122-1128.

Martin, P. and Leibovich, S. J. (2005) Inflammatory cells during wound repair: the good, the bad and the ugly. Trends in cell biology, 15, 599-607.

McBride, S., Tatrai, E., Blundell, R., Kovacikova, Z., Cardozo, L., Adamis, Z., Smith, T. and Harrison, D. (2000) Characterisation of lectin binding patterns of mouse bronchiolar and rat alveolar epithelial cells in culture. Histochem J, 32, 33-40.

McCormack, F. X. and Whitsett, J. A. (2002) The pulmonary collectins, SP-A and SP-D, orchestrate innate immunity in the lung. The Journal of clinical investigation, 109, 707-712.

McMahon, J. M., Conroy, S., Lyons, M., Greiser, U., O'Shea, C., Strappe, P., Howard, L., Murphy, M., Barry, F. and O'Brien, T. (2006) Gene transfer into rat mesenchymal stem cells: a comparative study of viral and nonviral vectors. Stem Cells Dev, 15, 87-96.

Medina, M. F., Kobinger, G. P., Rux, J., Gasmi, M., Looney, D. J., Bates, P. and Wilson, J. M. (2003) Lentiviral vectors pseudotyped with minimal filovirus envelopes increased gene transfer in murine lung. Mol Ther, 8, 777-789.

Mennesson, E., Erbacher, P., Piller, V., Kieda, C., Midoux, P. and Pichon, C. (2005) Transfection efficiency and uptake process of polyplexes in human lung endothelial cells: a comparative study in non-polarized and polarized cells. J Gene Med, 7, 729-738.

Metzger, R. J., Klein, O. D., Martin, G. R. and Krasnow, M. A. (2008) The branching programme of mouse lung development. Nature, 453, 745-750.

Meuwissen, R. and Berns, A. (2005) Mouse models for human lung cancer. Genes & development, 19, 643-664.

Meuwissen, R., Linn, S. C., Linnoila, R. I., Zevenhoven, J., Mooi, W. J. and Berns, A. (2003) Induction of small cell lung cancer by somatic inactivation of both Trp53 and Rb1 in a conditional mouse model. Cancer cell, 4, 181-189.

Meuwissen, R., Linn, S. C., van der Valk, M., Mooi, W. J. and Berns, A. (2001) Mouse model for lung tumorigenesis through Cre/lox controlled sporadic activation of the K-Ras oncogene. Oncogene, 20, 6551-6558.

Mishina, Y., Suzuki, A., Ueno, N. and Behringer, R. R. (1995) Bmpr encodes a type I bone morphogenetic protein receptor that is essential for gastrulation during mouse embryogenesis. Genes & development, 9, 3027-3037.

Miura, K., Bowman, E. D., Simon, R., Peng, A. C., Robles, A. I., Jones, R. T., Katagiri, T., He, P., Mizukami, H., Charboneau, L., Kikuchi, T., Liotta, L. A., Nakamura, Y. and Harris, C. C. (2002) Laser capture microdissection and microarray expression analysis of lung adenocarcinoma reveals tobacco smoking- and prognosis-related molecular profiles. Cancer research, 62, 3244-3250.

Miyazono, K., Maeda, S. and Imamura, T. (2005) BMP receptor signaling: transcriptional targets, regulation of signals, and signaling cross-talk. Cytokine & growth factor reviews, 16, 251-263.

Moffatt, S., Wiehle, S. and Cristiano, R. J. (2006) A multifunctional PEI-based cationic polyplex for enhanced systemic p53-mediated gene therapy. Gene Ther, 13, 1512-1523.

Moldovan, G. L., Pfander, B. and Jentsch, S. (2007) PCNA, the maestro of the replication fork. Cell, 129, 665-679.

Molloy, E. L., Adams, A., Moore, J. B., Masterson, J. C., Madrigal-Estebas, L., Mahon, B. P. and O'Dea, S. (2008) BMP4 induces an epithelial-mesenchymal transition-like response in adult airway epithelial cells. Growth factors (Chur, Switzerland), 26, 12-22.

Montesano, R. (2007) Bone morphogenetic protein-4 abrogates lumen formation by mammary epithelial cells and promotes invasive growth. Biochemical and biophysical research communications, 353, 817-822.

Montier, T., Delepine, P., Pichon, C., Ferec, C., Porteous, D. J. and Midoux, P. (2004) Non-viral vectors in cystic fibrosis gene therapy: progress and challenges. Trends in biotechnology, 22, 586-592.

Morrissey, J., Hruska, K., Guo, G., Wang, S., Chen, Q. and Klahr, S. (2002) Bone morphogenetic protein-7 improves renal fibrosis and accelerates the return of renal function. J Am Soc Nephrol, 13 Suppl 1, S14-21.

Moss, R. B., Rodman, D., Spencer, L. T., Aitken, M. L., Zeitlin, P. L., Waltz, D., Milla, C., Brody, A. S., Clancy, J. P., Ramsey, B., Hamblett, N. and Heald, A. E. (2004) Repeated adeno-associated virus serotype 2 aerosol-mediated cystic fibrosis

transmembrane regulator gene transfer to the lungs of patients with cystic fibrosis: a multicenter, double-blind, placebo-controlled trial. Chest, 125, 509-521.

Motti, M. L., Califano, D., Baldassarre, G., Celetti, A., Merolla, F., Forzati, F., Napolitano, M., Tavernise, B., Fusco, A. and Viglietto, G. (2005) Reduced E-cadherin expression contributes to the loss of p27kip1-mediated mechanism of contact inhibition in thyroid anaplastic carcinomas. Carcinogenesis, 26, 1021-1034.

Mucenski, M. L., Wert, S. E., Nation, J. M., Loudy, D. E., Huelsken, J., Birchmeier, W., Morrisey, E. E. and Whitsett, J. A. (2003) beta-Catenin is required for specification of proximal/distal cell fate during lung morphogenesis. The Journal of biological chemistry, 278, 40231-40238.

Mudway, I. S. and Kelly, F. J. (2000) Ozone and the lung: a sensitive issue. Molecular aspects of medicine, 21, 1-48.

Myllarniemi, M., Lindholm, P., Ryynanen, M. J., Kliment, C. R., Salmenkivi, K., Keski-Oja, J., Kinnula, V. L., Oury, T. D. and Koli, K. (2008) Gremlin-mediated decrease in bone morphogenetic protein signaling promotes pulmonary fibrosis. American journal of respiratory and critical care medicine, 177, 321-329.

Nagatake, M., Takagi, Y., Osada, H., Uchida, K., Mitsudomi, T., Saji, S., Shimokata, K., Takahashi, T. and Takahashi, T. (1996) Somatic in vivo alterations of the DPC4 gene at 18q21 in human lung cancers. Cancer research, 56, 2718-2720.

Nawrocki-Raby, B., Gilles, C., Polette, M., Bruyneel, E., Laronze, J. Y., Bonnet, N., Foidart, J. M., Mareel, M. and Birembaut, P. (2003) Upregulation of MMPs by soluble E-cadherin in human lung tumor cells. International journal of cancer, 105, 790-795.

Nishanian, T. G. and Waldman, T. (2004) Interaction of the BMPR-IA tumor suppressor with a developmentally relevant splicing factor. Biochemical and biophysical research communications, 323, 91-97.

Nohe, A., Hassel, S., Ehrlich, M., Neubauer, F., Sebald, W., Henis, Y. I. and Knaus, P. (2002) The mode of bone morphogenetic protein (BMP) receptor oligomerization determines different BMP-2 signaling pathways. The Journal of biological chemistry, 277, 5330-5338.

Nomoto, S., Haruki, N., Tatematsu, Y., Konishi, H., Mitsudomi, T., Takahashi, T. and Takahashi, T. (2000) Frequent allelic imbalance suggests involvement of a tumor suppressor gene at 1p36 in the pathogenesis of human lung cancers. Genes, chromosomes & cancer, 28, 342-346.

Norton, J. D. (2000) ID helix-loop-helix proteins in cell growth, differentiation and tumorigenesis. Journal of cell science, 113 (Pt 22), 3897-3905.

Oka, H., Shiozaki, H., Kobayashi, K., Inoue, M., Tahara, H., Kobayashi, T., Takatsuka, Y., Matsuyoshi, N., Hirano, S., Takeichi, M. and et al. (1993) Expression of E-cadherin cell adhesion molecules in human breast cancer tissues and its relationship to metastasis. Cancer research, 53, 1696-1701.

Okubo, T. and Hogan, B. L. (2004) Hyperactive Wnt signaling changes the developmental potential of embryonic lung endoderm. Journal of biology, 3, 11.

Owens, R. A. (2002) Second generation adeno-associated virus type 2-based gene therapy systems with the potential for preferential integration into AAVS1. Current gene therapy, 2, 145-159.

Paige, R. C., Royce, F. H., Plopper, C. G. and Buckpitt, A. R. (2000a) Long-term exposure to ozone increases acute pulmonary centriacinar injury by 1-nitronaphthalene: I. Region-specific enzyme activity. The Journal of pharmacology and experimental therapeutics, 295, 934-941.

Paige, R. C., Wong, V. and Plopper, C. G. (2000b) Long-term exposure to ozone increases acute pulmonary centriacinar injury by 1-nitronaphthalene: II. Quantitative histopathology. The Journal of pharmacology and experimental therapeutics, 295, 942-950.

Panchision, D. M., Pickel, J. M., Studer, L., Lee, S. H., Turner, P. A., Hazel, T. G. and McKay, R. D. (2001) Sequential actions of BMP receptors control neural precursor cell production and fate. Genes & development, 15, 2094-2110.

Pankiewicz, W., Minarowski, L., Niklinska, W., Naumnik, W., Niklinski, J. and Chyczewski, L. (2007) Immunohistochemical markers of cancerogenesis in the lung. Folia Histochem Cytobiol, 45, 65-74.

Park, K. S., Wells, J. M., Zorn, A. M., Wert, S. E., Laubach, V. E., Fernandez, L. G. and Whitsett, J. A. (2006) Transdifferentiation of ciliated cells during repair of the respiratory epithelium. American journal of respiratory cell and molecular biology, 34, 151-157.

Peake, J. L., Reynolds, S. D., Stripp, B. R., Stephens, K. E. and Pinkerton, K. E. (2000) Alteration of pulmonary neuroendocrine cells during epithelial repair of naphthalene-induced airway injury. The American journal of pathology, 156, 279-286.

Peinado, H., Olmeda, D. and Cano, A. (2007) Snail, Zeb and bHLH factors in tumour progression: an alliance against the epithelial phenotype? Nature reviews, 7, 415-428.

Pi, X., Ren, R., Kelley, R., Zhang, C., Moser, M., Bohil, A. B., Divito, M., Cheney, R. E. and Patterson, C. (2007) Sequential roles for myosin-X in BMP6-dependent filopodial extension, migration, and activation of BMP receptors. The Journal of cell biology, 179, 1569-1582.

Plopper, C. G., Mango, G. W., Hatch, G. E., Wong, V. J., Toskala, E., Reynolds, S. D., Tarkington, B. K. and Stripp, B. R. (2006) Elevation of susceptibility to ozone-induced acute tracheobronchial injury in transgenic mice deficient in Clara cell secretory protein. Toxicology and applied pharmacology, 213, 74-85.

Plovins, A., Alvarez, A. M., Ibanez, M., Molina, M. and Nombela, C. (1994) Use of fluorescein-di-beta-D-galactopyranoside (FDG) and C12-FDG as substrates for beta-galactosidase detection by flow cytometry in animal, bacterial, and yeast cells. Applied and environmental microbiology, 60, 4638-4641.

Pouliot, F., Blais, A. and Labrie, C. (2003) Overexpression of a dominant negative type II bone morphogenetic protein receptor inhibits the growth of human breast cancer cells. Cancer research, 63, 277-281.

Powell, C. A., Spira, A., Derti, A., DeLisi, C., Liu, G., Borczuk, A., Busch, S., Sahasrabudhe, S., Chen, Y., Sugarbaker, D., Bueno, R., Richards, W. G. and Brody, J. S. (2003) Gene expression in lung adenocarcinomas of smokers and nonsmokers. American journal of respiratory cell and molecular biology, 29, 157-162.

Ramanarayanan, J., Hernandez-Ilizaliturri, F. J., Chanan-Khan, A. and Czuczman, M. S. (2004) Pro-apoptotic therapy with the oligonucleotide Genasense (oblimersen sodium) targeting Bcl-2 protein expression enhances the biological anti-tumour activity of rituximab. British journal of haematology, 127, 519-530.

Ramos, M. F., Lame, M. W., Segall, H. J. and Wilson, D. W. (2008) Smad signaling in the rat model of monocrotaline pulmonary hypertension. Toxicologic pathology, 36, 311-320.

Ramsay, P. L., Luo, Z., Major, A., Park, M. S., Finegold, M., Welty, S. E., Kwak, I., Darlington, G. and Demayo, F. J. (2003) Multiple mechanisms for oxygen-induced regulation of the Clara cell secretory protein gene. Faseb J, 17, 2142-2144.

Rawlins, E. L., Ostrowski, L. E., Randell, S. H. and Hogan, B. L. (2007) Lung development and repair: contribution of the ciliated lineage. Proceedings of the National Academy of Sciences of the United States of America, 104, 410-417.

Reddel, R. R., Ke, Y., Gerwin, B. I., McMenamin, M. G., Lechner, J. F., Su, R. T., Brash, D. E., Park, J. B., Rhim, J. S. and Harris, C. C. (1988) Transformation of human bronchial epithelial cells by infection with SV40 or adenovirus-12 SV40 hybrid virus, or transfection via strontium phosphate coprecipitation with a plasmid containing SV40 early region genes. Cancer research, 48, 1904-1909.

Reissmann, P. T., Koga, H., Takahashi, R., Figlin, R. A., Holmes, E. C., Piantadosi, S., Cordon-Cardo, C. and Slamon, D. J. (1993) Inactivation of the retinoblastoma susceptibility gene in non-small-cell lung cancer. The Lung Cancer Study Group. Oncogene, 8, 1913-1919.

Reynolds, S. D., Giangreco, A., Power, J. H. and Stripp, B. R. (2000a) Neuroepithelial bodies of pulmonary airways serve as a reservoir of progenitor cells capable of epithelial regeneration. The American journal of pathology, 156, 269-278.

Reynolds, S. D., Hong, K. U., Giangreco, A., Mango, G. W., Guron, C., Morimoto, Y. and Stripp, B. R. (2000b) Conditional clara cell ablation reveals a self-renewing progenitor function of pulmonary neuroendocrine cells. American journal of physiology, 278, L1256-1263.

Reynolds, S. D., Zemke, A. C., Giangreco, A., Brockway, B. L., Teisanu, R. M., Drake, J. A., Mariani, T., Di, P. Y., Taketo, M. M. and Stripp, B. R. (2008) Conditional stabilization of beta-catenin expands the pool of lung stem cells. Stem cells (Dayton, Ohio), 26, 1337-1346.

Roberts, A. B., Piek, E., Bottinger, E. P., Ashcroft, G., Mitchell, J. B. and Flanders, K. C. (2001) Is Smad3 a major player in signal transduction pathways leading to fibrogenesis? Chest, 120, 43S-47S.

Robles, A. I., Linke, S. P. and Harris, C. C. (2002) The p53 network in lung carcinogenesis. Oncogene, 21, 6898-6907.

Roelen, B. A., Cohen, O. S., Raychowdhury, M. K., Chadee, D. N., Zhang, Y., Kyriakis, J. M., Alessandrini, A. A. and Lin, H. Y. (2003) Phosphorylation of threonine 276 in Smad4 is involved in transforming growth factor-beta-induced nuclear accumulation. American journal of physiology, 285, C823-830.

Rosendahl, A., Pardali, E., Speletas, M., Ten Dijke, P., Heldin, C. H. and Sideras, P. (2002) Activation of bone morphogenetic protein/Smad signaling in bronchial

epithelial cells during airway inflammation. American journal of respiratory cell and molecular biology, 27, 160-169.
Rosenzweig, B. L., Imamura, T., Okadome, T., Cox, G. N., Yamashita, H., ten Dijke, P., Heldin, C. H. and Miyazono, K. (1995) Cloning and characterization of a human type II receptor for bone morphogenetic proteins. Proceedings of the National Academy of Sciences of the United States of America, 92, 7632-7636.
Rubin, L. J. (1997) Primary pulmonary hypertension. The New England journal of medicine, 336, 111-117.
Ruiz, F. E., Clancy, J. P., Perricone, M. A., Bebok, Z., Hong, J. S., Cheng, S. H., Meeker, D. P., Young, K. R., Schoumacher, R. A., Weatherly, M. R., Wing, L., Morris, J. E., Sindel, L., Rosenberg, M., van Ginkel, F. W., McGhee, J. R., Kelly, D., Lyrene, R. K. and Sorscher, E. J. (2001) A clinical inflammatory syndrome attributable to aerosolized lipid-DNA administration in cystic fibrosis. Hum Gene Ther, 12, 751-761.
Saarikoski, S. T., Rivera, S. P. and Hankinson, O. (2002) Mitogen-inducible gene 6 (MIG-6), adipophilin and tuftelin are inducible by hypoxia. FEBS letters, 530, 186-190.
Saez, E., Nelson, M. C., Eshelman, B., Banayo, E., Koder, A., Cho, G. J. and Evans, R. M. (2000) Identification of ligands and coligands for the ecdysone-regulated gene switch. Proceedings of the National Academy of Sciences of the United States of America, 97, 14512-14517.
Saito, T., Oda, Y., Itakura, E., Shiratsuchi, H., Kinoshita, Y., Oshiro, Y., Tamiya, S., Hachitanda, Y., Iwamoto, Y. and Tsuneyoshi, M. (2001) Expression of intercellular adhesion molecules in epithelioid sarcoma and malignant rhabdoid tumor. Pathology international, 51, 532-542.
Samad, T. A., Rebbapragada, A., Bell, E., Zhang, Y., Sidis, Y., Jeong, S. J., Campagna, J. A., Perusini, S., Fabrizio, D. A., Schneyer, A. L., Lin, H. Y., Brivanlou, A. H., Attisano, L. and Woolf, C. J. (2005) DRAGON, a bone morphogenetic protein co-receptor. The Journal of biological chemistry, 280, 14122-14129.
Sater, A. K., El-Hodiri, H. M., Goswami, M., Alexander, T. B., Al-Sheikh, O., Etkin, L. D. and Akif Uzman, J. (2003) Evidence for antagonism of BMP-4 signals by MAP kinase during Xenopus axis determination and neural specification. Differentiation; research in biological diversity, 71, 434-444.
Satow, R., Kurisaki, A., Chan, T. C., Hamazaki, T. S. and Asashima, M. (2006) Dullard promotes degradation and dephosphorylation of BMP receptors and is required for neural induction. Developmental cell, 11, 763-774.
Sauer, J. M., Eversole, R. R., Lehmann, C. L., Johnson, D. E. and Beuving, L. J. (1997) An ultrastructural evaluation of acute 1-nitronaphthalene induced hepatic and pulmonary toxicity in the rat. Toxicology letters, 90, 19-27.
Sauer, T., Boudjema, G., Jebsen, P. W. and Naess, O. (2001) Immunocytochemical expression of E-cadherin on fine-needle aspirates from breast carcinomas correlate with the cell dissociation pattern seen on smears. Diagnostic cytopathology, 25, 382-388.
Schatzlein, A. G., Zinselmeyer, B. H., Elouzi, A., Dufes, C., Chim, Y. T., Roberts, C. J., Davies, M. C., Munro, A., Gray, A. I. and Uchegbu, I. F. (2005) Preferential liver

gene expression with polypropylenimine dendrimers. J Control Release, 101, 247-258.
Schmelzer, K. R., Wheelock, A. M., Dettmer, K., Morin, D. and Hammock, B. D. (2006) The role of inflammatory mediators in the synergistic toxicity of ozone and 1-nitronaphthalene in rat airways. Environmental health perspectives, 114, 1354-1360.
Schoch, K. G., Lori, A., Burns, K. A., Eldred, T., Olsen, J. C. and Randell, S. H. (2004) A subset of mouse tracheal epithelial basal cells generates large colonies in vitro. American journal of physiology, 286, L631-642.
Schubbert, S., Shannon, K. and Bollag, G. (2007) Hyperactive Ras in developmental disorders and cancer. Nature reviews, 7, 295-308.
Schuler, M., Rochlitz, C., Horowitz, J. A., Schlegel, J., Perruchoud, A. P., Kommoss, F., Bolliger, C. T., Kauczor, H. U., Dalquen, P., Fritz, M. A., Swanson, S., Herrmann, R. and Huber, C. (1998) A phase I study of adenovirus-mediated wild-type p53 gene transfer in patients with advanced non-small cell lung cancer. Hum Gene Ther, 9, 2075-2082.
Seiler, M. P., Miller, A. D., Zabner, J. and Halbert, C. L. (2006) Adeno-associated virus types 5 and 6 use distinct receptors for cell entry. Hum Gene Ther, 17, 10-19.
Sekido, Y., Fong, K. M. and Minna, J. D. (2003) Molecular genetics of lung cancer. Annual review of medicine, 54, 73-87.
Serrano-Mollar, A., Nacher, M., Gay-Jordi, G., Closa, D., Xaubet, A. and Bulbena, O. (2007) Intratracheal transplantation of alveolar type II cells reverses bleomycin-induced lung fibrosis. American journal of respiratory and critical care medicine, 176, 1261-1268.
Sheehan, G. M., Kallakury, B. V., Sheehan, C. E., Fisher, H. A., Kaufman, R. P., Jr. and Ross, J. S. (2005) Smad4 protein expression correlates with grade, stage, and DNA ploidy in prostatic adenocarcinomas. Human pathology, 36, 1204-1209.
Shimizu, E., Coxon, A., Otterson, G. A., Steinberg, S. M., Kratzke, R. A., Kim, Y. W., Fedorko, J., Oie, H., Johnson, B. E., Mulshine, J. L. and et al. (1994) RB protein status and clinical correlation from 171 cell lines representing lung cancer, extrapulmonary small cell carcinoma, and mesothelioma. Oncogene, 9, 2441-2448.
Shimshek, D. R., Kim, J., Hubner, M. R., Spergel, D. J., Buchholz, F., Casanova, E., Stewart, A. F., Seeburg, P. H. and Sprengel, R. (2002) Codon-improved Cre recombinase (iCre) expression in the mouse. Genesis, 32, 19-26.
Shultz, M. A., Choudary, P. V. and Buckpitt, A. R. (1999) Role of murine cytochrome P-450 2F2 in metabolic activation of naphthalene and metabolism of other xenobiotics. The Journal of pharmacology and experimental therapeutics, 290, 281-288.
Sibley, C. D., Rabin, H. and Surette, M. G. (2006) Cystic fibrosis: a polymicrobial infectious disease. Future microbiology, 1, 53-61.
Sinn, P. L., Burnight, E. R., Hickey, M. A., Blissard, G. W. and McCray, P. B., Jr. (2005) Persistent gene expression in mouse nasal epithelia following feline immunodeficiency virus-based vector gene transfer. J Virol, 79, 12818-12827.
Sinn, P. L., Hickey, M. A., Staber, P. D., Dylla, D. E., Jeffers, S. A., Davidson, B. L., Sanders, D. A. and McCray, P. B., Jr. (2003) Lentivirus vectors pseudotyped with

filoviral envelope glycoproteins transduce airway epithelia from the apical surface independently of folate receptor alpha. J Virol, 77, 5902-5910.
Sisson, T. H., Hansen, J. M., Shah, M., Hanson, K. E., Du, M., Ling, T., Simon, R. H. and Christensen, P. J. (2006) Expression of the reverse tetracycline-transactivator gene causes emphysema-like changes in mice. American journal of respiratory cell and molecular biology, 34, 552-560.
Sisson, T. H., Hanson, K. E., Subbotina, N., Patwardhan, A., Hattori, N. and Simon, R. H. (2002) Inducible lung-specific urokinase expression reduces fibrosis and mortality after lung injury in mice. American journal of physiology, 283, L1023-1032.
Solly, S. K., Trajcevski, S., Frisen, C., Holzer, G. W., Nelson, E., Clerc, B., Abordo-Adesida, E., Castro, M., Lowenstein, P. and Klatzmann, D. (2003) Replicative retroviral vectors for cancer gene therapy. Cancer Gene Ther, 10, 30-39.
Sonawane, N. D., Szoka, F. C., Jr. and Verkman, A. S. (2003) Chloride accumulation and swelling in endosomes enhances DNA transfer by polyamine-DNA polyplexes. J Biol Chem, 278, 44826-44831.
Soriano, P. (1999) Generalized lacZ expression with the ROSA26 Cre reporter strain. Nature genetics, 21, 70-71.
Stripp, B. R., Reynolds, S. D., Boe, I. M., Lund, J., Power, J. H., Coppens, J. T., Wong, V., Reynolds, P. R. and Plopper, C. G. (2002) Clara cell secretory protein deficiency alters clara cell secretory apparatus and the protein composition of airway lining fluid. American journal of respiratory cell and molecular biology, 27, 170-178.
Stuart-Harris, R., Caldas, C., Pinder, S. E. and Pharoah, P. (2008) Proliferation markers and survival in early breast cancer: a systematic review and meta-analysis of 85 studies in 32,825 patients. Breast (Edinburgh, Scotland), 17, 323-334.
Sumner-Jones, S. G., Davies, L. A., Varathalingam, A., Gill, D. R. and Hyde, S. C. (2006) Long-term persistence of gene expression from adeno-associated virus serotype 5 in the mouse airways. Gene Ther, 13, 1703-1713.
Sun, S., Schiller, J. H. and Gazdar, A. F. (2007) Lung cancer in never smokers--a different disease. Nature reviews, 7, 778-790.
Suzuki, J., Otsuka, F., Takeda, M., Inagaki, K., Miyoshi, T., Mimura, Y., Ogura, T., Doihara, H. and Makino, H. (2005) Functional roles of the bone morphogenetic protein system in thyrotropin signaling in porcine thyroid cells. Biochemical and biophysical research communications, 327, 1124-1130.
Symowicz, J., Adley, B. P., Gleason, K. J., Johnson, J. J., Ghosh, S., Fishman, D. A., Hudson, L. G. and Stack, M. S. (2007) Engagement of collagen-binding integrins promotes matrix metalloproteinase-9-dependent E-cadherin ectodomain shedding in ovarian carcinoma cells. Cancer research, 67, 2030-2039.
Tada, Y., Majka, S., Carr, M., Harral, J., Crona, D., Kuriyama, T. and West, J. (2007) Molecular effects of loss of BMPR2 signaling in smooth muscle in a transgenic mouse model of PAH. American journal of physiology, 292, L1556-1563.
Takeda, K., Miyahara, N., Rha, Y. H., Taube, C., Yang, E. S., Joetham, A., Kodama, T., Balhorn, A. M., Dakhama, A., Duez, C., Evans, A. J., Voelker, D. R. and Gelfand, E. W. (2003) Surfactant protein D regulates airway function and allergic

inflammation through modulation of macrophage function. American journal of respiratory and critical care medicine, 168, 783-789.
Tammemagi, M. C., McLaughlin, J. R. and Bull, S. B. (1999) Meta-analyses of p53 tumor suppressor gene alterations and clinicopathological features in resected lung cancers. Cancer Epidemiol Biomarkers Prev, 8, 625-634.
Terauchi, M., Kajiyama, H., Yamashita, M., Kato, M., Tsukamoto, H., Umezu, T., Hosono, S., Yamamoto, E., Shibata, K., Ino, K., Nawa, A., Nagasaka, T. and Kikkawa, F. (2007) Possible involvement of TWIST in enhanced peritoneal metastasis of epithelial ovarian carcinoma. Clinical & experimental metastasis, 24, 329-339.
Terry, S., Queires, L., Gil-Diez-de-Medina, S., Chen, M. W., de la Taille, A., Allory, Y., Tran, P. L., Abbou, C. C., Buttyan, R. and Vacherot, F. (2006) Protocadherin-PC promotes androgen-independent prostate cancer cell growth. The Prostate, 66, 1100-1113.
Theriault, B. L., Shepherd, T. G., Mujoomdar, M. L. and Nachtigal, M. W. (2007) BMP4 induces EMT and Rho GTPase activation in human ovarian cancer cells. Carcinogenesis, 28, 1153-1162.
Thiagalingam, S., Foy, R. L., Cheng, K. H., Lee, H. J., Thiagalingam, A. and Ponte, J. F. (2002) Loss of heterozygosity as a predictor to map tumor suppressor genes in cancer: molecular basis of its occurrence. Current opinion in oncology, 14, 65-72.
Thomson, J. R., Machado, R. D., Pauciulo, M. W., Morgan, N. V., Humbert, M., Elliott, G. C., Ward, K., Yacoub, M., Mikhail, G., Rogers, P., Newman, J., Wheeler, L., Higenbottam, T., Gibbs, J. S., Egan, J., Crozier, A., Peacock, A., Allcock, R., Corris, P., Loyd, J. E., Trembath, R. C. and Nichols, W. C. (2000) Sporadic primary pulmonary hypertension is associated with germline mutations of the gene encoding BMPR-II, a receptor member of the TGF-beta family. Journal of medical genetics, 37, 741-745.
Torbenson, M., Marinopoulos, S., Dang, D. T., Choti, M., Ashfaq, R., Maitra, A., Boitnott, J. and Wilentz, R. E. (2002) Smad4 overexpression in hepatocellular carcinoma is strongly associated with transforming growth factor beta II receptor immunolabeling. Human pathology, 33, 871-876.
Torchilin, V. (2008) Antibody-modified liposomes for cancer chemotherapy. Expert opinion on drug delivery, 5, 1003-1025.
Toyooka, S., Toyooka, K. O., Maruyama, R., Virmani, A. K., Girard, L., Miyajima, K., Harada, K., Ariyoshi, Y., Takahashi, T., Sugio, K., Brambilla, E., Gilcrease, M., Minna, J. D. and Gazdar, A. F. (2001) DNA methylation profiles of lung tumors. Molecular cancer therapeutics, 1, 61-67.
Tremblay, K. D., Dunn, N. R. and Robertson, E. J. (2001) Mouse embryos lacking Smad1 signals display defects in extra-embryonic tissues and germ cell formation. Development (Cambridge, England), 128, 3609-3621.
Umbas, R., Schalken, J. A., Aalders, T. W., Carter, B. S., Karthaus, H. F., Schaafsma, H. E., Debruyne, F. M. and Isaacs, W. B. (1992) Expression of the cellular adhesion molecule E-cadherin is reduced or absent in high-grade prostate cancer. Cancer research, 52, 5104-5109.
Vacherot, F., Terry, S., Faucon, H., Queires, L., Chen, M. W., Yang, X., Gil Diez de Medina, S., Verdier, A., Azoulay, S., Allory, Y., Abbou, C. C., Buttyan, R. and de

la Taille, A. (2005) [Protocadherin-PC discovery and its implication in prostate cancer progression]. Prog Urol, 15, 1294-1302.
van Baal, J. W., Milana, F., Rygiel, A. M., Sondermeijer, C. M., Spek, C. A., Bergman, J. J., Peppelenbosch, M. P. and Krishnadath, K. K. (2008) A comparative analysis by SAGE of gene expression profiles of esophageal adenocarcinoma and esophageal squamous cell carcinoma. Cell Oncol, 30, 63-75.
van Laar, T., Schouten, T., van der Eb, A. J. and Terleth, C. (2001) Induction of the SAPK activator MIG-6 by the alkylating agent methyl methanesulfonate. Molecular carcinogenesis, 31, 63-67.
Verheyen, E. M. (2007) Opposing effects of Wnt and MAPK on BMP/Smad signal duration. Developmental cell, 13, 755-756.
Verschoyle, R. D., Carthew, P., Wolf, C. R. and Dinsdale, D. (1993) 1-Nitronaphthalene toxicity in rat lung and liver: effects of inhibiting and inducing cytochrome P450 activity. Toxicology and applied pharmacology, 122, 208-213.
Vinals, F., Lopez-Rovira, T., Rosa, J. L. and Ventura, F. (2002) Inhibition of PI3K/p70 S6K and p38 MAPK cascades increases osteoblastic differentiation induced by BMP-2. FEBS letters, 510, 99-104.
Vincent, P., Collette, Y., Marignier, R., Vuaillat, C., Rogemond, V., Davoust, N., Malcus, C., Cavagna, S., Gessain, A., Machuca-Gayet, I., Belin, M. F., Quach, T. and Giraudon, P. (2005) A role for the neuronal protein collapsin response mediator protein 2 in T lymphocyte polarization and migration. J Immunol, 175, 7650-7660.
Wada, T. and Penninger, J. M. (2004) Mitogen-activated protein kinases in apoptosis regulation. Oncogene, 23, 2838-2849.
Walsh, M., Tangney, M., O'Neill, M. J., Larkin, J. O., Soden, D. M., McKenna, S. L., Darcy, R., O'Sullivan, G. C. and O'Driscoll, C. M. (2006) Evaluation of cellular uptake and gene transfer efficiency of pegylated poly-L-lysine compacted DNA: implications for cancer gene therapy. Molecular pharmaceutics, 3, 644-653.
Walters, R. W., Yi, S. M., Keshavjee, S., Brown, K. E., Welsh, M. J., Chiorini, J. A. and Zabner, J. (2001) Binding of adeno-associated virus type 5 to 2,3-linked sialic acid is required for gene transfer. J Biol Chem, 276, 20610-20616.
Wang, S. Z., Rosenberger, C. L., Espindola, T. M., Barrett, E. G., Tesfaigzi, Y., Bice, D. E. and Harrod, K. S. (2001) CCSP modulates airway dysfunction and host responses in an Ova-challenged mouse model. American journal of physiology, 281, L1303-1311.
Wang, W. J., Tai, C. K., Kasahara, N. and Chen, T. C. (2003) Highly efficient and tumor-restricted gene transfer to malignant gliomas by replication-competent retroviral vectors. Hum Gene Ther, 14, 117-127.
Wang, X. J., Liefer, K. M., Tsai, S., O'Malley, B. W. and Roop, D. R. (1999) Development of gene-switch transgenic mice that inducibly express transforming growth factor beta1 in the epidermis. Proceedings of the National Academy of Sciences of the United States of America, 96, 8483-8488.
Wang, X. Q., Li, H., Van Putten, V., Winn, R. A., Heasley, L. E. and Nemenoff, R. A. (2008) Oncogenic K-Ras Regulates Proliferation and Cell Junctions in Lung Epithelial Cells Through Induction of COX-2 and Activation of MMP-9. Molecular biology of the cell.

Warburton, D., Gauldie, J., Bellusci, S. and Shi, W. (2006) Lung development and susceptibility to chronic obstructive pulmonary disease. Proceedings of the American Thoracic Society, 3, 668-672.

Warming, S., Costantino, N., Court, D. L., Jenkins, N. A. and Copeland, N. G. (2005) Simple and highly efficient BAC recombineering using galK selection. Nucleic acids research, 33, e36.

Warrier, M. R. and Hershey, G. K. (2008) Asthma genetics: personalizing medicine. J Asthma, 45, 257-264.

Watanabe, H., Shionyu, M., Kimura, T., Kimata, K. and Watanabe, H. (2007) Splicing factor 3b subunit 4 binds BMPR-IA and inhibits osteochondral cell differentiation. The Journal of biological chemistry, 282, 20728-20738.

West, J., Fagan, K., Steudel, W., Fouty, B., Lane, K., Harral, J., Hoedt-Miller, M., Tada, Y., Ozimek, J., Tuder, R. and Rodman, D. M. (2004) Pulmonary hypertension in transgenic mice expressing a dominant-negative BMPRII gene in smooth muscle. Circulation research, 94, 1109-1114.

Wheelock, A. M., Boland, B. C., Isbell, M., Morin, D., Wegesser, T. C., Plopper, C. G. and Buckpitt, A. R. (2005) In vivo effects of ozone exposure on protein adduct formation by 1-nitronaphthalene in rat lung. American journal of respiratory cell and molecular biology, 33, 130-137.

Wheelock, A. M., Zhang, L., Tran, M. U., Morin, D., Penn, S., Buckpitt, A. R. and Plopper, C. G. (2004) Isolation of rodent airway epithelial cell proteins facilitates in vivo proteomics studies of lung toxicity. American journal of physiology, 286, L399-410.

Winnier, G., Blessing, M., Labosky, P. A. and Hogan, B. L. (1995) Bone morphogenetic protein-4 is required for mesoderm formation and patterning in the mouse. Genes & development, 9, 2105-2116.

Winter, J. M., Ting, A. H., Vilardell, F., Gallmeier, E., Baylin, S. B., Hruban, R. H., Kern, S. E. and Iacobuzio-Donahue, C. A. (2008) Absence of E-cadherin expression distinguishes noncohesive from cohesive pancreatic cancer. Clin Cancer Res, 14, 412-418.

Wistuba, II, Gazdar, A. F. and Minna, J. D. (2001) Molecular genetics of small cell lung carcinoma. Seminars in oncology, 28, 3-13.

Wistuba, II, Mao, L. and Gazdar, A. F. (2002) Smoking molecular damage in bronchial epithelium. Oncogene, 21, 7298-7306.

Wolff, J. A., Malone, R. W., Williams, P., Chong, W., Acsadi, G., Jani, A. and Felgner, P. L. (1990) Direct gene transfer into mouse muscle in vivo. Science, 247, 1465-1468.

Wozney, J. M., Rosen, V., Celeste, A. J., Mitsock, L. M., Whitters, M. J., Kriz, R. W., Hewick, R. M. and Wang, E. A. (1988) Novel regulators of bone formation: molecular clones and activities. Science (New York, N.Y, 242, 1528-1534.

Wu, X., Shi, W. and Cao, X. (2007) Multiplicity of BMP signaling in skeletal development. Annals of the New York Academy of Sciences, 1116, 29-49.

Xenariou, S., Griesenbach, U., Ferrari, S., Dean, P., Scheule, R. K., Cheng, S. H., Geddes, D. M., Plank, C. and Alton, E. W. (2006) Using magnetic forces to enhance non-viral gene transfer to airway epithelium in vivo. Gene Ther, 13, 1545-1552.

Xenariou, S., Griesenbach, U., Liang, H. D., Zhu, J., Farley, R., Somerton, L., Singh, C., Jeffery, P. K., Ferrari, S., Scheule, R. K., Cheng, S. H., Geddes, D. M., Blomley, M. and Alton, E. W. (2007) Use of ultrasound to enhance nonviral lung gene transfer in vivo. Gene Ther, 14, 768-774.

Xia, Y., Yu, P. B., Sidis, Y., Beppu, H., Bloch, K. D., Schneyer, A. L. and Lin, H. Y. (2007) Repulsive guidance molecule RGMa alters utilization of bone morphogenetic protein (BMP) type II receptors by BMP2 and BMP4. The Journal of biological chemistry, 282, 18129-18140.

Xu, D., Makkinje, A. and Kyriakis, J. M. (2005) Gene 33 is an endogenous inhibitor of epidermal growth factor (EGF) receptor signaling and mediates dexamethasone-induced suppression of EGF function. The Journal of biological chemistry, 280, 2924-2933.

Xu, J., Keeton, A. B., Wu, L., Franklin, J. L., Cao, X. and Messina, J. L. (2005) Gene 33 inhibits apoptosis of breast cancer cells and increases poly(ADP-ribose) polymerase expression. Breast cancer research and treatment, 91, 207-215.

Xu, W. Q., Jiang, X. C., Zheng, L., Yu, Y. Y. and Tang, J. M. (2007) Expression of TGF-beta1, TbetaRII and Smad4 in colorectal carcinoma. Experimental and molecular pathology, 82, 284-291.

Xu, X., Brodie, S. G., Yang, X., Im, Y. H., Parks, W. T., Chen, L., Zhou, Y. X., Weinstein, M., Kim, S. J. and Deng, C. X. (2000) Haploid loss of the tumor suppressor Smad4/Dpc4 initiates gastric polyposis and cancer in mice. Oncogene, 19, 1868-1874.

Xu, Y. and Szoka, F. C., Jr. (1996) Mechanism of DNA release from cationic liposome/DNA complexes used in cell transfection. Biochemistry, 35, 5616-5623.

Yamamoto, N., Hayashi, Y., Kagami, H., Fukui, T., Fukuhara, H., Tohnai, I., Ueda, M., Mizuno, M. and Yoshida, J. (2005) Suicide gene therapy using adenovirus vector for human oral squamous carcinoma cell line in vitro. Nagoya journal of medical science, 67, 83-91.

Yang, J., Zhou, W., Zhang, Y., Zidon, T., Ritchie, T. and Engelhardt, J. F. (1999) Concatamerization of adeno-associated virus circular genomes occurs through intermolecular recombination. J Virol, 73, 9468-9477.

Yang, N. S., Burkholder, J., Roberts, B., Martinell, B. and McCabe, D. (1990) In vivo and in vitro gene transfer to mammalian somatic cells by particle bombardment. Proceedings of the National Academy of Sciences of the United States of America, 87, 9568-9572.

Yang, P., Sun, Z., Krowka, M. J., Aubry, M. C., Bamlet, W. R., Wampfler, J. A., Thibodeau, S. N., Katzmann, J. A., Allen, M. S., Midthun, D. E., Marks, R. S. and de Andrade, M. (2008) Alpha1-antitrypsin deficiency carriers, tobacco smoke, chronic obstructive pulmonary disease, and lung cancer risk. Archives of internal medicine, 168, 1097-1103.

Yang, S., Du, J., Wang, Z., Yuan, W., Qiao, Y., Zhang, M., Zhang, J., Gao, S., Yin, J., Sun, B. and Zhu, T. (2007) BMP-6 promotes E-cadherin expression through repressing deltaEF1 in breast cancer cells. BMC cancer, 7, 211.

Yang, X., Li, C., Xu, X. and Deng, C. (1998) The tumor suppressor SMAD4/DPC4 is essential for epiblast proliferation and mesoderm induction in mice. Proceedings

of the National Academy of Sciences of the United States of America, 95, 3667-3672.
Yi, S. E., Daluiski, A., Pederson, R., Rosen, V. and Lyons, K. M. (2000) The type I BMP receptor BMPRIB is required for chondrogenesis in the mouse limb. Development (Cambridge, England), 127, 621-630.
Yu, D., Ellis, H. M., Lee, E. C., Jenkins, N. A., Copeland, N. G. and Court, D. L. (2000) An efficient recombination system for chromosome engineering in Escherichia coli. Proceedings of the National Academy of Sciences of the United States of America, 97, 5978-5983.
Yu, J. S., Koujak, S., Nagase, S., Li, C. M., Su, T., Wang, X., Keniry, M., Memeo, L., Rojtman, A., Mansukhani, M., Hibshoosh, H., Tycko, B. and Parsons, R. (2008) PCDH8, the human homolog of PAPC, is a candidate tumor suppressor of breast cancer. Oncogene, 27, 4657-4665.
Yu, P. B., Beppu, H., Kawai, N., Li, E. and Bloch, K. D. (2005) Bone morphogenetic protein (BMP) type II receptor deletion reveals BMP ligand-specific gain of signaling in pulmonary artery smooth muscle cells. The Journal of biological chemistry, 280, 24443-24450.
Zabner, J., Seiler, M., Walters, R., Kotin, R. M., Fulgeras, W., Davidson, B. L. and Chiorini, J. A. (2000) Adeno-associated virus type 5 (AAV5) but not AAV2 binds to the apical surfaces of airway epithelia and facilitates gene transfer. J Virol, 74, 3852-3858.
Zhang, H. and Bradley, A. (1996) Mice deficient for BMP2 are nonviable and have defects in amnion/chorion and cardiac development. Development (Cambridge, England), 122, 2977-2986.
Zhang, H. and Xue, Y. (2008) Wnt pathway is involved in advanced gastric carcinoma. Hepato-gastroenterology, 55, 1126-1130.
Zhang, X. and Chang, A. (2008) Molecular predictors of EGFR-TKI sensitivity in advanced non-small cell lung cancer. International journal of medical sciences, 5, 209-217.
Zhang, X., Ling, M. T., Wong, Y. C. and Wang, X. (2007a) Evidence of a novel antiapoptotic factor: role of inhibitor of differentiation or DNA binding (Id-1) in anticancer drug-induced apoptosis. Cancer science, 98, 308-314.
Zhang, X., Pickin, K. A., Bose, R., Jura, N., Cole, P. A. and Kuriyan, J. (2007b) Inhibition of the EGF receptor by binding of MIG6 to an activating kinase domain interface. Nature, 450, 741-744.
Zhang, Y. W., Staal, B., Su, Y., Swiatek, P., Zhao, P., Cao, B., Resau, J., Sigler, R., Bronson, R. and Vande Woude, G. F. (2007) Evidence that MIG-6 is a tumor-suppressor gene. Oncogene, 26, 269-276.
Zhang, Y. W., Su, Y., Lanning, N., Swiatek, P. J., Bronson, R. T., Sigler, R., Martin, R. W. and Vande Woude, G. F. (2005) Targeted disruption of Mig-6 in the mouse genome leads to early onset degenerative joint disease. Proceedings of the National Academy of Sciences of the United States of America, 102, 11740-11745.
Zheleva, D. I., Zhelev, N. Z., Fischer, P. M., Duff, S. V., Warbrick, E., Blake, D. G. and Lane, D. P. (2000) A quantitative study of the in vitro binding of the C-terminal

domain of p21 to PCNA: affinity, stoichiometry, and thermodynamics. Biochemistry, 39, 7388-7397.
Zhu, M., Tian, D., Li, J., Ma, Y., Wang, Y. and Wu, R. (2007) Glycogen synthase kinase 3beta and beta-catenin are involved in the injury and repair of bronchial epithelial cells induced by scratching. Experimental and molecular pathology, 83, 30-38.
Zou, H., Wieser, R., Massague, J. and Niswander, L. (1997) Distinct roles of type I bone morphogenetic protein receptors in the formation and differentiation of cartilage. Genes & development, 11, 2191-2203.
Zou, Y., Tornos, C., Qiu, X., Lia, M. and Perez-Soler, R. (2007) p53 aerosol formulation with low toxicity and high efficiency for early lung cancer treatment. Clin Cancer Res, 13, 4900-4908.

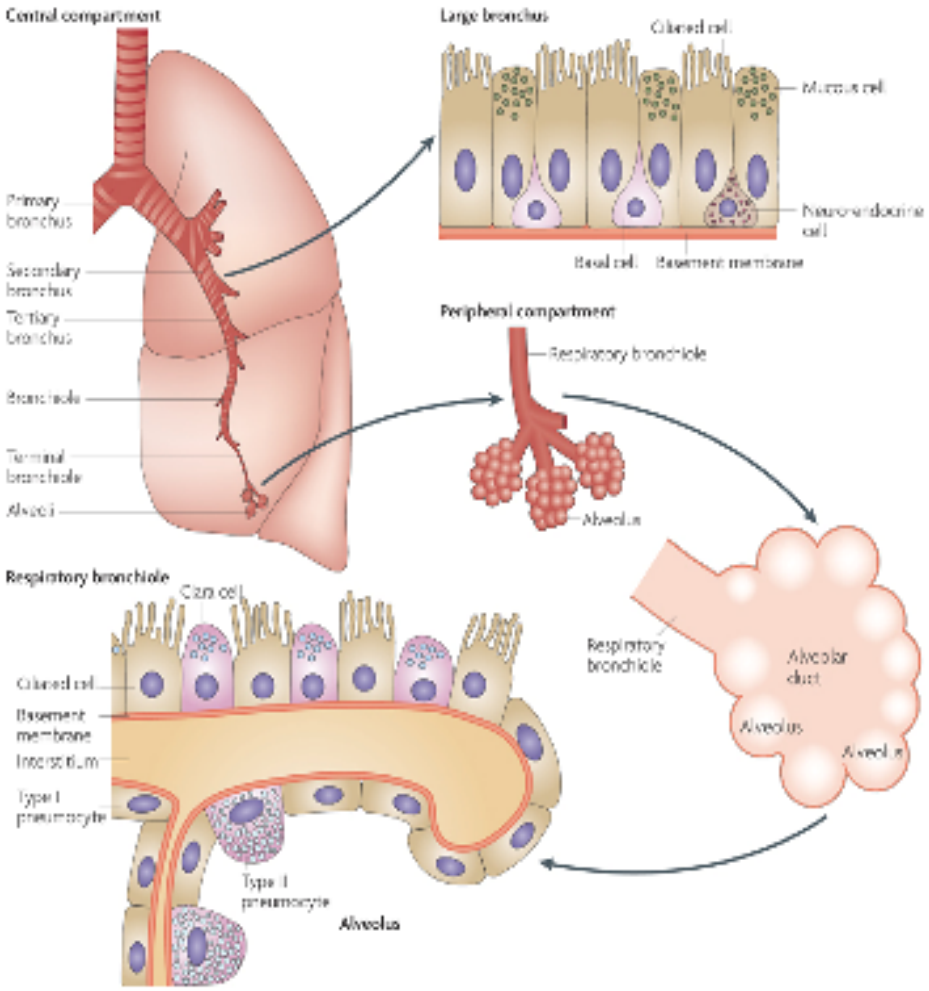

Figure 1.1: Cell structure and cells lining the airways

The mammalian conducting airways are composed of the trachea, secondary bronchus, tertiary bronchus, bronchioles and terminal bronchioles. The area at which respiration occurs is the alveolar duct region. A heterogeneous population of cells line the conducting and respiratory airways. The population of cells differ from proximal to distal regions. In the proximal regions ciliated and goblet cells predominant. In the distal regions Clara cells are the predominant cells type, pulmonary neuroendocrine cells (PNEC) and ciliated cells also reside in this location, though in lesser numbers. Figure from Sun, S *et al,* 2007

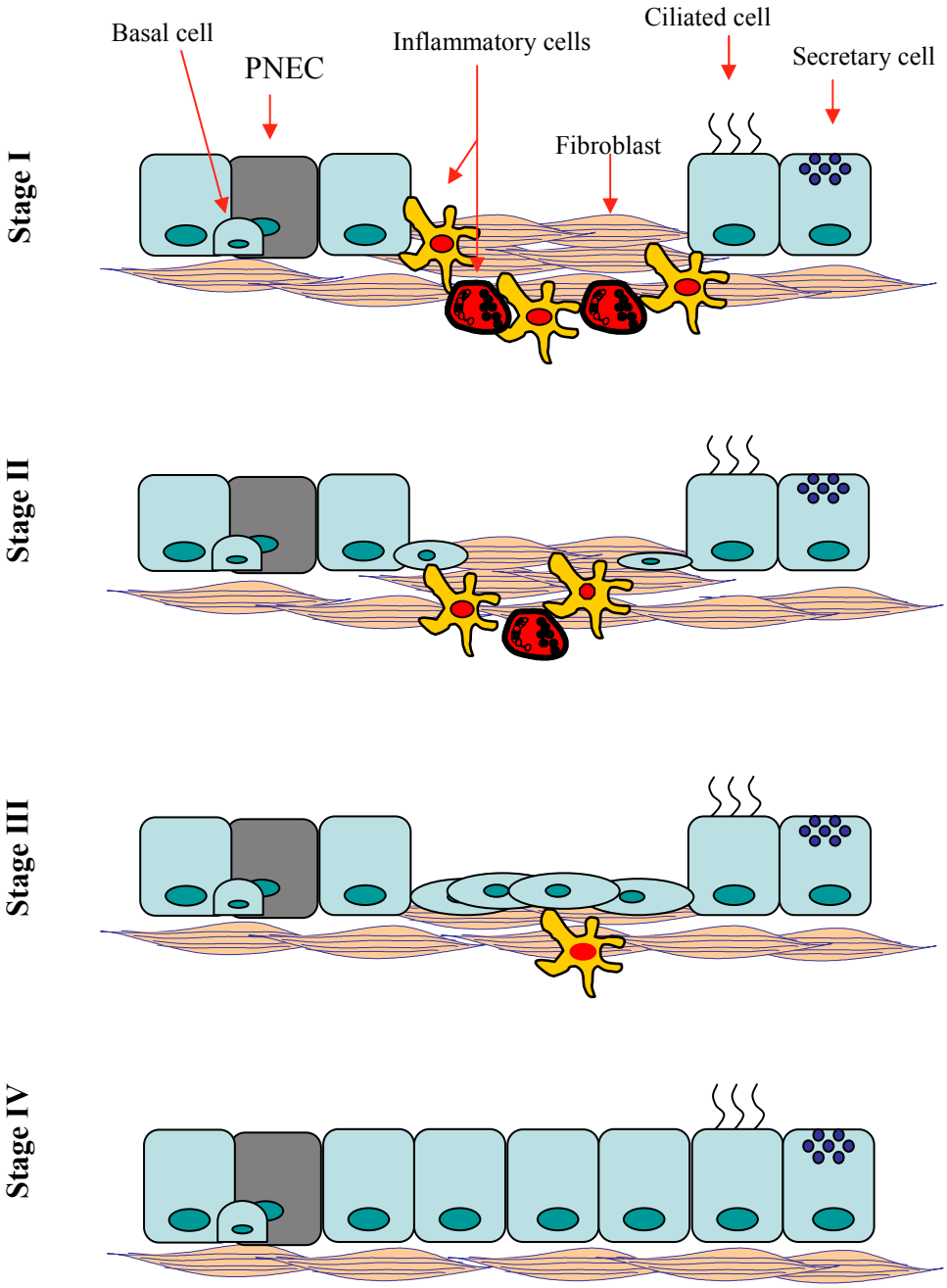
Basal cell
PNEC
Inflammatory cells
Ciliated cell
Secretary cell
Fibroblast
Stage I
Stage II
Stage III
Stage IV

Figure 1.2: Repair of the airway epithelium after injury

Cell loss from the epithelial membrane maybe caused by chemical or mechanical damage. Stage I) Loss of epithelial cells cause an immediate response in which cells of the mesenchymal layer proliferate, and immune cells infiltrate to the area to seal the wound, and prevent entry of pathogens. Stage II & III) Cells from the surrounding epithelial membrane begin to proliferate and migrate into the wounded area. Stage IV) Newly proliferated cells differentiate to regenerate the epithelial membrane of the lung.

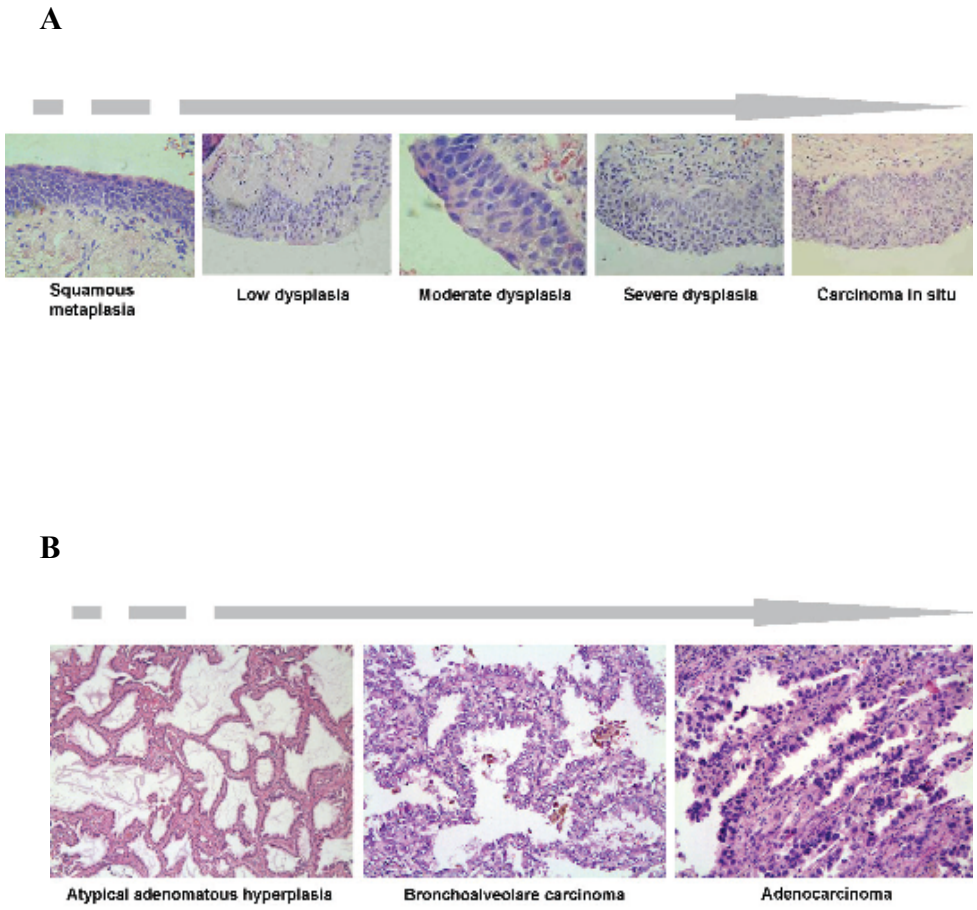

Figure 1.3: Progressive stages of NSCLC

NSCLC progress through numerous stages before forming a poorly differentiated tumour. A) Stages of progression for squamous cell carcinoma. B) Stages of progression for adenocarcinoma. Figure from Pankiewicz, *et al* 2007

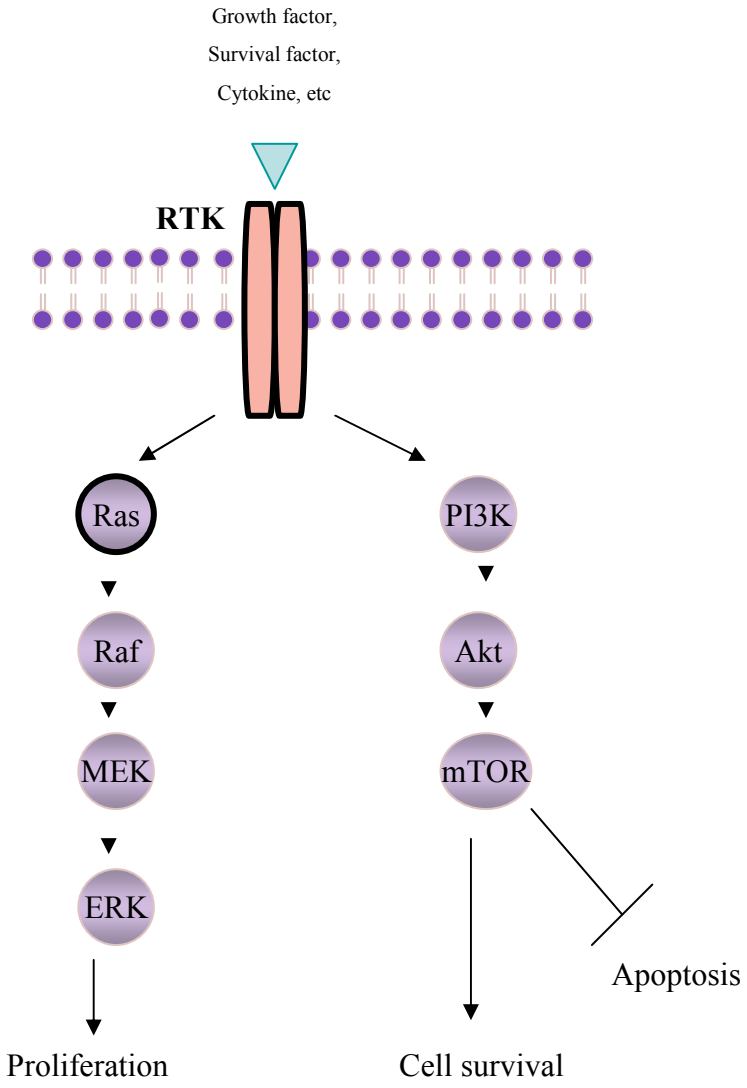

Figure 1.4: Signalling pathways effected during lung cancer

Tumours form when proliferation, pro-survival and/or anti-apoptotic signals are aberrantly expressed in the cell. Numerous mutation occur during lung cancer progression. Common mutations in NSCLC include activating mutations in the receptor thyrosine kinase (RTK) EGFR (extracellular growth factor), or in the ras protein. In this way pro-survival, proliferation and anti-apoptotic signals are constitutively activated to allow cells to proliferate out of control and contribute to tumour formation. → indicates initiation of signalling ⊣ indicates inhibition of signalling.

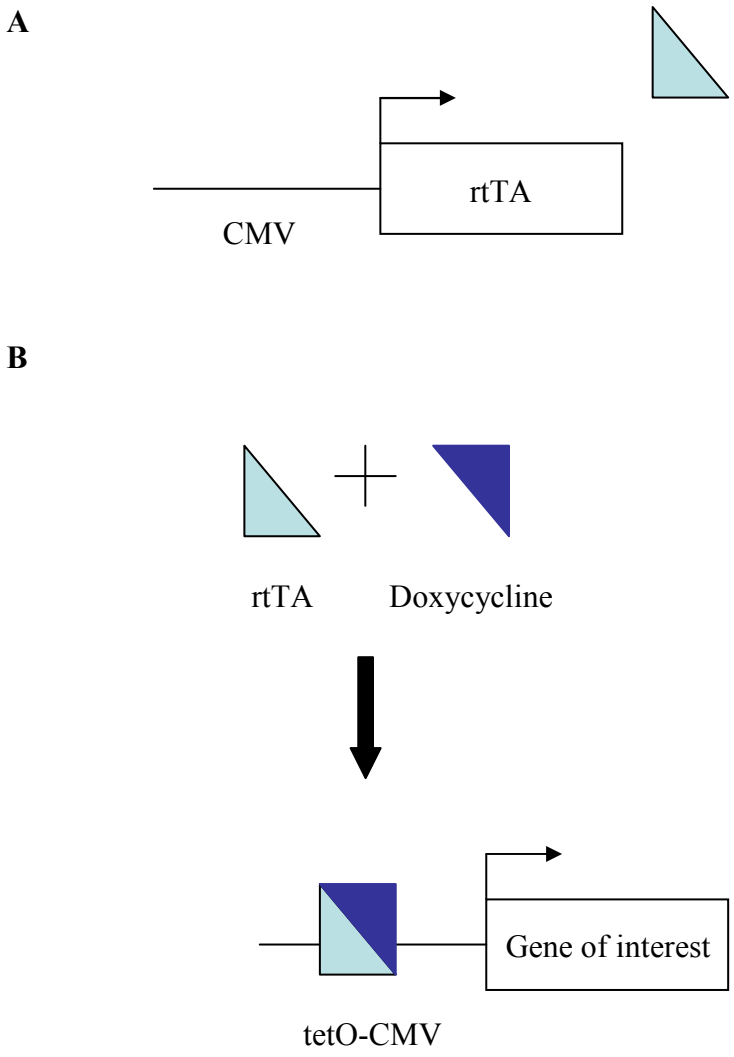

Figure 1.5: Tetracycline inducible system

The tetracycline inducible system allows temporal regulation of gene expression. A) The reverse tetracycline-controlled transactivator (rtTA) is expressed under the control of a CMV promoter allowing constitutive activation of the rtTA gene. B) In the presence of Doxycycline antibiotic (Dox) the rtTA protein recognises the specific DNA target sequence (tetO) allowing expression of the gene of interest.

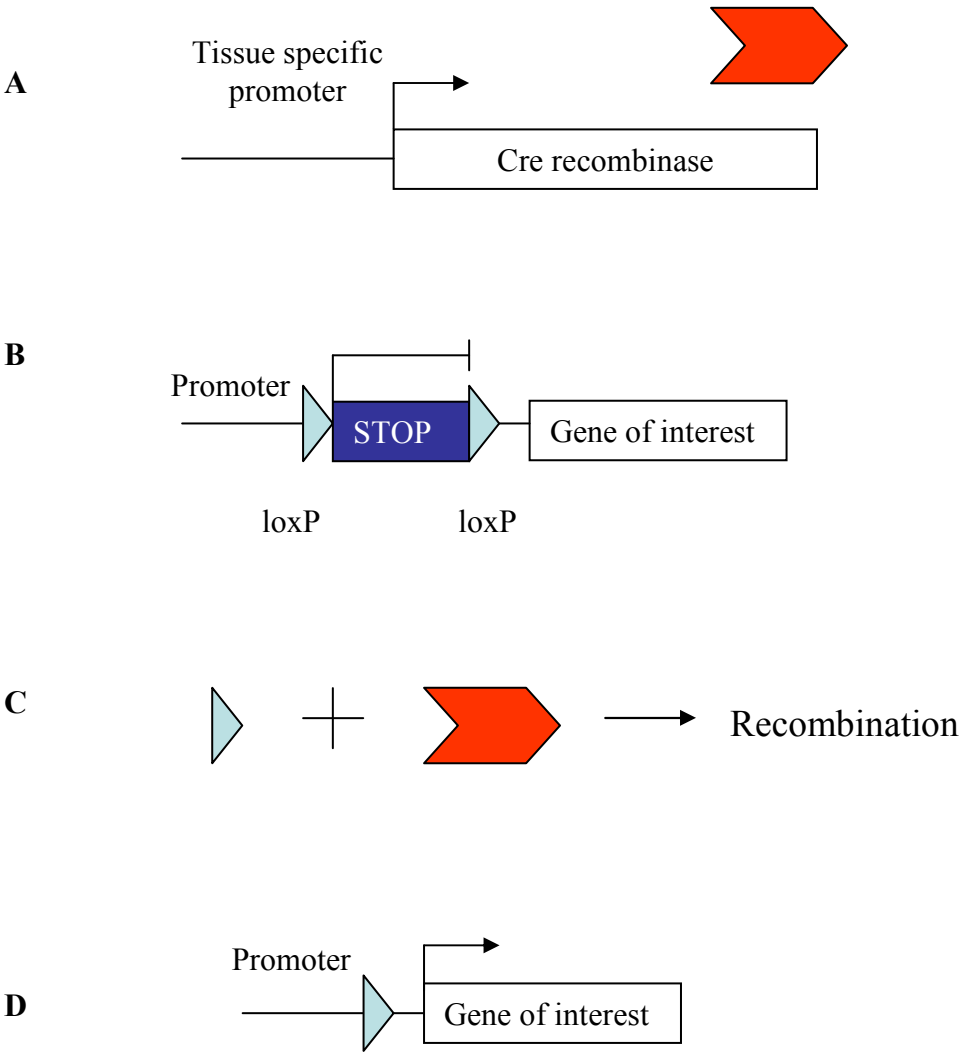

Figure 1.6: Cre-LoxP recombination system

The Cre-LoxP recombination system allows tissue specific induction (or deletion) of a gene of interest, dependant on the promoter controlling Cre recombinase. A) Cre recombinase is expressed under the control of a tissue specific promoter (for example the CCSP promoter expresses Cre recombinase in the Clara cells of the lungs). B) The gene of interest, downstream of a floxed stop cassette (loxP sites flanking the stop cassette), is not expressed in the presence of the stop cassette. C) Cre recombinase allows homologous recombination between the loxP sites thereby removing the stop cassette. D) Removal of the stop cassette allows expression of the gene of interest.

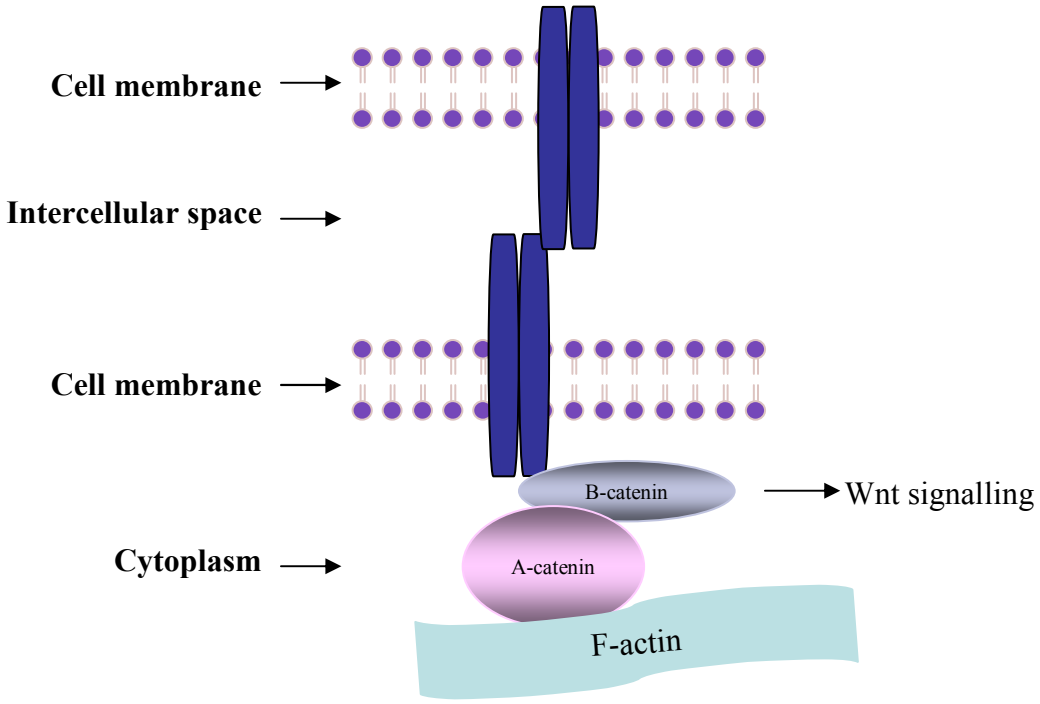

Figure 1.7: E-cadherin cell adhesion complex

Epithelial cell adhesion is achieved by interaction of E-cadherin molecules from adjacent cells. β-catenin binds to the cytoplasmic region of the E-cadherin molecule. α-catenin is recruited to the E-cadherin complex via β-catenin, and is responsible for binding actin filaments. In this way epithelial cells tightly adhere to one another and are polarised, with a structured cytoskeleton.

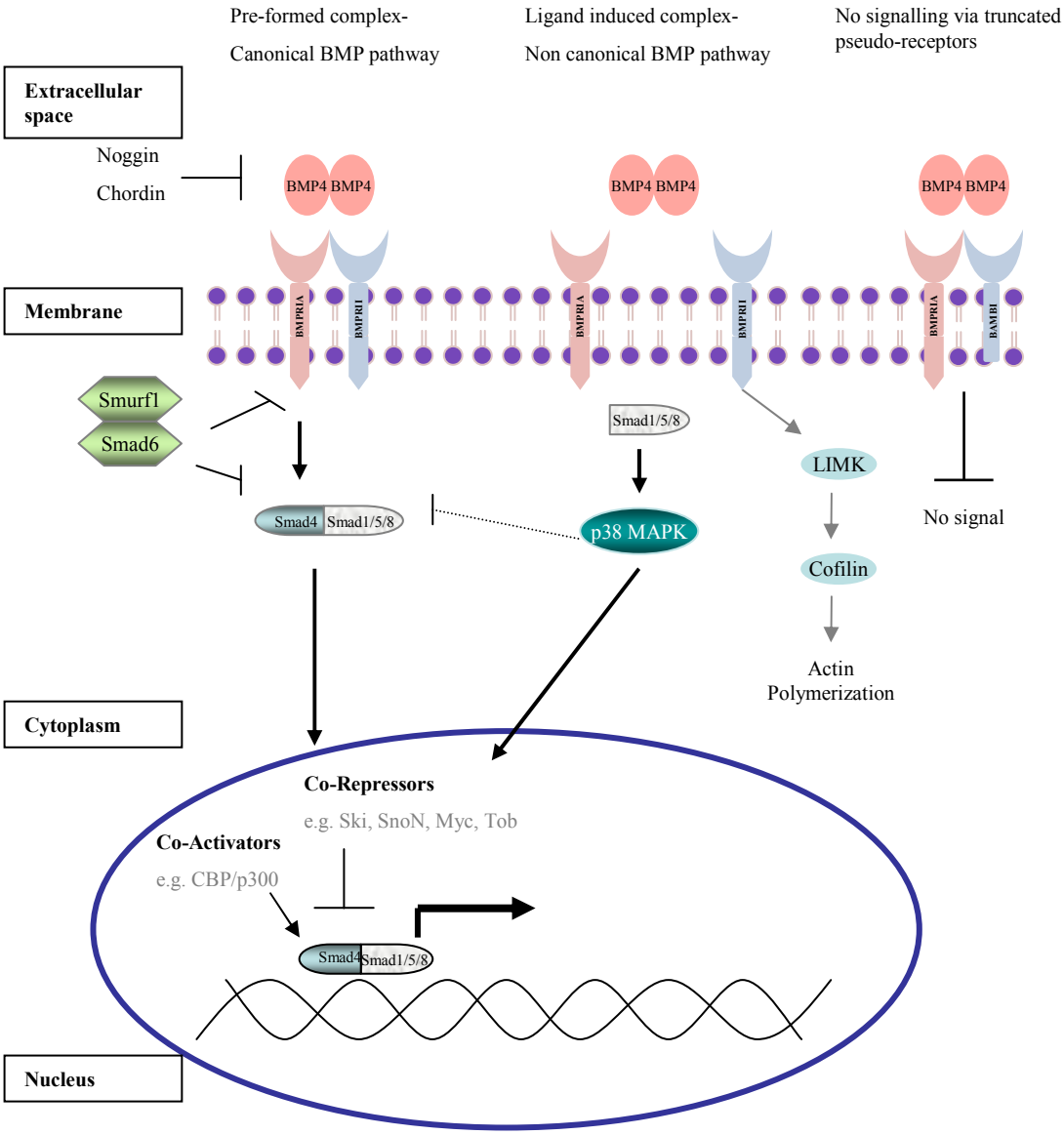

Figure 1.8: BMP signalling pathway

The BMP signalling pathway is initiated by ligand binding to either a pre-formed heterodimeric receptor complex or to a ligand induced receptor complex. Receptor smads (Smad 1, 5, 8) bind to and are activated by the phosphorylated BMPRI. During canonical signalling the activated R-Smad proteins bind to Smad 4 and translocates to the nucleus where it regulates gene transcription. MAPK signalling is activated via the ligand induced non-canonical pathway. There are numerous regulators of the pathway that reside in the extracellular, membranous, intracellular, and nuclear compartment of the cell.

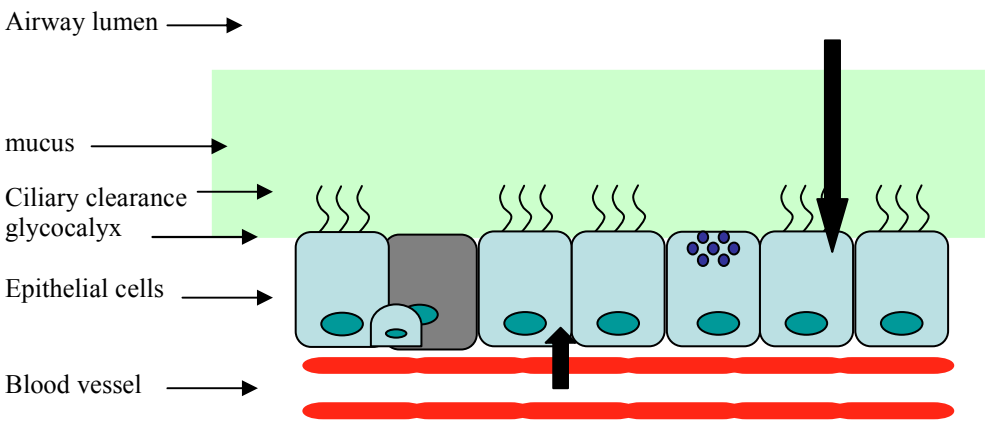

Figure 1.9: Routes of gene delivery to the airways

Intravenous or intraperitonelial administration of gene therapy vectors enter the epithelial cells in the airways via the blood vessels. Intratracheal delivery of gene therapy vectors enter the epithelial cells via the airways and must pass the mucocillary and glycocalyx layer before having the potential to enter into the epithelial cells.

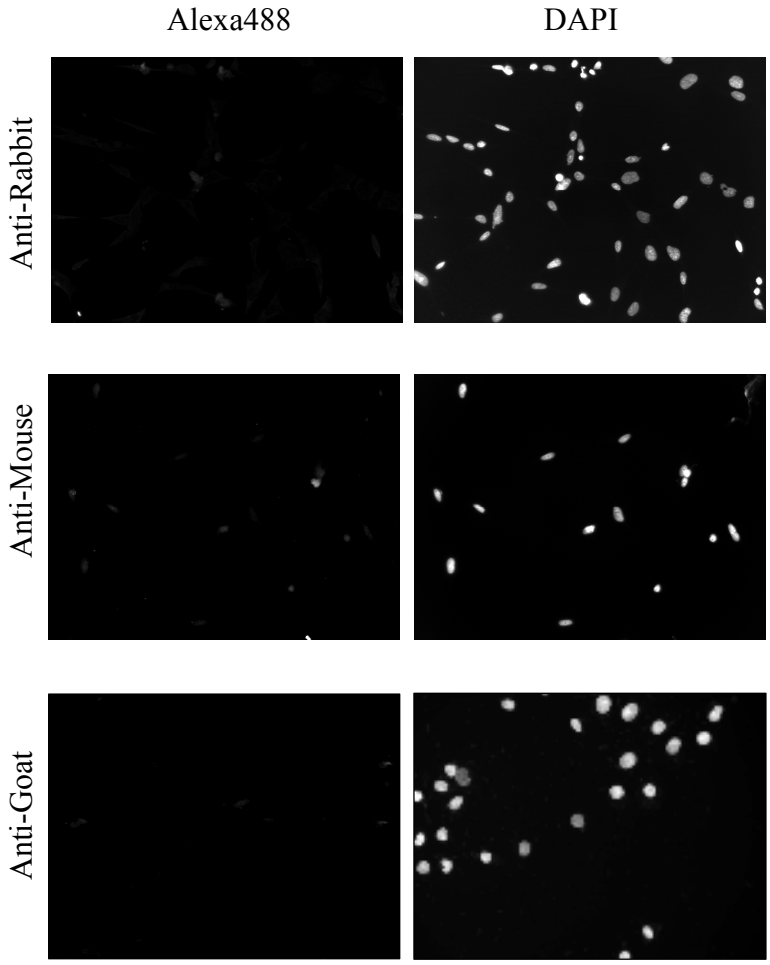

Figure 2.1: Immunofluorescent secondary controls

Representative photomicrographs show immunofluorescent secondary controls for anti-Rabbit, anti-Mouse and anti-Goat secondary antibodies conjugated with Alexa488 fluorophore. DAPI was used as a counter stain.

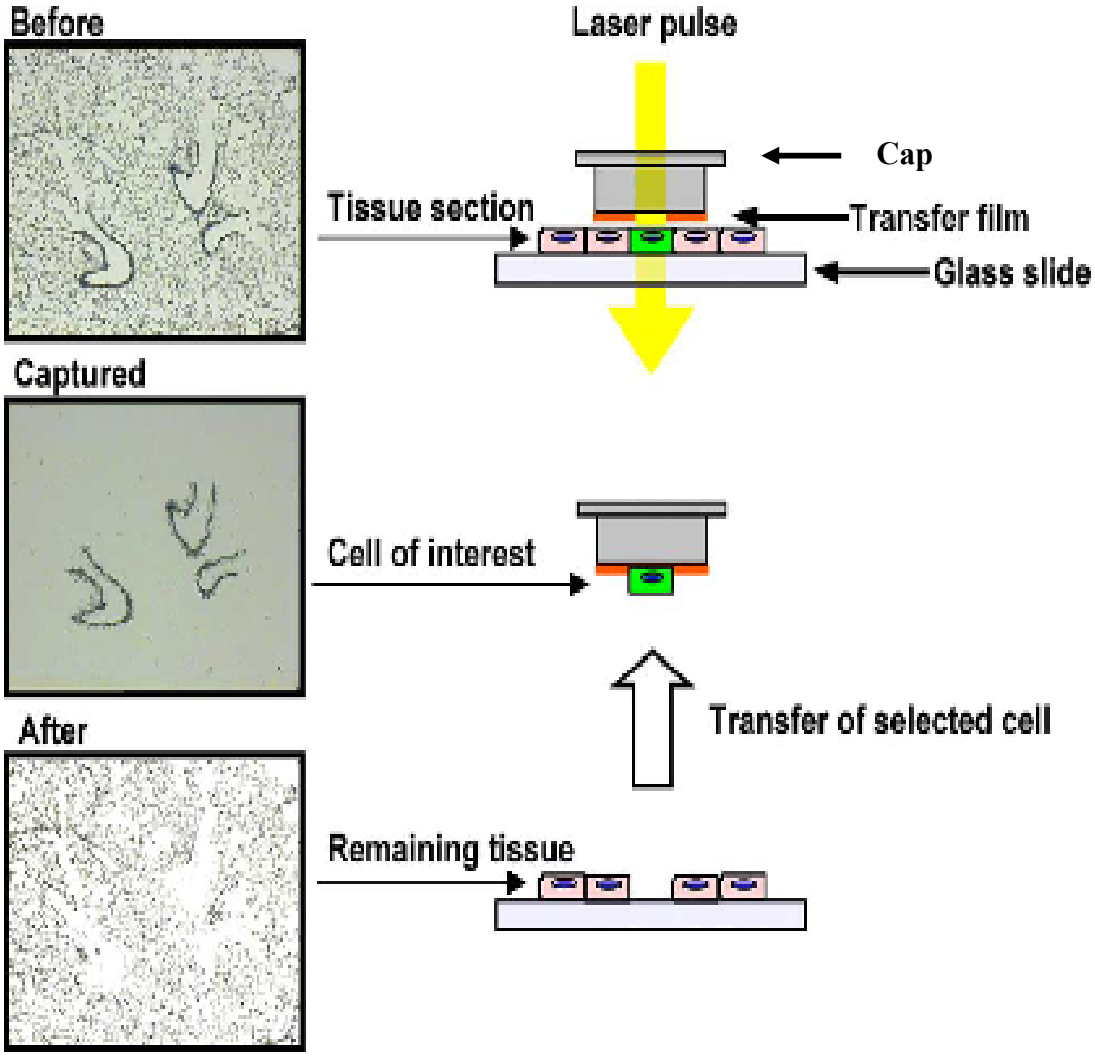

Figure 2.2: Laser capture microdissection technique

Cryosectioned tissue was sectioned onto a microscope slide and visualised under the microscope (Before). The cap, containing the transfer filament was placed over the tissue. The laser beamed down through the cap, capturing the cells of interest onto the cap for downstream isolation of RNA, DNA or protein (Captured). Uncaptured tissue remains on the microscope slide (After). Figure from Betsuyaku *et al* 2004.

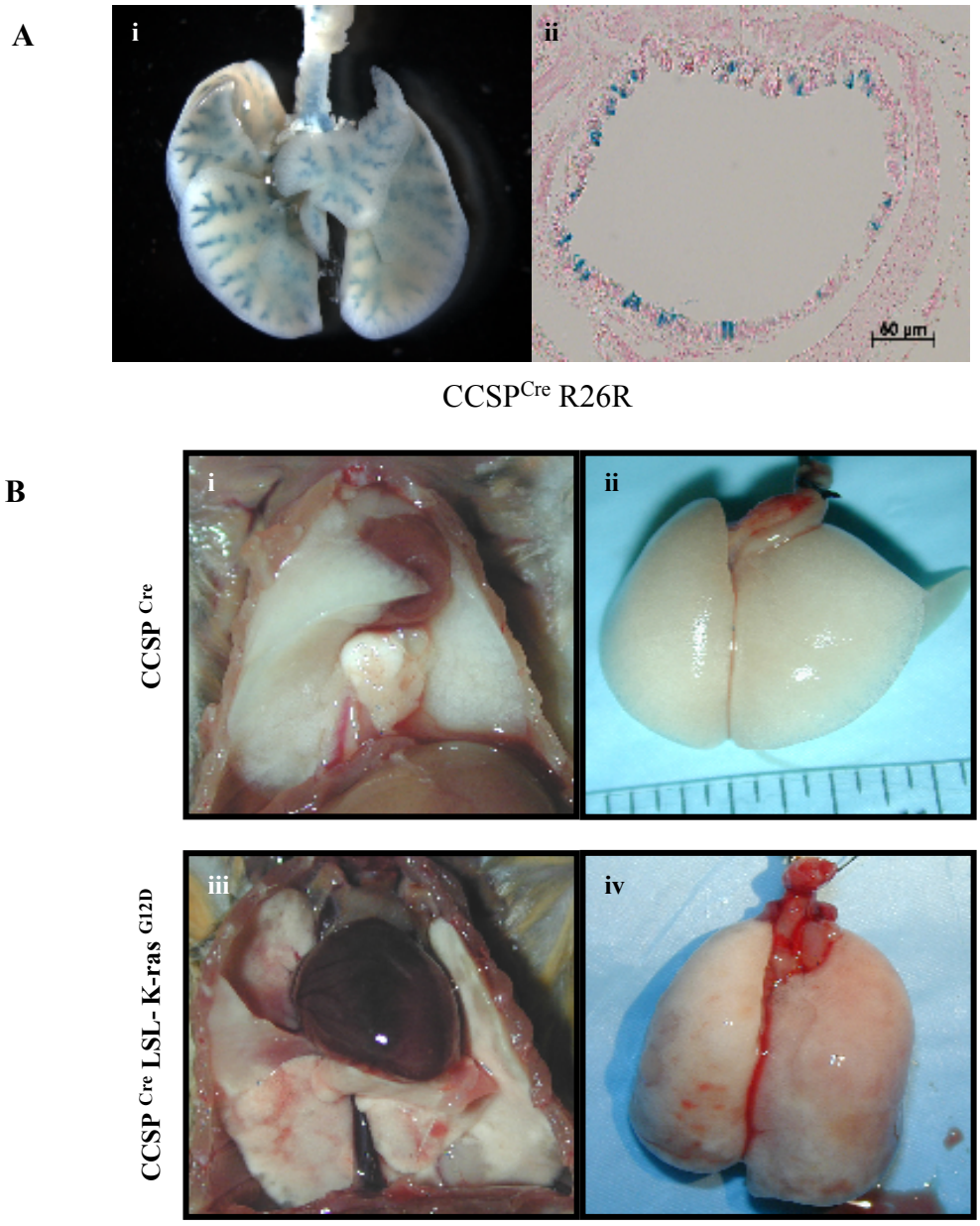

Figure 3.1: Lungs from control animals and K-ras^{G12D} lung cancer mouse model

The CCSP^{Cre} LSL-K-ras^{G12D} mouse model express the constitutively active K-ras^{G12D} gene in the Clara cells of the lungs. A) LacZ staining in the whole lung of CCSP^{Cre} R26R mice (i) lung (ii) H & E stained trachea tissue section mice act as proof of principal for the specificity of the CCSP^{Cre} promoter. B) 6 month old (i & ii) healthy control CCSP^{Cre} lungs. (iii & iv) tumour containing CCSP ^{Cre} LSL-K-ras^{G12D} lungs. (Figure A proved by Prof DeMayo)

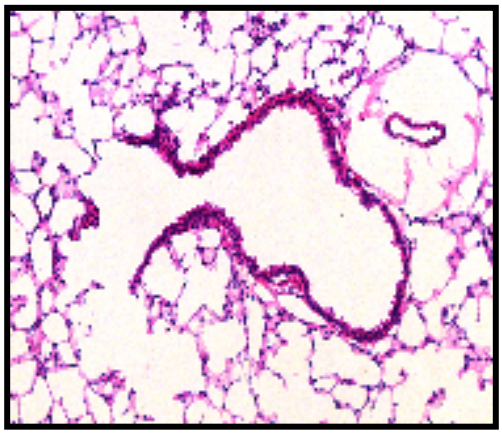

Normal Airway

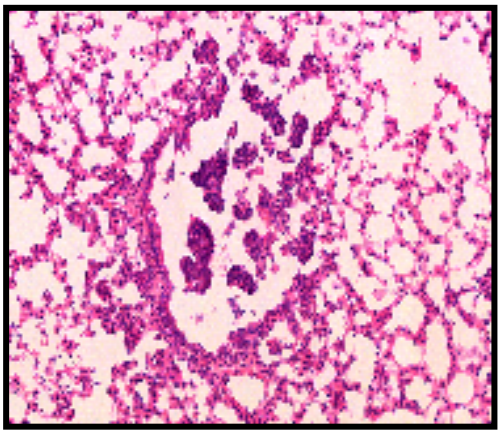

Hyperplasia

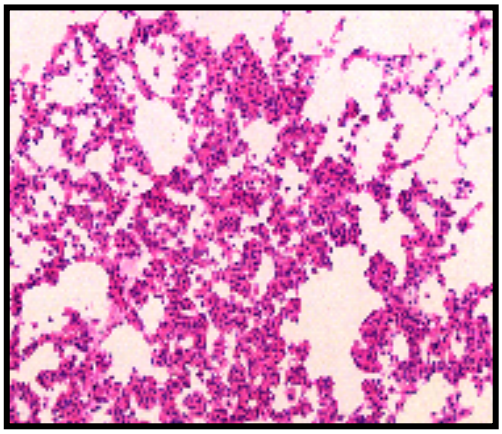

AAH
(Atypical Adenomatous Hyperplasia)

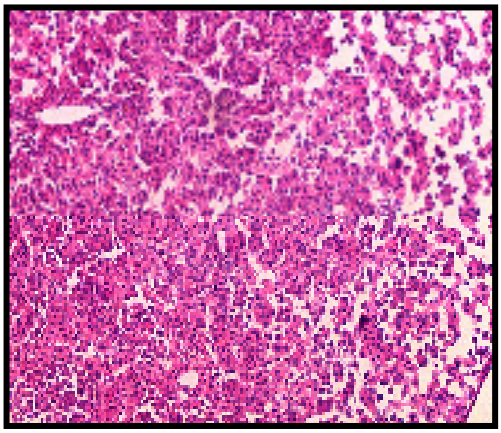

Adenoma

Figure 3.2: H & E staining of lung cancer pathologies

Haematoxylin & Eosin (H & E) staining of tissue sections cut from control mice ($CCSP^{Cre}$) resulted in normal airway architecture. H & E lung slices from $CCSP^{Cre}$ LSL-K-$ras^{G12D/}$ expressing mice showed hyperplasia within airways, AAH in alveolar regions and adenoma lung cancer pathologies in the lungs.

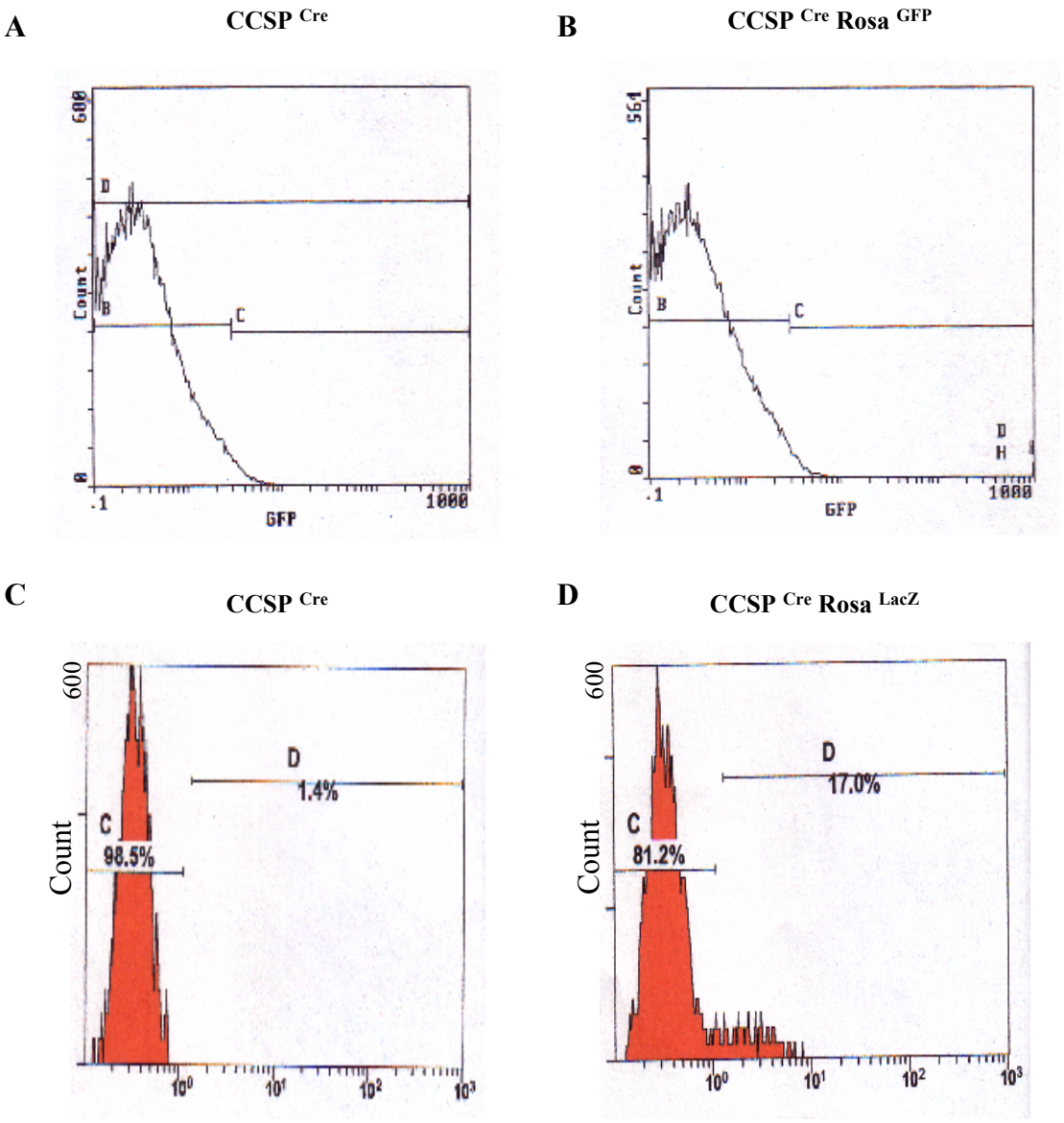

Figure 3.3: Flow cytometry identification of MAEC by reporter gene expression

MAECs were isolated from transgenic animals to identify reporter gene expression. Flow cytometry analysis was carried out to identify expression of the GFP or β-gal from transgenic mice. A) GFP (open histograms) expression from $CCSP^{Cre}$ negative control MAECs resulted in the same expression level as B) CCSP ^{Cre} $Rosa^{GFP}$ MAECs. D) LacZ (orange histogram) expression was higher in $CCSP^{Cre}$ $Rosa^{LacZ}$ MAECs compared to the C) $CCSP^{Cre}$ negative control.

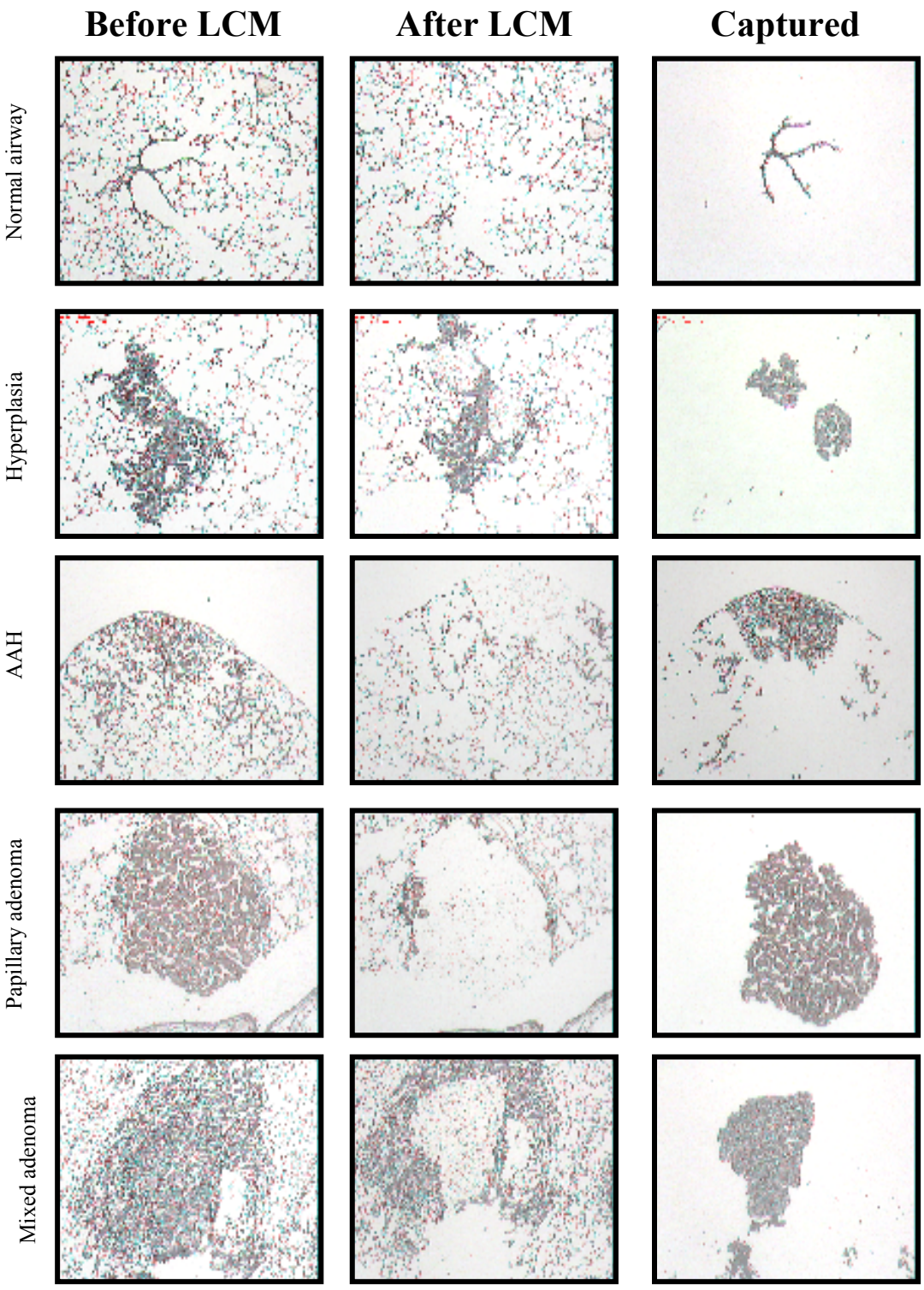
Before LCM
After LCM
Captured
Normal airway
Hyperplasia
AAH
Papillary adenoma
Mixed adenoma

Figure 3.4: Laser capture microdissection lung tissue slices

Laser capture microdissection was used to isolate purified populations of cells from normal ($CCSP^{Cre}$) and lung cancer ($CCSP^{Cre}$ LSL-K-ras^{G12D}) mice. Normal airways, hyperplasia, AAH and adenomas were captured and RNA was isolated from these purified populations of cells. Pictures were taken under 20X lens of: before LCM, after LCM, and the purified population of cells that were captured. (Cells were isolated under the supervision of Dr. Gabriella Raso)

Ear Tag	Sex	CCSP	Rosa	Age
4478	F	Cre/+	+/+	5.0
4513	F	Cre/+	+/+	7.0
4959	F	Cre/ +	+/+	6.9
4963	M	Cre/ +	+/+	6.6
4854	M	Cre/ +	+/+	6.6
5750	F	Cre/ +	+/+	5.2
6654	F	Cre/ +	+/+	4.5
6655	F	Cre/ +	+/+	4.5
4148	M	Cre/ +	+/+	8.3
6129	M	Cre/ +	+/+	4.3
4479	F	Cre/+	mt/+	5.0
4511	F	Cre/+	mt/+	7.0
4514	M	Cre/+	mt/+	7.0
4749	F	Cre/+	mt/+	7.0
5292	F	Cre/ +	mt/+	5.7
4954	F	Cre/ +	mt/+	6.6
4955	F	Cre/ +	mt/+	6.6
4752	M	Cre/ +	mt/+	7.1
5749	F	Cre/ +	mt/+	5.2
6128	M	Cre/ +	mt/+	4.0
6122	F	Cre/ +	mt/+	4.3
6432	M	Cre/ +	mt/+	5.0

(mt- mutant K-ras^{G12D} allele; + wild type allele)

Figure 3.5: List of mice taken for LCM

Lungs were harvested from control CCSP^{Cre} or CCSP^{Cre} LSL-K-ras^{G12D} (identified by ear tag number). Lungs were isolated from male and female mice that ranged in age between 4 and 8.3 months of age. Normal airway cells were taken from CCSP^{Cre} control animals. Pre-cancer lesions were taken from CCSP^{Cre} LSL-K-ras^{G12D} animals. (Animal colonies were cared for by SungNam Cho)

A

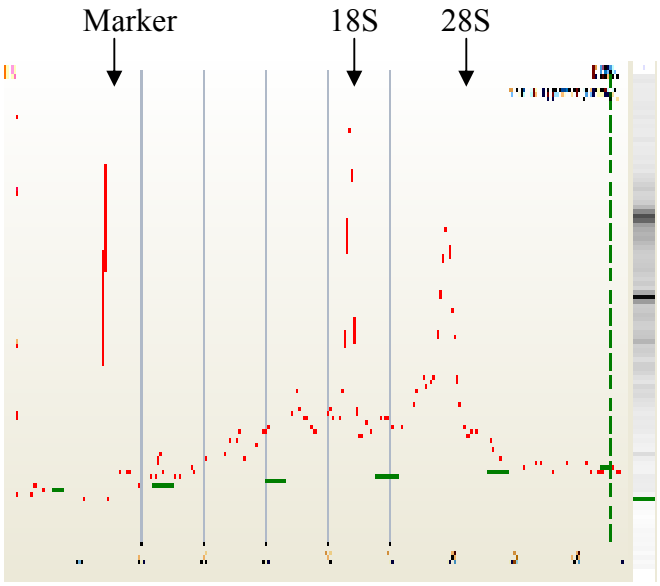

RNA quality assurance

B

Tissue type	Sex	Age	ng/ul	Cell no.
normal	F	5	3.43	879
	M	6.6	1.47	1493
	F	4.58	0.1	1555
hyperplasia	F	5	2.87	863
	F	5.7	9.55	1541
	F	4.3	0.6	1889
AAH	M	7.1	1.85	556
	F	7	3.16	632
papillary	F	5.2	1.25	1067
	M	5	1.99	1394
	F	6.6	2.5	1166
solid	M	4.81	5.58	2194

RNA samples taken for microarray analysis

Figure 3.6: RNA analysis for quality control

RNA isolated from laser captured cells was analysed to ensure high quality and sufficient quantity for Affymetrix microarray analysis. This analysis was carried out by the RNA core at Baylor College of Medicine. A) Agilent bioanalyzer was used to ensure the RNA was of high quality. The graph and gel represent peaks/bands of 18S and 28S ribosomal RNA. B) Tabulated information on samples utilised in microarray analysis, including tissue type, animal sex and age, concentration of RNA samples and approximate number of cells isolated by laser capture.

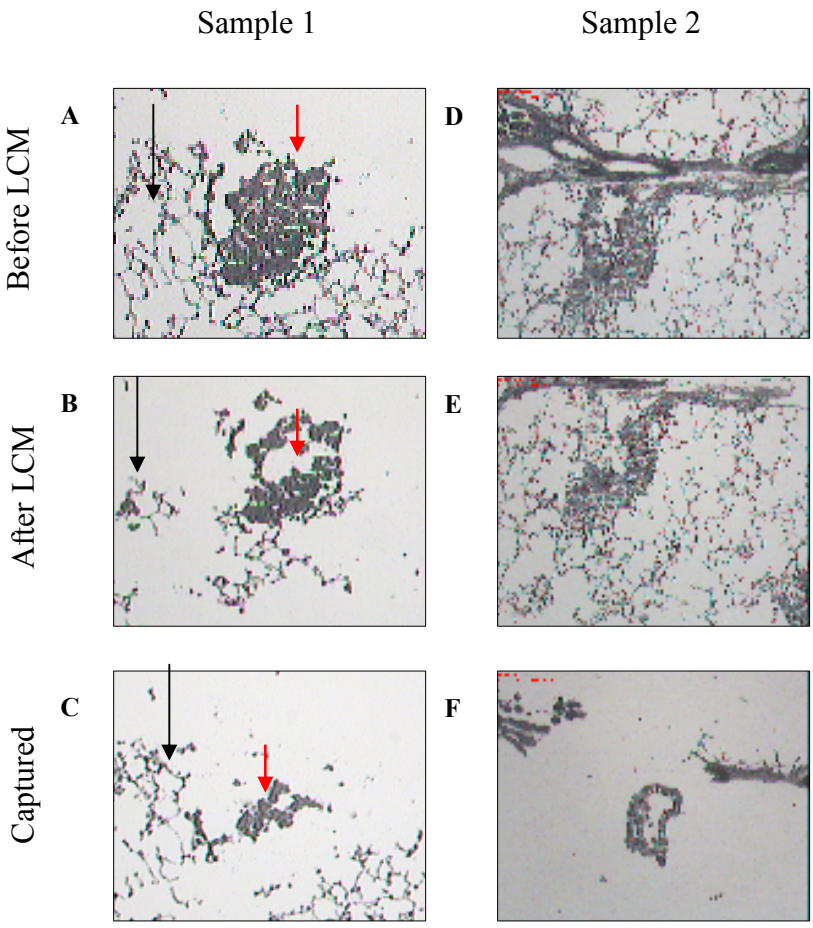

Figure 3.7: Contamination of uncaptured cells on the LCM cap

Photomicrographs were taken before laser capturing (A & D), after laser capturing (B & E) and the tissue captured (C & F). Two LCM samples (A, B,C or D, E, F) represents one technical difficulty of contamination of non-specific regions of lung tissue on the LCM cap due to the delicate architecture of the alveolar region. Photomicrographs were taken at 10x magnification. Red arrows indicate cells that were captured, black arrows indicate alveolar contamination.

Tissue	Age (months)	ng/ul	260/280	260/230
scrape	5	18.4	1.84	0.1
scrape	5	17.18	2.17	0.86
scrape	7	4.36	1.65	0.04
scrape	6.6	1.86	2.81	0.42
scrape	5.2	8.05	1.89	1.21
scrape	7.1	3.78	1.74	0.72

Figure 3.8: RNA positive control for LCM procedure

Tabulated information on RNA isolated from scrape control tissue, including animal age, RNA quantity (ng/ul) and RNA quality (Abs 260/280 and Abs 260/280). Scraped tissue was a control for cyrosectioning, haemotoxylin staining and dehydration to ensure this processing did not have adverse affects on RNA quantity and quality.

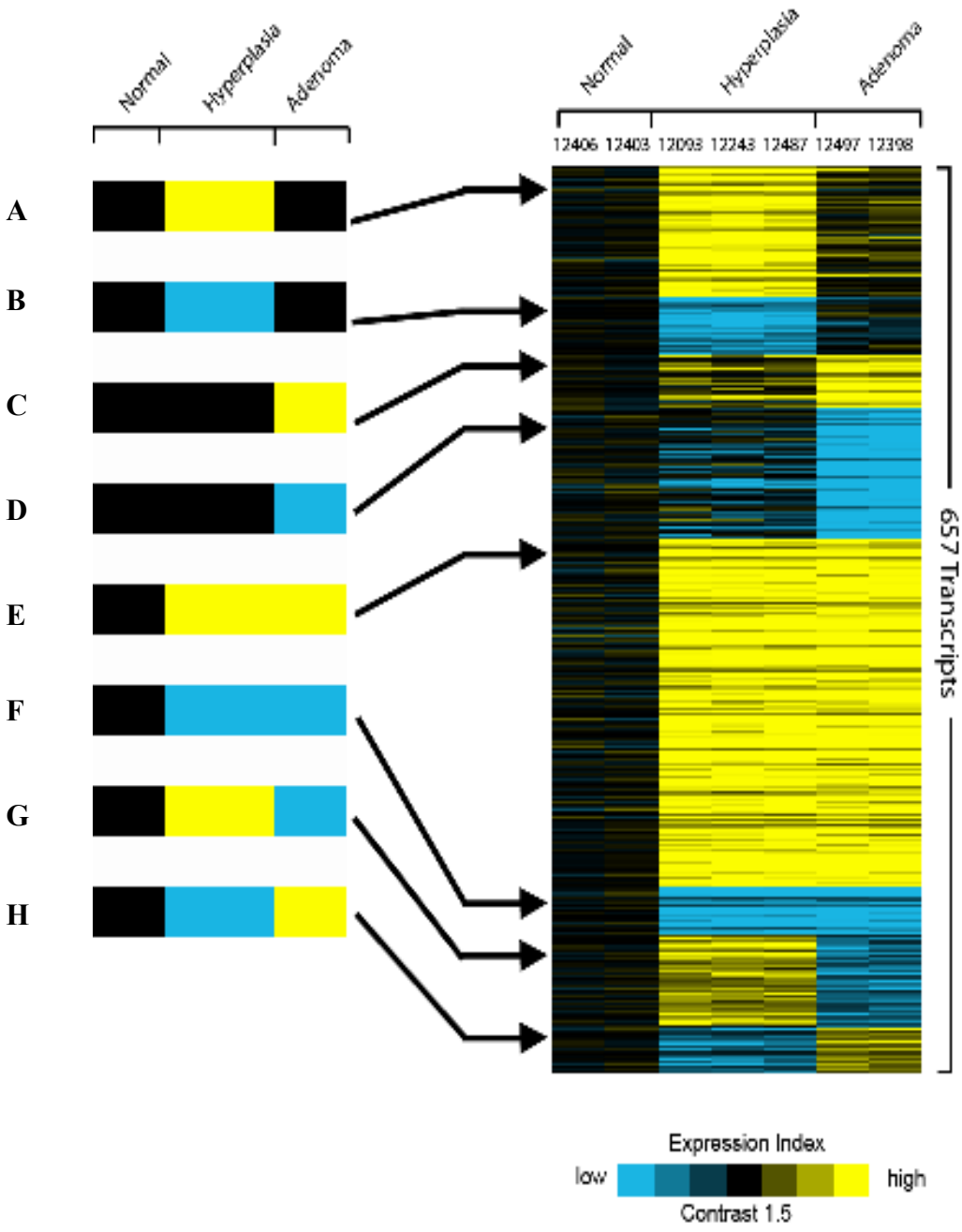

Figure 3.9: Heat map of microarray differential gene expression from the microarray analysis

Supervised clustering of genes differing by $p < 0.01$ (ANOVA) of normal, hyperplasia and adenoma samples. In this supervised clustering normal airway gene expression was normalized to a value of 1 and differential gene expression in the hyperplasia and adenoma were up or down regulated relative to the normal expression. Yellow represents high gene expression and blue denotes low gene expression. (Heat map carried out by Dr. Craig Creighton)

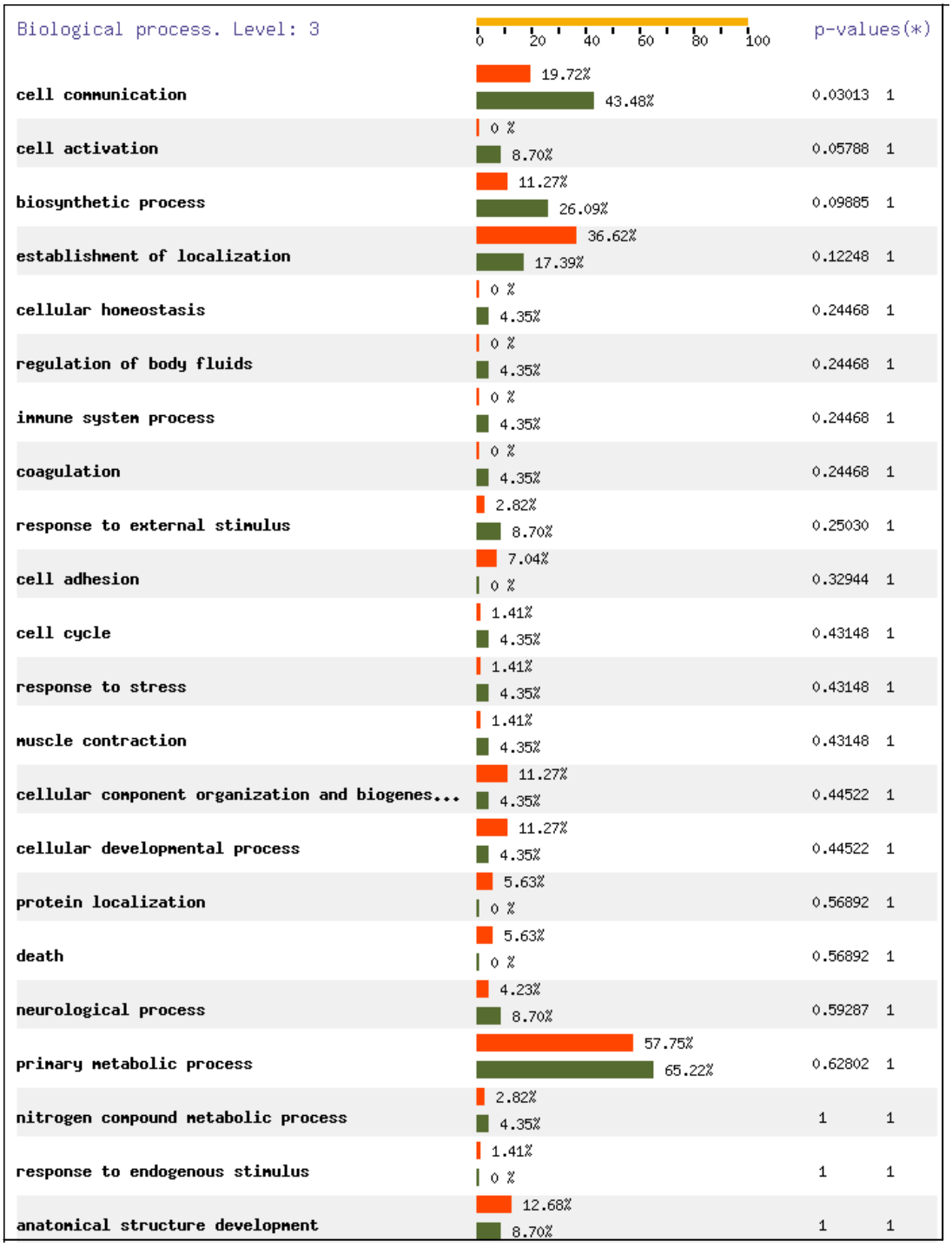

Figure 3.10- continued on next page

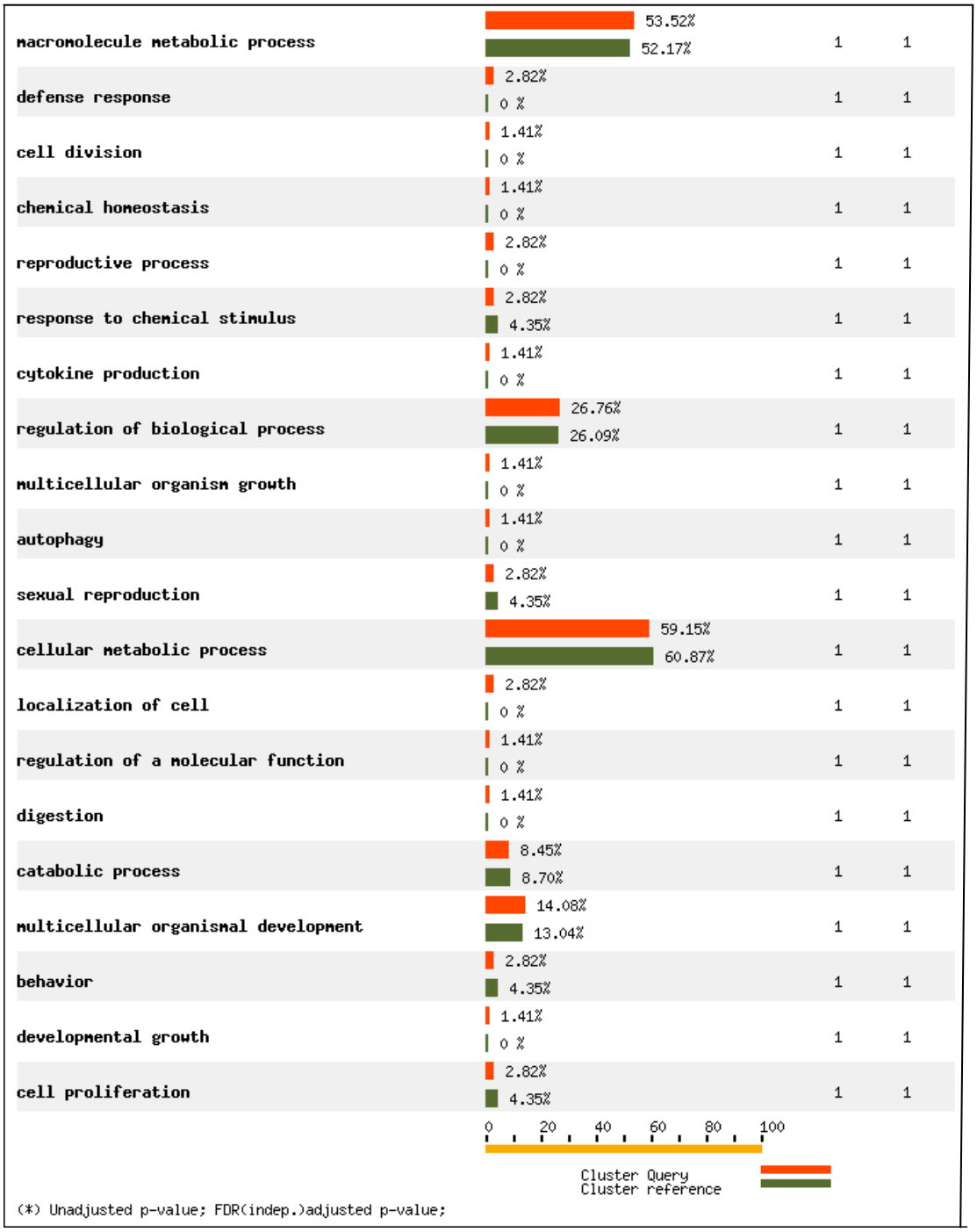

Figure 3.10: Hyperplasia up regulated genes compared to adenoma up regulated genes: Biological process, Level 3

The differential gene expression list of those gene up regulated in hyperplasia were compared to genes up regulated in adenoma samples. Functional gene analysis was carried out using FatiGO+ programme. Genes were analysed within biological function criteria. Red bars represent genes altered in hyperplasia, green bars represent genes altered in adenoma.

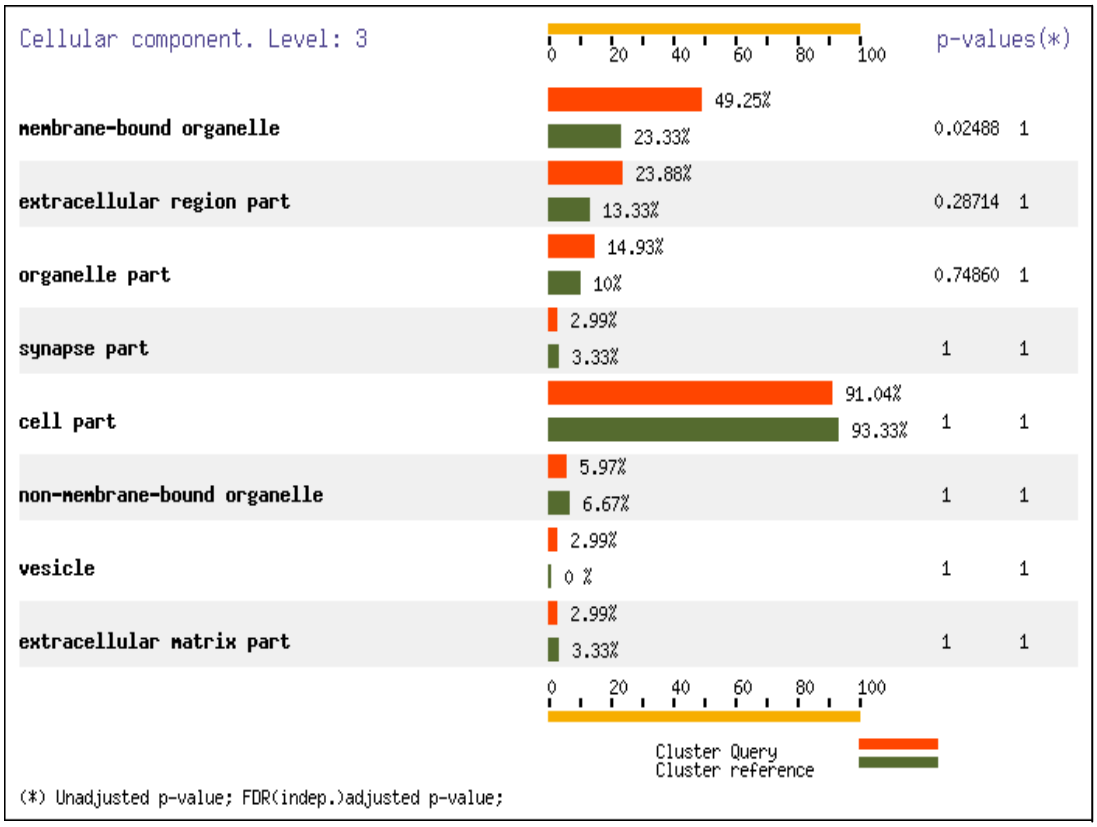

Figure 3.11: Hyperplasia up regulated genes compared to adenoma up regulated genes: Cellular component, Level 3

The differential gene expression list of those gene up regulated in hyperplasia were compared to genes up regulated in adenoma samples. Functional gene analysis was carried out using FatiGO+ programme. Genes were analysed within cellular component criteria. Red bars represent genes altered in hyperplasia, green bar represents genes altered in adenoma.

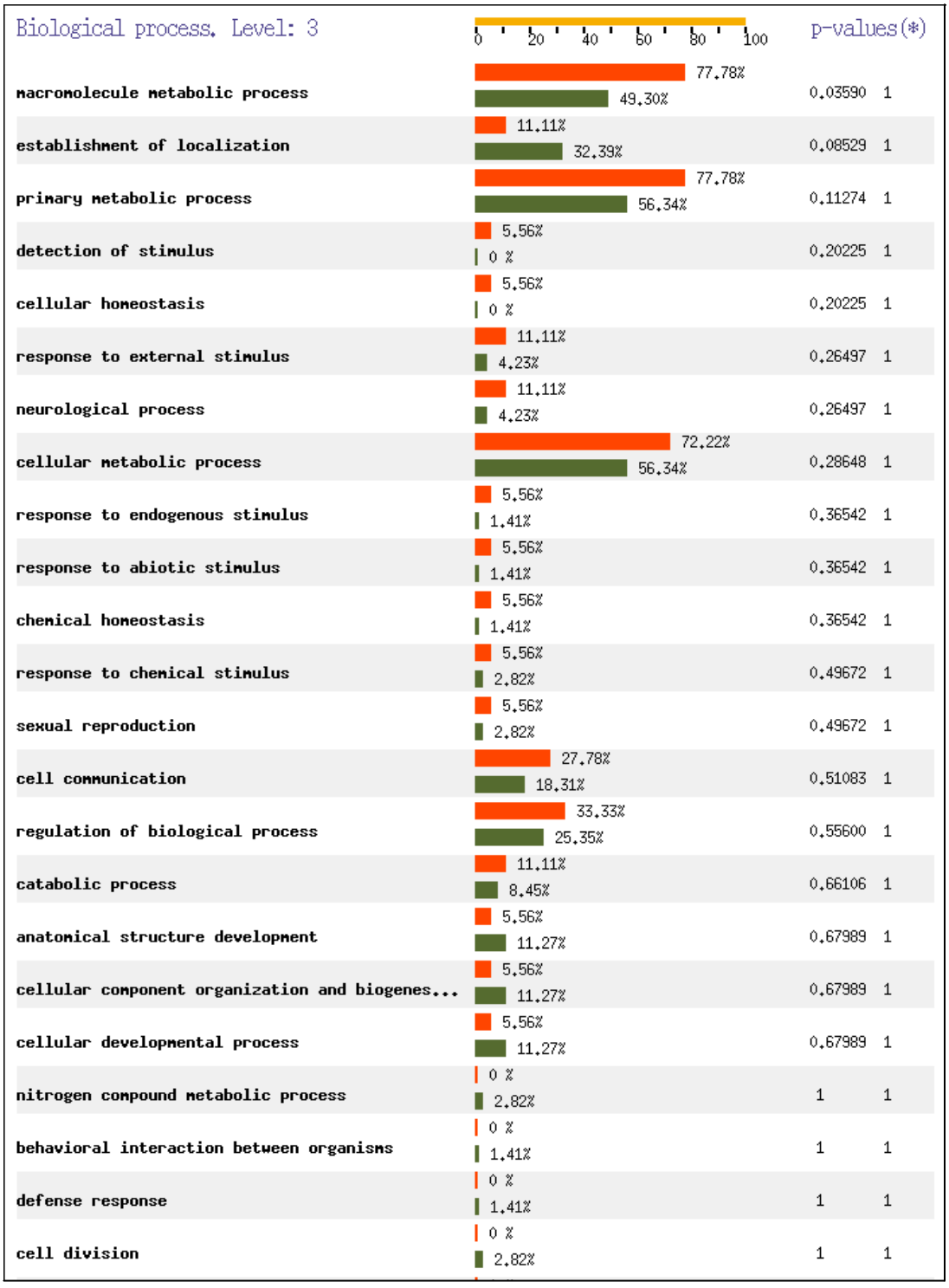

Figure 3.12 –continued on next page

Figure 3.12: Hyperplasia down regulated genes compared to adenoma down regulated genes: Biological process, Level 3

Comparative analysis was carried out on genes down regulated in hyperplasia and down regulated in adenoma, using FatiGO+ programme. Genes were analysed within biological function criteria. Red bars represent the percentage of genes altered in hyperplasia, green bars represent genes altered in adenoma.

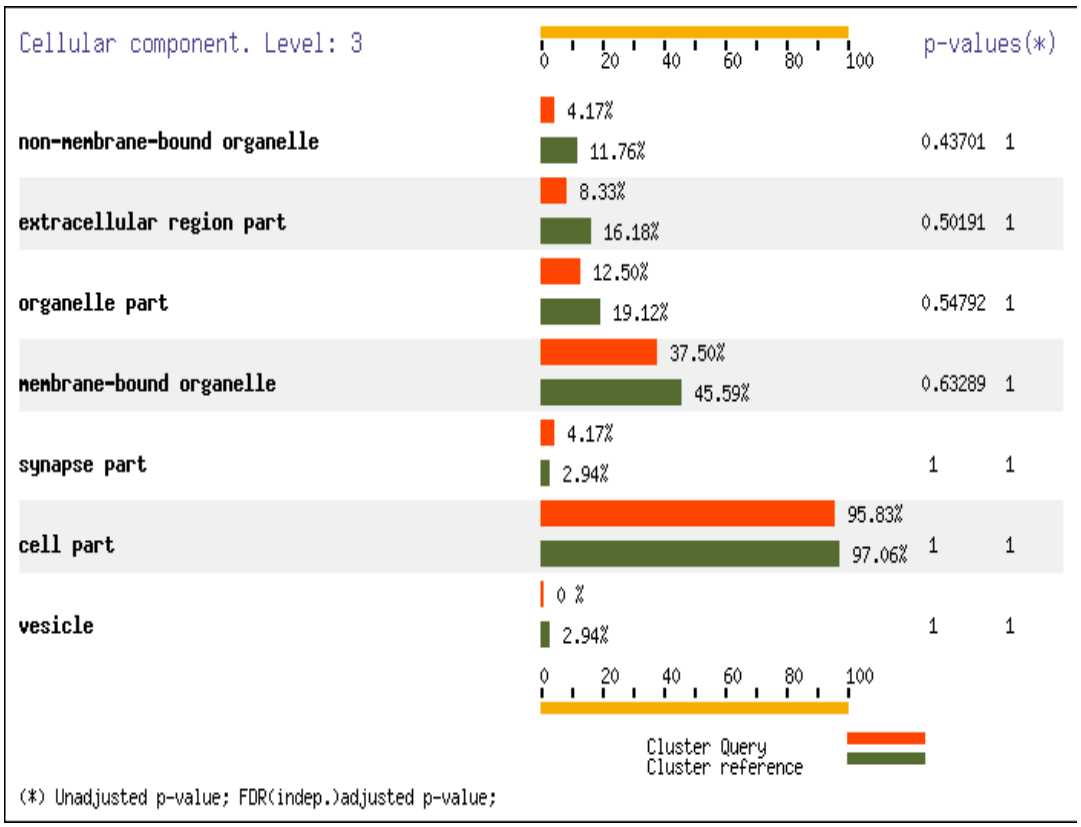

Figure 3.13: Hyperplasia down regulated genes compared to adenoma down regulated genes: Cellular component, Level 3

The differential gene expression list of those gene down regulated in hyperplasia were compared to genes down regulated in adenoma samples. Functional gene analysis was carried out using FatiGO+ programme. Genes were anaylsed within cellular component criteria. Red bars represent genes altered in hyperplasia, green bars represent genes altered in adenoma.

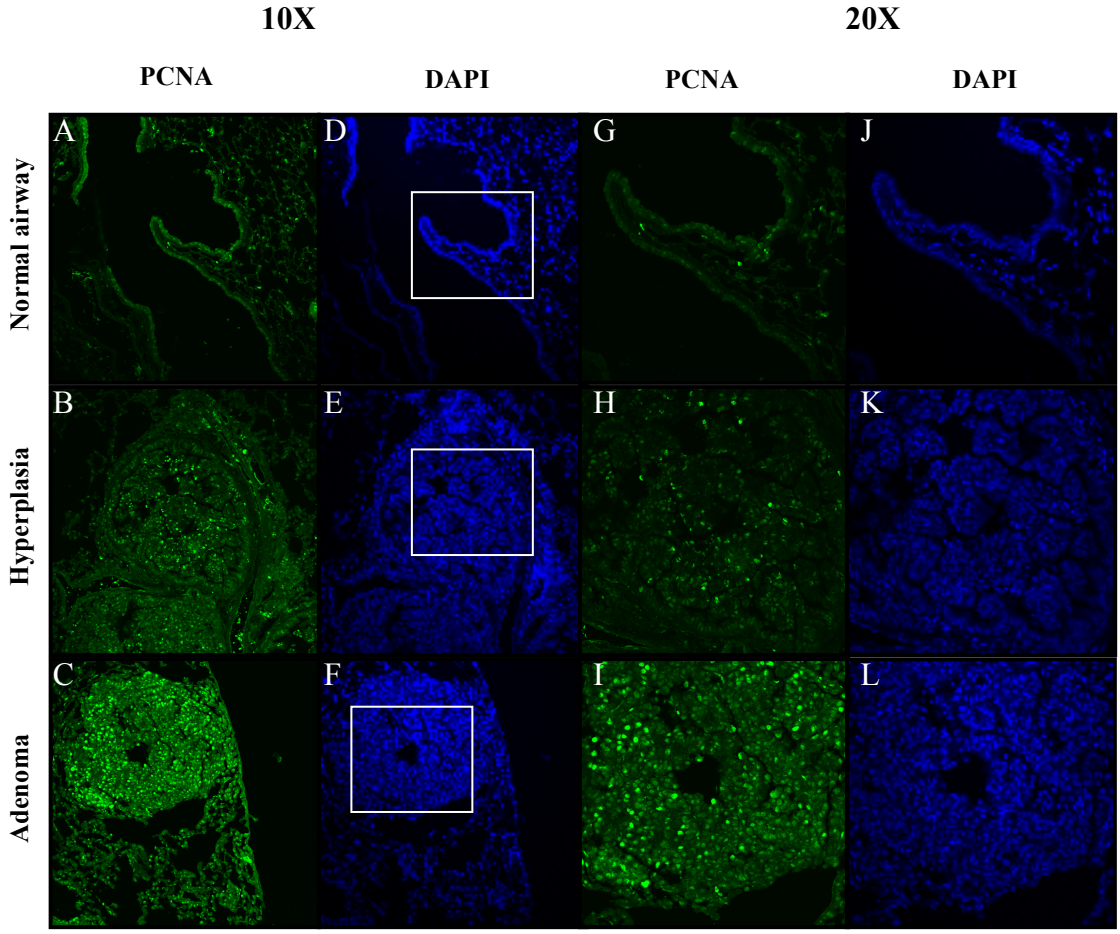

Figure 3.14: PCNA staining in normal, hyperplasia and adenoma cells

PCNA immunofluorescence was carried out on normal airway from control mice, and hyperplasia and adenoma lesions from K-ras^{G12D} expressing mice. The white boxes within 10x magnification indicate the regions zoomed in under 20x magnification. A, D, G, J normal airway, B, E, H, K hyperplasia region, C, F, I, L adenoma region. A, B, C 10 magnification of PCNA staining. D, E, F 10x magnification of DAPI nuclear counter stain. G, H, I 20x magnification of PCNA expression. J, K, L 20x magnification of DAPI nuclear counter stain. Images were taken on a confocal fluorescent microscope.

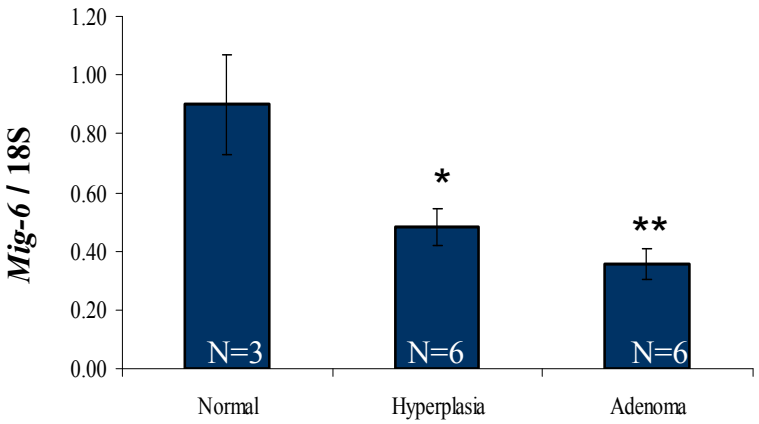

Figure 3.15: Down regulation of *Mig-6* in hyperplasia and adenoma samples

Real time PCR analysis of *Mig-6* expression was carried out on RNA isolated from laser captured normal, hyperplasia and adenoma samples. *Mig-6* expression was normalised to 18S expression in each sample and the fold expression graphed. N is the number of animals examined. * $p < 0.05$, ** $p < 0.01$

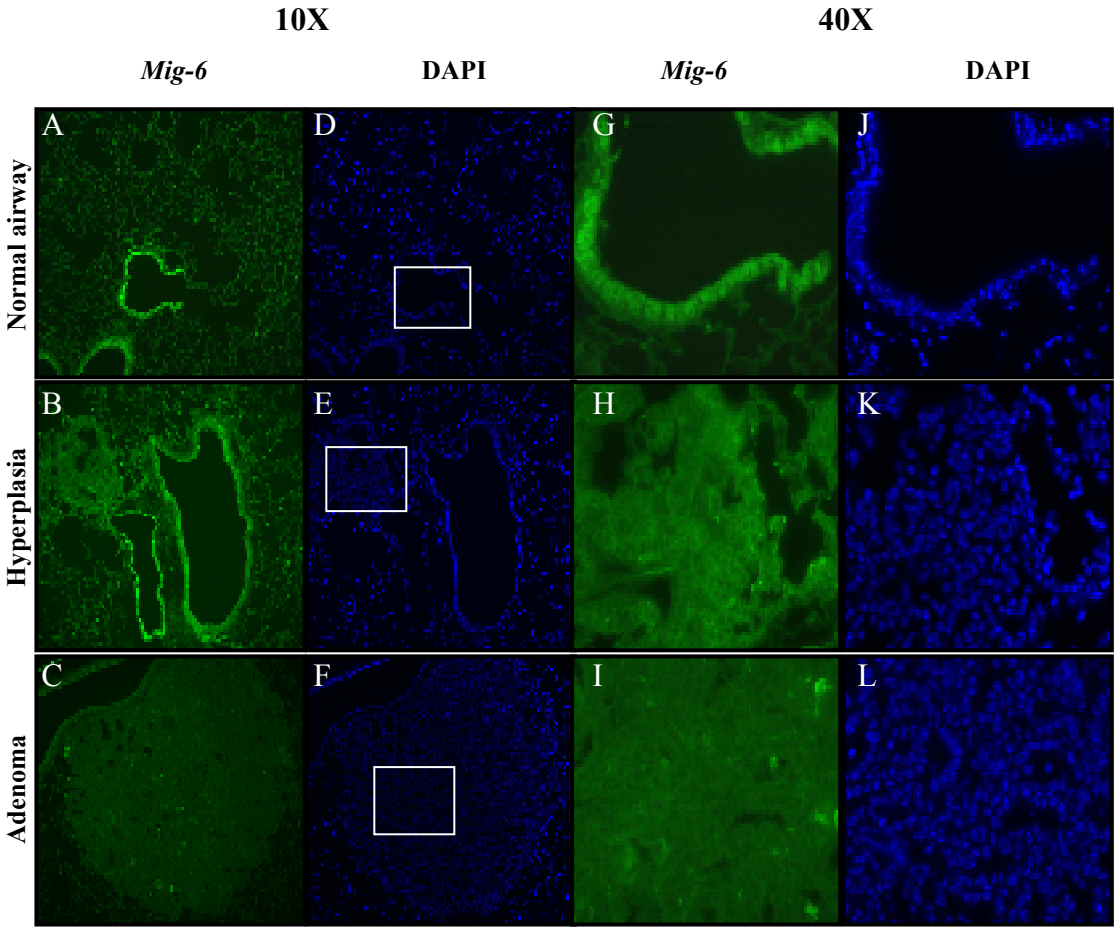

Figure 3.16: *Mig-6* staining in normal, hyperplasia and adenoma cells

Mig-6 immunofluorescence was carried out on normal airways from control mice and hyperplasia and adenoma lesions from K-ras^{G12D} expressing mice. The white boxes within 10x magnification indicate the regions zoomed in under 40x magnification. A, D, G, J normal airway, B, E, H, K hyperplasia region, C, F, I, L adenoma region. A, B, C 10x magnification of *Mig-6* staining. D, E, F 10x magnification of DAPI nuclear counter stain G, H, I 40x magnification of *Mig-6* expression. J, K, L 40x magnification of DAPI nuclear counter stain. Images were taken on a fluorescent microscope.

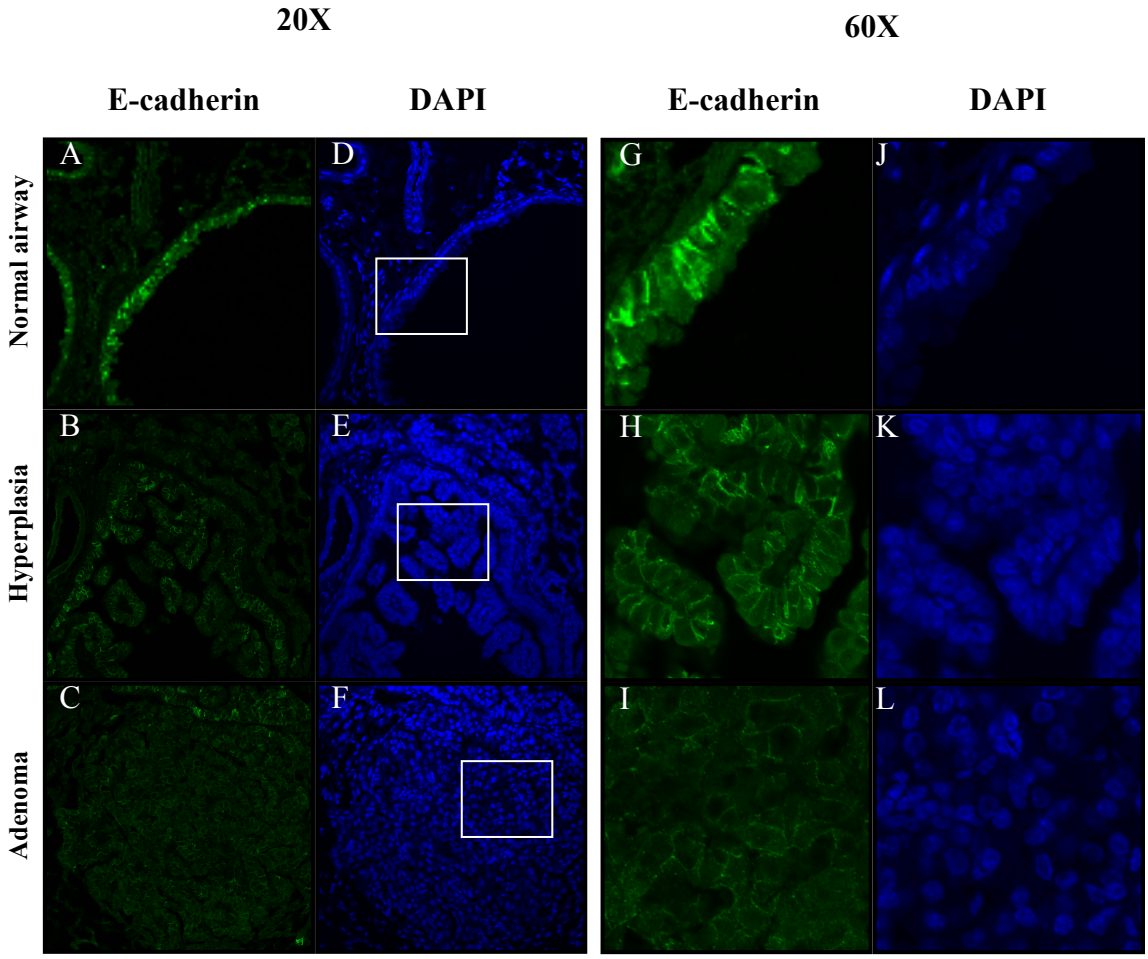

Figure 3.17: E-cadherin expression in early lung tumours

E-cadherin protein expression was examined by immunofluorescence in normal, hyperplasia and adenoma samples. The white boxes within 20x magnification indicate the regions zoomed in under 60x magnification. A, D, G, J normal airway, B, E, H, K hyperplasia region, C, F, I, L adenoma region. A, B, C 20x magnification of E-cadherin staining. D, E, F 20x magnification of DAPI nuclear counter stain G, H, I 60x magnification of E-cadherin expression. J, K, L 60x magnification of DAPI nuclear counter stain. Images were taken on a confocal fluorescent microscope.

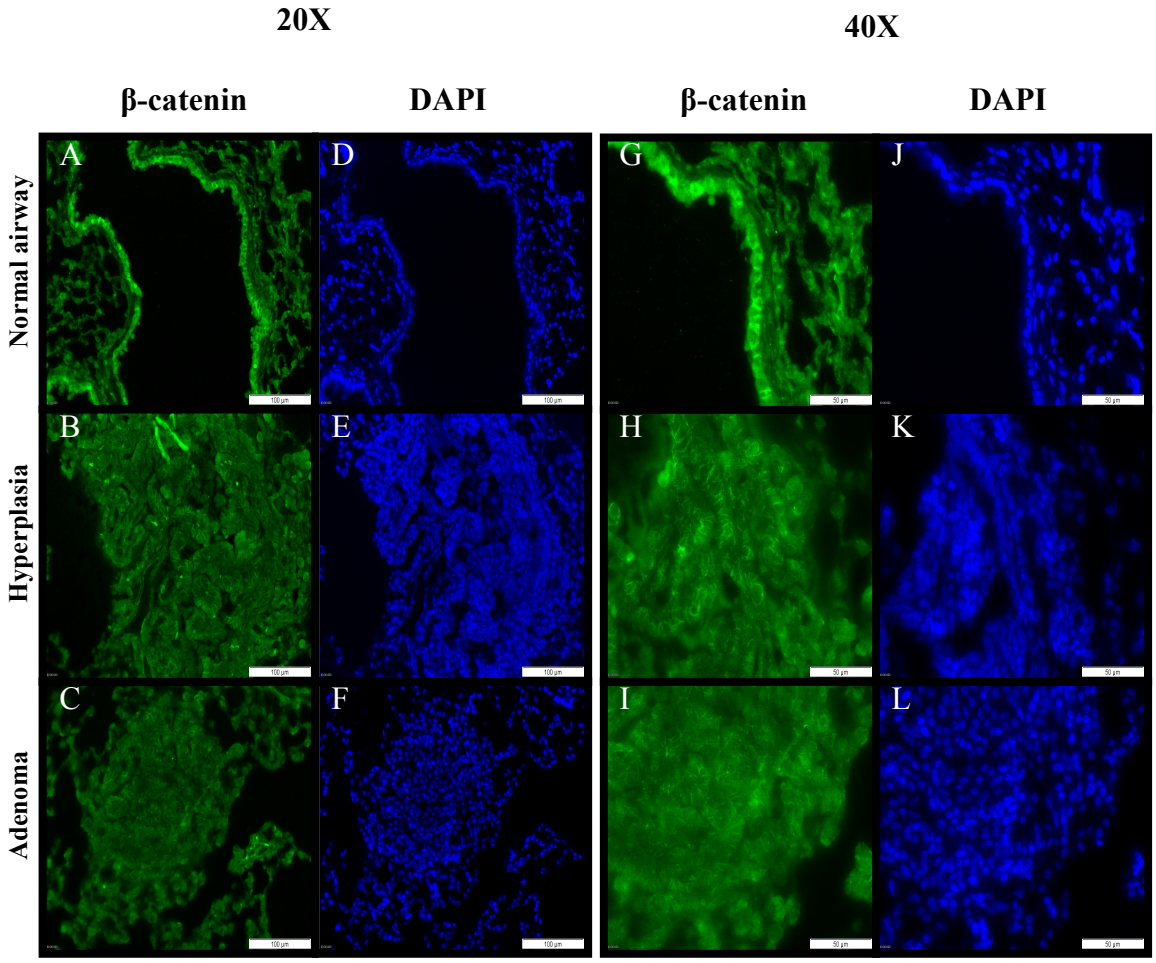

Figure 3.18: β-catenin in hyperplasia and adenoma cells

β-catenin protein expression was examined by immunofluorescence in normal, hyperplasia and adenoma samples. The white boxes within 20x magnification indicate the regions zoomed in under 40x magnification. A, D, G, J normal airway, B, E, H, K hyperplasia region, C, F, I, L adenoma region. A, B, C 20x magnification of β-catenin staining. D, E, F 20x magnification of DAPI nuclear counter stain G, H, I 40x magnification of β-catenin expression. J, K, L 40x magnification of DAPI nuclear counter stain. Images were taken on a fluorescent microscope.

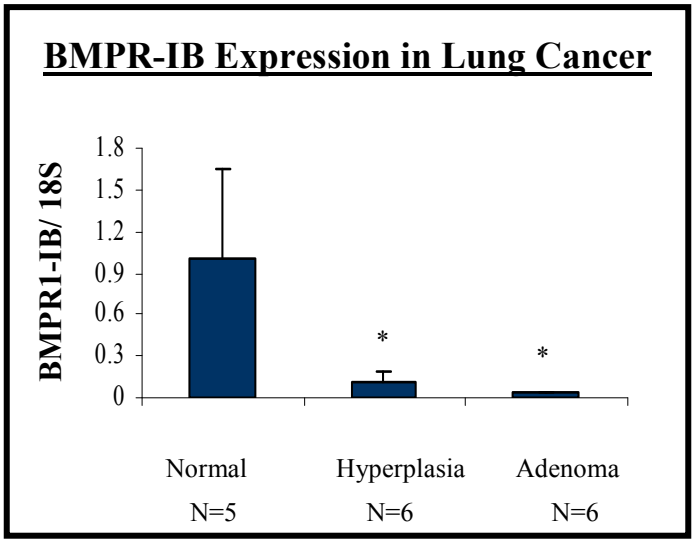

Figure 3.19: Down regulation of BMPR-IB expression in early lung cancer

Real time PCR analysis for BMPR-IB expression was carried out on RNA isolated from normal, hyperplasia and adenoma samples. BMPR-IB expression was normalised to 18S expression for each samples. N is the number of samples analysed. * $p < 0.05$.

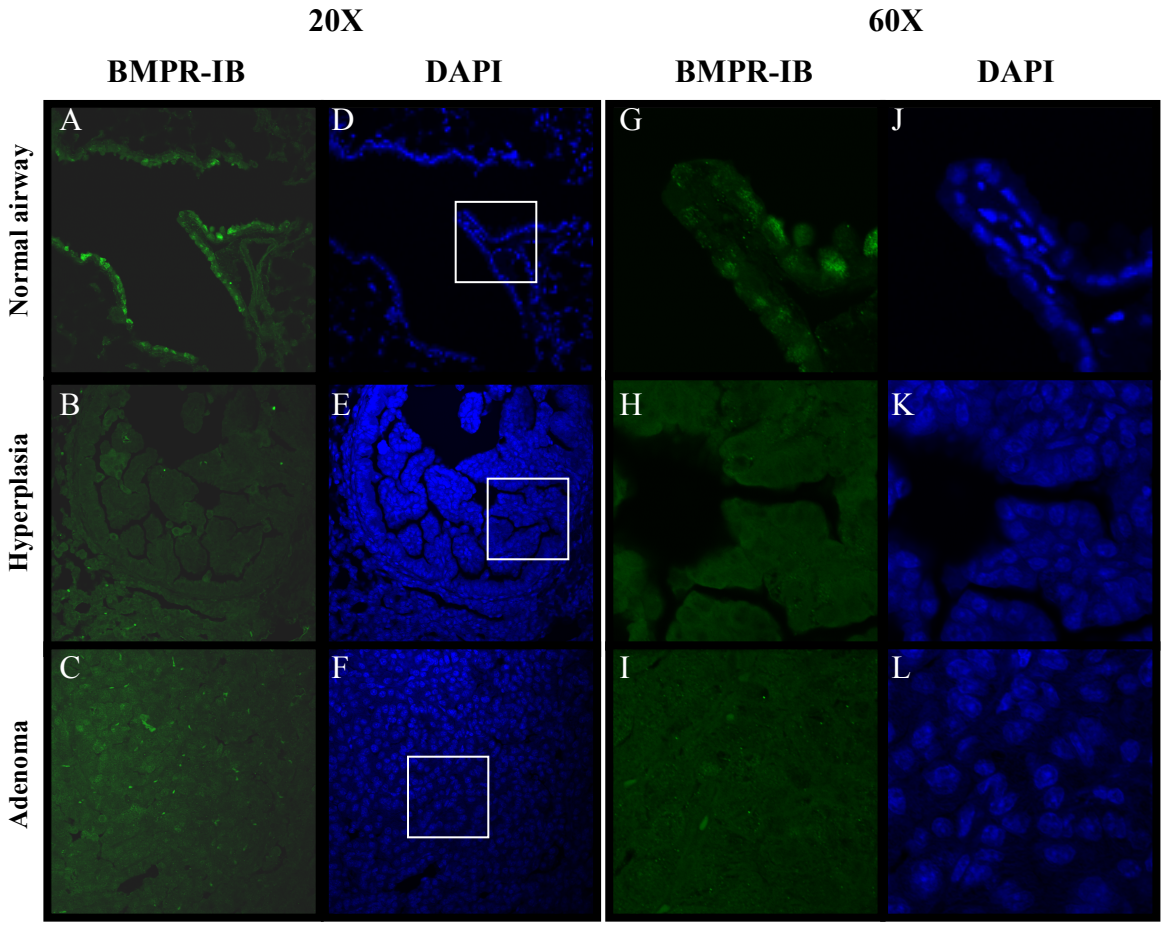

Figure 3.20: Loss of BMPR-IB in hyperplasia and adenoma

BMPRI-B protein expression was examined by immunofluorescence in normal, hyperplasia and adenoma samples. The white boxes within 20x magnification indicate the regions zoomed in under 60x magnification. A, D, G, J normal airway, B, E, H, K hyperplasia region, C, F, I, L adenoma region. A, B, C 20x magnification of BMPR-IB staining. D, E, F 20x magnification of DAPI nuclear counter stain G, H, I 60x magnification of BMPR-IB expression. J, K, L 60x magnification of DAPI nuclear counter stain. Images were taken on a confocal fluorescent microscope.

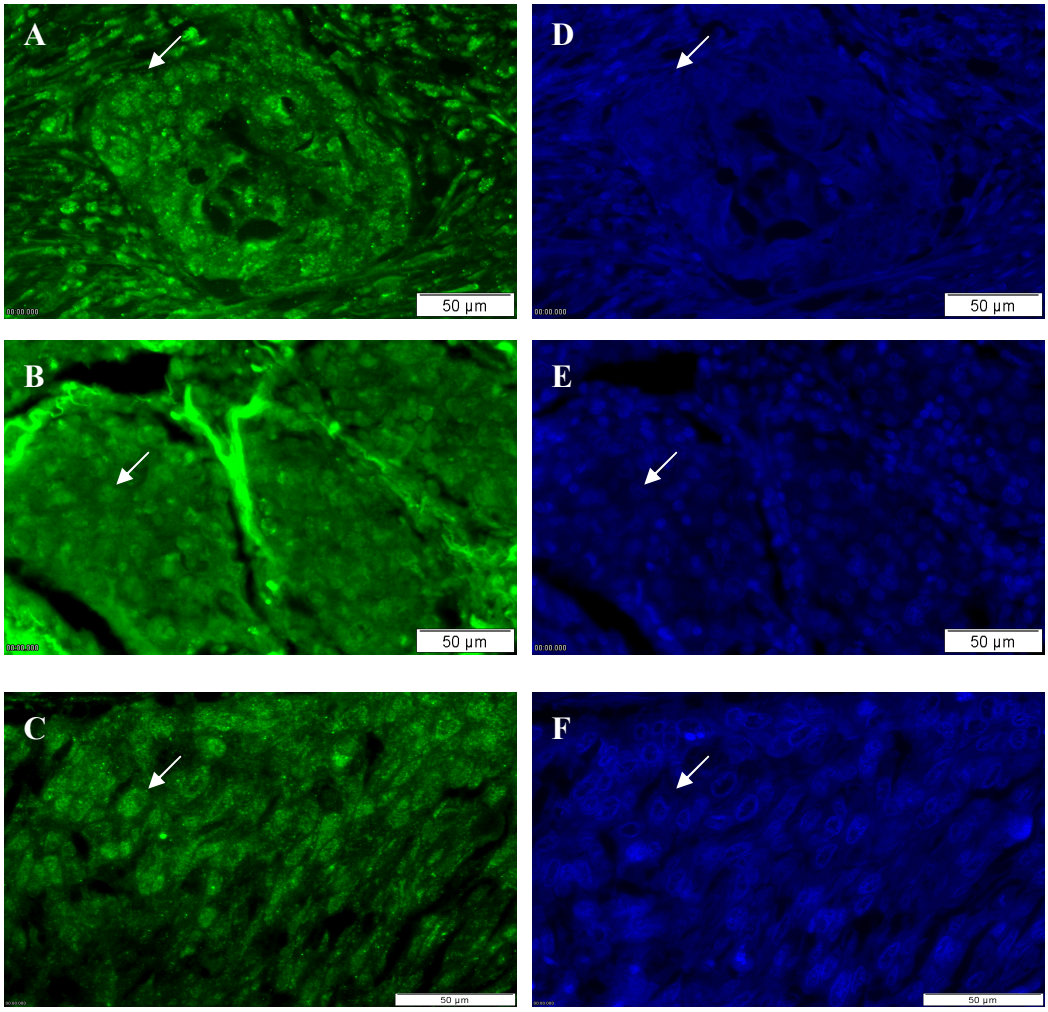

Figure 3.21: BMPR-IB expression in human adenocarcinoma tissue

BMPR-IB protein expression was analysed by immunofluorescence. Human adenocarcinoma tissue samples revealed BMPR-IB expression in the nuclei of the cells. A, B,C 40x photomicrographs of BMPR-IB staining. D, E, F 40x photomicrographs of DAPI counter nuclear staining. Arrows indicate an example of BMPR-IB in the nuclei cells.

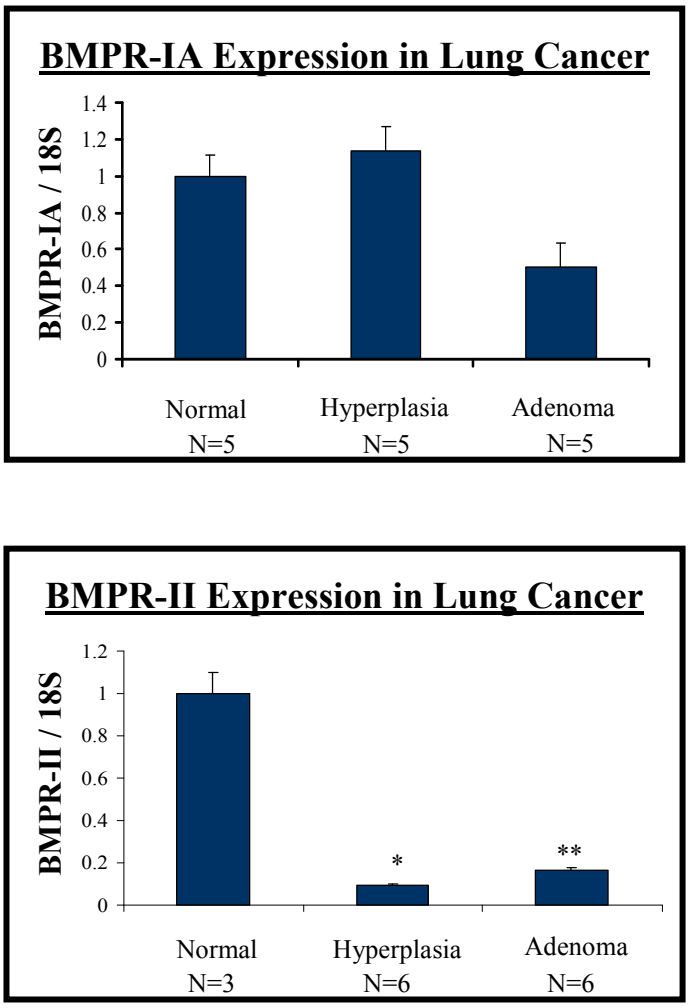

Figure 3.22: BMPR-IA and BMPR-II expression in early lung cancer

Real time PCR analysis was carried out on RNA isolated from LCM normal, hyperplasia and adenoma samples to analysed the expression of BMPR-IA and BMPR-II. BMPR-IA and BMPR-II expression were normalised to 18S expression for each samples. N is the number of samples analysed. * $p< 0.05$, ** $p< 0.01$.

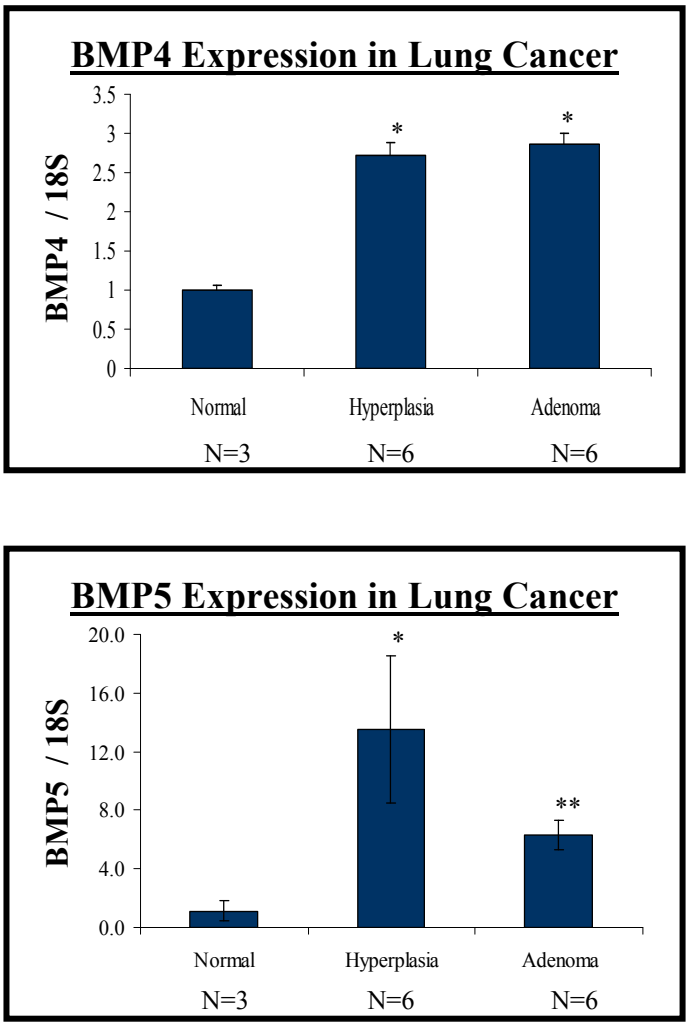

Figure 3.23: BMP4 and BMP5 expression in early lung cancer

Real time PCR analysis was carried out for BMP4 and BMP5 ligands. Real time PCR was carried out on RNA isolated from normal, hyperplasia and adenoma samples. BMP4 and BMP5 ligand expression levels were normalised to 18S in each sample. N indicates the number of samples analysed. * $p < 0.05$, ** $p < 0.01$

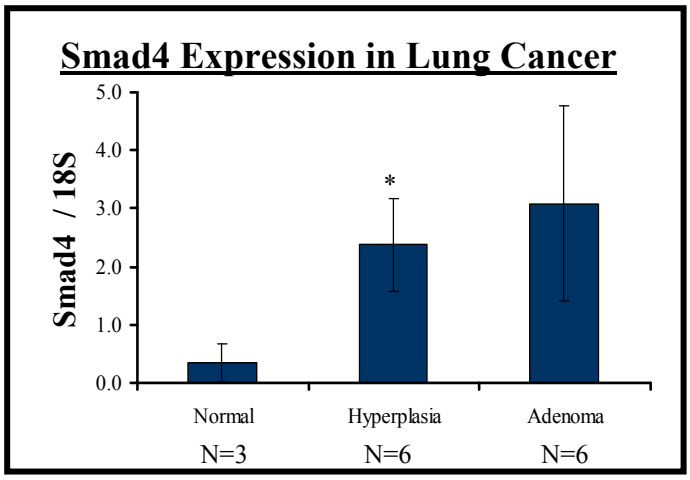

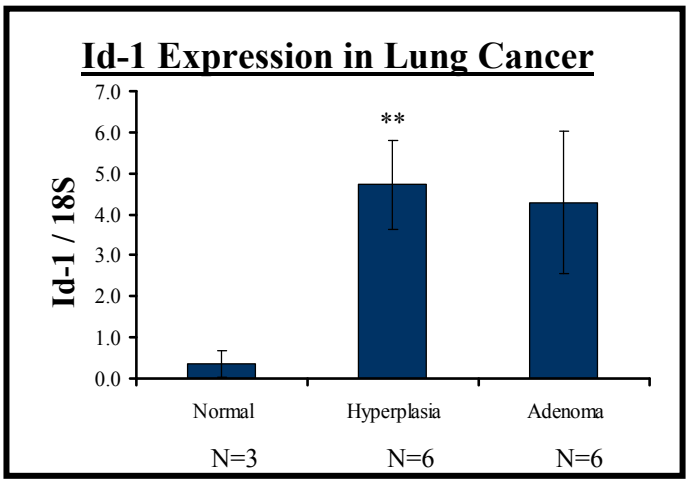

Figure 3.24: Smad4 and Id-1 expression in early lung cancer cells

Real time PCR analysis was carried out for Smad4, the BMP co-smad signalling molecule, and Id-1, an immediate downstream target of the BMP pathway. Real time PCR was carried out on RNA isolated from normal, hyperplasia and adenoma samples. Smad4 and Id-1 expression levels were normalised to 18S in each sample. N indicates the number of samples analysed. * $p < 0.05$, ** $p < 0.01$

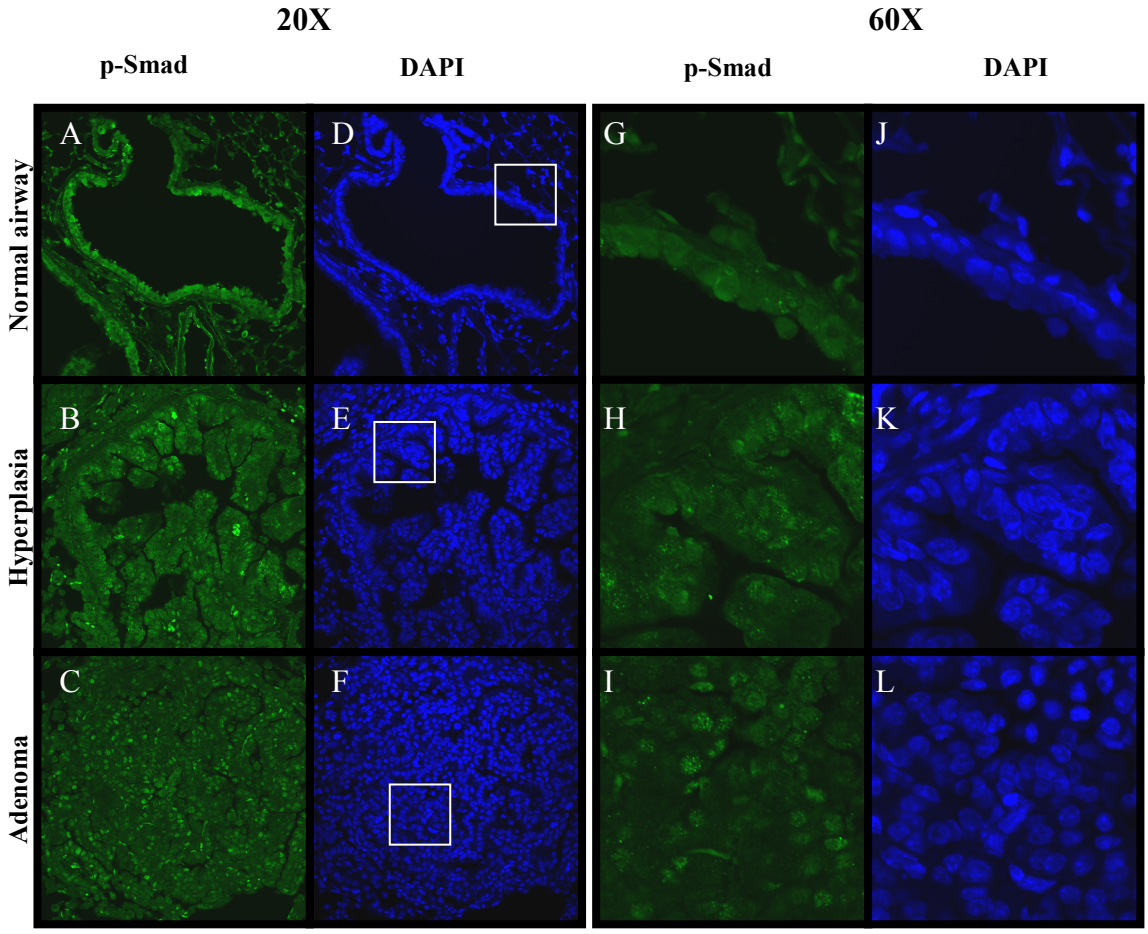

Figure 3.25: p-Smad staining in normal airway, hyperplasia and adenoma.

Representative photomicrographs of p-Smad staining in (A, D, G, J) normal, (B, E, H, K) hyperplasia and (C, F, I, L) adenoma lesions. White boxes in 20x photomicrographs represent the area imaged in the 60x photomicrograph. p-Smad 20x photomicrograph images were taken for (A) normal, (B) hyperplasia and (C) adenoma samples. p-Smad 60x photomicrograph images were taken for (G) normal, (H) hyperplasia, (I) adenoma samples. DAPI counterstained images correspond to p-Smad images.

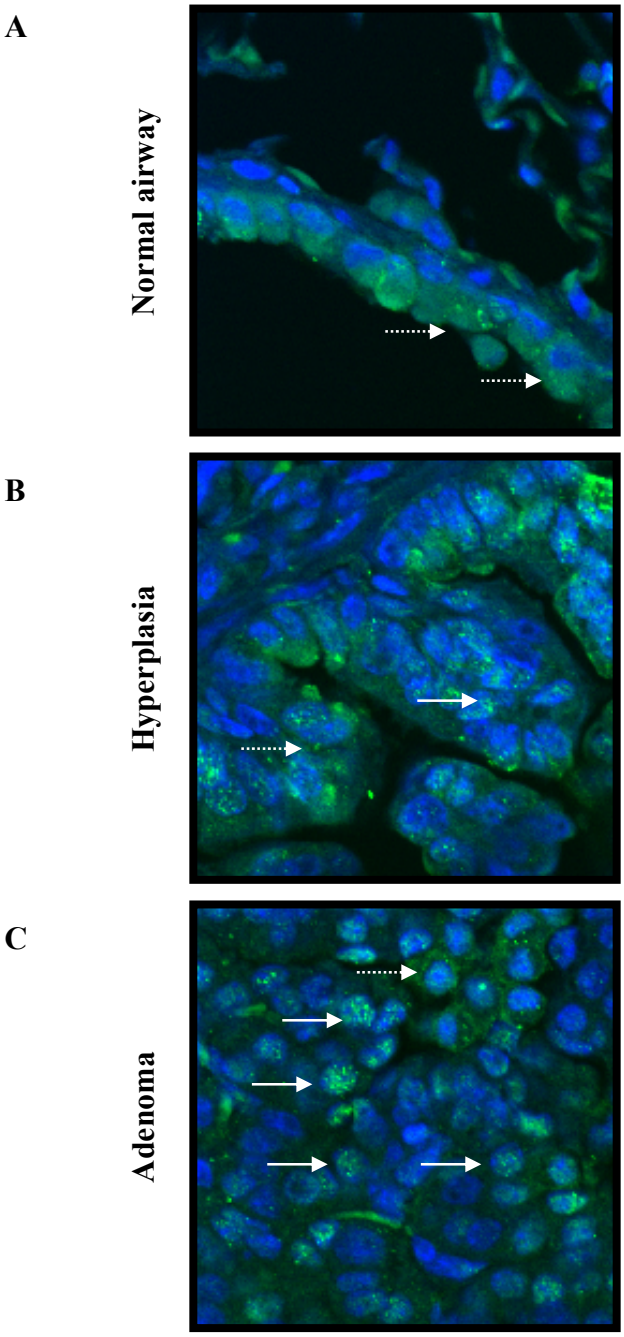

Figure 3.26: p-Smad and DAPI overlay of normal airways, hyperplasia and adenoma

DAPI nuclear counter stained images were over-layed with p-Smad Alexa 488 stained images to observe the localisation of p-Smad in the cells. Photomicrographs represent A) normal airway B) hyperplasia lesion C) adenoma lesions. Arrows indicates nuclear p-Smad staining, dashed arrows indicate cytoplasmic p-Smad staining.

Gene/Protein	Normal	Hyperplasia	Adenocarcinoma
PCNA	+	++	+++
Mig-6	+	-	--
E-cadherin	+	-	--
B-catenin	+	-	--
BMPR-IB	+	--	--
BMPR-IA	+	+	-
BMPR-II	+	--	--
BMP4	+	++	++
BMP5	+	+++	+++
Smad4	+	++	++
Id-1	+	+++	+++
p-Smad	+	++	+++

Figure 3.27: Summary table

This summary table represents alteration of expression levels during hyperplasia and adenoma stages of tumour progression. ++, +++ represents increasing in expression while --, --- represents decreasing expression.

A

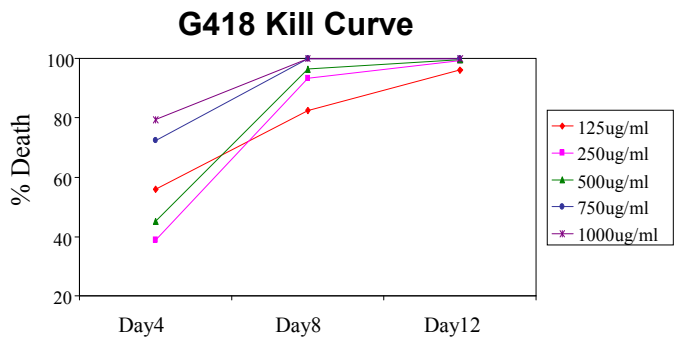

B

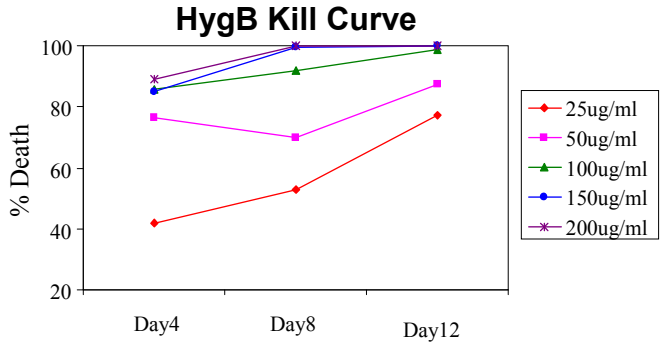

C

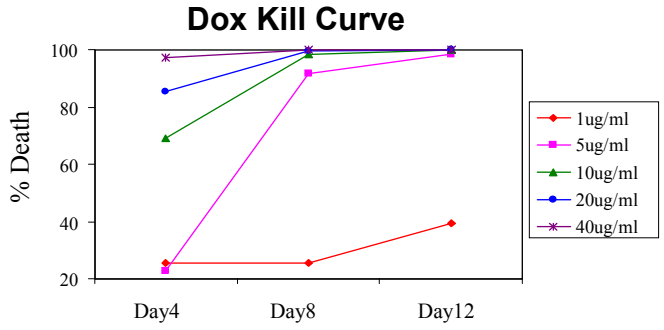

Figure 4.1: Antibiotic kill curves

Antibiotic kill curve were carried out on BEAS-2B cells to establish toxic concentration of the antibiotic. Cells were treated with various concentrations of A) G418 B) Hygromycin B (HygB) C) Doxycycline (Dox). Cell counts were carried out on day 4, 8 and 12. Percentage cell death was calculated as number of dead cells compared to the untreated control.

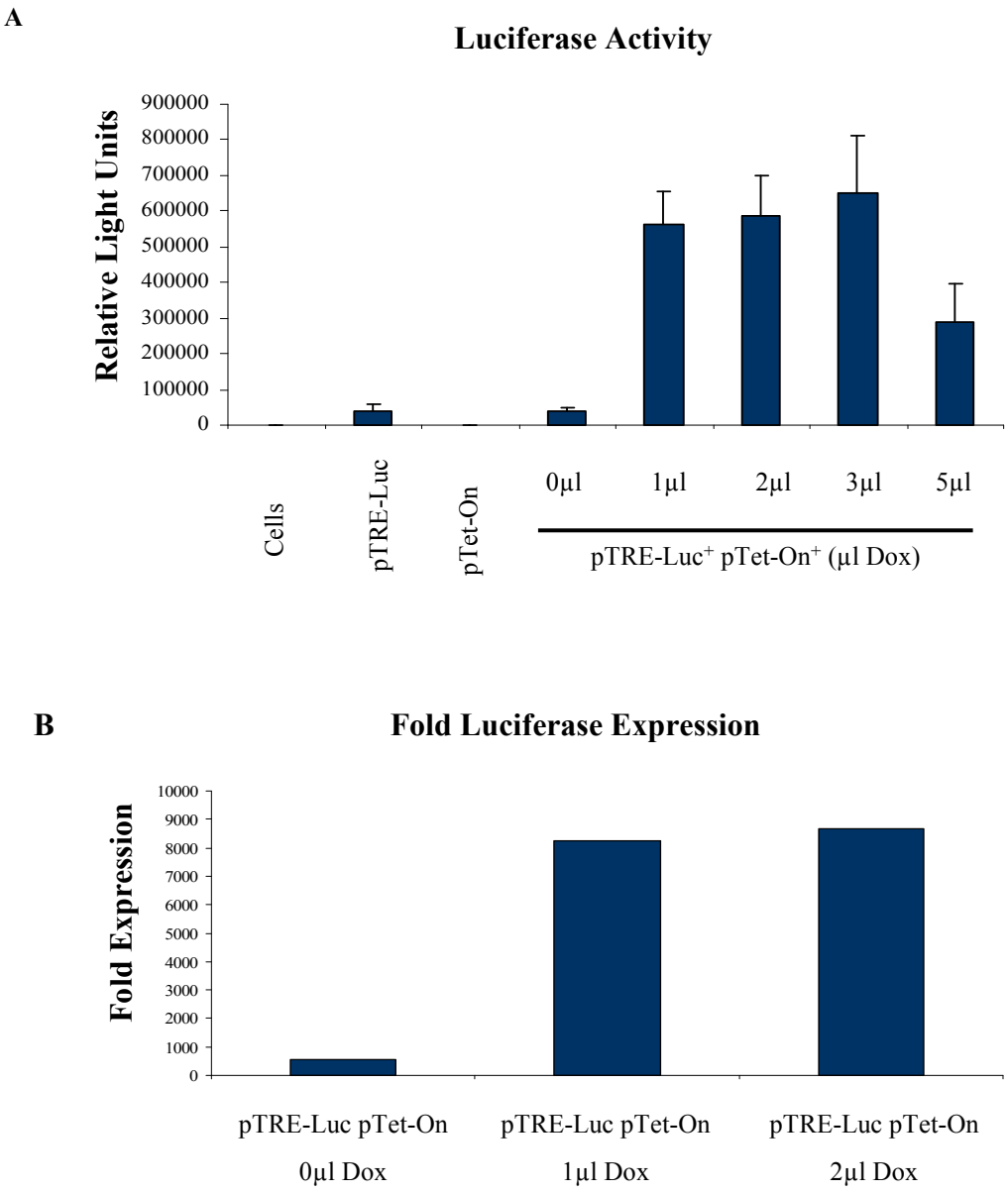

Figure 4.2: Luciferase induction after transient co-transfection of pTRE-Luc and pTet-On

pTRE-Luc and pTet-On were transiently co-transfected into BEAS-2B cells. Doxycycline was added to initiate expression of the luciferase reporter gene. A) Relative light units of transgene expression after doxycycline administration. B) Fold expression of luciferase activation relative to cells only control.

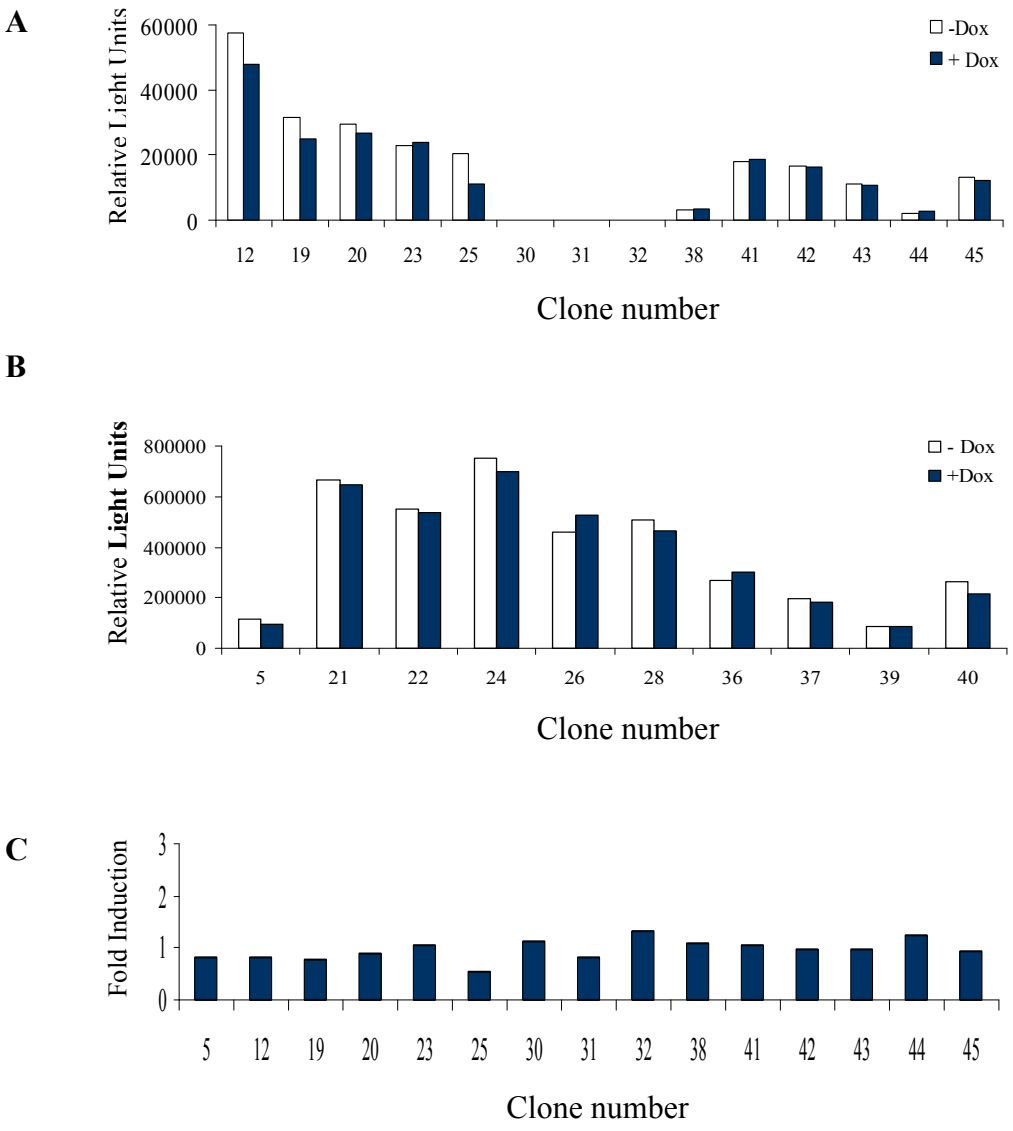

Figure 4.3: pTRE-Luciferase co-transfection into pTet-On BEAS-2B stable cell lines: Trial #1

pTet-On BEAS-2B stable clones were transiently transfected with pTRE-Luciferase to analyse luciferase reporter expression. A) & B) Expression of luciferase from clones in the presence or absence of Doxycycline C) Fold induction of luciferase for each clone: (+Dox/-Dox)

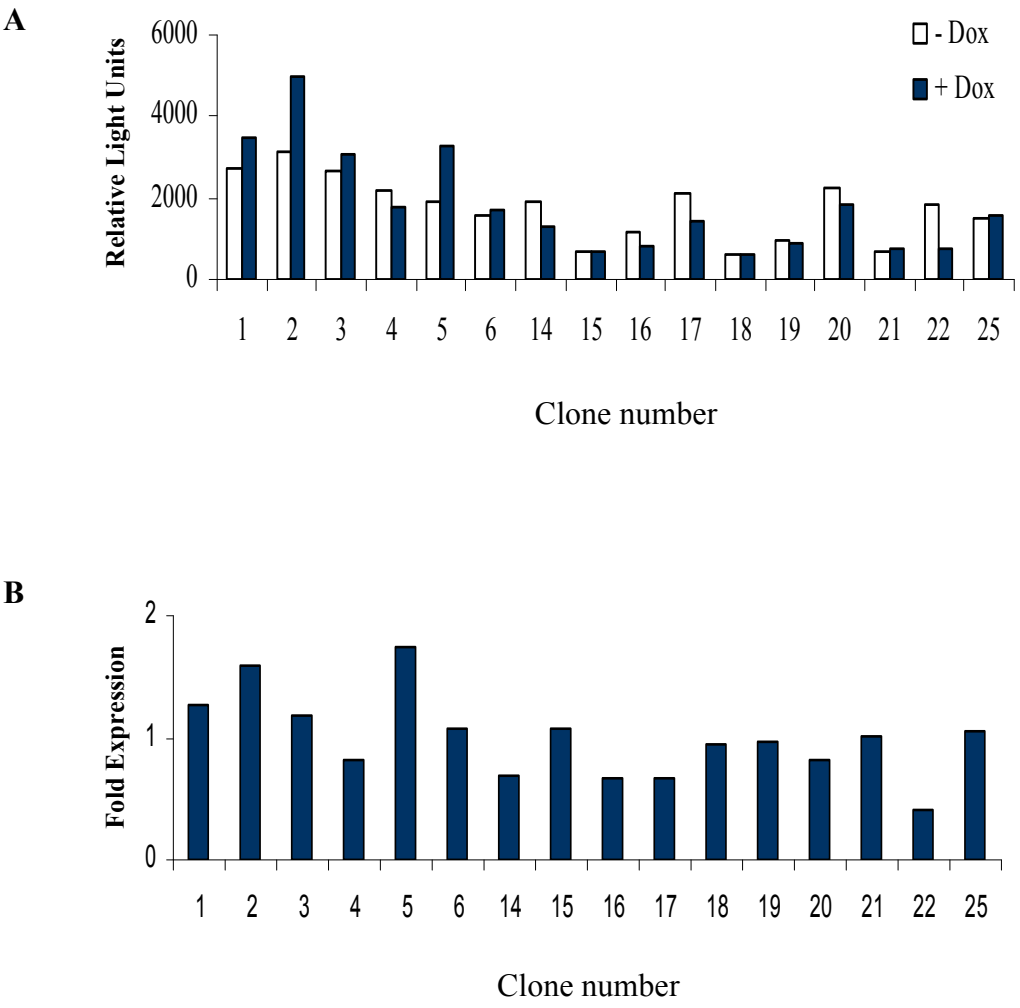

Figure 4.4: pTRE-Luciferase co-transfection into pTet-On BEAS-2B stable cell lines: Trial #2

pTet-On BEAS-2B stable clones were transiently transfected with pTRE-Luciferase to analyse luciferase reporter expression. A) Luicferase expression from clones: 1, 2, 3, 4, 5, 6, 14, 15, 16, 17, 18, 19, 20, 21, 22, 25 in the absence or presence of Doxycycline B) Fold induction of luciferase for each clone: (+Dox/-Dox)

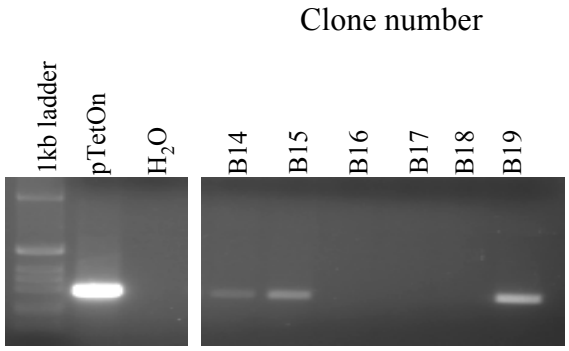

Figure 4.5: RT-PCR for pTetOn expression of rtTA (transactivator)

RT-PCR was carried out on BEAS-2B pTet-On trial 2 clone 14, 15, 16, 17, 18, 19 to establish if rtTA transactivator was being expressed at an mRNA level. Clone B14, B15 and B19 expressed the mRNA for the transactivator.

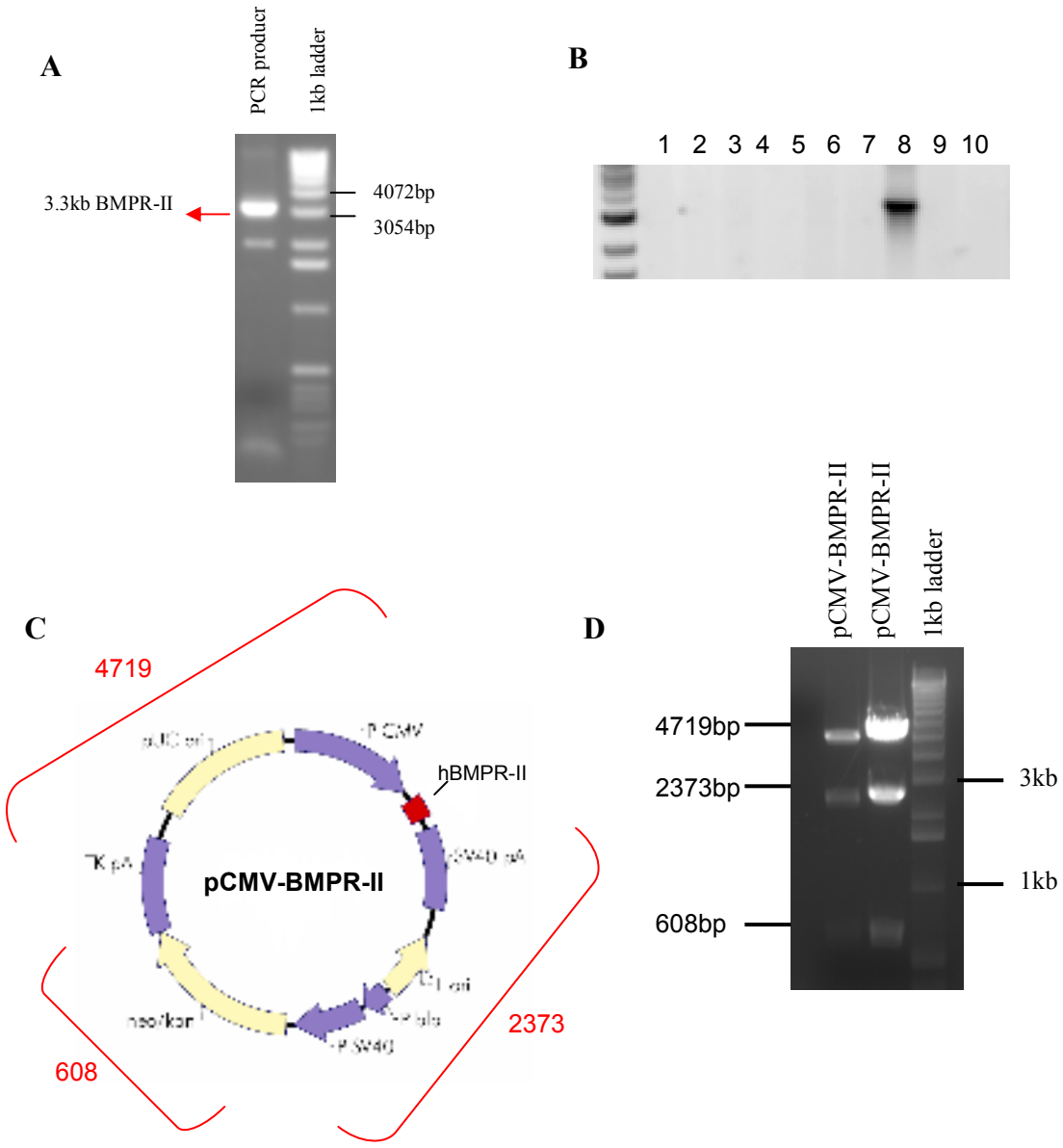

Figure 4.6: Generation of pCMV-BMPR-II expression plasmid

BMPR-II cloned from BEAS-2B cDNA was inserted into the pCMV-Script cloning vector. A) PCR amplification was used to clone the 3.3 kb BMPR-II gene from BEAS-2B cDNA. B) Lane 8 represents one of the pCMV-BMPR-II colonies screened that contained the BMPR-II gene in the correct orientation. C) BMPR-II cDNA was inserted into the multiple cloning site of pCMV-Script, restriction digest with *Pvu* II resulted in three digestion fragments. D) *Pvu* II cut pCMV-BMPR-II proves the inserted BMPR-II is in the correct orientation.

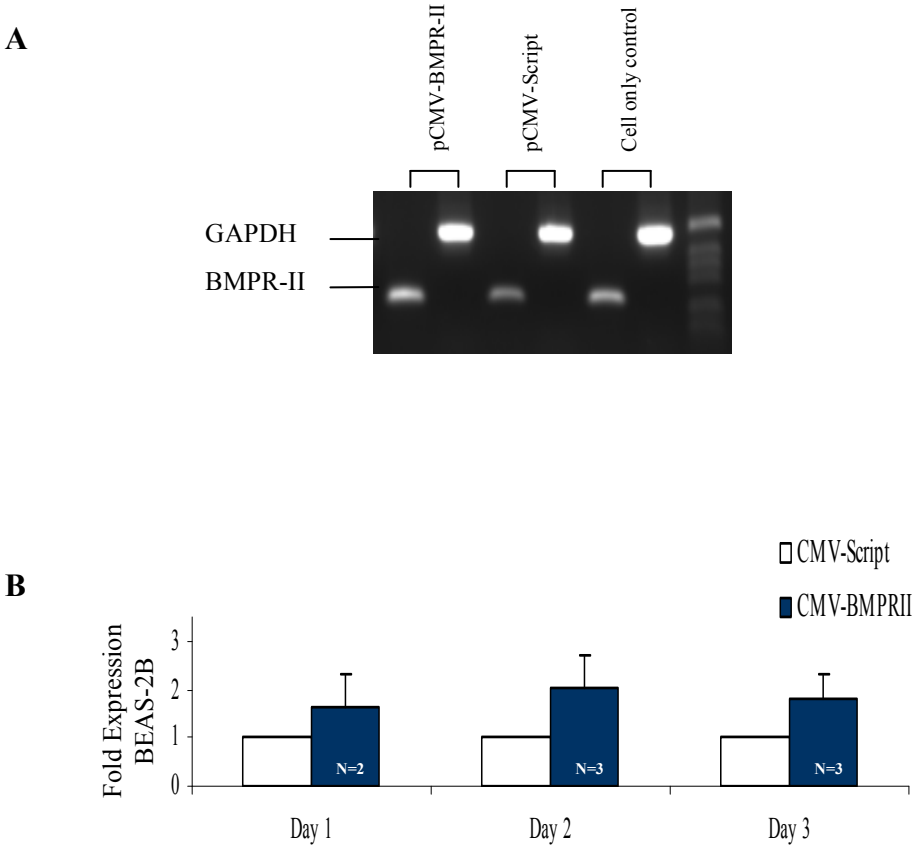

Figure 4.7: RT-PCR analysis of pCMV-BMPR-II expression

pCMV-BMPR-II was transiently transfected into BEAS-2B cells. RT-PCR and densitometry was carried out on the PCR bands to semi-quantify the rate of over-expression. A) DNA gel of GAPDH and BMPR-II was set up for no-vector control, empty vector control (pCMV-Script) and pCMV-BMPR-II expression vector. B) Densitometry results for pCMV-BMPR-II expression in BEAS-2B.

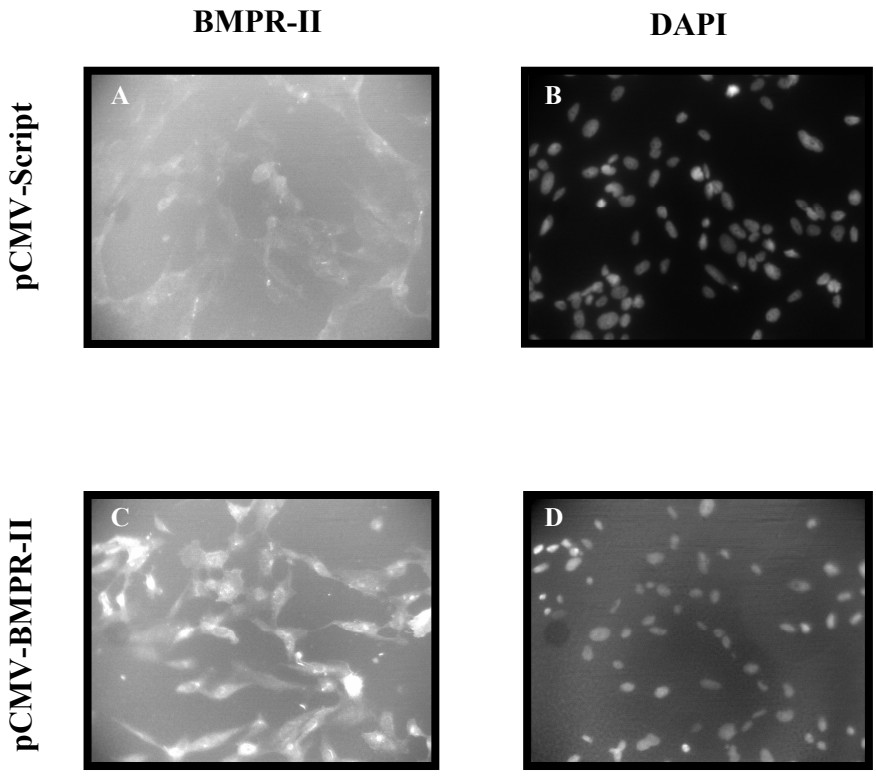

Figure 4.8: Immunofluorescence to detect pCMV-BMPR-II expression

Immunofluorescence for BMPR-II was carried out on BEAS-2B cells transiently transfected with pCMV-BMPR-II (C & D) and mock transfection control (A & B). Anti BMPR-II antibody was used to detect both endogenous and transiently transfected BMPR-II expression in the cells (A & C). Photomicrographs were taken of DAPI nuclear counterstain (B & D)

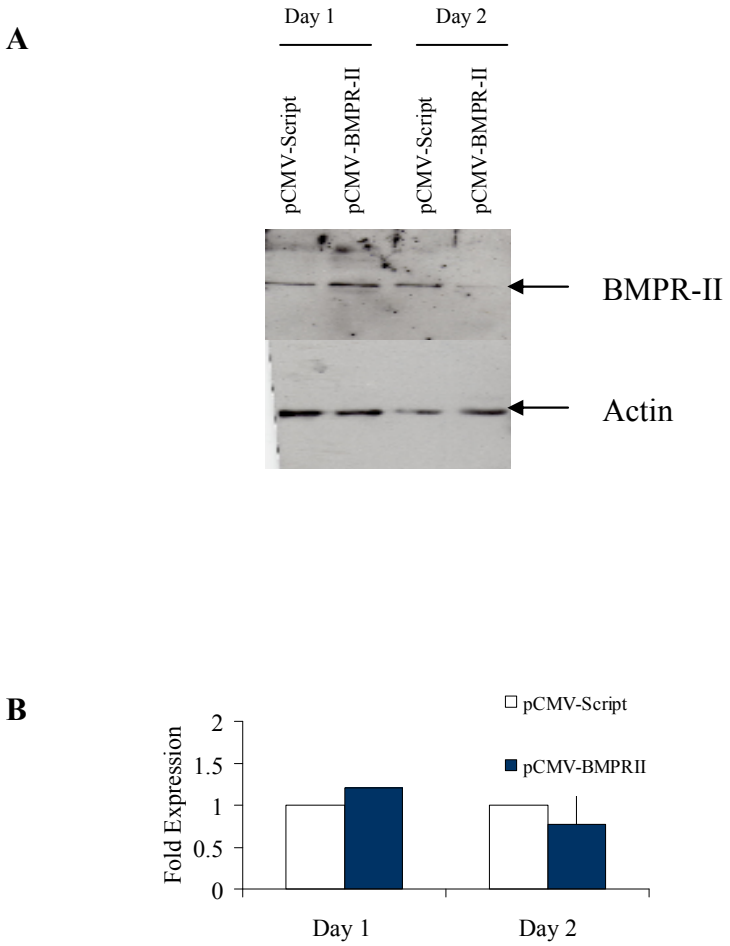

Figure 4.9: Western blot analysis of pCMV-BMPR-II expression

pCMV-BMPR-II was transiently transfected into BEAS-2B cells. Densitometry was carried out on Western blot bands to quantify BMPR-II protein expression. A) Western blot for BMPR-II and actin was set up for pCMV-Script control and pCMV-BMPR-II expression vector. B) The graph represents BMPR-II protein expression in control and pCMV-BMPR-II expressing cells.

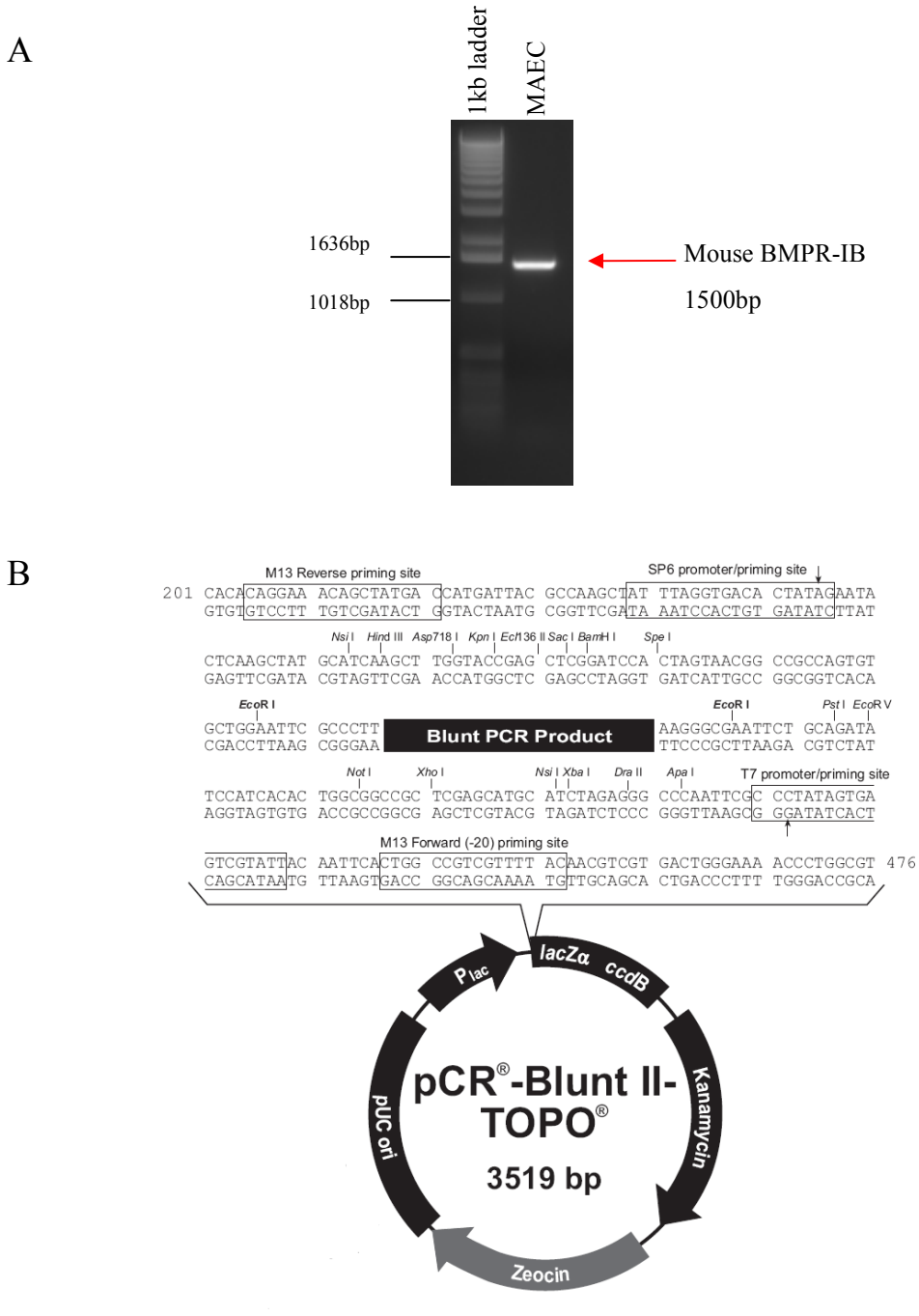

Figure 4.10: Cloning of mouse BMPR-IB from MAECs

A) Mouse BMPR-IB was cloned from MAEC cDNA using the cloning primers BMPR-IB-F-*BamH* I and BMPR-IB-R-*EcoR* I primers. B) BMPR-IB cDNA was ligated into the pCR-BluntII TOPO cloning vector.

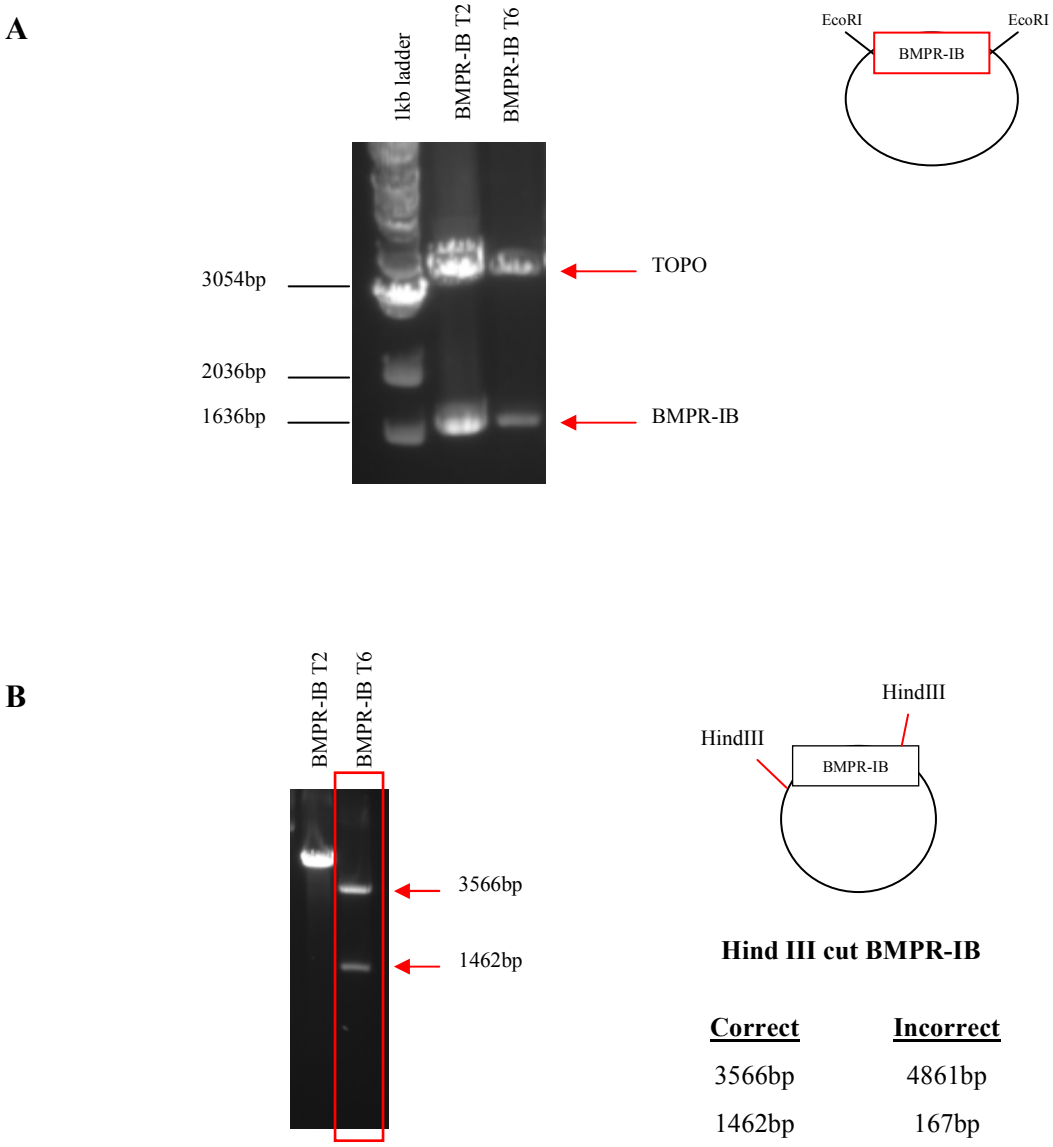

Figure 4.11: BMPR-IB-TOPO validation

BMPR-IB was cloned into the pCR-BluntII-TOPO cloning vector and the resulting clones were screened to identify clones which contained an insert of the correct size. A) BMPR-IB-TOPO ligation products were digested with *EcoR* I to identify clones containing BMPR-IB cDNA. B) BMPR-IB-TOPO clones were screened by *Hind* III restriction digest to identify the clones containing an insert in the correct orientation.

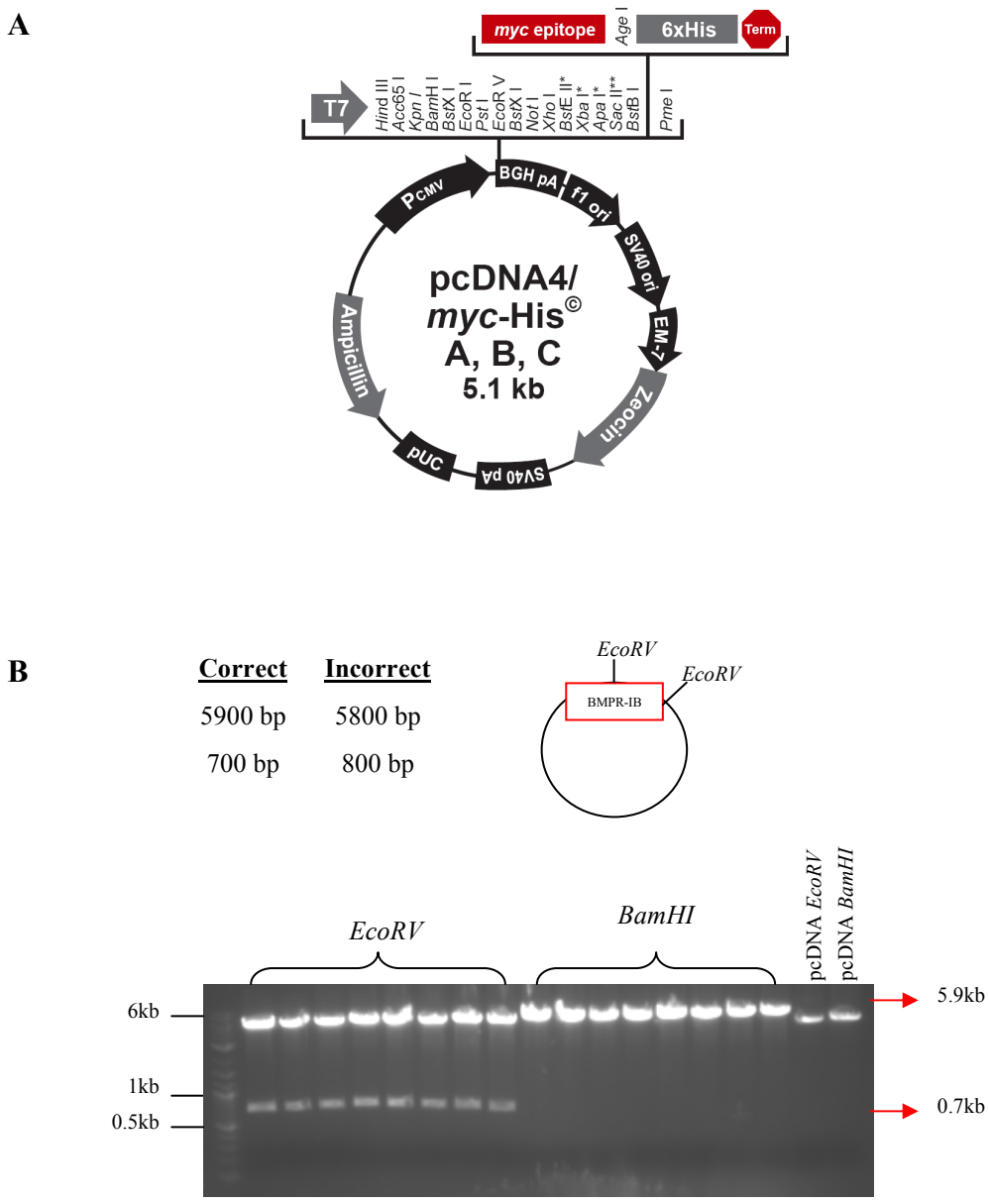

Figure 4.12: BMPR-IB-pcDNA4 sub-cloning

BMPR-IB was digested from pCR-BluntII TOPO cloning vector and ligated into *BamHI /EcoRI* digested pcDNA4. A) pcDNA4 plasmid map. B) BMPR-IB-pcDNA4 ligation product colonies were screened for insertion of the 1.5kb gene (*BamHI* digest), and correct orientation of the insert (*EcoRV* digest).

BMPR-IB NM_007560

ATG CTC TTA CGA AGC TCT GGA AAA TTA AAT GTG GGC ACC AAG AAG GAG GAT
GGA GAG AGT ACA GCC CCC ACC CCT CGG CCC AAG ATC CTA CGT TGT AAA TGC
CAC CAC CAC TGT CCG GAA GAC TCA GTC AAC AAT ATC TGC AGC ACA GAT GGG
TAC TGC TTC ACG ATG ATA GAA GAA GAT GAC TCT GGA ATG CCT GTT GTC ACC
TCT GGA TGT CTA GGA CTA GAA GGG TCA GAT TTT CAA TGT CGT GAC ACT CCC
ATT CCT CAT CAA AGA AGA TCA ATT GAA TGC TGC ACA GAA AGG AAT GAG TGT
AAT AAA GAC CTC CAC CCC ACT CTG CCT CCT CTC AAG GAC AGA GAT TTT GTT
GAT GGG CCC ATA CAC CAC AAG GCC TTG CTT ATC TCT GTG ACT GTC TGT AGT
TTA CTC TTG GTC CTC ATT ATT TTA TTC TGT TAC TTC AGG TAT AAA AGA CAA
GAA GCC CGA CCT CGG TAC AGC ATT GGG CTG GAG CAG GAC GAG ACA TAC ATT
CCT CCT GGA GAG TCC CTG AGA GAC TTG ATC GAG CAG TCT CAG AGC TCG GGA
AGT GGA TCA GGC CTC CCT CTG CTG GTC CAA AGG ACA ATA GCT AAG CAA ATT
CAG ATG GTG AAG CAG ATT GGA AAA GGC CGC TAT GGC GAG GTG TGG ATG GGA
AAG TGG CGT GGA GAA AAG GTG GCT GTG AAA GTG TTC TTC ACC ACG GAG GAA
GCC AGC TGG TTC CGA GAG ACT GAG ATA TAT CAG ACG GTC CTG ATG CGG CAT
GAG AAT ATT CTG GGG TTC ATT GCT GCA GAT ATC AAA GGG ACT GGG TCC TGG
ACT CAG TTG TAC CTC ATC ACA GAC TAT CAT GAA AAC GGC TCC CTT TAT GAC
TAT CTG AAA TCC ACC ACC TTA GAC GCA AAG TCC ATG CTG AAG CTA GCC TAC
TCC TCT GTC AGC GGC **CTA** TGC CAT TTA CAC ACG **GAA** ATC TTT AGC ACT CAA
GGC AAG CCA GCA ATC GCC CAT CGA GAC TTG AAA AGT AAA AAC ATC CTG GTG
AAG AAA AAT GGA ACT TGC TGC ATA GCA GAC CTG GGC TTG GCT GTC AAG TTC
ATT AGT GAC ACA AAT GAG GTT GAC ATC CCA CCC AAC ACC CGG GTT GGC ACC
AAG CGC TAT ATG CCT CCA GAA GTG CTG GAC GAG AGC TTG AAT AGA AAC CAT
TTC CAG TCC TAC ATT ATG GCT GAC ATG TAC AGC TTT GGA CTC ATC CTC TGG
GAG ATT GCA AGG AGA TGT GTT TCT GGA GGT ATA GTG GAA GAA TAC CAG CTT
CCC TAT CAC GAC CTG GTG CCC AGT GAC CCT TCT TAT GAG GAC ATG AGA GAA
ATT GTG TGC ATG AAG AAG TTA CGG CCT TCA TTC CCC AAT CGA TGG AGC AGT
GAT GAG TGT CTC AGG CAG ATG GGG AAG CTT ATG ACA GAG TGC TGG GCG CAG
AAT CCT GCC TCC AGG CTG ACG GCC CTG AGA GTT AAG AAA ACC CTT GCC AAA
ATG TCA GAG TCC CAG GAC ATT AAA CTC GGA

Point mutations:
Should be CTA (LEU) but is CTG (LEU)
Should be GAA (GLU) but is GAG (GLU)

Figure 4.13: BMPR-IB-pcDNA4 sequencing results

Sequencing of BMPR-IB-pcDNA4 exhibited two A-G point mutations. These mutations occurred in the third position of the codon. Both CTA and CTG code for leucine. Both GAA and GAG code for glutamine. The point mutations did not affect the amino acid sequence. The stop codon was mutated to glycine as intended.

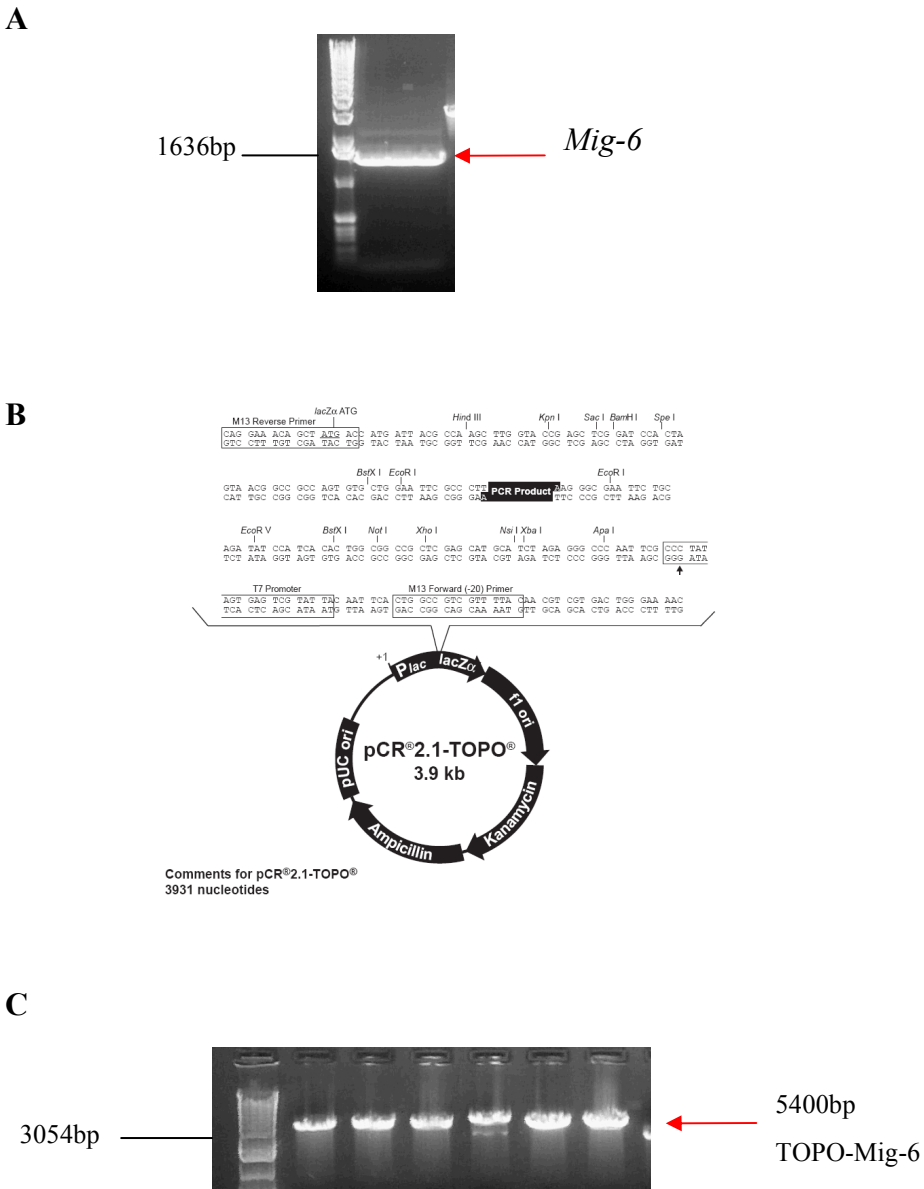

Figure 4.14: *Mig-6*-TOPO cloning

(A) Mig-6 was cloned from human uterine cDNA and ligated to (B) pCR2.1-TOPO cloning vector. This ligation was transformed into TOP10 bacteria and resulting colonies were screened for *Mig-6*-TOPO ligation vectors. (C) Positive vectors resulted in a 5400bp band (3900bp of TOPO and 1500bp of *Mig-6*)

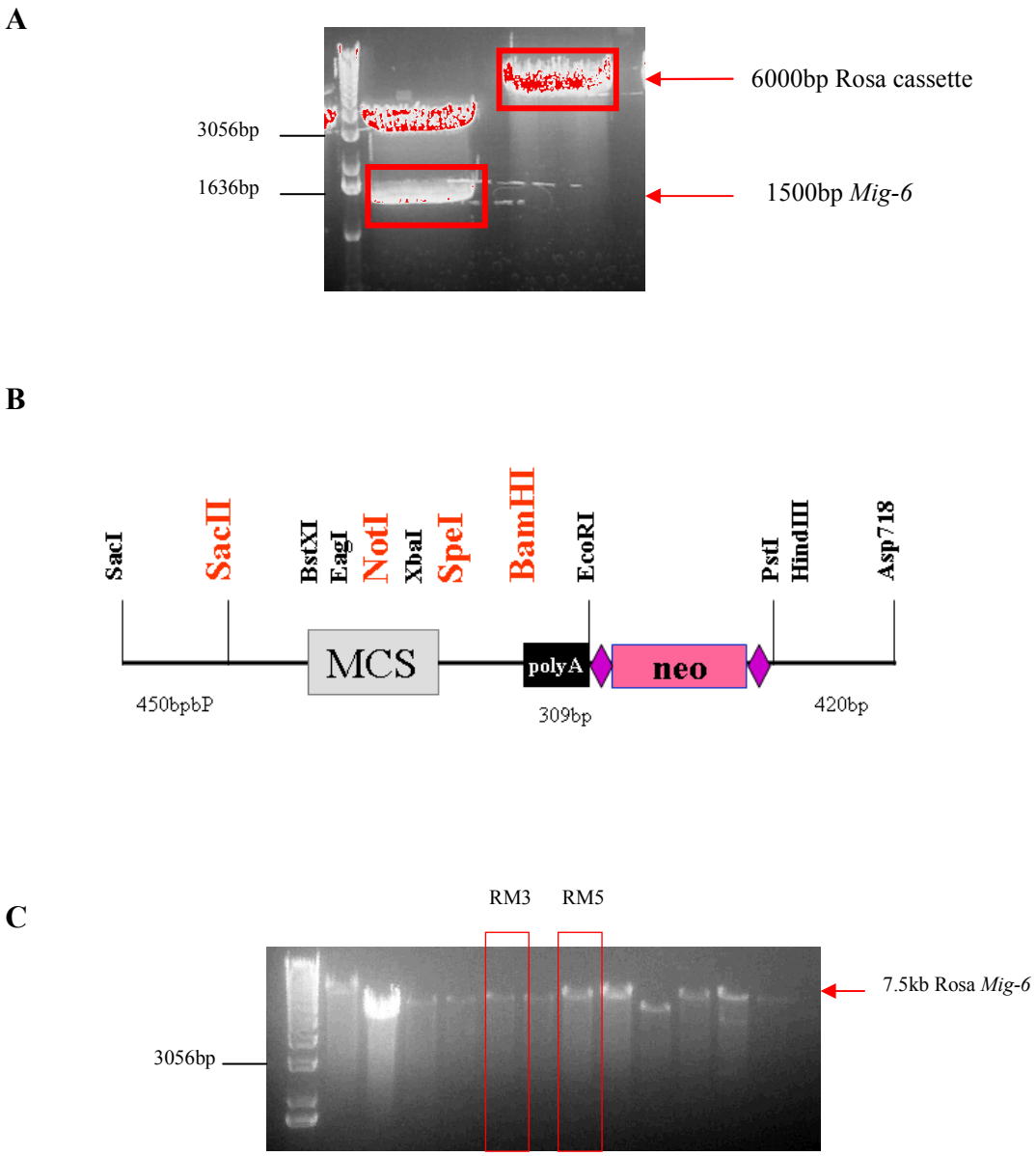

Figure 4.15: Cloning of *Mig-6* into the Rosa plasmid

Sac II and *BamH* I double digest of A) pCR2.1-TOPO-*Mig-6* and Rosa cassette for sub-cloning. B) The *Mig-6* gene was inserted into the Rosa cassette in the between the *SacII* and *BamHI* restriction sites. C) *BamH* I restriction digest was carried out on resulting colonies to identify a 7.5kb plasmid. Two clones (RM3 and RM5) were analysed further.

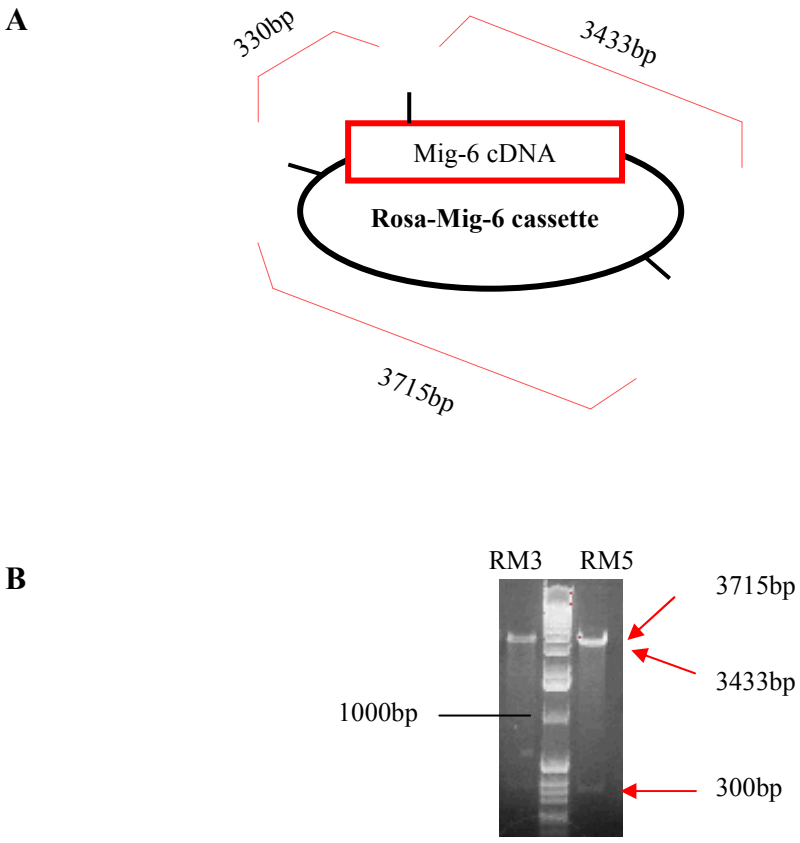

Figure 4.16: *Rosa Mig-6* ligation product

Rosa-Mig-6 clone 3 and 5 were digested with Hind *III* to identify if the Mig-6 gene had inserted in the correct orientation A) *Hind* III digest of the Rosa-Mig-6 vector results in three DNA products (330, 3433, 3715bp products). B) *Hind* III digest of Rosa-*Mig-6* clone 5 (RM5) resulted in the correct expected digestion pattern.

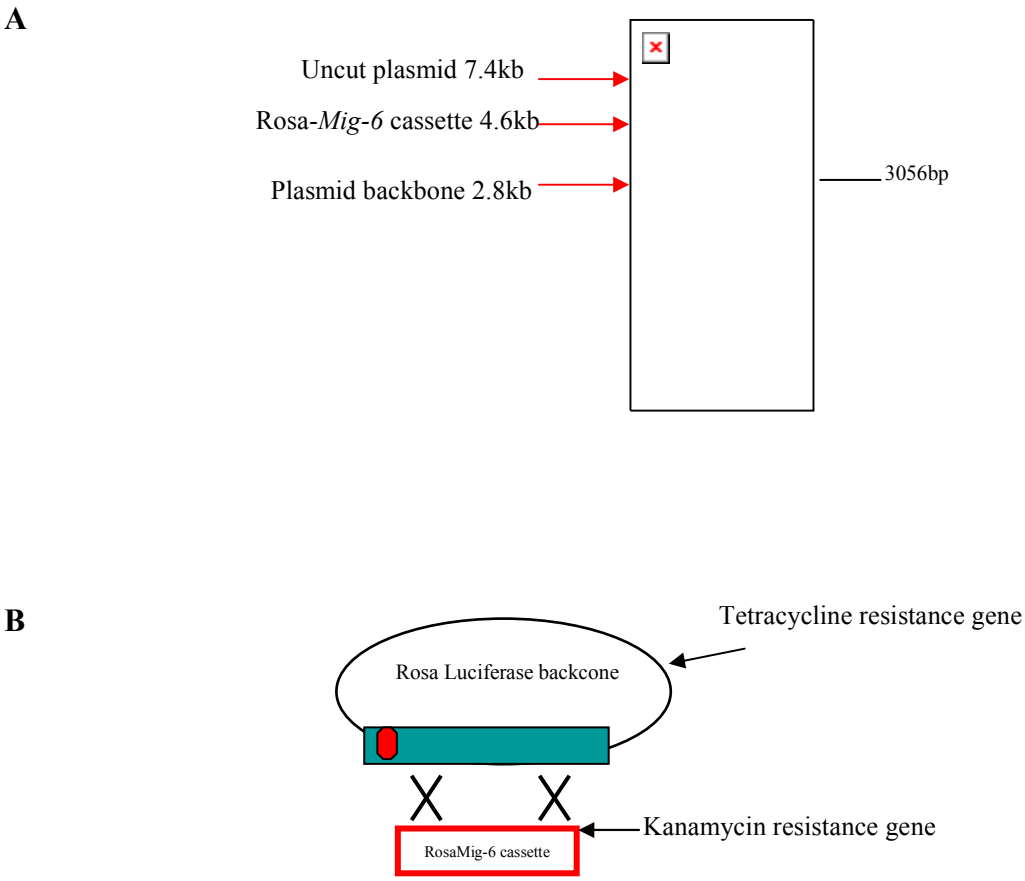

Figure 4.17: Generation of recombeered Rosa *Mig-6* plasmid

A) Rosa-*Mig-6* cassette was digested from the backbone with *SacI* and *KpnI* double digest. B) The linearised Rosa cassette was electroporated into DY380 bacteria containing the Rosa luciferase plasmid. Recombineered colonies were selected on kanamycin plates.

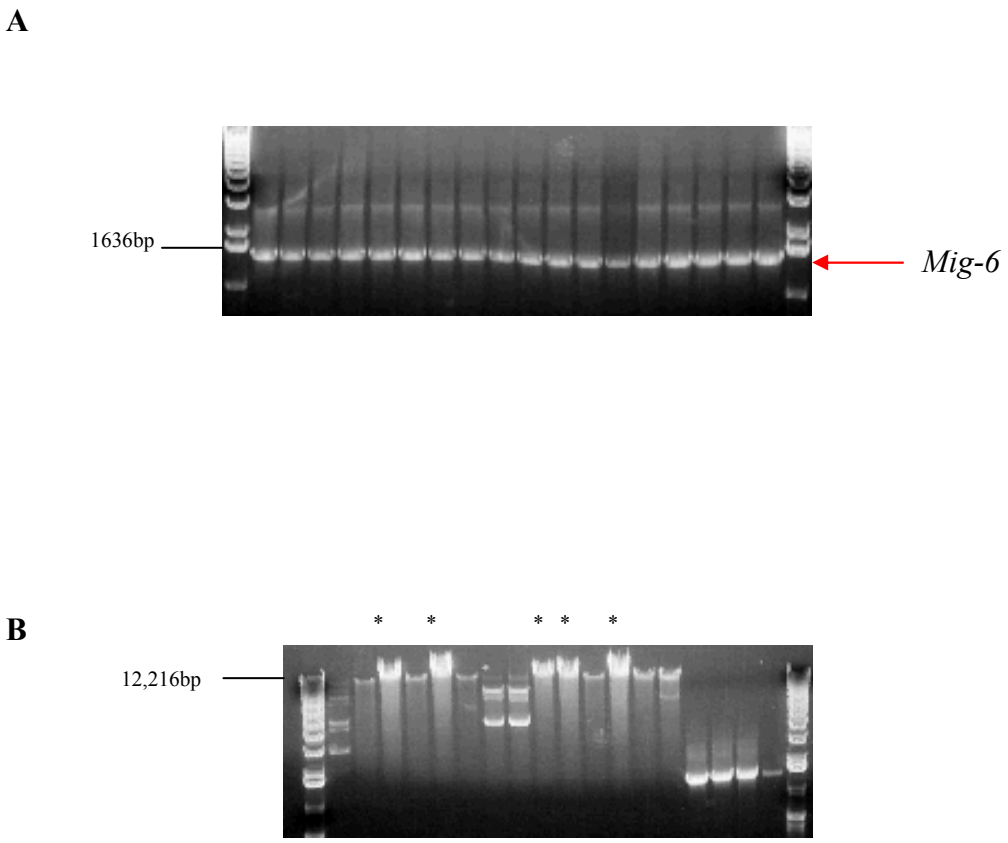

Figure 4.18: Screening of Recombineered Rosa *Mig-6* clones

Recombineered Rosa *Mig-6* colonies were screened for correctly recombined products. A) Colonies were screened by PCR for the presence of the *Mig-6* gene. B) Restriction digest analysis was carried out to ensure the recombineered plasmid was the correct size. *PacI* restriction enzyme was used to linearise the plasmid. All clones with a star were greater than 12 kb, large enough to be the correct product, and were analysed further.

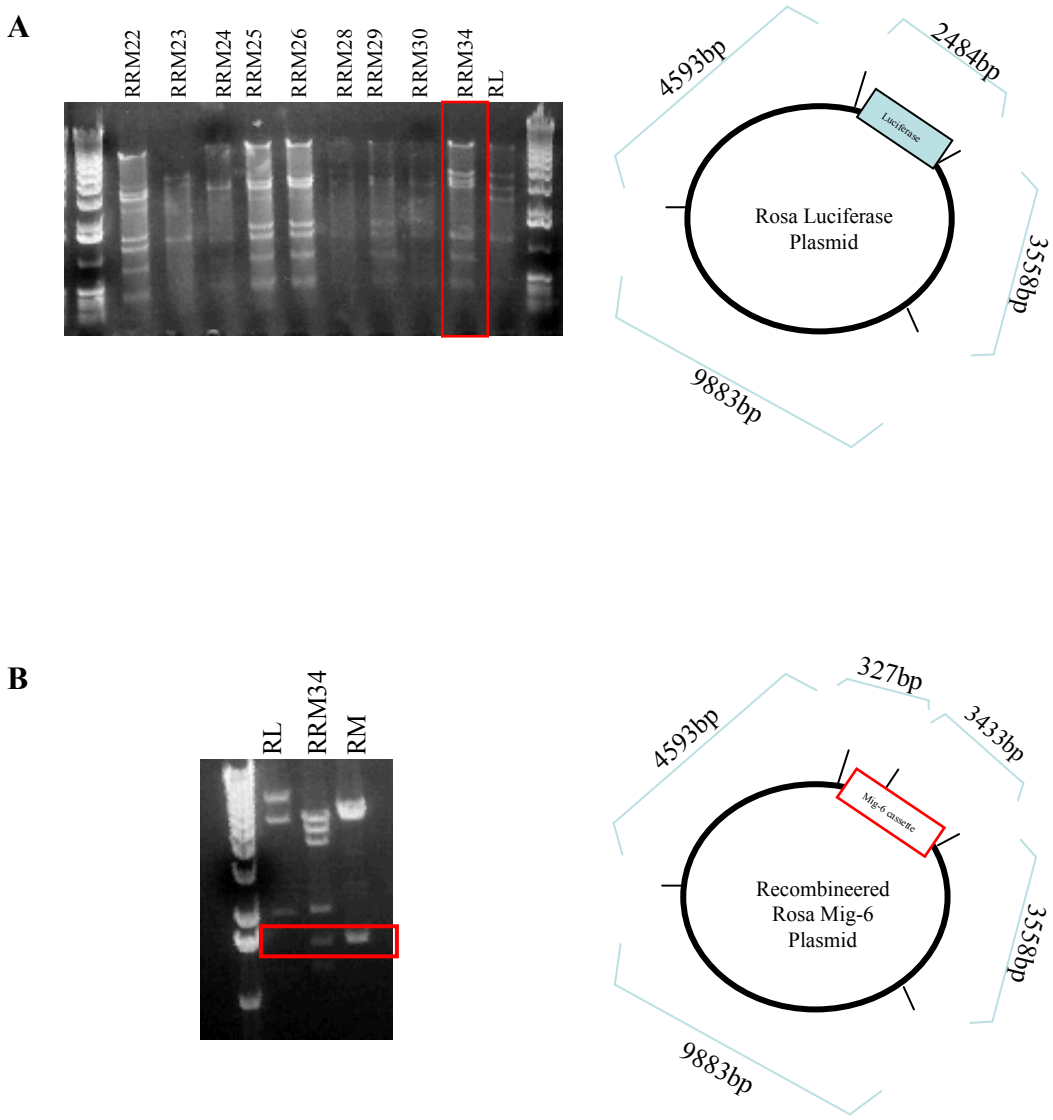

Figure 4.19: Screening for Recombineered Rosa *Mig-6* clones

A) HindIII digest of Recombineered Rosa *Mig-6* clones. RRM34 had the correct banding pattern. B) RRM34 was cut with *BamH* I and *Sac* I to excise out the *Mig-6* fragment. Rosa *Mig-6* cassette was used as a positive control and Rosa - luciferase plasmid was used as a negative control to identify *Mig-6* cDNA.

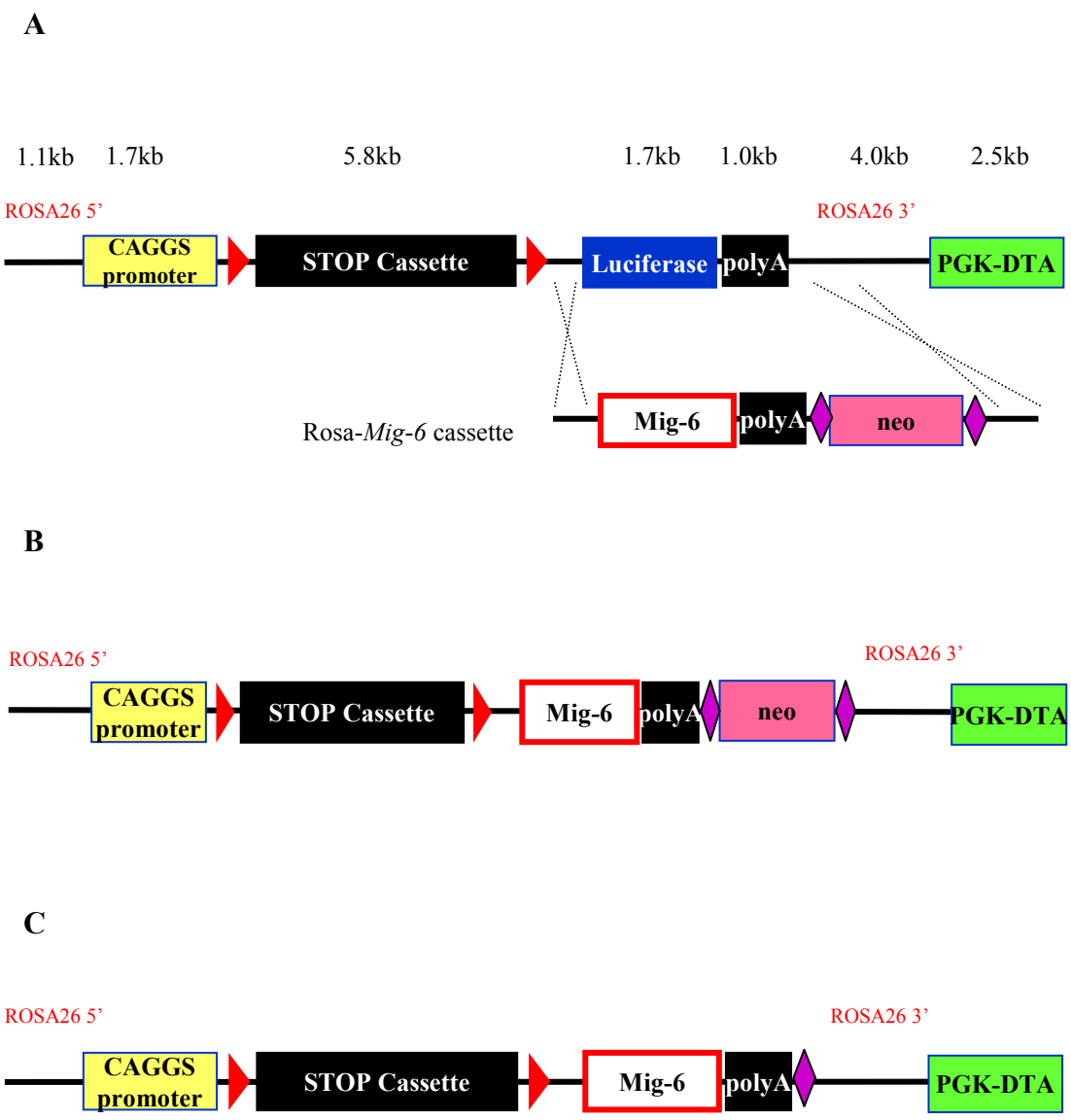

Figure 4.20: Recombineering process

A) Map of original Rosa Luciferase backbone containing the floxed stop cassette upstream of a luciferase reporter gene. B) The Rosa cassette contains homologous regions to the Rosa Luciferase plasmid allowing homologous recombination to occur thereby inserting the Mig-6 FLP-Neo sequence into the luciferase position. C) The neomycin selection marker is removed transformation into 295FLP bacteria, which contains the enzyme FLP, capable of recombining FRT sites, thereby removing the neomycin cassette.

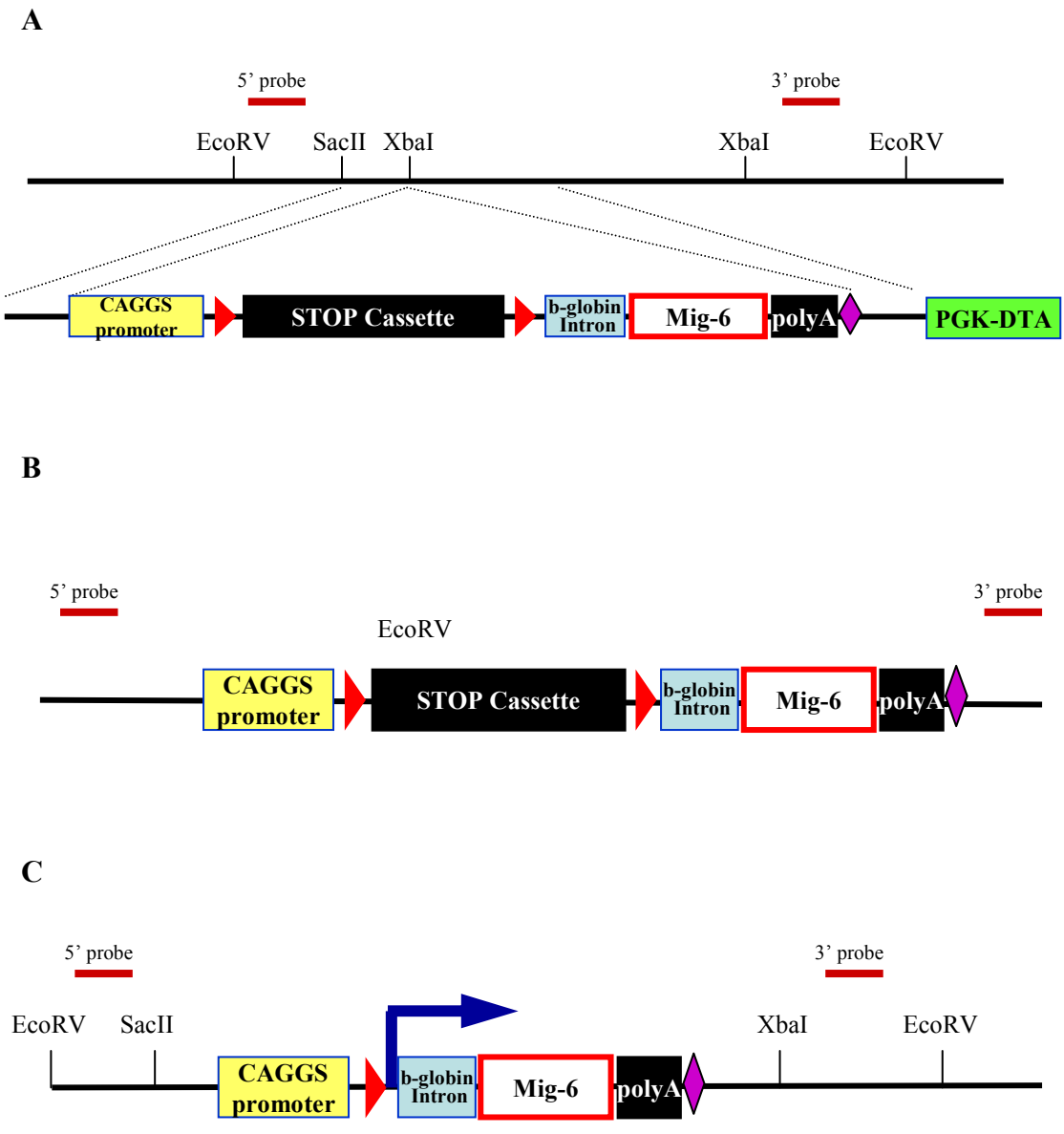

Figure 4.21: Generation of transgenic knock-in mouse

A) The Rosa-*Mig-6* plasmid contains regions homologous to the Rosa locus where homologous recombination can occur. B) 5' and 3' probes were generated to analyse insertion of LSL-*Mig-6* region by Southern blot analysis. C) Crossing of the LSL-*Mig-6* mouse with a mouse expressing Cre recombinase under the control of a tissue specific promoter will lead to the removal of the stop cassette and therefore tissue specific expression of the *Mig-6* transgene.

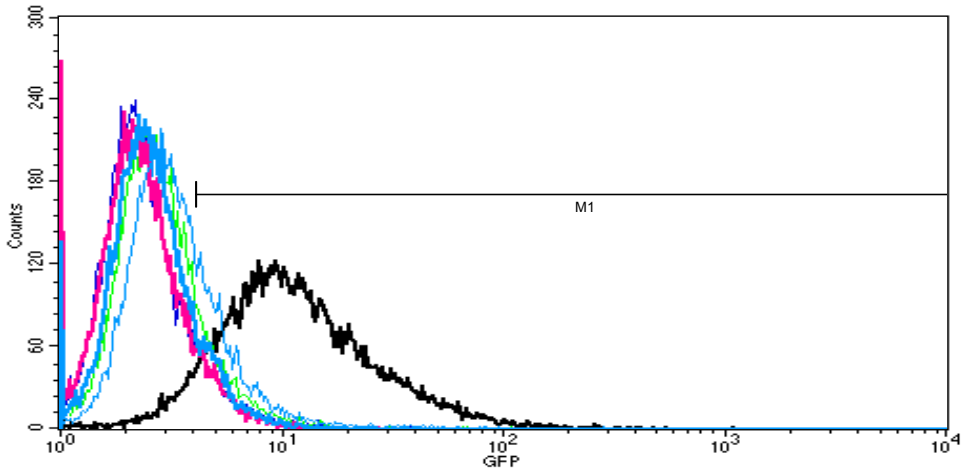

Figure 5.1: Flow cytometry analysis of endogenous GFP expression from CyclinD1-GFP clones

Flow cytometry analysis of GFP expression for: A549 (purple), A549-CyclinD1-GFP clone 5 (green), A549-CyclinD1-GFP clone 3 (pink), A549-CyclinD1-GFP clone 2 (blue), and A549-CyclinD1-GFP clone 1A (black).

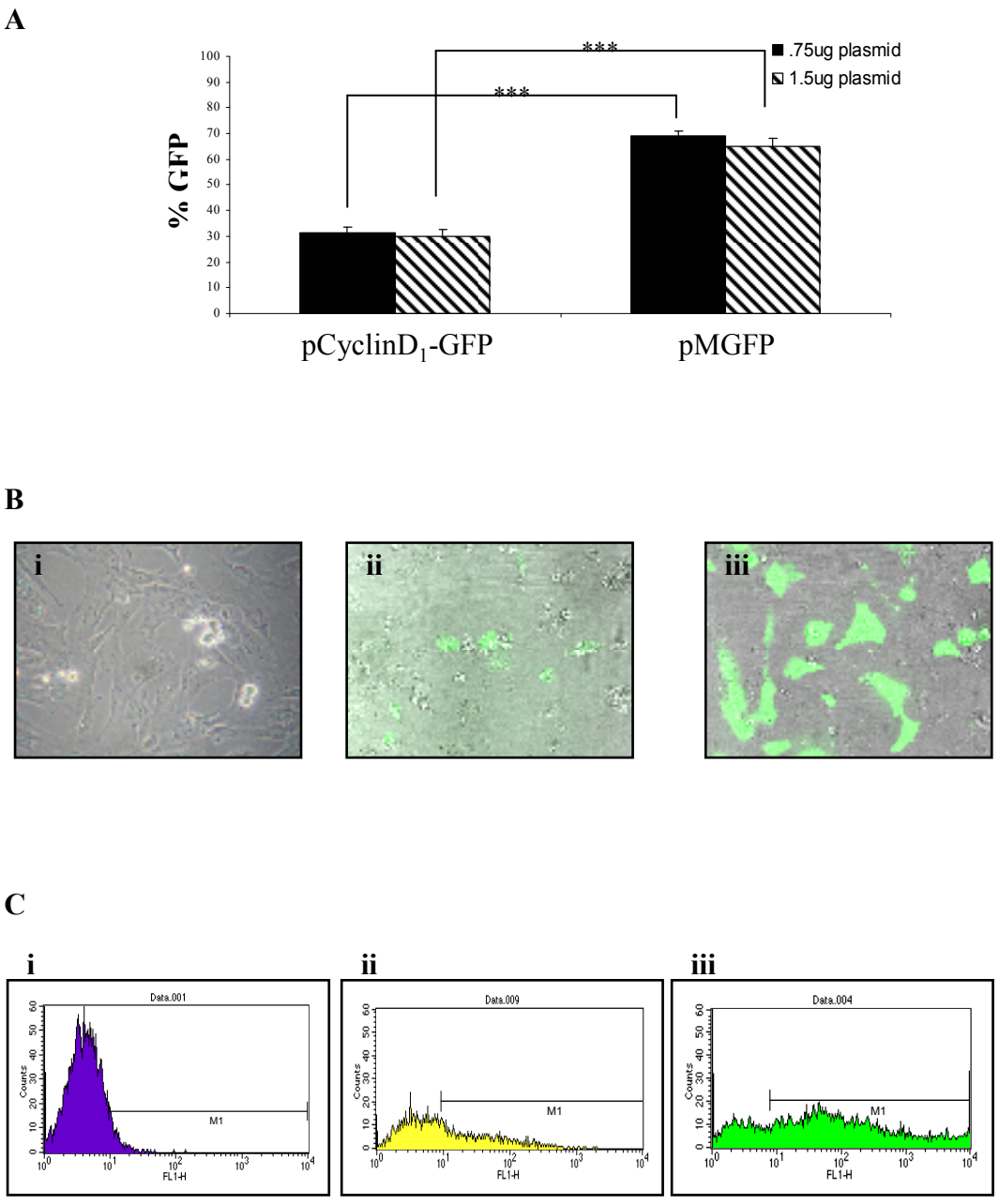

Figure 5. 2: Comparison of plasmids pCyclinD$_1$-GFP and pMGFP

Plasmids were transiently transfected into A549 cells. A) CyclinD$_1$-GFP results in significantly less GFP expression compared to pMGFP. B) Bright field and GFP overlayed photomicrographs of cells transfected with i) no vector ii) CyclinD$_1$-GFP and iii) pMGFP. C) Flow cytometry graphs of GFP fluorescent intensity (FL-1) of i) no vector ii)CyclinD$_1$-GFP and iii) pMGFP.

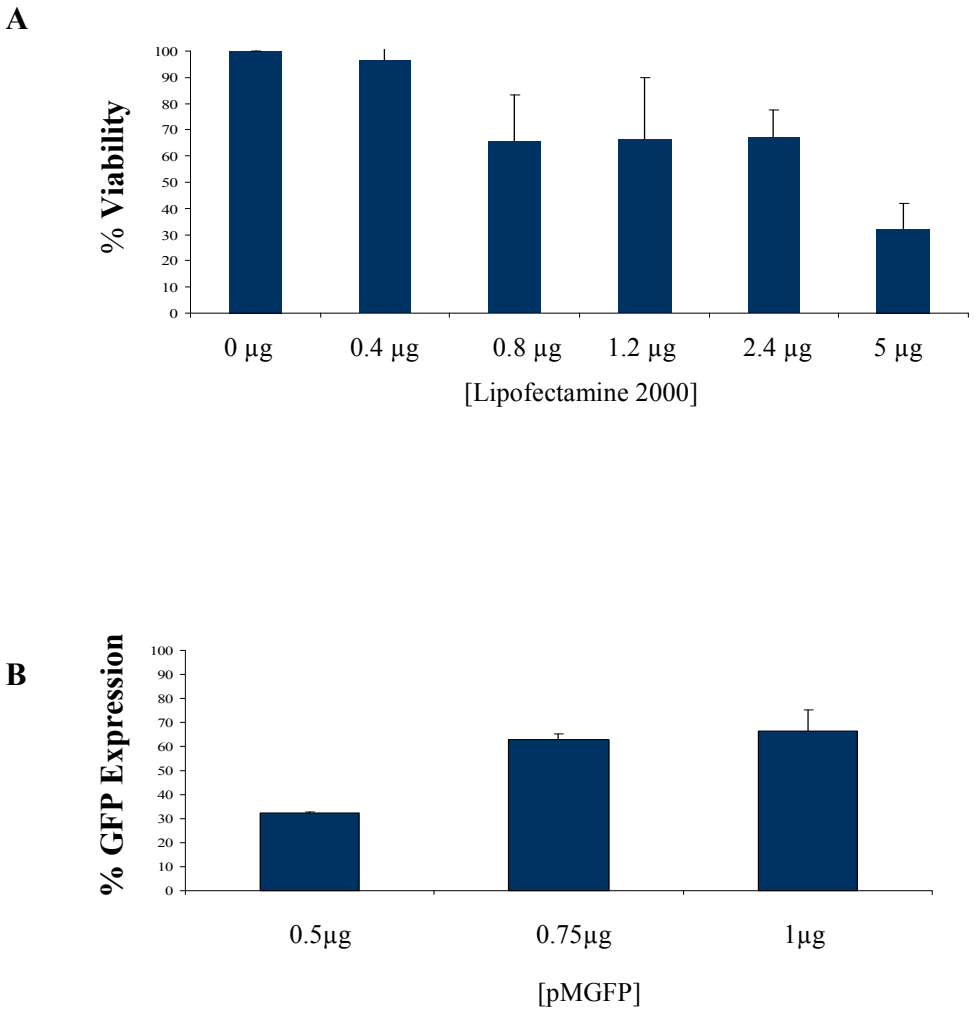

Figure 5.3: Optimisation of Lipofectamine 2000

A) A549 cells were treated with Lipofectamine 2000 to establish a range which was not toxic to the cells. The graph represents % viability after treatment with increasing concentrations of lipid, as determined by cell counts. B) 0.4 µl Lipofectamine 2000 was complexed with 0.5, 0.75 or 1ug of pMGFP to establish the ratio that results in the high transfection efficiency. The graph represents % GFP expression from varying ratios of Lipofectamine 2000 and pMGFP plasmid for n=2 experimental repeats.

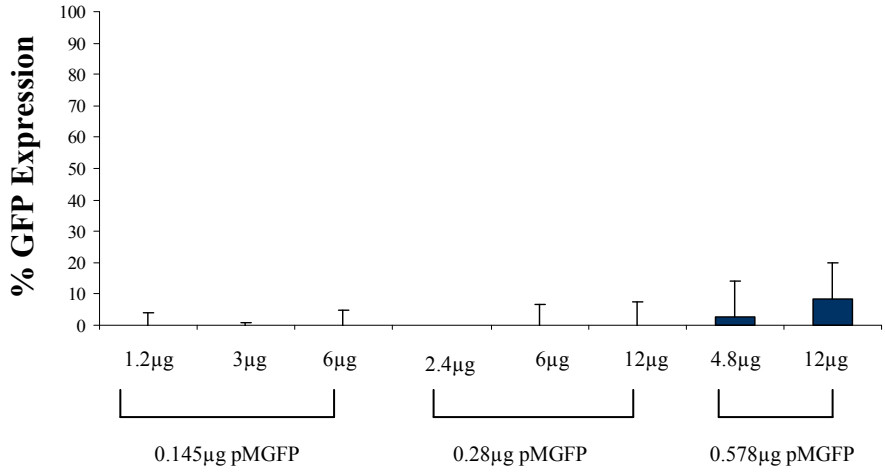

Figure 5.4: Optimisation of Superfect

Varying concentrations of Superfect and pMGFP were complexed together to establish the ratio which resulted in the highest transfection efficiency. The graph represents the percentage of cells expressing GFP for n=2 experimental repeats.

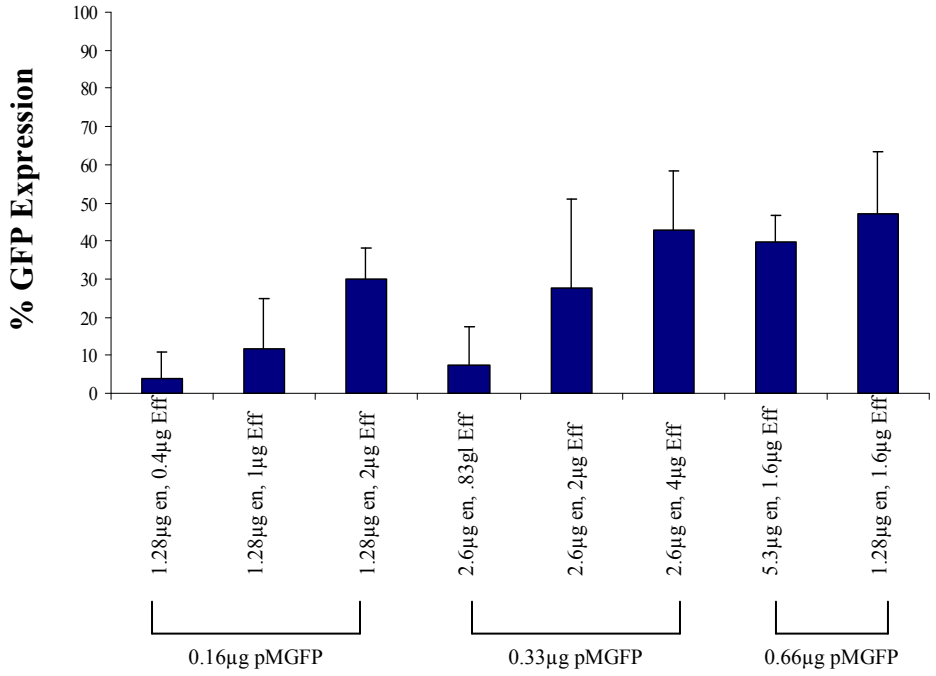

Figure 5.5: Optimisation of Effectene

Varying concentrations of Effectene (Eff), Enhancer (En) and pMGFP were complexed together to establish the ratio which resulted in the highest transfection efficiency. The graph represents the percentage of cells expressing GFP for n=2 experimental repeats.

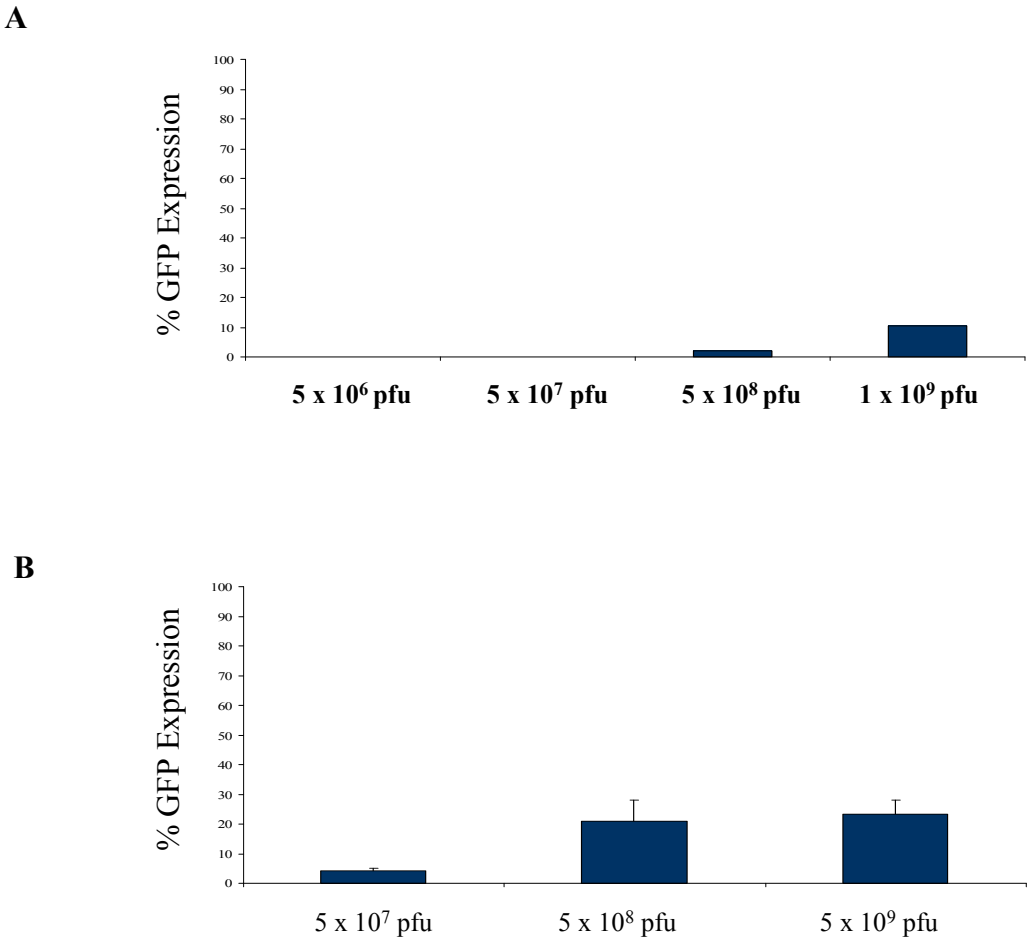

Figure 5.6: AAV optimisation

A549 cells, at low and high confluency, were transfected with a range of AAV2 virus to establish the optimum concentration. The efficiency of transfection was measured by flow cytometry. A) A wide range of AAV2 plaque forming units (pfu) were used to transfect a high confluency monolayer. B) A narrower range of AAV2 concentrations were utilised to transfect a sub-confluent monolayer of epithelial cells for n=2 experimental repeats.

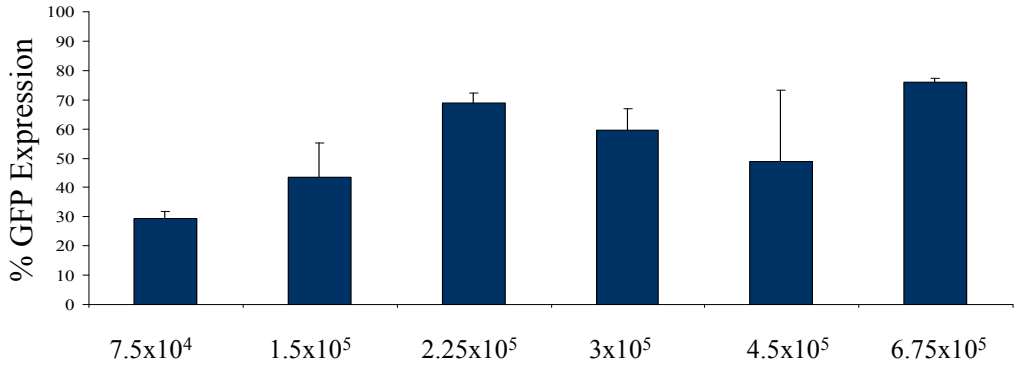

Figure 5.7: Lentivirus optimisation

A range of HIV-VSV-G lentivirus was transfected into a sub-confluent layer of BEAS-2B cells to determine the optimal range of lentivirus concentration for n=2 experimental repeats.

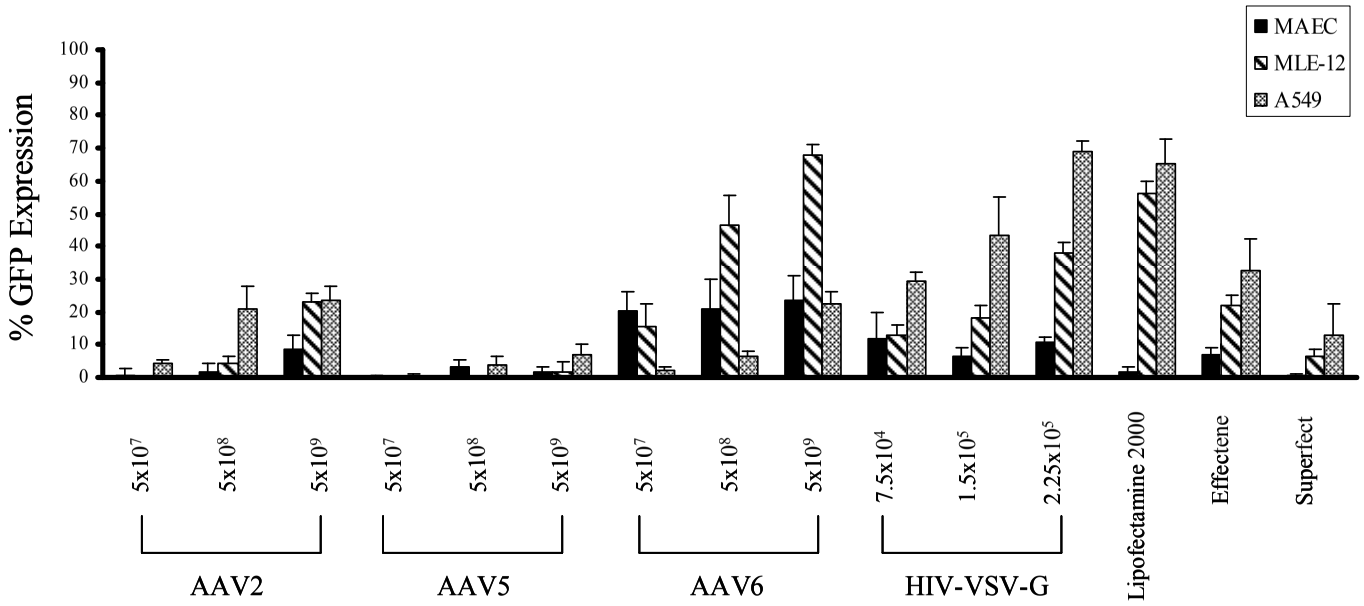

Figure 5.8: Day 1 % GFP transfection

Transfection efficiencies of viral and non-viral vectors delivery to MEACs, MLE-12 cells and BEAS-2B cells were measured by flow cytometry. Percentage of cells expressing GFP were measured at 24 hrs post transfection for n=3 experiments.

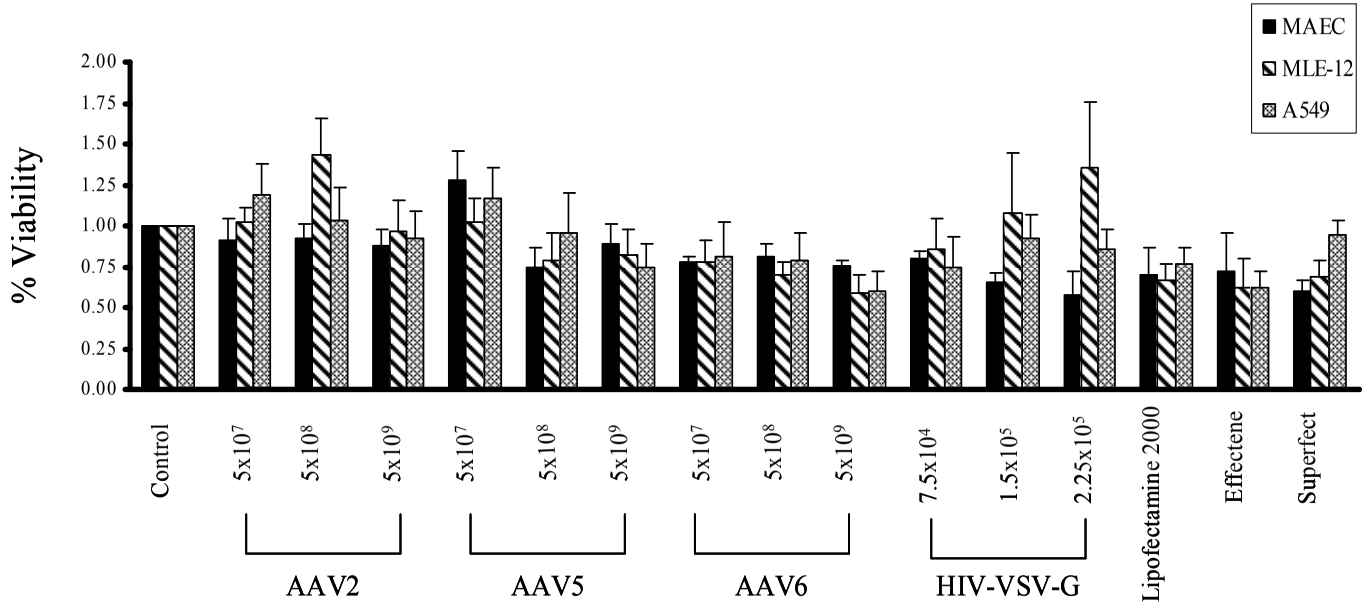

Figure 5. 9: Day 1 % viability

Levels of toxicity caused by viral and non-viral vectors delivery to MEACs, MLE-12 cells and BEAS-2B cells were measured by EBAO cell counts. Cell viability, as an indicator of toxicity, was represented as a percentage of untreated control 24 hrs post transfection for n=3 experimental repeats.

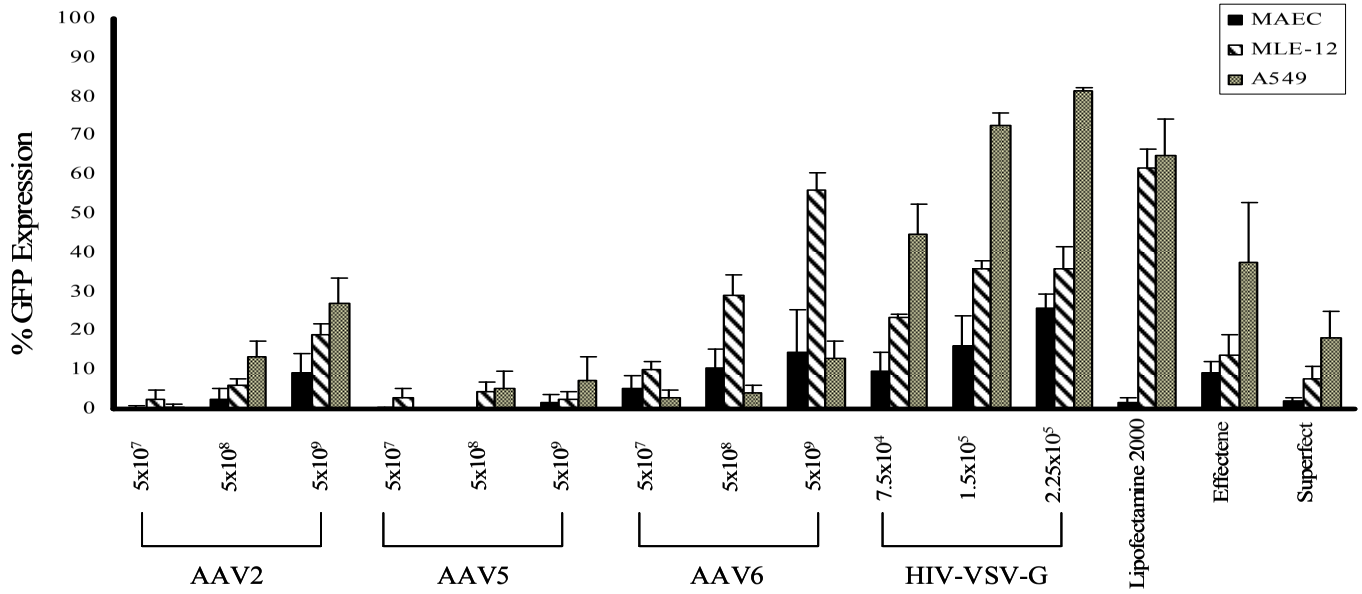

Figure 5.10: Day 2 % GFP expression

Transfection efficiencies of viral and non-viral vectors delivery to MEACs, MLE-12 cells and BEAS-2B cells were measured by flow cytometry. Percentage of cells expressing GFP were measured at 48 hrs post transfection for n=3 experiments.

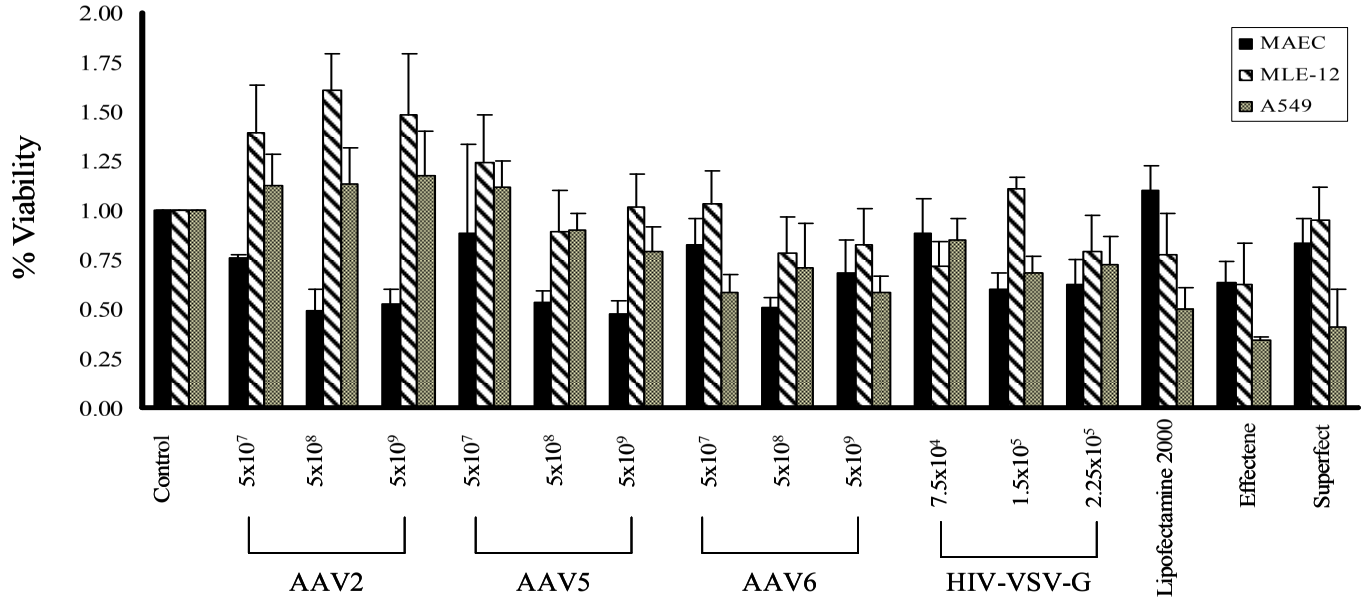

Figure 5.11: Day 2 % viability

Levels of toxicity caused by viral and non-viral vectors delivery to MEACs, MLE-12 cells and BEAS-2B cells were measured by EBAO cell counts. Cell viability, as an indicator of toxicity, was represented as a percentage of untreated control 48 hrs post transfection for n=3 experimental repeats.

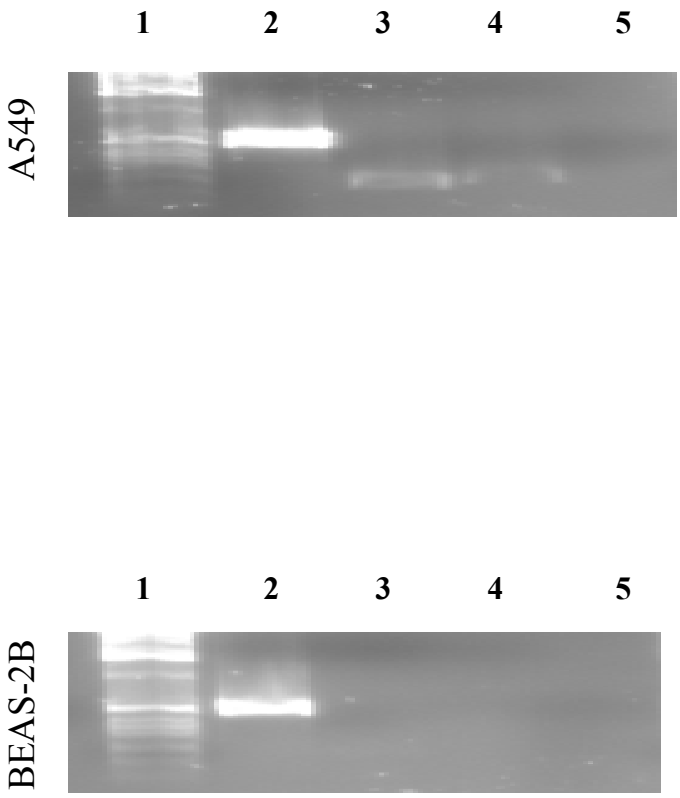

Figure 6.1: BMPR-IB endogenous mRNA expression in A549 and BEAS-2B

RT-PCR analysis was carried out utilising two independent sets of primers to verify the endogenous expression of BMPR-IB in the A549 and BEAS-2B cell lines. Lane 1- 1kb DNA ladder. Lane 2- GAPDH. Lane 3- BMPR-IB internal primer set 1. Lane 4 BMPR-IB internal primer set 2. Lane 5- no cDNA control.

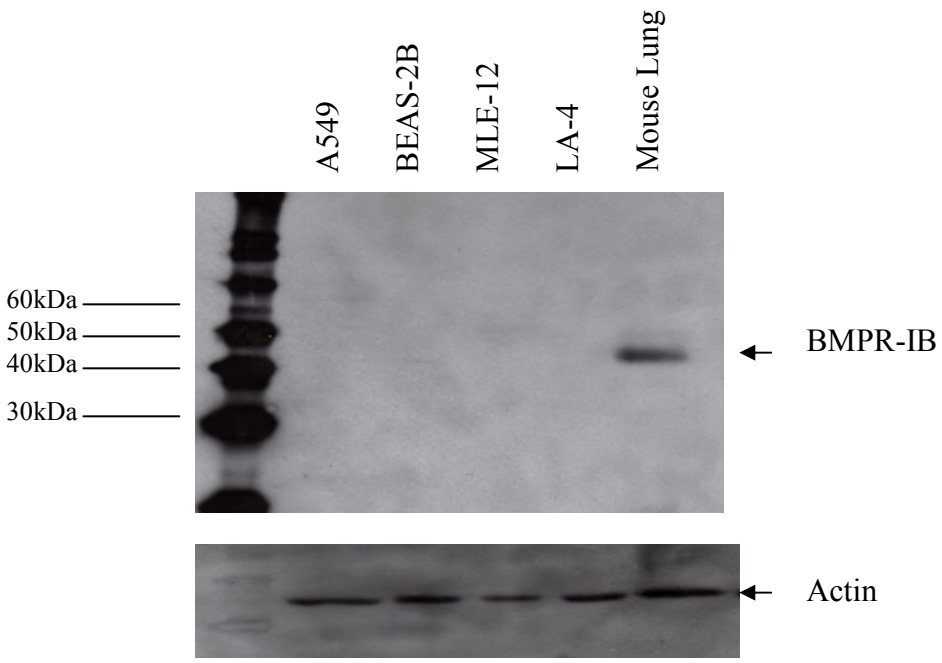

Figure 6.2: BMPR-IB endogenous protein expression

Western blot analysis was carried out using 1:100 dilution of anti-BMPR-IB antibody (R&D Systems) to detect endogenous expression of BMPR-IB protein in A549, BEAS-2B, MLE-12, LA-4 cells lines and mouse lung protein.

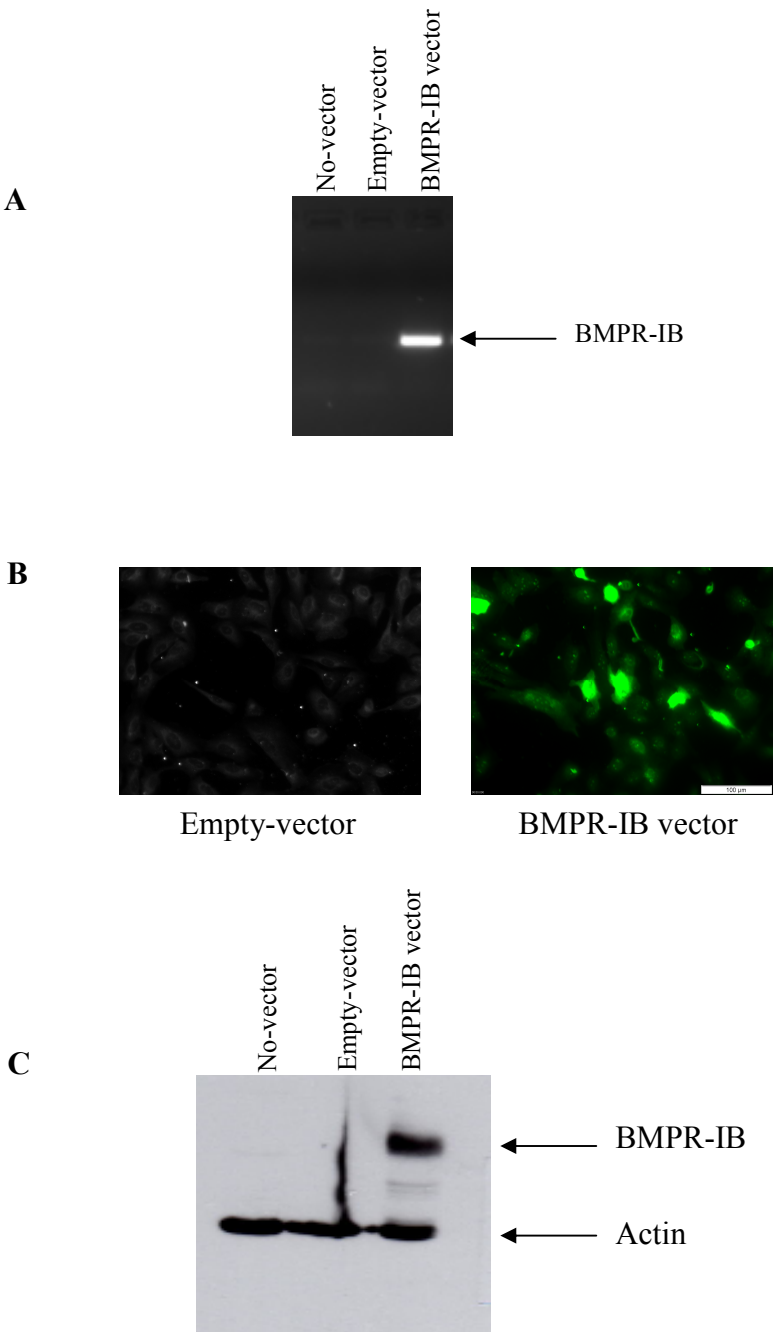

Figure 6.3: Validation of BMPR-IB over expression in BEAS-2B cells

BMPR-IB-pcDNA4 plasmid was transiently transfected into BEAS-2B cell line using Lipofectamine 2000 reagent. Cells were harvested at Day 1. A) RT-PCR was carried out to identify mRNA expression using BMPR-IB internal primer set 1 B) Immunofluorescence using anti-myc (1:1000) antibody and C) Western blot using anti-myc antibody (1:1000) was used to validate the protein over expression

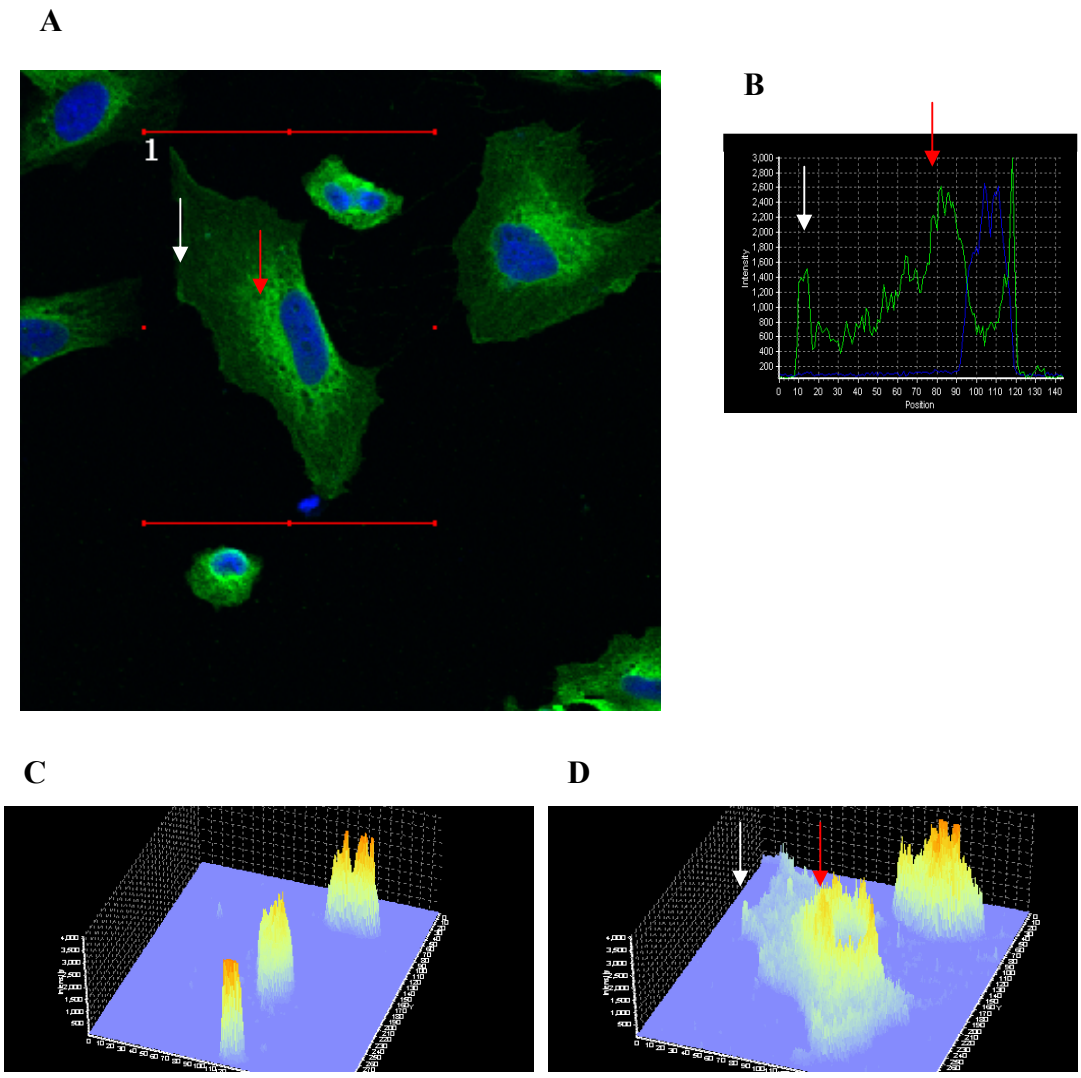

Figure 6.4: BMPR-IB localisation in BEAS-2B cells

Confocal immunofluorescent photomicrographs were taken of BMPR-IB-pcDNA4, detected by anti-myc tag antibody. A) Green fluorescence represents BMPR-IB protein localisation, blue fluorescence represents DAPI nuclear counter stain. B) 2D graph identifies the localisation of BMPR-IB (green line) and the nucleus (blue line) through one position in the cell. C) 3D graph of DAPI nuclear counter stain for the area inside the red box in A. D) 3D image was taken of BMPR-IB localisation, for the area inside the red box in A. White arrow indicates cell membrane localised BMPR-IB expression, red arrow represents possible endoplasmic reticulum localisation.

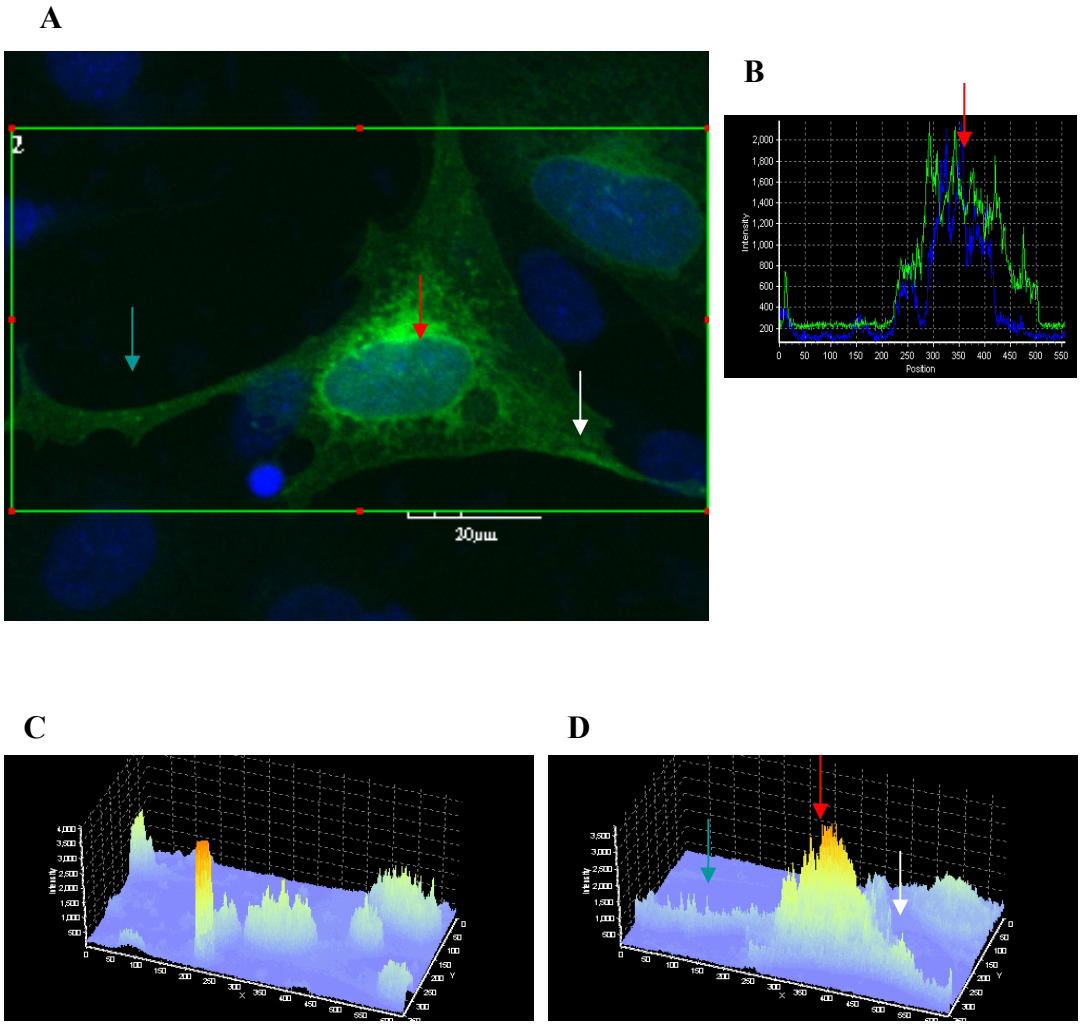

Figure 6.5: The effects of BMP4 ligand stimulation on BMPR-IB localisation in BEAS-2B

Confocal microscopy was carried out on cells transfected with BMPR-IB-pcDNA4 and stimulated with BMP4 ligand (100ng/ml). A) Green fluorescence represents BMPR-IB protein localisation, blue fluorescence represents DAPI nuclear counter stain. B) 2D graph identifies the localisation of BMPR-IB (green line) and the DNA (blue line) through one position in the cell. C) 3D graph of DAPI nuclear counter stain for the area inside the green box in A. D) 3D graph of BMPR-IB localisation, for the area inside the green box in A. Arrows highlight BMPR-IB staining at the cell membrane (white arrow), nucleus (red arrow), filipodia of cell (blue arrow).

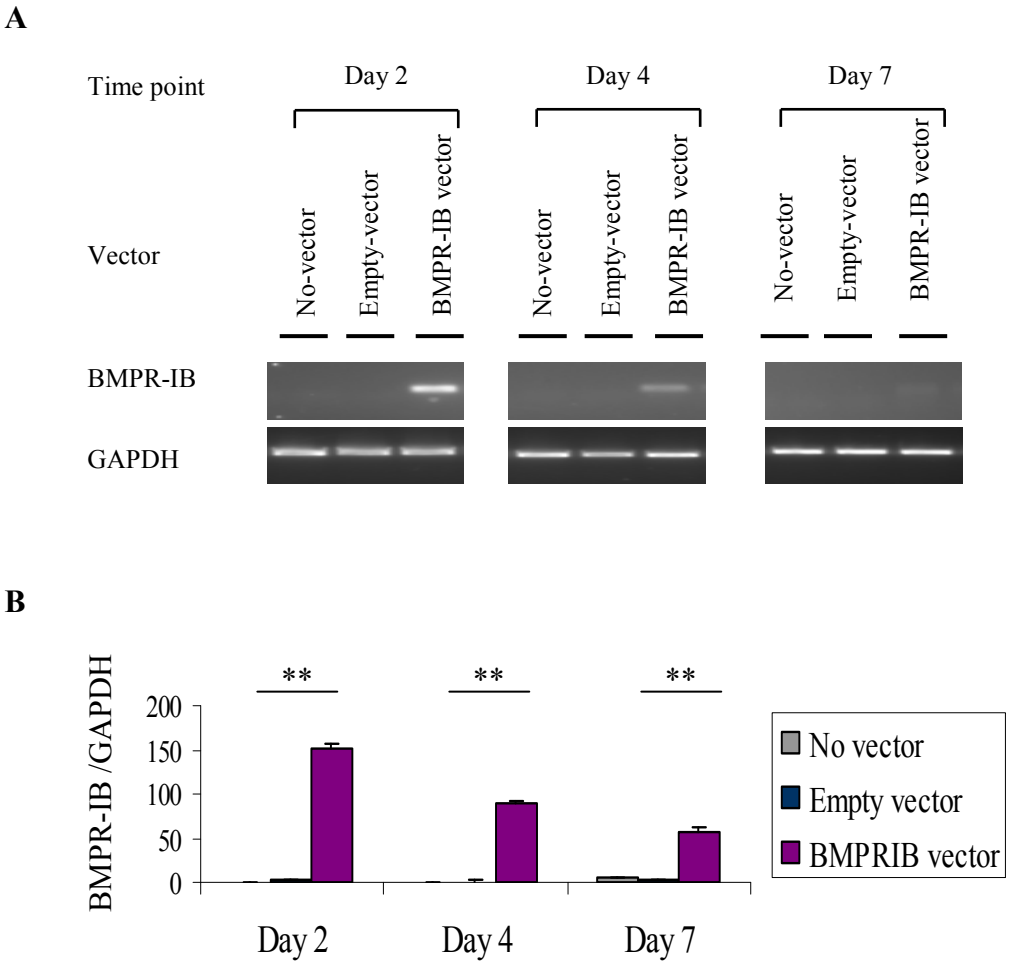

Figure 6.6: Duration of BMPR-IB mRNA expression in BMPR-IB-pcDNA4 transfected BEAS-2B cells

A time course experiment was set up to establish the duration of expression of BMPR-IB-pcDNA4 from a transient transfection in the BEAS-2B cell line. A) RT-PCR was carried out on no-vector control cells, empty-vector control cells and BMPR-IB expressing cells on day 2, 4, 7 post transfection. B) Densitometry values show the level of mRNA over expression over the time course, relative to day 2 untreated control cells. * $p < 0.05$ (results represent the average of 2 experimental repeats).

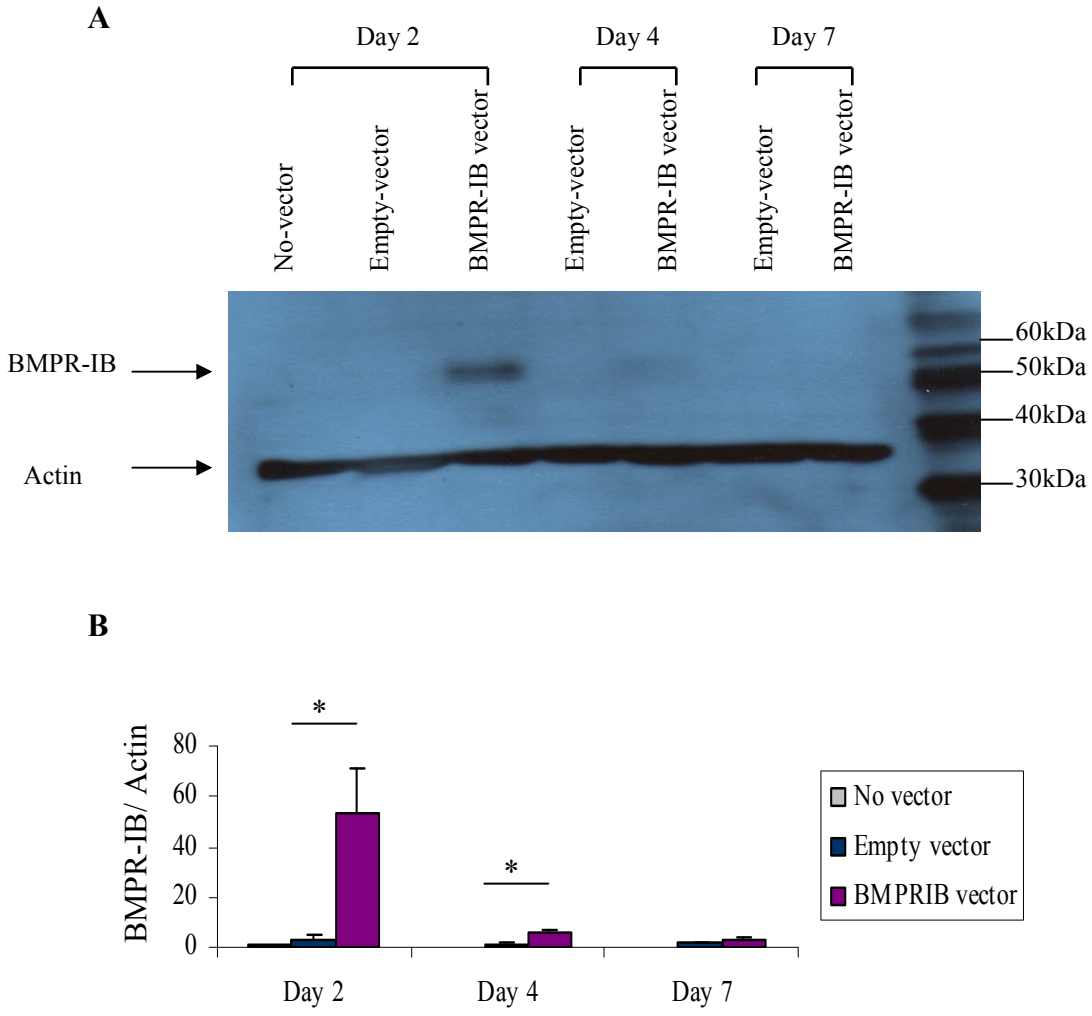

Figure 6.7: Duration of BMPR-IB protein expression in BMPR-IB-pcDNA4 transfected BEAS-2B cells

A time course experiment was set up to establish the duration of expression of BMPR-IB-pcDNA4 from a transient transfection in the BEAS-2B cell line. A) Western blot analysis was carried out on no-vector control cells, empty-vector control cells and BMPR-IB-pcDNA4 over expression cells on day 2, 4, and 7 post transient transfection, using anti-myc antibody. B) Densitometry values show the level of over expression of the plasmid over the time course, relative to day 2 untreated control cells. * $p < 0.05$ (The results represent the average of 2 experimental repeats)

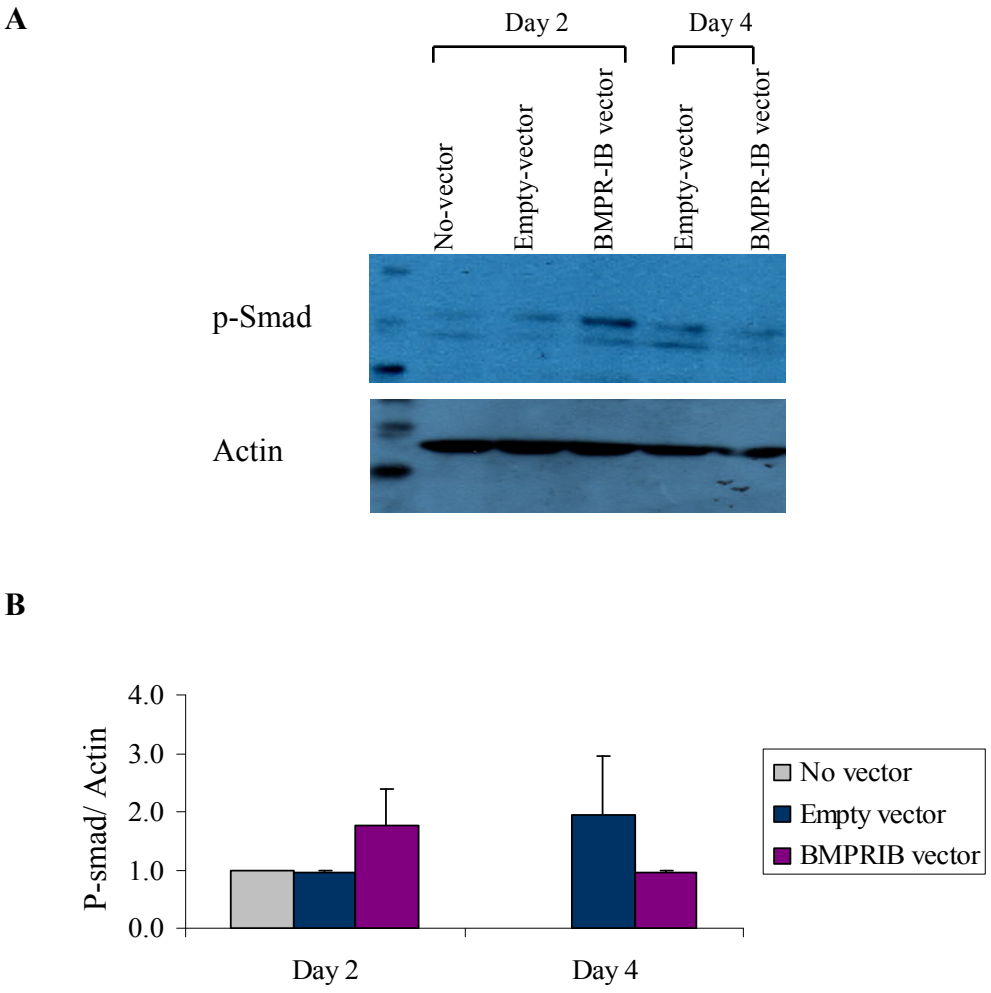

Figure 6.8: p-Smad protein expression in BMPR-IB-pcDNA4 transfected BEAS-2B cells

Analysis of p-Smad expression by Western blot analysis was carried out on day 2 and 4 post BMPR-IB-pcDNA4 transfection. A) Western blot represents p-Smad expression in no-vector control, empty-vector control and BMPR-IB expressing cells. B) p-Smad expression was normalised to actin. p-Smad expression is relative to day 2 untreated control cells for n=3 experimental repeats.

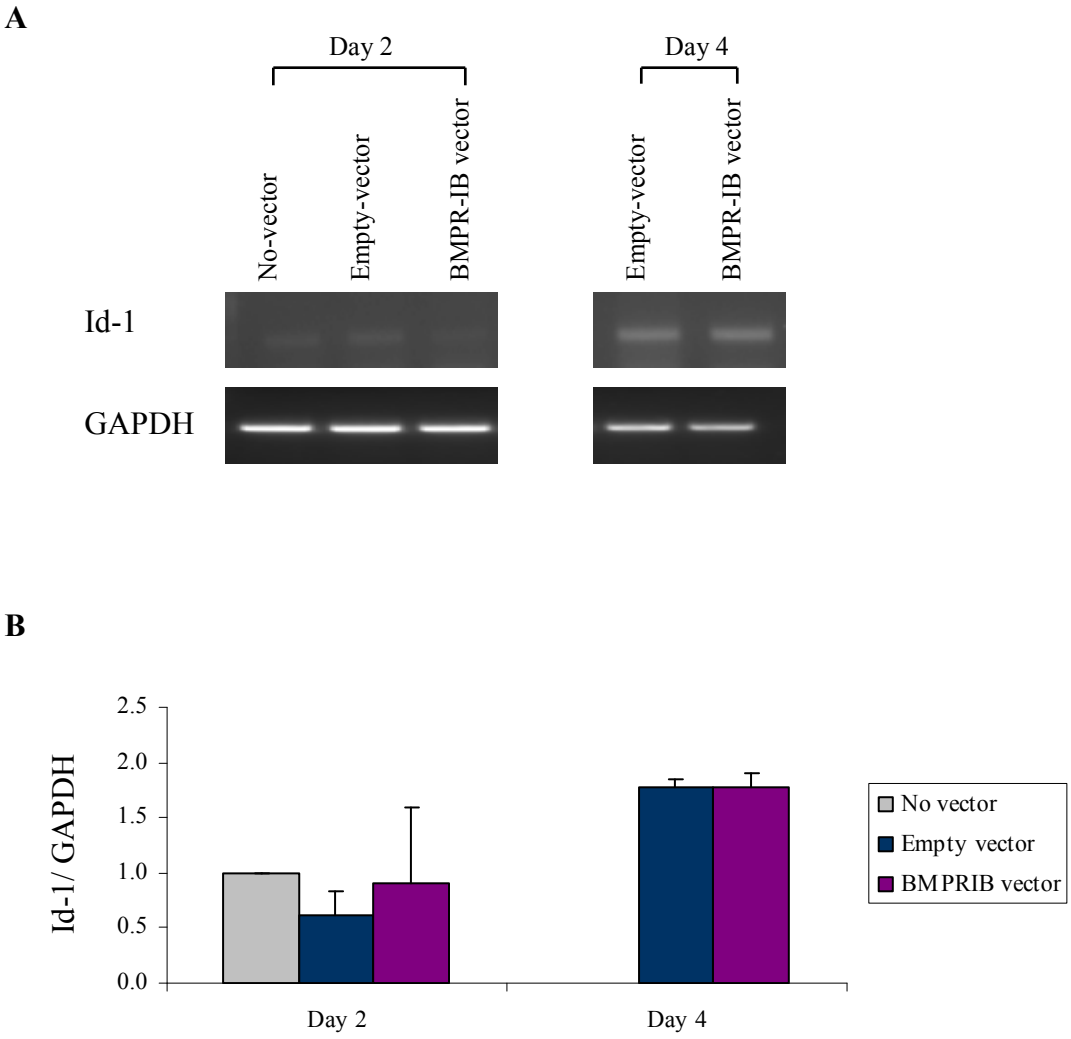

Figure 6.9: Id-1 expression in BMPR-IB-pcDNA4 transfected BEAS-2B cells

Analysis of Id-1 expression by RT-PCR was carried out on day 2 and 4 post transfection. A) DNA electrophoresis gel represents Id-1 expression in no-vector control, empty-vector control and BMPR-IB expression vector. B) Id-1 densitometry values were normalised to GAPDH for each sample. Id-1 expression for each treatment was expressed relative to day 2 untreated control for n=3 experimental repeats.

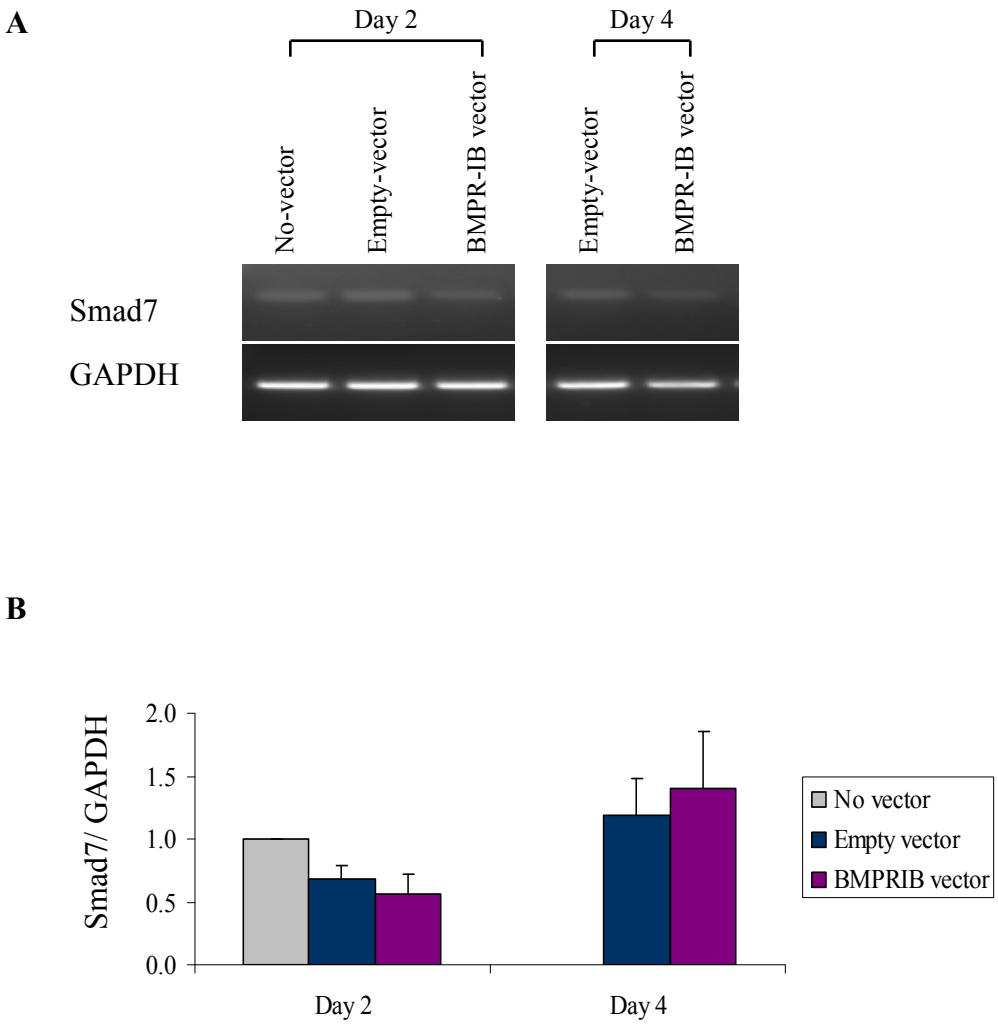

Figure 6.10: Smad7 expression in BMPR-IB-pcDNA4 transfected BEAS-2B cells

Analysis of Smad7 mRNA expression was carried out on day 2 and 4 post BMPR-IB-pcDNA4 transfection. A) DNA electrophoresis gel represents Smad7 expression in no-vector control, empty-vector control and BMPR-IB expression vector transfected cells. B) Densitometry values for Smad7 expression were normalised to GAPDH, and represented relative to no-vector day 2 control for n=3 experimental repeats.

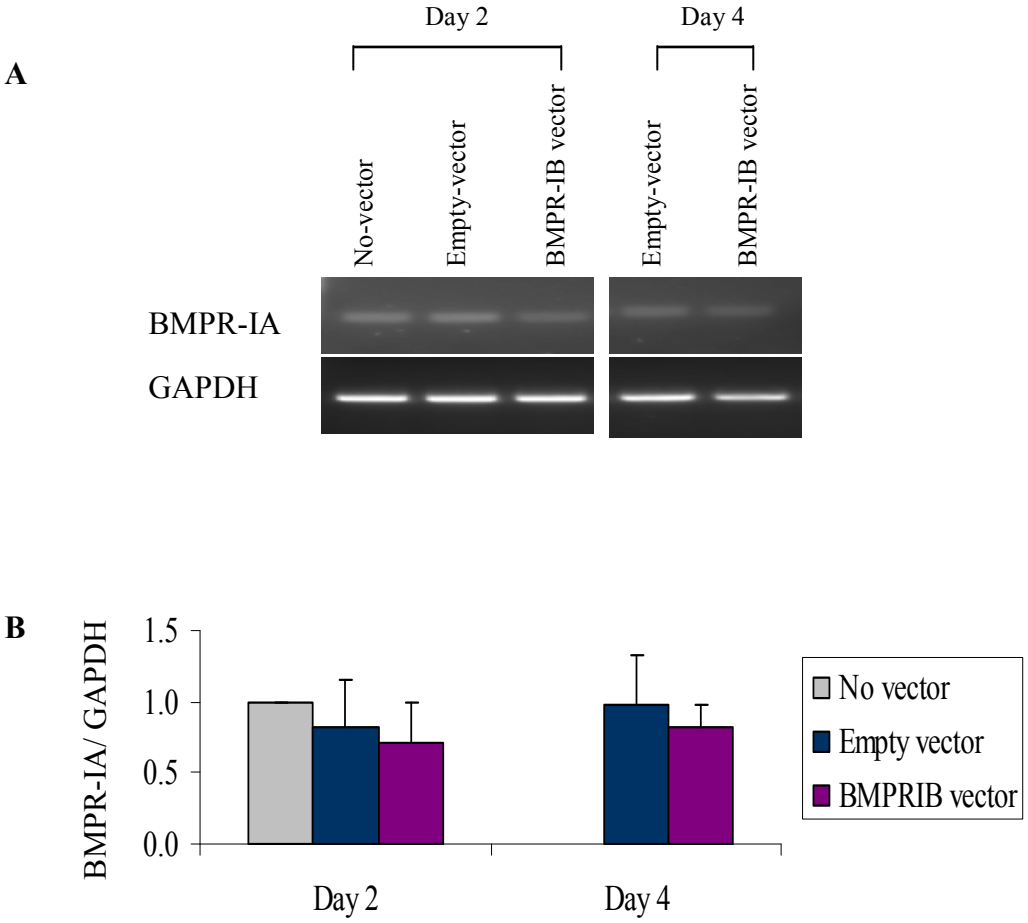

Figure 6.11: BMPR-IA expression in BMPR-IB-pcDNA4 transfected BEAS-2B cells

Analysis of BMPR-IA mRNA expression was carried out on day 2 and 4 post BMPR-IB-pcDNA4 transfection. A) DNA electrophoresis gel represents BMPR-IA expression in no-vector control, empty-vector control and BMPR-IB-pcDNA4 expressing cells. B) BMPR-IA densitometry values were normalised to GAPDH for each sample. BMPR-IA expression for each treatment is represented relative to day no-vector control cells for n=3 experimental repeats.

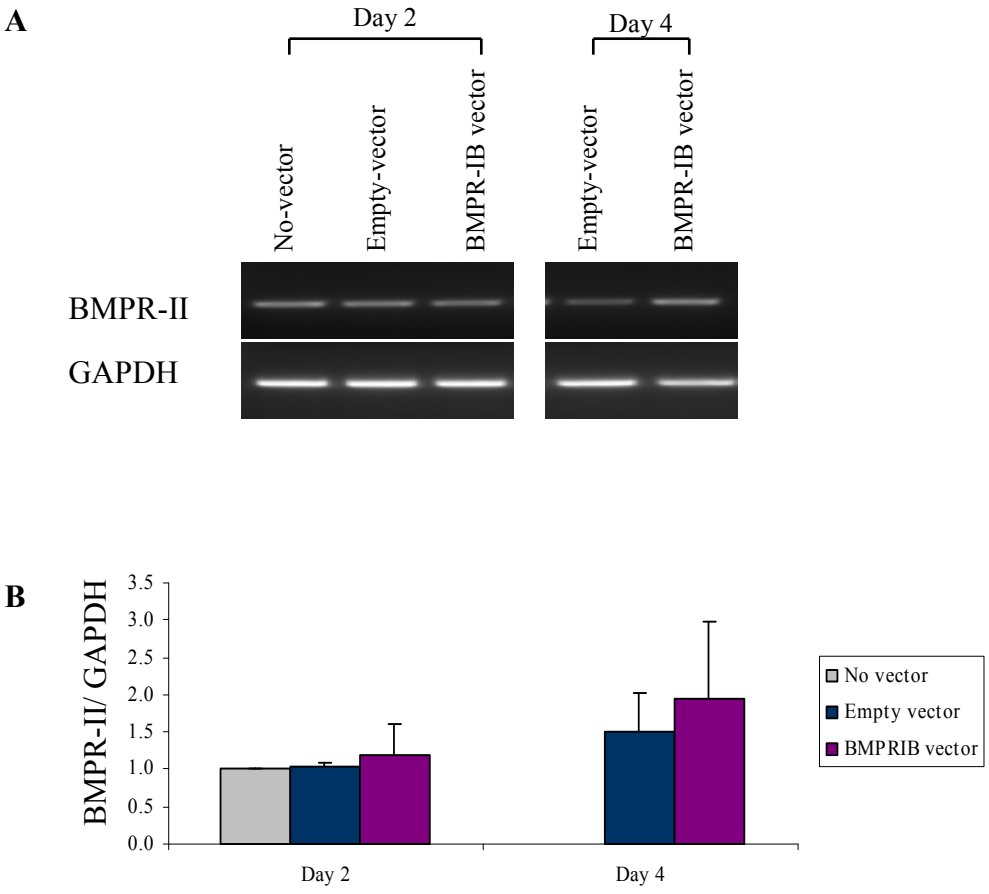

Figure 6.12: BMPR-II expression in BMPR-IB-pcDNA4 transfected BEAS-2B cells

Analysis of BMPR-II mRNA expression was carried out on day 2 and 4 post BMPR-IB-pcDNA4 transfection. A) DNA electrophoresis gel represents BMPR-II expression in no-vector control, empty-vector control and BMPR-IB-pcDNA4 transfected cells. B) Densitometry values for BMPR-II expression were normalised to GAPDH for each sample. BMPR-II expression was normalised to day 2 no-vector control cells for n=3 experimental repeats.

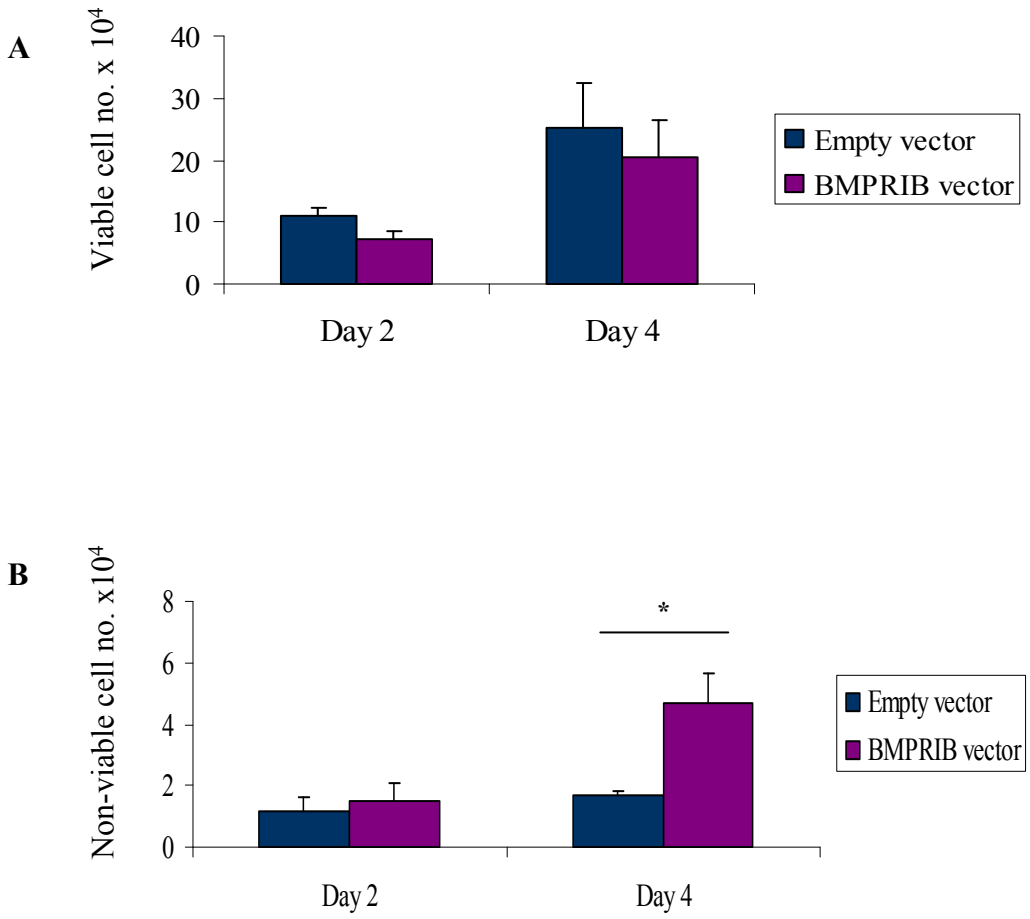

Figure 6.13: BMPR-IB-pcDNA4 expressing BEAS-2B cell counts

EBAO cell counts were carried out on BEAS-2B cells transfected with empty-vector and BMPR-IB-pcDNA4 over expression vector. A) Graph represents viable cells that were counted on day 2 and 4 post transfection. B) Graph represents non-viable cells counted on days 2 and 4 post transfection. Results represent n=3 experimental repeats. * $p < 0.05$

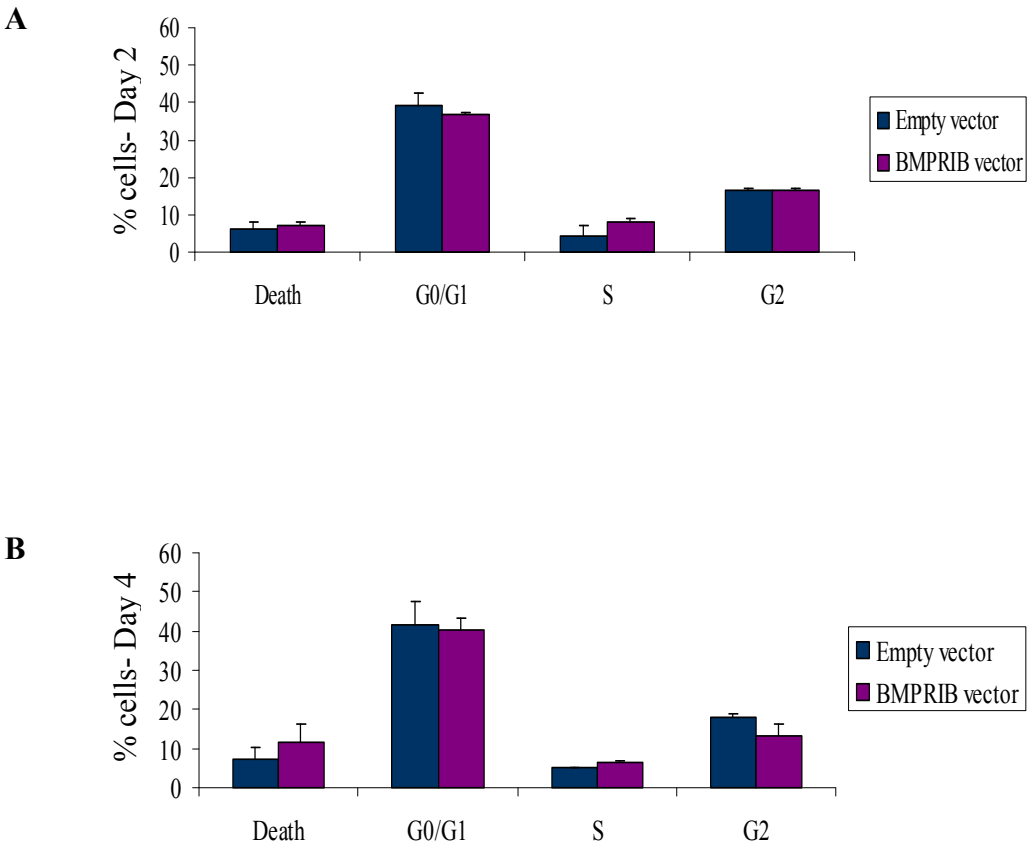

Figure 6.14: Cell cycle analysis of BMPR-IB-pcDNA transfected cells

Flow cytometry analysis was carried out on propidium iodide stained cells from empty-vector control and BMPR-IB-pcDNA4 transfected BEAS-2B cells. Graphs represent analysis of A) Day 2 and B) Day 4 cell cycle progression post transfection. (Graphs represent minimum n=2)

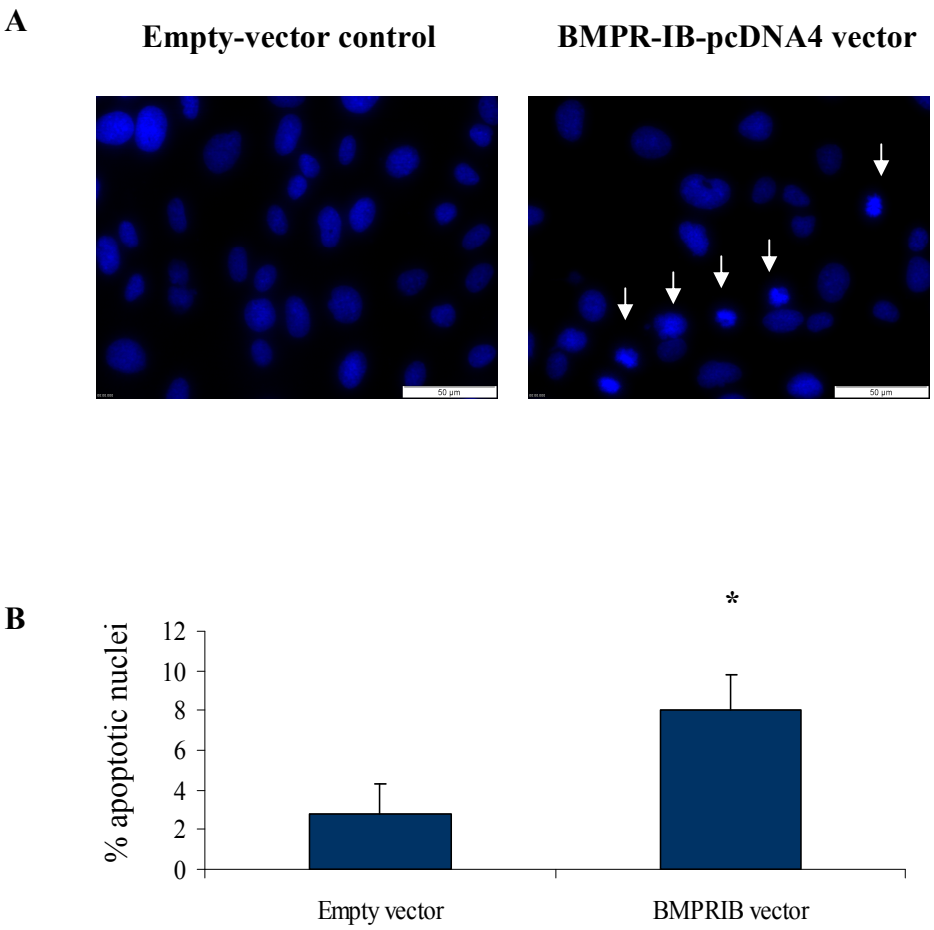

Figure 6.15 : BMPR-IB expression results in an increase in apoptotic cells

40x photomicrographs were taken of DAPI staining of BEAS-2B cells transfected with empty-vector control and BMPR-IB vector control. An increase in apoptotic nuclei is apparent in BMPR-IB transfected cells. Arrows indicate apoptotic nuclei. Graph represents an average of % apoptotic nuclei taken from 3 photomicrographs from 3 independent experiments. * $p < 0.05$

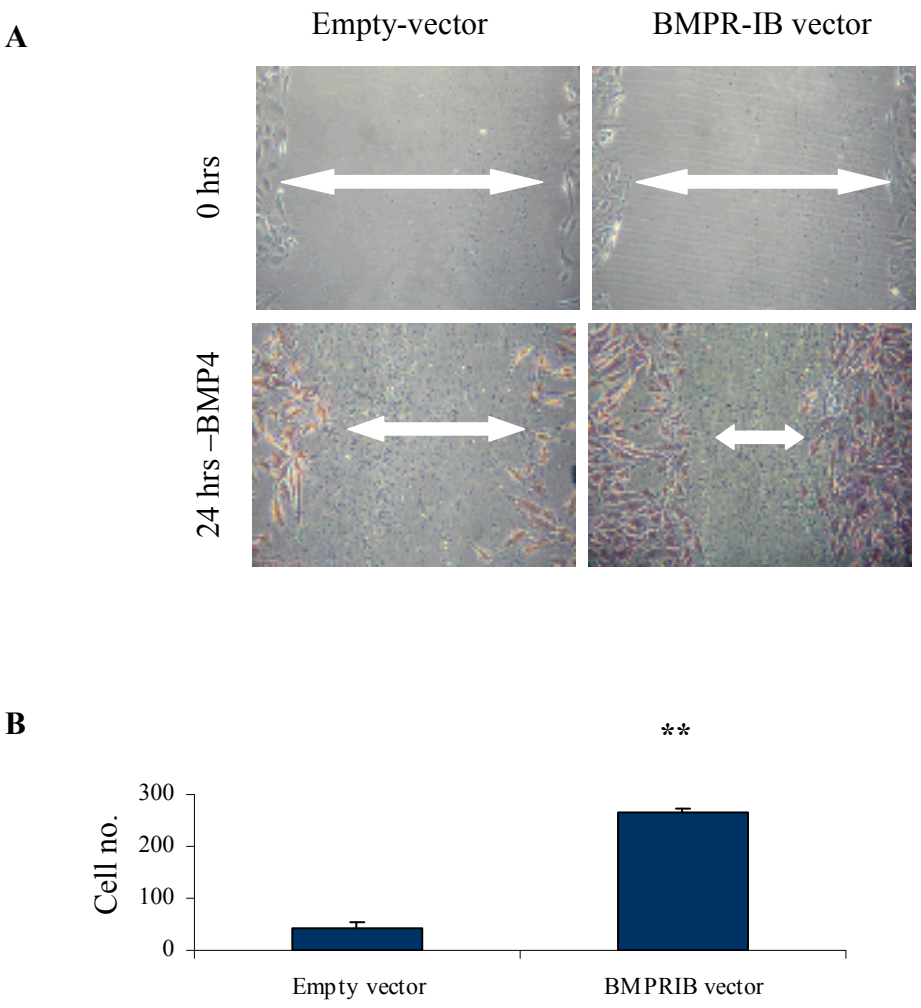

Figure 6.16: Motility of BMPR-IB-pcDNA4 transfected BEAS-2B cells

A) Phase-contrast photomicrographs demonstrate the rate of migration into the denuded area in empty-vector control cells and BMPR-IB expressing cells 0hrs when the area was initially denuded and 24 hrs post denuding. Cell numbers that had migrated into the denuded area were counted after 24 hours cultured in defined serum free media. B) The graph represents cell counts that were carried out on the cells which had migrated into the denuded area. The graph represents n=2. ** $p < 0.01$

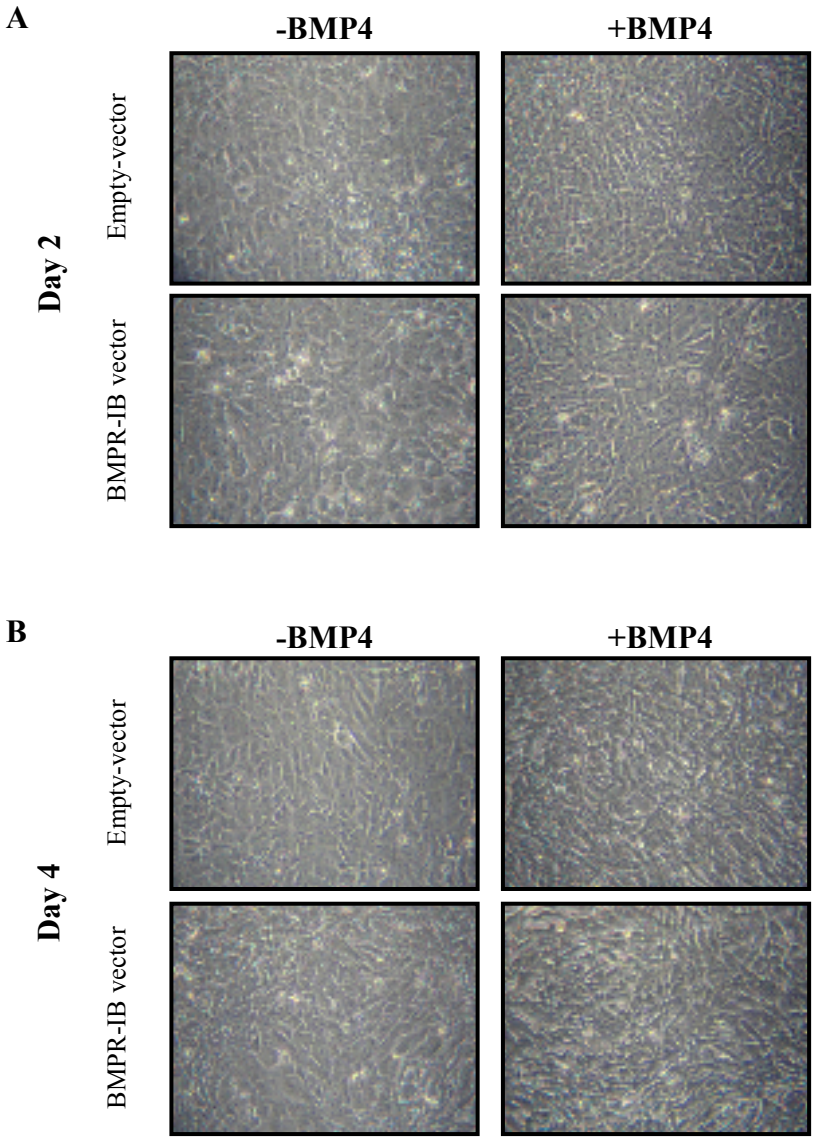

Figure 6.17: Cell morphology of BMPR-IB-pcDNA4 transfected BEAS-2B cells in the absence or presence of BMP4 ligand

BEAS-2B cells were transfected with empty-vector control or BMPR-IB-pcDNA4 expression vector. Cells were grown in DSFM in the presence (+ BMP4) or absence (- BMP4) of 100ng/ml BMP4 ligand. Phase contrast photomicrographs were taken on (A) day 2 or (B) day 4, post transfection.

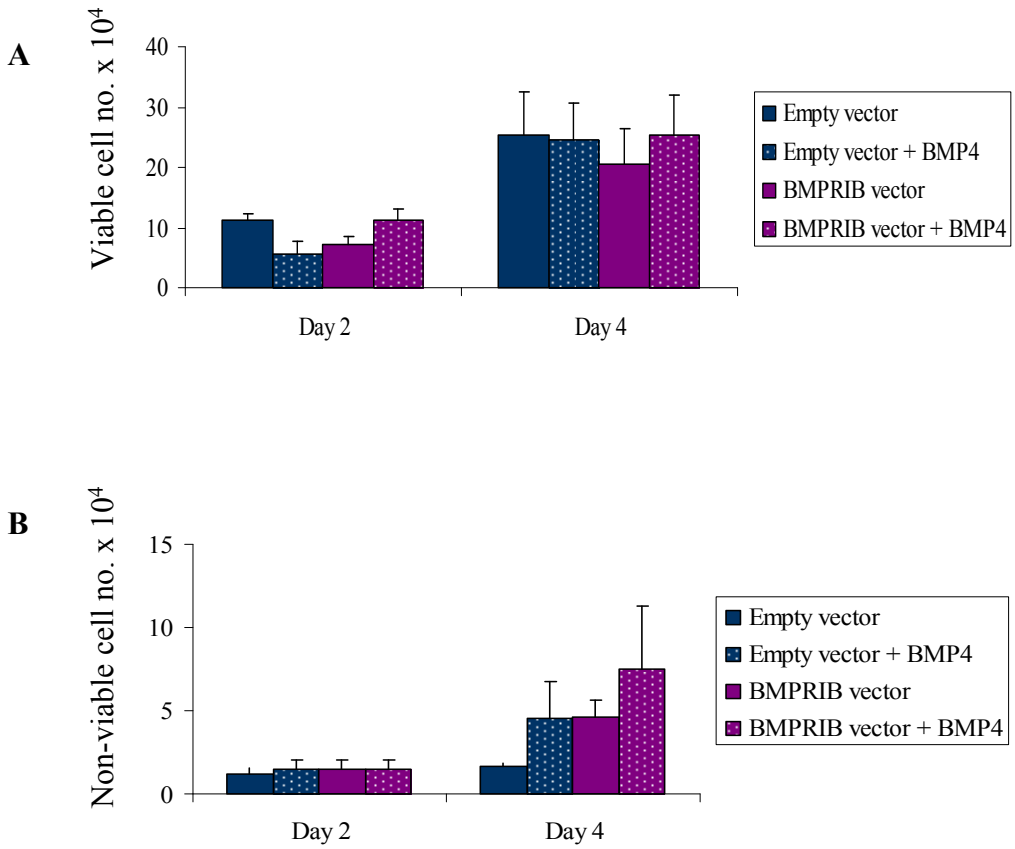

Figure 6.18: Cell counts for BMPR-IB-pcDNA4 transfected BEAS-2B cells in the presence or absence BMP4 ligand

EBAO cell counts were carried out on BEAS-2B cells transfected with empty-vector and BMPR-IB-pcDNA4 expression vector in the absence or presence of BMP4 ligand. A) Graph represents viable cell counts on day 2 and day 4 post transfection. B) Graph represents non-viable cells counted on day 2 and day 4 post transfection. Results represent n=3 experimental repeats.

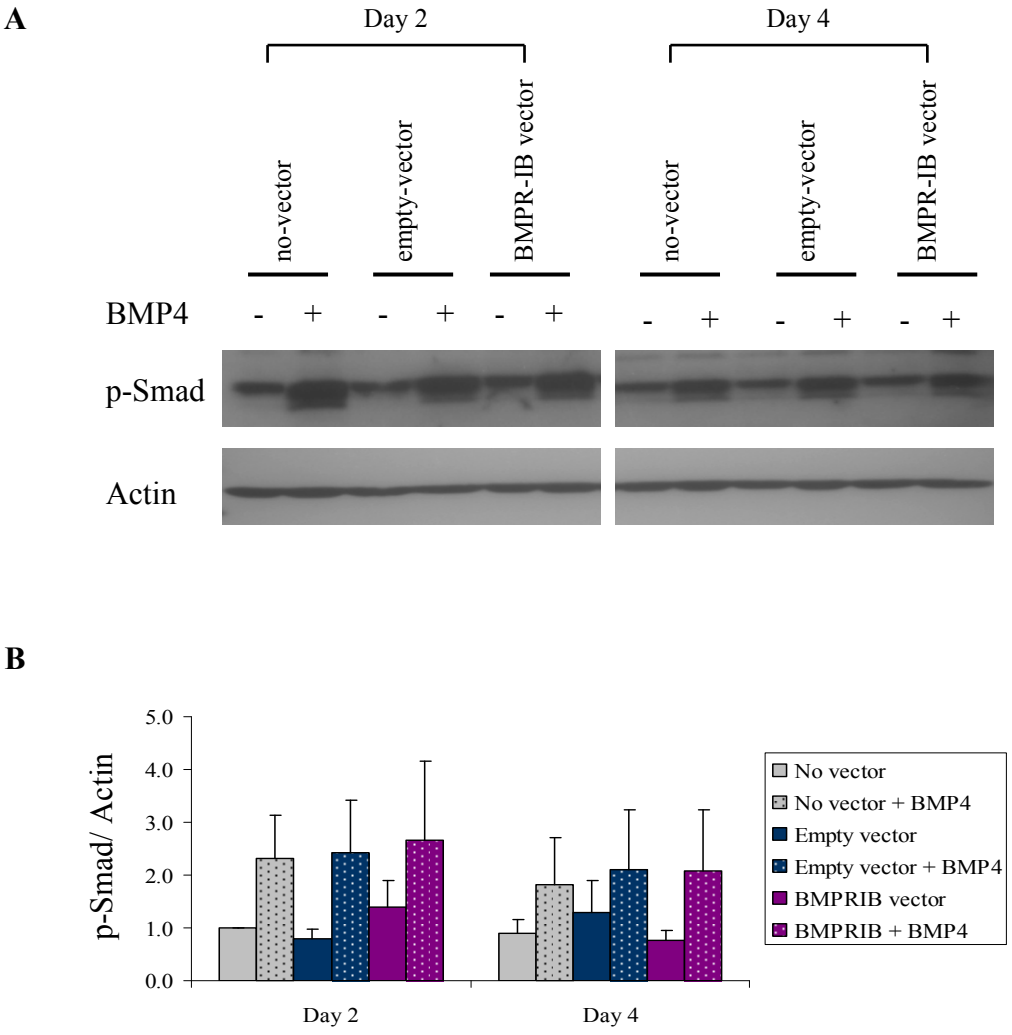

Figure 6.19: p-Smad protein expression in BMPR-IB-pcDNA4 transfected BEAS-2B cells in the presence or absence of BMP4 ligand

Western blot analysis was carried out on protein extracted from BEAS-2B cells transfected with no-vector control, empty-vector control or BMPR-IB-pcDNA4, and cultured in the absence or presence of BMP4 ligand. A) Western blot image representing p-Smad expression. B) Densitometry results for p-Smad expression. p-Smad expression for each sample was normalised to actin. The quantity of p-Smad was represented relative to day 2 no-vector control. The graph represents n=3 experimental repeats.

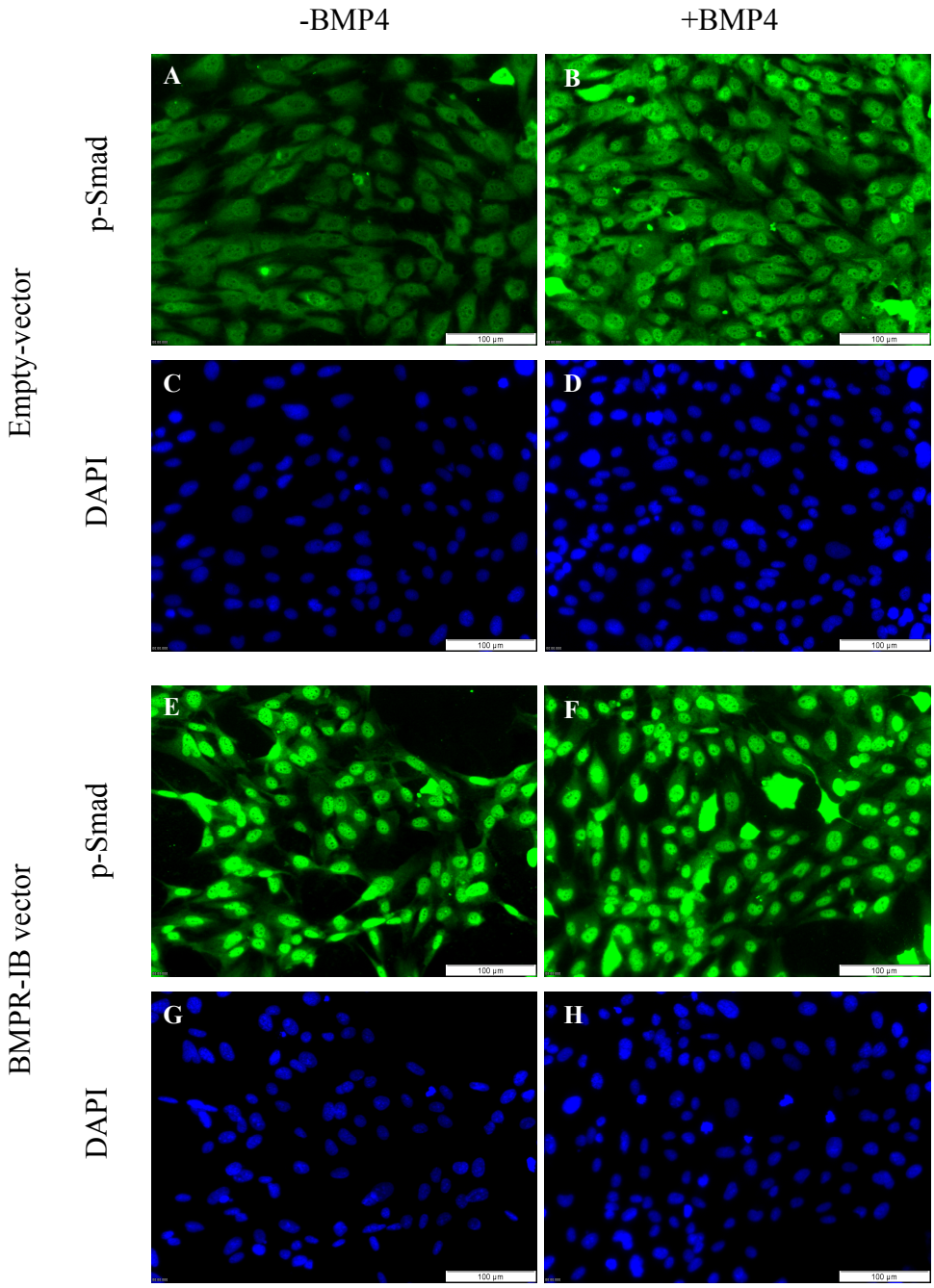

Figure 6.20: p-Smad localisation in BMPR-IB-pcDNA4 transfected BEAS-2B cells cultured in the absence or presence of BMP4 ligand

Immunofluorescence analysis of: A) p-Smad expression in empty-vector transfected cells in the absence (-BMP4) of BMP4 ligand. B) p-Smad expression in empty-vector transfected cells in the presence (+ BMP4) of BMP4 ligand. E) p-Smad expression in BMPR-IB-pcDNA4 transfected cells in absence of BMP4 ligand. F) p-Smad expression in BMPR-IB-pcDNA4 transfected cells in the presence of BMP4 ligand. C, D, G, H represent DAPI nuclear counter stained cells.

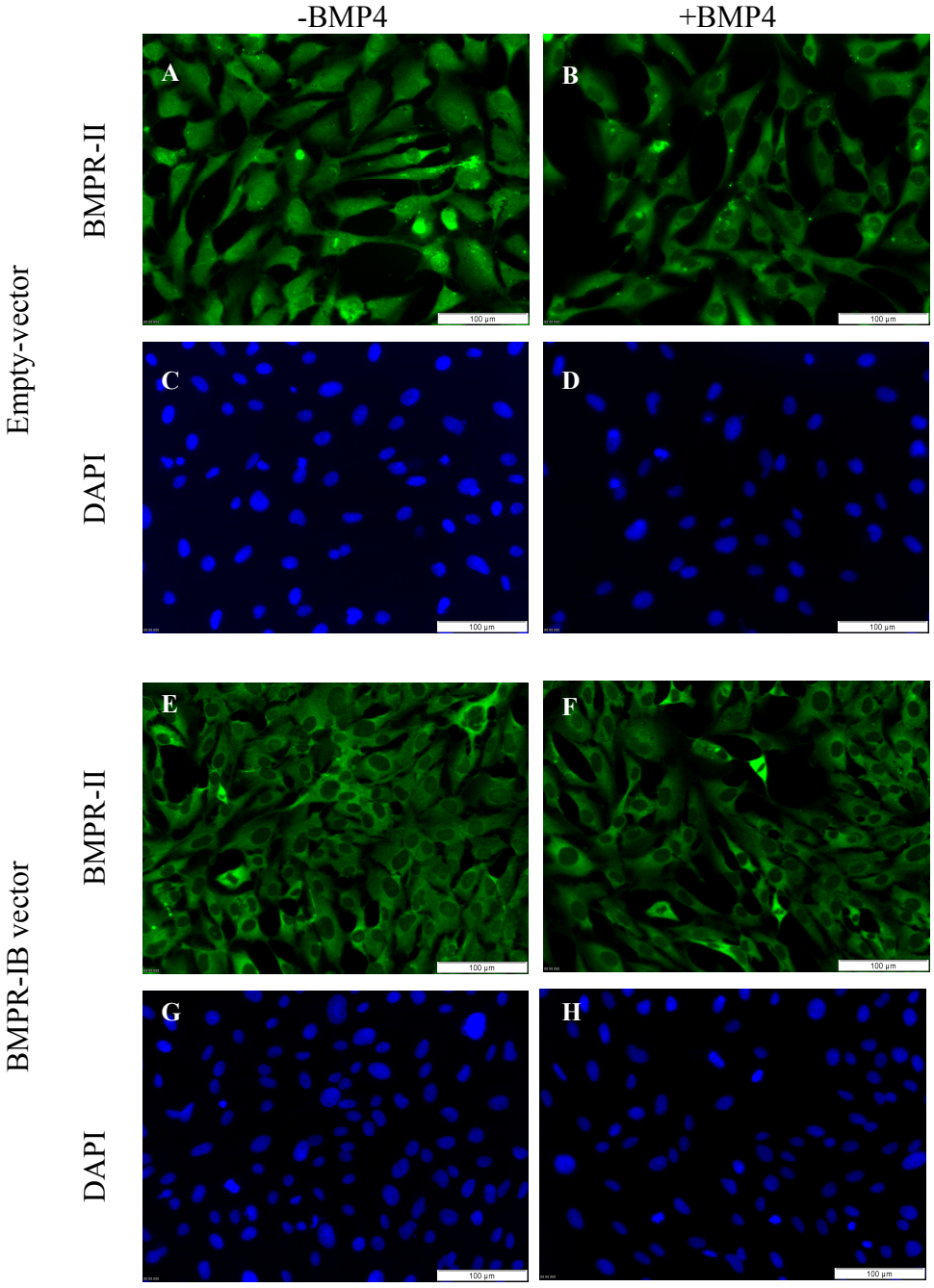

Figure 6.21: BMPR-II localisation in BMPR-IB expressing BEAS-2B cells cultured in the absence or presence of BMP4 ligand

Immunofluorescence analysis of: A) BMPR-II expression in empty-vector transfected cells in the absence (-BMP4) of BMP4 ligand. B) BMPR-II expression in empty-vector transfected cells in the presence (+BMP4) of BMP4 ligand. E) BMPR-II expression in BMPR-IB-pcDNA4 transfected cells in absence of BMP4 ligand. F) BMPR-II expression in BMPR-IB-pcDNA4 transfected cells in the presence of BMP4 ligand. C, D, G, H represent DAPI nuclear counter stained cells.

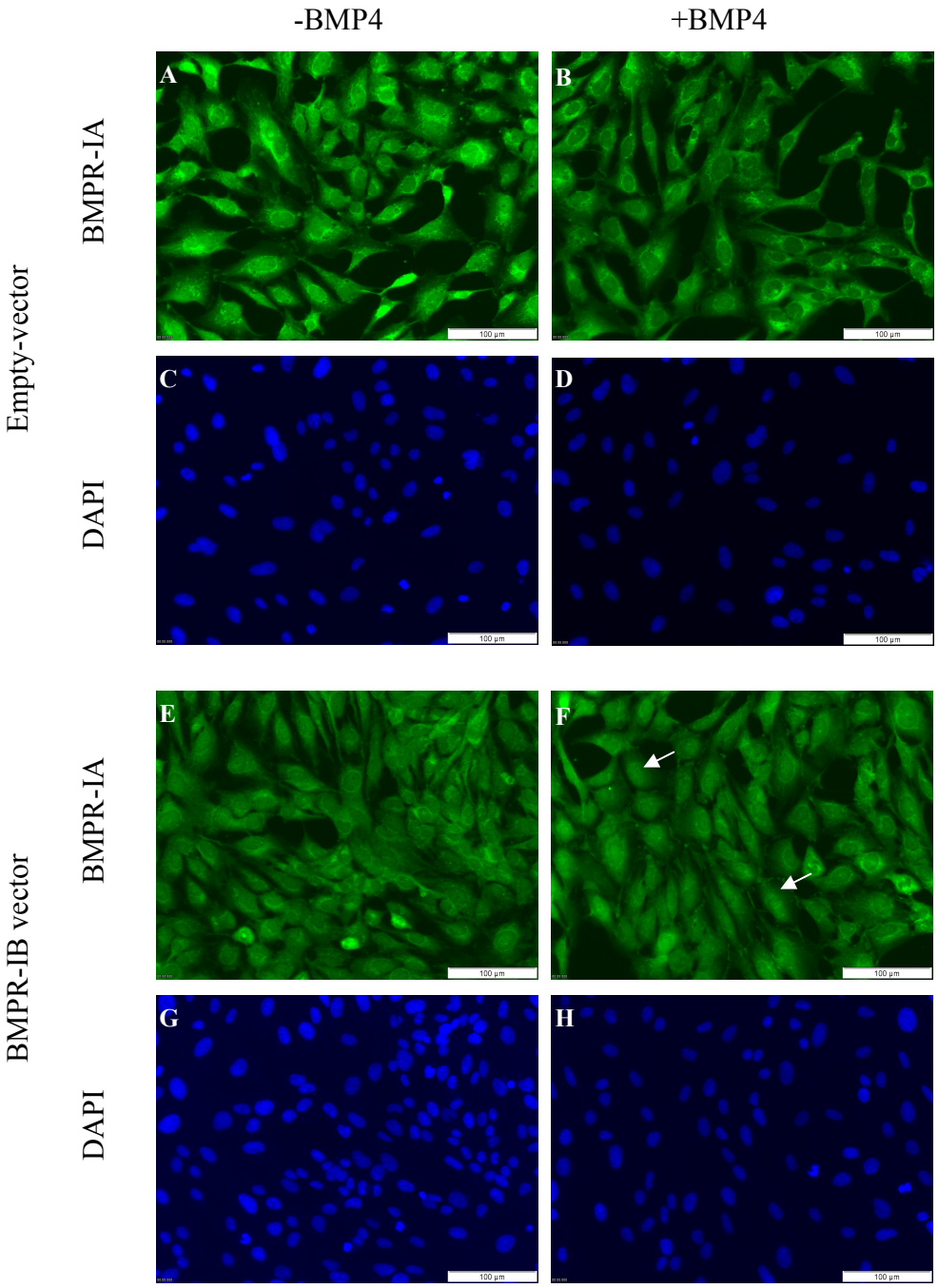

Figure 6.22: BMPR-IA localisation in BMPR-IB-pcDNA4 transfected cells cultured in the absence or presence of BMP4 ligand

Immunofluorescence analysis of: A) BMPR-IA expression in empty-vector transfected cells in absence of BMP4 ligand. B) BMPR-IA expression in empty-vector transfected cells in the presence of BMP4 ligand. E) BMPR-IA expression in BMPR-IB-pcDNA4 transfected cells in absence of BMP4 ligand. F) BMPR-IA expression in BMPR-IB-pcDNA4 transfected cells in the presence of BMP4 ligand. C, D, G, H represent DAPI nuclear counter stained cells. White arrows indicate nuclear staining.

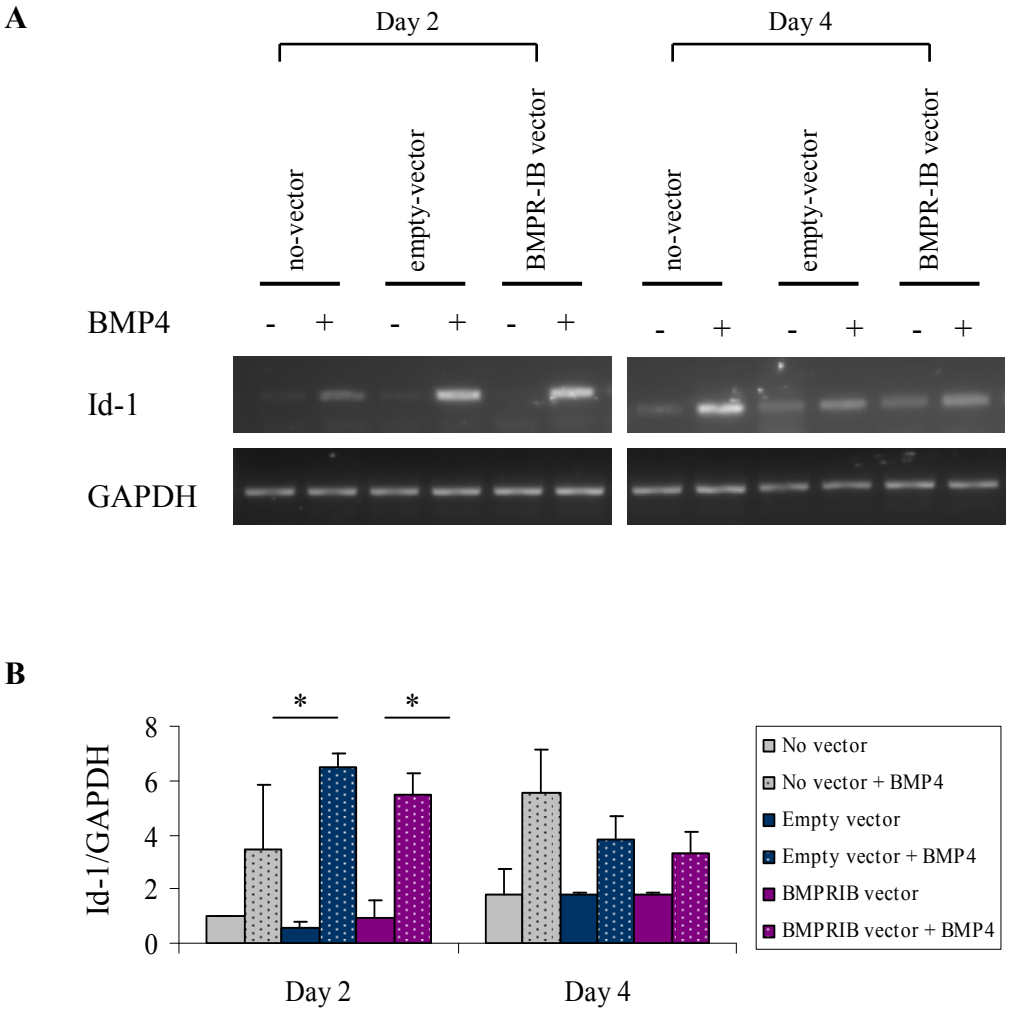

Figure 6.23: Id-1 mRNA expression in BMPR-IB-pcDNA4 transfected cells in the absence or presence of BMP4 ligand

Id-1 RT-PCR analysis was carried out on mRNA isolated from no-vector, empty-vector and BMPR-IB expressing cells. A) DNA gel electrophoresis represents Id-1 expression. B) The graph represents Id-1 densitometry values. Id-1 expression for each sample was presented relative to the GAPDH value. The value for day 2 no-vector control was normalised to a value of 1. All samples were quantified relative to the day 2 no-vector control value. The graph represents n=3 experimental repeats.

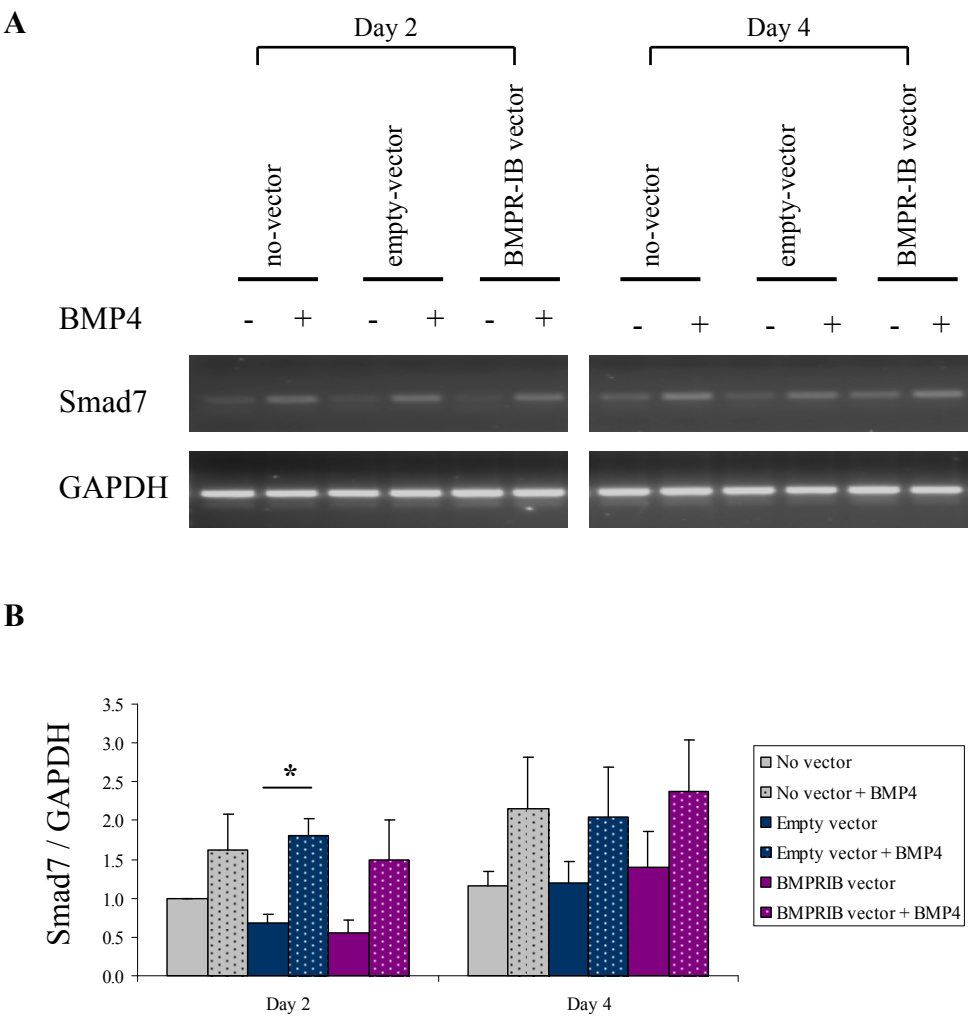

Figure 6.24: Smad7 expression in BMPR-IB-pcDNA4 transfected cells in the absence or presence of BMP4 ligand

Analysis of Smad7 mRNA expression was carried out on day 2 and 4 post transfection, for cells cultured in the absence or presence of BMP4 ligand. A) DNA electrophoresis gel represents Smad7 expression in no-vector control, empty-vector control and BMPR-IB-pcDNA4 expressing cells. B) Smad7 densitometry values were normalised to GAPDH for each sample. Smad7 expression for each treatment is represented relative to day 2 untreated control cells for n=3 experimental repeats.

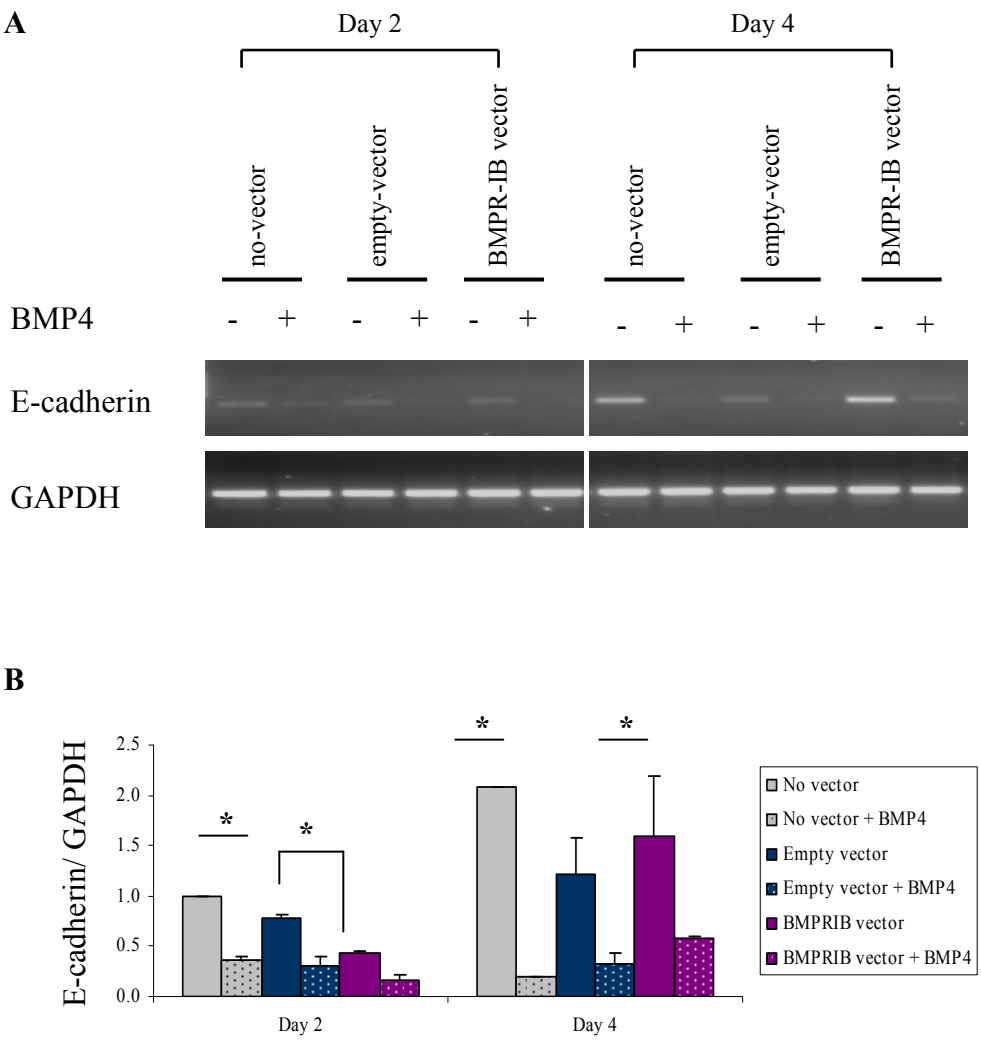

Figure 6.25: E-cadherin expression in BMPR-IB-pcDNA4 transfected cells in the absence or presence of BMP4 ligand

Analysis of E-cadherin mRNA expression was carried out on day 2 and 4 post BMPR-IB-pcDNA4 transfection, for cells cultured in the absence or presence of BMP4 ligand. A) DNA electrophoresis gel represents E-cadherin expression in no-vector control, empty-vector control and BMPR-IB-pcDNA4 expressing cells. B) E-cadherin densitometry values were normalised to GAPDH for each sample. E-cadherin expression for each treatment is represented relative to day 2 untreated control cells for n=2 experimental repeats.

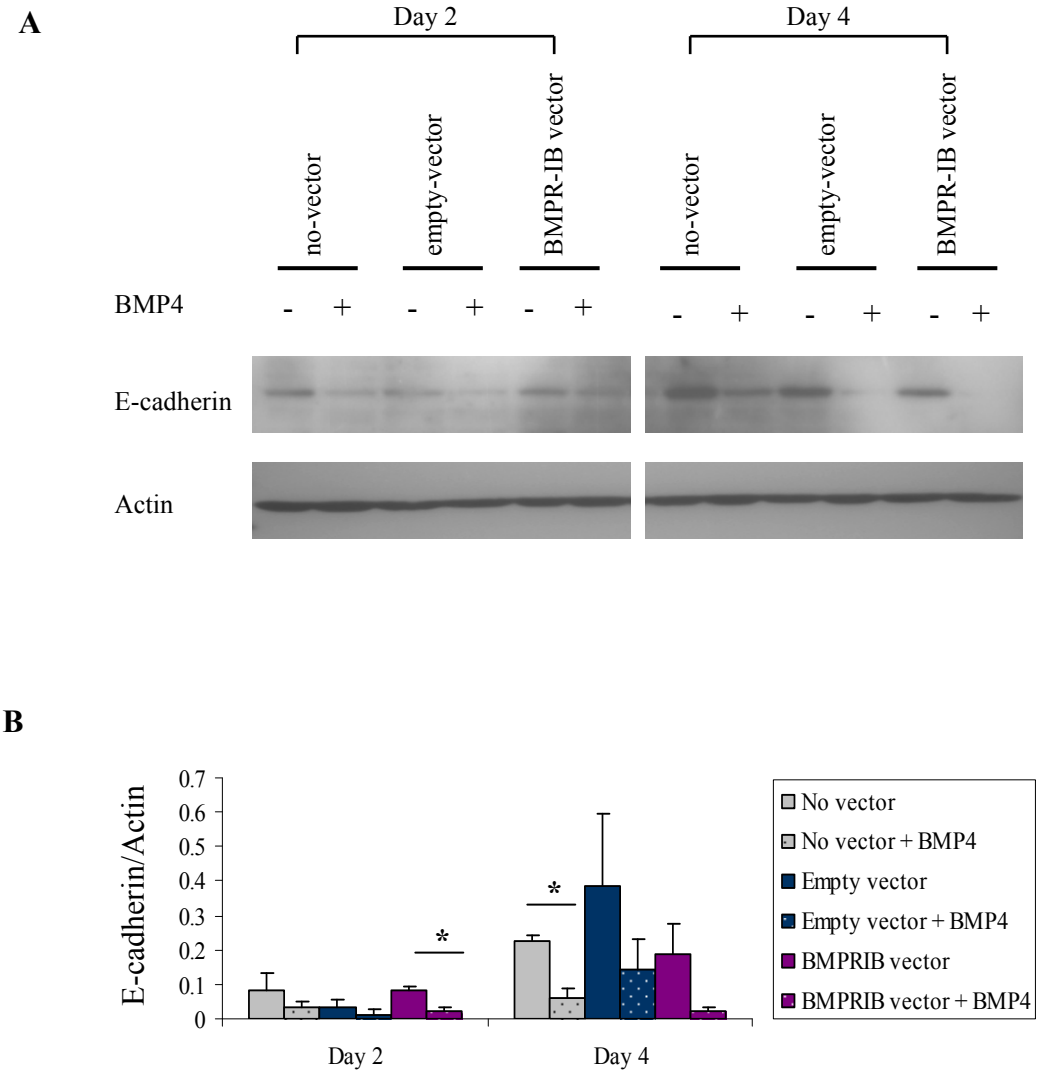

Figure 6.26: E-cadherin protein expression in BMPR-IB-pcDNA4 transfected BEAS-2B cells in the presence or absence of BMP4 ligand

Western blot analysis was carried out on protein extracted from BEAS-2B cells transfected with no-vector control, empty-vector control or BMPR-IB-pcDNA4, and cultured in the absence or presence of BMP4 ligand. A) Representative Western blot image of E-cadherin expression. B) E-cadherin expression for each sample was normalised to actin. The graph represents n=2 (day 2) and n=3 (day 4) experimental repeats.

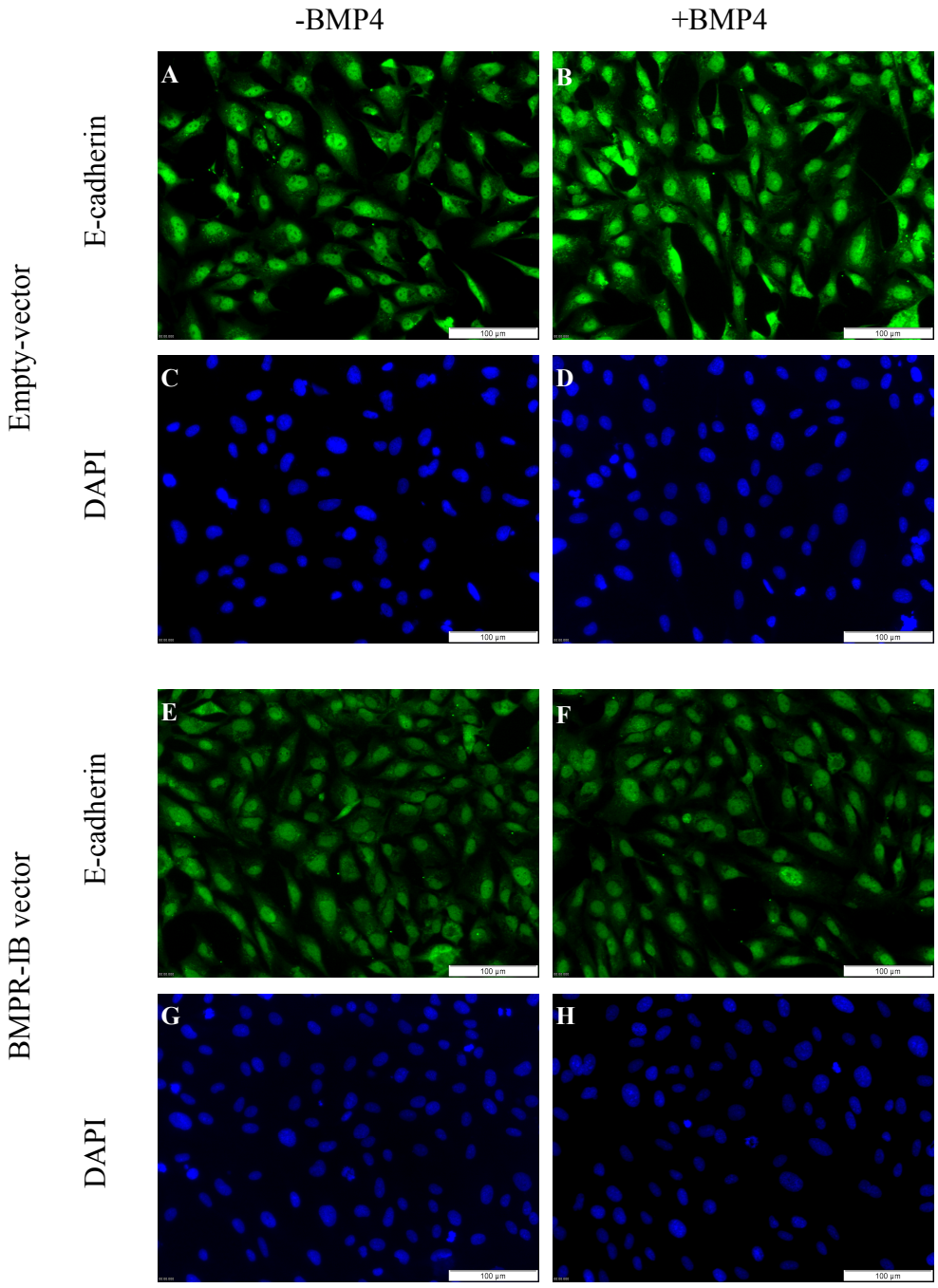

Figure 6.27: E-cadherin protein localisation in BMPR-IB-pcDNA4 transfected cells cultured in the absence or presence of BMP4 ligand

Immunofluorescence analysis of: A) E-cadherin expression in empty-vector transfected cells in absence of BMP4 ligand. B) E-cadherin expression in empty-vector transfected cells in the presence of BMP4 ligand. E) E-cadherin expression in BMPR-IB-pcDNA4 transfected cells in absence of BMP4 ligand. F) E-cadherin expression in BMPR-IB-pcDNA4 transfected cells in the presence of BMP4 ligand. C, D, G, H represent DAPI nuclear counter stained cells.

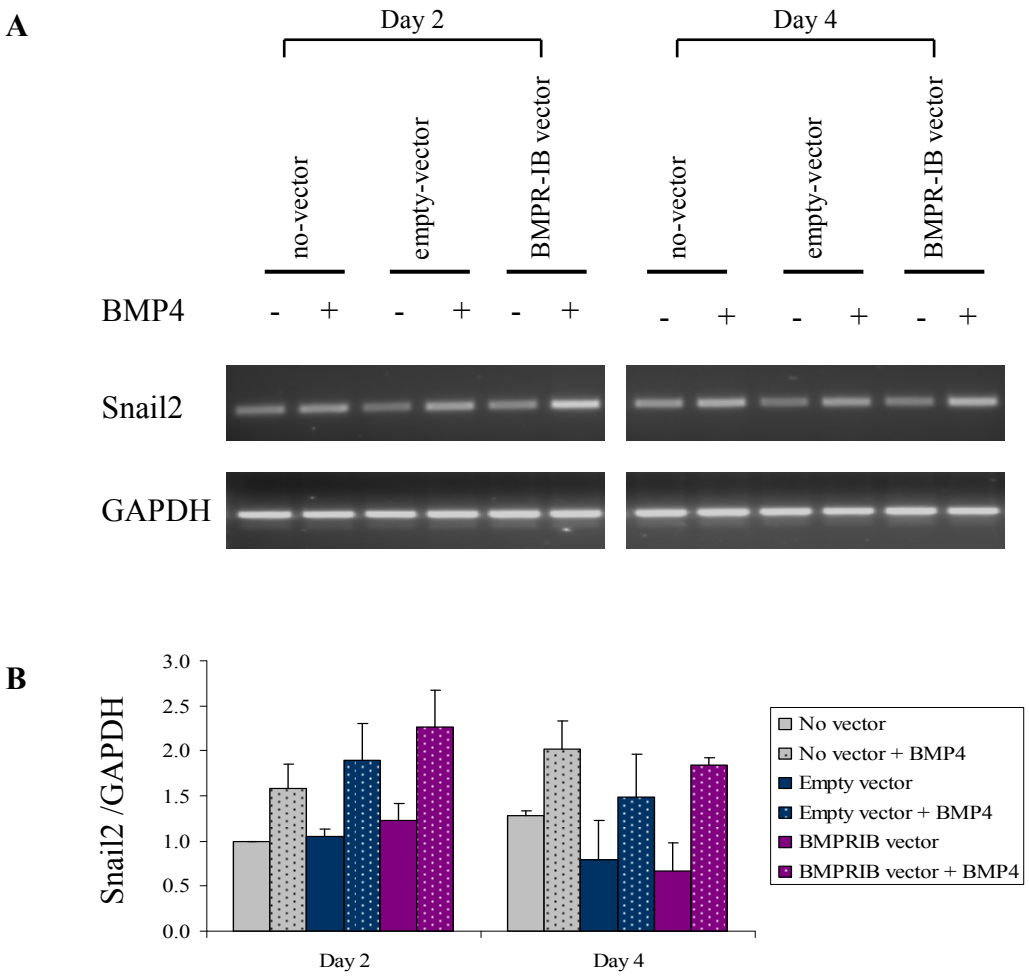

Figure 6.28: Snail2 expression in BMPR-IB-pcDNA4 transfected cells in the absence or presence of BMP4 ligand

Analysis of Snail2 mRNA expression was carried out on day 2 and 4 post transfection, for cells cultured in the absence or presence of BMP4 ligand. A) DNA electrophoresis gel representing Snail2 expression in no-vector control, empty-vector control and BMPR-IB-pcDNA4 expressing cells. B) Snail2 densitometry values were normalised to GAPDH for each sample. Snail2 expression for each treatment is represented relative to day 2 untreated control cells for n=3 experimental repeats.

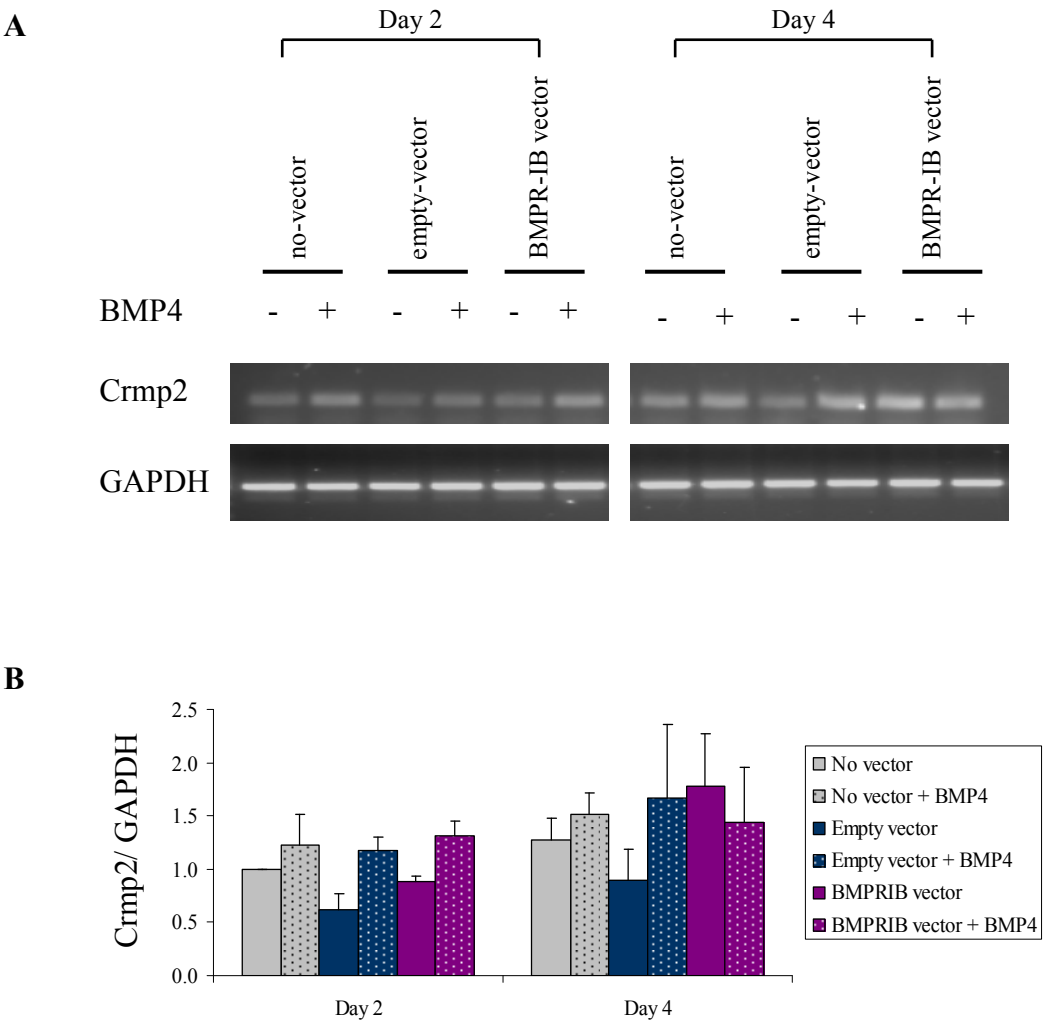

Figure 6.29: Crmp2 expression in BMPR-IB-pcDNA4 transfected cells in the absence or presence of BMP4 ligand

Analysis of Crmp2 mRNA expression was carried out on day 2 and 4 post transfection, for cells cultured in the absence or presence of BMP4 ligand. A) DNA electrophoresis gel representing Crmp2 expression in no-vector control, empty-vector control and BMPR-IB-pcDNA4 expressing cells. B) Crmp2 densitometry values were normalised to GAPDH for each sample. Crmp2 expression for each treatment is represented relative to day 2 untreated control cells for n=3 experimental repeats.

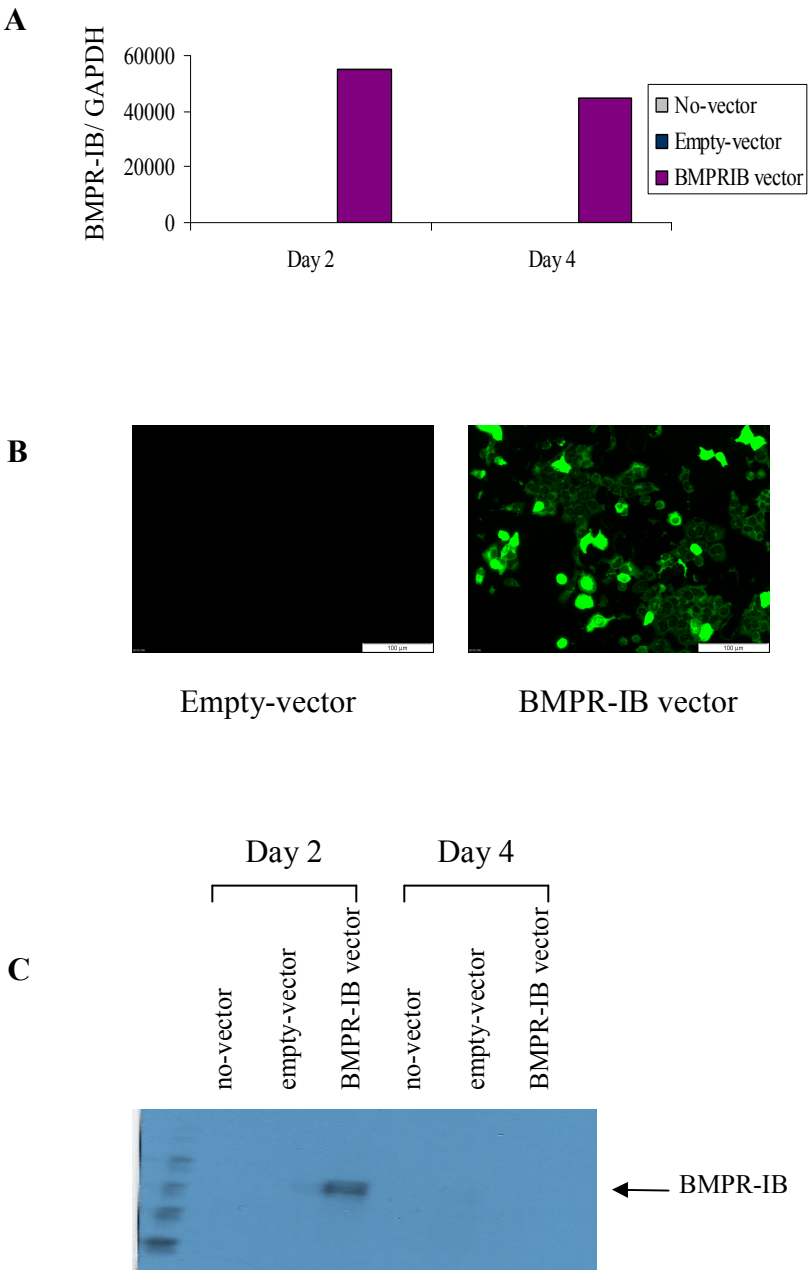

Figure 6.30: Validation of BMPR-IB-pcDNA4 expression in MLE-12 cells

BMPR-IB-pcDNA4 plasmid was transiently transfected into MLE-12 cell line using Lipofectamine 2000 reagent and cells were harvested at Day 1. A) qPCR was carried out to quantify mRNA expression using BMPR-IB F1 and R1 primers (Section 2.1.). B) Immunofluorescence using anti-myc (1:1000) antibody and C) Western blot using anti-myc antibody (1:1000)identified BMPR-IB-pcDNA4 protein expression.

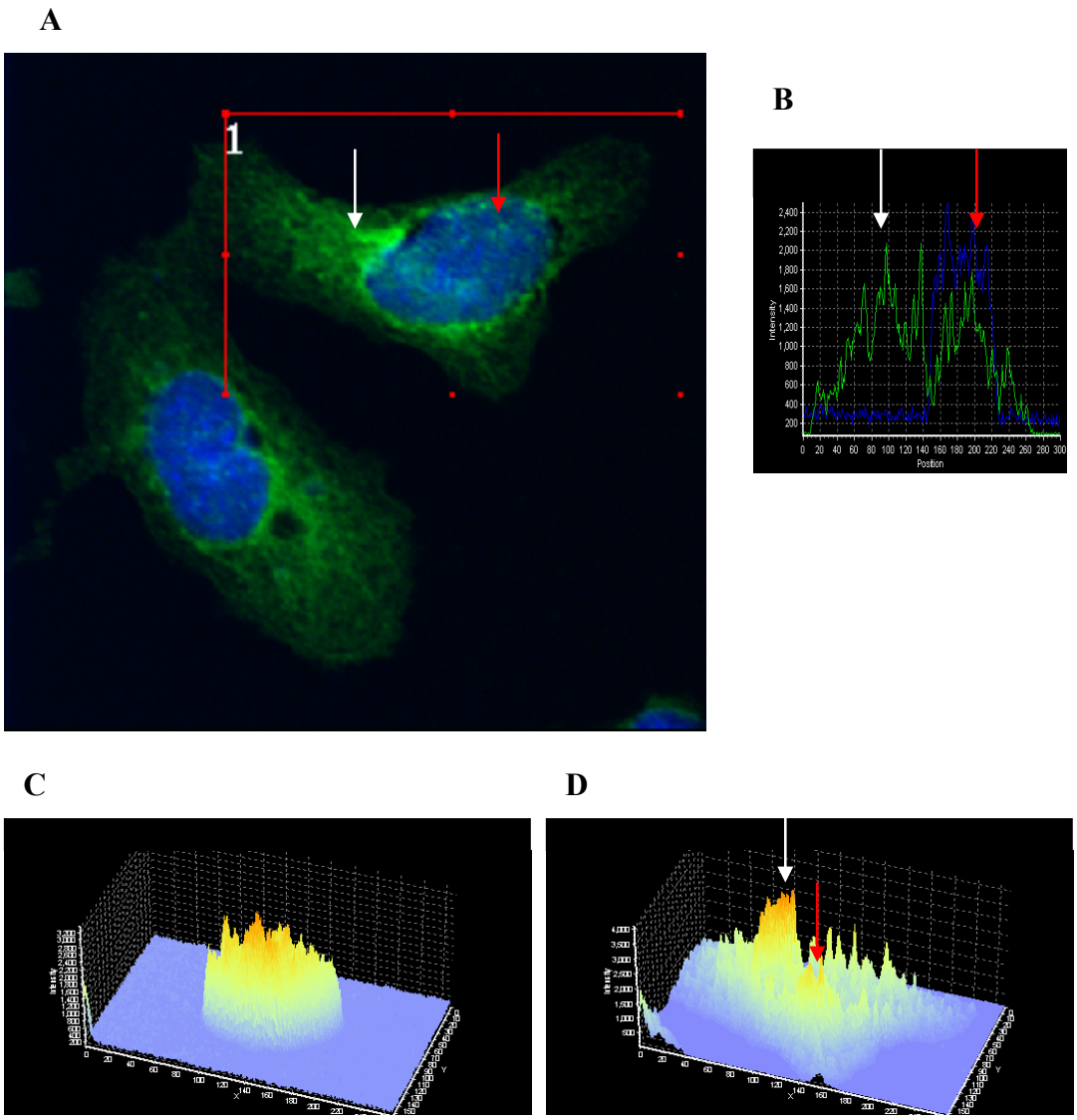

Figure 6.31: Localisation of BMPR-IB in MLE-12 cells

Confocal immunofluorescence photomicrographs were taken of BMPR-IB-pcDNA4, detected by anti-myc tag antibody. A) Green fluorescence represents BMPR-IB protein localisation, blue fluorescence represents DAPI nuclear counter stain. B) 2D graph identifies the localisation of BMPR-IB (green line) and the nucleus (blue line) through one position in the cell. C) 3D graph of DAPI nuclear counter stain for the area inside the red box in A. D) 3D graph of BMPR-IB localisation for the area inside the red box in A. White arrows identify possible endoplasmic reticulum BMPR-IB localisation, red arrows represent nuclear localisation.

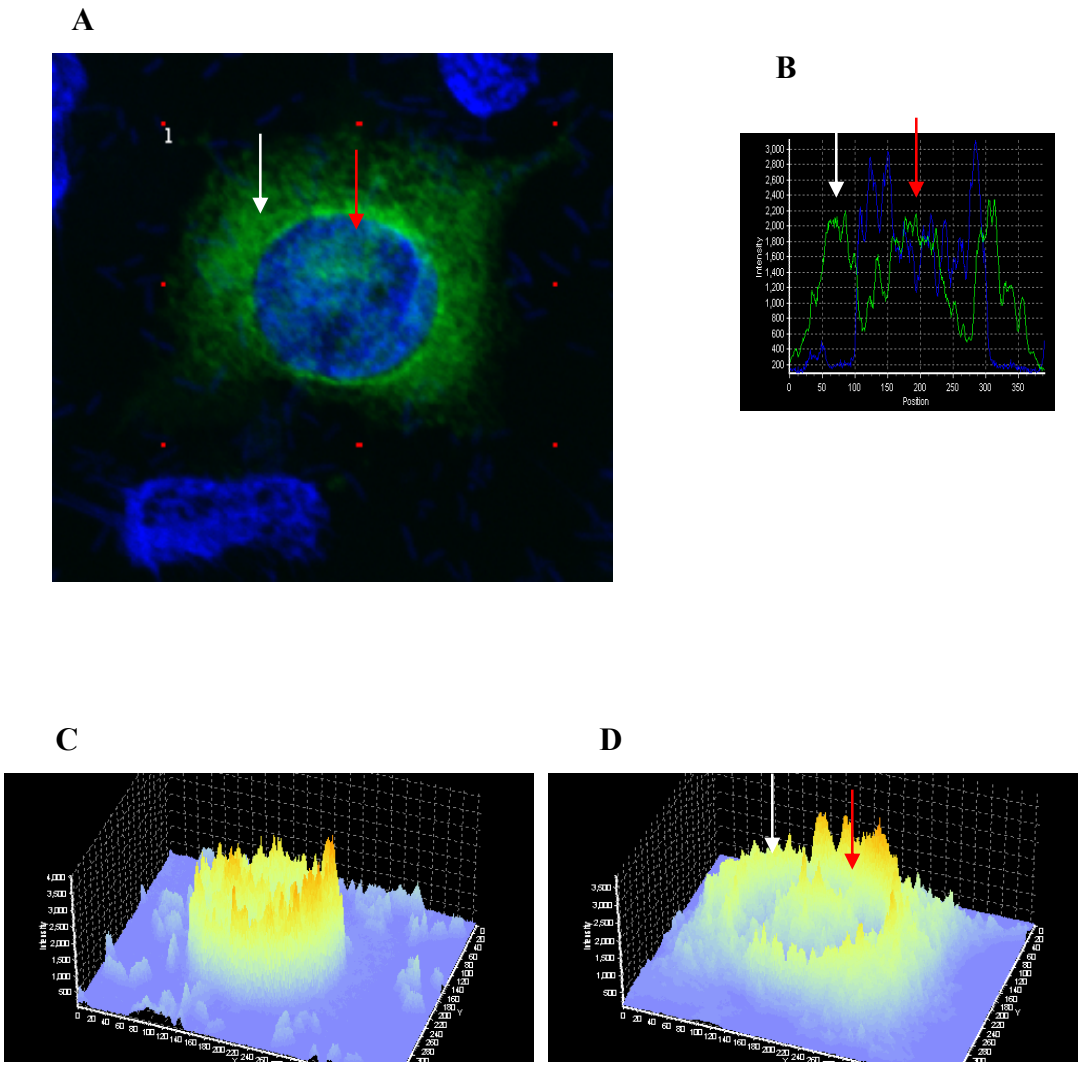

Figure 6.32: The effects of BMP4 ligand stimulation on BMPR-IB localisation in MLE-12 cells

Confocal microscopy was carried out on cells transfected with BMPR-IB-pcDNA4 and stimulated with BMP4 ligand (100ng/ml). A) Green fluorescence represents BMPR-IB protein localisation, blue fluorescence represents DAPI nuclear counter stain. B) Graph identifies the localisation of BMPR-IB (green line) and the nucleus (blue line) through one position in the cell. C) 3D image of DAPI nuclear counter stain for the area inside the green box in A. D) 3D image was taken of BMPR-IB localisation. White arrows identify possible endoplasmic reticulum BMPR-IB localisation, red arrows represent nuclear localisation.

.

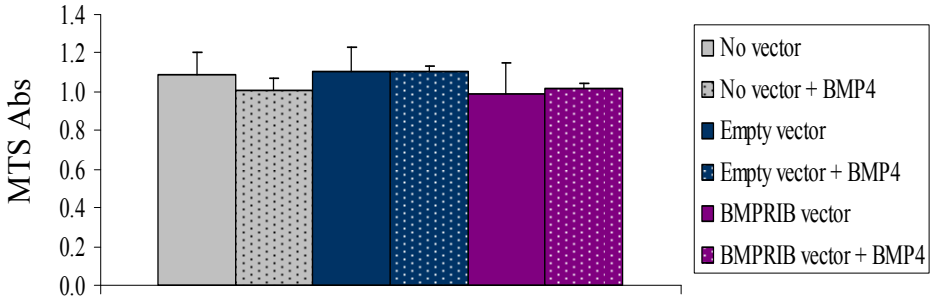

Figure 6.33: MTS assay of BMPR-IB-pcDNA4 transfected MLE-12 cells in the absence or presence of BMP4

An MTS assay was carried out on day 2 cells to establish if BMPR-IB expression or BMP4 treatment had an effect on cell proliferation. Neither BMPR-IB expression nor BMP4 treatment had an effect on MLE-12 cell proliferation.

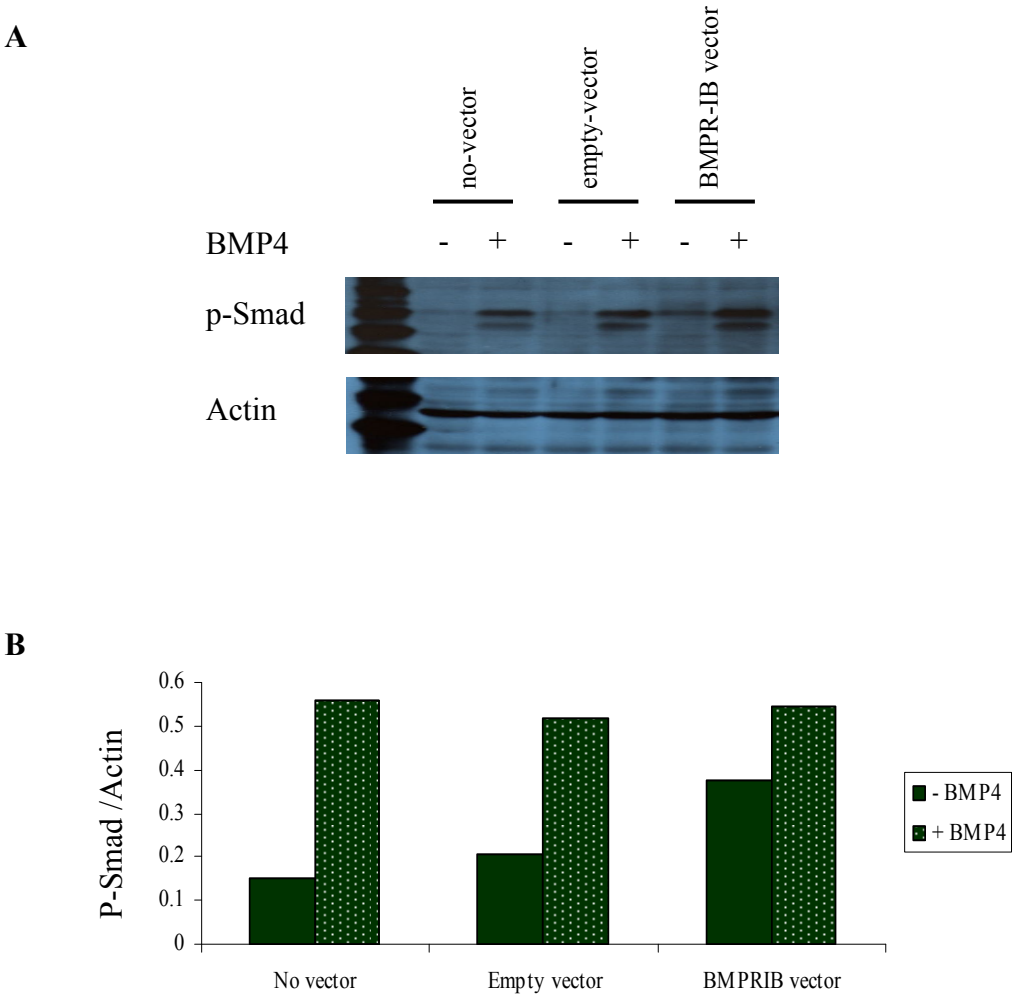

Figure 6.34: p-Smad protein expression in BMPR-IB-pcDNA4 transfected MLE-12 cells

Western blot analysis was carried out to investigate the expression of p-Smad in no-vector control, empty-vector control and BMPR-IB-pcDNA4 transfected cells cultured in the absence or presence of BMP4 ligand. A) Western blot gel image of p-Smad expression. B) Densitometry results for n=1 p-Smad expression normalised to actin in each sample.

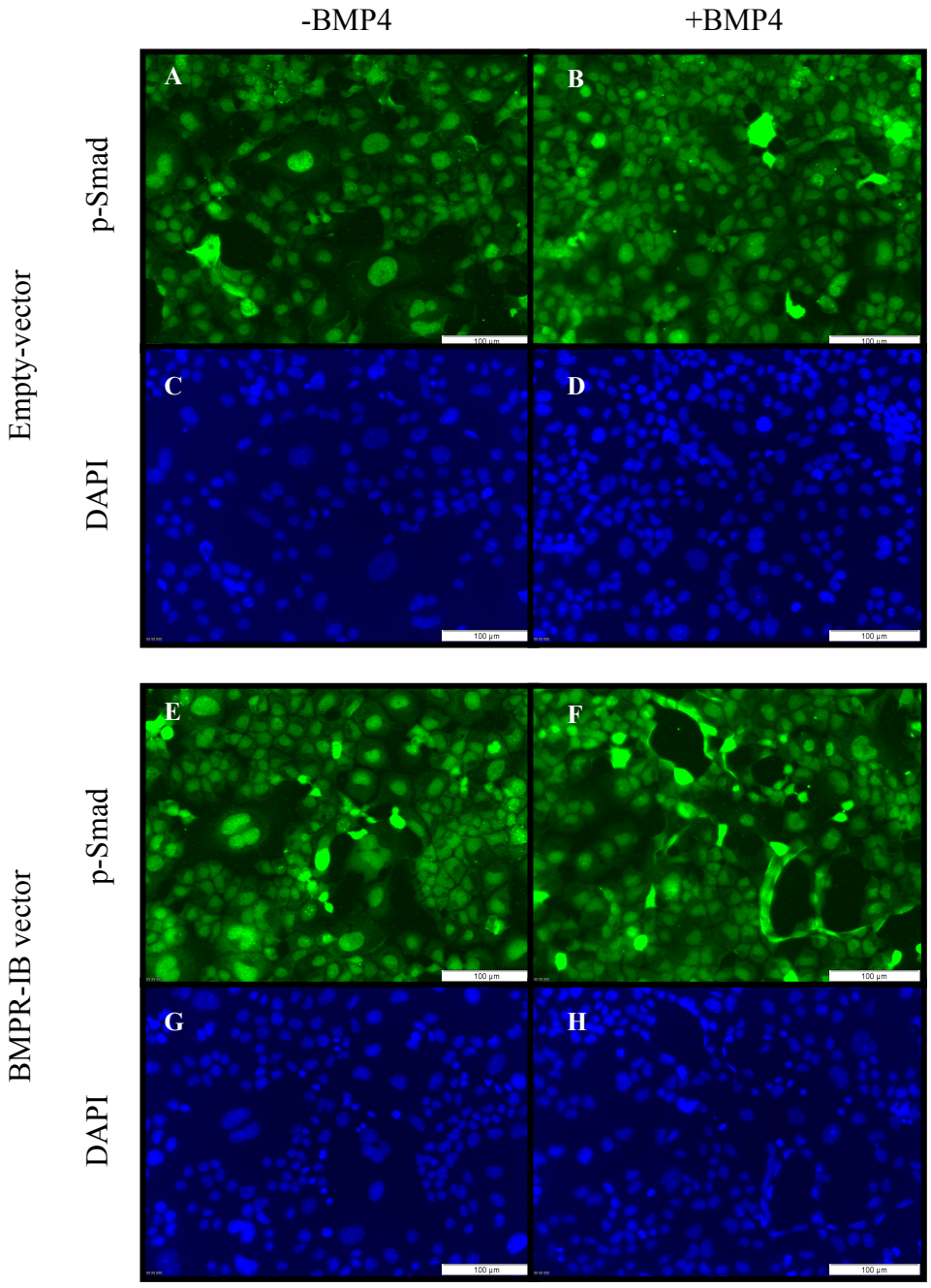

Figure 6.35: p-Smad localisation in BMPR-IB-pcDNA4 transfected MLE-12 cells cultured in the absence or presence of BMP4 ligand

Immunofluorescence analysis of: A) p-Smad expression in empty-vector transfected cells in absence of BMP4 ligand. B) p-Smad expression in empty-vector transfected cells in the presence of BMP4 ligand. E) p-Smad expression in BMPR-IB-pcDNA4 transfected cells in absence of BMP4 ligand. F) p-Smad expression in BMPR-IB-pcDNA4 transfected cells in the presence of BMP4 ligand. C, D, G, H represent DAPI nuclear counter stained cells.

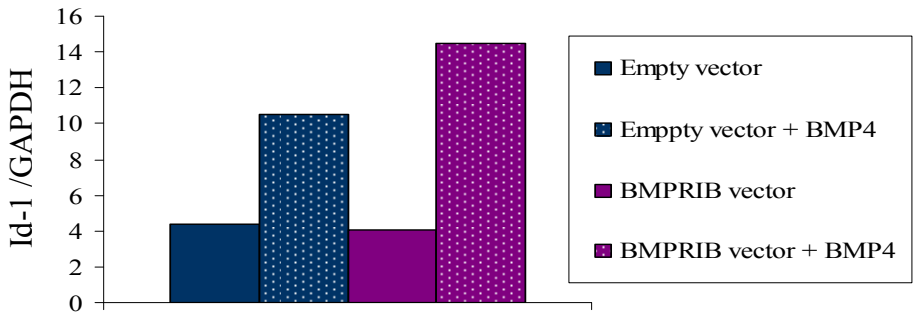

Figure 6.36: Id-1 expression in BMPR-IB-pcDNA4 transfected MLE-12 cells in the absence or presence of BMP4

Real time PCR analysis was carried out to investigate the expression of Id-1 in no-vector control, empty-vector control and BMPR-IB-pcDNA4 transfected cells cultured in the absence or presence of BMP4 ligand. Id-1 expression increased in the presence of BMP4 ligand. BMPR-IB expression did not effect Id-1 expression. Graph represent 1 experimental repeat.

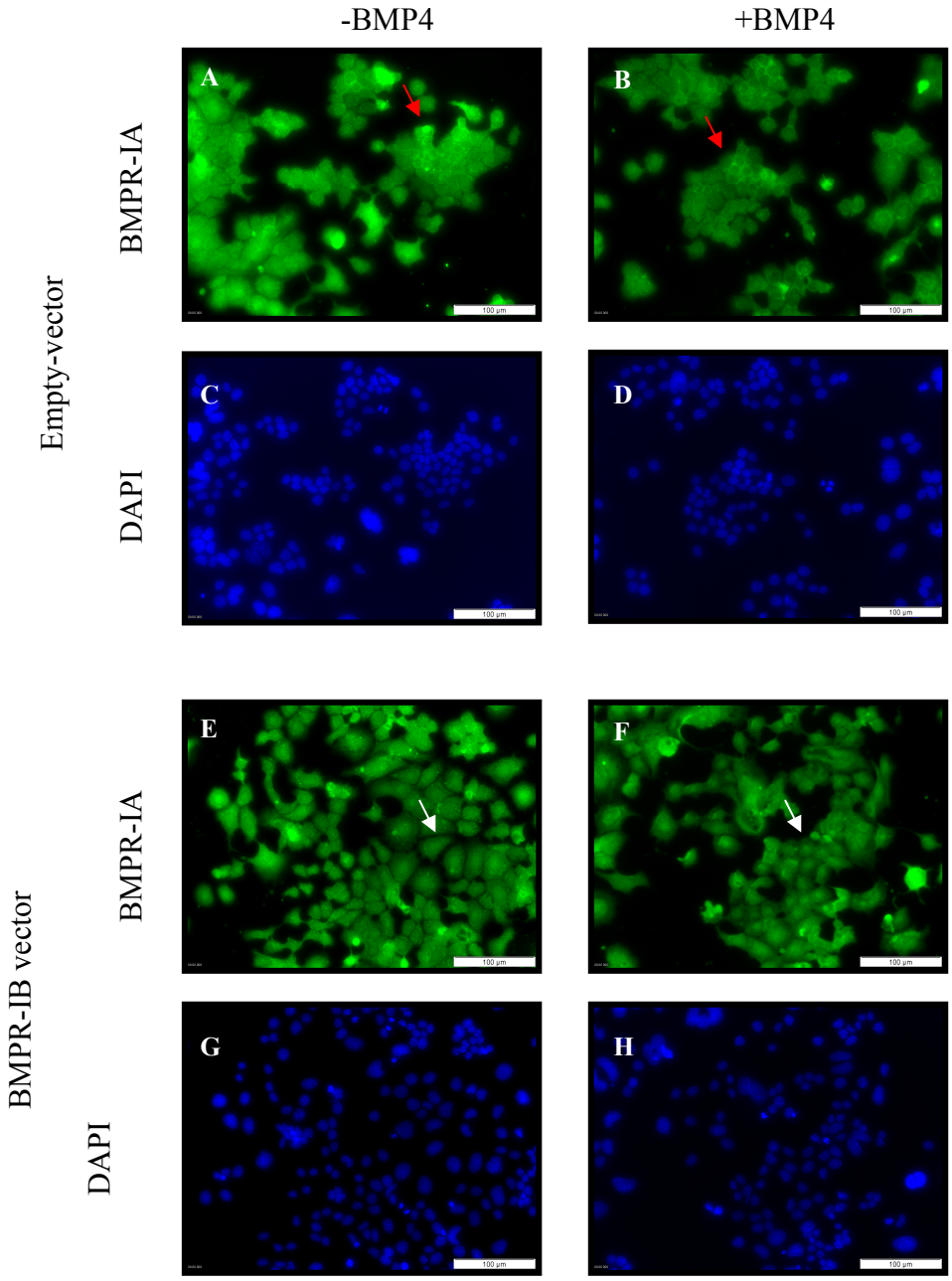

Figure 6.37: BMPR-IA localisation in BMPR-IB-pcDNA4 transfected MLE-12 cells cultured in the absence or presence of BMP4 ligand

Immunofluorescence analysis of: A) BMPR-IA expression in empty-vector transfected cells in absence of BMP4 ligand. B) BMPR-IA expression in empty-vector transfected cells in the presence of BMP4 ligand. E) BMPR-IA expression in BMPR-IB-pcDNA4 transfected cells in absence of BMP4 ligand. F) BMPR-IA expression in BMPR-IB-pcDNA4 transfected cells in the presence of BMP4 ligand. C, D, G, H represent DAPI nuclear counter stained cells. Red arrows indicate membrane staining, white arrows indicate nuclear staining.

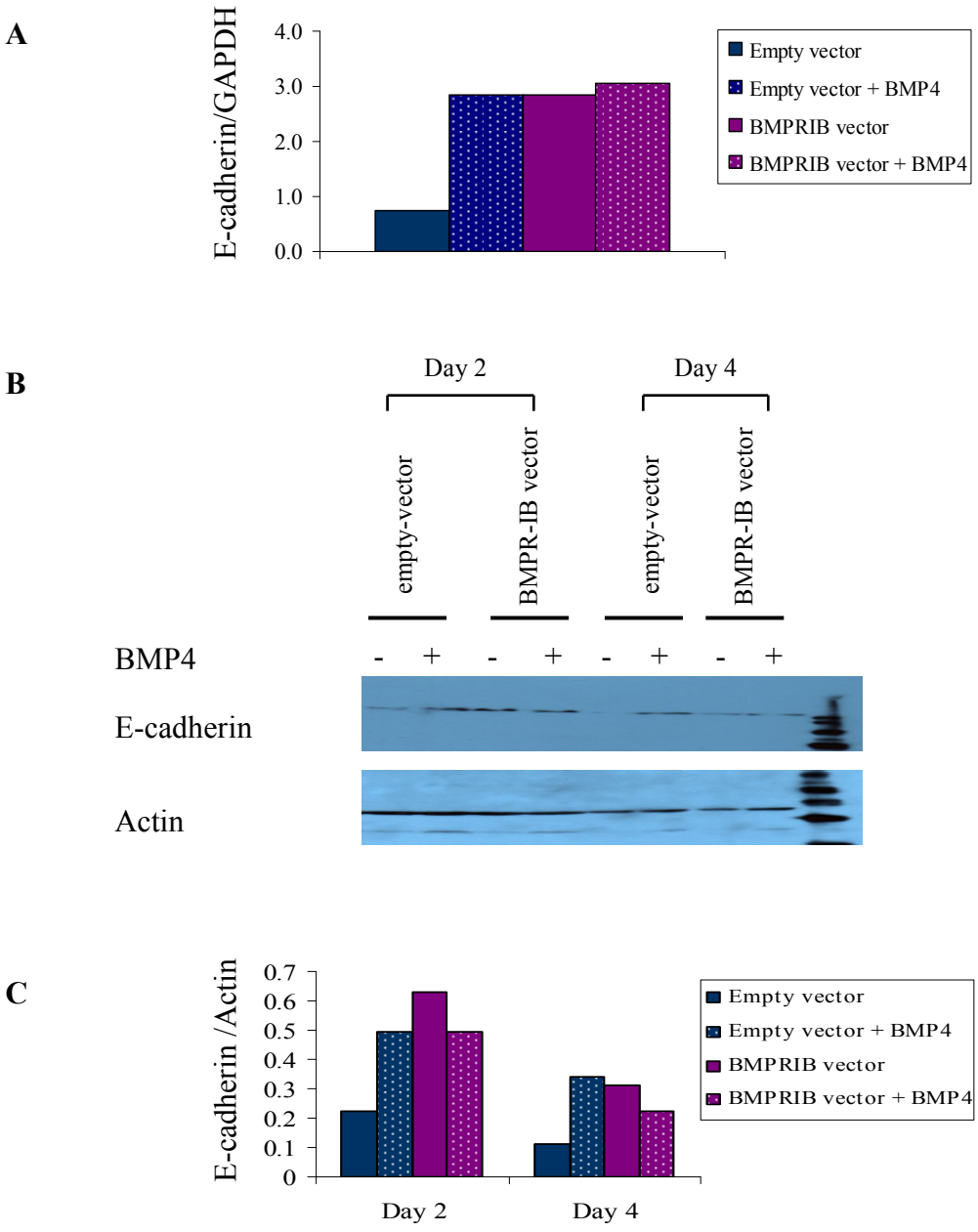

Figure 6.38: E-cadherin expression in MLE-12 cells transfected with BMPR-IB-pcDNA4 and cultured in the absence or presence of BMP4 ligand

A) Real time PCR analysis of E-cadherin mRNA expression. B) Western blot of E-cadherin protein expression. C) Densitometry was carried out on Western blot analysis, E-cadherin expression was normalised to actin in each sample for an n=1 experiment.

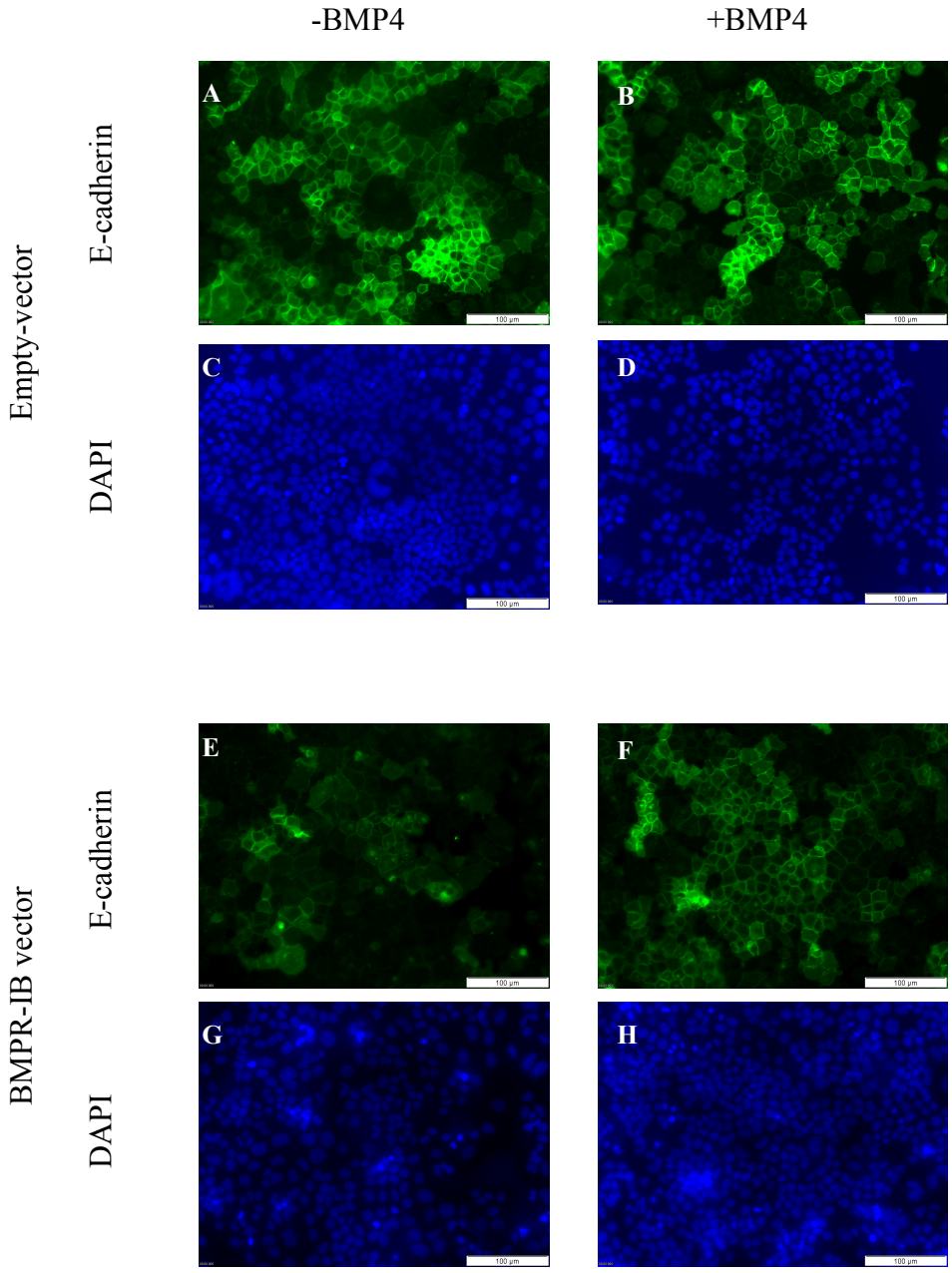

Figure 6.39: E-cadherin localisation in BMPR-IB-pcDNA4 transfected MLE-12 cells cultured in the absence or presence of BMP4 ligand

Immunofluorescence analysis of: A) E-cadherin expression in empty-vector transfected cells in absence of BMP4 ligand. B) E-cadherin expression in empty-vector transfected cells in the presence of BMP4 ligand. E) E-cadherin expression in BMPR-IB-pcDNA4 transfected cells in absence of BMP4 ligand. F) E-cadherin expression in BMPR-IB-pcDNA4 transfected cells in the presence of BMP4 ligand. C, D, G, H represent DAPI nuclear counter stained cells.

	pcDNA4	pcDNA4 + BMP4	BMPR-IB	BMPR-IB + BMP4
Function				
Viable cells day 2	+	-	-	+
Viable cells day 4	++	++	++	++
Non-viable cells day 2	+	+	+	+
Non-viable cells day 4	+	+++	+++	++++
Apoptotic nuclei	+		+++	
Migration	+		+++	
mRNA				
Id-1	+	+++	+	+++
Smad7	+	++	+	++
E-cadherin	+	--	-	--
Snail2	+	++	+	++
crmp2	+	+++	++	+++
Western blot				
p-Smad	+	+++	++	+++
E-cadherin	+	--	++	-
Immunofluorescence				
p-Smad	nuclear	nuclear	nuclear	nuclear
BMPR-II	dispersed	cytoplasmic	cytoplasmic	cytoplasmic
BMPR-IA	dispersed	dispersed	nuclear +	nuclear ++

Figure 6.40: Summary table

This table summarises some of the main results of functional studies, mRNA expression and protein expression (examined by Western blot and immunofluorescence) after BMPR-IB expression in the absence and presence of BMP4 ligand. Levels of expression are presented by + indicating up-regulation of expression or – indicating down-regulation of expression.

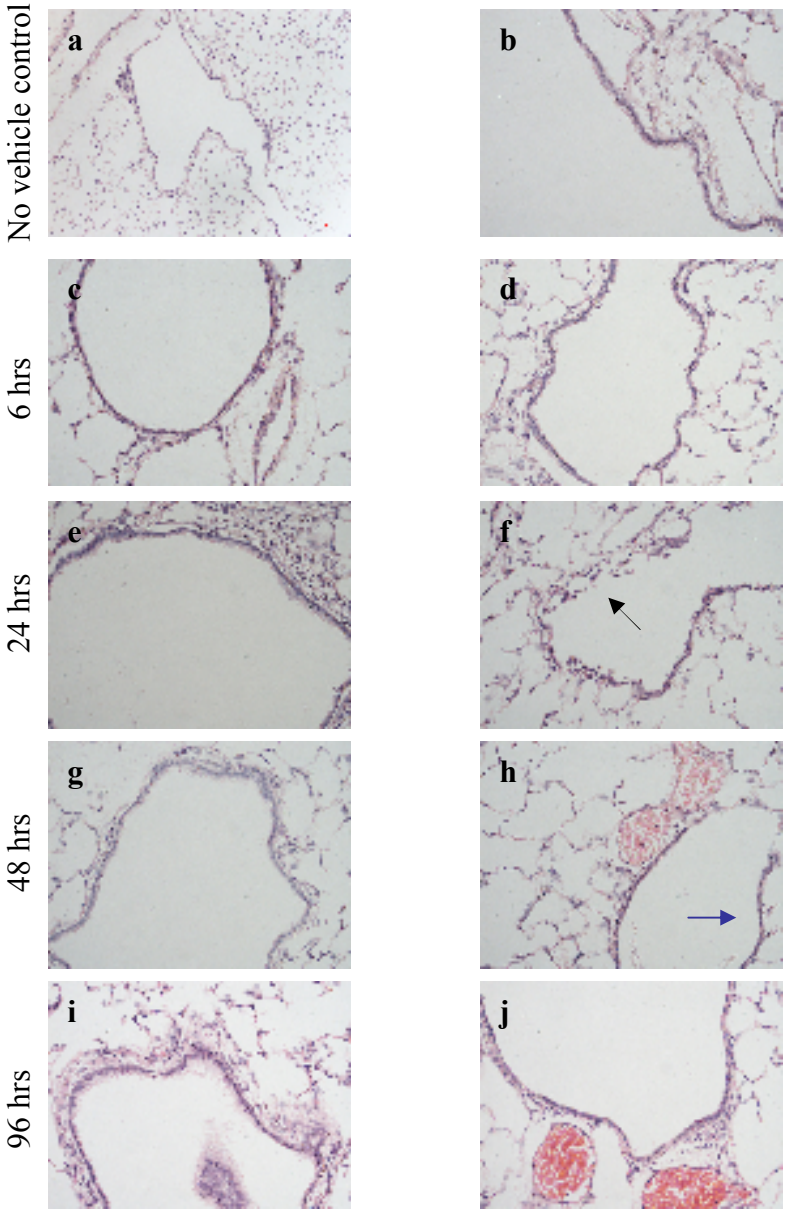

Figure 7.1: H&E staining of rat 1-NN treatment

Photomicrographs were taken of H&E stained tissue from the lungs of untreated control, vehicle control and 1-NN treated rats. a) 10X magnification of untreated control lungs b) 40X magnification of untreated control lungs. Bright field images were taken at 40X magnification of vehicle control airways at c) 6 hrs, e) 24 hrs, g) 48 hrs and i) 96 hrs. 1-NN treated lungs were observed under 40X magnification at d) 6 hrs, f) 24 hrs, h) 48 hrs, j) 96 hrs. Black arrow indicated denuding epithelial cells, blue arrow indicated flattened epithelial cells.

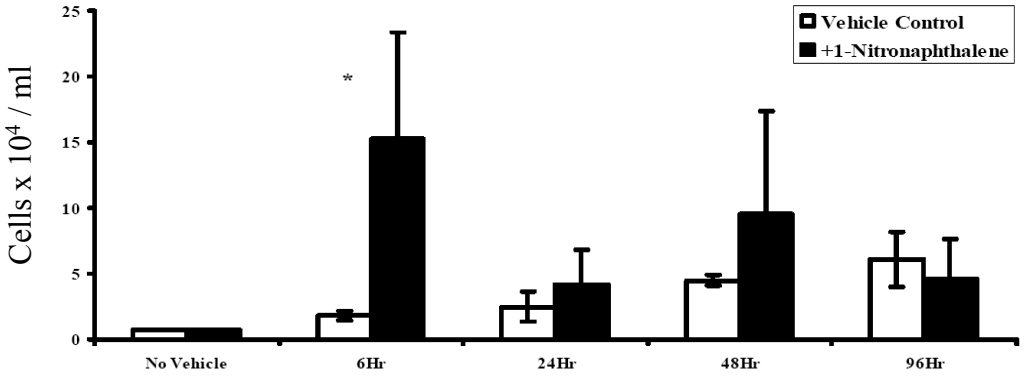

Figure 7.2: Bronchoalveolar lavage fluid (BALF) cell count

BALF was harvested during the lysis lavage procedure at each time point. Cell counts were carried out on the BALF. One no vehicle (untreated) control animal was used to indicate the base line number of cells in the lungs of untreated animals. Error bars represent ± SEM preformed on 3 animals, except for no vehicle control which was representative of 1 animal. (Figure provided by Dr. Joanne Masterson)

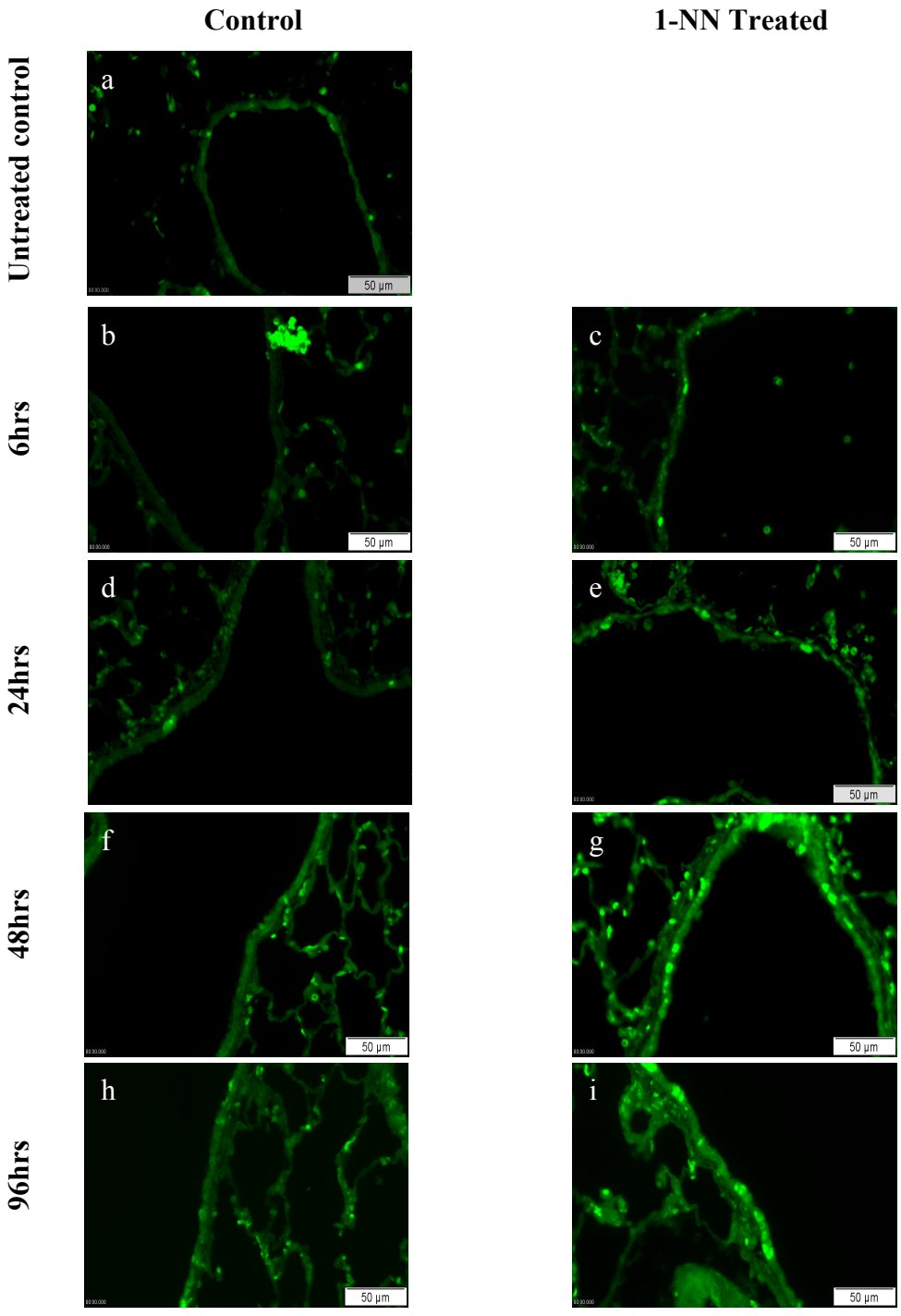
Control
1-NN Treated
Untreated control
6hrs
24hrs
48hrs
96hrs
a
b
c
d
e
f
g
h
i
50 µm

Figure 7.3 A

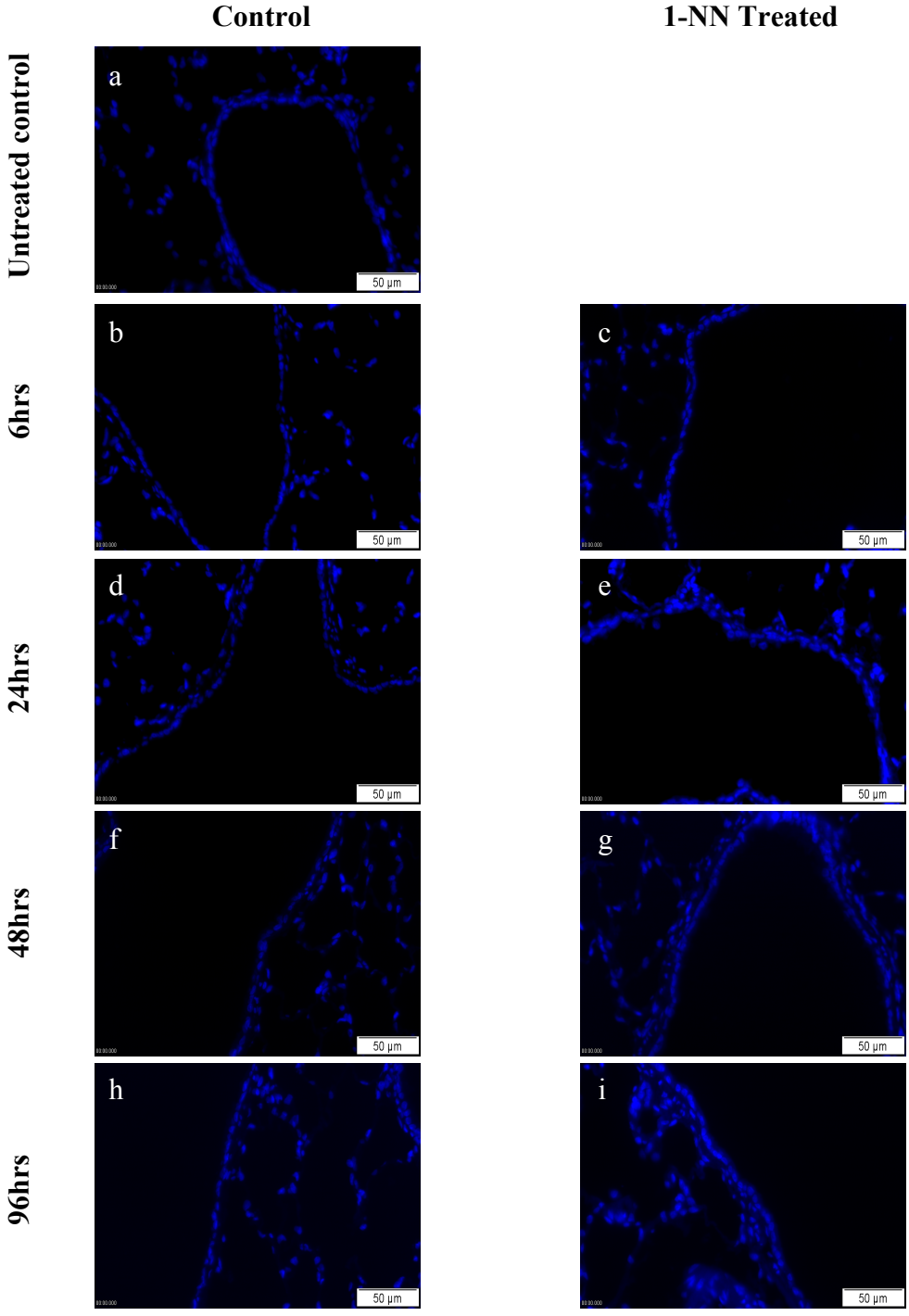
Control
1-NN Treated
Untreated control
6hrs
24hrs
48hrs
96hrs
a
b
c
d
e
f
g
h
i
50 µm

Figure 7.3 B

Figure 7.3: Increased PCNA expression was observed at 48 hrs and 96 hrs post 1-NN treatment

Immunofluorescence was carried out on lung tissue from vehicle control and 1-NN animals using anti-PCNA antibody at 1/3000 dilution. A) PCNA expression is found in the nucleus in a) untreated control animal, b) 6 hr vehicle control, c) 6 hr 1-NN treated, d) 24 hr vehicle control, e) 24 hr 1-NN treated, f) 48 hr vehicle control, g) 48 hr 1-NN treated, h) 96 hr vehicle control and i) 96 hr 1-NN treated animals. B) Corresponding DAPI counter-stained images.

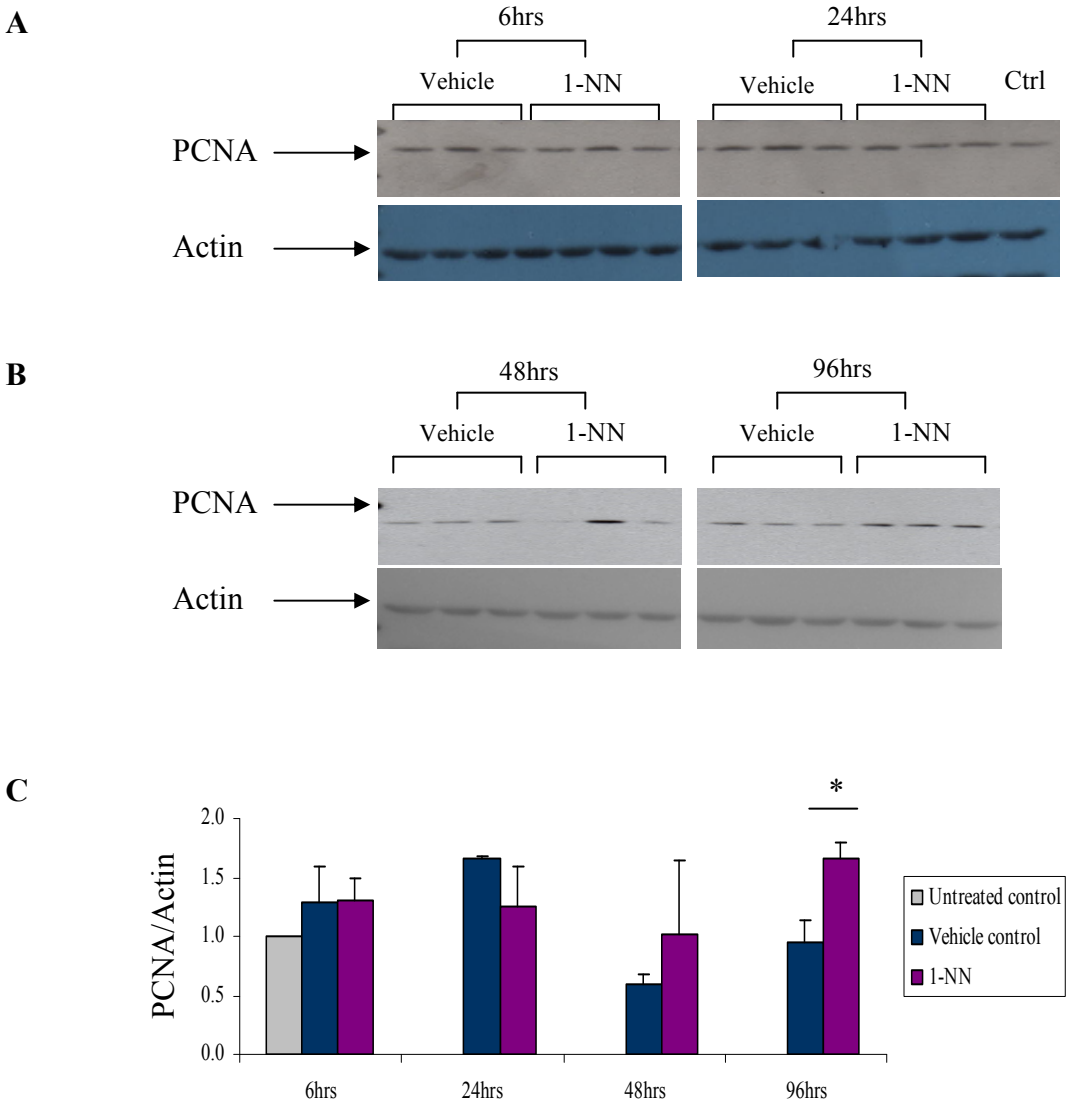

Figure 7.4: PCNA expression increased 96 hrs after 1-NN treatment

Lung lysis lavage protein from untreated control, vehicle control and 1-NN animals were examined by Western blot analysis for PCNA expression, using anti-PCNA antibody (1/3000). Western blot gels for PCNA and actin expression in vehicle control and 1-NN treated animals at A) 6 hrs and 24 hrs B) 48 hrs, 96 hrs and (Ctrl) untreated control. C) Densitometric quantification data of each treatment and time point is presented, actin was used to normalise for loading. Bars represent mean ± SEM based on 3 animals, normalised to the 1 untreated control animal. * $p < 0.05$.

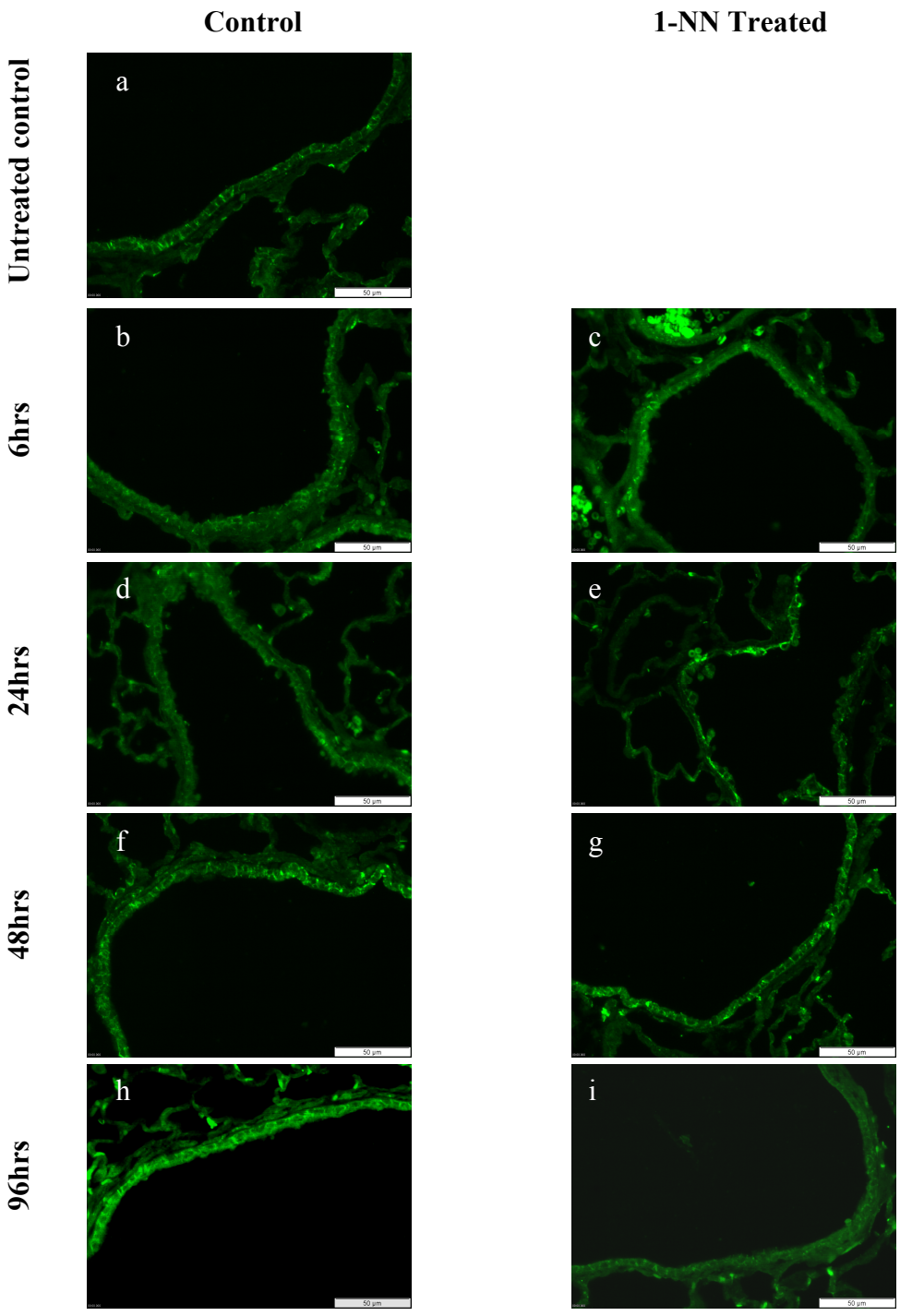
Control
1-NN Treated
Untreated control
6hrs
24hrs
48hrs
96hrs
a
b
c
d
e
f
g
h
i

Figure 7.5 A

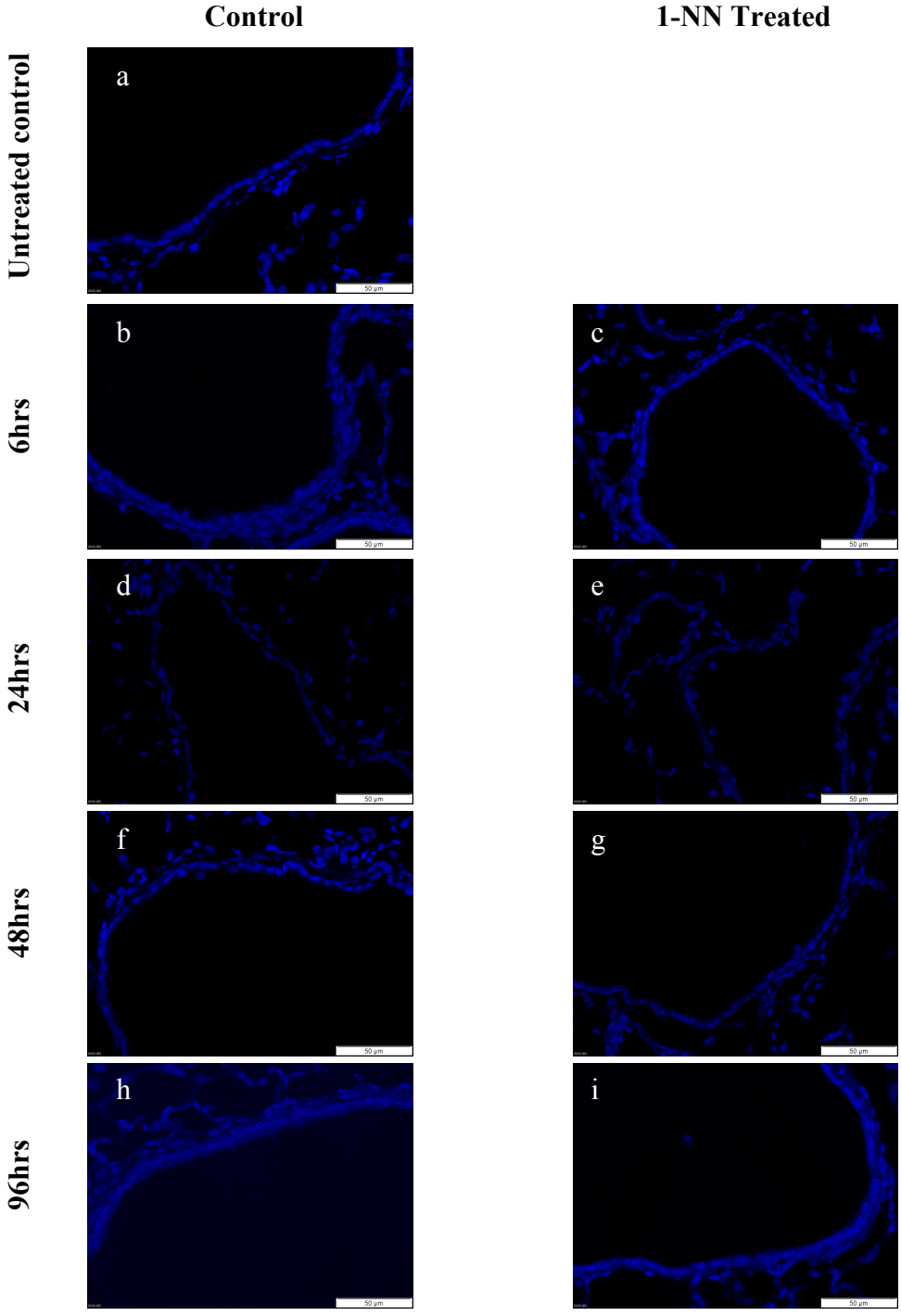
Control
1-NN Treated
Untreated control
6hrs
24hrs
48hrs
96hrs
a
b
c
d
e
f
g
h
i

Figure 7.5 B

Figure 7.5: E-cadherin expression at the epithelial membrane junction

40X immunofluorescence photomicrograph images were taken of E-cadherin expression and DAPI nuclear counter stained airways. A) E-cadherin expression was found at the epithelial membranes of a) untreated control animal, b) 6 hr vehicle control, c) 6 hr 1-NN treated, d) 24 hr vehicle control, e) 24 hr 1-NN treated, f) 48 hr vehicle control, g) 48 hr 1-NN treated, h) 96 hr vehicle control and i) 96 hr 1-NN treated animals. B) Corresponding DAPI counter-stained images.

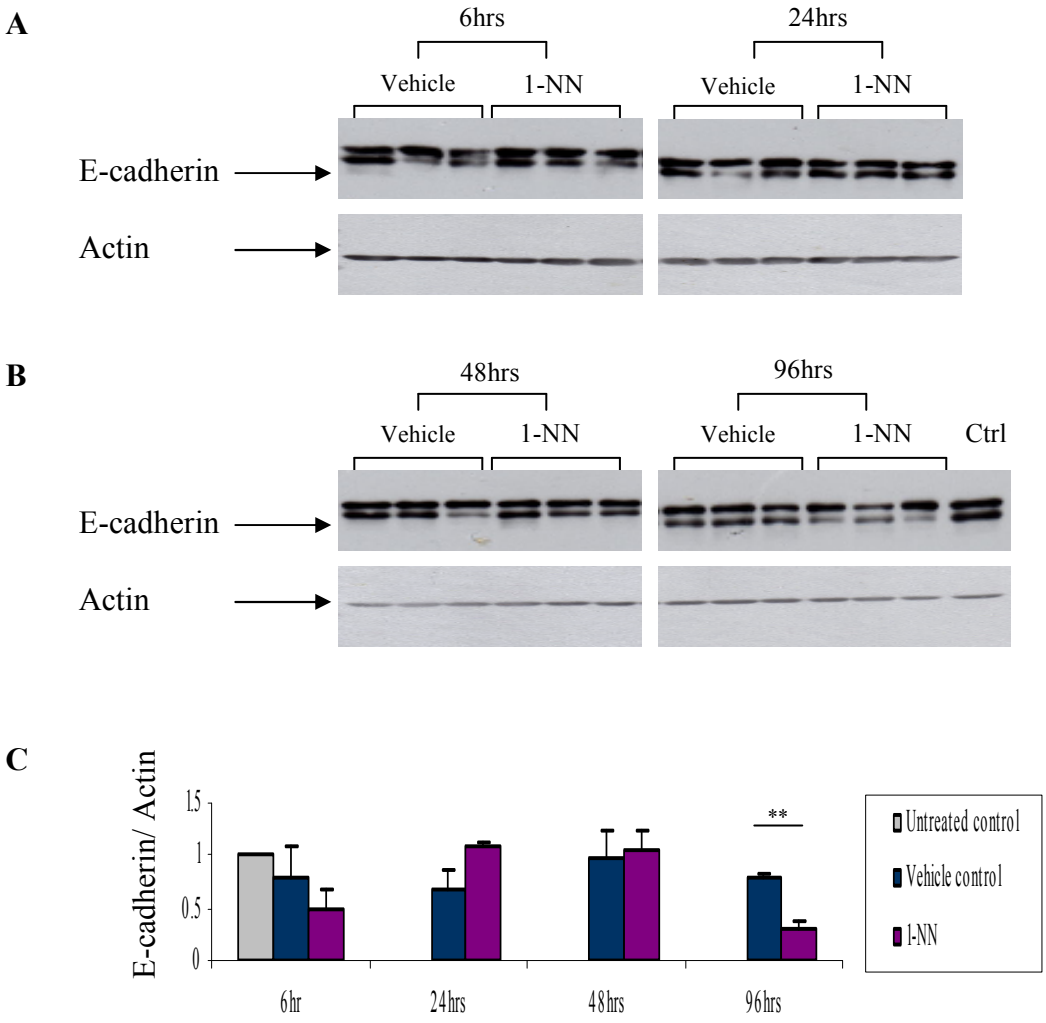

Figure 7.6: E-cadherin expression was reduced at 96 hrs post 1-NN administration

Lung lysis lavage protein from untreated control, vehicle control and 1-NN animals were examined by Western blot analysis for E-cadherin expression, using anti-E-cadherin antibody (1/2000). Western blot gels for E-cadherin and actin expression in vehicle control and 1-NN treated animals at A) 6 hrs and 24 hrs B) 48 hrs, 96 hrs and (Ctrl) untreated control. C) Densitometric quantification data of each treatment and time point is presented, actin was used to normalise for loading. Bars represent mean ± SEM based on 3 animals, normalised to 1 untreated control animal. ** $p < 0.01$

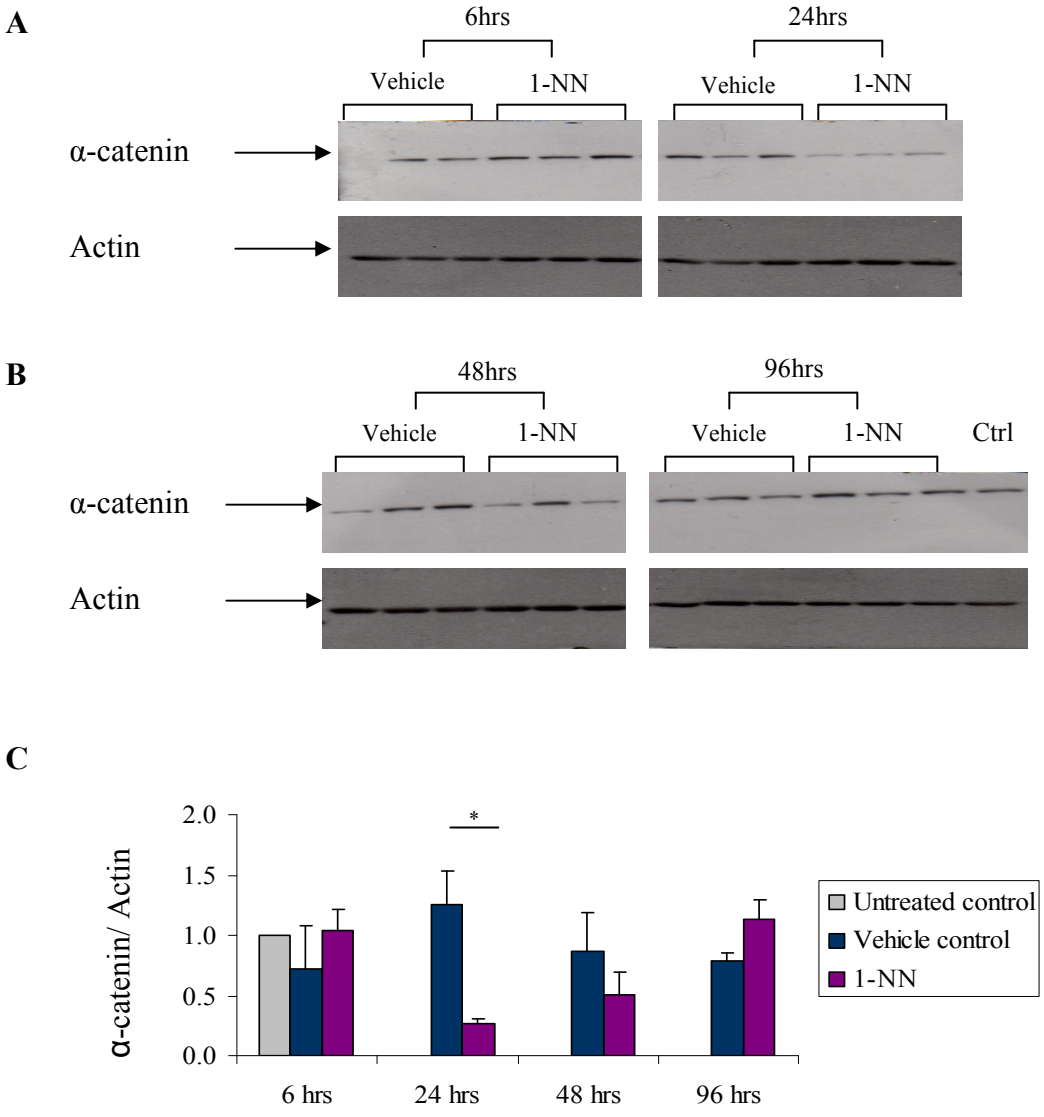

Figure 7.7: α-catenin protein reduction 24 hrs after 1-NN treatment

Lung lysis lavage protein from untreated control, vehicle control and 1-NN animals were examined by Western blot analysis for α-catenin expression, using anti-α-catenin antibody (1/250). Western blot gels for α-catenin and actin expression in vehicle control and 1-NN treated animals at A) 6 hrs and 24 hrs B) 48 hrs, 96 hrs and (Ctrl) untreated control. C) Densitometric quantification data of each treatment and time point is presented, actin was used to normalise for loading. Bars represent mean ± SEM based on 3 animals, normalised to 1 untreated control animal . * $p < 0.05$.

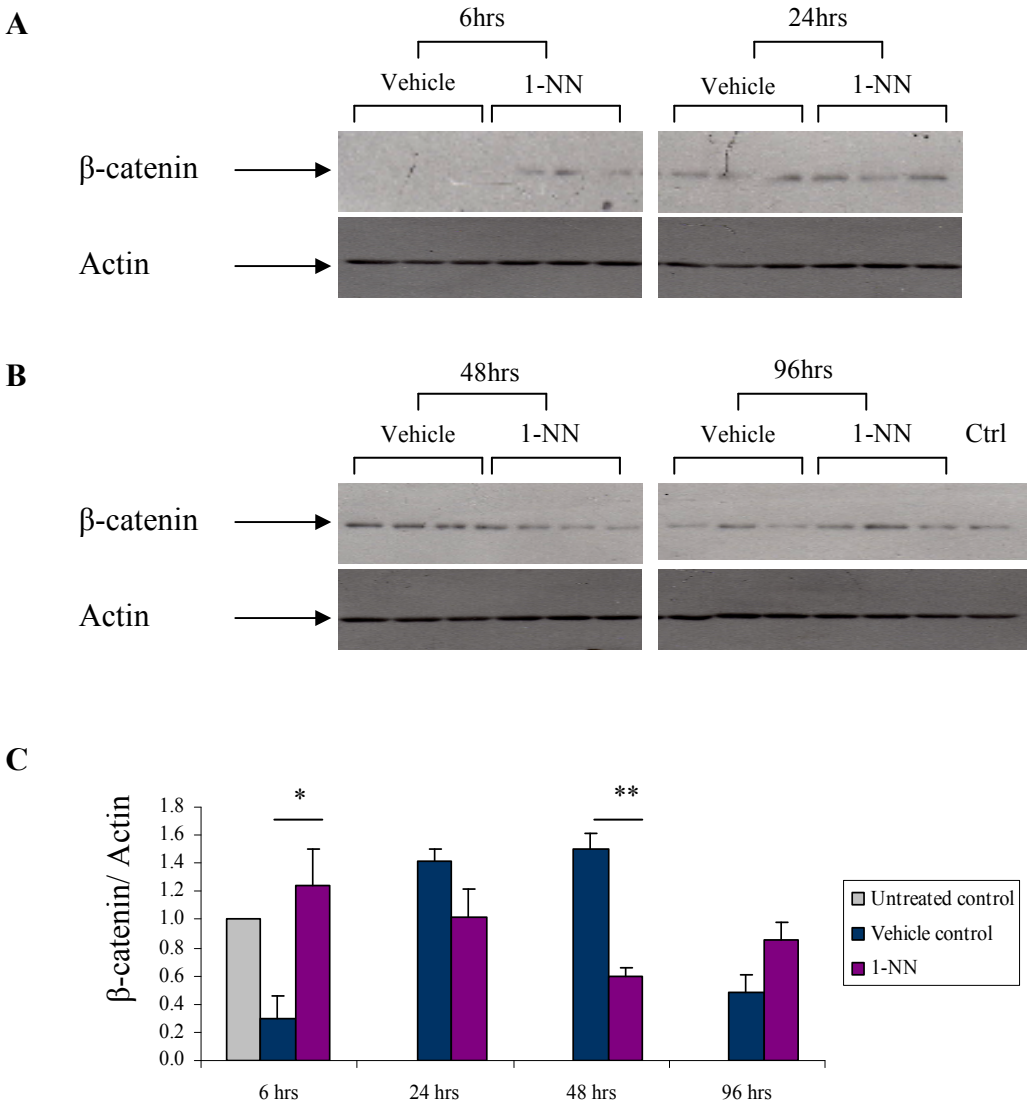

Figure 7.8: 1-NN alters β-catenin protein expression 6 hrs and 48 hrs post treatment

Lung lysis lavage protein from untreated control, vehicle control and 1-NN animals were examined by Western blot analysis for β-catenin expression, using anti-β-catenin antibody (1/250). Western blot gels for β-catenin and actin expression in vehicle control and 1-NN treated animals at A) 6 hrs and 24 hrs B) 48 hrs, 96 hrs and (Ctrl) untreated control. C) Densitometric quantification data of each treatment and time point is presented, actin was used to normalise for loading. Bars represent mean ± SEM based on 3 animals, normalised to 1 untreated control animal. * $p < 0.05$, ** $p < 0.01$.

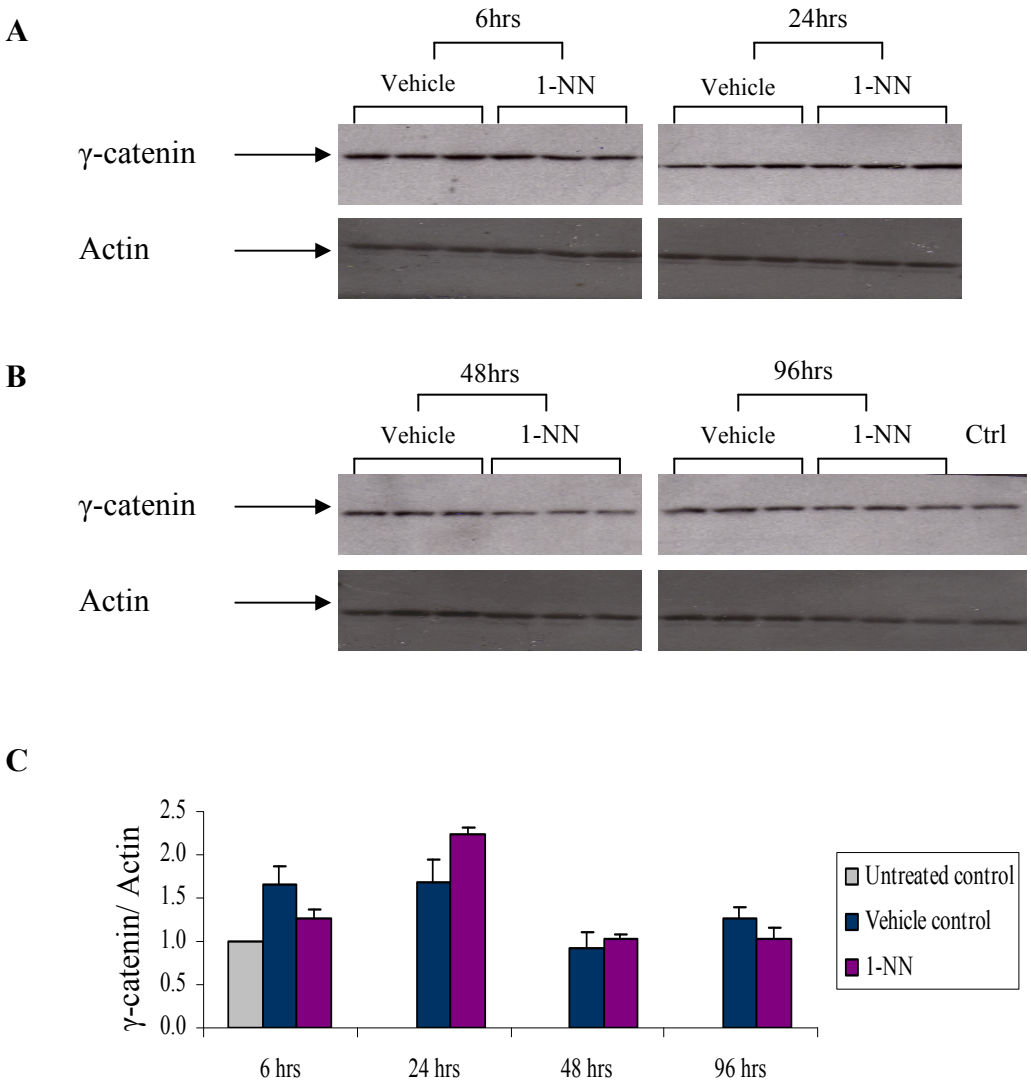

Figure 7.9: γ-catenin expression is not significantly altered by 1-NN treatment

Lung lysis lavage protein from untreated control, vehicle control and 1-NN animals were examined by Western blot analysis for γ-catenin expression, using anti-γ-catenin antibody (1/250). Western blot gels for γ-catenin and actin expression in vehicle control and 1-NN treated animals at A) 6 hrs and 24 hrs B) 48 hrs, 96 hrs and (Ctrl) untreated control. C) Densitometric quantification data of each treatment and time point is presented, actin was used to normalise for loading. Bars represent mean ± SEM based on 3 animals, normalised to 1 untreated control animal.

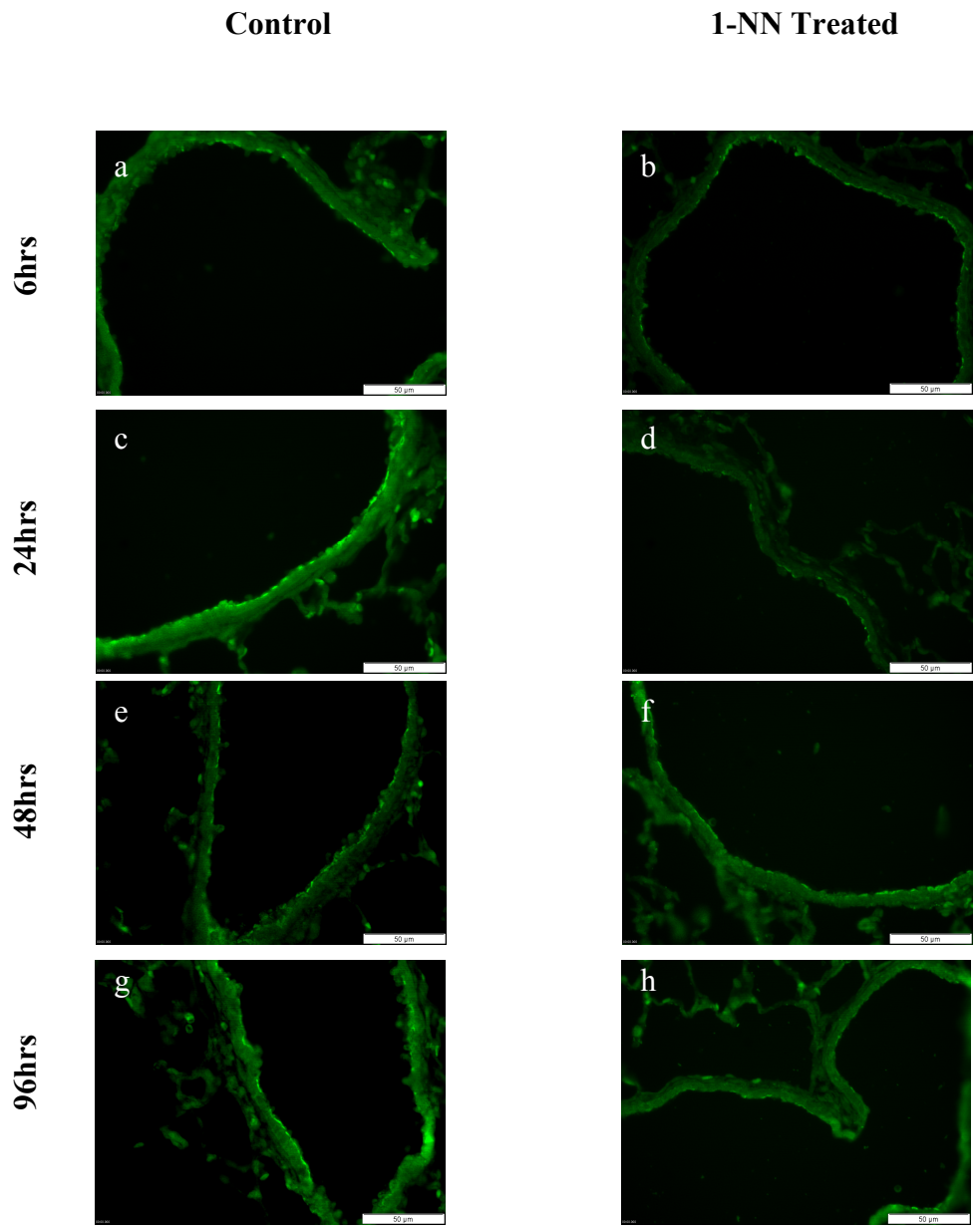

Figure 7.10 A

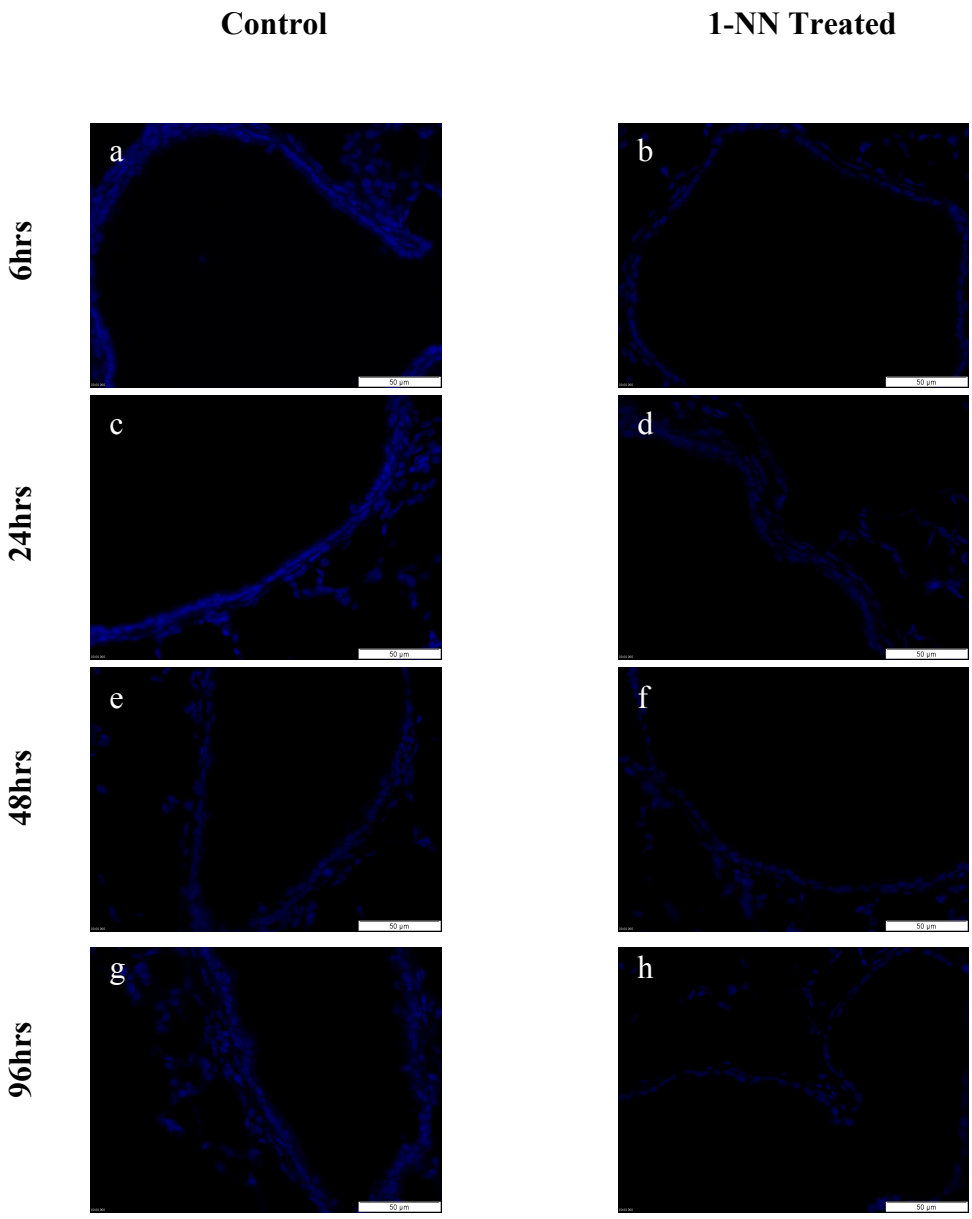

Figure 7.10 B

Figure 7.10: BMPR-IA expression during epithelial damage and repair

Immunofluorescence was carried out on lung tissue from vehicle control and 1-NN animals. A) BMPR-IA expression was found in the cytoplasm of a) 6 hr vehicle control, b) 6 hr 1-NN treated, c) 24 hr vehicle control, d) 24 hr 1-NN treated, e) 48 hr vehicle control, f) 48 hr 1-NN treated, g) 96 hr vehicle control and h) 96 hr 1-NN treated animals. B) Corresponding DAPI counter-stained images.

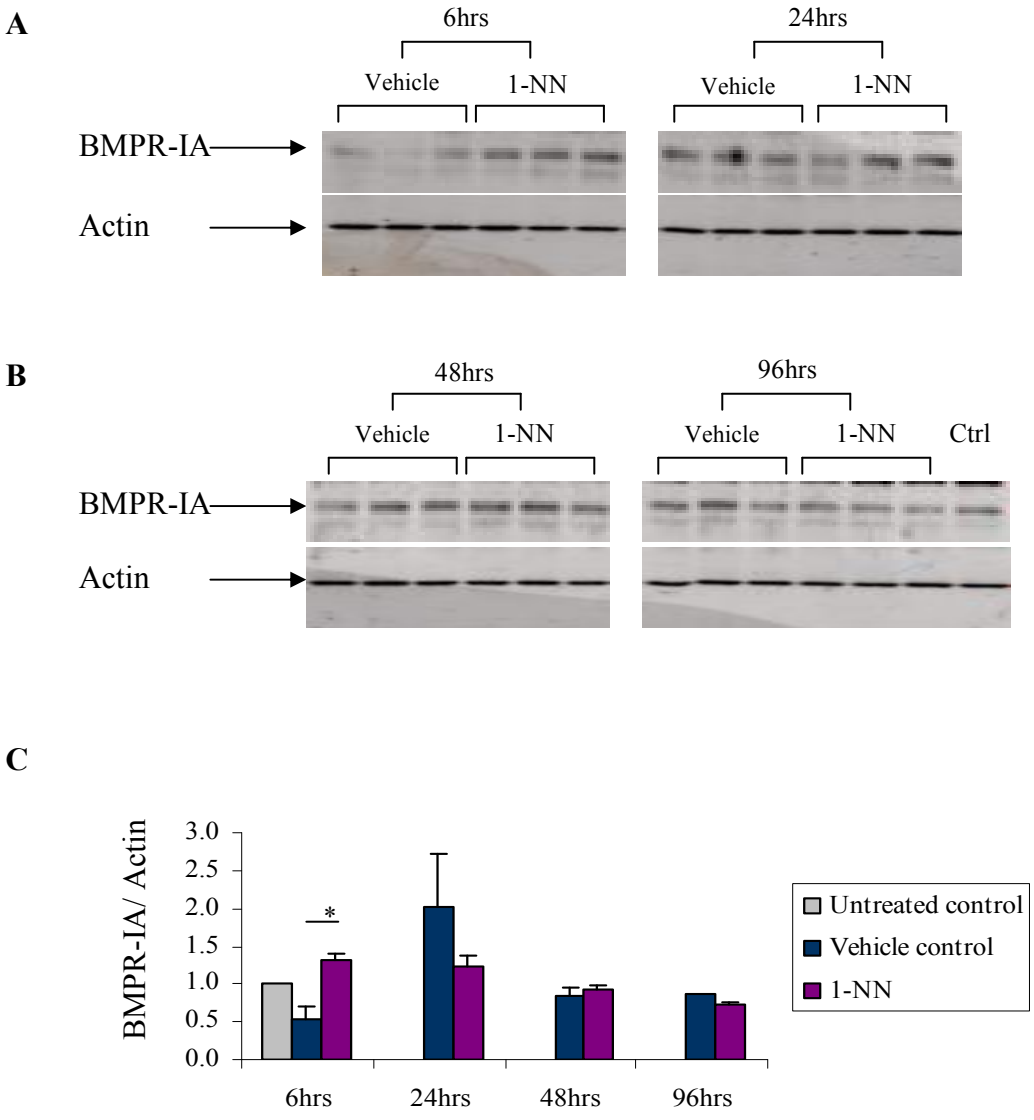

Figure 7.11: BMPR-IA protein expression is increased 6 hrs after 1-NN treatment

Lung lysis lavage protein from untreated control, vehicle control and 1-NN animals were examined by western blot analysis for BMPR-IA expression, using anti-BMPR-IA antibody (1/200). Western blot gels for BMPR-IA and actin expression in vehicle control and 1-NN treated animals at A) 6 hrs and 24 hrs B) 48 hrs, 96 hrs and (Ctrl) untreated control. C) Densitometric quantification data of each treatment and time point is presented, actin was used to normalise for loading. Bars represent mean ± SEM based on 3 animals, normalised to 1 untreated control animal. * $p < 0.05$.

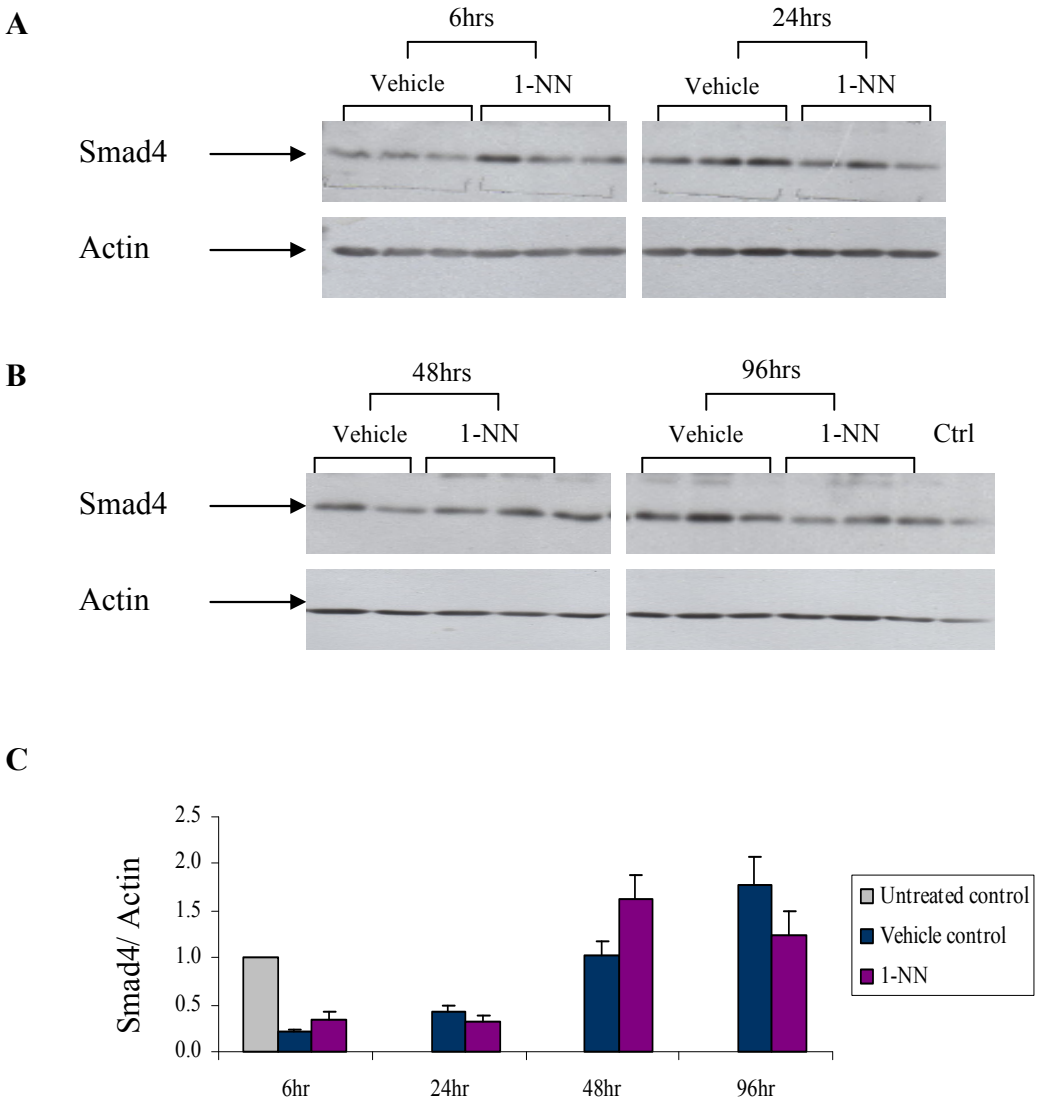

Figure 7.12: Smad4 expression was not significantly altered by 1-NN treatment

Lung lysis lavage protein from untreated control, vehicle control and 1-NN animals were examined by western blot analysis for Smad4 expression, using anti-Smad4 antibody (1/100). Western blot gels for Smad4 and actin expression in vehicle control and 1-NN treated animals at A) 6 hrs and 24 hrs B) 48 hrs, 96 hrs and (Ctrl) untreated control. C) Densitometric quantification data of each treatment and time point is presented, actin was used to normalise for loading. Bars represent mean ± SEM based on 3 animals (except 48 hrs ctrl which is based on 2 animals), normalised to 1 untreated control animal.

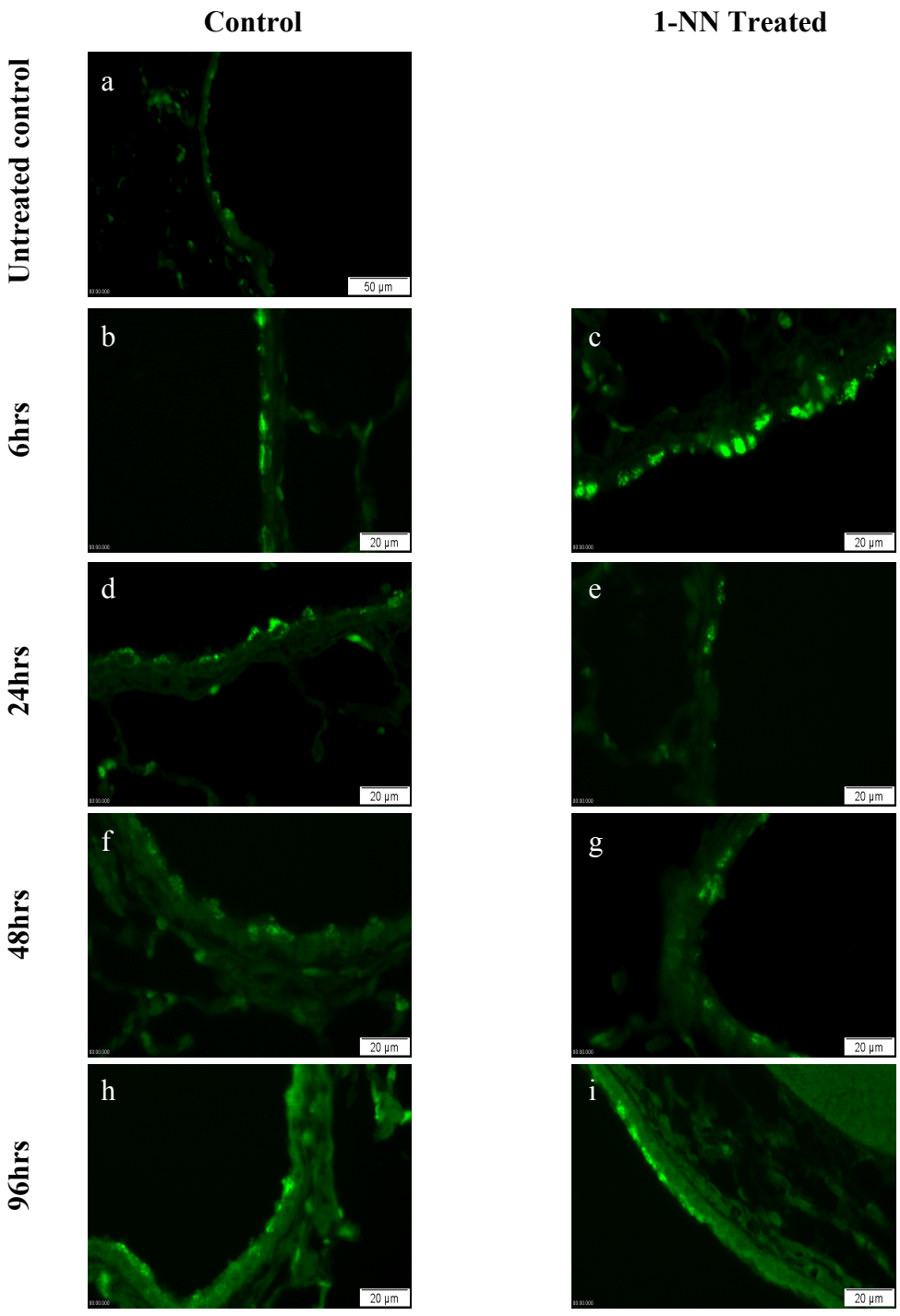
Control
1-NN Treated
Untreated control
6hrs
24hrs
48hrs
96hrs
a
b
c
d
e
f
g
h
i
50 µm
20 µm

Figure 7.13 A

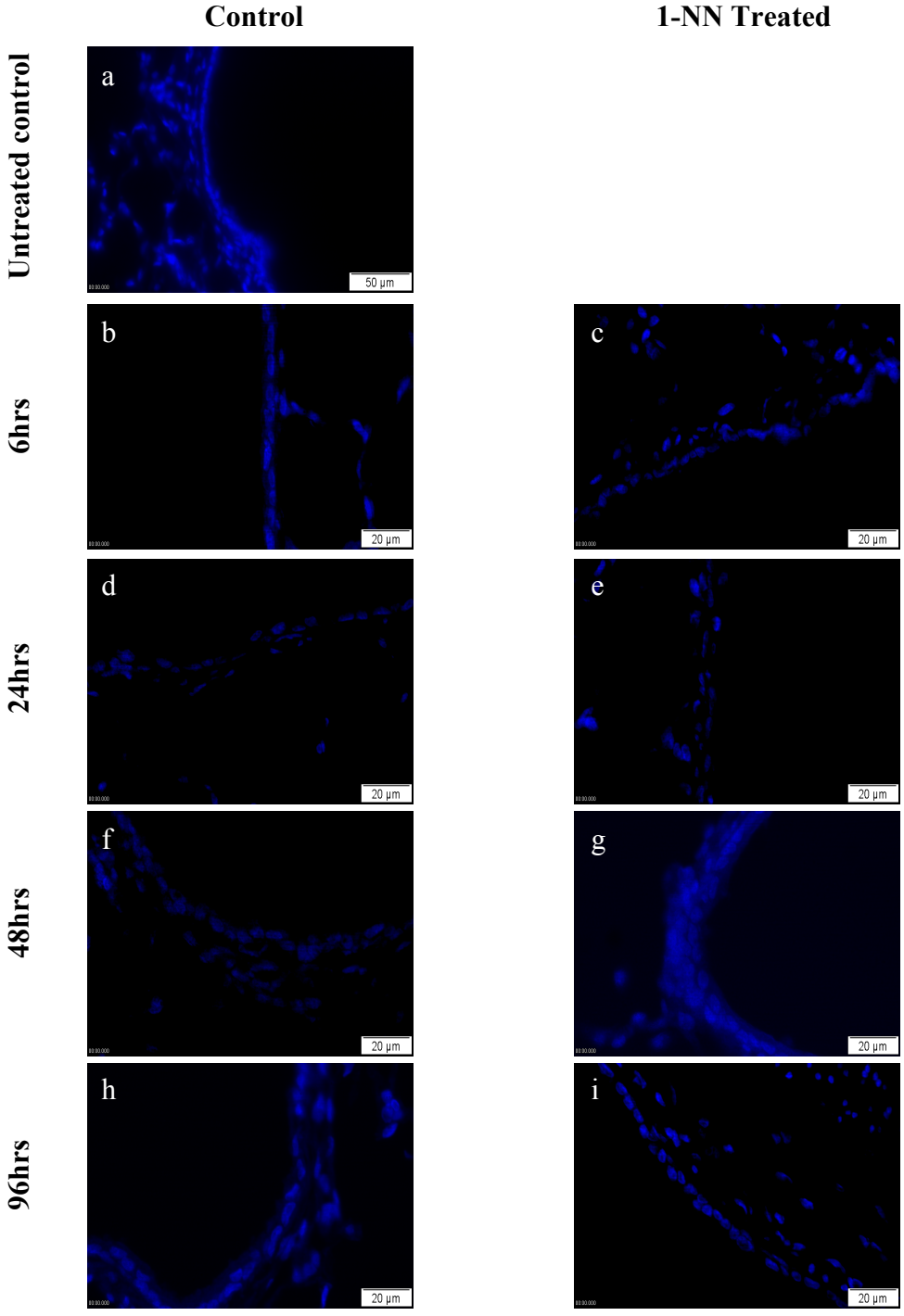
Control
1-NN Treated
Untreated control
6hrs
24hrs
48hrs
96hrs
a
b
c
d
e
f
g
h
i
50 µm
20 µm

Figure 7.13 B

Figure 7.13: p-Smad expression during epithelial damage and repair

Immunofluorescence was carried out on lung tissue from vehicle control and 1-NN animals using anti-p-Smad antibody at 1/50 dilution. A) p-Smad expression was found in the cytoplasm of a) untreated control animal, b) 6 hr vehicle control, c) 6 hr 1-NN treated, d) 24 hr vehicle control, e) 24 hr 1-NN treated, f) 48 hr vehicle control, g) 48 hr 1-NN treated, h) 96 hr vehicle control and i) 96 hr 1-NN treated animals. B) Corresponding DAPI counter-stained images.

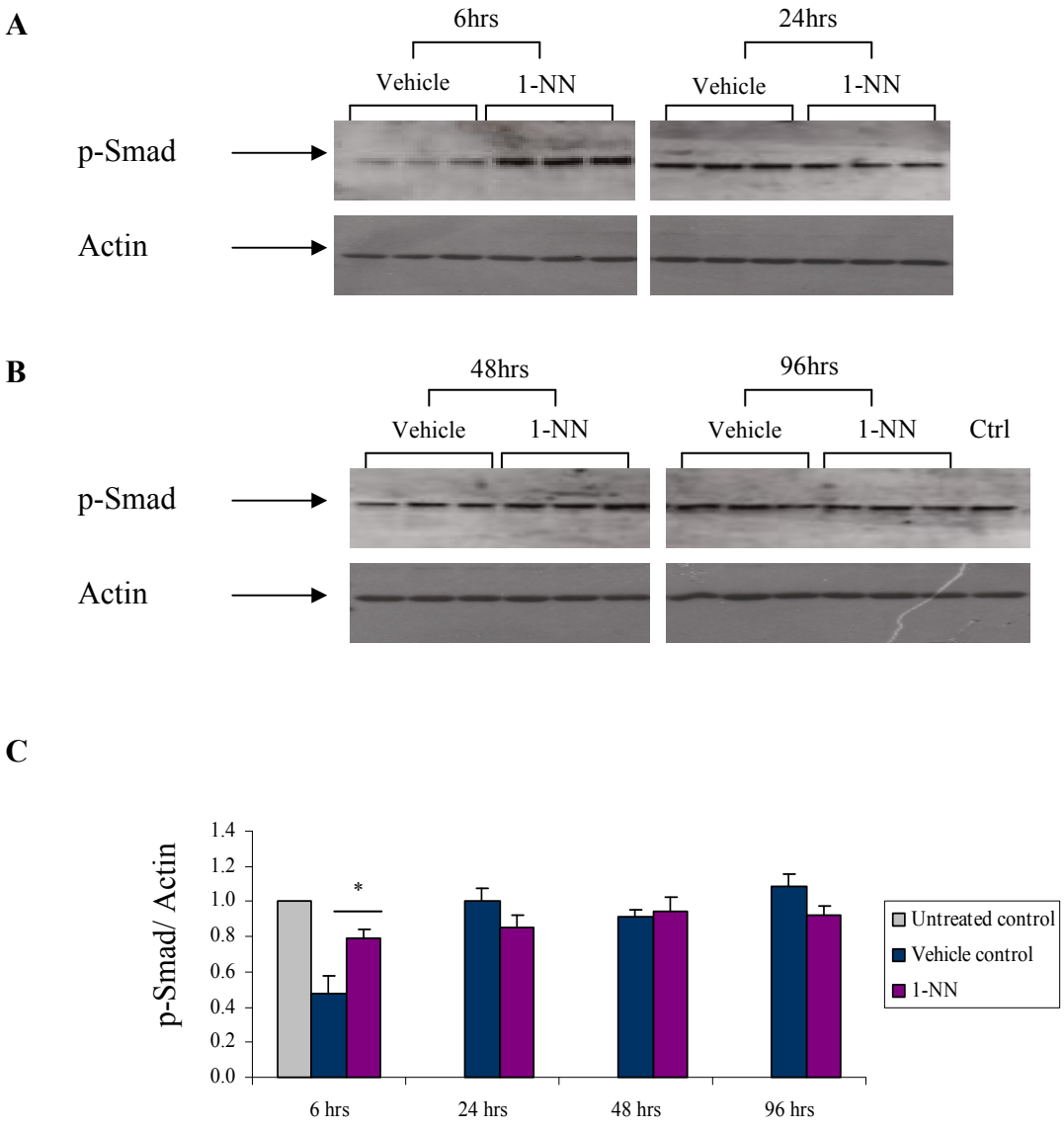

Figure 7.14: p-Smad protein expression after 1-NN treatment

Lung lysis lavage protein from untreated control, vehicle control and 1-NN animals were examined by Western blot analysis for p-Smad expression, using anti-p-Smad antibody (1/1000). Western blot gels for p-Smad and actin expression in vehicle control and 1-NN treated animals at A) 6 hrs and 24 hrs B) 48 hrs, 96 hrs and (Ctrl) untreated control. C) Densitometric quantification data of each treatment and time point is presented, actin was used to normalise for loading. Bars represent mean ± SEM based on 3 animals, normalised to 1 untreated control animal. * $p < 0.05$.

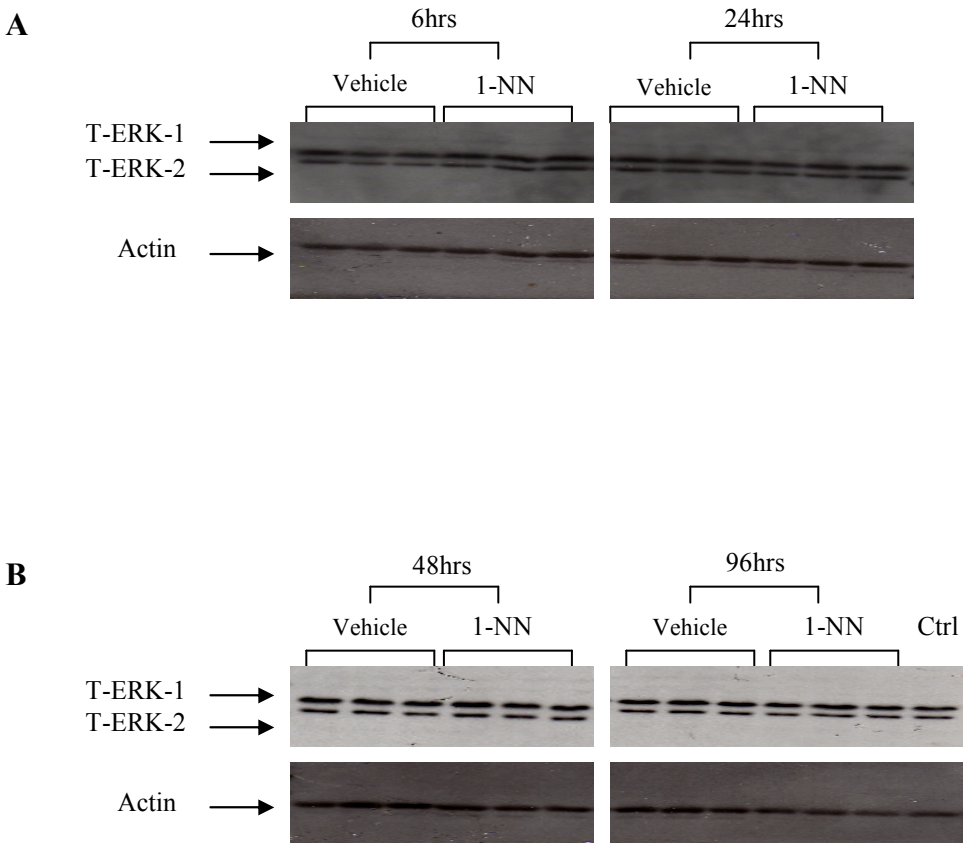

Figure 7.15: T-ERK protein expression following 1-NN treatment

Western blot analysis was carried out on lung lysis lavage protein to quantify T-ERK protein in A) 6 hr and 24 hr, vehicle control and 1-NN treated animals and B) 48 hr and 96 hr, vehicle control and 1-NN treated animals, and untreated control animal (Ctrl).

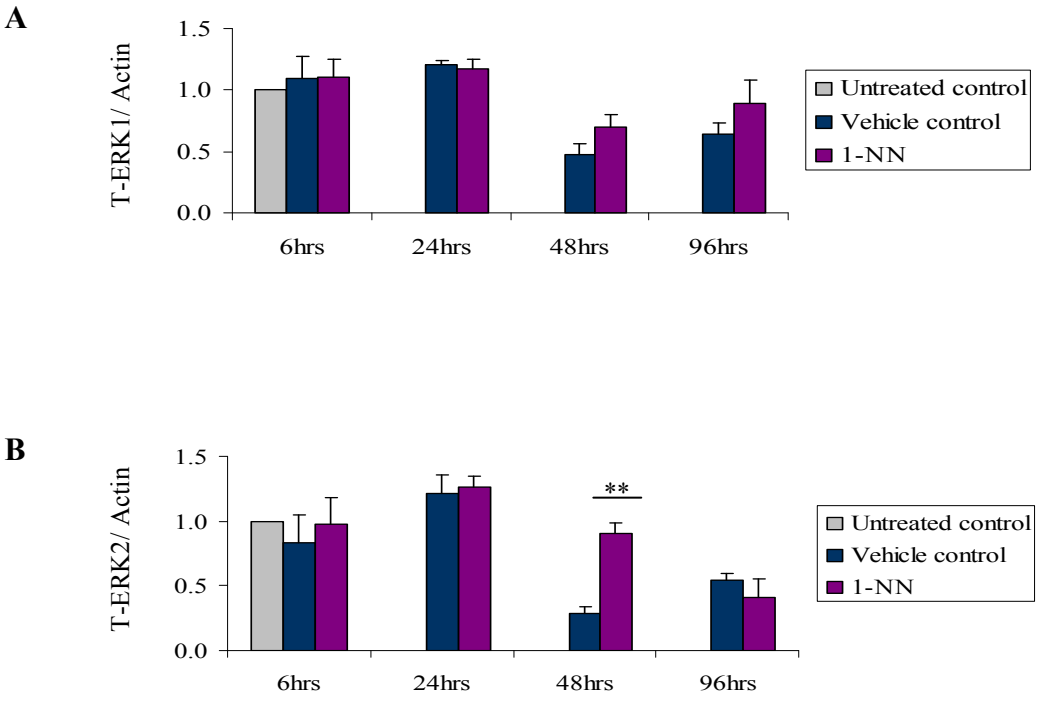

Figure 7.16: Quantification of T-ERK expression following 1-NN treatment

Densitometry was carried out on Western blot results in figure 7.15. T-ERK expression in each sample was normalised to its respective actin value. Graphs represent A) Mean densitometry values for T-ERK-1. B) Mean densitometry values for T-ERK-2. Bars represent mean ± SEM based on 3 animals, normalised to 1 untreated control animal. * $p < 0.05$.

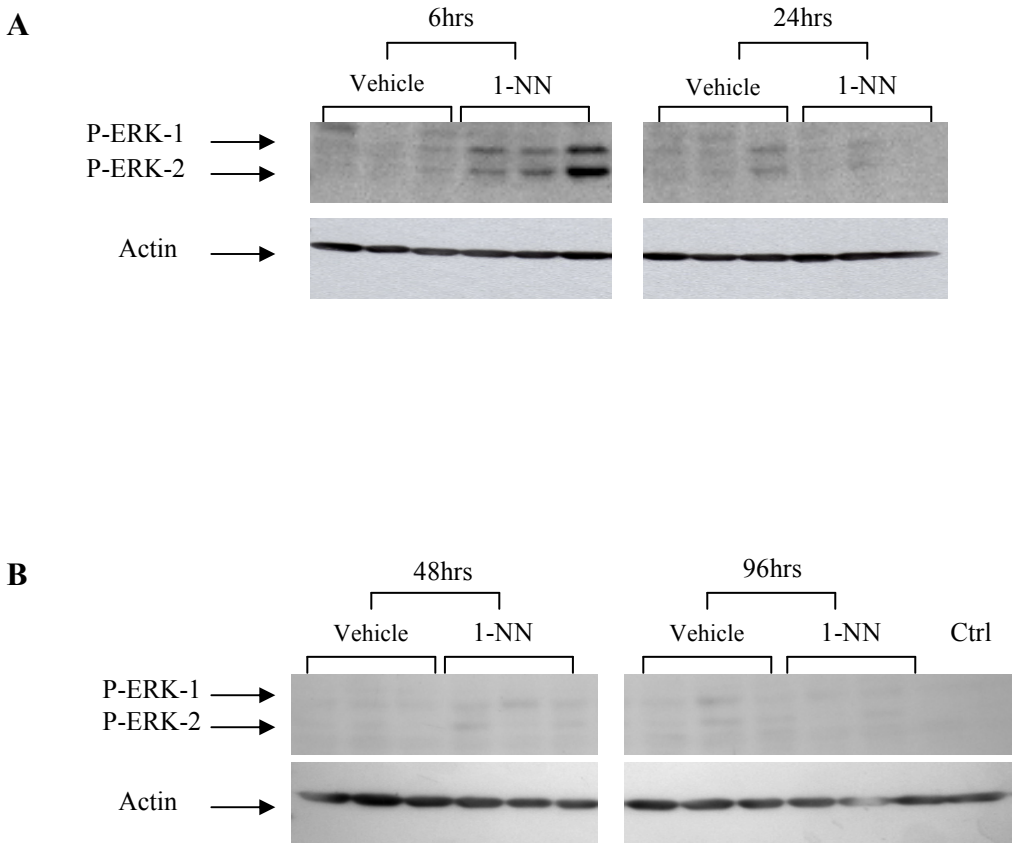

Figure 7.17: P-ERK protein expression following 1-NN treatment

Lung lysis lavage protein from untreated control, vehicle control and 1-NN animals were examined by Western blot analysis for P-ERK expression, using anti-P-ERK antibody (1/1000). Western blot gels for P-ERK and actin expression in vehicle control and 1-NN treated animals at A) 6 hrs and 24 hrs B) 48 hrs, 96 hrs and (Ctrl) untreated control.

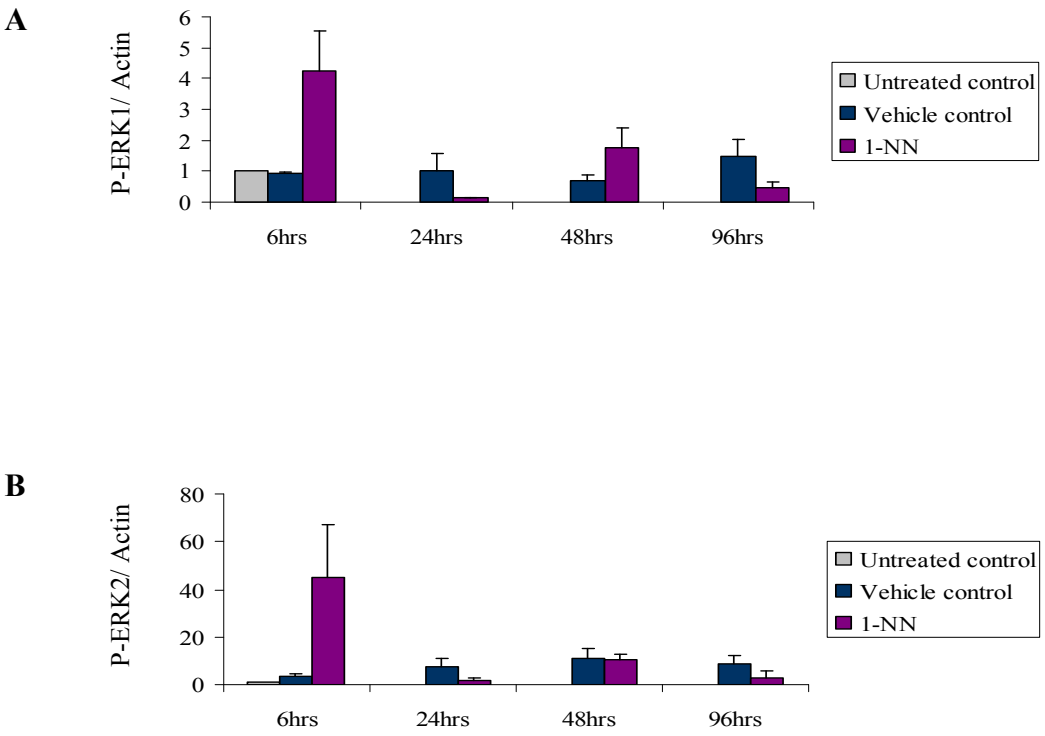

Figure 7.18: P-ERK expression in rat 1-NN time course model

Densitometry was carried out on Western blot results from figure 7.17. P-ERK expression in each sample was normalised to its respective actin value. Graphs represent A) Mean densitometry values for P-ERK-1,with each value normalised to actin. B) Mean densitometry values for P-ERK-2, with each value normalised to actin. Bars represent mean ± SEM based on 3 animals, normalised to 1 untreated control animal. * $p < 0.05$.

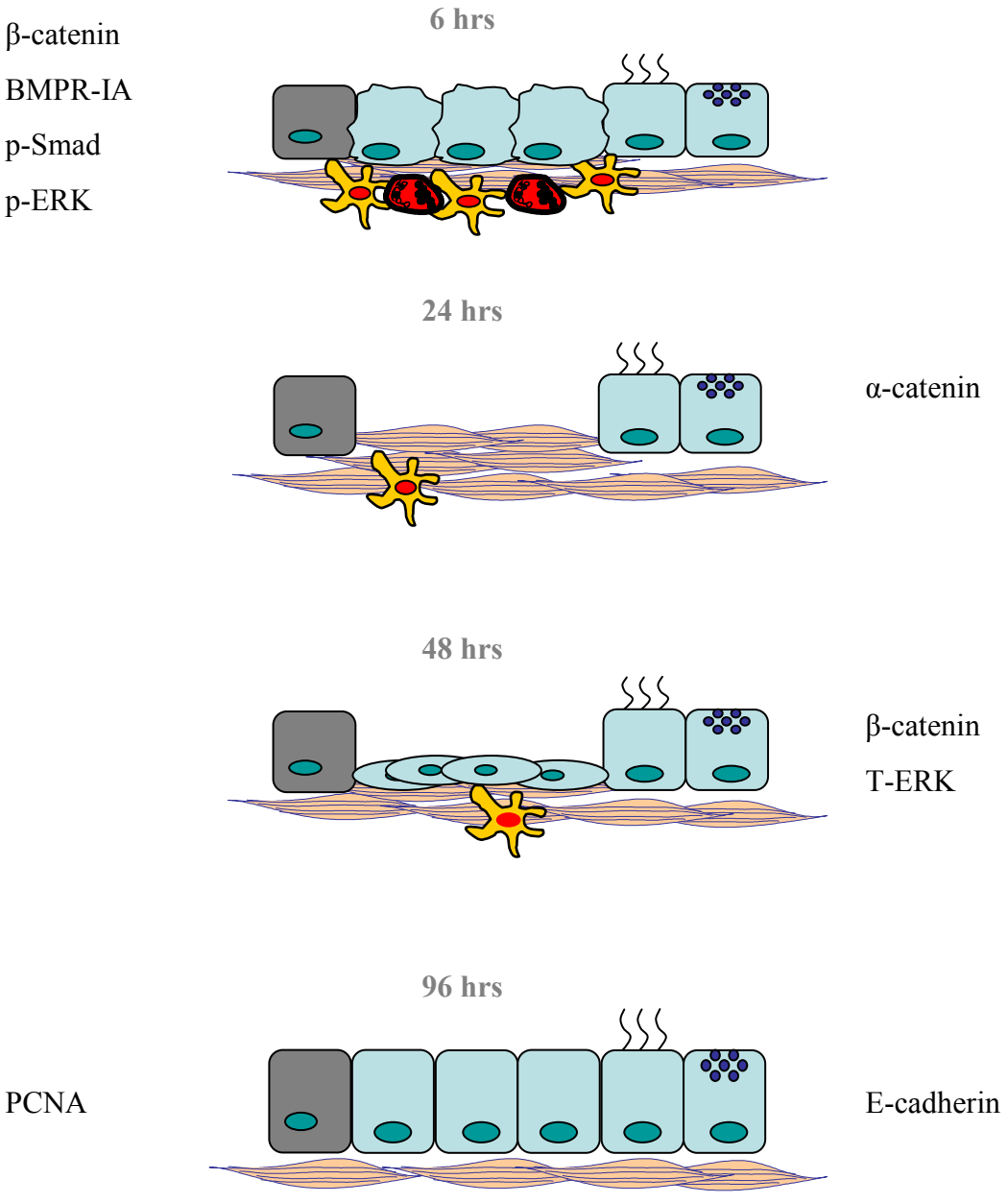

Figure 7.19: Effects of 1-NN damage on protein expression

This summary diagram represents protein expression that was either up-regulated or down-regulated at each of the time points after 1-NN treatment. Inflammatory cell infiltration was evident at 6 hrs; epithelial damage occurred at 24 hrs; squamous cell infiltration occurred at 48 hrs; epithelial repair occurred at 96 hrs.

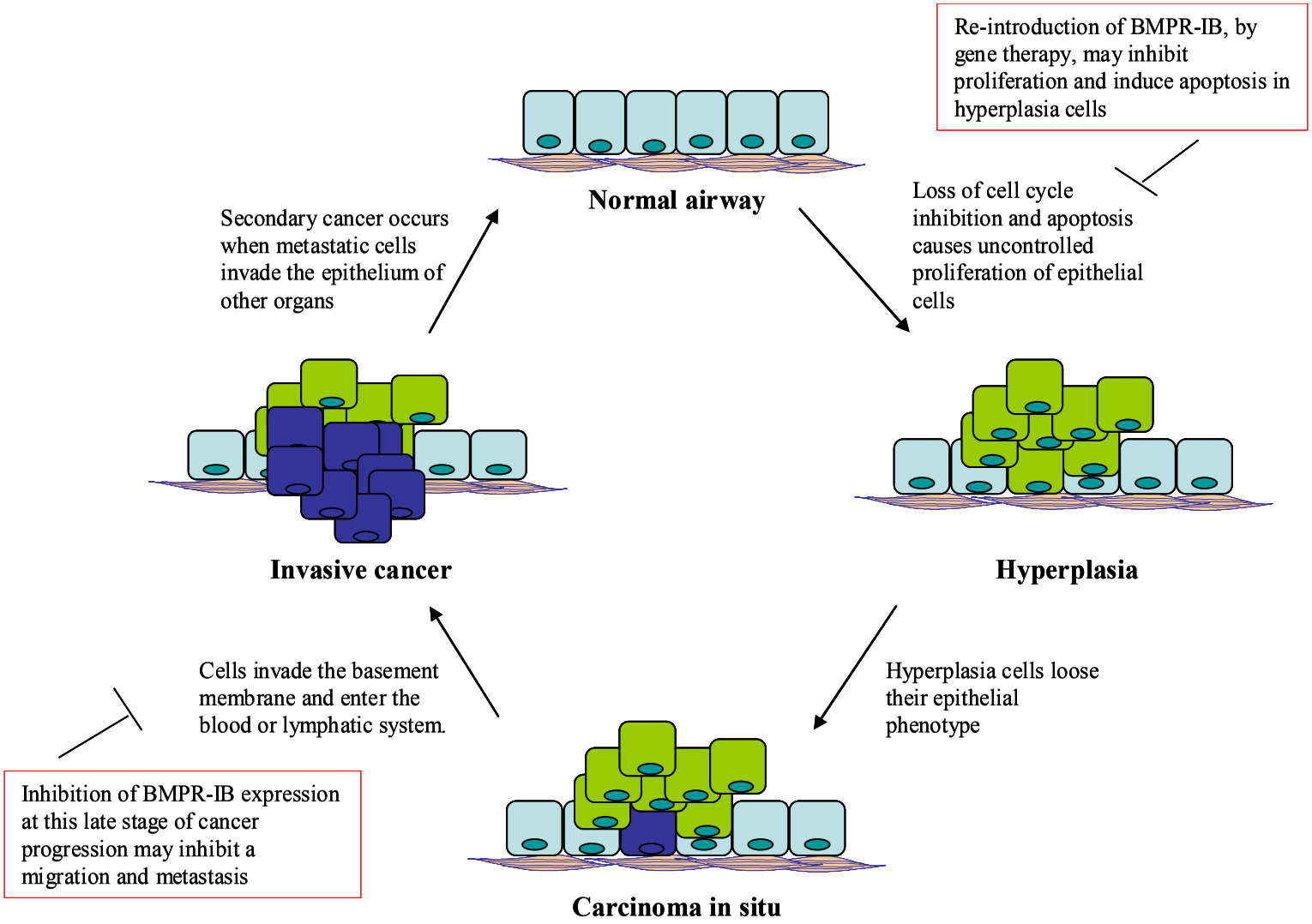
Re-introduction of BMPR-IB, by gene therapy, may inhibit proliferation and induce apoptosis in hyperplasia cells
Normal airway
Loss of cell cycle inhibition and apoptosis causes uncontrolled proliferation of epithelial cells
Secondary cancer occurs when metastatic cells invade the epithelium of other organs
Hyperplasia
Invasive cancer
Hyperplasia cells loose their epithelial phenotype
Cells invade the basement membrane and enter the blood or lymphatic system.
Inhibition of BMPR-IB expression at this late stage of cancer progression may inhibit a migration and metastasis
Carcinoma in situ